

2007

# Experimental and numerical studies for evaluating dynamic behaviour of prestressed concrete sleepers subject to severe impact loading

Sakdirat Kaewunruen  
*University of Wollongong*

---

## Recommended Citation

Kaewunruen, Sakdirat, Experimental and numerical studies for evaluating dynamic behaviour of prestressed concrete sleepers subject to severe impact loading, PhD thesis, School of Civil, Mining & Environmental Engineering, University of Wollongong, 2007.  
<http://ro.uow.edu.au/theses/277>

## **NOTE**

This online version of the thesis may have different page formatting and pagination from the paper copy held in the University of Wollongong Library.

## **UNIVERSITY OF WOLLONGONG**

### **COPYRIGHT WARNING**

You may print or download ONE copy of this document for the purpose of your own research or study. The University does not authorise you to copy, communicate or otherwise make available electronically to any other person any copyright material contained on this site. You are reminded of the following:

Copyright owners are entitled to take legal action against persons who infringe their copyright. A reproduction of material that is protected by copyright may be a copyright infringement. A court may impose penalties and award damages in relation to offences and infringements relating to copyright material. Higher penalties may apply, and higher damages may be awarded, for offences and infringements involving the conversion of material into digital or electronic form.

**EXPERIMENTAL AND NUMERICAL STUDIES FOR  
EVALUATING DYNAMIC BEHAVIOUR OF PRESTRESSED  
CONCRETE SLEEPERS SUBJECT TO SEVERE IMPACT LOADING**

A thesis submitted in fulfillment of  
the requirements for the award of the degree

**DOCTOR OF PHILOSOPHY**

(Civil Engineering)

from

**UNIVERSITY OF WOLLONGONG**

by

**SAKDIRAT KAEWUNRUEN**

BEng (Hons), MEng (Civil)

School of Civil, Mining, and Environmental Engineering

Faculty of Engineering

2007

## **CERTIFICATION**

I, Sakdirat Kaewunruen, declare that this thesis, submitted in fulfillment of the requirements for the award of Doctor of Philosophy, in the School of Civil, Mining, and Environmental Engineering, University of Wollongong, is wholly my own work unless otherwise referenced or acknowledged. The document has not been submitted for qualifications at any other academic institution

The published documents and presented materials, which are fully or partly related to the research work conducted in this PhD program, are included in Section R2 of the Reference.

Sakdirat Kaewunruen

19 November 2007

## ABSTRACT

Rail operators are consistently demanding higher axle loads to compete effectively with other modes of transport, particularly for heavy haul freight of minerals. However, high axle loads can only be achieved by ensuring that the existing rail infrastructure can cope with the greater static and dynamic loads associated with the wheel-rail interactions. Premature cracking of prestressed concrete sleepers is often the result of high-intensity dynamic loading caused by wheel or rail irregularities. The high-magnitude wheel loads produced by a small percentage of “bad” wheels or rail head surface defects are crudely accounted for in the Australian Standard AS 1085.14 by a single load amplification factor. In addition, there is a widespread perception within the railway engineering community that the carrying capacity of the existing track infrastructure is not fully utilised, and concrete sleepers possess significant amounts of untapped reserve strength. This can be attributed to the current design philosophy for concrete sleepers, outlined in AS 1085.14. This is based on the assessment of permissible stresses resulting from quasi-static wheel loads and essentially the static response of concrete sleepers, making it unduly conservative and very costly for the railway organisations. This thesis addresses the identified deficiencies of the current design method through an in-depth analysis of the dynamic response of concrete sleepers under realistic loading conditions and proposes a more rational design procedure.

In order to shift the conventional methodology to a more rational design method that involves more realistic dynamic response of concrete sleepers and performance-based design methodology, a significant research effort within the framework of the Cooperative Research Centre (CRC) for Railway Engineering and Technologies has been carried out to perform comprehensive studies of the loading conditions, the dynamic response, and the dynamic resistance of prestressed concrete sleepers. The collaborative research between the University of Wollongong (UoW) and Queensland University of Technology (QUT) has addressed such important issues as the spectrum and amplitudes of dynamic forces applied to the railway track, evaluation of the reserve capacity of typical prestressed concrete

sleepers designed to the current code AS 1085.14, and the development of a new limit states design concept.

The comprehensive literature review highlighted the extremely limited research work that previously had been done in this field of research. In order to enhance an understanding of the dynamic performance of railway tracks, the first part of this thesis investigates the dynamic characteristics of the global railway track and its individual components with particular reference to rail pads and prestressed concrete (PC) sleepers. The experimental techniques for extracting dynamic properties of track components, developed in the laboratory, have been successfully applied in field trials. Moreover, this thesis provides an intensive review aimed at predicting wheel impact loads due to the wheel/rail irregularities at different return periods (based on the field data from wheel impact detectors).

The experimental and numerical investigations into the dynamic behaviour of prestressed concrete sleepers subjected to severe impact loading are then presented. The impact tests were carried out using the prestressed concrete sleepers manufactured in Australia. A track test bed was simulated in the laboratory and calibrated against the frequency response functions obtained for real tracks. A series of incremental impact loading tests for the prestressed concrete sleepers was performed, ranging from a typical design load to a severe wheel load. The cumulative impact damage and crack propagation in concrete sleepers were identified. The effects of track environment together with the relationship between the bending moment of prestressed concrete sleepers and the applied impact force are also presented.

The later part of this thesis identifies the responses of prestressed concrete sleepers in railway track structures under both single and repeated impact loads associated with different probabilities of occurrence. The residual capacities of the damaged prestressed concrete sleepers are studied in order to clarify the notion about the reserve strength of the concrete sleepers. The numerical investigations of the static and impact behaviours of railway prestressed concrete sleepers under static and dynamic loads were also undertaken to supplement the experimental findings in this thesis.

A proposal for the reliability-based design concepts and rationales associated with the development of limit states design procedures for the conversion of AS 1085.14 to a limit states design format is one of the key outcomes of this thesis. The new limit states design concepts and procedures for railway prestressed concrete sleepers are presented as the design guidelines for the railway engineers. The new methodology is aimed not only to save the material resources to achieve financial gains, but also to reduce the amount of cement production which would otherwise emit carbon dioxide as a contributing factor towards global warming.

## ACKNOWLEDGEMENTS

This thesis could not have been successfully completed without the help received from many people. Firstly, the author is highly grateful to his supervisor, Dr. Alex Remennikov, for his thoughtful guidance, invaluable support, encouragement and patience in completing this thesis. Dr. Remennikov's willingness to help at all stages of this thesis and the 'open door policy' was deeply appreciated.

The author would like to express his sincere appreciation to the technical officers and colleagues at the University of Wollongong, including Alan Grant, Ian Bridge, Bob Rowland, Jason Knust, Ken and Ian Laird, and Ee Loon Tan for their active assistance throughout the test rig construction and experimental stages of the research project. He would like to thank the following people for the valuable comments, suggestions, and support, including Professors Jens Nelsen of Chalmers University of Technology, Sweden; Brian Uy of University of Western Sydney, Australia; William N Sharpe Jr of Johns Hopkins University, USA; and, N. Kishi of Muroran Institute of Technology Japan. The copy editing for English by Mr. Bill Clayton (Bill Clayton Writing Services) is gratefully acknowledged.

The author wishes to express his gratitude to the Australian Cooperative Research Centre for Railway Engineering and Technologies (RailCRC) for the PhD scholarship and financial support to this research project. He would also like to thank the Rail CRC steering committee for Project 5/23, including Messrs Karl Ikaunieks, Ric Lewtas, Steve Douglas, John Cowie, Jeffrey Leong, and Dr Martin Murray for their expertise, guidance, and support. The assistance of the Royal Thai Government is appreciated throughout the permission for sabbatical leave from the Department of Public Works and Town & Country Planning, Ministry of Interior.

The author is profoundly grateful for the continuous support and patience to his family and friends who have given him their time, enjoyment, and support during the course of his candidature. Special thanks are also given to those who gave the assistance, support, and compliments to the author but would like to remain anonymous.



# TABLE OF CONTENTS

	<b>Page</b>
ABSTRACT	iii
ACKNOWLEDGEMENTS	vi
TABLE OF CONTENTS	vii
LIST OF FIGURES	xiv
LIST OF TABLES	xxiii
NOMENCLATURES	xxv
<b>CHAPTER 1 INTRODUCTION</b>	<b>1</b>
1.1 GENERAL BACKGROUND	1
1.2 STATEMENT OF THE PROBLEM	4
1.3 SCOPE OF STUDY	5
1.4 OBJECTIVES OF THE STUDY	6
1.5 ORGANISATION OF THE THESIS	7
<b>CHAPTER 2 REVIEW OF THE DYNAMICS OF RAILWAY TRACK AND ITS COMPONENTS</b>	<b>9</b>
2.1 BALLASTED RAILWAY TRACKS	9
2.1.1 Rail	10
2.1.2 Fastening Systems	10
2.1.3 Fasteners	12
2.1.4 Rail Pads	12
2.1.5 Sleepers	12
2.1.6 Ballast	13
2.1.7 Sub-ballast	15
2.1.8 Subgrade	15
2.2 MODAL TESTING	15
2.3 DYNAMICS OF RAIL PADS	18
2.3.1 Linear and nonlinear model of rail pads	18
2.3.2 Dynamic testing of rail pads	19

2.4 VIBRATIONS OF CONCRETE SLEEPERS	21
2.5 DYNAMICS OF RAILWAY TRACKS	24
2.5.1 In-situ dynamic testing	25
2.5.2 Field trials	26
2.6 SUMMARY	27
<b>CHAPTER 3 DYNAMIC CHARACTERISTICS OF RAILWAY TRACK AND ITS COMPONENTS</b>	<b>29</b>
3.1 RAIL PADS	29
3.1.1 Analytical Modal Analysis	33
3.1.1.1 SDOF Dynamic Model	35
3.1.1.2 Vibration Measurements	36
3.1.1.3 Parameter Optimization	36
3.1.2 New Rail Pad Tester	36
3.1.2.1 Design Attributes	36
3.1.2.2 Preload Control	37
3.1.2.2 Modal Testing	37
3.1.3 Applications of the new rail pad tester	40
3.1.3.1 Determination of Dynamic Rail Pad Characteristics	40
3.1.3.2 Monitoring Deterioration of Worn Pads	41
3.1.4 Results of dynamic rail pad characteristics	41
3.2 PRESTRESSED CONCRETE SLEEPERS	46
3.2.1 Analytical Modal Analysis	48
3.2.2 Experimental Overview	50
3.2.3 Experimental Results	51
3.3 IN SITU RAILWAY TRACK	59
3.3.1 Modal results	61
3.3.2 Three-dimensional Finite Element Model	62
3.4 FIELD TRIALS	64
3.4.1 General Background	64
3.4.2 Track Simulation	66
3.4.3 System Identification	67

3.4.4 Condition Assessment	70
3.4.5 Field Trials	72
3.4.5.1 Good condition tracks	74
3.4.5.2 Loosening rail fastening system	77
3.4.5.3 Cracked sleeper	78
3.4.6 Full-Scale Modal Testing of In-situ Concrete Sleeper	79
3.5 SUMMARY	81
3.5.1 Rail Pads	81
3.5.2 Prestressed Concrete Sleepers	81
3.5.3 In situ Railway Track	82
3.5.4 Field Trials	82
<b>CHAPTER 4 REVIEW OF LOADING CONDITIONS ON RAILWAY</b>	<b>84</b>
<b>TRACK STRUCTURES AND THEIR RESPONSES</b>	
4.1 BASIC CONCEPTS	84
4.2 STATIC AND QUASI-STATIC (DYNAMIC RIDE) LOADING	89
4.3 IMPACT LOADING ON RAILWAY TRACKS	98
4.3.1 Impact loads due to worn wheel/rail surface profiles	98
4.3.2 Impact loads due to wheel flats and shells	103
4.3.3 Impact loads due to bad welds, joints, and switches	110
4.3.4 Impact loads due to rail corrugation	115
4.3.5 Impact loads due to unsupported sleepers	118
4.4 IMPACT RESISTANCE OF CONCRETE SLEEPERS	119
4.4.1 Experimental Techniques for Impact Testing	120
4.4.2 Evaluation of Impact Resistance in Laboratories	121
4.4.3 In-field Impact Tests	122
4.5 SUMMARY	123
<b>CHAPTER 5 INVESTIGATION ON STATIC ULTIMATE LOAD-</b>	<b>126</b>
<b>CARRYING CAPACITY OF PRESTRESSED CONCRETE SLEEPERS</b>	
5.1 OVERVIEW	126
5.2 NEGATIVE MOMENT TEST AT MID-SPAN	130
5.2.1 Load-deflection relationship	132

5.2.2 Energy absorption characteristics	132
5.2.3 Rotational capacity	135
5.2.4 Stress-strain curves	136
5.2.5 Mode of failure	138
5.2.6 Post-failure mechanisms and crack propagation	139
<b>5.3 POSITIVE MOMENT TEST AT RAILSEAT</b>	<b>144</b>
5.3.1 Load-deflection relationship	146
5.3.2 Energy absorption characteristics	148
5.3.3 Rotational capacity	148
5.3.4 Stress-strain curves	150
5.3.5 Mode of failure	151
5.3.6 Post-failure mechanisms and crack propagation	152
<b>5.4 SECTIONAL ANALYSIS</b>	<b>158</b>
5.4.1 Railseat section	158
5.4.2 Mid-span section	161
<b>5.5 SUMMARY</b>	<b>163</b>
<b>CHAPTER 6 IMPACT TESTING OF PRESTRESSED CONCRETE</b>	<b>166</b>
<b>SLEEPERS</b>	
6.1 OVERVIEW	166
6.2 TEST SPECIMENS	167
6.3 SUPPORT CONDITIONS	168
6.3.1 Alternative support	169
6.3.2 Test sample	170
6.3.3 Load-displacement analysis	172
6.3.4 2DOF modal analysis	174
6.3.5 MDOF modal analysis	177
6.4 IMPACT TESTING FACILITY	181
6.4.1 High-capacity drop-weight impact testing machine	182
6.4.2 Calibration of impactor using a high-speed camera	183
6.5 TEST INSTRUMENTATION	184
6.5.1 Measurement devices	184

6.5.2 Data acquisition system	187
6.6 IMPACT ANALYSIS	188
6.6.1 Effect of inertia load	188
6.6.2 Energy of the impactor	189
6.6.3 Energy loss in the impactor	189
6.7 SIMULATION OF IMPACT LOADS	190
6.7.1 Drop impact tests	193
6.7.2 Impact loads	196
6.8 SUMMARY	199
<b>CHAPTER 7 PROGRESSIVE IMPACT RESPONSES OF PRESTRESSED</b>	<b>201</b>
<b>CONCRETE SLEEPERS</b>	
7.1 OVERVIEW	201
7.2 EXPERIMENTAL PROGRAM	203
7.3 RELATION BETWEEN IMPACT FORCE AND DYNAMIC MOMENT	205
7.3.1 D-TRACK for dynamic analysis of railway tracks	205
7.3.2 Benchmarking	206
7.3.3 Case studies: computer simulations	209
7.3.4 Case studies: experiments	211
7.4 IMPACT PERFORMANCE	215
7.4.1 Crack propagations	215
7.4.2 Progressive failure	220
7.5 IMPACT DAMAGE CLASSIFICATION	225
7.6 SUMMARY	229
<b>CHAPTER 8 REPEATED IMPACT BEHAVIOUR AND RESIDUAL</b>	<b>231</b>
<b>CAPACITY OF PRESTRESSED CONCRETE SLEEPERS</b>	
8.1 OVERVIEW	231
8.2 EXPERIMENTAL PROGRAM	235
8.3 CRACK PROPAGATION UNDER SINGLE IMPACT CONDITIONS	238
8.3.1 Cracks of prestressed concrete sleeper in soft track condition	238
8.3.2 Cracks of prestressed concrete sleeper in hard track condition	241
8.3.3 Crack propagations under single impact loading	243

8.4 CRACK PROPAGATION UNDER REPEATED IMPACT CONDITIONS	244
8.4.1 Cracks of prestressed concrete sleeper in soft track condition	244
8.4.2 Cracks of prestressed concrete sleeper in hard track condition	248
8.4.3 Crack propagations under single impact loading	251
8.5 SINGLE IMPACT RESPONSES	254
8.5.1 Dynamic strains	254
8.5.2 Accelerations	255
8.6 REPEATED IMPACT RESPONSES	256
8.6.1 Dynamic strains	256
8.6.2 Accelerations	260
8.7 RESIDUAL CAPACITY	263
8.7.1 Residual capacity of prestressed concrete sleeper under single impacts	264
8.7.2 Residual capacity of prestressed concrete sleeper under repeated impacts	269
8.7.3 Reserve strength of prestressed concrete sleepers	277
8.8 SUMMARY	281
<b>CHAPTER 9 NUMERICAL ANALYSES OF PRESTRESSED CONCRETE SLEEPERS</b>	<b>285</b>
9.1 OVERVIEW	285
9.2 MATERIAL MODEL	288
9.3 FINITE ELEMENT MODELLING	291
9.3.1 Static modelling	291
9.3.2 Impact modelling	292
9.4 NONLINEAR STATIC ANALYSIS	295
9.5 PREDICTION OF IMPACT LOADS AND RESPONSES	298
9.5.1 Model verification	298
9.5.2 Impact simulations	298
9.6 SUMMARY	307
<b>CHAPTER 10 DEVELOPMENT OF LIMIT STATES DESIGN CONCEPT FOR PRESTRESSED CONCRETE SLEEPERS</b>	<b>309</b>
10.1 OVERVIEW	310

10.2 CURRENT DESIGN STANDARD AS1085.14-2003	313
10.3 STATISTICS OF DYNAMIC LOAD ON TRACKS	314
10.4 CAPACITY OF PRESTRESSED CONCRETE SLEEPERS	316
10.5 RELIABILITY CONCEPT	321
10.6 CONVERSION OF AS1085.14	323
10.7 LIMIT STATE DESIGN OF PRESTRESSED CONCRETE SLEEPERS	326
10.8 ECONOMIC ASPECTS OF THE NEW DESIGN APPROACH	340
10.9 SUMMARY	341
<b>CHAPTER 11 CONCLUSIONS AND RECOMMENDATIONS</b>	342
11.1 CONCLUSIONS	343
11.1.1 Dynamic properties of railway track's components	343
11.1.2 Capacity of prestressed concrete sleepers	346
11.2 RECOMMENDATIONS FOR FUTURE RESEARCH	355
11.2.1 Dynamic properties of railway track's components	356
11.2.2 Capacity of prestressed concrete sleepers	356
<b>REFERENCES</b>	359
R1 References from literature survey	359
R2 References from the author's publications	371
<b>APPENDIX</b>	379
A OCCUPATIONAL HEALTH AND SAFETY PROCEDURE	380

## LIST OF FIGURES

	<b>Page</b>
Figure 2.1 Typical ballasted track profile	9
Figure 2.2 Typical fastening system for concrete sleepers (Steffens, 2005)	12
Figure 2.3 Types of concrete sleepers	13
Figure 2.4 Typical construction of a ballasted track	15
Figure 3.1 Available types of rail pads in Australia	31
Figure 3.2 Rail pad models	31
Figure 3.3 Typical ballasted railway track	34
Figure 3.4 Schematic diagram of the rail pad tester developed at UoW	34
Figure 3.5 The alternative rail pad tester at UoW	38
Figure 3.6 Frequency response function and its coherence of the tested studded rail pad (10mm) under a preload of 20kN	40
Figure 3.7 Worn rail pads	42
Figure 3.8 Load-deflection curves of worn rail pads	43
Figure 3.9 Curve fitting of frequency response functions at 20 kN preload	43
Figure 3.10 Dynamic behaviour of new rail pads under large preloads	44
Figure 3.11 Concrete sleepers	47
Figure 3.12 Free-free condition	51
Figure 3.13 Ballast condition	51
Figure 3.14 Effect of sleeper/ballast interaction on vibration properties of sleepers	57
Figure 3.15 Experimental modal result of UoW track test bed	61
Figure 3.16 Two-dimensional finite element analysis of railway track	62
Figure 3.17 Typical ballasted track on a coal line in Central Queensland	65
Figure 3.18 Ballasted track components (Kaewunruen and Remennikov, 2005c)	67
Figure 3.19 Modal testing schematic scenario (5-point test)	68
Figure 3.20 Modal results from 5-point tests of railway track	69
Figure 3.21 2DOF dynamic models of railway track	70
Figure 3.22 Dynamic testing installation	71
Figure 3.23 Visual inspection	73
Figure 3.24 Field measurements	74



Figure 3.25 Best curve fitting of measured data at a good condition site	75
Figure 4.1 A typical railway track configuration	85
Figure 4.2 Railway track design procedure (Jeffs and Tew, 1991)	88
Figure 4.3 Accelerance responses at a site obtained from field trials (Kaewunruen and Remennikov, 2005b)	89
Figure 4.4 Static, quasi-static, and dynamic loading time histories	90
Figure 4.5 Schematic diagrams of vertical axle force measurements on rails (Fryba, 1996)	91
Figure 4.6 Track test bed at the University of Wollongong	92
Figure 4.7 Relationship between wheel load, wheel diameter, and tread profile for a limiting mean peak contact stress of $1,260 \text{ MN/m}^2$ (Rail Safety and Standards Board, 1993; 1995)	95
Figure 4.8 Axle load distribution factor	96
Figure 4.9 Example of wheel profiles used in the experiments (Ahlbeck and Hadden, 1985)	100
Figure 4.10 Impact loads measured from the worn wheel profiles (Ahlbeck and Hadden, 1985)	101
Figure 4.11 Rail running surface profile measured at engine burn (Ahlbeck and Hadden, 1985)	102
Figure 4.12 Impact loads due to burned rail running surface profile (Ahlbeck and Hadden, 1985)	102
Figure 4.13 Typical idealized profile of wheel flats (Wu and Thompson, 2001)	103
Figure 4.14 Impact signal from wheel flat (Dukkipati and Dong, 1999)	104
Figure 4.15 Effect of wheel flat size on impact loads: $L_f$ and $D_f$ are the length and depth of flat, respectively (Dukkipati and Dong, 1999)	104
Figure 4.16 Impact forces due to 2 mm rounded wheel flat (Wu and Thompson, 2001)	105
Figure 4.17 Impact forces due to 2 mm newly formed wheel flat (Wu and Thompson, 2001)	106
Figure 4.18 Impact forces due to wheel flats varying with speeds (Wu and Thompson, 2001)	107

Figure 4.19 Effect of sleeper types on impact forces due to wheel flat (Esveld, 2001)	107
Figure 4.20 Axle-box acceleration waveform due to wheel flat (Wakui and Okuda, 1999)	108
Figure 4.21 Wheel/rail impacts due to a) 100 mm wheel flat; b) 0.5 m long local deflect – at train speed of 50 km/h (Johansson and Nielsen, 2003)	109
Figure 4.22 Wheel/rail impacts due to a) 100 mm wheel flat; b) 0.5 m long local deflect – at different train speeds and axle loads (Johansson and Nielsen, 2003)	110
Figure 4.23 Impact forces from a typical dipped joint (Zhai and Cai, 1997)	111
Figure 4.24 Impact forces from a bad weld (Esveld, 2001)	112
Figure 4.25 Effect of train speed on loading from a bad weld (Esveld, 2001)	113
Figure 4.26 Impact forces from high speed trains (Rochard and Schmid, 2004)	114
Figure 4.27 Wheel/rail impact loads from a corrugated rail (Cai, 1992)	116
Figure 4.28 Time histories of wheel/rail impact loads from a corrugated rail (Cai, 1992)	117
Figure 4.29 Axle-box acceleration from a rail corrugation (Wakui and Okuda, 1999)	118
Figure 4.30 Impact forces due to unsupported sleepers (Lundqvist and Dahlberg, 2005)	119
Figure 5.1 Pressure distribution (AS1085.14, 2003)	128
Figure 5.2 Centre-negative moment test (AS1085.15-2003, L1)	130
Figure 5.2 Centre-negative moment test (AS1085.15-2003, L1)	131
Figure 5.3 Experimental setup for centre-negative moment test	131
Figure 5.4 Instrument in the test	132
Figure 5.5 Load-deflection curve of centre negative moment test	133
Figure 5.6 Moment-deflection curve of centre negative moment test	133
Figure 5.7 Measured cracking load of centre negative moment test	134
Figure 5.8 Energy absorption characteristic due to centre negative moment test	134
Figure 5.9 Load-rotation relation from centre negative moment test	135
Figure 5.10 Moment-rotation relation from centre negative moment test	136
Figure 5.11 Compressive stress-strain curve of centre negative moment test	137
Figure 5.12 Tensile stress-strain curve of centre negative moment test	137

Figure 5.13 Moment-curvature relation of negative middle section – End rotations	138
Figure 5.14 Moment-curvature relation of negative middle section – Strain diagram	139
Figure 5.15 Initial flexure cracks at middle span of AUS-BG Sleeper	140
Figure 5.16 Failure of middle span of AUS-BG Sleeper	140
Figure 5.17 Damage of the lowest-layer prestressing wires of AUS-BG Sleeper	141
Figure 5.18 Load-deflection analysis of AUS-BG Sleeper	142
Figure 5.19 Crack pattern of AUS-BG Sleeper	143
Figure 5.20 Rail Seat-positive moment test (AS1085.15-2003, P2)	144
Figure 5.21 Experimental setup for rail seat- positive moment test	145
Figure 5.22 Load-deflection curve of rail seat positive moment test	146
Figure 5.23 Moment-deflection curve of rail seat positive moment test	147
Figure 5.24 Measured cracking load of rail seat positive moment test	147
Figure 5.25 Energy absorption characteristic due to rail seat positive moment test	148
Figure 5.26 Load-rotation relation from centre negative moment test	149
Figure 5.27 Moment-rotation relation from centre negative moment test	149
Figure 5.28 Compressive stress-strain curve of railseat positive moment test	150
Figure 5.29 Tensile stress-strain curve of railseat positive moment test	151
Figure 5.30 Moment-curvature relation of positive rail seat section – End rotations	151
Figure 5.31 Flexure cracks at rail seat	153
Figure 5.32 Crush and spalling along diagonal crack at rail seat	154
Figure 5.33 Prestressing wire inspection at rail seat	154
Figure 5.34 Remaining concrete core at rail seat	155
Figure 5.35 Load-deflection curve of rail seat positive moment test	156
Figure 5.36 Crack pattern at railseat	157
Figure 5.37 Rail seat section of AUS-BG Sleeper	158
Figure 5.38 Ultimate positive behaviour of AUS-BG Sleeper at rail seat	159
Figure 5.39 Positive moment-curvature of rail seat section of AUS-BG Sleeper	159
Figure 5.40 Crack width of AUS-BG Sleeper at ultimate, positive rail seat moment	159
Figure 5.41 Ultimate negative behaviour of AUS-BG Sleeper at rail seat	160
Figure 5.42 Negative moment-curvature of rail seat section of AUS-BG Sleeper	160
Figure 5.43 Crack width of AUS-BG Sleeper at ultimate, negative rail seat moment	160

Figure 5.44 Middle section of AUSTRAK broad gauge Sleeper	161
Figure 5.45 Ultimate positive behaviour of AUS-BG Sleeper at centre	161
Figure 5.46 Positive moment-curvature of middle section of AUS-BG Sleeper	162
Figure 5.47 Crack width of AUS-BG Sleeper at ultimate, positive centre moment	162
Figure 5.48 Ultimate negative behaviour of AUS-BG Sleeper at centre	162
Figure 5.49 Negative moment-curvature of middle section of AUS-BG Sleeper	163
Figure 5.50 Crack width of AUS-BG Sleeper at ultimate, negative centre moment	163
Figure 6.1 Cross sectional area of the test specimens	168
Figure 6.2 Conveying belt used in mining processes	170
Figure 6.3 Dynamic properties of a single-layer conveying belt: a) natural frequency; b) dynamic stiffness; and c) damping factor	171
Figure 6.4 Load-deflection test setups	173
Figure 6.5 Load-deflection curves of rubber mat	174
Figure 6.6 Experimental rigs	175
Figure 6.7 Schematic test setup for 2DOF modal testing	175
Figure 6.8 Frequency response functions of 2DOF test rig under different conditions	176
Figure 6.9 Experimental setups for a) on ballast bed and b) on 6-layer rubber mat	178
Figure 6.10 Steel frame for the strong floor	181
Figure 6.11 Schematic layout of the drop-weight impact test rig	182
Figure 6.12 1200 kN standard high capacity load cell ( <a href="http://www.interfaceforce.com">http://www.interfaceforce.com</a> )	184
Figure 6.13 Calibration curve for the 1200 kN standard high capacity load cell	185
Figure 6.14 3200B Dytran Accelerometer ( <a href="http://www.dytran.com">http://www.dytran.com</a> )	185
Figure 6.15 National Instrument DAQ	187
Figure 6.16 A setup of the in-situ prestressed concrete sleeper	188
Figure 6.17 High-capacity drop-weight impact machine at the University of Wollongong	192
Figure 6.18 Schematic impact load history for a tough material (Saxton, et al., 1974); time $t_2$ results from a linear extrapolation	194
Figure 6.19 Schematic impact load histories for general materials (Saxton, et al., 1974)	196

Figure 6.20 Impact forces at different drop heights	197
Figure 7.1 General profile and cross-sections of prestressed concrete sleepers	203
Figure 7.2 Analytical relation between bending moment and impact force at a railseat	211
Figure 7.3 Example of typical impact forces from the impact testing	212
Figure 7.4 Accelerations due to 200 mm drop height	212
Figure 7.5 Dynamic strain at sleeper railseat due to 200 mm drop-weight impact	213
Figure 7.6 Experimental relation between bending moment and impact force at a railseat	214
Figure 7.7 Progressive impact response of a railway sleeper in soft track environment	217
Figure 7.8 Progressive impact response of a railway sleeper in hard track environment	219
Figure 7.9 Ultimate impact forces failing railway concrete sleepers (after the low-frequency-pass filtering)	222
Figure 7.10 Impact failure at 1,910 kN of a railway sleeper in soft track environment	223
Figure 7.11 Impact failure at 1,780 kN of a railway sleeper in hard track environment	224
Figure 7.12 Cracking damage index of railway concrete sleepers in different track environments	226
Figure 7.13 Incremental damage of railway concrete sleepers in different track environments	227
Figure 8.1 A typical statistical data of loading on tracks (Leong, 2007)	233
Figure 8.2 Flow chart of the repeated impact and residual capacity toughness tests	235
Figure 8.3 Schematic experimental setup for impact testing	237
Figure 8.4 Cracks in a sleeper in soft track after a single impact of 500 kN	238
Figure 8.5 Cracks in a sleeper in soft track after a single impact of 740 kN	239
Figure 8.6 Cracks in a sleeper in soft track after a single impact of 810 kN	240
Figure 8.8 Cracks in a sleeper in soft track after a single impact of 1,500 kN	240
Figure 8.9 Cracks in a sleeper in hard track after a single impact of 500 kN	241

Figure 8.10 Cracks in a sleeper in hard track after a single impact of 740 kN	242
Figure 8.11 Cracks in a sleeper in hard track after a single impact of 810 kN	242
Figure 8.12 Cracks in a sleeper in hard track after a single impact of 1,500 kN	243
Figure 8.13 Crack propagations in the sleepers under single impact loads	244
Figure 8.14 Cracks in a sleeper in soft track after 50 repeated impact of 500 kN	245
Figure 8.15 Cracks in a sleeper mid-span in soft track after 50 drops of 500 kN	245
Figure 8.16 Cracks in a sleeper in soft track after 50 repeated impact of 740 kN	246
Figure 8.17 Cracks in a sleeper mid-span in soft track after 50 drops of 740 kN	246
Figure 8.18 Cracks in a sleeper in soft track after 50 repeated impact of 810 kN	247
Figure 8.19 Cracks in a sleeper mid-span in soft track after 50 drops of 810 kN	247
Figure 8.20 Cracks in a sleeper in hard track after 50 repeated impact of 500 kN	248
Figure 8.21 Cracks in a sleeper mid-span in hard track after 50 drops of 500 kN	249
Figure 8.22 Cracks in a sleeper in hard track after 50 repeated impact of 740 kN	249
Figure 8.23 Cracks in a sleeper mid-span in hard track after 50 drops of 740 kN	250
Figure 8.24 Cracks in a sleeper in hard track after 50 repeated impact of 810 kN	250
Figure 8.25 Cracks in a sleeper mid-span in hard track after 50 drops of 810 kN	251
Figure 8.26 Crack propagations in concrete sleepers under multiple impact loads	252
Figure 8.27 Crack distributions in the concrete sleepers under multiple impact loads	253
Figure 8.28 Strains due to the impact load of 500 kN	254
Figure 8.29 Acceleration responses due to the impact load of 500 kN	255
Figure 8.30 Dynamic strains after 10 drop tests of impact load of 500 kN	257
Figure 8.31 Dynamic strains after 20 drop tests of impact load of 500 kN	258
Figure 8.32 Dynamic strains after 50 drop tests of impact load of 500 kN	259
Figure 8.33 Accelerations after 10 drop tests of impact load of 500 kN	260
Figure 8.33 Accelerations after 10 drop tests of impact load of 500 kN	261
Figure 8.34 Accelerations after 20 drop tests of impact load of 500 kN	261
Figure 8.35 Accelerations after 50 drop tests of impact load of 500 kN	262
Figure 8.36 Schematic full load-deflection curve of structural member	264
Figure 8.37 Residual load-deflection relation for sleepers subjected to a 500 kN impact	265
Figure 8.38 Residual energy absorption for sleepers subjected to a 500 kN impact	265

Figure 8.39 Residual load-deflection relation for sleepers subjected to a 740 kN impact	266
Figure 8.40 Residual energy absorption for sleepers subjected to a 740 kN impact	266
Figure 8.41 Residual load-deflection relation for sleepers subjected to a 810 kN impact	267
Figure 8.42 Residual energy absorption for sleepers subjected to a 810 kN impact	267
Figure 8.43 Residual load-deflection relation for sleepers subjected to a 1,500 kN impact	268
Figure 8.44 Residual energy absorption for sleepers subjected to a 1,500 kN impact	269
Figure 8.45 Residual load-deflection relation for sleepers subjected to 50 repeated impact loads of 500 kN impact	270
Figure 8.46 Residual energy absorption for sleepers subjected to 50 repeated impact loads of 500 kN impact	270
Figure 8.47 Residual static failure mode of the sleepers subjected to 50 repeated impact loads of 500 kN impact	271
Figure 8.48 Residual load-deflection relation for sleepers subjected to 50 repeated impact loads of 740 kN impact	272
Figure 8.49 Residual energy absorption for sleepers subjected to 50 repeated impact loads of 740 kN impact	273
Figure 8.50 Residual static failure mode of the sleepers subjected to 50 repeated impact loads of 740 kN impact	273
Figure 8.51 Residual load-deflection relation for sleepers subjected to 50 repeated impact loads of 810 kN impact	275
Figure 8.52 Residual energy absorption for sleepers subjected to 50 repeated impact loads of 810 kN impact	275
Figure 8.53 Residual static failure mode of the sleepers subjected to 50 repeated impact loads of 810 kN impact	276
Figure 8.54 Reserve fracture toughness of the concrete sleepers	278
Figure 8.55 Post-failure fracture energy of the concrete sleepers	279
Figure 8.56 Post-failure fracture energy of the concrete sleepers	280
Figure 9.1 Material models for static analysis	289

Figure 9.2. Finite element mesh of railway prestressed concrete sleeper	292
Figure 9.3 Impact model of a prestressed concrete sleeper	294
Figure 9.4 Pre-camber, displacement, and fibre stress diagrams due to pre-tensioned strain	295
Figure 9.5 Load-deflection responses	297
Figure 9.6 Comparison of numerical and experimental results (0.1 m drop)	299
Figure 9.7 Influence of ballast elasticity on contact impact forces and dynamic responses	300
Figure 9.7 Influence of ballast elasticity on contact impact forces and dynamic responses	302
Figure 9.8 Influence of rail pad stiffness on contact impact forces and dynamic responses	304
Figure 9.9 Influence of rail pad stiffness on impact responses of the prestressed concrete sleeper	306
Figure 10.1 Typical ballasted railway tracks from D-Track (Steffens, 2005)	310
Figure 10.2 Frequency of occurrence of impact forces, derived from (Leong, 2007)	314
Figure 10.3 Static test setup	317
Figure 10.4 A static moment-displacement relationship (at railseat)	318
Figure 10.5 Crack propagation of PC sleeper under static loading (at railseat)	319
Figure 10.6 Progressive impact response of a PC sleeper in soft track environment	320
Figure 10.7 Probabilistic density functions for reliability (Standards Australia, 1981)	322
Figure 10.8 Relationship between safety index and probability of failure (Standards Australia, 2005)	323
Figure 10.9 Safety indices for steel beams and columns (Standards Australia, 1981)	324
Figure 10.10 Safety indices (rail seat positive moment)	339
Figure 10.11 Safety indices (rail seat negative moment)	339



## LIST OF TABLES

	<b>Page</b>
Table 2.1 Types of rail profiles and their applications (Esveld, 2001)	11
Table 2.2 Discrete sleeper support models	23
Table 3.1 Review of current rail pad testers	33
Table 3.2 2DOF finite element model and parametric analyses	39
Table 3.3 General data of rail pad specimens	41
Table 3.4 Dimensions and masses of the test sleepers	51
Table 3.5 Modal parameters of sleeper no.1 – ROCLA Heavy Duty	53
Table 3.6 Modal parameters of sleeper no.2 - ROCLA Medium Duty	54
Table 3.7 Modal parameters of sleeper no.3 - AUSTRAK Broad Gauge	55
Table 3.8 Modal parameters of sleeper no.4 - AUSTRAK Narrow Gauge	56
Table 3.9 Dynamic behaviour of simplified railway tracks	68
Table 3.10 Summary of average parameters of the components of well conditioned railway track	76
Table 3.11 Summary of average parameters of the railway track with broken fastening system	77
Table 3.12 Summary of average parameters of the railway track with cracked sleeper	78
Table 3.13 Comparison of modal parameters of concrete sleeper with different support conditions	80
Table 4.1 Train records on a very heavily trafficked CSD bridge	93
Table 4.2 Statistical records of axle forces on a very heavily trafficked CSD bridge	93
Table 4.3 Static axle loading of various types of rolling stocks	94
Table 4.4 Types and shapes of abnormalities (Steffen, 2005)	99
Table 5.1 Test results of concrete sleepers	164
Table 5.2 Prediction of static performance of concrete sleepers	164
Table 5.3 Experimental results of static performance of concrete sleepers	165
Table 6.1 Dimensions and masses of the test sleepers (Austrak Broad Gauge Sleeper)	168

Table 6.2 Energy absorption and dissipation capacities of rubber mat	173
Table 6.3. Modal data of rubber mat using 2DOF test assembly	177
Table 6.4 Comparison of modal parameters of test sleeper with different support conditions	180
Table 6.4 Efficiency of high capacity impact testing machine	183
Table 6.5 Common specification of 3200B Dytran accelerometer	186
Table 6.6 Experimental programs for impact load duplication	195
Table 6.7 Impact load characteristics in the soft track with rail pad	198
Table 6.8 Impact load characteristics in the soft track without rail pad	198
Table 6.9 Impact load characteristics in the hard track with rail pad	199
Table 6.10 Impact load characteristics in the hard track without rail pad	199
Table 7.1 Summary of experimental programs	204
Table 7.2 Benchmark participants	207
Table 7.3 Benchmark I scenarios (Steffens, 2005)	207
Table 7.4 Benchmark II scenarios (Leong, 2007)	208
Table 7.5 Correlation between computer packages' analytical results and field data (Leong, 2007)	209
Table 7.6 D-TRACK simulation scenarios (Murray and Leong, 2006)	210
Table 7.7 Impact crack identification of railway prestressed concrete sleepers	216
Table 7.8 Accumulative impact damage of railway prestressed concrete sleepers	221
Table 7.9 Damage classification of prestressed concrete sleepers	228
Table 8.1 Summary of impact and static testing programs	237
Table 9.1 Material models used in finite element analyses	290
Table 10.1 Track importance categories and related factors (Leong, 2007)	331
Table 10.2 Track maintenance factor, $k_{tf}$ (Leong, 2007)	332
Table 10.3 Wheel maintenance factor, $k_{vf}$ (Leong, 2007)	332
Table 10.4 Design results for the selected PC sleeper	334
Table 10.5 Statistical model of the selected PC sleeper	336
Table 10.6 Reliability indices of railseat section of Austrak broad gauge sleepers	338

## NOMENCLATURES

$a(t)$	acceleration along the sleeper in $x$ direction
$A_g$	gross sectional area
$A_z$	0.020 rad (total angle of vertical ramp discontinuity)
$c$	speed of elastic wave propagation
$c_1$	damping coefficients of the rail
$c_2$	damping coefficients of ballast supporting system
$c_p$	damping of a rail pad
$c_{max}$	maximum bending crack lengths
$C_z$	$55.4 \times 10^3$ Ns/m (effective rail damping rate per wheel)
$[C]$	damping matrix
$d$	total depth of the sleeper
$D$	wheel tread diameter (mm); damage index
$DF$	axle load distribution factor
$e$	effective eccentricity
$E$	elastic modulus of the test specimen
$E_A$	actual energy absorbed by the sleepers
$E_c$	modulus of elasticity of concrete
$EI$	bending stiffness of the rail
$f$	pin-pin resonance frequency; excitation frequency; stress
$f'_c$	ultimate compressive strength at 28 days
$f'_{c,dyn}$	dynamic compressive strength
$f'_{c,st}$	static compressive strength of concrete
$f'_{ct}$	tensile strength of concrete at 28 days
$f_{y,dyn}$	dynamic upper yield point stress of prestressing wires
$f_{y,st}$	the static upper yield point stress of prestressing wires
$F$	harmonic force magnitude
$F_i$	dynamic wheel load
$F_s$	static wheel load

$F^*$	design wheel load
$g$	gauge length; gravitational acceleration
$g(x)$	limit states function
$g_{\text{ult}}(\mathbf{X})$	ultimate limit states function
$h$	drop height
$H(f)$	magnitude of the frequency response function
$I$	impact force transferring onto the railseat
$I_g$	gross moment of inertia of the cross section
$I$	impulse; area under the impact load history diagram
$I_1$	impulse due to the 1 <sup>st</sup> drop
$I_f$	total impulse at failure
$I_R$	cumulative impulse ratio
$j$	dynamic amplification factor
$k_1$	stiffness of the rail
$k_2$	stiffness of ballast supporting system
$k_i$	stiffness of the $i^{\text{th}}$ layer of rubber mat
$k_p$	stiffness of a rail pad
$k_t$	track importance factor
$k_{tf}$	track maintenance factor
$k_{\text{total}}$	stiffness of combined system
$k_r$	factor associated with the basic return period of loading
$k_{vf}$	maintenance factor on vehicle wheels
$K_z$	$62.0 \times 10^6$ N/m (effective vertical rail stiffness per wheel)
$[K]$	stiffness matrix
$L$	sleeper spacing; length of simple beam; sleeper length
$m$	mass of the rail per unit length; mass per unit length of the test specimen
$m_1$	mass of rail
$m_2$	mass of sleeper
$m_p$	effective rail mass of a rail pad
$M$	drop mass

$M_{C-}$	maximum negative design bending moment at mid span
$M_{R+}$	maximum positive design bending moment at railseat
$M_u$	ultimate moment capacity
$M_v$	effective vertical unsprung mass per wheel (kg)
$M_z$	245 kg (effective vertical rail mass per wheel)
$M^*$	resultant bending moment at railseat
$[M]$	mass matrix
$p_F$	probability of failure
$P$	prestressing force
$P_0$	static wheel load
$P_1$	first peak of impact load due to dipped joint
$P_2$	second peak of impact load due to dipped joint
$P_{axle}$	nominal axle load in tonnes
$P_b(t)$	true bending load
$P_i(t)$	generalized inertia load
$P_{mp}$	mean plastic impact force
$P_t(t)$	recorded impact load history
$P_D$	design wheel load
$Q$	maximum static wheel load (kN)
$Q_{dyn}$	dynamic component of quasi-static design wheel load
$Q_k$	characteristic value of load
$Q_{st}$	static component of quasi-static design wheel load
$Q^*$	design value of load
$r^2$	correlation index
$R$	rail seat load; return periods
$R_b$	basic return period of load occurrence
$R_c$	characteristic flexural compressive strength of concrete
$R_k$	characteristic value of resistance
$R_t$	characteristic flexural tensile strength of concrete

$R^*$	design value of resistance
$S_k$	characteristic value of load effect
$S^*$	load effect
$SF$	factor of safety
$u_o$	displacement at the load point of time $t$
$\ddot{u}_o(t)$	acceleration at the load point of time $t$
$v$	wheel running speed
$V$	drop velocity in impact testing
$V_m$	maximum normal operating speed (m/s)
$V_t$	estimated traffic volume
$w_l$	impact energy input of the 1 <sup>st</sup> drop
$w_n$	impact energy input of the n <sup>st</sup> drop
$W$	net impact energy absorbed at failure
$X_N$	random variables
$y_b$	distance between bottom fibre and neutral axis of a cross section
$y_t$	distance between top fibre and neutral axis of a cross section
$Z$	mechanical or acoustical impedance of the test specimen
$\beta$	safety index or reliability index
$\beta_{bi}$	reliability index with respect to bottom fibre stress at initial stage
$\beta_{bf}$	reliability index with respect to bottom fibre stress at final stage
$\beta_{cf}$	reliability index with respect to cross-sectional stress at final stage
$\beta_{ti}$	reliability index with respect to top fibre stress at initial stage
$\beta_{tf}$	reliability index with respect to top fibre stress at final stage
$\beta_{wi}$	reliability index with respect to wire stress at initial stage
$\beta_{wf}$	reliability index with respect to wire stress at final stage
$\Delta E$	energy loss in impactor
$\sigma$	stress; dynamic stress
$\sigma_b$	stress at the bottom fibre
$\bar{\sigma}_b$	permissible stresses at the bottom fibre
$\sigma_t$	stress at the top fibre

$\bar{\sigma}_t$	permissible stresses at the top fibre
$\alpha_1$	model variation coefficients with respect to the resistance
$\alpha_2$	model variation coefficients with respect to the load action
$\varepsilon$	strain; dynamic strain
$\varepsilon_0$	strain at the ultimate compressive strength at 28 days
$\varepsilon_{c0,st}$	static ultimate strain
$\dot{\varepsilon}$	strain rate in concrete fibre
$\rho$	density of the test specimen
$\omega$	arbitrary frequency; loading frequency
$\omega_i$	resonant frequency
$\omega_n$	natural frequency
$\phi$	dynamic impact factor
$\phi_i$	mass-normalized mode shape
$\xi_i$	modal damping ratio
$\eta_i$	hysteretic damping
$\lambda$	wavelength of a sinusoidal rail irregularity
$\delta u_0$	virtual displacement at the load point
$\delta u(x)$	generalised virtual displacement
$\delta W$	virtual work done by an external force
$\gamma$	load factor
$\gamma_Q$	design coefficient for load
$\gamma_S$	design coefficient for load effect
$\Phi$	cumulative frequency distribution function
$\Theta_R$	model uncertainty coefficient for resistance
$\Theta_S$	model uncertainty coefficient for load effect

## **CHAPTER 1**

### **INTRODUCTION**

Contemporary knowledge has led to two key paradoxical interests and concerns in the railway engineering community. First, track maintenance engineers pay more attention to the observable cracks and damage caused to concrete sleepers by the high-intensity dynamic loading due to wheel irregularities or defects in the rails. On the other hand, structural engineers are concerned about whether the concrete sleepers are over designed despite the fact that they possess large amounts of untapped reserve strength. These parallel issues are due to an insufficient insight into the dynamic behaviour of concrete sleepers under realistic conditions and impact loads. This lack of insight will be addressed in this thesis.

#### **1. 1 GENERAL BACKGROUND**

Prestressed concrete sleepers are a major part of ballasted railway tracks. It is the cross-tie beam that distributes service loads from the rails to the supporting formation. A notion has long been established that concrete sleepers have a large redundant capacity. Nevertheless, premature cracking of concrete sleepers in North America and Europe raised a widespread concern about their reaction to high intensity impact loads from wheel or rail irregularities. In addition to their high magnitude, short-duration impact loads can initiate resonances in the track and components. The dynamic characteristics of a railway track and its components are important indicators of any resonant vibration where excessive flexural movement of the sleepers exist and cause cracks. Structural problems could result in serious failures and design restrictions over a wide range of engineering structures because natural phenomena and human activities often impart a time-dependent burden on every accessible structure. Analysis and design of structures subjected to dynamic loads are based on parameters such as natural frequency, damping constant, and corresponding mode shape. As a consequence it is imperative that the



dynamic properties of an object associated with various sources of noise and vibration be thoroughly investigated.

In general, railways play a major role in transporting population, resources, and merchandise, etc., over a continent as large as Australia. The railway industry has grown significantly over the past century and continuously developed new technology suitable for a particular solution to a specific local area. In Australia the traditional ballasted track system of steel rails, rail pads, fasteners, and concrete sleepers laid on ballast and subgrade is still used widely, but the demand for transportation and logistics has increased greatly over recent years. An increasing frequency of passenger and freight trains has been a significant factor in the steady deterioration of the track system. This increase has been stimulated by the growing need of industry, especially Australian coal mines, for long distance freight conveyancing. Railway tracks in Australia have been deteriorating due, not only to increased traffic, but also heavier wheel loads and improper maintenance. The undetermined ultimate load capacity of track components has been under suspicion for some time, regardless of the fact that they are subjected to impact dynamics induced by wheel/rail interaction, irregularities, and so on.

The problem of cracking sleepers and corollary damage are largely due to the high intensity loads from wheel or rail irregularities such as wheel burns, dipped joints, rail corrugation, or defective track stiffness. Although most problems in North America and Europe were primarily associated with wheel defects, similar effects from rail abnormalities could also be found on the tracks (Grassie, 1987). The principal cause of cracking is the high magnitude of the loads, although the duration of the pulse also contributes to excessive flexural vibrations. These high frequency impacts commonly excite resonance in the tracks and sleepers. For instance, the first bending resonance of concrete sleepers would accelerate cracking at mid span, while the second and third bending modes enlarge the cracks at the rail seats. There was no report about whether those cracks were severe or detrimental to the structural condition of individual sleepers. They were a major concern however, because cracks could be tolerated during the 50 year service life, as stated in the current (Standards Australia, 2003) permissible design. This is because of the lack of knowledge of the dynamic behaviour, failure, and residual capacity of concrete sleepers under severe impact loads. It was also found that using a very high impact factor in the current design (from 50% to 200%) did not prevent the sleepers from cracking (Wang, 1996). This implied the need for further

research related to the reaction of concrete sleepers under more realistic loads and surrounding conditions.

As a result, the present research aims at providing rail track owners/designers with the up to date knowledge related to the dynamic behaviour of prestressed concrete sleepers, rail pads, and other track components. The ultimate goal is to shift the current permissible stress design concept to the new limits for prestressed concrete sleepers. Based on the fact that the rail firms do run their own business, this project attempts to give them the opportunity to use the existing railway structures more efficiently and in particular, more cost effectively. Limited information on the static and dynamic behaviour of railway tracks and components permits only a simplified method and procedure for over analysing and designing railway structures, particularly concrete sleepers. In order to either devise a novel economical analysis and design, or exploit the applicable capacity of existing structures, an in-depth analysis of the static, dynamic, and impact of concrete sleepers must be carried out.

The Cooperative Research Centre for Railway Engineering and Technologies (Rail CRC) was established and based on the awareness of those problems. Its mission has been to become an internationally recognised National Research Centre for the Australian Railway Industry and to deliver the decision making tools, knowledge, and technology necessary to address industry needs for effective rail management, operation, maintenance, and development. To accomplish this mission Rail CRC promotes several research projects in coordination with industry partners and six universities. This research is a funded project of Rail CRC No.5/23: “Dynamic analysis of track and the assessment of its capacity with particular reference to concrete sleepers”, which is allocated into Research Theme # 2 “Innovative Track Maintenance and Upgrading Technologies”. The University of Wollongong’s contribution to the project includes the integration of experiments and simulations with reference to concrete sleepers and railway tracks, and the development of a new limit states design philosophy of concrete sleepers, with a close relationship to a computer package for track analysis and factored load analysis carried out at Queensland University of Technology (QUT).

## 1.2 STATEMENT OF THE PROBLEM

Earlier investigations have shown that the majority of cracks in concrete sleepers are due to impact loading caused by wheel/rail interaction with or without wheel/rail irregularities (Cai, 1992; Wang, 1996; Wakui and Okuda, 1999; Stiffen, 2005; and Leong, 2007). The current design philosophy for prestressed concrete sleepers is based on the permissible stress principle that only considers static and quasi-static loads which are unrealistic compared to the actual dynamic loads on tracks. The discussion papers prepared by Murray and Leong (2006a; 2006b) were released in October 2005 and September 2006 where the limit states design concept and load factors for a revamped standard AS1085.14 were proposed. The papers revealed that based on the field data from the QR WILD Impact detector and DTRACK simulations, impact forces over 300kN and up to 400-500 kN were detected (Murray and Leong, 2006a). There also existed the certainty that a high magnitude impact can occur at particular return periods. Leong (2007) then developed the expressions for predicting impact loads at different return periods (based on the field data from impact detectors at two sites). It has been suggested that a simple pseudo-static (using factored load) approach can be used when designing prestressed concrete sleepers subject to routine traffic. For sleepers subjected to non-routine traffic it is suggested that dynamic analysis be used as part of the design process.

In order to devise a new limit states design concept where there are more logical loads and surrounding conditions, further comprehensive studies of the loading conditions, static behaviour, dynamic characteristic and response, and the impact resistance of prestressed concrete sleepers are required. The University of Wollongong (UoW) has been developing both numerical and experimental programs to investigate the ultimate impact resistance of prestressed concrete sleepers that compliments the limit states design approach. This research involves determining the dynamic characteristics of tracks and components, including rail pads and concrete sleepers. This is because in a track system the sleepers interact with the other components such that the resonance often results in excessive degradation of specific components. It is therefore important to identify the critical vibrations in the track and each particular component so that the dynamic effects can be evaluated. Static tests of the sleepers provide some understanding of the ultimate failure and energy absorption mechanisms.

The static and dynamic behaviour of concrete sleepers forms the fundamental basis and cornerstone of impact studies to develop new limit states design concepts.

To achieve the next phase a new, large capacity impact testing rig was constructed at the UoW to test prestressed concrete sleepers under impulsive loads similar to the wheel/rail forces stemming from wheel and rail imperfections. The challenge and originality of this study are in simulating both the dynamic loading and surrounding conditions of railway tracks. An insight into the behaviour of prestressed concrete sleepers under severe impact results in optimising their design and performance. The residual capacity of concrete sleepers is also determined in order to indicate the ultimate failure mode and serviceability required.

### **1.3 SCOPE OF STUDY**

The scope of this study covers the experimental and numerical approach used to better understand the high-intensity impact resistance and dynamic characteristics of prestressed concrete sleepers. This study reviews our fundamental understanding of the dynamic characteristics of railway tracks and components including the at-large loading conditions on railway tracks.

This experimental work extends to an in-situ simulation in the laboratory and also the in-field track environment. The dynamic integrity of railway tracks and an assessment of the components are carried out. The load carrying capacity and energy absorption mechanisms of prestressed concrete sleepers under different loading conditions are evaluated. Static tests comply with “AS1085.14 Prestressed concrete sleepers,” which captures the general understanding of engineering practitioners in the railway industry. Dynamic and impact tests convey the probability concept of loading to the limit states design philosophy. The experimental program and simulated track set up developed to complement the reliability concepts for the impulsive response and severe impact resistance of prestressed concrete sleepers is discussed. Crack propagations indicate the dynamic performance of the concrete sleepers. Numerical analyses of prestressed concrete sleepers under static and impact loads help predict the dynamic response and broaden the impact of sleepers in various environments. Since it is expected that they can still perform after repeated impact loads, the residual static load

carrying capacity and fracture energy of damaged sleepers is investigated as a performance index. This thesis also describes the reliability concepts and rationales associated with the development and conversion of current permissible stress design concept to limit states format codes.

#### **1.4 OBJECTIVES OF THE STUDY**

This thesis involved a comprehensive study of the loading conditions and response and resistance of pre-stressed concrete sleepers. This includes an analysis of the track and inter-action between the sleepers and other components with the ultimate goal being to rationalise the present design method into a more realistic response. The objective was to explore the static, dynamic, and impact of prestressed concrete sleepers to understand how they interact with the track and its components. These specific objectives are highlighted below:

- a) Identify the critical parameters, methods for dynamic modelling and simulation of track structure;
- b) Use an impact hammer on tracks in the laboratory and in the field, under various conditions, to test and measure the properties of individual and assembled track components.
- c) Develop and update finite element models of global tracks and individual concrete sleepers coupled with measurements to study their response to impact, monitor their health, and detect any damage.
- d) Perform static, repeated low-velocity and ultimate impact tests on concrete sleepers to study cracking, toughness, capacity, and resistance to impact loads, and evaluate the load attenuation, properties and degradation of rail pads from impact and,
- e) Review and devise the new limit states design philosophy (load distribution, impact strength, and impact load factor) of concrete sleepers, contributing to amending Australian Standard: AS 1085.14.

## 1.5 ORGANISATION OF THE THESIS

This thesis comprises 11 Chapters followed by the bibliography and appendices. The total number of pages is 381 excluding the table of contents, abstract and acknowledgements.

Chapter 1 contains a general introduction to the present research, background to the study, statement of the problem, and scope of study.

Chapter 2 gives a survey of literature on the static and dynamic behaviour of railway tracks and components, with particular reference to concrete sleepers. The technical procedures and testing methods for evaluating the dynamic characteristics of the ballasted track components are reviewed and summarised. Previous analytical models and experimental work to determine the response of railway track and components to vibration, are reviewed.

Chapter 3 describes an investigation of the dynamic properties of railway track and its main components. The emphasis is on prestressed concrete sleepers, rail pads, and ballast. Modal analysis is used in order to obtain modal parameters of the track components.

Chapter 4 is devoted to reviewing the various parameters governing the characteristics of impact forces on railway track structures. Wheel and rail abnormalities, which could significantly affect them are discussed. Wheel impact detection and probabilistic analysis of impact loading are described. The treatment of impact forces and the common procedures of the current design approach for prestressed concrete sleepers are also presented.

Chapter 5 presents the experiments and analyses used to determine the ultimate capacity, failure and post-failure mechanisms, and crack propagations of concrete sleepers in accordance with AS1085.14 Prestressed concrete sleepers.

Chapter 6 describes the impact testing apparatus and experimental programmes on the resistance of prestressed concrete sleepers to impact.

Chapter 7 describes the impact resistance, responses, and behaviour of prestressed concrete sleepers based on the experiments. The relationship between the impact forces and bending moment at the rail seat are investigated.

Chapter 8 describes the analysis of the residual capacity of in-situ prestressed concrete sleepers under single and repeated impact loads.

Chapter 9 provides details of the numerical modelling of concrete sleepers for static, dynamic, and impact analyses. Validation between numerical and experimental results is presented. Parametric studies to identify the key influences of each component on impact and the response of concrete sleepers are highlighted.

Chapter 10 describes the reliability analysis and proposes limit state design concepts for prestressed concrete sleepers. Conversion from the permissible stress design concept to the limit states design concept is discussed.

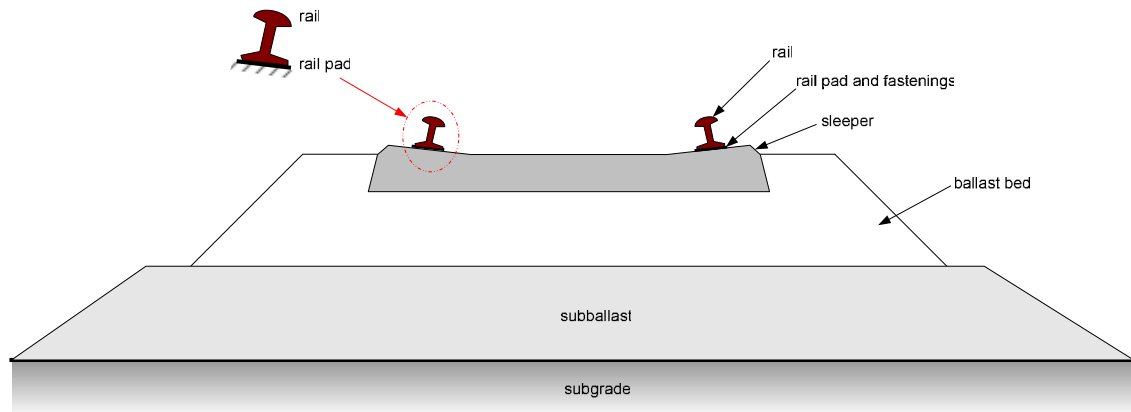
Chapter 11 presents the conclusions and recommendations for future research.

## CHAPTER 2

### REVIEW OF THE DYNAMICS OF RAILWAY TRACK AND ITS COMPONENTS

#### 2.1 BALLASTED RAILWAY TRACKS

Rail track is a fundamental part of railway infrastructure and its components can be classified into two main categories: superstructure and substructure. The most obvious parts of the track as the rails, rail pads, concrete sleepers, and fastening systems are referred to as the superstructure while the substructure is associated with a geotechnical system consisting of ballast, sub-ballast and subgrade (formation). Both superstructure and substructure are mutually important in ensuring the safety and comfort of passengers and quality of the ride. The typical shape and construction profiles of a ballasted track are illustrated in Figure 2.1.



**Figure 2.1.** Typical ballasted track profile



### 2.1.1 Rails

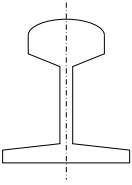
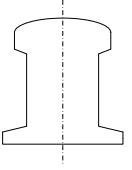
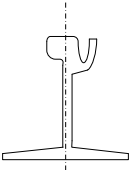
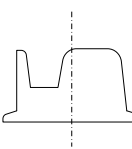
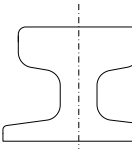
Rails are longitudinal steel members that are placed on spaced sleepers to guide the rolling stock. Their strength and stiffness must be sufficient to maintain a steady shape and smooth track configuration (Selig and Waters, 1994), and resist various forces exerted by travelling rolling stock. One of their primary functions is to accommodate and transfer the wheel/axle loads onto the supporting sleepers. Esveld (2001) reported that a modern rail track also conveys signals and acts as a conductor on an electrified line. Adopted from Esveld (2001), Table 2.1 describes typical rail profiles and their applications. The most commonly used profile is flat-bottom rail, also called Vignole rail, and is divided into three parts:

- *rail head*: the top surface that contacts the wheel tire
- *rail web*: the middle part that supports the rail head, like columns
- *rail foot*: the bottom part that distributes the load from the web to the underlying superstructure components.

### 2.1.2 Fastening Systems

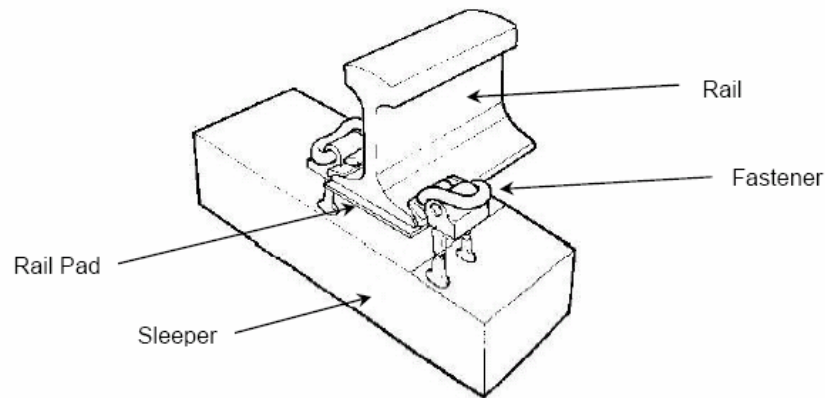
The fastening system, or “*fastenings*,” includes every component that connects the rail to the sleeper. Fastenings clamp the rail gauge within acceptable tolerances and then absorb forces from the rails and transfer them to the sleepers. Vibration and impact from various sources e.g. traffics, natural hazards, etc. are also dampened and decelerated by fastenings. Fastenings sometimes act as electrical insulation between the rail and the sleepers. Their primary components are fastener and rail pad. Some tracks might have base plates with or without pads, which helps the workmen to remove damaged rails without having to untie the fastenings and immediately replace them with new rails. In this case the rail is only connected to the immediate base plate. This system is called *indirect fastenings*, which differs from the usual *direct fastenings* in that the latter device is built-in and holds the rail directly onto the sleepers (Esveld, 2001; Smutny, 2004). A typical concrete fastening system is shown in Figure 2.2.

**Table 2.1** Types of rail profiles and their applications (Esveld, 2001).

Shape	Profile type:	Applications:
	Flat-bottom rail	Standard rail track
	Construction rail	Manufacturing of automobiles and switch parts
	Grooved rail	Railway track embedded in pavements, roads, yards
	Block rail	Railway track used in concrete slab as part of Nikex-structure
	Crane rail	Heavy load hoisting cranes with high wheel loads

### 2.1.3 Fasteners

Because there are many different types of fasteners, their application depends on the characteristics, patterns, and structure of the sleepers to be used. The fasteners withstand the vertical, lateral, and longitudinal forces, and overturning moments of the track, as well as keeping the rails in place. They also transfer all the forces caused by the wheels, thermal change, and natural hazards, from the rails to the adjacent sleepers.



**Figure 2.2.** Typical fastening system for concrete sleepers (Steffens, 2005)

### 2.1.4 Rail Pads

Rail pads are placed on the rail seat to filter and transfer the dynamic forces from rails and fasteners to the sleepers. The high dashpot value of rail pads reduces excessive high-frequency forces and provides a resiliency between rail and sleeper that helps alleviate rail seat cracking and contact attrition.

### 2.1.5 Sleepers

Sleepers are transverse beams resting on ballast and support. Wooden sleepers were used in the past because timber was readily available in the local area. However, pre-stressed or reinforced concrete sleepers, and to a limited extent steel sleepers, have been adopted in modern railway tracks over the past decades because of their durability and long service life. Esveld (2001) grouped timber sleepers into two types: softwood (e.g. pinewood) and hardwood (e.g. beech, oak, tropical tree). Concrete sleepers are

described as either twin-block or mono-block (FIP Commission on Prefabrication, 1987), and are illustrated in Figure 2.3. Within all these types, concrete sleepers are more widely used because they are not affected very much by either climate or weather.

The important functions of sleepers are:

- To uniformly transfer and distribute loads from the rail foot to the underlying ballast bed;
- To provide an anchorage for the fastening system that holds the rails at their correct gauge and preserves inclination, and
- To support the rail and restrain longitudinal, lateral and vertical movement by embedding itself onto the substructures.



a) monoblock concrete sleeper



b) twin-block concrete sleeper

**Figure 2.3.** Types of concrete sleepers

### **2.1.6 Ballast**

Ballast is a layer of free draining coarse aggregate used as a tensionless elastic support for resting sleepers. This layer comprises graded crushed stone, gravel, and crushed gravel such as granite and basalt which depends on local availability. It not only provides support, it also transfers the load from the track to the sub-ballast and drains water away from the rails and sleepers. For a heavy haul freight line, individual axle loads on rails can be up to 50 tons or around 80 tons. Thus, in addition to the weight of the track, heavy cyclic loading, tamping and impact from rolling stock, ballast provides

a static and dynamic stability to the sleepers by distributing a uniform load and reduction over the sub-ballast and subgrade.

The fundamental functions of ballast can be summarised from previous research as follows (Hay, 1982; Selig and Waters, 1994; Esveld, 2001).

- Resist vertical, lateral and longitudinal forces applied to the sleepers, to retain the track in its proper position because the submergence and interlocking of irregularly shaped ballast tends to confine the sleepers, as shown in Figure 2.4.;
- Absorb shock and impact from the rough interlocking particles acting as a simple spring element with limited action;
- Give resiliency and energy absorption to the sleeper;
- Assist track maintenance in surfacing and lining operations (track geometry adjustment and sleeper replacement) by the ability to manipulate ballast with low energy tamping;
- Reduce bearing stresses from the sleeper to acceptable stress levels for underlying layers;
- Allow optimum global and local settlement;
- Provide some large voids for controlling the storage of internal fouling materials enable small particles to pass through;
- Provide fast drainage of fluid;
- Avoid freezing and thawing problems by being unsusceptible to frost;
- Provide an insulating layer with some electrical resistance;
- Prohibit vegetation growth because of unsuitable cover layer for vegetation
- Absorb airborne noise from travelling traffic, and
- Facilitate reconstruction of the track.



**Figure 2.4.** Typical construction of a ballasted track

### 2.1.7 Sub-ballast

Sub-ballast that may be called *the capping layer* is a layer of granular material between the ballast and underlying subgrade. It is generally composed of broadly graded slag or crushed aggregate, although a broadly graded sand-gravel compound is sometimes used. Sub-ballast is usually impervious and therefore its general functions are to:

- Reduce stress at the bottom of the ballast layer to a reasonable level for the top of the subgrade;
- Prevent inter-penetration from the upward migration of fine particles from the layer of subgrade to the upper layer of ballast;
- Provide good drainage that is ascribed to the non-obstructed voids by inter-penetration;
- Also act as a shedding layer to keep water away from subgrade;
- Protect the subgrade from attrition by the hard ballast; and
- Inhibit freezing and thawing problems in the subgrade.

### 2.1.8 Subgrade

Subgrade is also referred to as *the formation*. It includes the existing soil and rock, which possess slopes, verges, ditches and other structures or materials within. The subgrade is the last support which bears and distributes the dynamic loading resultant downward along its infinite depth. This deep layer must have sufficient bearing capacity, provide good drainage and yield a tolerably smooth settlement in order to prolong track serviceability. Some synthetic materials such as geo-textile, fabric, etc., have recently been used to upgrade the capacity of the subgrade.

## 2.2 MODAL TESTING

Experimental modal analysis (EMA) or *modal testing* is a non-destructive testing strategy based on the response of structures to vibration. Since the 1940s, modal testing has been widely used to help understand the dynamic behaviour of structures. The original modal testing technique was based on the simple sine dwell method. After some years, innovations based on Fast Fourier Transform (FFT) have been developed

and are currently used (Brown, 1982; Allemang and Brown, 1986; Mitchell, 1986; Allemang, 1993; Ewin, 1995; He and Fu, 2001). This vast improvement of modal analysis results in the more precise and accurate vibration measurements. In addition, the integration of analytical models and experimental results has led to the sensitivity analysis of structural behaviour.

To solve dynamic problems or analyse and design structures, experimental modal analysis becomes one of the most significant methodologies. It promises civil/mechanical engineers practical procedures and a prompt and reasonable solution to structural dynamic problems.

Numerous researches have been investigated from the modal analysis perspective and have shown substantial efficiency in engineering uses, even if the modal analysis is comparatively young. Assumptions involved in modal testing include the linearity of structures, time-invariant structural parameters, and observability in measurements (Allemang, 1993). It is noteworthy that linear systems mean that the superposition of forces can be applied, although linearity may be inapplicable for some structures (Zaveri, 1985). Besides the time invariant properties mean that structural parameters such as stiffness and damping remain constant, depending on factors excluded in the model, during a time. Observability arises when the input-output measurements have sufficient information to create a characteristic model of the structure, although the forcing and response functions must be measurable for the structure to be observed.

In addition to the generic assumptions, there are five more options to be assumed when one performs an excitation on a structure. They are whether the excitation is impulsive; or white noise; or a step; or a Wiener-Levy signal; and or that there is no excitation (free decay or free response) (Allemang and Brown, 1986). Various methods for performing experimental modal analysis had been categorised by Allemang and Brown (1986) into:

- Forced-normal-mode excitation,
- Frequency response function,
- Damped complex exponential response, and
- Mathematical input-output model

The forced-normal-mode function method is the oldest modal testing approach that uses multiple inputs to approximate the modal parameters but it does not take the complex modes of vibration into account. The frequency response function (FRF) method is currently the most common one to use for assessing modal parameters. It contains spectra computed from the auto-spectrum and cross-spectrum that are measured from the structure. The damped complex exponential response method makes use of the information acquired from the free decay of a system, which is generated by the release of an initial condition. There are two similar approaches, which occur through the development of a damped complex exponential response method. They are the Ibrahim time domain method and Poly reference approach.

- The Ibrahim time domain (ITD) method uses data received from the impulse response function (IRF) to identify the modal parameters of a structure. This approach requires the response measurements simultaneously at a number of locations on the structure. However, a universal position can be chosen for measurements if multiple data collection is unobtainable. Then the displacement and acceleration, or velocity of free response data is used to form the eigenvalue matrix to be solved (He and Fu, 2001).
- The poly reference approach uses FRF data from multi-input multi-output testing to carry out the natural frequency, modal constants and damping loss factors. All data measured simultaneously are used to identify the modal frequencies (Allemang and Brown, 1986).

The mathematical input-output model method considers the input and output responses independently. Applications can be extended to both time and frequency domain models with no limitation in the number of degrees of freedom (dof). The approaches based on this methodology are the auto-regressive moving average approach and the reduced structural matrix approach.

- The auto-regressive moving average approach makes the excitation assumption that the responses obtained at various points are induced by white random noise input to the structure. The two-stage least square method is needed. From statistical results, the confidence factor (coefficients of variation), which are the ratio of the standard deviation of each parameter compared to its real counterpart, can be computed for natural frequencies and damping (Allemang and Brown, 1986).



- The reduced structural matrix approach is based on the condensed matrix obtained from incomplete responses. However, its estimated solution is not unique, and the frequency range is reduced because the matrix is weighted to represent an incomplete model. Besides, the sensitivity needed to reduce the matrix will be decreased due to the limited precision of modal results from experimental errors. As a result, this method is not very successful (Allemang and Brown, 1986).

## 2.3 DYNAMICS OF RAIL PADS

The standard rail pads used in the Australian track system are usually made from polymeric compound materials. They are installed on rail seats to reduce the dynamic stress from axle loads and wheel impact from both regular and irregular train movements. These pads are highly important because of their dynamic softening between track and sleepers. Inappropriate or inadequate uses of rail pads exacerbate the cracking of sleepers at rail seats. Besides, misuse causes high settlements of global and local tracks, and ballast/subgrade breakage from heavier tamping (Remennikov and Kaewunruen, 2004). This negative effect can be extended to the capacity and integrity of a railway system unless this helps to gain a better understanding of the structural behaviour of them. Based on these grounds Australia has launched a standard referred to as AS1085.19 for testing bearing pads. (Standards Australia, 2003b). The dynamic behaviour of rail pads is not well known, although some publications can be found, as presented:

### *2.3.1 Linear and nonlinear model of rail pads*

Many investigations have been carried to describe the dynamic behaviour of rail pads mathematically; they are either linear or nonlinear models. Dynamic rail pad models are usually on the fundamental basis of either time or frequency domain. The literature review shows that most are in relation to the frequency domain because this model implicates dynamic properties such as resonant frequencies and damping (Fahey and Pratt, 1998).

A suitable linear '*Fractional derivative model*' was developed by Fenander (1997; 1998) and adopted into a linear track model. In this approach the rail pad model

had to be linear. Various damping or viscoelasticity models were included; for example, the viscous model where the loss factor is proportional to frequency. Since the stiffness of a rail pad is nonlinearly dependent on the preload and the fractional derivative model is linear, a different set of parameters, which were fitted to the experimental data, was needed for each preload. This model seems to be a good fit, especially for testing the stiffness of the rail pads.

Sjoberg (2002) developed a time domain model, which uses compressive actions as component forces and accounts for the effect of pre-load, and the frequency and dynamic amplitude dependence. The nonlinear shape factor, neo-Hookean hyper-elastic model, fractional derivative element model, and Coulomb forcing function were included in the proposed model. It is a one dimensional component model using a few parameters whilst giving reasonably measured characteristics. It was proposed initially for rubber isolators but could for other rubber elements.

Since the complex properties of rail pads are frequency dependent, Knothe et al. (2003) developed a frequency domain model which assumed that for each frequency the equivalent complex stiffness can be approximated by a bi-linear function associated with load amplitude and preload. The latter assumption is that the modal parameters rely linearly on the frequency. The estimated values fitted the measured results quite well.

### ***2.3.2 Dynamic testing of rail pads***

The dynamic testing of rail pads has been of interest for many years and many different methods have been developed to determine their dynamic properties. The response of a rail system comprising a concrete sleeper, rail section, and various types of rail pads to vibration were measured (Ford, 1988b) and a series of FRFs was presented to identify the effects that various pads had on the wave signals.

Several types of resilient rail pads with various materials and different surface profiles had been tested in the laboratory and on a track (Grassie, 1989). The average attenuation of the pads was indicated and the results from the laboratory showed that they were conservative. Their dynamic stiffness increases with normal load and is more than or identical to the tangent stiffness from the load deflection curves. Although rail

pad damping has almost no effect on the dynamic behaviour of a well compacted ballasted track, more damping causes the pad itself to heat up.

Van't Zand (1993) used FFT technique to measure and assess the dynamic characteristics of pads through impact load tests. The curve fitting method was used to fit an SDOF equation of motion to the experimental results. It was carried out at a specific frequency of 400-2000 Hz. The results were compared with another research and seemed to be in a good agreement. This method was then extended to the urban track structures (Esveld, 1997; Esveld, Kok, and De Man, 1998).

Later, Fenander (1997) studied the vertical stiffness and damping of studded rail pads on a complete track and in a laboratory test rig. Stiffness increased substantially with preload but only weakly with frequency. The fractional derivative model of their dynamic behaviour was presented in this investigation. The 2DOF testing apparatus was developed from research done by Verheij (1982). It consisted of two steel blocks with the resilient element mounted between them. To approximate the dynamic stiffness of the pads, the stiffness of the lower spring supporting the lower block was neglected. The measurements of several new pads indicated that stiffness tends to increase slightly with frequency whilst the effect of the preload is more pronounced.

Thompson et al. (1998) developed an indirect method for measuring the high frequency dynamic stiffness of resilient elements by applying the theory of two-degree-of-freedom (2DOF) system. The resilient element was mounted between two large blocks on a floor, one of which was supported by soft springs beneath it. The resilient element was assumed to be much stiffer than the soft springs. Two exciters were used in the measurement apparatus and some approximations were made to reduce some difficulties with the 2DOF system. This proposed methodology can be extended to elements with low frequency stiffness by rearranging the equations of motion. The results of this case study seem to be reliable and it is noteworthy that this approximated method is being included in international standards.

Another rail pad tester has been constructed based on the SDOF viewpoint, to examine their dynamic properties in controlled conditions in the laboratory (De Man and Esveld, 2000; De Man, 2002). New and worn pads were tested in the laboratory. They are considered to be the only elastic components in the tester, which is an

apparatus of tuned masses, preloading springs and elastic supports. In this investigation the 2DOF-based tests on real track had also been done. However, it is noteworthy that this tester gives realistic results and becomes a better way for determining their properties.

There has been a recent investigation by Knothe et al. (2003) dealing with the measurement and modelling of resilient rubber pads. The quasi-static and dynamic measurements were done in the low frequency (0-40 Hz.) and high frequency range (100-2000 Hz.). With dynamic testing two pads are placed between three steel plates which then introduces the secant, tangent and equivalent stiffness. This test showed that the stiffness of the pads are frequency dependent and thus conform to previous researches. They were also hinged on the preload and amplitude of the harmonically varying load. It can be concluded that the equivalent stiffness increases with increasing preload and decreasing amplitude. These tests showed the hyper-elastic action of the rubber in the quasi-static test, its visco-plastic action in the low frequency cyclic load test, and especially its viscoelastic action in the high frequency range test.

At the UoW an alternative method for determining the dynamic properties of rail pads based on measuring the response to SDOF vibration has been proposed. The simplicity and reliability of this method has been shown. It proved to be a fast and non-destructive method for accurately assessing the dynamic stiffness and damping constant of every type of rail pad available in Australia. This strategy enables new types of rail pads to be tested as well as evaluate how ageing affects their dynamic characteristics (Remennikov and Kaewunruen, 2004).

## **2.4 VIBRATIONS OF CONCRETE SLEEPERS**

Apart from the rail pads, concrete sleepers have also played a crucial role in this country for many years. Many investigations dealing with the dynamic properties of concrete sleepers have been performed, modal testing in particular (Ford, 1988a). Ballasted track can be divided into five groups of discrete support models (Knothe and Grassie, 1993), as shown in Table 2.2. To get a better insight into the dynamic strength of sleepers, their response to various dynamic loadings has been studied (Grassie and Cox, 1984; Esveld et al., 1996; De Man, 2002). Standards Australia (2003) developed AS1085.14 for

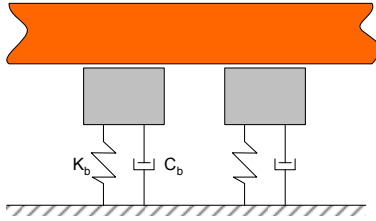
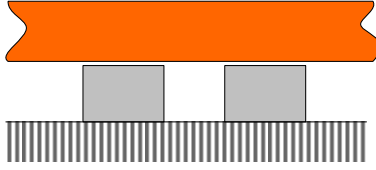
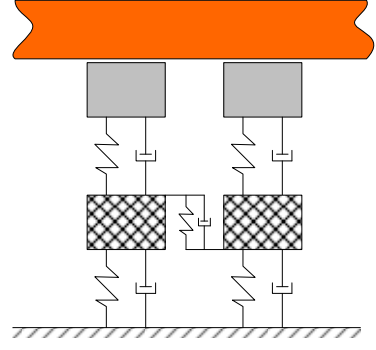
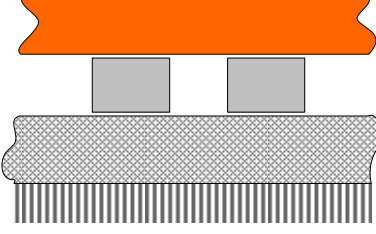
analysing and designing concrete sleepers, including procedures for sampling and testing materials. It also contains the methods for testing static, quasi-static, and dynamic cyclic loading and the allowable limits and serviceability of sleepers.

Modal testing has been very significant as a method for non-destructive dynamic testing of concrete sleepers for over five decades. Ford (1988a) performed a modal analysis on a concrete railway sleeper. It was suspended at each end by soft springs which allowed for “free-free” support. An electro-dynamic shaker was used to excite the sleeper at a single point, an accelerometer was used to measure the response at the remaining points, and then a series of FRFs were obtained. In this test the natural frequencies and corresponding mode shapes were extracted using modal analysis software (SMS modal).

Vincent (2001) carried out modal testing and numerical modelling of a reinforced concrete sleeper. It was laid on a very soft spring support and excitations were done with an impact hammer and a swept sine loading of a shaker with different load amplitudes. Different types of modal parameter extraction methods were used and showed that linear behaviour arises in the low frequency range but is less in the higher frequency range. Also, a 3D linear finite element model was developed by *I-deas* to compare the experimental and numerical results. However, excluding the steel reinforcement, the model only contains sleeper geometry with the material property updating with modal testing results. A comparison of those results shows good agreement. A sensitivity analysis was done by modifying the structural properties.

Various boundary conditions such as free-free, perfectly coupled to the subsoil, and voided sleepers, were investigated for their effects on the dynamic behaviour of concrete sleepers (Plenge and Lammering, 2003). Excitations were given laterally and vertically. FRFs were obtained and became a means to study the effects of various boundary conditions on their response to vibration. A numerical investigation was done and if the sleeper was modelled as a rigid beam the results were not very good but by using the thin layer method, the simulated FRFs coincided with the measured results much better when the frequency was up to 2000 Hz. Additionally, a static load on a sleeper increases the bond with the ballast to stiffen the whole system. These experiments confirmed the results observed by Wu and Thompson (1999).

**Table 2.2** Discrete sleeper support models

Models	Assumptions
	<p><u>Type A</u></p> <ul style="list-style-type: none"> <li>- discrete sleeper support</li> <li>- ballast: spring and damper</li> </ul>
	<p><u>Type B</u></p> <ul style="list-style-type: none"> <li>- discrete sleeper support</li> <li>- half-space modeling of ballast and substrate</li> </ul>
	<p><u>Type C</u></p> <ul style="list-style-type: none"> <li>- discrete sleeper support</li> <li>- ballast: spring and damper</li> <li>- interconnected ballasted masses</li> <li>- substrate: spring and damper</li> </ul>
	<p><u>Type D</u></p> <ul style="list-style-type: none"> <li>- discrete sleeper support</li> <li>- continuous ballast layer</li> <li>- half-space substrate model</li> </ul>

## 2.5 DYNAMICS OF RAILWAY TRACKS

Timoshenko (1926) was one of the first to model the dynamic behaviour of a railway track. In that model, the rail was considered as an infinite uniform Euler beam, laid on a continuous damped elastic Winkler foundation. Grassie (1982) then found in some experiments that there are only two dominant resonances in the frequency range of interest. The first in-phase mode at about 100 Hz corresponds to the sleeper and rail moving together on the ballast while the second out-of-phase mode at a frequency somewhere between 300-500 Hz depending on the rail pad parameters, corresponds to the opposite vibration of sleepers on ballast and rails on the rail pad. The dynamic moment and impact attenuation were subsequently observed. It was concluded from much research that a rail pad which was resilient at frequencies of several hundred Hertz would substantially reduce the dynamic loads on concrete sleepers. Some rail pads attenuate dynamic bending strains in concrete sleepers by more than 50%. Their stiffness has a greater effect on reducing strain in a sleeper than its depth (Grassie, 1988). The dynamic loading on sleepers was also studied and revealed that when ballast is packed loosely, the dynamic loads become significantly higher and the resilient pads have less effect. Selig and Waters (1994) studied the ground formation of a railway track and found that the subgrade is the one component of the substructure that has the greatest affect on track stiffness. Raymond (1978) also found that stiffer tracks have smaller differential settlements or unevenness and cause lower impact loading. Coincidentally, Liang and Zhu (2001) found the lower subgrade stiffness leads to greater elastic deformation and less stability of the ballast layer and upper part of the track structure.

In-situ and in-field experiments for determining global ballasted track were mostly done using the instrumented impact hammer technique because an impact hammer is mobile and self-supporting (De Man, 1996) and can be used without damaging or obstructing traffic. The FRF measurements can be obtained through a handy laptop and immediately extracted for such modal properties as resonant frequency, damping constant, and corresponding mode shape. However, these parameters are susceptible to factors such as duration of pad usage, temperature, and preload (Wu and Thompson, 1999). Previous investigations into this kind of tests are summarised below.

### ***2.5.1 In-situ dynamic testing***

An in-situ dynamic test was done by Ford (1988b) to determine how systems comprising a concrete sleeper, rail section, and rail pads respond to vibration. In a laboratory, a sleeper was embedded in ballast contained by a wooden box on a concrete floor. The tests were done using an electro-dynamic shaker to excite the top surface of the rail in the frequency of 0-1000 Hz. The frequency of vibration of the rail at the same point and at three points near the rail seat, were measured by the accelerometers.

Sadeghi (1997) observed that by performing modal testing, the natural frequencies obtained from a test on individual concrete sleepers in the laboratory are higher than those obtained from the in-situ track test bed. These results could indicate that ballast and subgrade cause a slight reduction in the natural frequencies of sleepers. It was also found that the components of the substructure have a very strong non-linear stress-strain relationship and non-homogeneous properties.

Plenge and Lammering (2003) developed full scale laboratory experiments in order to measure the dynamic behaviour of a segment ballasted track and its constituents. The effects of voids between the sleepers and underlying ballast were considered, especially in the partially unsupported sleepers. The two kinds of voided sleepers tested were limited to sleepers with a hovering end and with 2 sided hovering ends. The dynamic displacements were measured by the holographic interferometry in addition to the common accelerometers. The results of these experiments agreed with the field data from the previous record. It also showed that deviations from coupling to the subgrade lead to remarkable changes in the dynamic behaviour.

Until now, very few investigations have been conducted to study the dynamic interaction between the ballast and railway track, or its components such as sleepers, adjacent sleepers, and global systems connected by the rail track. Therefore, at the UoW, there are a number of investigations into the dynamic interaction of ballast and sleeper with various types of realistic voids and pockets in a ballasted track system, with varying wet/dry properties and static preloads (Kaewunruen and Remennikov, 2004; Remennikov and Kaewunruen, 2005).



### ***2.5.2 Field trials***

Apparently the field trials seem to be the most realistic ones because there are no standard methods currently accepted by the industry for determining the dynamic parameters of track components required to successfully model their dynamics. The industry does not have methods for investigating dynamic parameters and responses. Instead, designers usually calculate the dynamic response based on the static loading specified in the Australian Standards and apply factors that incorporate dynamic loading. Nevertheless these experiments may lead to extremely unreliable results due to unpredictable problems in the rail track itself, e.g., the nonlinearity attributed to voided sleepers, rail impurities, corrugation, worn pads, voided sleepers, and so on.

Grassie (1989a) investigated the properties of a number of rail pads with different materials (synthetic and natural rubber, plastics, and composites) and surfaces (plain, grooved and studded surfaces), to find that the relative correlation coefficients of the relationship between data in a laboratory and on the track, were reasonable. The fractional impact attenuation of a particular pad in the field relies considerably on track conditions, and the amplitudes of dynamic and quasi-static loads. It was shown that the impact test is a good, conservative method for determining its performance.

De Man (1996), and De Man and Esveld (2000) carried out the in-field trials to determine dynamic track properties by using excitation hammer testing. In this test the track was simplified as a 2DOF, discretely supported continuous rail system representing two effective masses of rail and sleeper, as well as two dynamic stiffness and two dashpots of rail pad and ballast-formation, respectively. Based on FRF measurements and FFT, the modal parameters of the track were extracted by an automatic curve fitting optimisation procedure. In the test example two resonance frequencies were clearly obtained and the first 'pin-pin' resonance was noticed in the FRFs measured. In 2002 Colla et al. combined several techniques for a site investigation of non-ballasted railway tracks. The radar technique was used for the layer interface bonding tests, ultrasound helped detect the contact conditions between sleepers and subgrade, and an impact echo technique played a vital role in investigating the structural integrity of those tracks.

However Knothe et al. (2003), reported that the values obtained from the field could only be reliable in the frequency range of the second resonance peak. These field measurements could be obtained when:

- The excitation of a train travelling on the track can be measured;
- A shaker can be used to excite the rail; and
- A calibrated impact hammer can be successfully used to hit the rail.

At the UoW two 2DOF models have been developed based on the FFT analysis and mode superposition method to extract the dynamic properties of ballasted track systems. Responses to ambient vibration induced by normal traffic from the Lara site in Victoria are recorded by a CRC-Rail project. The signal analyses are being done to extract the dynamic properties of the track and field tests will be conducted to investigate more precise results (Kaewunruen and Remennikov, 2005).

## **2.6 SUMMARY**

Rail track is a fundamental part of railway infrastructure and its components are divided into superstructure and substructure. The most observable parts such as the rails, rail pads, concrete sleepers, and fastening systems are referred to as the superstructure while the substructure is associated with a geotechnical system consisting of ballast, sub-ballast and subgrade. The dynamic testing of railway tracks and its components are of interest, particularly the concrete sleepers and rail pads. In this chapter the technical procedures and testing methods for evaluating the components of ballasted track have also been reviewed and summarised. The ballasted track system and the well-known modal testing technique have been described. Previous analytical models and experiments into the vibration of track components have also been included and practical tests methods used in the field and in situ have been highlighted.

Rail pads are usually installed on rail seats to reduce the stress from axle loads and wheel impact from regular and irregular train movements. They are very important because they soften the interaction between the track and the sleepers. Several time and frequency domain modelling of rail pads had been done as well as a number of experiments of their dynamic parameters.

Some investigations dealing with the dynamic properties of concrete sleepers can be found in this paper. Most are based on the experimental modal testing technique. In addition the various boundary conditions of sleepers, such as free-free, perfectly coupled to the subsoil, and voided sleepers, were investigated for their effect on the dynamic behaviour of concrete sleepers. However, some limitations still remain, as reported.

Until now, very few investigations have been conducted into studying the dynamic interaction between the ballast and track or components such as sleepers, adjacent sleepers, and global systems connected by the rail track. In addition, although the field tests seem to be realistic, the experiments may lead to extremely unreliable results due to many unpredictable problems in the track such as nonlinearity that is attributed to voided sleepers, rail impurities, track corrugations, worn pads, and voided sleepers.

## CHAPTER 3

### DYNAMIC CHARACTERISTICS OF RAILWAY TRACK AND ITS COMPONENTS

In this chapter, the dynamic characteristics of global railway track and its individual components particularly with regards to rail pads and prestressed concrete (PC) sleepers are described. The experimental techniques and procedures developed in laboratory have been successfully applied to field trials and will be discussed later. This chapter is one of the major tasks in order to establish realistic mechanical properties of railtrack components to be used in the computer program, DTRACK, developed by Queensland University of Technology. These data also assist the explanation of experimental outcomes as well as numerical predictions of dynamic responses and behaviour of prestressed concrete sleepers to impact loading.

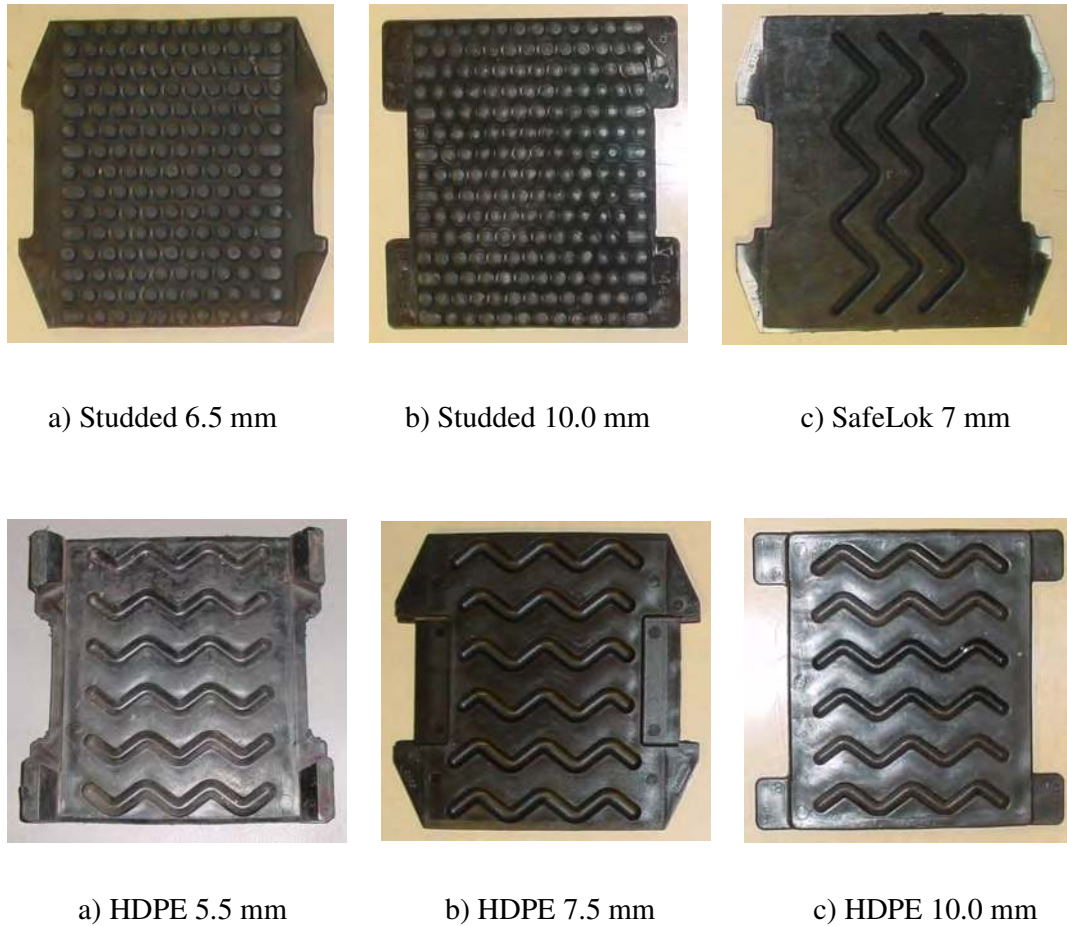
#### 3.1 RAIL PADS

Rail pad is an important track component usually used in ballasted railway tracks. It is mostly made from polymeric compound, rubber, or composite materials. Mounted on rail seats, the rail pads are designed to attenuate the dynamic stress from axle loads and wheel impacts caused by both regular and irregular train movements. In terms of track analysis and design, rail pads take part in the attenuation of dynamic forces and high-frequency content that is transferred from the rails to concrete sleepers. The physical attribute and dynamic properties of rail pads are an indicator for scheduling the track maintenance and renewal program of rail pads.

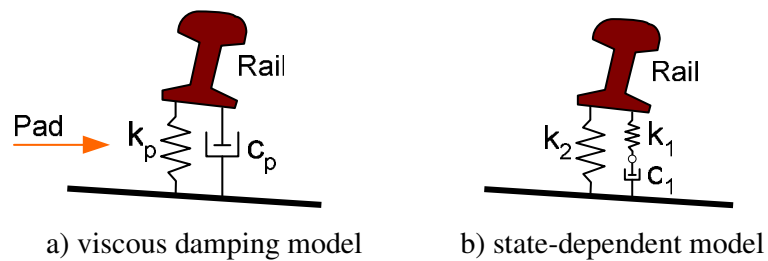
It is known that the bogie burden and the rail fastening system impart dynamic and static preloading to the track, respectively. The toe load can escalate to as much as 150-200 kN when a wheel burn strikes the railhead (Cai, 1992; Remennikov and Kaewunruen, 2006). Nonetheless, the current numerical models or simulations of

railway tracks often exclude the effect of preloading on the nonlinear dynamic behaviour of rail pads, although it is evident that preloading has significant influence on dynamic rail pad properties that affect the dynamic responses of railway tracks (Grassie and Cox, 1984; Wu and Thompson, 1999; Kaewunruen and Remennikov, 2006; 2007). This could be explained by the lack of information on the behaviours of rail pads under variable preloads, and the limited knowledge of the dynamic wheel-load distribution to rail pads and other track components. This section presents information on a rail pad tester for large preload control and discusses the experimental results of testing several types of railway pads manufactured in Australia. The developed relationships between dynamic pad stiffness and preload could be incorporated into track analysis and design tools for a more realistic representation of the dynamic load transfer mechanisms in railway tracks.

In general, dynamic responses of railway tracks are directly associated with noise and wear problems in railway track environments. There are currently many types of rail pads such as high-density polyethylene (HDPE) pads, resilient rubber pads, and resilient elastomer pads, all of which have different surface profiles and distinctive engineering properties. Figure 3.1 features some available types of pads in Australia, namely the HDPE, EVA, Studded, or Rubber rail pads. The dynamic behaviour of rail pads is generally represented by two important parameters: dynamic stiffness and damping coefficient. Sometimes, more variables are needed and nonlinear dynamic model or so-called '*state-dependent viscoelastic model*' might be adopted. To obtain such properties, the dynamic testing of rail pads in laboratory or on track is required. From the dynamic response measurements, both linear and nonlinear properties can be estimated by optimizing the objective formulations of the desired dynamic model. Modeling rail pads as a '*spring and viscous dashpot in parallel*' seems to be a very practical means for railway industry. Not only can the parameters be obtained conveniently, this model is usually applied to the studies on vertical vibrations of railway tracks (Cai, 1992; Grassie and Cox 1984; Knothe and Grassie, 1993; Oscarsson, 2002).



**Figure 3.1** Available types of rail pads in Australia



**Figure 3.2** Rail pad models

The state-dependent model of rail pads, where an additional spring is presented in series with the dashpot as illustrated in Figure 3.2, has been recently proposed but the interpretation of the mathematical model and its influence on dynamic responses of a

track are still unclear and need further investigation (Fenander, 1998; De Man, 2002; Nielsen and Oscarsson, 2004; Maes et. al, 2006). Alternatively, De Man (2002) noted a benefit of the state-dependent models in that the model can separate influences of loading frequency from the influences of preload, in case of harmonic or cyclic testing on frequency-dependent materials. With regard to identifying the properties of the track components, e.g. rail pads, Grassie and Cox (1984) recommended that the best way to determine the dynamic parameters is by extracting from operational vibration measurements or field testing by an impact hammer or dynamic exciter. It should be noted that the dynamic properties could only be determined at the resonance frequency, when using an impact hammer.

A number of publications have recently addressed the dynamic characteristics of resilient pads (Grassie, 1989; Van't Zand, 1993; Kaewunruen and Remennikov, 2005a, 2005b, 2006; Remennikov and Kaewunruen, 2006a, 2006b; Remennikov et. al, 2006; Maes et. al, 2006; Carrascal et. al, 2007). It is noted that some studies included a two-degree-of-freedom (2DOF) rail pad models (Fenander, 1997; Thompson et. al, 1998; Knothe et. al, 2003). Except Maes's work (2006) that measured the input acceleration directly, the technique of '*indirect measurement*' was generally utilised. Indirect measurement is an approach that measures the dynamic responses due to dynamic input force or excitation. The direct method is possible to use when the test specimens are very small and the exciter is very powerful. A variety of previous rail pad testers were illustrated in Maes et. al (2006). The preload capacities of those rail pad testers are presented in Table 3.1. It is found that the capacities of previous rail pad testers had been limited. From the literature, single-degree-of-freedom (SDOF) dynamic model of rail pads has been used in a number of investigations as well. Instrumented hammer impact technique is widely used in this kind of tests due to its proven effectiveness and mobility. Most of above-mentioned studies discussed the effects of loading frequency that tend to induce potential problems to railway tracks (e.g., noise, wear, etc). It has been showed that the loading frequency may increase the dynamic stiffness of rail pads, and plays significant role in the level of damping provided. However, the influence of large preload, which might be inducted by dynamic wheel/rail interaction, has not been studied adequately so far.

**Table 3.1.** Review of current rail pad testers.

Place	Excitation	Method	Model	Preload Capacity
TU-Delft <sup>a</sup>	Impact	Direct	SDOF	0-25 kN
VUB-Belgium <sup>b</sup>	Harmonic	Direct	SDOF	0-1 kN
UNICAN-Spain <sup>c</sup>	Harmonic	Direct	SDOF	20-95 kN
TNO-UK <sup>d</sup>	Harmonic	Indirect	2DOF	0-80 kN
TU-Berlin <sup>e</sup>	Harmonic	Indirect	2DOF	0-95 kN
UoW-Australia	Impact	Direct	SDOF	0-400 kN

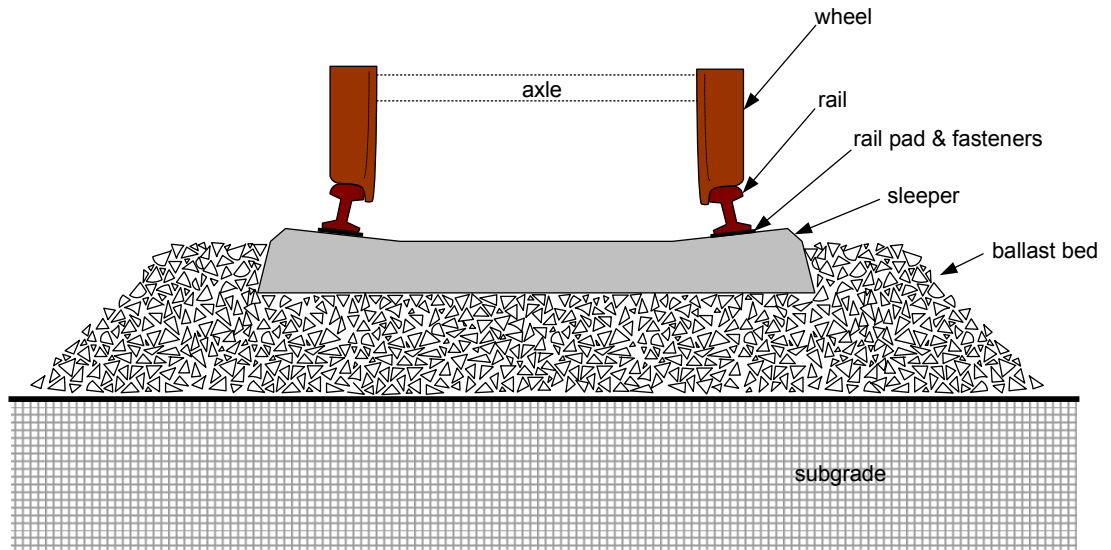
<sup>a</sup>(Van't Zand, 1993; De Man, 2002); <sup>b</sup>(Maes et. al, 2006); <sup>c</sup>(Carrascal et. al, 2007); <sup>d</sup>(Thompson et. al, 1998); <sup>e</sup>(Knothe et. al, 2003).

In this study, a SDOF-based method is employed that allows evaluating the dynamic properties of rail pads. Instrumented hammer impact technique is adopted in order to benchmark with the field trials in Sections 3.3 and 3.4. Figure 3.3 demonstrates a typical ballasted railway track. Figure 3.4 shows the schematic test setup of the rail pad tester developed at University of Wollongong. This test rig has adopted the benefit of modern force sensing bolt that can resist large load up to 100 kN each. An analytical solution for a frequency response function was used to best fit the vibration responses. Vibration response recordings were obtained by impacting the rail with an instrumented hammer. In this investigation, the effective mass, dynamic stiffness and damping of resilient-type rail pads are obtained from the least-square optimisation of the frequency response functions (FRFs) obtained from the modal testing measurements. Demonstrations shown are focused on both new and worn pads.

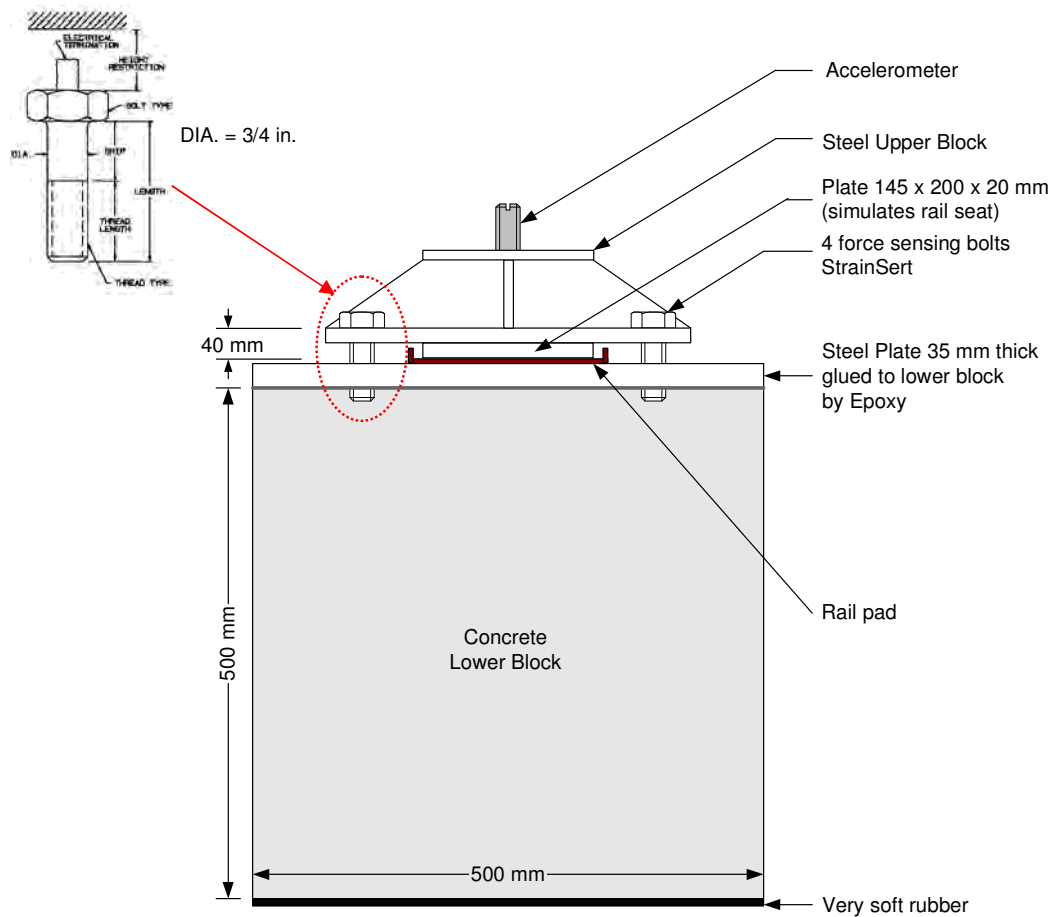
### 3.1.1 Analytical Modal Analysis

In this study, the rail pad is considered as the only elastic element in the test rig, as shown in Figure 3.4. This test rig has been developed to perform indirect measurement of pad properties. A single degree of freedom (SDOF) system has been proven to be a suitable model for use in the determination of the dynamic characteristics of the rail pad (Remennikov and Kaewunruen, 2005). The dynamic model of rail pads includes the following two parameters: dynamic stiffness and damping constant.





**Figure 3.3.** Typical ballasted railway track



**Figure 3.4.** Schematic diagram of the rail pad tester developed at UoW

### 3.1.1.1 SDOF Dynamic Model

Rail pads can be simplified as the elastic and dashpot components of a simple mass-spring-damper SDOF system by installing the pads between a steel rail and a rigid block, as shown in Figure 3.2a. The dynamic characteristics of rail pads in the vertical direction can be described by the well-known equation of motion:

$$m_p \ddot{x} + c_p \dot{x} + k_p x = f(t) \quad (3.1)$$

$$\omega_n^2 = k_p / m, \quad 2\zeta\omega_n = c_p / m, \quad \text{or} \quad \zeta = c_p / 2\sqrt{k_p m} \quad (3.2a, b, c)$$

where  $m_p$ ,  $c_p$ , and  $k_p$  generally represent the effective rail mass, damping and stiffness of a rail pad, respectively. Taking the Fourier transformation of (3.1), the frequency response function can be determined. The magnitude of FRF is given by

$$H(\omega) = \frac{1/m_p}{\sqrt{(\omega_n^2 - \omega^2)^2 + (2\zeta\omega\omega_n)^2}} \quad (3.3)$$

Substituting equations (3.2) into equation (3.3) and using  $\omega = 2\pi f$ , the magnitude of the frequency response function  $H(f)$  can be represented as follows:

$$H(f) = \frac{1}{m_p} \frac{4\pi^2 \beta f^2}{\sqrt{\left[1 - 4\pi^2 \beta f^2\right]^2 + \left[4\pi^2 \beta \left(\frac{c_p^2}{k_p m_p}\right) f^2\right]}} \quad (3.4)$$

where,

$$\beta = \frac{m_p}{k_p} \quad (3.5)$$

This expression contains the system parameters  $m_p$ ,  $k_p$  and  $c_p$  that will later be used as the curve-fitting parameters.

### 3.1.1.2 Vibration Measurements

To measure the vibration response of the rail pads, an accelerometer was placed on the top surface of the railhead, as illustrated in Figure 3.4. The mass of the upper segment is 30.30 kg, and the mass of each preloading bolt is 0.75 kg. It should be noted that a test rig was rigidly mounted on a “strong” or “isolated” floor (1.5 m deep of heavily reinforced concrete), the frequency responses of which are significantly higher than those of interest for the rail pads. The floor also isolates ground vibration from surrounding sources. To impart an excitation on the upper mass, an impact hammer was employed within a capable frequency range of 0–3,500 Hz. The FRF could then be measured by using the PCB accelerometer connected to the Bruel&Kjaer PULSE modal testing system, and to a computer. Measurement records also included the impact forcing functions and the coherence functions

### 3.1.1.3 Parameter Optimization

Parts of FRFs, especially in the vicinity of the resonant frequencies, provide detailed information on the properties of the tested component. Using a curve-fitting approach the dynamic properties can be extracted. In this approach, the theoretical FRF from Equation (3.4) will be tuned to be as close as possible to the experimental FRF in a frequency band around the resonant frequency. Optimization algorithms were programmed using DataFit (2005). The dynamic properties can be obtained from the optimization. The correlation index ( $r^2$ ) is the target function while each parameter will be utilized in the least square algorithm as the objective solutions. Iterations will converge when the residual tolerance of the objective parameters is less than  $10^{-3}$ .

## 3.1.2 New Rail Pad Tester

### 3.1.2.1 Design Attributes

A base-isolated experimental rig for dynamic testing of rail pads (so-called ‘*pad tester*’) has been developed at the University of Wollongong. As shown in Figure 3.5, the test rig consists of a concrete block that supports steel mass, preloading bolt system, and a rail pad. The concrete block is isolated from surrounding noise by placing on the very soft rubber plate between the block and strong floor representing the absolutely rigid foundation. The very soft rubber plate was chosen based on the 2DOF finite

element analyses in which its characteristics allow the upper block vibrates freely but prohibits the surrounding noise and dynamic interaction from the lower mass, as exemplified in Table 3.2. An accelerometer and dial gauges are installed on the upper steel mass, as illustrated in Figure 3.4. An instrumented impact hammer is employed to impart excitation to the assembly of components for 10 times. The frequency response function (FRF) is then obtained using the PULSE dynamic analyser in a frequency range of interest, from 0 to 1,000 Hz. The coherence function is also obtained to evaluate the quality of FRF measurements, which were averaged from the 10 hits.

#### 3.1.2.2 Preload Control

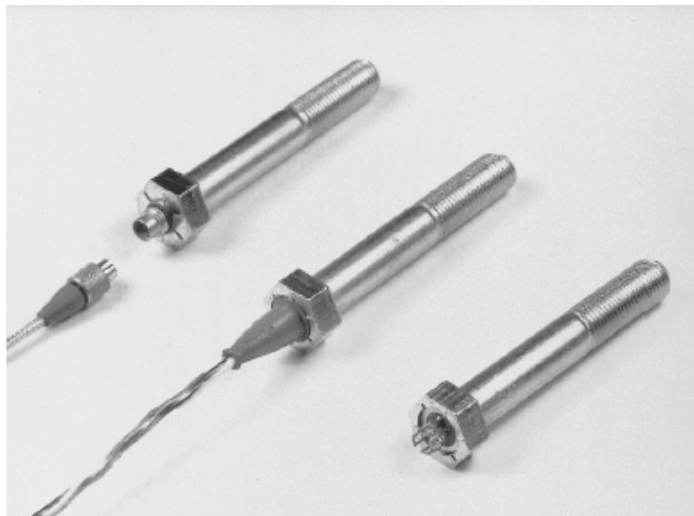
The test rig was designed to apply preloads up to a maximum of approximately 400 kN in total. Each calibrated force-sensing bolt is connected to a real-time data logger and to a computer (see Figures 3.5a and 3.5b). Using four force-sensing bolts (StranSert), the preloading can be introduced, incrementally adjusted and recorded through a computer screen. Ten levels of preload of rail pads in the range between 0 to 200 kN were considered. Dynamic performance of rail pads under this large amount of preload has not been investigated so far. It should be noted that the preload of 20 kN is equivalent to an average preload of the PANDROL e-Clip fastening system on the rail. Also, the preload of 200 kN is comparable to a 40-ton axle load (Esveld, 2001).

#### 3.1.2.3 Modal Testing

The upper mass was impacted using an instrumented hammer. The accelerometer was used to measure the vibration response that was processed by the PULSE Dynamic Analyzer to produce FRFs. As an example, the properties of the PANDROL resilient rubber pad (studded type, 10 mm thick) were determined using the test rig and the results are presented in Figure 3.6. Parameter optimization was then applied to the experimental FRFs, yielding the dynamic properties of rail pads under various conditions.



a) Experimental setup



b) Examples of force sensing bolts

**Figure 3.5.** The alternative rail pad tester at UoW

**Table 3.2.** 2DOF finite element model and parametric analyses.

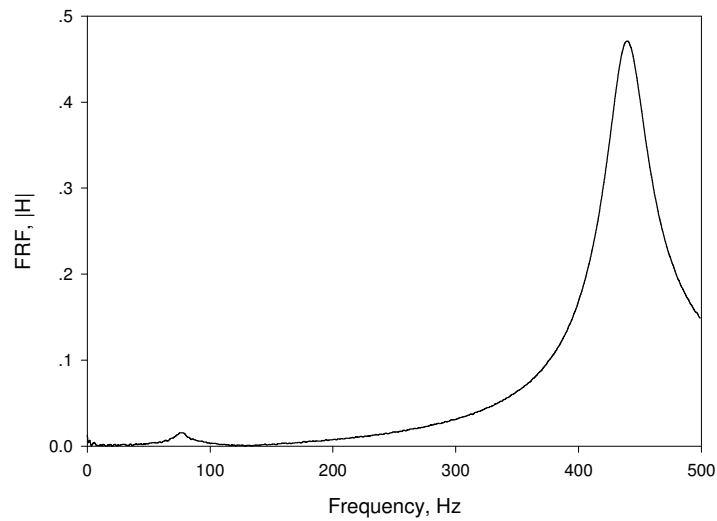
Rubber base stiffness MN/m	Natural frequency, Hz.		Type of Rail Pad
	First resonance	Second resonance	
0.01	1.42	286.06	<b>Studded Pad</b> $k_1 = 65 \text{ MN.m}$ $c_1 = 5.5 \text{ kNs/m}$
0.10	4.49	286.06	
1.00	14.19	286.14	
10.00	44.73	286.95	
100.00	136.57	297.22	
0.01	1.42	883.45	<b>HDPE Pad</b> $k_1 = 620 \text{ MN.m}$ $c_1 = 3.0 \text{ kNs/m}$
0.10	4.49	883.45	
1.00	14.19	883.48	
10.00	44.85	883.73	
100.00	141.43	886.36	

*Note that:*

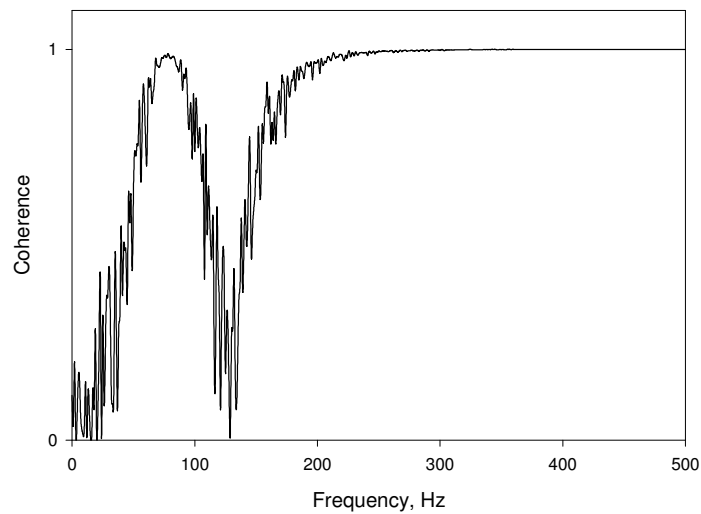
For rubber base parameters  
 $c_2 = 10 \text{ kNs/m}$

FEM model is illustrated:  
 $m_1 = 25 \text{ kg}$   
 $m_2 = 75 \text{ kg}$

The diagram illustrates the finite element model (FEM) for a rail pad. It consists of two masses,  $m_1$  and  $m_2$ , connected by a spring and damper in parallel. A force  $F(t)$  is applied to mass  $m_1$ . The displacement of mass  $m_1$  is  $u_1$  and the displacement of mass  $m_2$  is  $u_2$ . The spring constant is  $k_1$  and the damping coefficient is  $c_1$ . The spring constant of the base is  $k_2$  and the damping coefficient is  $c_2$ .



a) FRF



b) Coherence

**Figure 3.6.** Frequency response function and its coherence of the tested studded rail pad (10mm) under a preload of 20kN.

### 3.1.3 Applications of the new rail pad tester

#### 3.1.3.1 Determination of Dynamic Rail Pad Characteristics

All standard sizes of rail pads can be tested using the developed rail pad tester. Two types of new rail pads were chosen (Figure 3.1), that included the high-density polyethylene (HDPE) and studded rubber pads. As supplied by the manufacturer (PANDROL), the dynamic stiffness of HDPE pads ranges between 700 and 900 MN/m,

while the dynamic stiffness of studded rubber pads is about 45-65 MN/m. Table 3.3 gives the general data of the pad specimens. These two specimens of rail pads (HDPE 5.5 mm and Studded 10 mm) are selected from the available types, which are widely used in Australian railway networks for either passenger or heavy haul rolling stocks, i.e. Sydney Suburban Network, Queensland Rails' tracks, etc. In this case study, the testing procedures are identical to those previously described. The influence of large preloads on the dynamic behaviour of new rail pads has been firstly highlighted.

**Table 3.3.** General data of rail pad specimens.

Type	Area cm <sup>2</sup>	Thickness mm	Shape
Studded rubber	225	7.5	Studded, double side
Studded rubber	267	10.0	Studded, double side
Safelok7	254	7.0	Plane, black
Poly Urethylene	271	7.0	Plane, white
HDPE5.5	208	5.5	Plane
HDPE7.5	208	7.5	Plane
HDPE10	246	10.0	Plane

### 3.1.3.2 Monitoring Deterioration of Worn Pads

The worn rail pads were collected from a railway network operated by Rail Corporation (RailCorp) in areas of New South Wales, Australia. Two groups of used rail pads, after 99 MGT (18 years in service) and 110 MGT (20 years in service), were evaluated. The innovative rail pad tester can be used to trace and monitor the deterioration of worn rail pads on the modal data basis (Remennikov et. al, 2006). Details can be found in References, R2.

### 3.1.4 Results of dynamic rail pad characteristics

Variations of the incremental preload during excitation have been statistically detected of about 1%-4% of each instant preload during the tests. The excitation was given



through the impact hammer and the frequency response function was obtained using PULSE after each preloading. The load-deflection curve can be recorded using Dial Gauges, for instance as shown in Figure 3.8. Figure 3.9 shows the examples of curve fitting using DataFit.



a) after 99 MGT in service on RailCorp track

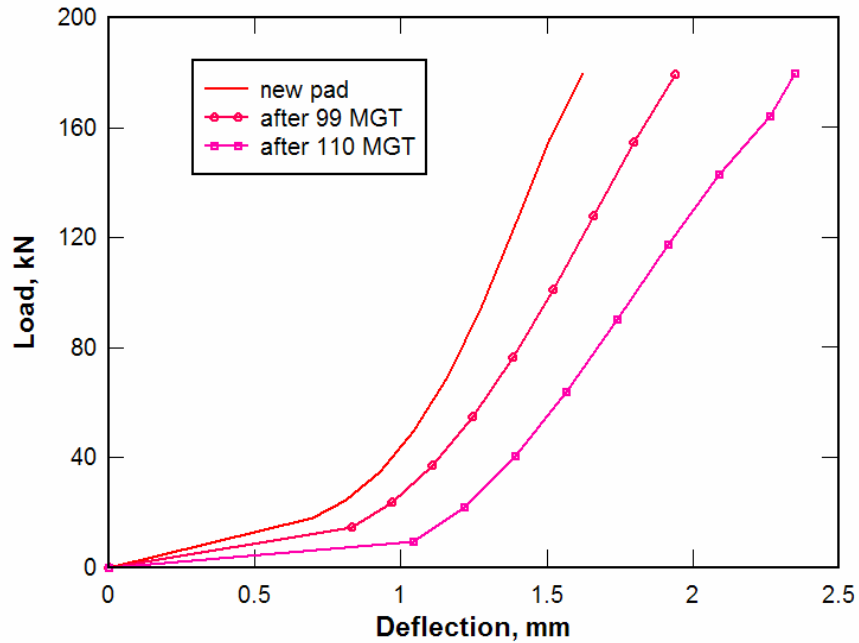


b) after 110 MGT in service on RailCorp track

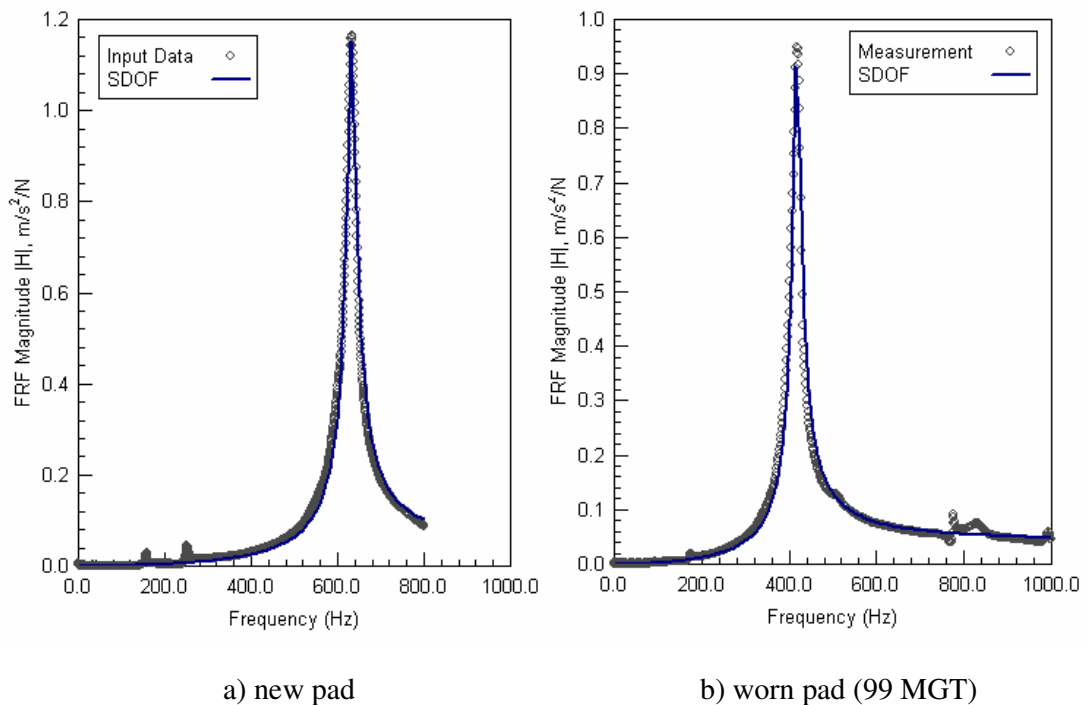
**Figure 3.7** Worn rail pads

The resonance frequencies and corresponding dynamic properties of HDPE and rubber pads are presented in Figure 3.10. The results at preload of 20 kN are comparable to the previous experimental results published by the Track Testing Center

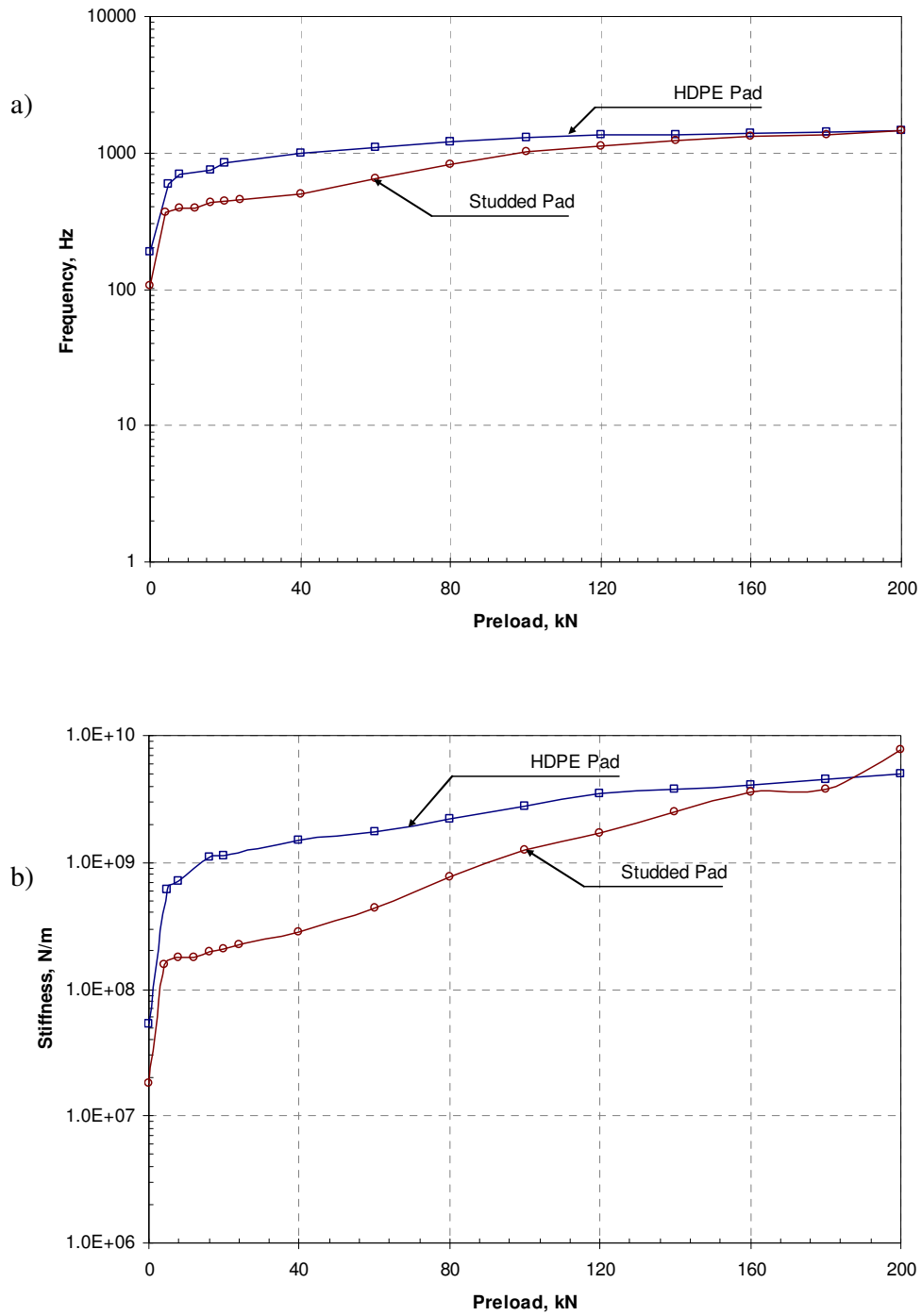
(TTC) of Spoomet, South Africa, and by TU Delft (DUT) of the Netherlands (Van't Zand, 1993). The correlation indices are found less than 2% error.



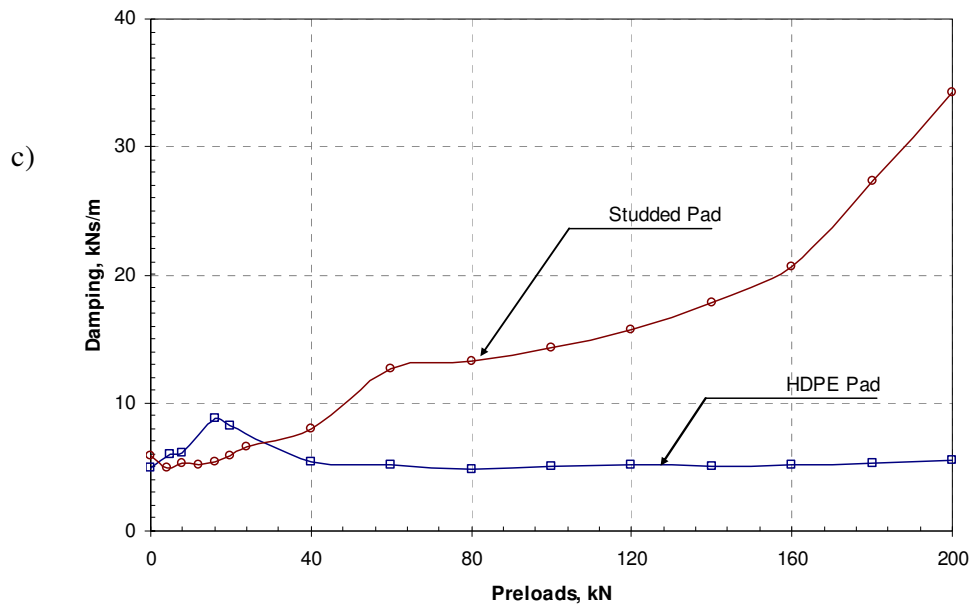
**Figure 3.8.** Load-deflection curves of worn rail pads



**Figure 3.9.** Curve fitting of frequency response functions at 20 kN preload.



**Figure 3.10.** Dynamic behaviour of new rail pads under large preloads.



**Figure 3.10.** Dynamic behaviour of new rail pads under large preloads.

It is seen from Figure 3.10a that at low to moderate amount of preloads, the effect of preloading on resonance frequencies of studded pad is significant. This effect fades away when the preload exceeds 100-150 kN. Figures 3.10b and 3.10c show the tendency of substantial increases in both dynamic stiffness and damping values with incremental preloads. On the other hand, Figure 3.10 also demonstrates that only very low preloads have effect on resonance frequencies and corresponding dynamic characteristics of the HDPE pads. At moderate to high levels of preload, the preloading seems to have small influence on the dynamic stiffness and no impact on either resonance frequencies or damping coefficients.

Resonance frequencies of the studded rubber pads tend to be less than those for the HDPE pads at low to moderate preloads. However, at high preloads, the effect of preloading on the resonance frequencies seems to be significantly less, resulting in similar values of the natural frequencies. Although the studded pads have lower dynamic stiffness than the HDPE pads at low amount of preloading, they are likely to gain benefit from high preloads and behave considerably stiffer. Interestingly, the damping mechanism of studded rubber pads is susceptible to incremental preloads, while in the HDPE pads damping mechanism needs a certain level of preload for driving full mechanism and is therefore not sensitive to any further preloads.

It should be noted that the dynamic rail pad characteristics depend on the type of rail pads. This is because each type of rail pad has different chemical combination of substances, different choices of materials, and also different thickness and area subjecting to toe load.

### 3.2 PRESTRESSED CONCRETE SLEEPERS

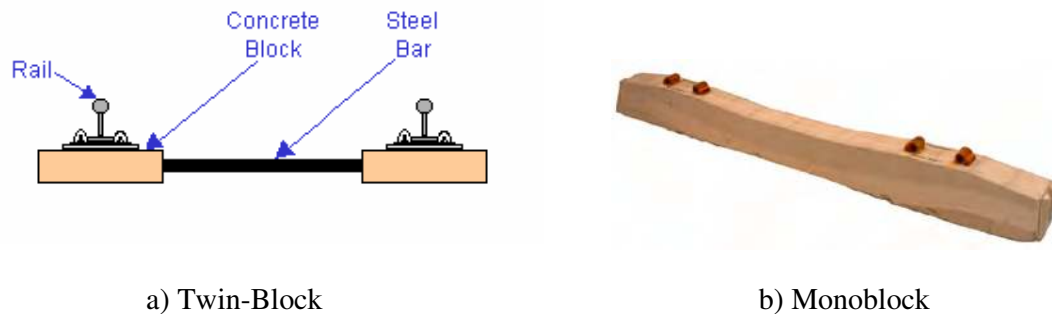
Australian railway industry paid approximately 25–35 percent of its 1998 annual budget on rail track maintenance, and the replacement costs of rails and sleepers were a considerable part of the expense (Yun and Ferreira, 2003). It shows the importance of concrete sleepers as part of ballasted track, in particular in Australian coal and mining industries. Two major parts of ballasted track are the super-structure and the sub-structure. The super-structure is made up of steel rails, the fastening systems and sleepers; whilst the ballast, sub-ballast, sub-grade and formation, form the sub-structure. Figure 3.3 illustrates the ballasted track components. Esveld (2001) noted that ballasted track has many advantages; for example, the construction costs are comparatively low, the maintenance and repair of track and its components are convenient, it has high damping and very good drainage properties, and noise can be controlled. Since railway track is always subjected to a variety of time-dependent loads, understanding the dynamic track behaviour is essential in order to evaluate the structural safety and service life of the railway track components.

Traditionally, sleepers are the track components resting on the ballast formation transversely as shown in Figure 3.3. Railway sleepers were first made in timber, and then a limited number of steel sleepers were used, followed by the now popular concrete sleepers. The majority of modern railway sleepers used in Australia are the prestressed concrete sleepers. In general, the sleepers are required to:

- support and restrain the rail foot;
- sustain and distribute loads from the rail foot to the underlying ballast;
- maintain the rail gauge and shape, and preclude rail inclination and track instability;
- withstand longitudinal, lateral and vertical rail movements;

- provide insulation between parallel rails, and
- resist wearing and loading, and endure extreme weather conditions from cold to hot, and from rain to drought.

There are two commercially available types of concrete sleepers: twin-block and monoblock sleepers, as shown in Figure 3.11. The former sleepers were originally developed in France and used in Europe, India, Brazil, and Mexico. The later ones first came from the UK and have been adopted in countries such as Australia, Canada, China, Japan, the UK, the USA, and the former USSR (FIP Commission, 1987). Due to the nature of dynamic loadings on railway track, the vibration characteristics of concrete sleepers are essential in analysis and design procedures. Also, to develop and validate a numerical simulation of rail track, the free vibration characteristics of the sleepers in various conditions are needed. Archives of vibration response measurements and parameters of sleepers can help engineers to identify the vibration-based damage or remotely monitor the sleeper health, since it is clear that the sleeper damage occurs mostly at resonant frequencies of the sleepers (Grassie, 1995). The resonant vibrations of sleepers affect not only the sleepers themselves, but also the wheel–rail interaction forces. These effects have been analytically studied by Clark et al. (1982), Grassie and Cox (1984), and Knothe and Grassie (1993). Due to their wide use, the design and maintenance of prestressed concrete sleepers is a major concern to Australian track engineers.



**Figure 3.11** Concrete sleepers

There have been a number of studies related to the determination of dynamic properties of concrete sleepers. Modal analysis is one of the widely used techniques to examine the

vibration characteristics of concrete sleepers. Ford (1988) performed modal analysis on a concrete sleeper in free-free condition using an electrodynamic shaker. Dahlberg and Nielsen (1991) developed an analytical model for analysing dynamic behaviour of concrete sleepers in both free-free and in-situ conditions. Based on the experimental results, a two-dimensional dynamic modelling for vibration analysis of concrete sleepers was done by Grassie (1995). It was found that the Timoshenko beam element was the best approximation of the concrete sleepers, even though the elastic properties of prestressed concrete sleepers may not be precise. Recently, Gustavson (2000) and Vincent (2001) performed the three-dimensional finite element modelling and modal testing of concrete sleepers in free-free condition. The results were in good agreement between numerical and experimental data. In reality, however, the sleepers are placed on ballast/subgrade formation. A comprehensive sleeper-ballast dynamic interaction has rarely been studied (Remennikov and Kaewunruen, 2005).

This part presents results of an experimental modal analysis of prestressed concrete sleepers in both free-free and in-situ conditions. Four types of prestressed concrete sleepers were provided by the Australian manufacturers. The concrete sleepers were tested using an impact hammer excitation technique over the frequency range of interest: 0 to 1600 Hz. Frequency response functions (FRFs) were measured using the Bruel&Kjaer PULSE dynamic analyser. The FRFs were processed using the STARModal analysis package to identify natural frequencies and the corresponding mode shapes for the sleepers. The conclusions are presented on the effect of boundary conditions on the dynamic properties of prestressed concrete sleepers and their use for predicting railway track dynamic responses. Vibration parameters of concrete sleepers are required for the development of a realistic dynamic model of railway track capable of predicting its responses to impact loads due to wheel burns, irregularities of the rail, so on.

### 3.2.1 Analytical Modal Analysis

Measurements of vibration responses in structures result in the modal parameter identification to obtain the dynamic characteristics of the structures. There are a number of methods to extract the dynamic characteristics, depending on the format of data obtained (Ewins, 1995; He and Fu, 2001).

In a dynamic system, the equation of motion of the system can usually be represented by

$$[M]\{\ddot{x}\} + [C]\{\dot{x}\} + [K]\{x\} = \{f\} \quad (3.6)$$

where  $[M]$  is the mass matrix,  $[C]$  is the damping matrix, and  $[K]$  is the stiffness matrix. The harmonic force applied to the system with magnitude  $F$  and loading frequency  $\omega$  is given by

$$\{f\} = F \sin \omega t \quad (3.7)$$

As known, a non-trivial solution to Equation (1) is  $\{x\} = \{X\} e^{j\omega t}$ . Substituting this solution to Equation (3.6) and manipulating it with Equation (3.7), the equation of motion becomes

$$(-\omega^2 [M] + j\omega [C] + [K])\{X\} = \{F\} \quad (3.8)$$

With some manipulations, transforming Equation (3.8) using modal coordinates by using  $\{X\} = [\Phi]\{Q\}$  and the orthogonality principle, and it then yields

$$Q_i = \frac{\{\phi_i^T\}}{\omega_i^2 - \omega^2 + 2\xi_i \omega_i \omega j} \{F\} \quad (3.9)$$

Recalling  $\{X\} = [\Phi]\{Q\} = Q_1 \phi_1 + \dots + Q_n \phi_n$ , Equation (3.9) can be re-written as

$$\{X\} = \left( \sum_{i=1}^n \frac{\phi_i \phi_i^T}{\omega_i^2 - \omega^2 + 2\xi_i \omega_i \omega j} \right) \{F\} \quad (3.10)$$

Then, the receptance of the system can be identified by

$$H_{ij}(\omega) = \frac{X_i(\omega)}{F_j(\omega)} = \sum_{i=1}^n \frac{\phi_i \phi_i^T}{\omega_i^2 - \omega^2 + 2\xi_i \omega_i \omega j} \quad (3.11)$$



Herein,  $\omega_i$  denotes the resonant frequency,  $\phi_i$  is the mass-normalized mode shape, and  $\xi_i$  represents the modal damping ratio.

Note that for viscous damping (with critical damping  $c_r$ ),  $\xi_i = \frac{c_i}{c_r}$ ; for proportional

damping ( $[C] = a[M] + b[K]$ ),  $\xi_i = \frac{a}{2\omega_i} + \frac{b\omega_i}{2}$ ; and for hysteretic damping ( $\eta_i$ ),

$$\xi_i = \frac{\eta_i}{2}.$$

### 3.2.2 Experimental Overview

All test specimens were prestressed concrete sleepers designed in accordance with AS1085.14-2003. The dimensions and masses of the test sleepers are tabulated in Table 3.4. Sleepers No. 1 and 2 are the heavy- and medium-duty sleepers provided by ROCLA. Sleepers No.3 and 4 are the broad- and narrow-gauge sleepers provided by AUSTRAK. The excitation points were located on the top surface of the sleeper at every 150 mm along the perimeter. It should be noted that the number of these positions should be sufficient to represent the vibration modes of interest. In this case, an accelerometer had a fixed position whilst an instrumented impact hammer was roved along the excitation points. Figure 3.12 shows the experimental setup of a sleeper in free-free condition. The sleepers were suspended by very soft springs to simulate free-free boundary conditions. After performing the modal testing, the sleepers were then placed on the ballast bed that imitated the actual track construction, as illustrated in Figure 3.13. The ballast containment was designed based on the information of track geometry and sleeper spacing obtained from the railway organisations.

From experience, the best position for mounting the accelerometer is at the end of the sleeper. At this point, the FRFs recorded are clear at all modes of vibration without any noise. The instruments used in this study were a PCB accelerometer, the PCB impact hammer, and the Bruel&Kjaer PULSE vibration analyser. The accelerometer was mounted at the sleeper end. Using the hammer to excite vibrations in the sleeper over the frequency range 0 to 1600 Hz, the 10-time average vibration responses represented by the FRFs were obtained using the PULSE system. Then, processing the recorded

FRFs by STARModal gave the natural frequencies and modal damping constants of the sleeper. All procedures were performed twice per a sleeper for free-free and ballasted-support conditions.

**Table 3.4** Dimensions and masses of the test sleepers

Sleeper No.	Mass (kg)	Total length (m)	At railseat (m)		At centre (m)	
			width	depth	width	depth
1	206.0	2.50	0.20	0.23	0.21	0.18
2	198.1	2.47	0.22	0.18	0.21	0.17
3	299.5	2.85	0.22	0.21	0.22	0.18
4	283.0	2.15	0.18	0.25	0.16	0.24



**Figure 3.12** Free-free condition



**Figure 3.13** Ballast condition

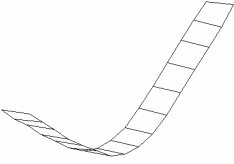
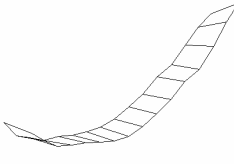
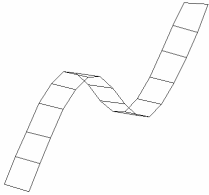
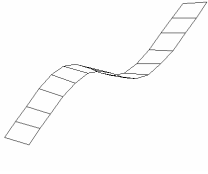
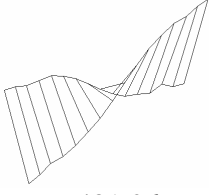
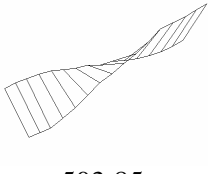
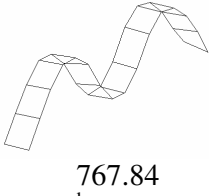
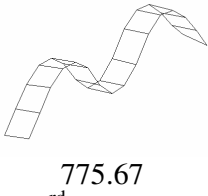

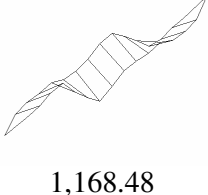
### 3.2.3 Experimental Results

The results of vibration tests for Sleepers No. 1–4 are depicted in Tables 3.5–3.8. In these tables, the first five modes of vibration are presented. For all sleepers, it was found that the first bending mode in a vertical plane clearly dominated the first resonant

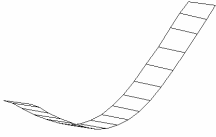
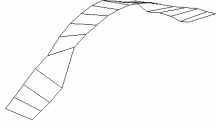
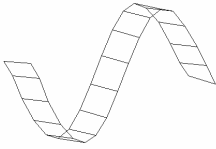
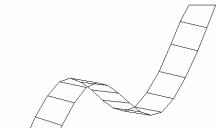
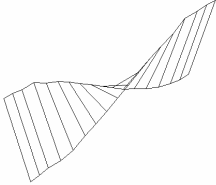
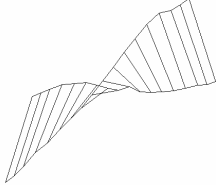
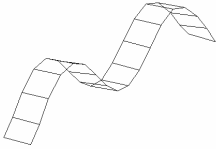
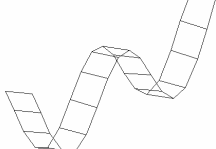
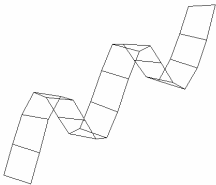
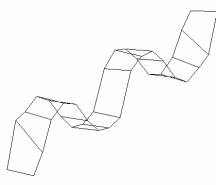
mode of vibration both in free-free and ballast conditions. Table 3.5 shows the experimental dynamic properties of Sleeper No. 1 (ROCLA Heavy Duty). For a free-free condition, the lowest frequency corresponded to the fundamental bending mode, the second frequency to the second bending mode, the third frequency to the lowest torsional mode, the fourth frequency to the third bending mode, and the fifth mode to the second torsional mode. Similar modes of vibration were identified for the sleeper in the in-situ boundary condition. Of all five modes, the most significant change in natural frequencies between the free-free and in-situ conditions was the first bending mode. The maximum frequency increase was about 15 percent. However, it was found that at higher resonant frequencies, the effect of boundary conditions was remarkably decreased to only two percent difference in the fourth and fifth vibration modes. Also, it should be noted that the ballast support played a significant role in increasing the damping values of all vibration modes. The maximum damping increase due to sleeper-ballast interaction was more than 50-fold in the first bending mode and the average change in other modes was between five and 10-fold. The mode shapes of ballasted sleepers were quite difficult to identify since some mode shapes were sometimes too closely spaced between each mode of vibration. The effect of boundary conditions on vibration properties of sleepers is depicted in Figure 3.14.

The experimental modal results for Sleeper No. 2 (ROCLA Medium Duty) are presented in Table 3.6. The frequency change between the free-free and in-situ conditions ranged from approximately one to 12 percent. The ballast support augmented the damping values of all vibration modes, varying from four to 35 times. As the sleeper dimension is fairly different from other sleepers whereas its depth over width ratio is less than unity, the fifth mode of vibration is rather a bending type. Table 3.7 gives the results of the experimental modal analysis of Sleeper No. 3 (AUSTRAK Broad Gauge). Up to a 34 percent frequency increase was found in the lowest mode which was considerably reduced to just a few percent in the higher frequency modes. At all frequencies, with one exception, the damping ratios on the ballast condition increased in the range from six up to 25 times. The one exception was the maximum increase in the first torsional frequency. Table 3.8 presents the modal properties of Sleeper No. 4 (AUSTRAK Narrow Gauge). The same trends in frequencies and damping constants for the sleepers in free-free and in-situ conditions were observed. Kaewunruen and Remennikov (2006) have recently found that the rails and rail pads also play a role in the alteration of such dynamic properties of the concrete sleepers.

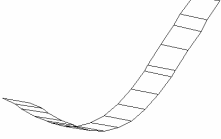
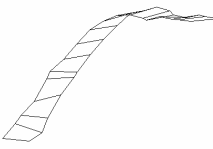
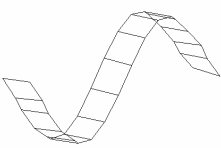
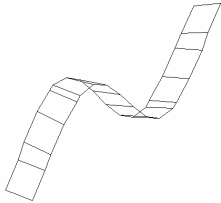
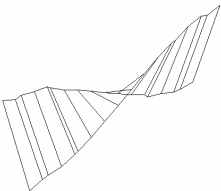
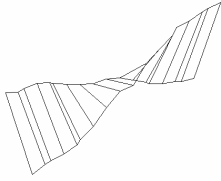
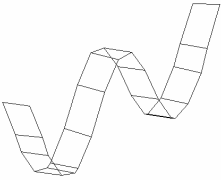
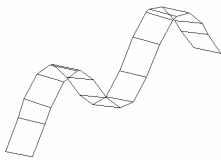
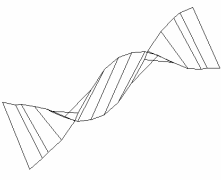
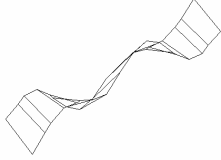
**Table 3.5** Modal parameters of sleeper no.1 – ROCLA Heavy Duty

Mode	Free-Free Condition		Ballast Support	
	Frequency (Hz)	Damping (%)	Frequency (Hz)	Damping (%)
1	 135.71 (1 <sup>st</sup> bending)	0.266	 155.22 (1 <sup>st</sup> bending)	15.92
2	 404.83 (2 <sup>nd</sup> bending)	0.298	 413.70 (2 <sup>nd</sup> bending)	3.09
3	 481.36 (1 <sup>st</sup> twisting)	0.331	 503.85 (1 <sup>st</sup> twisting)	5.58
4	 767.84 (3 <sup>rd</sup> bending)	0.279	 775.67 (3 <sup>rd</sup> bending)	1.74
5	 1,155.31 (2 <sup>nd</sup> twisting)	0.292	 1,168.48 (2 <sup>nd</sup> twisting)	1.03

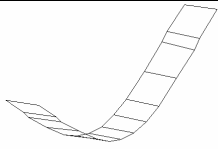
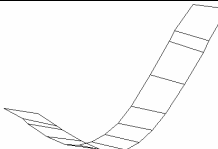
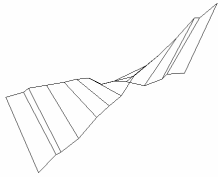
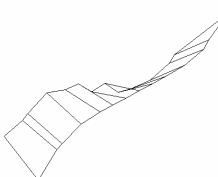
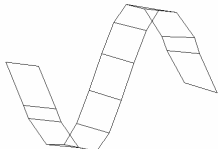
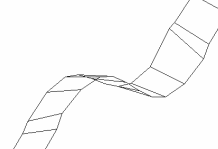
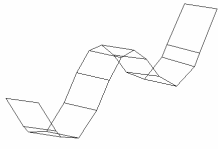
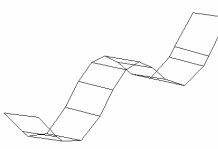
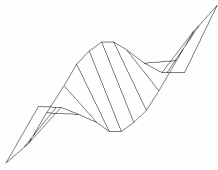
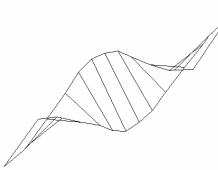
**Table 3.6** Modal parameters of sleeper no.2 - ROCLA Medium Duty

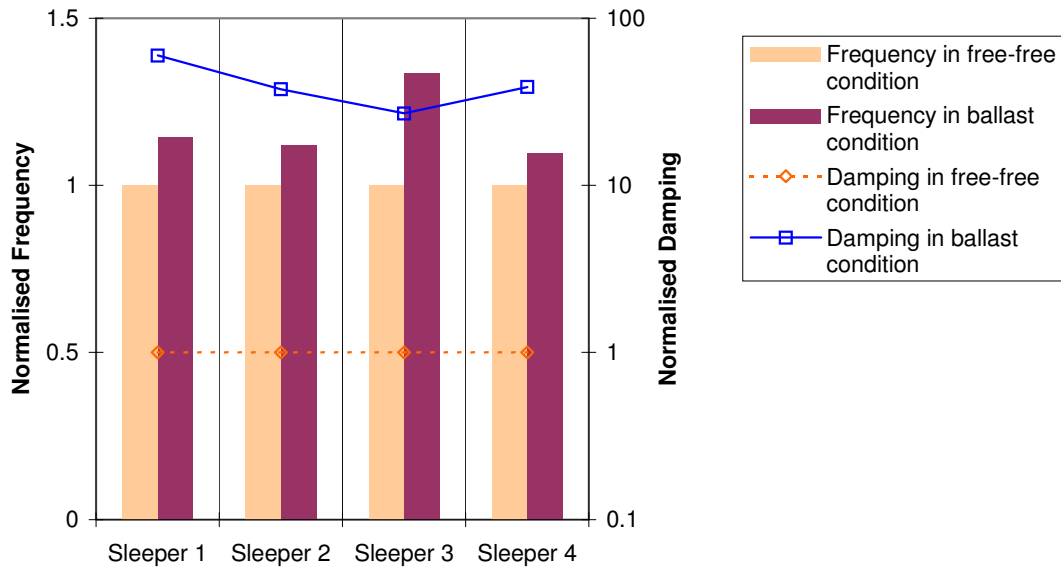
Mode	Free-Free Condition		Ballast Support	
	Frequency (Hz)	Damping (%)	Frequency (Hz)	Damping (%)
1	 123.47 (1 <sup>st</sup> bending)	0.236	 138.13 (1 <sup>st</sup> bending)	8.88
2	 340.49 (2 <sup>nd</sup> bending)	0.333	 361.08 (2 <sup>nd</sup> bending)	4.44
3	 497.70 (1 <sup>st</sup> twisting)	0.308	 512.47 (1 <sup>st</sup> twisting)	5.42
4	 651.50 (3 <sup>rd</sup> bending)	0.297	 661.72 (3 <sup>rd</sup> bending)	2.40
5	 1,026.15 (4 <sup>th</sup> bending)	0.334	 1,035.98 (4 <sup>th</sup> bending)	1.63

**Table 3.7** Modal parameters of sleeper no.3 - AUSTRAK Broad Gauge

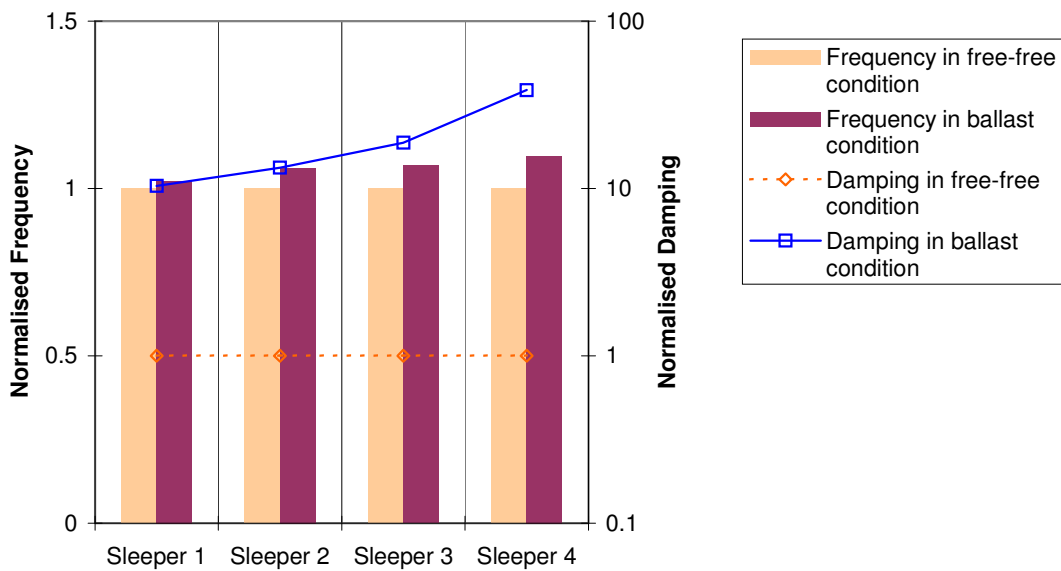
Mode	Free-Free Condition		Ballast Support	
	Frequency (Hz)	Damping (%)	Frequency (Hz)	Damping (%)
1	 112.64 (1 <sup>st</sup> bending)	0.192	 150.21 (1 <sup>st</sup> bending)	5.16
2	 312.50 (2 <sup>nd</sup> bending)	0.269	 334.13 (2 <sup>nd</sup> bending)	5.05
3	 436.60 (1 <sup>st</sup> twisting)	0.274	 449.05 (1 <sup>st</sup> twisting)	8.05
4	 605.51 (3 <sup>rd</sup> bending)	0.239	 617.98 (3 <sup>rd</sup> bending)	3.20
5	 943.53 (2 <sup>nd</sup> twisting)	0.220	 963.88 (2 <sup>nd</sup> twisting)	1.77

**Table 3.8** Modal parameters of sleeper no.4 - AUSTRAK Narrow Gauge

Mode	Free-Free Condition		Ballast Support	
	Frequency (Hz)	Damping (%)	Frequency (Hz)	Damping (%)
1	 223.09 (1 <sup>st</sup> bending)	0.216	 244.59 (1 <sup>st</sup> bending)	8.36
2	 561.62 (1 <sup>st</sup> twisting)	0.173	 565.70 (1 <sup>st</sup> twisting)	4.08
3	 593.19 (2 <sup>nd</sup> bending)	0.209	 603.00 (2 <sup>nd</sup> bending)	2.60
4	 1,092.68 (3 <sup>rd</sup> bending)	0.236	 1,100.38 (3 <sup>rd</sup> bending)	1.08
5	 1,266.67 (2 <sup>nd</sup> twisting)	0.242	 1,275.00 (2 <sup>nd</sup> twisting)	1.75



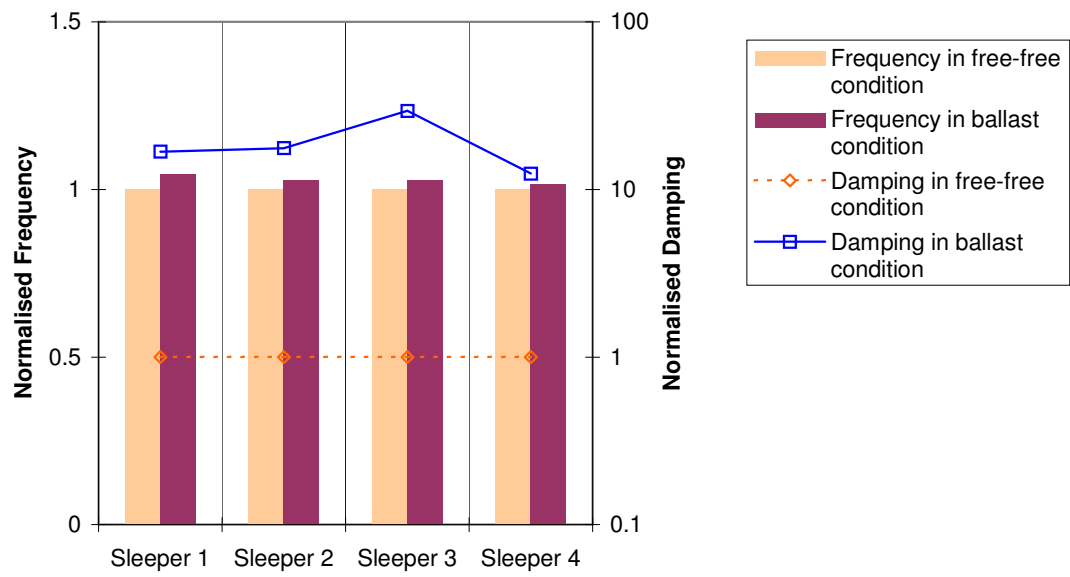
a) the lowest mode



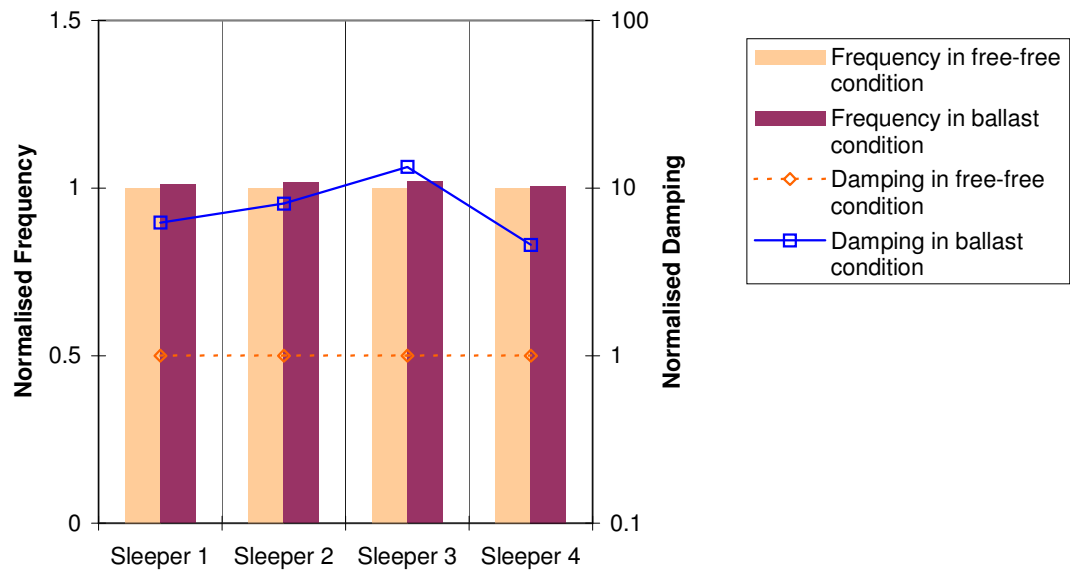
b) the second mode

Figure 3.14 Effect of sleeper/ballast interaction on vibration properties of sleepers



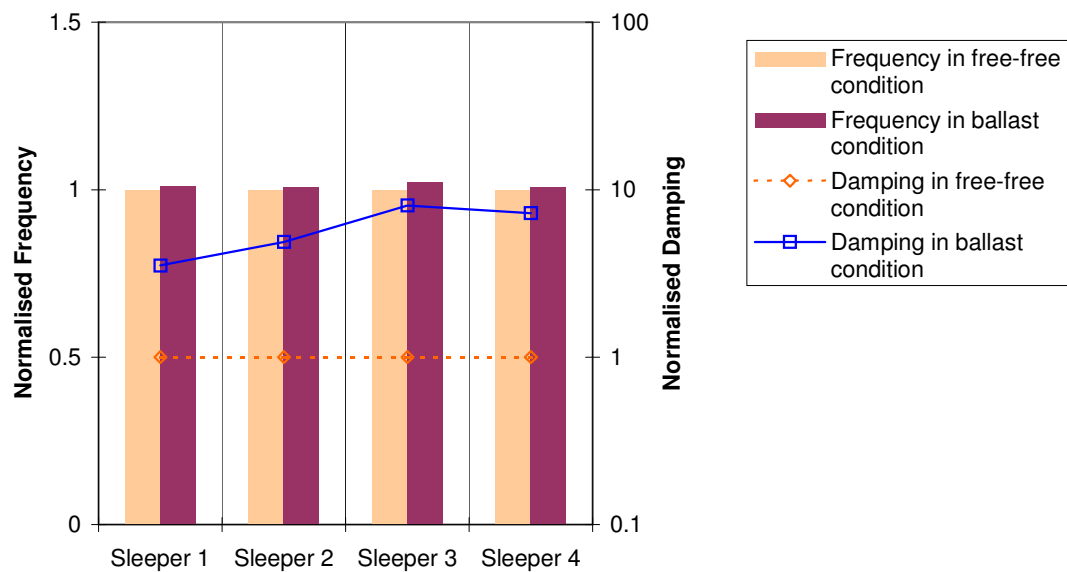


c) the third mode



d) the fourth mode

Figure 3.14 Effect of sleeper/ballast interaction on vibration properties of sleepers



e) the fifth mode (see distinction in bending/torsion modes in Tables 3.6-3.8)

**Figure 3.14** Effect of sleeper/ballast interaction on vibration properties of sleepers

### 3.3 IN SITU RAILWAY TRACK

One of major challenges in railway engineering is the non-destructive evaluation of railway track infrastructure. Applications of non-destructive testing (NDT) techniques are attributed to comprehensive backgrounds in mathematics and physics. Recently, a NDT technique on a basis of vibration theory has been adopted in railway engineering in order to measure track behaviours under either train services or man-made loadings. This NDT strategy is so-called '*modal analysis*'. Over the past decade, the modal testing has become an effective means for identifying, understanding, and simulating dynamic behaviour and responses of structures. One of the techniques widely used in modal analysis is based on an instrumented hammer impact excitation. By using signal analysis, the vibration response of the structures to the impact excitation is measured and transformed into frequency response functions (FRFs) using Fast Fourier Transformation (FFT) technique. Subsequently, the series of FRFs are used to extract such modal parameters as natural frequency, damping, and corresponding mode shape. In a wide range of practical applications the modal parameters are required to avoid

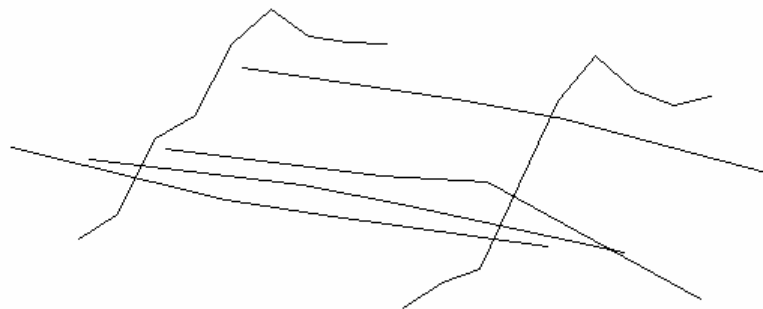
resonance in structures affected by external periodic dynamic loads. Practical applications of modal analysis span over various fields of science, engineering and technology.

A number of testing approaches is available to undertake the evaluation and monitoring of the dynamic integrity of building structures using wave signals. It is however found that the most practical strategy for railway track structures is to use an instrumented impact hammer to impart excitations into the in-situ tracks and to mount accelerometers for measuring the dynamic responses. This analogy has been successfully extended to the railway track structures in an urban environment (Esveld, 2001). To explain this, a two-degree-of-freedom (2DOF) dynamic system was used to simplify the railway track as a discretely supported continuous rail system. It consisted of two effective masses of rail and sleeper, two dynamic stiffness values, and two dashpots of rail pad and ballast formation, respectively. This part presents the in-situ tests and modellings of the track test bed constructed at University of Wollongong. The aim is to present the effectiveness of modal testing and full track finite element analysis to understand the dynamic behaviours of railway tracks.

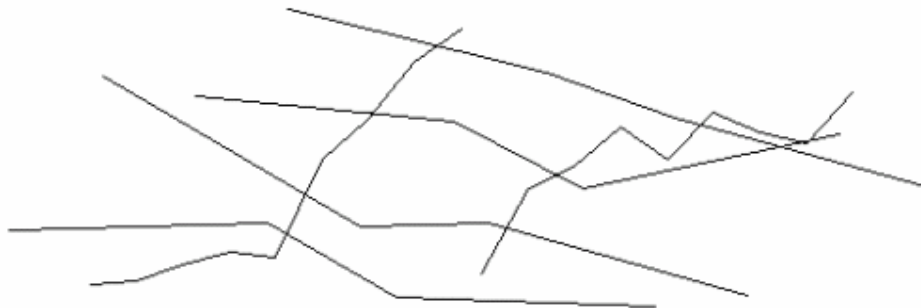
On the basis of three-dimensional elastic theory, free dynamic behaviours of global railway track are investigated. An in-situ ballasted track lying on the laboratory at University of Wollongong is modelled using elastically coupled beam elements on Winkler foundation. The rails and sleepers are modelled using beam elements while the rail pads and ballast support are represented as spring dampers. The two- and three-dimensional finite element (FE) models of the global track are developed using a FE package, STRAND7. Based on the natural frequency analysis, solutions are provided for the natural frequencies and corresponding mode shapes of railway track comprising of rails and sleepers in three dimensions. Symmetrical and asymmetrical modes of vibration are described. Also, influences of wheel load frequency on dynamic properties of railway track are additionally discussed, hence enabling ones to better understand the dynamic behaviours of track in any deteriorated circumstances. These free vibration results can also be used to predict the dynamic acceleration responses of the in-situ track.

### 3.3.1 Modal results

Modal testing was performed on the in-situ track test bed. An accelerometer was installed on the rail head. The impact excitation was exerted by hitting on the rail head and along sleepers. Full scale modal testing on the in-situ track over the frequency range of 0 to 1,600 Hz provides the frequency response functions and those responses were analyzed using STAR Modal Analysis package for experimental modal results. This frequency range was found sufficient for track structures under dynamic loading conditions (Remennikov and Kaewunruen, 2007). Figure 3.15a shows the first mode found at about 591 Hz. It corresponds to in-phase mode of vibration.



a) in-phase vibration



b) out-of-phase vibration

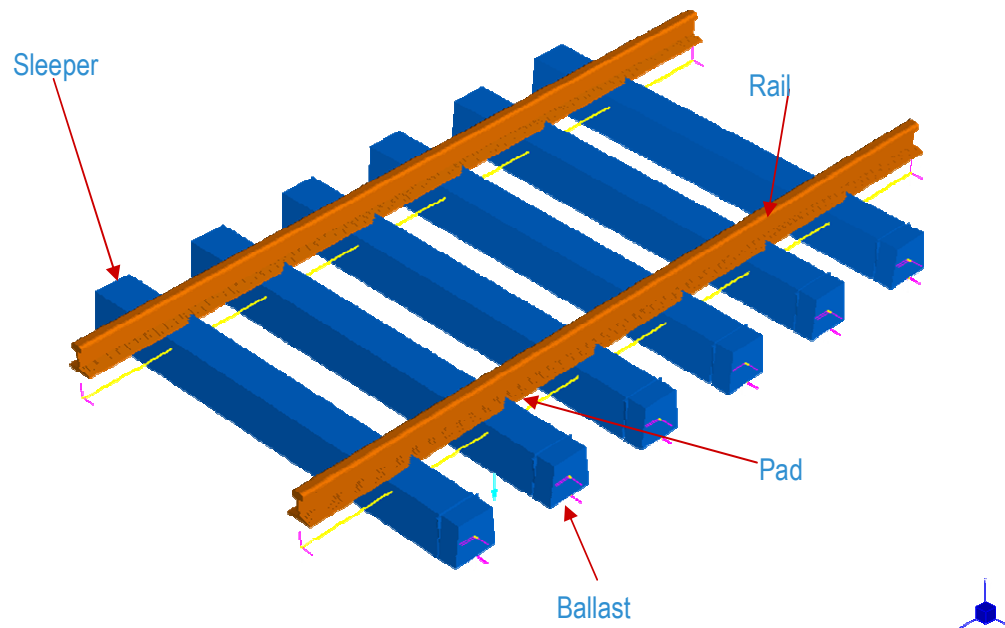
**Figure 3.15** Experimental modal result of UoW track test bed

Figure 3.15b depicts the out-of-phase vibration of in-situ railway track at the frequency of about 651 Hz. It is not very clear how each component behave from the modal mode shapes. The two- and three-dimensional finite element analyses have thus been

developed and calibrated to get better insight into the dynamic behaviours of in-situ railway tracks.

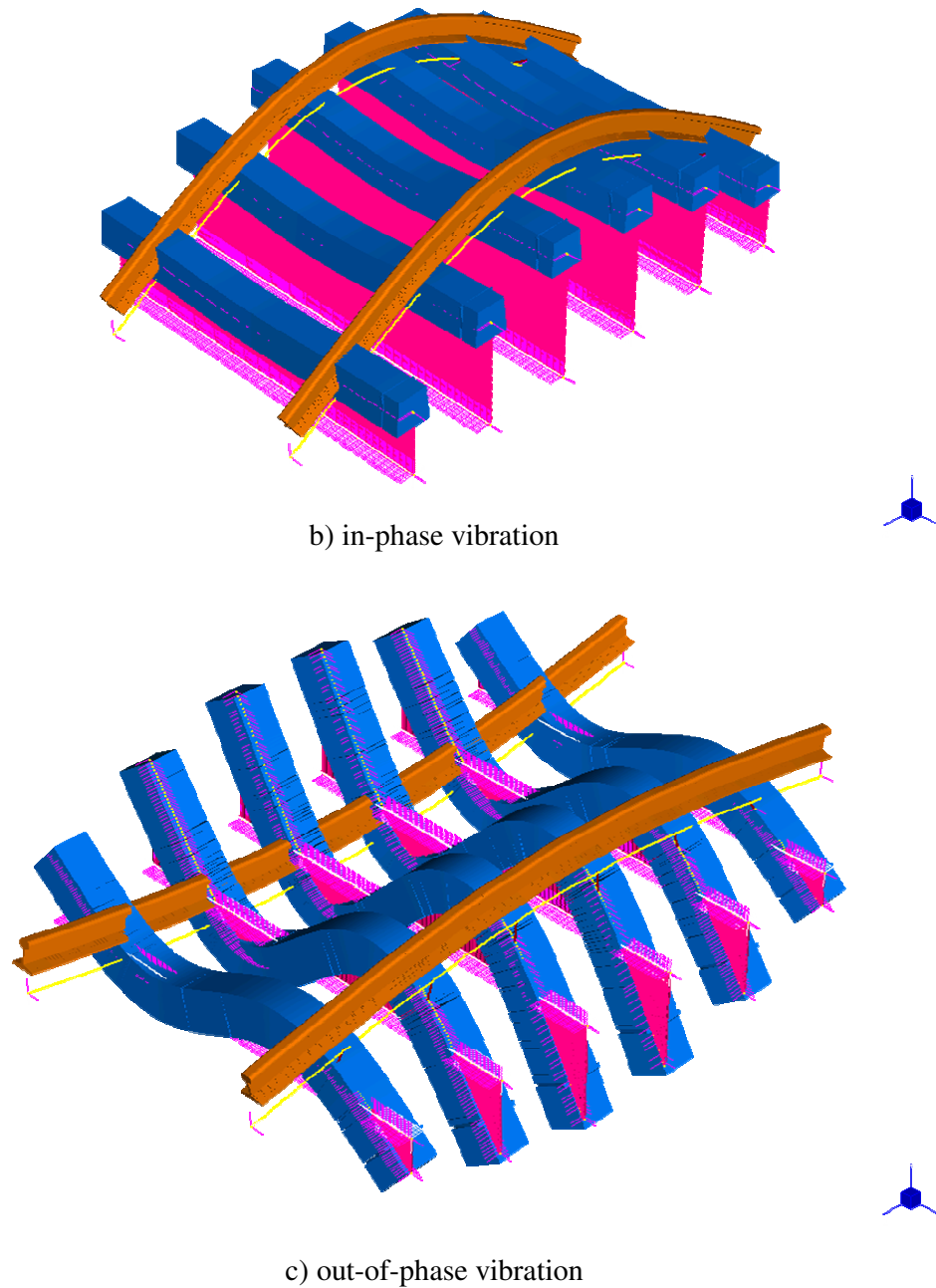
### 3.3.2 Three-dimensional Finite Element Model

The two-dimensional finite element model developed elucidates the dynamic behaviours of railway tracks only in two dimensions where the sleeper was modelled as a lump mass on the basis of discrete support model as described in Chapter 2. However, to understand the dynamic sleeper behaviour under track resonances, it is much better to develop a three-dimensional finite element model. In this study, the three-dimensional model has been extended from the two-dimensional finite element model developed using a commercial finite element package, STRAND7. The computational results were then verified against the experimental results. The rail (60kg section) and sleepers have been modelled using three-dimensional beam elements with updated dynamic properties, as illustrated in Figure 3.16a. Rail pads were simulated by spring-dashpot element while the ballast support was approximated by the elastic support feature in STRAND7 (G+D Computing, 2001; 2005). Figures 3.16b and 3.16c, show the dynamic mode shape of in-situ track in three dimensions (in-phase and out-of-phase vibrations).



a) finite element model

**Figure 3.16** Two-dimensional finite element analysis of railway track



**Figure 3.16** Two-dimensional finite element analysis of railway track

It is found that the in-phase and out-of-phase track resonances are likely to associate with the first bending and second bending mode of vibration, respectively. This confirms the knowledge that at certain wheel loading frequencies the sleepers tend to dramatically vibrate and develop cracks at bottom of rail seat or at top surface of mid-span.

### 3.4 FIELD TRIALS

#### 3.4.1 General Background

Demand for mass transportation, freight, and coal transport across a continent has become a major contribution driving research and development in railway industry to build railway tracks meeting such variety of services. Everyday there exist increasingly the needs of railway utilization (e.g. heavier axle loads, faster speeds, more frequent, etc) whilst the existing track infrastructure is questioned for its current capacity, functionality, and remaining service life. As well known, the railway structures are inevitably degrading and deteriorating due to the everyday services. Information on the structural integrity and deterioration of railway tracks is very limited. The relationships between deterioration and maintenance/renewal associated with railway infrastructure would be of great interest to track engineers and managers concerned with minimising maintenance/renewal costs. Having better understanding of maintenance and renewal and the deterioration rates could lead to the improved strategic planning and implementation (Andersson et al., 2004). In reality, structural conditions of railway tracks are typically not known either before or after maintenance procedures since in practice the maintenance and renewal operations are usually based on empirical criteria.

At present, accelerating degradation of railway tracks creates many problems to railway engineers. In order to both maximize safety and minimize costs of track maintenance and renewal, assessment and monitoring of the structural health of railway track and its components must be done. There are a number of testing methodologies available to undertake the identification and monitoring of the conditions of the track structures (Esveld, 2001). However, one of the most practical approaches is to use an instrumented impact hammer to impart excitations into the in-situ/in-field tracks and to measure the dynamic responses for condition assessment (De Man, 1996; 2002). This method has been successfully extended to the track structures in an urban environment (Esveld, 1997; Esveld et al., 1998). In those studies, the track was simplified as a two-degree-of-freedom (2DOF) discretely supported continuous rail system representing two effective masses of rail and sleeper, as well as two dynamic stiffness and two dashpots of rail pad and ballast-formation, respectively. Modal testing has been found to be a very useful tool in assessing the properties of railway tracks. In this study, modal testing was

adopted for the field investigations while the analytical and FEM models were used to evaluate the structural conditions of the railway tracks.

In Queensland, Australia, there are various problems identified on the coal lines due to the heavy axle loads and tilt topography. The structural integrity of the track components on some of the lines needed to be investigated. As part of the Rail-CRC project, the University of Wollongong (UoW) together with Queensland Rail (QR) and Queensland University of Technology (QUT) joined forces in to investigate the conditions of a heavy haul railway track in Mackay, Central Queensland (Kaewunruen and Remennikov, 2005c; 2005d; 2006c; 2006d), as illustrated in Figure 3.17. Modal results were obtained from field measurements and used to assess the current structural conditions of the railway track. Based on the discrete support model, equations of motion of a 2DOF dynamic model of railway track has been formulated using fast fourier transform (FFT) approximation technique, in order to extract the modal properties of track components from the field dynamic testing results obtained using an instrumented hammer impact technique. However, the dynamic responses obtained imply the local track behaviours only. Thus, random positions to be tested must be of a wide range that could represent the integrity of whole area.



**Figure 3.17.** Typical ballasted track on a coal line in Central Queensland



This part presents an integrated approach that combines field testing, experimental modal analysis and finite element modelling to evaluate the dynamic parameters of in-situ railway track components. Six sleeper-fastening-rail assemblies were selected for dynamic testing. The frequency response functions (FRFs) were recorded by using Bruel & Kjaer PULSE vibration analyser in a frequency domain between 0 and 1,600 Hz. The data obtained were processed using least-square curve fitting technique to determine the dynamic stiffness and damping constants of the tested track components. These results can supply a track maintenance engineer with very important information on the current structural conditions of the railway track. In addition, system identification to evaluate the track system dynamics has been developed and performed. The experimentally determined resonance frequencies together with the dynamic properties of each track component can provide a significant input for determining the maximum speed and axle load for the future track upgrades. However, in this study only ballasted railway tracks are considered.

### 3.4.2 Track Simulation

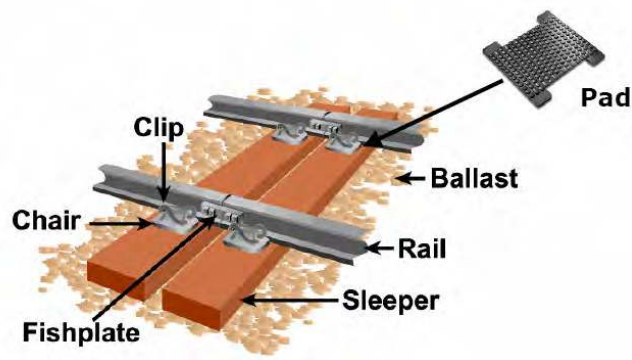
One of the first analytical models of railway track dynamics was developed by Timoshenko (1926). In that model, the rail was considered as an infinite uniform Euler beam, laid on a continuous damped elastic Winkler foundation. Later, Grassie and Cox (1984) found from the experiments that there are only two dominant resonances in the frequency range of interest for railway track. The first resonance, an in-phase mode at about 100 Hz, corresponds to the sleeper and rail moving together on the ballast. The second resonance, the out-of-phase mode at the frequency somewhere between 300-500 Hz depending on the rail pad parameters, corresponds to the opposite vibration of sleepers on ballast and rails on the rail pad. Cai (1992) found that modelling the rail and sleeper as Timoshenko beam provides the best analytical results.

For design and maintenance purposes, complicated models of railway tracks seem to be impractical when considering the field testing (Esveld, 2001). It has been demonstrated that simple analytical and finite element models calibrated using experimental data are capable of providing reliable predictions of railway track vibration response. In this study, the ballasted tracks are considered as shown in Figure 3.18. The Grassie's model (Knothe and Grassie, 1993) based on discrete sleeper support model has been employed for track simulations. The results of the finite element model of railway track show that

there are three dominant resonances, which are in a very good agreement with previous findings (Knothe and Grassie, 1993). The dominating resonance frequencies represent the in-phase, out-of-phase, and pin-pin vibration modes of railway track. As shown in Table 3.9, the in-phase and out-of-phase modes can also be represented using a simple 2DOF mass-spring system. As a result, the 2DOF mass-spring models have been widely used to identify the in-field dynamic conditions of railway tracks using the impact excitation techniques (De Man, 1996; Kaewunruen and Remennikov, 2005c; 2005d; 2006c; 2006d).

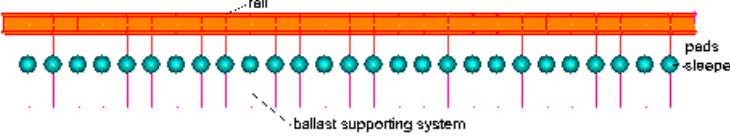
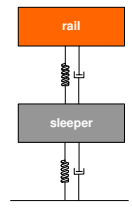
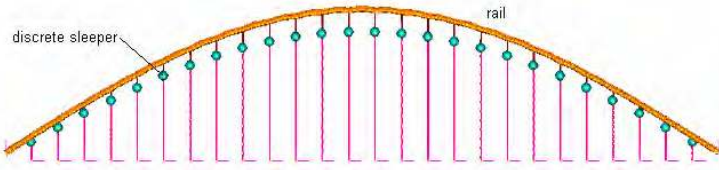
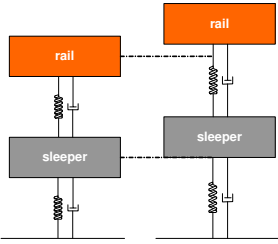
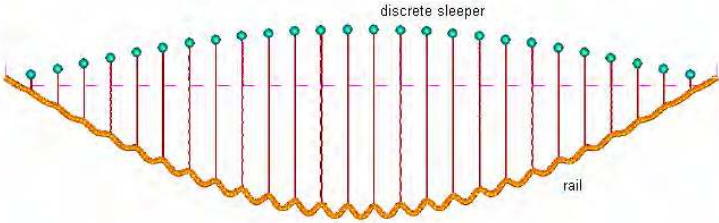
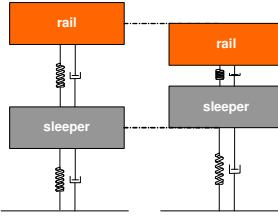
### 3.4.3 System Identification

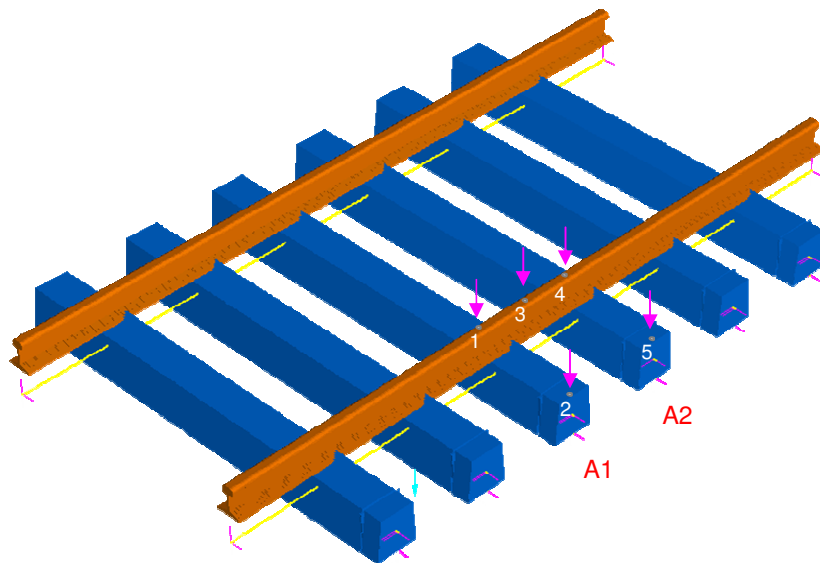
On the basis of 2DOF system, the actual global track vibration is under suspicion in that the dynamic behaviour may not be identical to the model assumed. System identification of the railway track is therefore important. Full track testing is time consuming and impractical. Five point tests at a part of the track are the better choice to estimate the system vibrations, see Figure 3.19. Few parts of the railway track were randomly selected for tests. Figure 3.19 shows the impacting point arrangement on the part of track. The points are selected as to implicate the global track responses associated with both rail and sleeper. Each point was impacted using an instrumented hammer. The accelerometer was installed at Location No 1 where provides the clearest dynamic responses to impact excitations at all excited locations. The vibration responses were processed by the PULSE Dynamic Analyzer to produce FRFs. The frequency response functions have been employed in Star Modal Testing Analysis Package to identify the resonance frequencies and corresponding dynamic mode shapes.



**Figure 3.18.** Ballasted track components (Kaewunruen and Remennikov, 2005c)

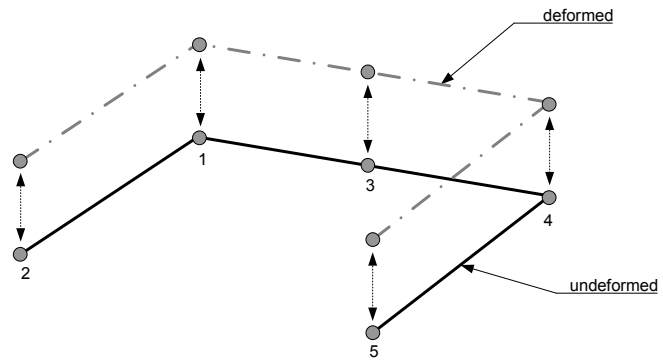
**Table 3.9** Dynamic behaviour of simplified railway tracks

Finite element model	2DOF mass-spring system
 <p>FEM</p>	
 <p>in-phase vibration</p>	
 <p>out-of-phase vibration</p>	

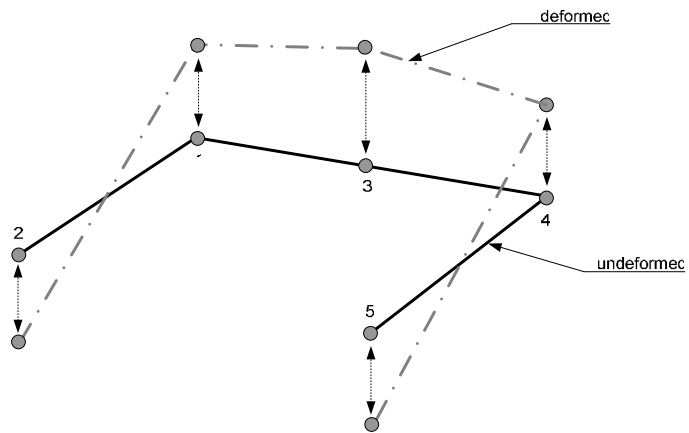


**Figure 3.19.** Modal testing schematic scenario (5-point test)

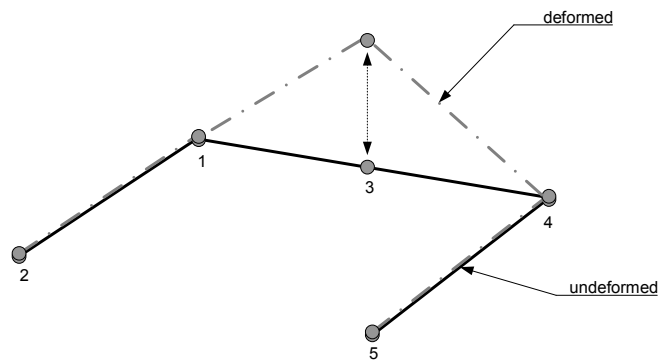




a) In-phase mode of vibration (150-250 Hz)



b) Out-of-phase mode of vibration (400-600 Hz)



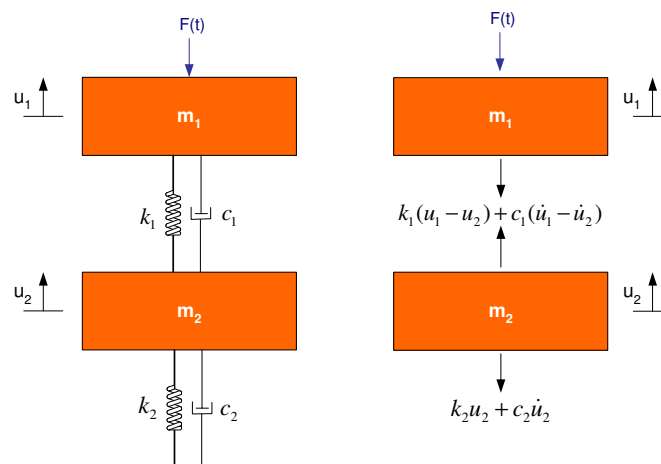
c) Pin-pin mode of vibration (700-850 Hz)

**Figure 3.20.** Modal results from 5-point tests of railway track

The results as shown in Figure 3.20 have led to the clear understanding into vibratory behaviour of the present track system. It is found that the resonance frequency ranging from 150 to 250 Hz at the track site is associated with the in-phase mode of vibration (Figure 3.20a). The out-of-phase mode of vibration is found at the frequency range between 400 and 600 Hz (Figure 3.20b) while the pin-pin vibration prevails over the frequency range of 700 to 850 Hz (Figure 3.20c). This information has confirmed with the field measurements using 2DOF idealization of railway tracks.

### 3.4.4 Condition Assessment

The in-field testing was carried out by means of excitation hammer testing. A small instrumented hammer and a large sledge hammer were used to evaluate the dynamic properties of a railway track. In this test, the track was simplified as a 2DOF discretely supported continuous rail as shown in Figure 3.21. The hammer was used to hit railhead to impart excitation to the track system. An accelerometer was mounted on the railhead as illustrated in Figure 3.22. Both the impact hammer and accelerometer were connected to the B&K FFT PULSE acquisition system through which the frequency response functions (FRFs) could be measured.



**Figure 3.21** 2DOF dynamic models of railway track



**Figure 3.22** Dynamic testing installation

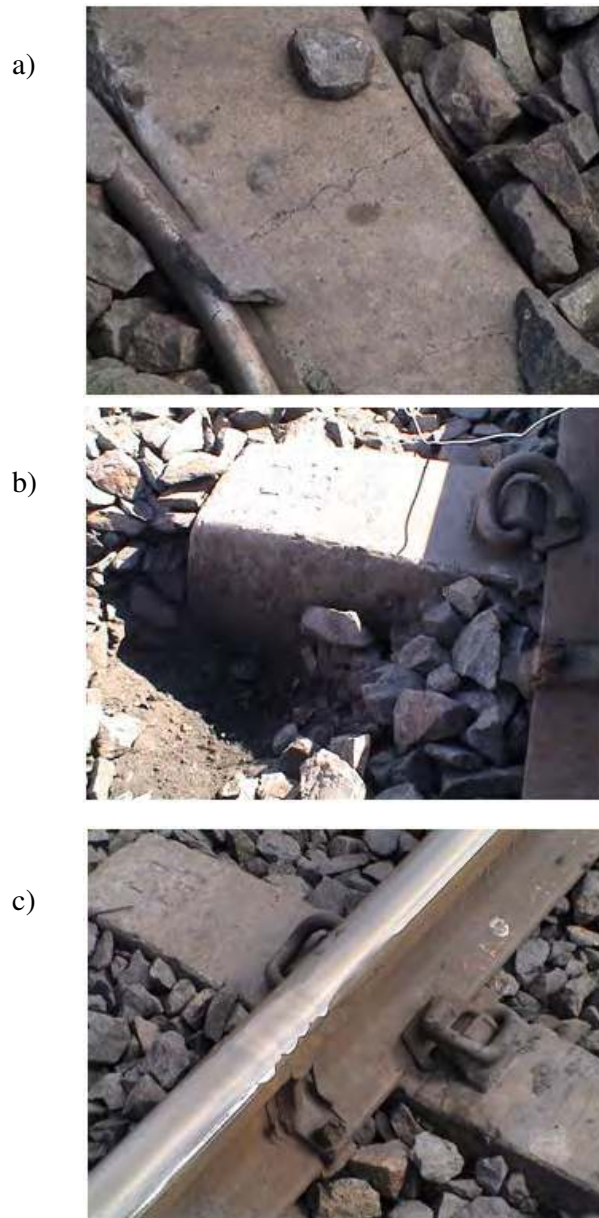
In order to extract the dynamic properties of the ballasted track systems, the analytical models of the 2DOF model depicted in Figure 3.21 have been developed based on the Fast Fourier Transform (FFT) and Mode Superposition (MS) methods. The developed analytical expressions are given in Equations (3.12) and (3.13) for FFT and MS methods, respectively. In these equations,  $m_1$  and  $m_2$  are masses of rail and sleeper,  $k_1$  and  $c_1$  represent stiffness and damping coefficients of the rail, and  $k_2$  and  $c_2$  represent stiffness and damping coefficients of ballast supporting system. It should be noted that system parameters in Equation (3.12) represent the actual stiffness, actual damping value, and actual mass. In contrast, Equation (3.13) is formulated in terms of modal stiffness, modal damping, and modal mass based on MS method. These equations are to be used in least square optimisation for the estimation of the dynamic system parameters.

$$H_{11}(f) = \frac{\sqrt{[k_1 + k_2 - 4\pi^2 f^2]^2 + [2\pi f (c_1 + c_2)]^2}}{\sqrt{[(k_1 - 4m_1\pi^2 f^2)(k_2 - 4m_2\pi^2 f^2) - 4\pi^2 f^2 (k_1 m_1 + c_1 c_2)]^2 + 4\pi^2 f^2 [k_1 c_2 + k_2 c_1 - (m_1 (c_1 + c_2) + c_1 m_2) 4\pi^2 f^2]^2}} \quad (3.12)$$

$$H_{11}(f) = \frac{\frac{1}{m_1} \frac{4\pi^2 \left(\frac{m_1}{k_1}\right) f^2}{\sqrt{\left[1 - 4\pi^2 \left(\frac{m_1}{k_1}\right) f^2\right]^2 + \left[4\pi^2 \left(\frac{m_1}{k_1}\right) \left(\frac{c_1^2}{k_1 m_1}\right) f^2\right]}}}{\frac{1}{m_2} \frac{4\pi^2 \left(\frac{m_2}{k_2}\right) f^2}{\sqrt{\left[1 - 4\pi^2 \left(\frac{m_2}{k_2}\right) f^2\right]^2 + \left[4\pi^2 \left(\frac{m_2}{k_2}\right) \left(\frac{c_2^2}{k_2 m_2}\right) f^2\right]}}} + \quad (3.13)$$

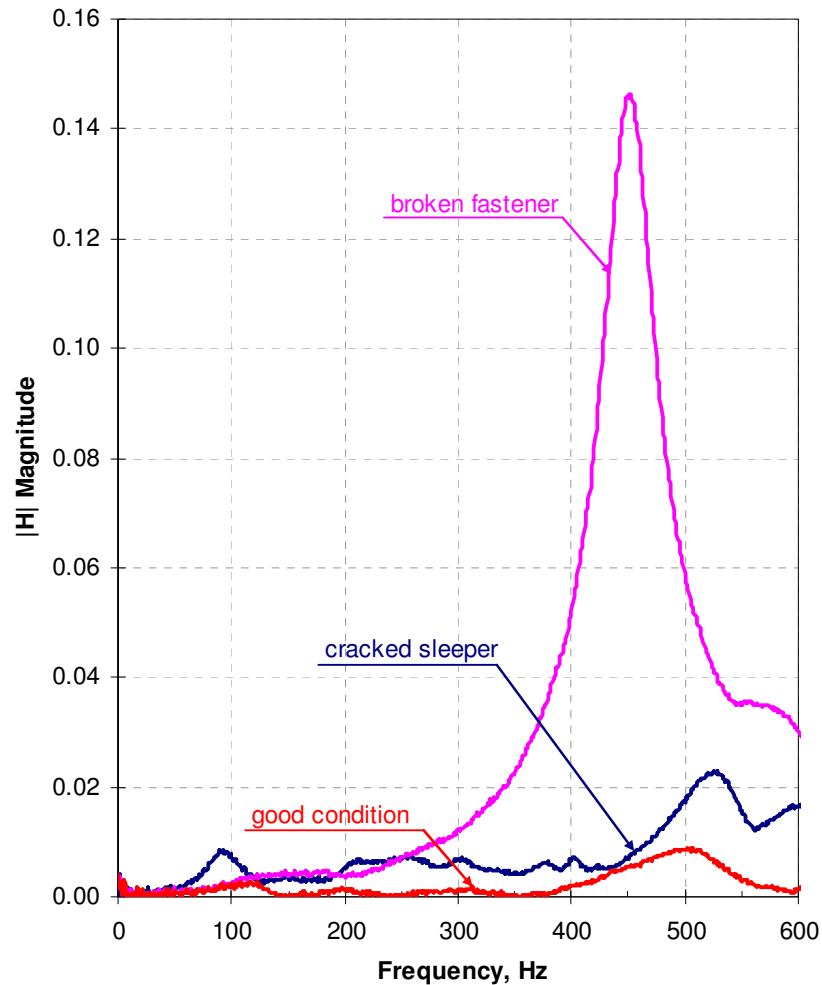
### 3.4.5 Field Trials

The field measurements were carried out in March 2005 on the existing track of a coal line between Nebo and Hay Point Port in Mackay, Central Queensland, Australia. The track has been in service since 1991. The line provides services to the coal mines at Goonyella utilising the 2-kilometre long heavy-haul coal trains passing by every 20 minutes (Kaewunruen and Remennikov, 2005d; 2006d). Referring to Figure 3.17, the ballasted track system is thoroughly used in this region. At the test sites, visual inspection for observable defects and faults was carried out. Overall conditions of rail track structures were found in good status with respect to both superstructure and substructure. There are not many irregularities found on the railhead surface, such as dip-joints, squats, wheel burns, wears, and so on. However, in few places, damage of rail fastening system, cracks in concrete sleepers, and so on, incurred as depicted in Figure 3.23. Figure 3.23a) shows the cracks on the mid span of sleepers, Figure 3.23b) shows the coal-ballast mixture and Figure 3.23c) is the short-pitch corrugation on rails. In this chapter, the experimental data are exemplified aiming at enhancing the insight into the non-destructive testing and its interpretation. Three samples of field data, including the good condition areas, broken fastening system site, and a track with cracked sleeper, are illustrated as follows.



**Figure 3.23.** Visual inspection



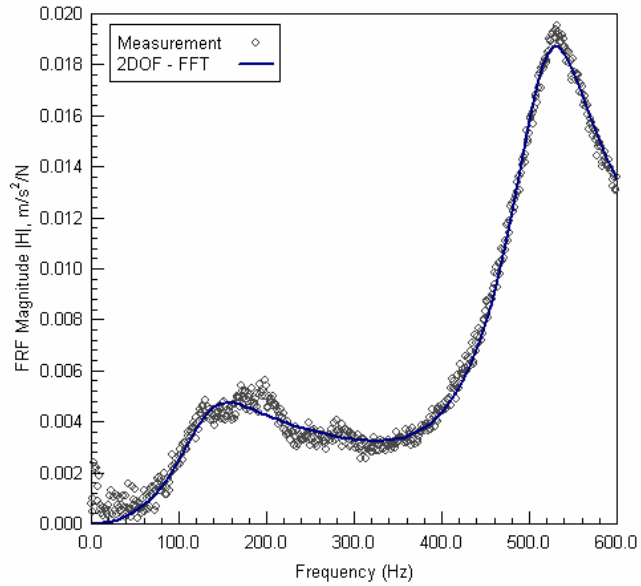


**Figure 3.24.** Field measurements

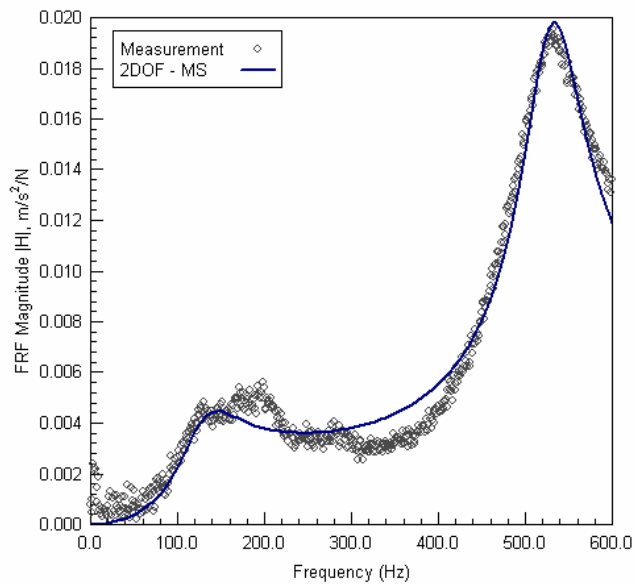
#### 3.4.5.1 Good condition tracks

The field measurements produced the FRF data sets to be processed for assessing the structural conditions of the railway track. Figure 3.24 shows the example of FRF measured in the field within a frequency range from 0 to 600 Hz of the good condition railway tracks. FRF represents the dynamic responses of local system to given excitation, while the coherence provides the quality level of the response signals. Based on the visual inspection, the track was in good conditions. The rail gauge was normal in general. The sleeper and ballast supporting system were in good conditions. In the frequency range of interest, the quality of the response is very high. Based on the previous experimental work (Kaewunruen and Remennikov, 2005d; 2006d), the

frequency range of 0 to 600 Hz was of practical interest in this study. The in-phase and out-of-phase resonance frequencies were found to about 130 Hz and 520 Hz, respectively.



a) FFT Best Fitting



b) MS Best Fitting

**Figure 3.25** Best curve fitting of measured data at a good condition site

The data sets obtained from field measurements were processed using two approaches: FFT and MS. The curve fitting operations were done using a curve-fitting package DataFit (2003). The best-fit algorithm was set in order to determine the parameters at 99% confidence level. An example of the curve-fitting results is presented in Figures 3.25a) and 3.25b) for the two analytical approaches used. From the curve fittings, it was found that the correlation error of the curve fitting is less than 3% for FFT procedure and 5% for MS algorithm. The results obtained using both approaches were in a good agreement with the industry-accepted data used in track design. Also, the results obtained are consistent for all tested sleepers. Using FFT, the stiffness of pads was found to be about 850-1050 MN/m, whereas the MS algorithm resulted in 1,100-1,500 MN/m. The ballast stiffness was determined to be within range of 140 to 270 MN/m using both FFT and MS techniques. The damping constants for rail pads varied from 1 to 23 and 1 to 58 kNs/m based on FFT and MS, respectively, while the damping values of ballast varied from 140 to 270 kNs/m based on both FFT and MS. It was found that the damping coefficients of the track components tested were in the acceptable ranges. Table 3.10 summarizes the average parameters of railway track components determined in the field investigations. Overall, the conditions of railway track components could be considered acceptable since the stiffness of rail pads and their damping characteristics have not deteriorated below the industry acceptable limits.

**Table 3.10** Summary of average parameters of the components of well conditioned railway track

Track Components	Methodologies	Average Parameters	
		Damping (kNs/m)	Stiffness (MN/m)
Rail pad	FFT	9.430	925.280
	MS	16.438	1,315.296
	FFT+MS	12.934	1,120.287
Ballast	FFT	225.698	246.847
	MS	220.562	333.632
	FFT+MS	223.130	290.240

### 3.4.5.2 Loosening rail fastening system

From visual inspection, at a glance it was not possible to notice that the rail fastening system was broken. The modal testing was performed. The frequency response functions (FRFs) were recorded on the site as shown in Figure 3.24. From the FRF, it can be read clearly in the frequency range of interest (up to 600 Hz) that there must be a defect in that local track system. The search on track was carefully performed. It was found that the rail fastening system (e-Clip) was broken and did not hold the rail gauge to the concrete sleeper.

The FRF of the track with loosening rail fastening system looks similar to those found in a SDOF dynamic model, see Figure 3.24. There is only one dominant peak during the frequency range of interest and very clear signal as seen in Figure 3.24. The dynamic responses of substructure in low frequency diminished since there is no connection between superstructure and substructure. Due to the broken fastener, the dynamic mass of the ballast could not be excited from the railhead. Table 3.11 shows the curve fitting results in which poor integrity of the substructure is evident. The average dynamic stiffness of rail pads was found to be about 513 MN/m whilst its damping constant was about 17 kNs/m. Noteworthy, this is the sign of a defect in the fastening system that track engineers should be aware of for maintenance purposes.

**Table 3.11** Summary of average parameters of the railway track with broken fastening system

Track Components	Methodologies	Average Parameters	
		Damping (kNs/m)	Stiffness (MN/m)
Rail pad	FFT	19.081	590.764
	MS	15.683	435.372
	FFT+MS	17.382	513.068
Ballast	FFT	0.000	0.000
	MS	0.000	0.000
	FFT+MS	0.000	0.000

### 3.4.5.3 Cracked sleeper

As illustrated in Figure 3.23a, the track with cracked sleeper at mid span was tested. Figure 3.24 illustrate the dynamic responses by means of FRF and coherence functions. It is found in the FRF that many peaks occur between the first and second peak. In case of the track with cracked sleeper, the FRF signal presents not much information for judgment on any observable defects. However, it can be noticed from the FRF in the frequency range between 0 and 600 Hz that there are a number of small but strong peaks arisen. This would result in a difficulty in best curve fitting processes. From curve fitting results in Table 3.12, it can be found that the cracked sleeper significantly reduces the dynamic mass and stiffness of substructure, whilst cracking remarkably increases the damping of system, in terms of increased friction in concrete material. The average stiffness of rail pad is about 744 MN/m while the average ballast stiffness remains only 80 MN/s. It should be noted that the ballast damping is much lesser than that of the well conditioned tracks in general.

**Table 3.12** Summary of average parameters of the railway track with cracked sleeper

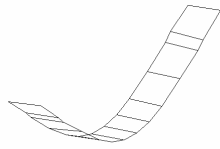
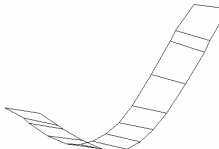
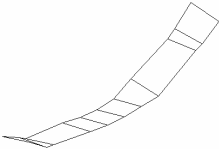

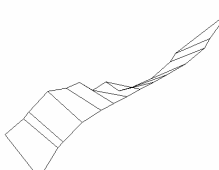

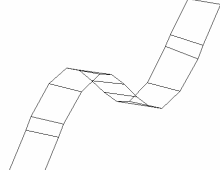
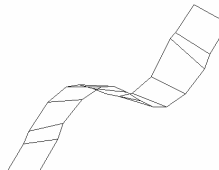
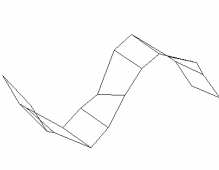
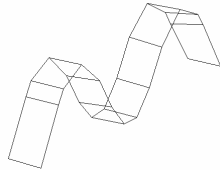
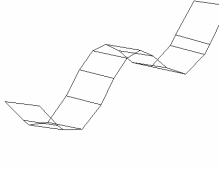
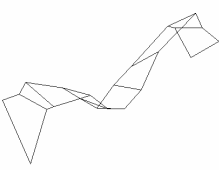
Track Components	Methodologies	Average Parameters	
		Damping (kNs/m)	Stiffness (MN/m)
Rail pad	FFT	5.000	564.983
	MS	5.000	923.367
	FFT+MS	5.000	744.175
Ballast	FFT	97.921	50.276
	MS	77.877	108.885
	FFT+MS	87.899	79.581

### 3.4.6 Full-Scale Modal Testing of In-situ Concrete Sleeper

From the previous investigations, the identification of system dynamics has been presented. There has been a concern regarding the concrete sleeper in flexural vibration modes whether the major resonances of railway tracks (in-phase and out-of-phase) are associated to the natural vibrations of an individual concrete sleeper. As a result, the full-scale modal testing was performed on an in-situ concrete sleeper in the good-condition site. The experimental procedures and arrangements were identical to previous research published elsewhere (Remennikov and Kaewunruen, 2005; 2006). The excitation was given in the frequency band between 0 and 1,600 Hz.

Table 3.13 shows the comparison of vibration characteristics of the identical type of concrete sleepers (AUSTRAK Narrow Gauge Sleeper) in different circumstances: free-free condition (Remennikov and Kaewunruen, 2005), ballast condition (Remennikov and Kaewunruen, 2006), and in-field condition. It is found that the first bending mode of vibration of the in-field concrete sleeper exists close to the in-phase vibration of the present railway track at about 250 Hz. Of interest, the first anti-symmetrical mode of vibration is clearly associated with the out-of-phase mode of vibration of the railway track. It should be noted that the second and third flexural modes of vibration have the significant influence on cracks of concrete sleepers. Nonetheless, the pin-pin vibration of the railway track is unlikely to interact with the vibrations of the in-field concrete sleeper because the first torsional vibration of the in-field concrete sleeper resonates at around 900 Hz whilst the third bending mode corresponds with the natural frequency of 1,225 Hz.

**Table 3.13** Comparison of modal parameters of concrete sleeper with different support conditions

Mode	Free-Free Condition (freq 0-1.6k Hz, 3200 line)		Ballast Condition (freq 0-2k Hz, 3200 lines)		In-field Condition (freq 0-2k Hz, 3200 lines)	
	Frequency (Hz)	Damping (%)	Frequency (Hz)	Damping (%)	Frequency (Hz)	Damping (%)
1						
	223.04 (1 <sup>st</sup> bending)	0.218	244.59 (1 <sup>st</sup> bending)	8.36	251.96 (1 <sup>st</sup> bending)	30.41
2						
	561.49 (1 <sup>st</sup> twisting)	0.224	565.70 (1 <sup>st</sup> twisting)	4.08	897.92 (1 <sup>st</sup> twisting)	6.81
3						
	593.04 (2 <sup>nd</sup> bending)	0.215	603.00 (2 <sup>nd</sup> bending)	2.60	518.73 (2 <sup>nd</sup> bending)	6.48
4						
	1,092.50 (3 <sup>rd</sup> bending)	236.66m	1,100.00 (3 <sup>rd</sup> bending)	1.08	1,225.36 (3 <sup>rd</sup> bending)	6.74

### **3.5 SUMMARY**

#### **3.5.1 Rail Pads**

An alternative, innovative rail pad tester based on the SDOF vibration response measurement for determining the dynamic properties of rail pads subjected to large preloads has been devised. The impact excitation technique has been found to be a simple, reliable, fast and non-destructive test method for assessing the dynamic stiffness and damping constant of all kinds of rail pad types available in Australia. This approach enables testing of new types of rail pads as well as identification of the influences of incremental preloading on their dynamic characteristics. It has been found that the preloads could have significant influence on the natural frequencies and the corresponding dynamic properties of the studded rubber pads. It has also been demonstrated that the damping mechanism of the studded rubber pads is much more susceptible to preloads than the HDPE pads.

Dynamic properties of structural/mechanical components can be used for a number of applications to railway track dynamics such as analysis, modelling and, as presented in References R2, for monitoring the structural degradation rate. The more comprehensive results of condition assessments of rail pads at more different ages, the degradation rates, and the optimum renewal period will be a new challenge for future studies.

#### **3.5.2 Prestressed Concrete Sleepers**

As mentioned, the vibration characteristics and dynamic interaction of concrete sleepers and ballast support system are very important for the development of a realistic dynamic model of railway track capable of predicting its dynamic responses. The results of the experimental modal analysis for prestressed concrete sleepers under different boundary conditions are presented in this chapter. The dynamic effects of sleeper/ballast interaction are illustrated. Four types of prestressed concrete sleepers manufactured in Australia were tested using an impact hammer excitation technique over the frequency range of interest: from 0 to 1600 Hz. It was found that the resonant frequencies and damping ratios associated with the lower mode of vibration of prestressed concrete sleepers were considerably affected by the support boundary conditions. However, the influence of the ballast condition was reduced in the higher frequency range. The dominant effect of the in-situ support was placed on the modal damping in the ballast-



sleeper interaction. In addition, the mode shapes, which can indicate the deteriorated state of concrete sleepers, were affected by the ballast condition. In summary, the in-situ boundary condition had a remarkable influence on the natural frequency, modal damping, and vibration mode shape of prestressed concrete sleepers, especially in the low frequency range. It is recommended that the determined parameters of concrete sleepers be used in modelling of railways tracks where the effect of the boundary condition and dynamic sleeper/ballast interaction will be taken into account.

The results of the dynamic characteristics of prestressed concrete sleepers under wet and dry ballast conditions, improper packing of ballast, rail pad stiffness, voids and pockets of ballast, and other boundary conditions were presented elsewhere as listed in the Reference R2.

### **3.5.3 In situ Railway Track**

Free vibration behaviours of global railway track can be investigated experimentally and computationally using an in-situ ballasted track lying on the laboratory at University of Wollongong. Using modal testing, the experimental modal results can be obtained. For the sake of better understanding, two- and three-dimensional finite element (FE) models of the global track were developed using a FE package, STRAND7. Based on the natural frequency analysis, numerical solutions have been validated against experimental results of the natural frequencies and corresponding mode shapes of railway track. Symmetrical and asymmetrical modes of vibration were discovered, enabling ones to better understand the dynamic behaviours of track in that wheel loading frequencies might deteriorate support and components of railway tracks.

### **3.5.4 Field Trials**

Accelerating degradation of railway track creates many problems for railway track engineers. In order to both maximize safety and minimize costs of track maintenance and renewal, assessment and monitoring of the structural health of railway track and its components must be done. The in-field dynamic testing in combination with track modeling represents an efficient strategy for identification of the current condition of railway track structure and its components.

In the field investigations described in this chapter, the experimental modal testing was employed. Modal results were obtained from the field measurements and used to assess the current state of the railway track. For practical purposes, this chapter integrates field measurements, experimental modal analysis and finite element modelling to evaluate the dynamic parameters of in-situ railway track components. Based on the discrete support model, the railway track is simplified as a two-degree-of-freedom (2DOF) dynamic system. Analytical formulation of the 2DOF model has been developed in order to extract the modal properties of track components from the field dynamic testing results obtained using an instrumented hammer impact technique. A railway track site in Central Queensland managed by Queensland Rail (QR) has been selected to perform the field tests. Six sleeper-fastening-rail assemblies have been randomly selected for dynamic testing. The frequency response functions (FRFs) have been recorded by using Bruel & Kjaer PULSE vibration analyser in a frequency domain between 0 and 1,600 Hz. However, it is found that only from 0 to 600 Hz is sufficient for the optimisations. The data collected in that frequency range have been simulated using least-square curve fitting to determine the dynamic stiffness and damping constants of the tested track components. Based from the analysed results, the correlation of the curve fitting seems to be very good in both methods: FFT and MS. However, FFT tend to better fit the experimental data. The dynamic properties at the track site with good conditions are consistent as can be seen that the stiffness of pad and ballast lies in the narrow ranges: 800-1500 MN/m for rail pads and 150-470 MN/m for ballast. Nonetheless, the damping for rail pads is varied from 1 to 58 kNs/m and for ballast is from 140 to 270 kNs/m.

The advances of this part are the non-destructive testing technique and criteria to evaluate the integrity of track structure. These could supply railway industry for the evaluation on the current state and also for health monitoring of the railway tracks. Three samples that include major defects found in general track problems, e.g. loosening e-Clip and cracked sleeper, are clearly illustrated. These results can supply a track maintenance engineer with very important information on the current state of the railway track and also as the benchmark for health monitoring. In addition, the experimentally determined resonance frequencies along with the dynamic properties of the track components can provide an important input in the dynamic analysis of railway track package for determining the maximum speed and axle load for the future track upgrades or functional changes.

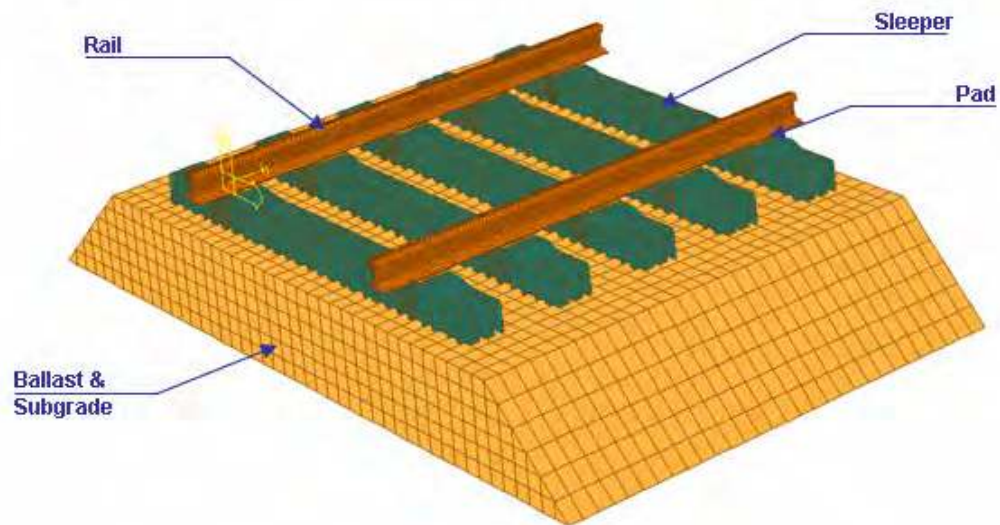
## CHAPTER 4

### REVIEW OF LOADING CONDITIONS ON RAILWAY TRACK STRUCTURES AND THEIR RESPONSES

#### 4.1 BASIC CONCEPTS

Railway tracks are built to transport either passengers or merchandises across areas. The track structures are expected to guide and facilitate the safe, economic, and smooth passages of any rolling stocks. Analysis and design of railway track structures consider static and dynamic loads acting on the track structures because excessive loading may induce damage to the track components such as rail, rail pad, sleeper, fastening system, and foundation. Figure 4.1 portrays a typical configuration of a ballasted railway track. Its components can be subdivided into the two main groups: superstructure and substructure. The rails, rail pads, concrete sleepers, and fastening systems form a group that is referred to as the superstructure. The substructure consists of ballast, sub-ballast and subgrade (formation). Both superstructure and substructure interacts as to efficiently distribute the dynamic wheel loads from the rails onto the ground during the train passages.

It should be noted that rails are longitudinal steel members placed on the equally spaced sleepers. The rails are the critical component in guiding the rolling stocks. Their strength and stiffness must be sufficiently designed in order to maintain a steady shape and the smooth track configuration, and to resist various dynamic forces exerted by the wheel and rail interactions of travelling rolling stocks. A main function of the rails is to accommodate and transfer the wheel/axle loads on track to the supporting sleepers. Its additional functions in modern rail track include that the rail, which conducts signal currents, also serves as an electrical conductor on an electrified line.



**Figure 4.1** A typical railway track configuration

The primary components of the fastening systems are the mechanical fasteners and the rail pads. The fasteners withstand the vertical, lateral and longitudinal forces and overturning moments of the track in addition to keeping the rails in position on sleepers. They also transfer forces, caused by wheels, thermal change, and natural hazard, from rails to the adjacent sleepers. Rail pads, which are placed on the rail seat, are very essential to filter and transfer the dynamic forces from the rails and fastenings to the sleepers. The high damping coefficient of the rail pads considerably reduces the excessive high-frequency force components. Also, the pads provide resiliency to rail-sleeper interaction, resulting in the alleviation of rail seat cracking and contact attrition.

Sleepers are cross-tie beams resting on ballast and support. From the past, the wooden sleepers had been employed as the timber could be easily sought from the local area. At present, due to the higher durability and longer service life span of concrete and steel materials, the prestressed concrete sleepers and to a limited extent steel sleepers have been used in modern track constructions. The sleeper duties are to: (1) uniformly transfer and distribute loads from the rail foot to underlying ballast bed; (2) sustain and retain the rails at the proper gauge by keeping anchorage for the rail fastening system; (3) preserve rail inclination; and (4) provide support for rail by restraining longitudinal, lateral and vertical rail movements.

Ballast is a free-draining coarse aggregate layer that is used as tensionless elastic support for resting sleepers. This layer is typically composed of crushed stones, gravel and crushed gravel such as granite and basalt depending on the local availability. It is provided to not only give support, but also transfer loads from the track to sub-ballast and drainage water away from the rails and sleepers. Sub-ballast, which is sometimes called the capping layer, is the layer of a granular material between ballast and the underlying subgrade. Usually found in general, broadly graded slag or crushed aggregate is the major composition of the sub-ballast, although broadly graded sand-gravel compound is also employed sometimes. Subgrade is also referred to as the formation. It includes the existing soil and rock, which possess slopes, verges, ditches and other structures or materials within. The subgrade is the last support to bear and distribute the dynamic loading resultant downward along its infinite depth. This deep layer must have sufficient bearing capacity, provide good drainage and yield the tolerable smooth settlement to prolong the track serviceability. Recently, new high-performance materials such as geotextiles and geofabrics have been applied for upgrading the capacity of subgrade (Indraratna and Salim, 2005).

Typically, the design of a railway system is divided into the design of trains or rollingstock and the design of the supporting track structure. The most common design procedures for the Australian railway tracks have been presented in Jeffs and Tew (1991). A design flow chart based on the permissible stress concept for conventional ballasted track structures is used by the track design engineers for undertaking a design of new railway track. The design flow chart is illustrated in Figure 4.2 (Jeffs and Tew, 1991). This permissible stress approach makes use of an empirical function taking into account the static wheel load ( $P_0$ ) with a dynamic impact factor ( $\phi$ ) to account for the dynamic vehicle/track interactions.

$$P_D = \phi P_0 \quad (4.1)$$

where  $P_D$  is the design wheel load,  $P_0$  is static wheel load, and  $\phi$  is the dynamic impact factor ( $>1.0$ ). Significant research attention has been devoted to vertical static and dynamic forces as they are the main source of railway track problems when trains are operated at different speeds and static axle loads. When vehicle and track are free from abnormalities, a moving vehicle exert certain low-frequency forces (below 20 Hz)

known as ‘*quasi-static*’ or ‘*dynamic ride*’ forces (Steffens, 2005). Over time, significant abnormalities arise in either the track structure or the vehicle. They induce much higher-frequency and much higher-magnitude forces than quasi-static loads. These forces are referred to as ‘*dynamic wheel/rail*’ or ‘*impact*’ forces.

In general, dynamic effects seem to govern the design of track structures and their components. Resonance frequencies of track structures are often obtained by means of modal testing (Ewins, 1995). There are three major track resonances usually obtained from the field trials: in-phase (50-200 Hz), out-of-phase (200-600 Hz), and pin-pin (800-1,200 Hz) vibrations, as illustrated in Figure 4.3 (Kaewunruen and Remennikov, 2005a, b). In-phase vibration occurs when rails and sleepers (as a mass) in the track structures vibrate on the ballast formation (as a spring). The out-of-phase vibration describes the bounce of rails on the rail pads. In this case, the pad act as a spring inserted between two masses: the rail and sleeper. The pin-pin resonance is induced by the bending wave of the rail when its wavelength is twice the sleeper spacing. Based on the Euler-Bernoulli beam theory, the pin-pin resonance frequency  $f$  (Hz) can be roughly estimated from the lowest bending frequency of a simple beam of length  $L$ , as shown in Dahlberg (2003):

$$f = \frac{\pi}{2} \sqrt{\frac{EI}{mL^4}} \quad (4.2)$$

where  $EI$  is the bending stiffness of the rail,  $m$  is the mass of the rail per unit length, and  $L$  is the sleeper spacing.

Not only do sources of loading on tracks derive from axle carriages, but on top of those, abnormalities of track geometry, track settlement, train speeds, wheel/rail irregularities, or rail joints also play a vital role in imparting excessive dynamic impacts to the track structures. The large amount of excitations may cause oscillations, vibrations, noise, damage, and deterioration to tracks and their environments. The typical characteristics of the impact loadings on track structures due to the wheel/rail interaction have not been thoroughly reported, although each particular wheel/rail interaction has been studied over the past decade. This chapter presents a variety of typical dynamic impact loadings imparted by wheel/rail interaction and irregularities. The summary of typical impact loadings due to train and track vertical interaction is

presented herein with particular reference to the shapes of the typical waveforms of impact loads generally found in railway track structures.

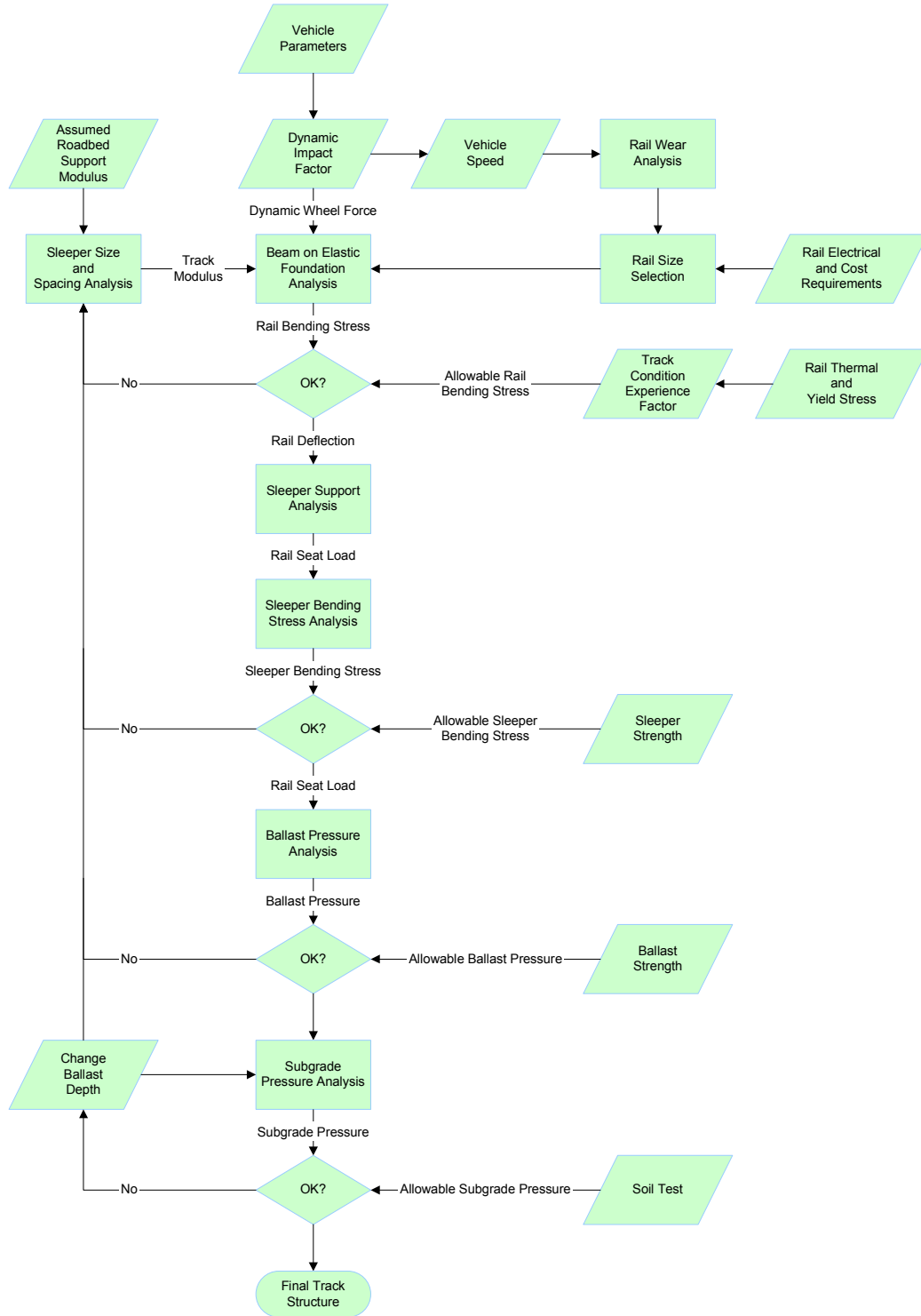
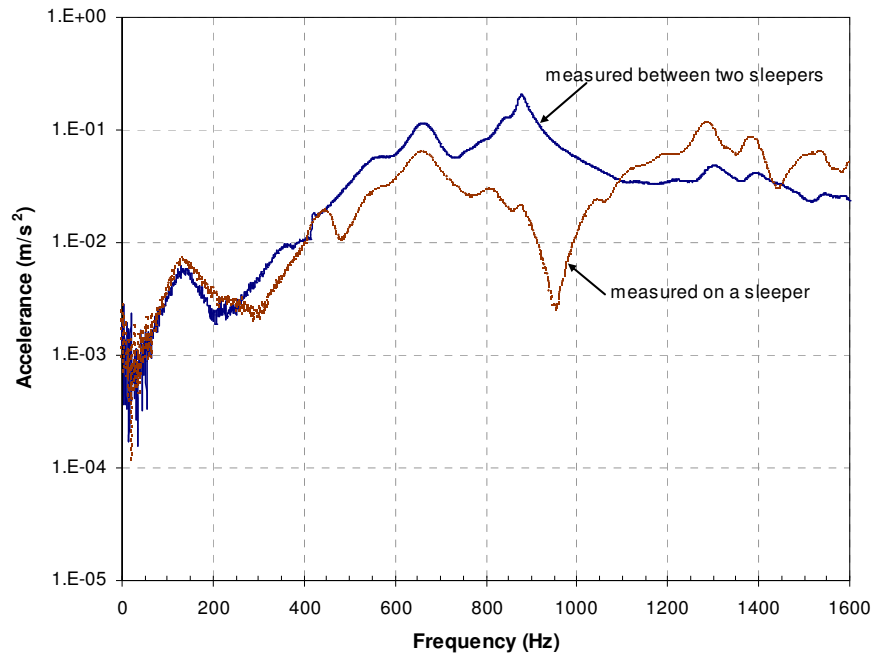


Figure 4.2 Railway track design procedure (Jeffs and Tew, 1991)

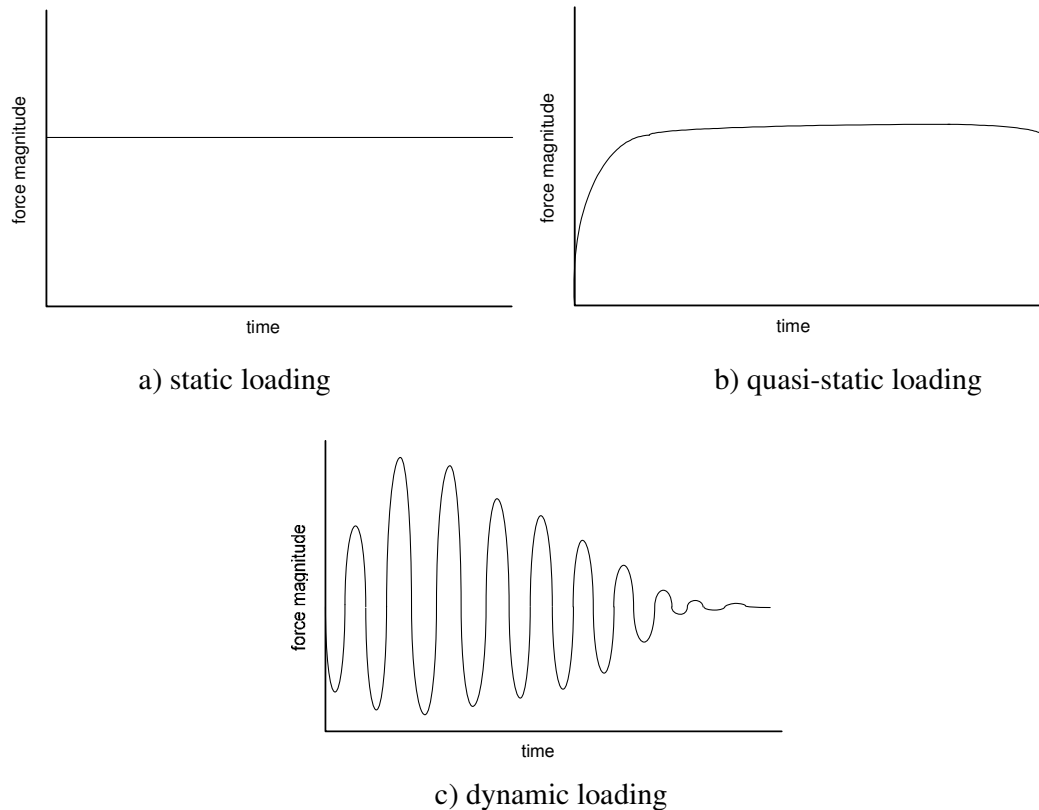


**Figure 4.3** Accelerance responses at a site obtained from field trials (Kaewunruen and Remennikov, 2005b)

## 4.2 STATIC AND QUASI-STATIC (DYNAMIC RIDE) LOADING

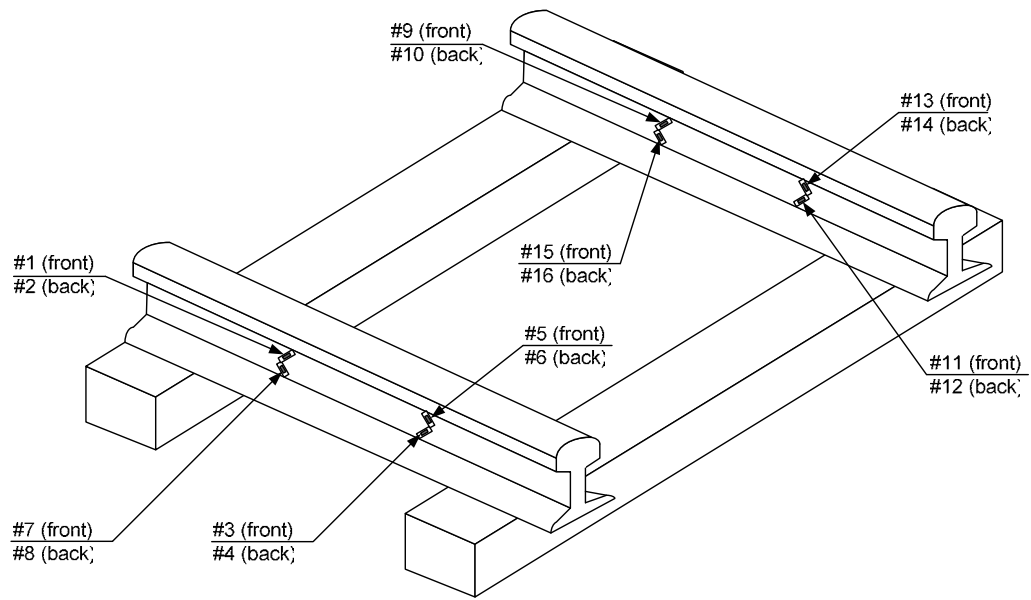
The static loading represents the mean weight of rail freight wagons, unchanged during reasonably long period of time. The wheel/rail contact force would be identical to static wheel load when the ideal conditions of perfect wheel tread and rail surface are found. Usually adopted in design procedure, quasi-static loading slightly changes its magnitude over a long period of time. It is the sum of the static load and the effect of vehicle speed, together with track support and geometry (curvature, superelevation, and roughness). In contrast, the dynamic loading is time dependent. Its magnitude changes rapidly within the short period of time, which is dependent on the type of abnormalities. Figure 4.4 depicts the typical time histories of static, quasi-static, and dynamic loads.



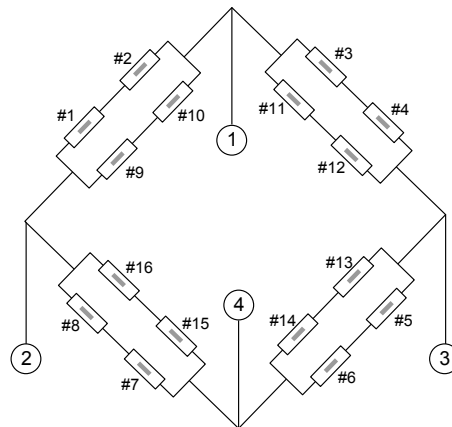


**Figure 4.4** Static, quasi-static, and dynamic loading time histories

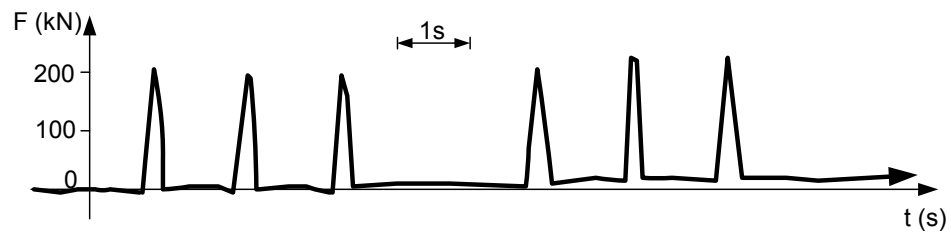
Fryba (1996) described the traffic loads on railway bridges. The traffic loads measured seem to be the quasi-static loading. The axle or wheel loads were suggested to be measured in one of three following manners. First, using the weightbridge weighs the static vertical forces. Second, the strain on wheel discs, on axles, or on bearing housings could be measured to obtain the time history of the wheel forces. In this way, the forces obtained represent only the specific vehicle. The third procedure deals with the strain measurement on rails. In this case, the dynamic axle or wheel forces at the time of train passages can be recorded instantaneously for any rolling stocks over the installation site. The last technique is advantageous for the case of measuring the mean typical operation loads at the certain location. Figure 4.5 shows the schematic diagrams of the axle force measurement on rails. The similar measurements were performed on the track test bed in the Highbay Laboratory at University of Wollongong (Sadeghi, 1997), as shown in Figure 4.6.



a) strain gauge installation



b) full bridge connection



c) dynamic shear forces

**Figure 4.5** Schematic diagrams of vertical axle force measurements on rails (Fryba, 1996).



**Figure 4.6** Track test bed at the University of Wollongong.

The statistical data of train operations measured on heavy haul railway bridges in Czech Republic are summarized in Tables 4.1 and 4.2. The measurements were performed over 24-hour period so that the annual data could be derived using extrapolation. From extensive experiments, Fryba (1996) found the following important issues regarding the vertical axle forces:

- Instantaneous dynamic axle load relies on dynamic interaction of rail and vehicle;
- From the statistical analysis of traffic on the railway line, there are three major loading ranges. The first range under fully loaded freight cars and locomotives is about 180-200 kN. The second range presenting the passenger cars and partially loaded freight cars is about 100 kN, while the third one under empty freight cars is about 50 kN; and,
- The loading data recorded from traffic in each operation were in relatively good agreement with the sum of the measured axle forces.

**Table 4.1** Train records on a very heavily trafficked CSD bridge

Services	Number of trains	Number of axles	Measured weight of trains		From traffic statistics (kN)
			Off bridge (kN)	On bridge (kN)	
Passenger	57	2,272	259,770	282,510	301,330
Freight	95	11,306	1,643,640	1,736,700	1,631,870
Work	10	55	10,905	11,265	10,515
Calibration	18	100	18,270	19,170	17,310
Total	180	13,733	1,932,585	2,049,645	1,961,025

(adopted from [8])

**Table 4.2** Statistical records of axle forces on a very heavily trafficked CSD bridge

Services	Records	Axle load	
		Off bridge (kN)	On bridge (kN)
Passenger	Maximum axle force	255.00	255.00
	Mean axle force	114.30	124.30
	Standard deviation of maximum force	35.97	36.49
	Standard deviation of average force	0.755	0.766
Freight	Maximum axle force	255.00	285.00
	Mean axle force	145.40	153.60
	Standard deviation of maximum force	49.27	53.20
	Standard deviation of average force	0.463	0.500
Work	Maximum axle force	225.00	255.00
	Mean axle force	198.30	204.80
	Standard deviation of maximum force	36.80	41.66
	Standard deviation of average force	5.00	5.62
Calibration	Maximum axle force	195.00	225.00
	Mean axle force	182.70	191.70
	Standard deviation of maximum force	19.10	14.07
	Standard deviation of average force	1.91	1.41
Overall	Maximum axle force	225.00	285.00
	Mean axle force	140.70	149.30
	Standard deviation of maximum force	48.78	51.99
	Standard deviation of average force	0.416	0.444

(adopted from [8])

In general track design, three important pieces of information are required to be specified; they are the static axle loads, the sum of axle loads (tonnage borne), and the running speeds of train. The nominal axle forces used in static track design in the EU, USA, and Australia are displayed in Table 4.3 (Esveld, 2001).

In UK, the permissible vertical static forces for railway vehicles can be calculated depending on the type of vehicles (Rail Safety and Standards Board, 1993; 1995). It is required that the vehicles be designed so that the combined effect of static wheel loading, wheel diameter and wheel tread profile does not compromise safety by causing excessive stresses and deformation in the contact zones between wheel treads and rail heads under all normal track conditions. Unless the appropriate technical justification

regarding the safe wheel-to-rail contact stress is provided, the static wheel load (for generic UK P5 Profile) shall not exceed the lower values of the following two values:

$$Q = 0.130D \text{ or } Q = 125 \text{ kN} \quad (4.3)$$

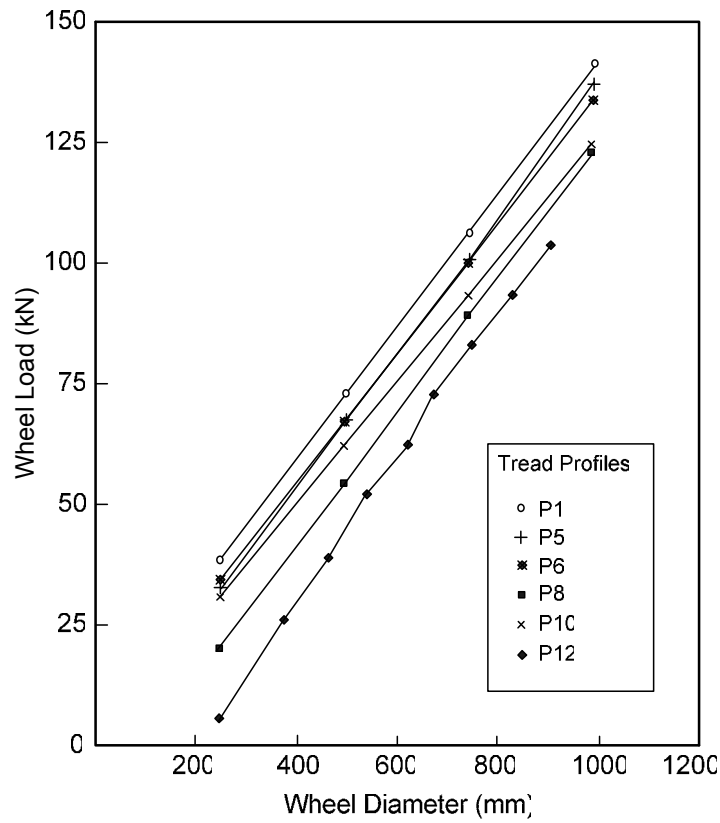
where  $Q$  = maximum static wheel load (kN);  $D$  = wheel tread diameter (mm). It is found that the wheel treads have linear relationships with static wheel load as shown in Figure 4.7. The values in the graph are based on the constant contact stress level at  $1,260 \text{ MN/m}^2$ .

**Table 4.3** Static axle loading of various types of rolling stocks

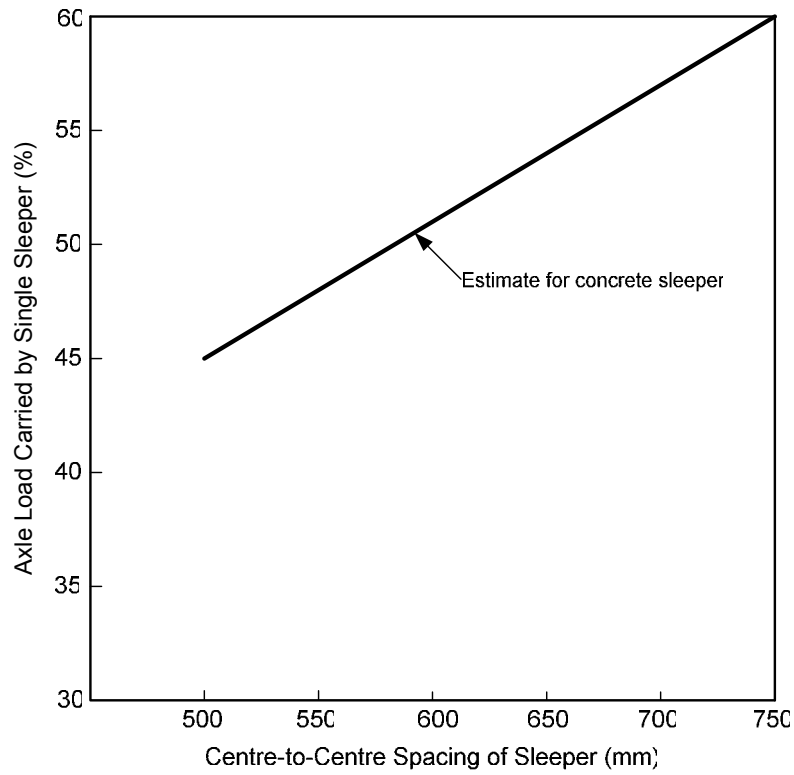
Train types	Number of axles	Axle loads under services:	
		Empty (kN)	Fully loaded (kN)
Trams	4	50	70
Light-rail	4	80	100
Passenger coach	4	100	120
Passenger motor coach	4	150	170
Locomotives	4 or 6	215	n/a
Freight wagon	2	120	225
Heavy haul (USA, Australia)	2	120	250-350

(adopted from Esveld, 2001)

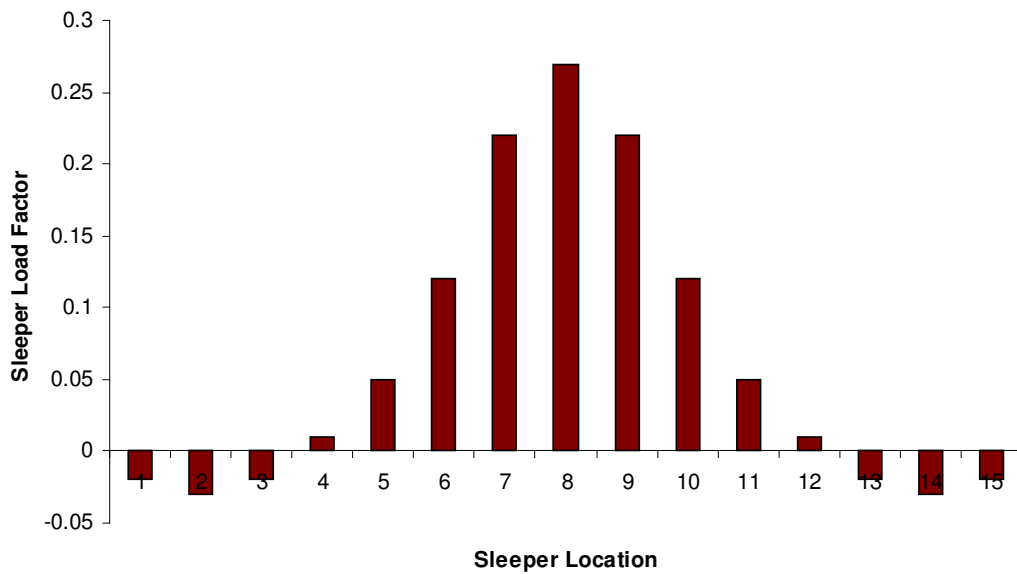
Australia Standard (AS1085.14) (Standards Australia, 2003) defines the vertical design loads intended for prestressed concrete sleeper design. The quasi-static loads are determined from the static loads and the effects of train speed. The typical values of such quasi-static loads are around 1.4 to 1.6 times the static wheel load excluding unbalanced super-elevation effects. In addition, the dynamic loading due to high frequency effects of wheel/rail interaction is required greater than 1.5 times of the static wheel load. Hence, the design load is the combination of both quasi-static and dynamic loads. It shall be not less than 2.5 times the static wheel load. At the point of wheel/rail contact over a sleeper, the force will be distributed to the adjacent sleepers in structural track system due to the rail stiffness, which is considered by introducing the load distribution factor. The estimation of the axle load distribution factor for a sleeper under the wheel in the track systems varying the sleeper spacing is given in Figure 4.8a (Standards Australia, 2003) while the load distribution factor for a group of sleepers is presented in Figure 4.8b (Murray and Cai, 1996).



**Figure 4.7** Relationship between wheel load, wheel diameter, and tread profile for a limiting mean peak contact stress of  $1,260 \text{ MN/m}^2$  (Rail Safety and Standards Board, 1993; 1995)



a) for the sleeper under the wheel with different sleeper spacing (Standards Australia, 2003)



b) for a group of sleeper (Murray and Cai, 1996)

**Figure 4.8** Axle load distribution factor

The quasi-static loads usually arise from the gross tare, centrifugal force, centering force in curves and switches, and cross winds. The dynamic loads are frequently caused by the track irregularities, irregular track stiffness due to variable properties and settlement of ballast bed and formation, corrugations (irregular rail surface), discontinuities at welds, joints, and switches, vehicle deflections such as wheel burns, wheel flats, hunting, or resonance vibrations, and so on (Esveld, 2001). Moreover, environment temperatures may cause instability to the railway tracks. The vertical wheel load in design procedure is reckoned from the combination of static wheel load (half the static axle load on straight track), incremental load from curved track, cross wind, and dynamic wheel loads. The wheel running with speed  $v$  (m/s) over a sinusoidal rail irregularity of wavelength  $\lambda$  (m) will induce an excitation frequency  $f$  (Hz), predicted by

$$f = \frac{v}{\lambda} \quad (4.4)$$

In short wavelength irregularities, e.g. corrugation, irregular track stiffness, wheel out-of-roundness, the wavelength may vary from 0.030 to 0.30 m; while long wavelength irregularities, e.g. track settlement, sleeper spacing, track geometric irregularities, or sometimes wheel out-of-roundness, will introduce longer wavelength. The forcing frequencies of the dynamic loading vary from 0 to 2000 Hz; for example, 0-20 Hz for sprung mass; 20-125 Hz for unsprung mass; or about 0-2000 Hz for defects such as corrugations, welds, switch, or wheel flats (Clark et al., 1982; Grassie et al., 1982; Grassie and Cox, 1984; Alias, 1986; Sato et al., 1988; Knothe and Grassie, 1993; Grassie and Kalousek, 1994; Grassie, 1996; Andersson and Dahlberg, 1999; Nielsen and Johansson, 2000; Fryba, 1996; Esveld, 2001). These frequencies may induce the resonance vibrations of railway tracks, resulting in the degradation of railway track components (Remennikov and Kaewunruen, 2005a; 2005b; 2006a; 2006b; Kaewunruen and Remennikov, 2005c; 2006; Remennikov et al., 2006). The cases of very-short-duration dynamic loading due to wheel/rail irregularities are referred to as transient dynamic loading. More details of such cases will be given in the following section.



### 4.3 IMPACT LOADING ON RAILWAY TRACKS


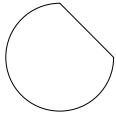




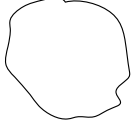

The transient dynamic loading is the dynamic loading occurring over a very short period of time. The causes of transient loading are usually from collisions, sudden loading, blast, shock, etc. Particularly in modern railway tracks, the transient loading is usually caused by the abnormalities in wheel/rail interaction. The magnitude of the forces is very high within the very short impulse duration, for instance, 2 to 10 milliseconds (msec) (Lee et al., 2005). Such loading is hereafter referred to as impact loads. The effects of impact forces are very significant in the design and utilization of concrete sleepers as parts of the railway track structures (Kumaran et al., 2002). Table 4.4 depicts the typical shape and approximate formulas for each corresponding shape of various irregularities (Steffen, 2005).

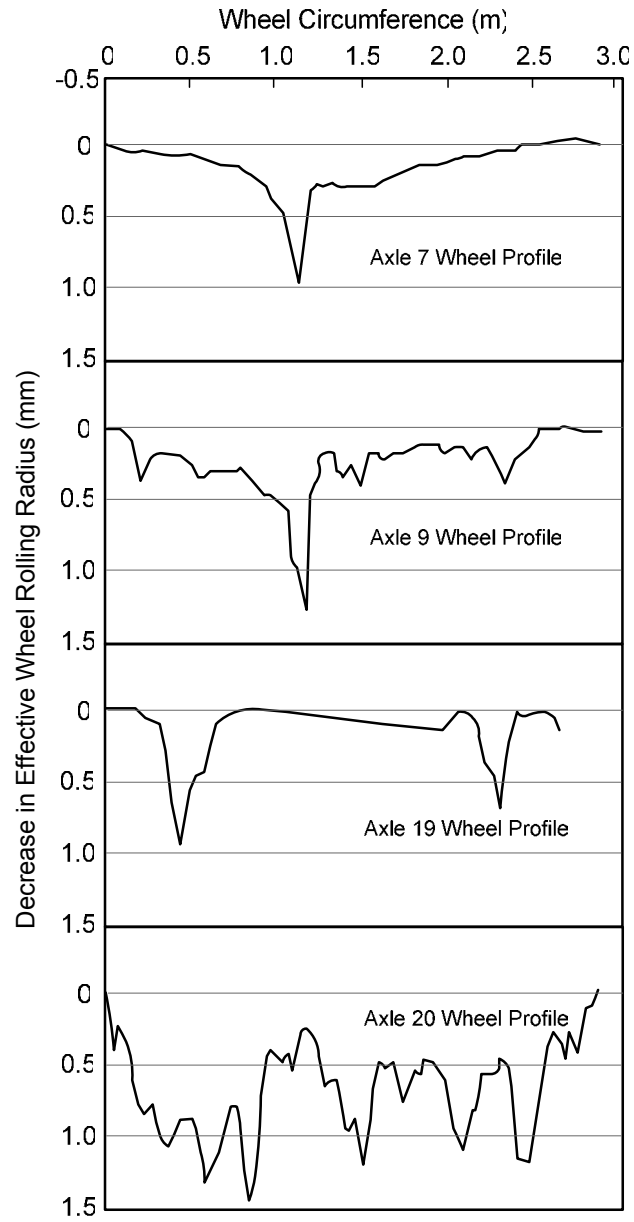
#### 4.3.1 Impact loads due to worn wheel/rail surface profiles

In 1985 Ahlbeck and Hadden (1985) measured impact loads on tracks and developed a computer model to predict the impact loads from worn railroad wheel and rail surface profiles. The experiments were done in northeast corridor networks operated by Amtrak in the United States. A wide range of train speeds that affects the wheel/rail contact forces was investigated. The computer model was developed based on energy approach using seven degrees of freedom idealization. However, only half the track was considered in the model. Figure 4.9 shows the examples of worn wheel profiles used in experiments. The tests were performed using anomaly wheels: No #7 and #19 (see Figure 4.9). The impact loads from the tests are presented in Figures 4.10a and 4.10b, respectively. It was found that the magnitudes of worn wheel profiles are about 214 kN to 312 kN, depending on the roughness of surface profiles, whereas the durations of the impulses are about 2 to 5 msec, respectively.

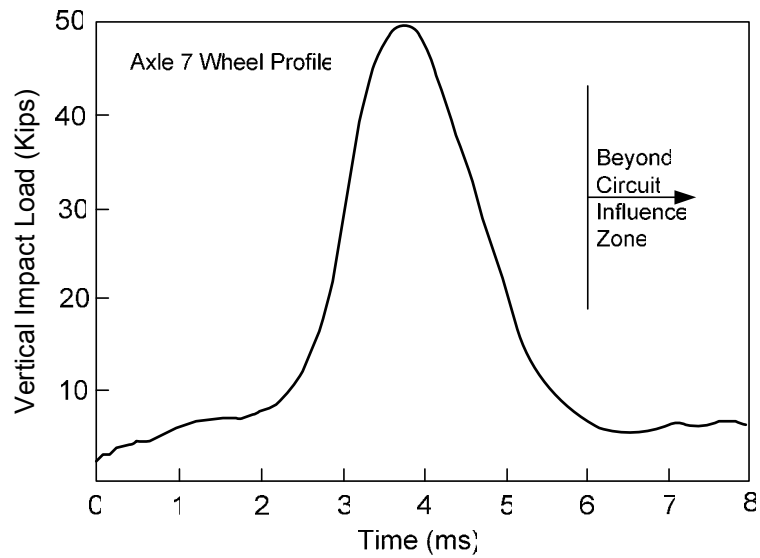
The experiments were extended to worn rail surfaces due to engine burns. Figure 4.11 shows the running surface profile at engine burn. The measurements of impact loads due to such defects were obtained as displayed in Figure 4.12. At low speeds, the magnitudes of impact forces are relatively lower when compared with the counterparts at the higher speeds, for instance, varying from 100 kN-force for speed 32 km/h to 133 kN for 177 km/h. It should be noted that the duration of forces can considerably change because of the train speeds: from 40 to 5 msec for increasing speeds from 32 to 177 km/h.

**Table 4.4** Types and shapes of abnormalities (Steffen, 2005)

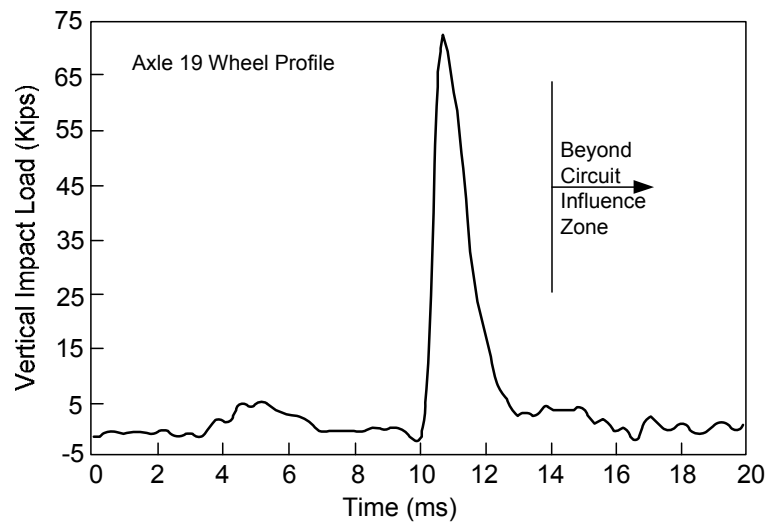
Irregularity	Equation	Shape
No irregularity	nil	
Wheel flat	$f(x) = \frac{d}{2} \left( 1 - \cos \frac{2\pi x}{L} \right)$	
Sinusoidal corrugation	$f(x) = \frac{d}{2} \left( \sin \frac{2\pi x}{L} \right)$	
Dipped joint	$f(x) = \frac{d}{2} \left( 1 \pm \cos \frac{\pi x}{L} \right)$	
Hollow weld	$f(x) = \frac{d}{2} \left( 1 - \cos \frac{2\pi x}{L} \right)$	
Humped weld	$f(x) = -\frac{d}{2} \left( 1 - \cos \frac{2\pi x}{L} \right)$	
Arbitrary wheel surface profile	x and y coordinates must be defined	
Arbitrary rail surface profile	x and y coordinates must be defined	
Note that	$f(x)$ = shape function of the irregularity $x$ = current coordinate on the rail $d$ = depth of the irregularity $L$ = total length of the irregularity	



**Figure 4.9** Example of wheel profiles used in the experiments (Ahlbeck and Hadden, 1985)

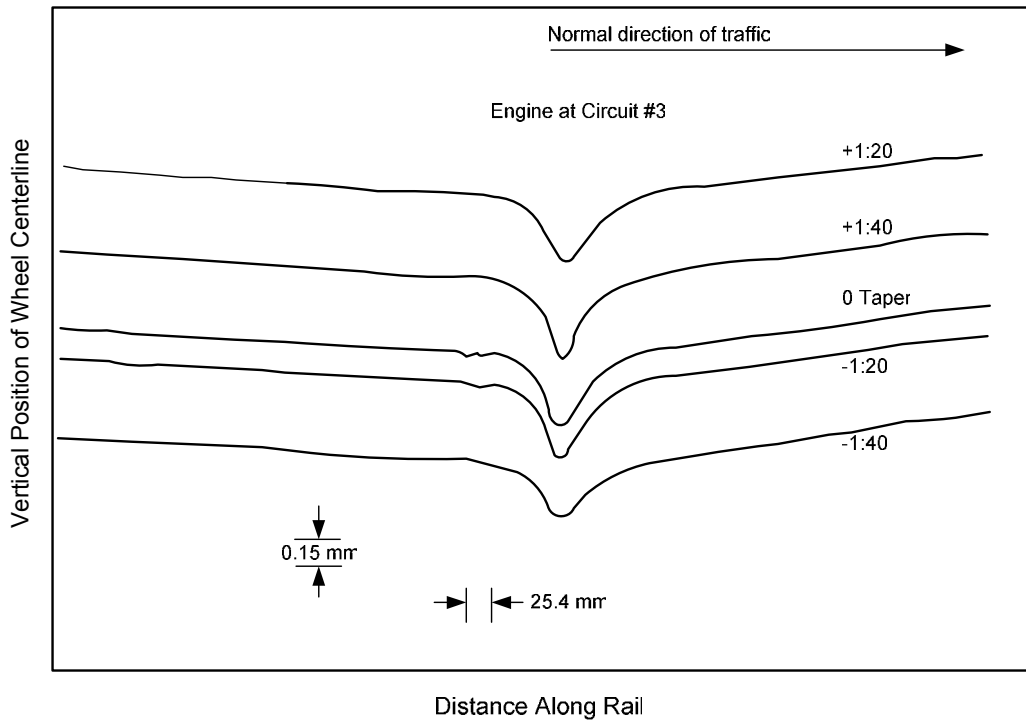


a) loads from wheel profile #7

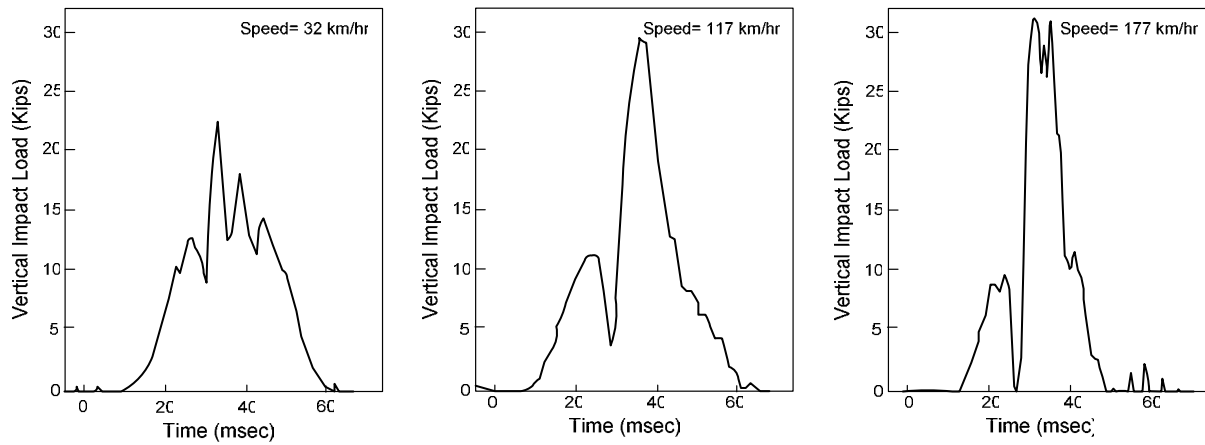


b) loads from wheel profile #19

**Figure 4.10** Impact loads measured from the worn wheel profiles (Ahlbeck and Hadden, 1985)



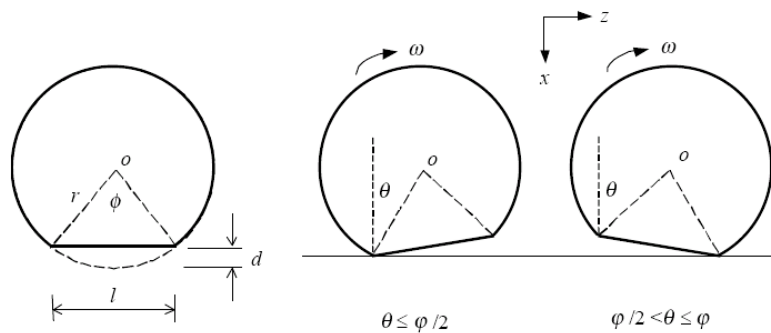
**Figure 4.11** Rail running surface profile measured at engine burn (Ahlbeck and Hadden, 1985)



**Figure 4.12** Impact loads due to burned rail running surface profile (Ahlbeck and Hadden, 1985)

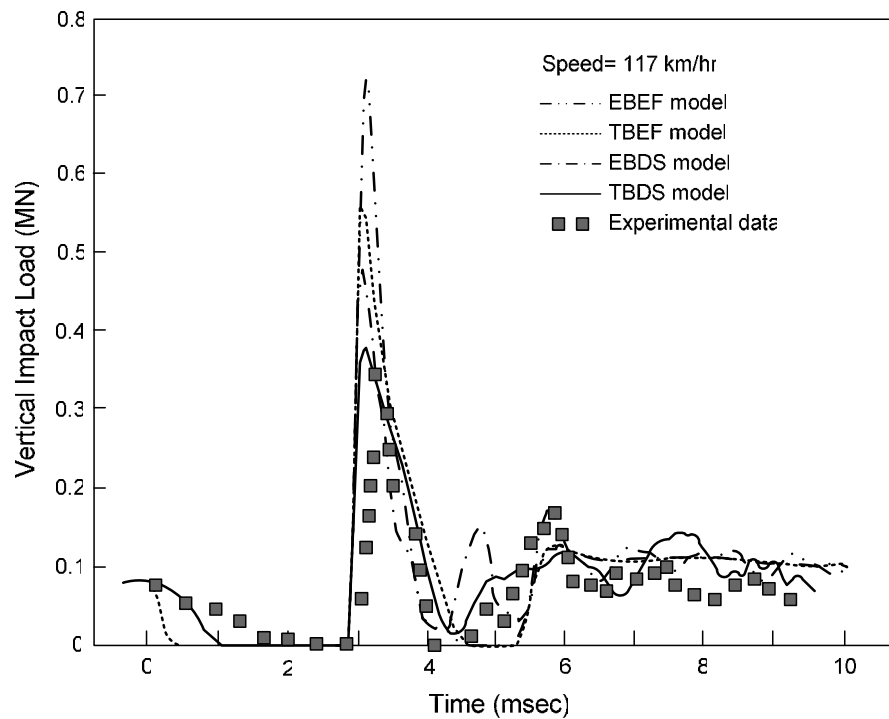
### 4.3.2 Impact loads due to wheel flats and shells

In general, the greatest and most common dynamic loads on tracks caused by vehicle/track interaction arise from the wheel irregularities, especially wheel flats and shells. The abnormally high impact loading on track due to wheel flats and wheel shells depends on the size and shape of defect, axle load, and train speed. Usually, wheel flats are generated by braking when the vehicle wheels become locked and slide along the track. In contrast, the wheel shells are mainly caused by micro-cracks initiated by high strains in wheel/rail contact region due to high axle load and creep forces. Dukkupati and Dong (1999) reported that despite the different appearances between wheel flats and wheel shells, the irregularity functions measured are similar and the basic characteristics of the resulting impact forces should be analogous. Based on the multiple measurements of the forcing signals from the wheel-flat and wheel-shell test wagons, a number of analytical models were developed to simulate the impact forces from such defects as wheel flats and shells (Newton and Clark, 1979; Knothe and Grassie, 1993; Dukkupati and Dong, 1999; Wakui and Okuda, 1999; Esveld, 2001; Wu and Thompson, 2001). Figure 4.13 shows the typical idealized wheel flats.

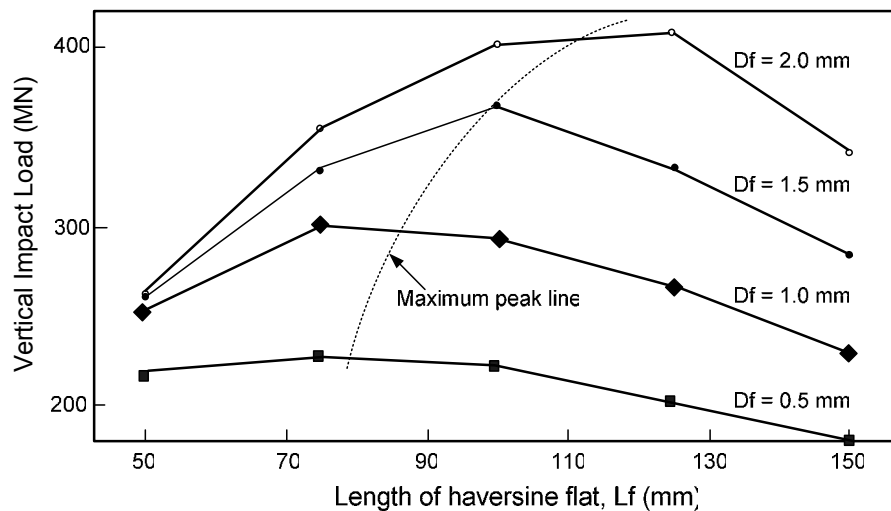


**Figure 4.13** Typical idealized profile of wheel flats (Wu and Thompson, 2001)

In the experiments done by British Rail (Dukkupati and Dong, 1999), it was found that there are two obvious impact peaks, and the first peak (so-called  $P_1$ ) is sensitive to the track equivalent mass, while the second peak (so-called  $P_2$ ) is somewhat unclear and is related to track stiffness. If a train is running at 117 km/h, the main frequency associated with the first peak is around 1,000 Hz, and it lasts only about 1 msec, as depicted in Figure 4.14. Figure 4.15 shows the effect of the flat size on the magnitude of impact forces.



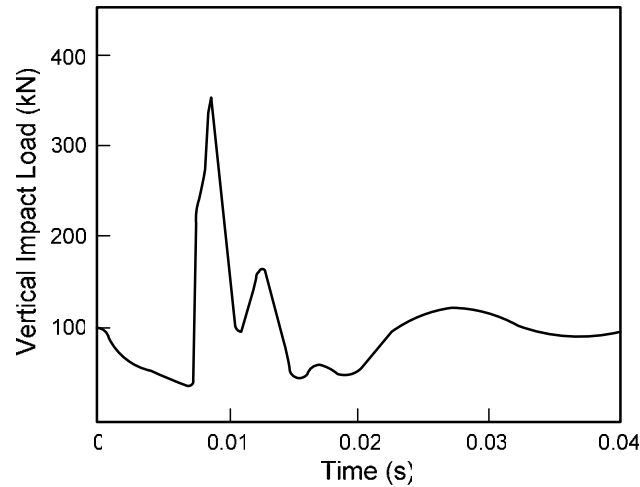
**Figure 4.14** Impact signal from wheel flat (Dukkipati and Dong, 1999)



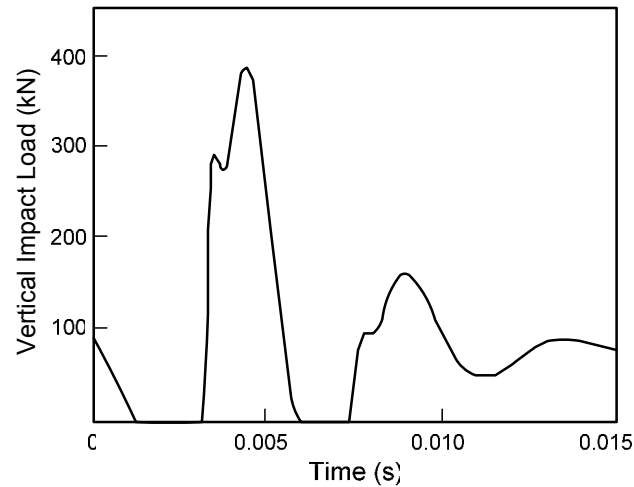
**Figure 4.15** Effect of wheel flat size on impact loads:  $L_f$  and  $D_f$  are the length and depth of flat, respectively (Dukkipati and Dong, 1999)

Effect of speeds on the impact forces from wheel flats has been studied analytically by Wu and Thompson (2001). Figure 4.16 shows the sample results of contact forces from wheel flat, simulated using vehicle weight of 100 kN, wheel radius 0.46 m, wheel mass 600 kg, and Hertzian constant  $93.7 \text{ GN/m}^{3/2}$ . It was found that at

higher speed the magnitude of impact force is greater (increasing from about 350 to nearly 400 kN), whilst the duration of the force is also shorter (decreasing from 3.5 to 2.5 ms).



a) at train speed 30 km/hr



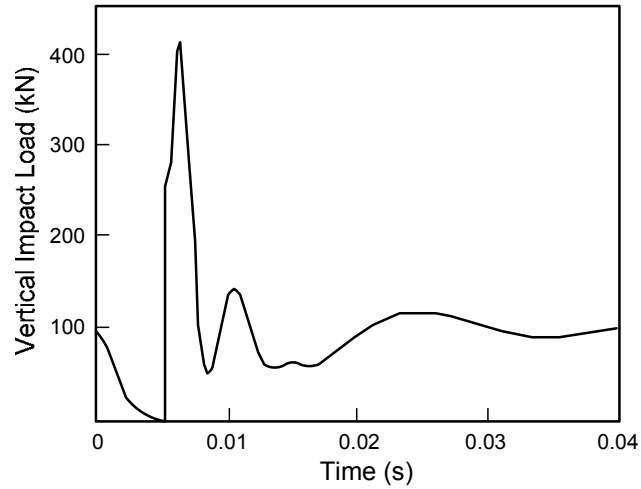
b) at train speed 80 km/hr

**Figure 4.16** Impact forces due to 2 mm rounded wheel flat (Wu and Thompson, 2001)

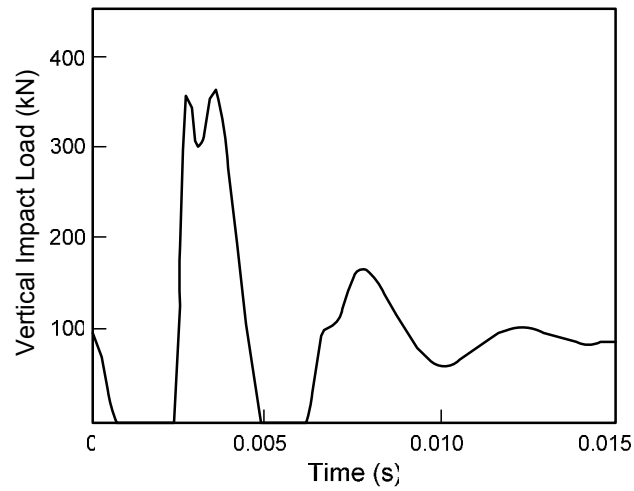
In case of a newly formed wheel flat with depth of about 2 mm and length 86 mm, the effect of train speed on the impact force is different as shown in Figure 4.17. It could be seen that at lower train speed the magnitude of impact force is higher than that at higher speed. Figure 4.18 summarizes the effect of train speed on different types of wheel flats (Wu and Thompson, 2001). Esveld (2001) presented the effect of sleeper



types on the magnitude of impulse load as illustrated in Figure 4.19. It was found that the concrete sleepers would interact with the rail and wheel causing higher impact forces than the timber ones.

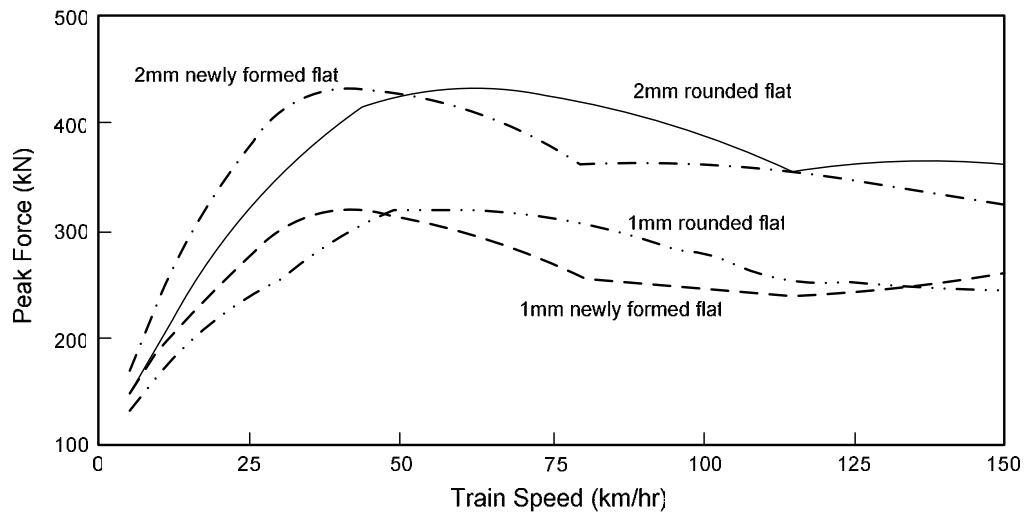


a) at train speed 30 km/hr

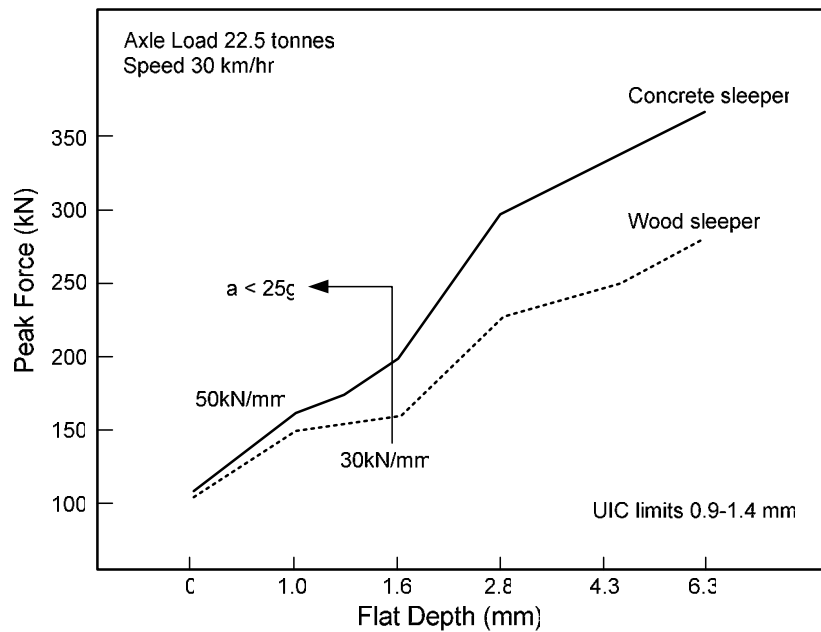


b) at train speed 80 km/hr

**Figure 4.17** Impact forces due to 2 mm newly formed wheel flat (Wu and Thompson, 2001)



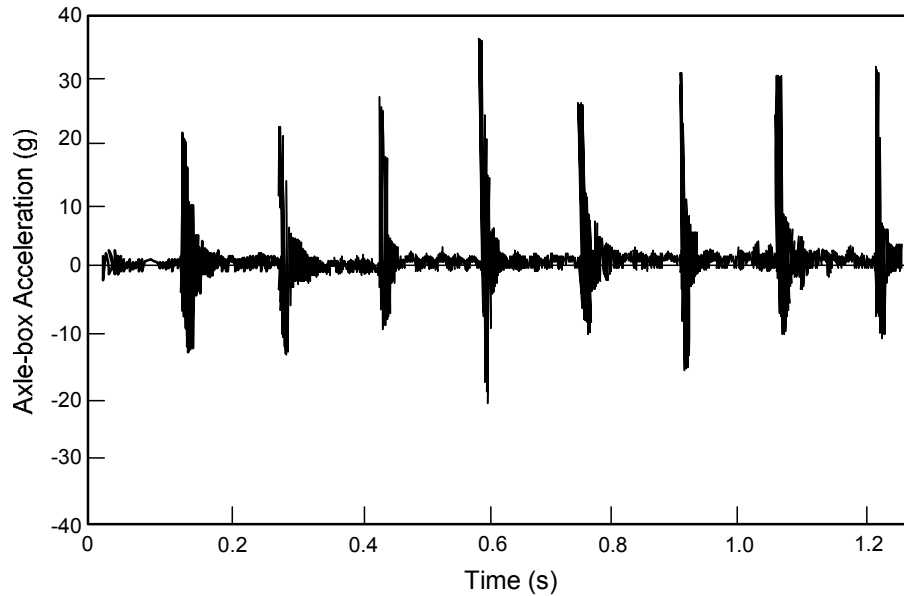
**Figure 4.18** Impact forces due to wheel flats varying with speeds (Wu and Thompson, 2001)



**Figure 4.19** Effect of sleeper types on impact forces due to wheel flat (Esveld, 2001)

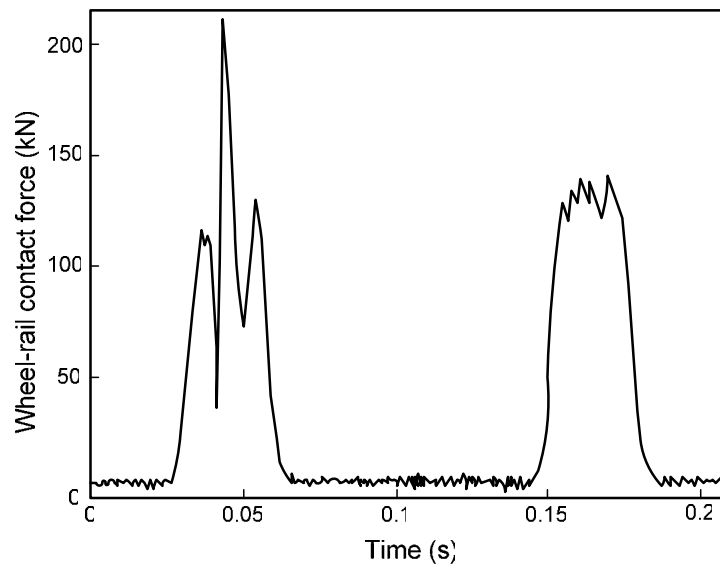
Wakui and Okuda (1999) studied the effect of extreme wheel flat. A wheel flat spot, 75 mm long and 3 mm deep, was artificially made on a wheel of a test wagon. Typical records by installing accelerometers on a wheel axle box are presented in Figure 4.20. It was found that the maximum axle box acceleration due to the wheel flat was 51g. The peaks over 30g are usually with the duration range from 1 to 6 msec. The pulse duration tends to decrease with higher speeds, e.g. 5-6 msec at 10 km/h, 2-3 msec

at 60 km/h, and 1 msec at 85 km/h. The impact forces can be obtained by multiplying the acceleration with unsprung effective wheel mass (in ref: Wu and Thompson (2001): the unsprung mass is 800 kg, the peak force is about 408 kN).

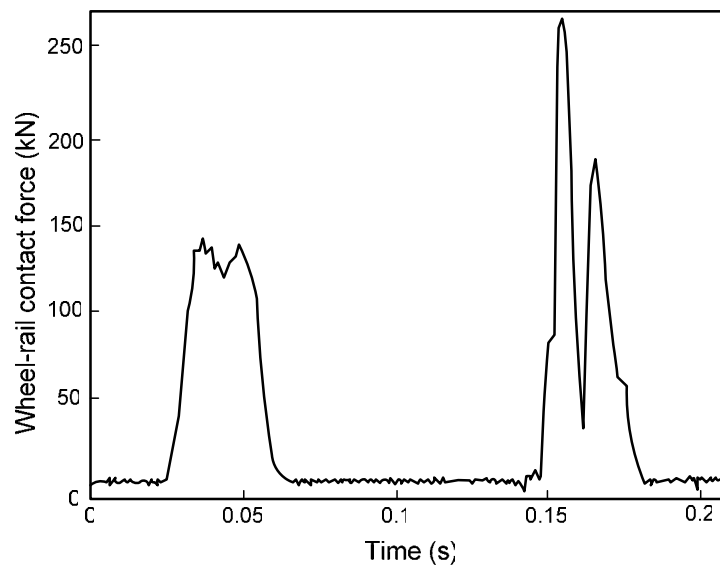


**Figure 4.20** Axle-box acceleration waveform due to wheel flat (Wakui and Okuda, 1999)

In addition, the effect of out-of-round wheels on wheel/rail impact forces has been found significant. The effect of rail pad stiffness on impact forces demonstrated that the higher the stiffness the larger the impact (Johansson and Nielsen, 2003; Fermer and Nielsen, 1994; Nielsen and Igeland, 1995; Wu and Thompson, 2004). Johansson and Nielsen (2003) developed numerical simulations to predict the vertical wheel/rail impact loading due to the out-of-round wheels. Field measurements were also performed at a site on Svealandsbanan, Sweden, since the Swedish standard allows the measured wheel/rail impact force not greater than 290 kN (independent of the axle load). If so, the wheel shall be repaired or replaced. Figure 4.21 shows time history of wheel/rail impact forces measured due to 100 mm wheel flat and 0.5 m defect at train speed of 50 km/h. The effects of train speeds versus train axle loads from the work of Johansson and Nielsen (2003) are presented in Figure 4.22.

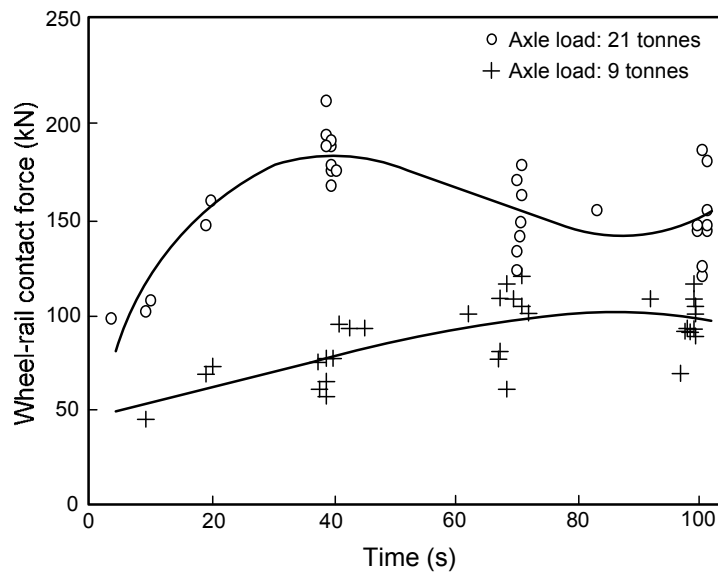


a) 100 mm wheel flat

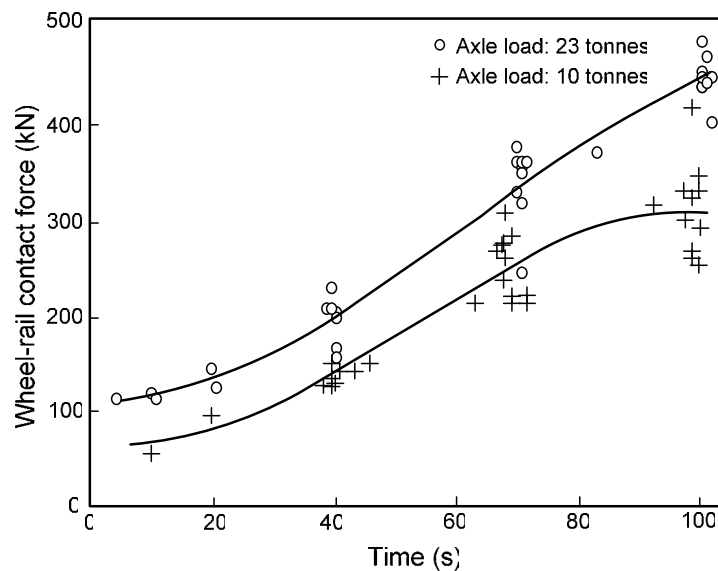


b) 0.5 m long local defect

**Figure 4.21** Wheel/rail impacts due to a) 100 mm wheel flat; b) 0.5 m long local defect – at train speed of 50 km/h (Johansson and Nielsen, 2003)



a) 100 mm wheel flat



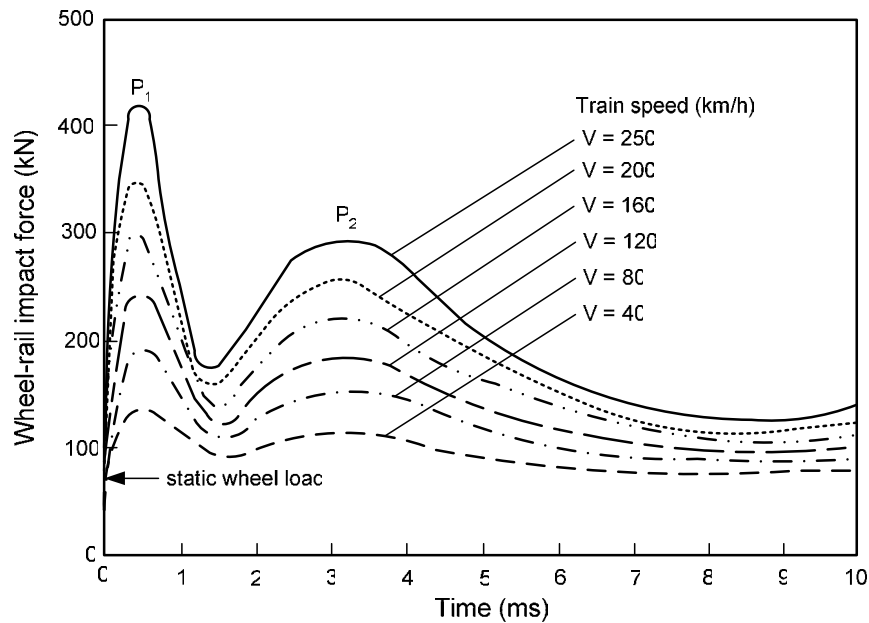
b) 0.5 m long local deflect

**Figure 4.22** Wheel/rail impacts due to a) 100 mm wheel flat; b) 0.5 m long local deflect – at different train speeds and axle loads (Johansson and Nielsen, 2003)

#### 4.3.3 Impact loads due to bad welds, joints, and switches

Rail joint or weld geometry and switches plays a vital role in imparting the impact loads on tracks. Usually, dipped welds are recognized as an important irregularity (Zhai and Cai, 1997; Andersson and Dahlberg, 1999). Also, it was reported that even small vertical deviations in weld geometry could generate large impact on rails (Esveld,

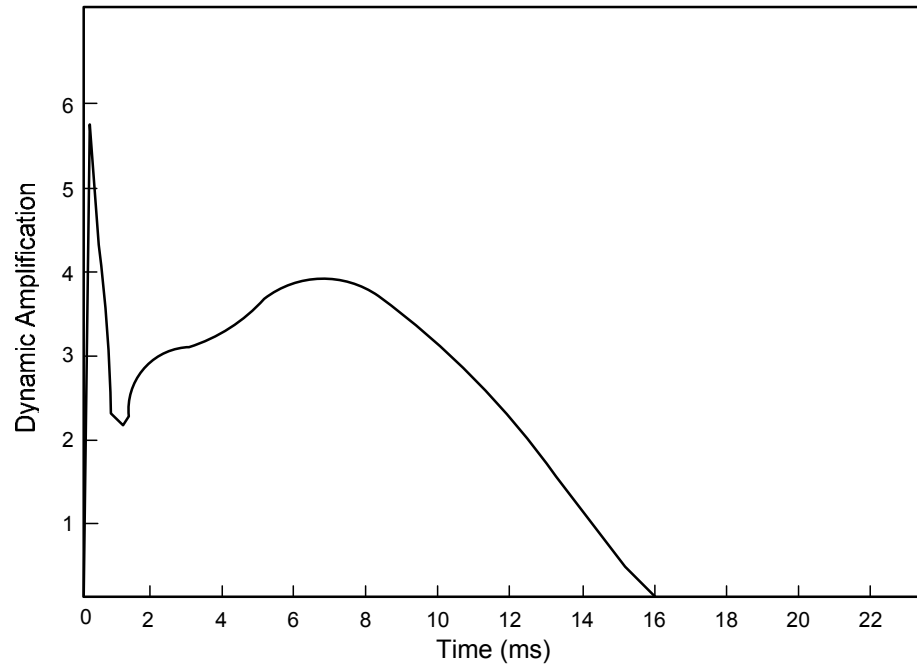
2001). Figure 4.23 illustrates the simulated effect of train speed on the impact force due to a typical dipped rail joint (about 0.2 rad). It was discovered that the second peak ( $P_2$ ) has a significant influence on primary crack and degradation of adjacent sleepers and underlying ballast formation (Bona, 2004).



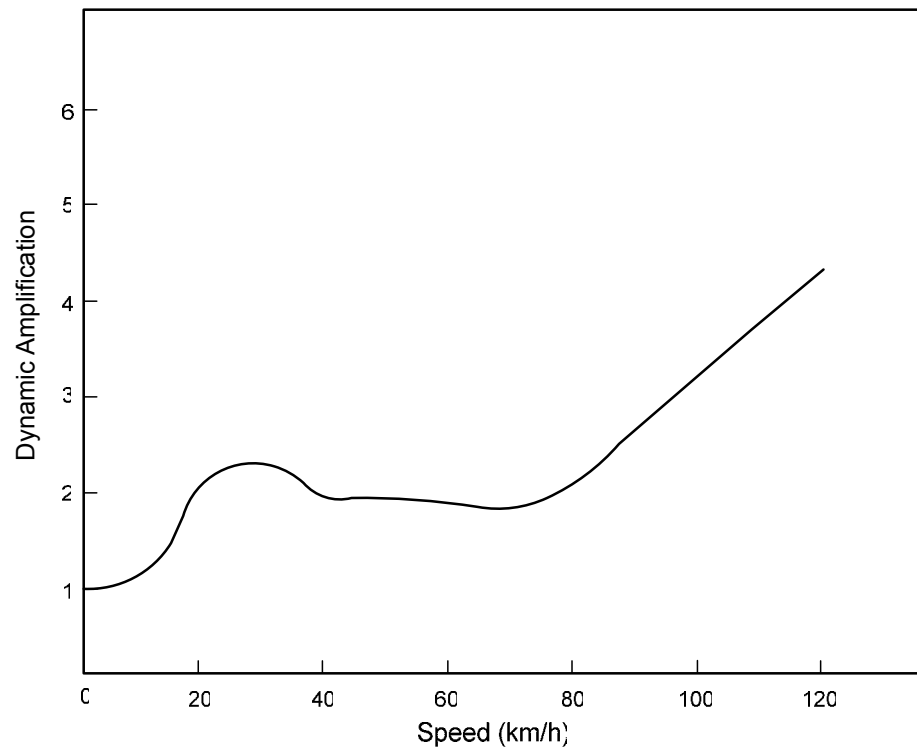
**Figure 4.23** Impact forces from a typical dipped joint (Zhai and Cai, 1997)

In relation to poor workmanships, it is found that the bad welds or weld misalignments can be seen quite often along the railway lines. Esveld (2001) studied the effect of bad welds on impact forces. Figure 4.24 presents the typical load distribution of the impact load due to bad welds (misaligned welds). Note that the dynamic amplification factor is the ratio between dynamic and static loads. It can be seen that the shape of the signal is similar to those from wheel flats.

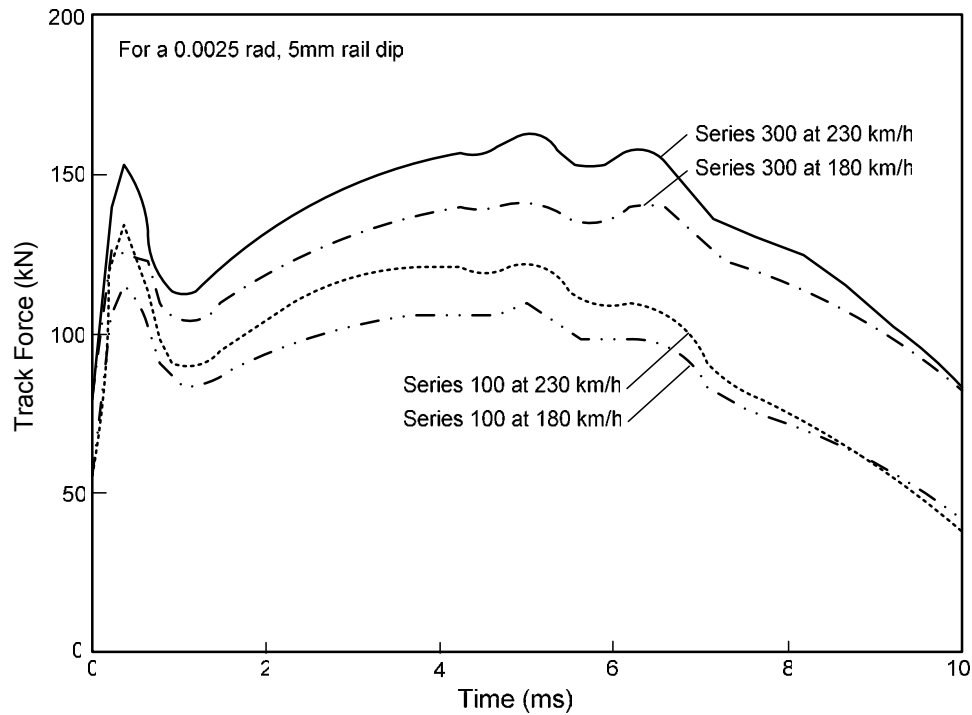
In good agreement between results of Zhai and Cai (1997) and Esveld (2001), it was found that the dynamic amplification of the impact forces from bad welds can be substantially increased with the increments of train speeds as illustrated in Figure 4.25. It should be noted that in order to attain acceptable dynamic loads from such bad welds the geometrical defects of welds should be less than a few tenths of a millimeter.



**Figure 4.24** Impact forces from a bad weld (Esveld, 2001)



**Figure 4.25** Effect of train speed on loading from a bad weld (Esveld, 2001)



**Figure 4.26** Impact forces from high speed trains (Rochard and Schmid, 2004)

The similarity of impact pulse due to the dipped joints between both studies can also be found. The first peak  $P_1$  lasts 1-2 msec while the second peak  $P_2$  lasts longer, 9-10 msec. Figure 4.26 shows the track force measurement under the high speed train (Shinkansen) in Japan. The speed of trains and the type of vehicle play vital role on the impact forces on the tracks (Rochard and Schmid, 2004).

Usually, the track degradation is driven by the wheel/rail impact loads, referred to as  $P_0$  (static load),  $P_1$  (first peak), and  $P_2$  (second peak).  $P_1$  is a high-frequency dynamic load when a vibration mode between the wheel and rail (coupled by the very stiff contact patch) is excited, whilst  $P_2$  is a low-frequency dynamic load when the coupled wheel-rail vibrate in phase on the ballast (Bona, 2004, Rochard and Schmid, 2004). Since  $P_2$  is the force that has direct influence on the degradation of track bed, UK Railway group standards (Rail Safety and Standards Board, 1993; 1995) provide a simplified formula (Equation 4.5) to compute for  $P_2$  force as an input related to track and vehicle characteristics.

$$P_2 = Q + (A_z V_m MCK) \quad (4.5)$$



where

$$M = \sqrt{\frac{M_V}{M_V + M_Z}} \quad (4.6)$$

$$C = 1 - \left[ \frac{\pi C_Z}{4\sqrt{K_Z(M_V + M_Z)}} \right] \quad (4.7)$$

$$K = \sqrt{K_Z M_V} \quad (4.8)$$

and,

$Q$  = maximum static wheel load (N)

$V_m$  = maximum normal operating speed (m/s)

$M_V$  = effective vertical unsprung mass per wheel (kg)

$A_z$  = 0.020 rad (total angle of vertical ramp discontinuity)

$M_Z$  = 245 kg (effective vertical rail mass per wheel)

$C_Z$  =  $55.4 \times 10^3$  Ns/m (effective rail damping rate per wheel)

$K_Z$  =  $62.0 \times 10^6$  N/m (effective vertical rail stiffness per wheel)

These formulae are based on the assumptions that a vehicle shall be able to negotiate a vertical ramp discontinuity in rail top profile, equivalent to a dipped rail joint on straight track, at its maximum design operating speed without exceeding a total (static plus dynamic)  $P_2$  force per wheel of 322 kN. If the forces proposed exceed 322 kN, technical support should be provided for safety. It is noteworthy that the maximum permissible  $P_2$  force of 322 kN per wheel corresponds to that which was theoretically induced by a high-speed vehicle class in UK standard (Vehicle Class 55 'Deltic' locomotive) when running over the prescribed rail joint at 161 km/h. The relevant

parameters for the Class 55 locomotive are as follows (Rail Safety and Standards Board, 1993; 1995):

$$Q = 86,000 \text{ N (maximum static wheel load)}$$

$$V_m = 44.7 \text{ m/s (maximum normal operating speed)}$$

$$M_v = 1,680 \text{ kg (effective vertical unsprung mass per wheel)}$$

$$A_z = 0.020 \text{ rad (total angle of vertical ramp discontinuity)}$$

$$M_z = 245 \text{ kg (effective vertical rail mass per wheel)}$$

$$C_z = 55.4 \times 10^3 \text{ Ns/m (effective rail damping rate per wheel)}$$

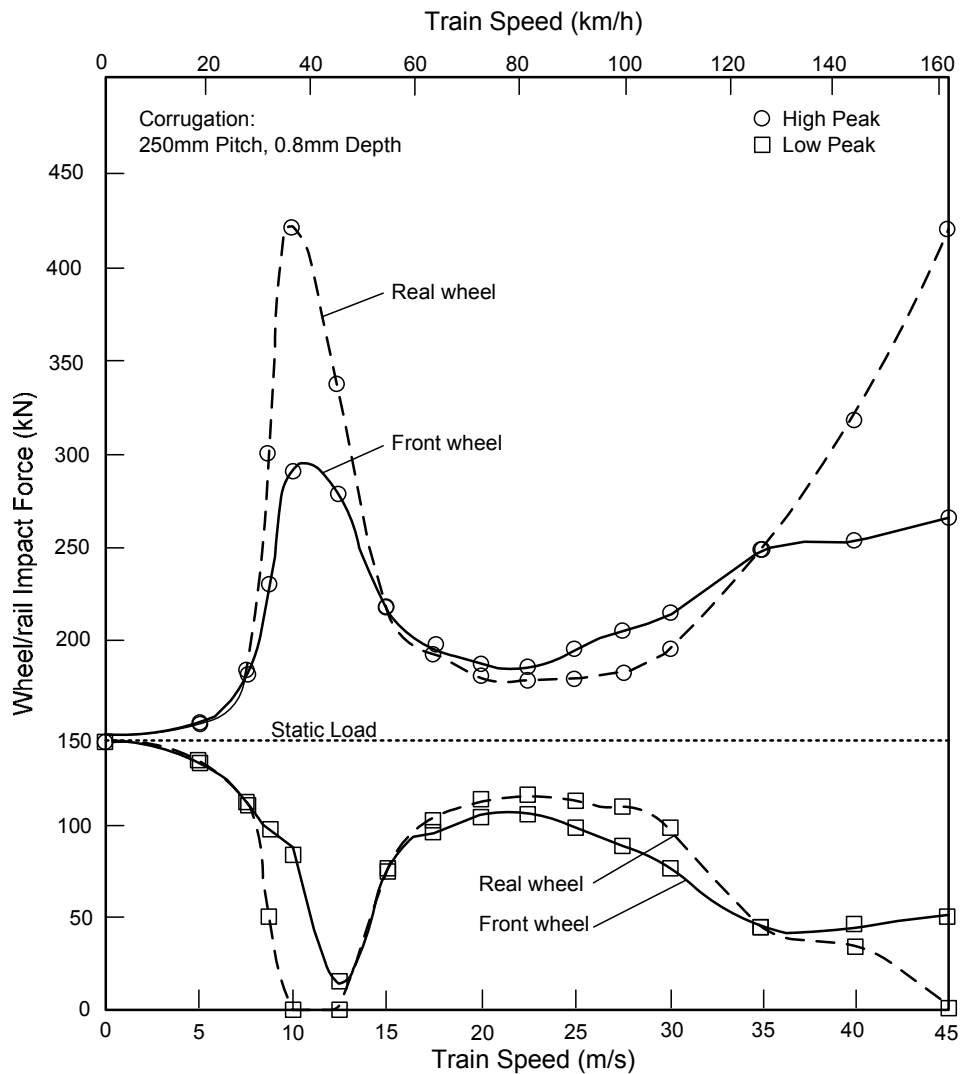
$$K_z = 62.0 \times 10^6 \text{ N/m (effective vertical rail stiffness per wheel)}$$

#### 4.3.4 Impact loads due to rail corrugation

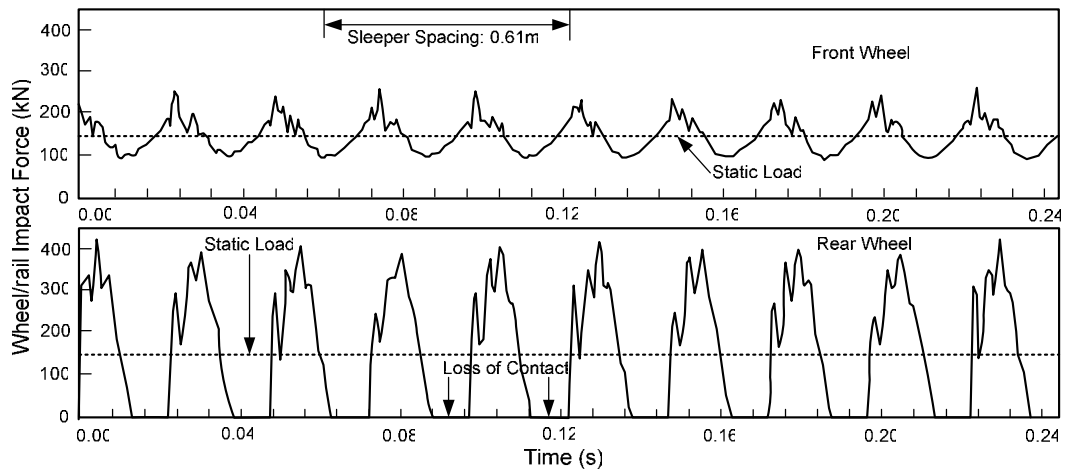
Rail corrugation, either short or long wavelength, is one of the major causes of the high impact loading. Cai (1992) and Murray and Cai (1998) developed the finite element model predicting the effect of corrugated rail on wheel/rail contact forces. A long-pitch rail corrugation with a sinusoidal wave pattern, 250 mm in pitch and 0.8 mm in depth, was created in the track model. It was found that the magnitude of the forces significantly depends on the train speeds as displayed in Figure 4.27. Time histories of impact forces at different train speeds are shown in Figure 4.28. It can be seen that the magnitude as well as the duration of the impact forces is dependent on the train speeds.

Impact force detection system was installed on a section of high speed Shinkansen railway line to study the impact forces due to the corrugations caused by corrosion in a submarine tunnel (slab track with 60 kg rail) (Wakui, H. & Okuda, 1999). Figure 4.29 shows the recorded axle-box acceleration in terms of waveforms. It was found that there is some negative acceleration recorded just before a shock pulse. This was caused by the effect called '*wheel fly*' when the wheel treads leave the railhead due to the gaps in

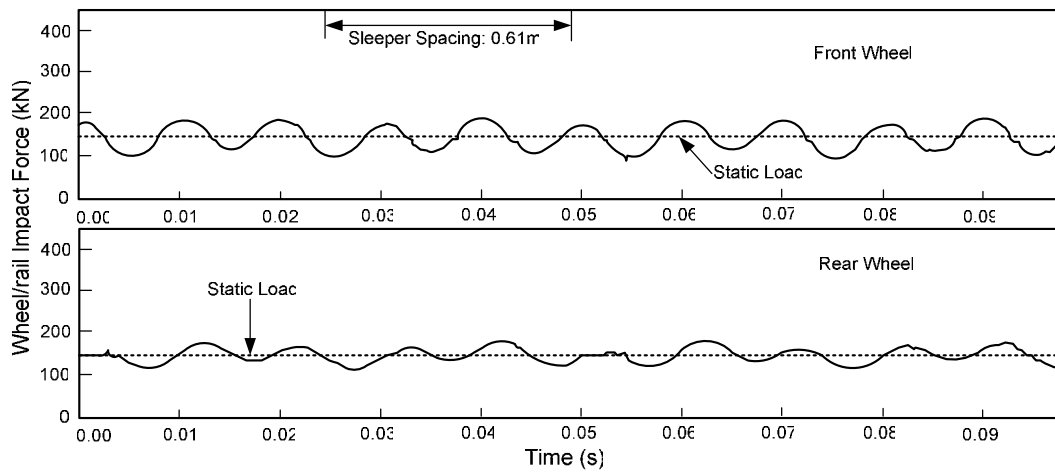
either short- or long-pitch corrugations on the rail; and subsequently, the wheel strikes the railhead with the axle sprung mass weight. It was also found that the maximum peak is about 54.3g (535 kN) and the peaks of over 30g have durations ranging from 5 to 10 msec.



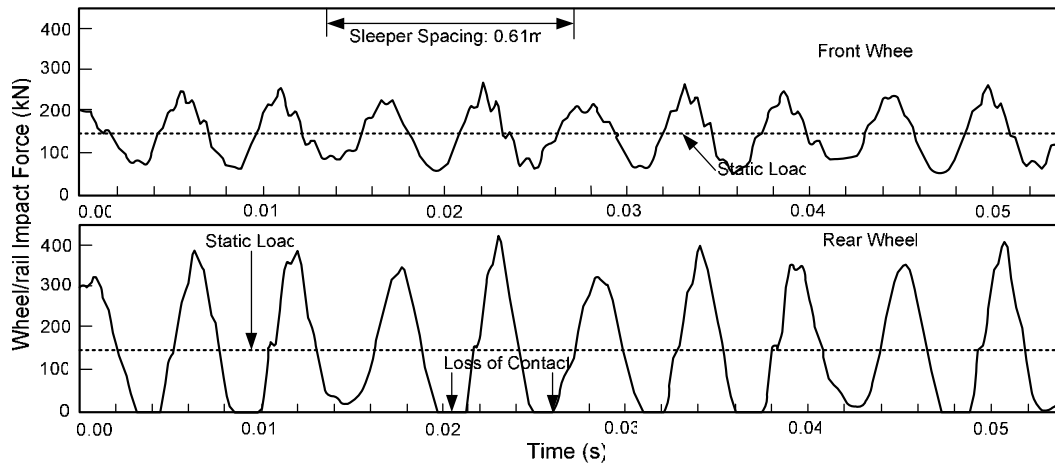
**Figure 4.27** Wheel/rail impact loads from a corrugated rail (Cai, 1992)



a) at train speed 36 km/h

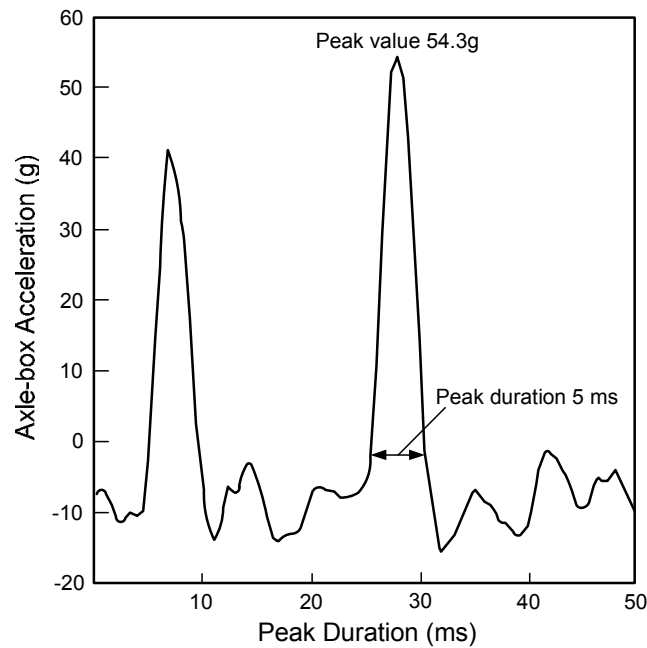


b) at train speed 90 km/h



c) at train speed 162 km/h

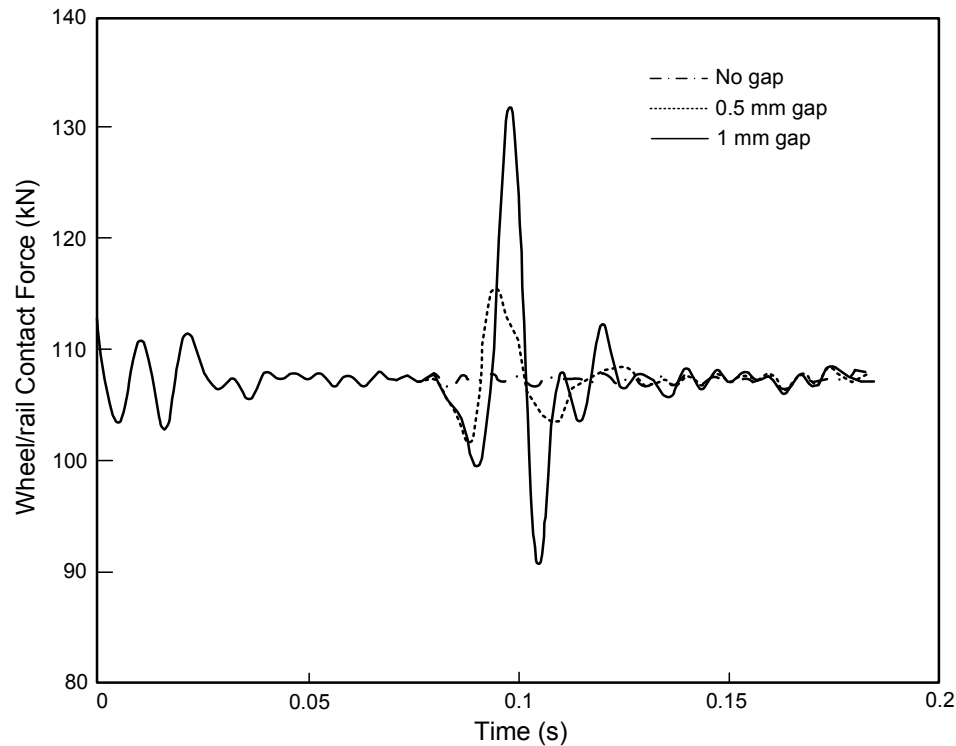
**Figure 4.28** Time histories of wheel/rail impact loads from a corrugated rail (Cai, 1992)



**Figure 4.29** Axle-box acceleration from a rail corrugation (Wakui and Okuda, 1999)

#### 4.3.5 Impact loads due to unsupported sleepers

Interestingly, the unsupported sleepers can result in unexpected impact loading. The voids and pockets underneath a sleeper in track system are generally caused by the wet beds from natural water springs, high percentage of subgrade breakage, or poor drainage of track substructure (Kaewunruen and Remennikov, 2006b). Those voids might be very large and allow the sleeper hanging to the rails (the so-called ‘*unsupported or hung sleeper*’). Lundqvist and Dahlberg (2005) developed a computer model simulating the dynamic train/track interaction. The effects on wheel/rail contact forces of one or several voided sleepers on tracks have been evaluated. It was found that the worst case occurs when one fully supported sleeper is surrounded by two unsupported sleepers. Figure 4.30 shows the typical wheel/rail contact force due to the 90 m/s train speed with 3 unsupported sleepers in the middle of a track.



**Figure 4.30** Impact forces due to unsupported sleepers (Lundqvist and Dahlberg, 2005)

#### 4.4 IMPACT RESISTANCE OF CONCRETE SLEEPERS

Train and track interactions during services normally generate substantial forces on railway tracks. Such forces are transient by nature and of relatively large magnitude and are referred to as impact loading. There has been no comprehensive review of the typical characteristics of the loading conditions for railway track structures, in particular, impact loads due to the wheel/rail interaction, published in the literature. The previous section presents a review of basic design concepts for railway tracks, abnormalities on tracks, and a variety of typical dynamic impact loadings imparted by wheel/rail interaction and irregularities. The characteristics of typical impact loads due to wheel and rail irregularities, e.g. rail corrugation, wheel flats and shells, worn wheel and rail profiles, bad welds or joints, and track imperfections, are presented with particular emphasis on the typical shapes of the impact load waveforms generally found on railway tracks.

As mentioned, railway track experiences multiple impact loading. The behaviour of concrete sleepers under impact loads is of great significance in order to predict their

dynamic responses and resistance to impact loading. Although there have been an extensive number of impact investigations, the majority of those were performed on individual materials such as polymer, steel, or plain concrete (Banthia, 1987), and composite sections such as fiber reinforced concrete (Abbate, 1998). Impact tests were introduced for prestressed concrete structures by Military forces and nuclear industry (Remennikov, 2003). The aim of that project was to investigate the effect of blast loads on the prestressed concrete members.

In the 1980s, the impact testing of concrete sleepers was performed to investigate the flexural cracks that were noticed at the rail seats of over 50 percent of concrete sleepers in the United States, although the sleepers were installed in service for a few months (Grassie, 1987). Cracks in concrete sleepers led to serious concerns about the concrete sleepers' durability, serviceability, and load-carrying capacity. Clearly, the major factors that cause sleepers cracking response mostly were due to the wheel/rail interactions, rail irregularities, or wheel defects. It was also found that those impact loads were greater than usual quasi-static ones as much as three times (Wang, 1996).

#### 4.4.1 Experimental Techniques for Impact Testing

The impact investigations were usually done to understand how much energy consumed to fracture, how many blows of multiple impact causing the first crack or the prescribed distress, and how bad of damaged zone under various aspects (ACI, 1990). Those aspects imply the toughness and resistance of such systems under extreme loading.

Impact testing devices have been developed for more than two decades. There are two types of those devices representing their own physical features: former, drop weight hammer; and later, pendulum machine. The drop weight hammer, which is the most common technique, has been adopted worldwide in impact testing on concrete structures (Banthia et al., 1989). In that test, the number of blows required to create the first visible crack was reported in addition to the ultimate impact force. This technique was proven versatile to be applied in railway engineering research as it could simulate both single and repeated impact loading on the actual tracks (Wang, 1996). Later, this drop-weight hammer technique has been extended to various research, for instance, investigations on bending-failure-mode and shear-failure-mode reinforced/prestressed

concrete beams (Ando et al., 1999; 2000; Kishi et al., 2001a; 2001b; 2002), sandwiched plates/beams (Abbate, 1998), etc.

The pendulum apparatus has been used commonly in the pulse tests on walls or the measurements of the resulting support reactions of columns or composites, and vice versa (Gopalaratnam et al., 1984). This pendulum method was also applied to reinforced concrete slabs under impulsive loads (Miyamoto et al., 1991). Either a uniformly distributed or a point load could be applied on the slabs, while the duration of impact pulses could be managed by varying the filter materials on the place between the force transducer and the steel hammer.

#### 4.4.2 Evaluation of Impact Resistance in Laboratories

As mentioned, railseat cracks motivated a number of investigations on impact testing of concrete sleepers/ties. The forensic discovery of those cracks was initiated by Dean et al. (1983). The impact loading tests were done on the single sleeper arrangements with the single drops using drop-weight hammer, varying amplitudes of loading and frequency contents. To measure the impact strain, the dynamic strain gauges were installed at the rail seats. By using different pads, it was found that the pad stiffness could remarkably decrease the bending moments at the dropping position, eliminate the cracking of concrete sleepers, and attenuate the bending strain by 25 percent.

Ahlbeck et al. (1986) found that the second and third bending modes of vibration of sleepers play an important role in their cracking behaviors. The resonant responses at these peaks are corresponding to the whole track natural frequencies, hence resulting in the crack initiation at either top or bottom surface in the rail seat region of sleepers. It was also found that the impact loading would be attenuated by the filter effect of resilient pads. Igwemezie and Mirza (1989) carried out a series of impact tests on prestressed concrete sleepers in railway bridges by using a drop-weight impact machine. From the results, the softer pads tend to decrease the peak impact load. Different hammer drop heights created the load-time diagrams with mostly the same pulse durations, except for the use of softer pads that provided the longer duration. With the tests of nine sleepers, the load distribution was found that using softer pads decreases the load transmitted to the sleepers about 40 percent. The impact loading attenuation



behavior of rail pads were studied by Grassie (1989a). The on-track and laboratory tests were done and both results were compared. These results were later served for few dynamic models of railway track (Cai, 1992; Knothe and Grassie, 1993; Cai and Raymond, 1994). In those models, the sleepers were deemed to be whether uniform Euler's or Timoshenko's beams, not only masses, since the flexural stiffness and shear deformation became important.

According to Igwemezie et al. (1992), a half-track bed consisting of 5.5 m rail and eight concrete sleepers was performed impact tests in the laboratory. Using shear gauges attached on the rail web and force transducer, the dynamic load patterns were obtained. The gauges were found to underestimate the impact force magnitude as much as 80 percent. The results showed that the concrete sleepers imparted higher wheel/rail impact loading to the track than the timber sleepers did for the same input energy. In contrast, the bending stress at the railhead was found lower because of their heavier and stiffer properties. It was found that the fastening system transferred most of the impact energy to the sleeper, which could be harmful both to the track and to the stock rolling.

Recently, Canadian manufactured prestressed concrete sleepers with steel and polypropylene fibre concrete materials had been tested for their fatigue toughness and impact resistance using drop-weight machines with drop masses of 345 kg and 578 kg, and with heights of up to 1524 mm (Mindess et al., 1991a, 1991b, 1992; Wang, 1996). The deflection and inertia load of the sleeper was obtained by using accelerometers. The results showed that the fibre reinforced sleepers possessed the higher fracture energies and deflection at mid-span than has the plain concrete sleeper. In those tests, the sleepers were placed on various supports i.e. neoprene, rubber, and plywood. However, the ballast-sleeper interaction was not taken into account.

#### 4.4.3 In-field Impact Tests

Impact on tracks in the worst case usually comes from wheels with a flattening or chording of the wheel circumference over a length of 305-457 mm, referred to as "wheel flat". Field trials on tracks in service were mostly investigated for the impact loading occurred on track components. Dean et al. (1983) measured the impact load history (e.g. duration and amplitude) using strain gauge coupons installed on the sleepers. It was found that the wheel flats hit on the rail only 1-3 ms with the bending

moment about 600 inch-kip. The maximum wheel/rail impact force was about 82 kips or around 4 times the mean static load given by the same axle. Grassie (1989b) investigated the behaviors of in-field concrete sleepers with various resilient rail pads. It was found that the rail pads attenuated significantly the dynamic moment in concrete sleepers, but they also increased the moment if the ballast was loosely packed

Igwemezie (1992) recorded the wheel/rail impact loads in an open deck railway bridge with concrete ties. The special work train with some flat wheels was arranged to generate the impact loading. The responses of the concrete ties were found dependent on the speed of the train. It was also found that there was a complete unloading of the tie accompanied with over loading due to on impact at low speeds (0-64 km/h), whilst the unloading was followed by over two impact loads at speeds more than 80 km/h. It is worth to note that the impact factor was about 300 percent, since the average strain for un-defected wheels was  $120 \mu\epsilon$ , while that under wheel flat was  $476 \mu\epsilon$ . However, the load distribution factor, proportioning the wheel/rail contact load transferred to the underneath tie at the loading point, was much higher than that used in the track design. The fatigue results showed the insubstantial effect of cracks on the service life of the concrete ties.

#### 4.5 SUMMARY

This chapter summarizes the typical dynamic impact loadings imparted by wheel/rail interaction and wheel/rail/track irregularities. This comprehensive overview starts with general static and dynamic forces on railway track structures. Its main emphasis is however placed on the typical impact loadings, which are attributed to certain sources, such as rail corrugation, wheel flats and shells, worn wheel and rail profiles, bad welds or joints, switches, and track imperfections. In this chapter, the comprehensive typical shapes of the dynamic, impact axle force waves in time history domain generally found on railway track structures are reviewed.

All static, quasi-static, and impact loads are very important in design and analysis of railway track and its components. Generally, dynamic/impact loading is associated with frequency range from 0 to 2000 Hz due to modern track vehicles. The shape of impact loading varies depending on various possible sources of such loading,

e.g. wheel flats, out-of-round wheels, wheel corrugation, short and long wavelength rail corrugation, dipped welds and joints, pitting, and shelling. Wheel/rail irregularities induce high dynamic impact forces along the rails that may greatly exceed the static wheel load. In all cases, the impact forces are significantly dependent on the train speed. These impulses would occur repetitively during the roll. Loss of contact between wheel/rail, so-called “wheel fly”, will occur if the irregularity is large enough, or the speed is fast enough. Nonetheless, the impact force could be simplified as a shock pulse acting after the static wheel load is removed.

In summary, the typical magnitude of impact loads from the above reviewed cases varies roughly between 100 kN and up to 750 kN, depending on the causes and the traveling speed of train. The durations of such loads are quite similar, varying between 1 and 10 msec. However, the representative values of the first peak ( $P_1$ ) of the forces caused by dipped joints should be about 400 kN magnitude with 1 to 5 msec time duration. For the second peak ( $P_2$ ), the average values are about 80 kN magnitude and 5 to 12 msec time duration. Therefore, it should be taken into account that the typical duration of impact wheel forces varies widely between 1 and 12 msec.

Based on the review, there exists the need to develop the experiment programs to achieve the impact resistance behaviours of prestressed concrete sleepers. The first step of the experimental study is to imitate the impact pulses of interest and then apply those impact forces onto the setup in-situ railway prestressed concrete sleepers. Subsequently, the numerical modelling becomes an effective and significant option because the repetitive experimental investigations in this regard would be time and resources consuming, and costly. It provides the virtual tests to develop the broader and deeper perspectives than those of the limited experiments. Currently, there is no analytical or numerical model for predicting the dynamic responses of prestressed concrete sleepers to impact loading. This study would thus provide the profound insight into the impact behaviours of railway concrete sleepers under various conditions.

As aforementioned, cracking of prestressed concrete sleepers has been investigated by many railway organisations. The principal cause of cracking is the infrequent but high-magnitude wheel loads produced by a small percentage of “bad” wheels or rail head surface defects which are crudely accounted for in AS 1085.14 by a

single load factor. The current design philosophy, outlined in AS 1085.14, is based on assessment of permissible stresses resulting from quasi-static wheel loads and essentially the static response of concrete sleepers. In order to shift the conventional methodology to a more rational design method that involves more realistic dynamic response of concrete sleepers and performance-based design methodology, a significant research effort is imperative to perform comprehensive studies of the loading conditions, the dynamic response, and the impact resistance of the prestressed concrete sleepers. This chapter has addressed such important issues as the spectrum and amplitudes of dynamic forces applied to the railway track. This background will lead to the evaluation of the reserve capacity of typical prestressed concrete sleepers designed to the current code AS 1085.14, and the development of a new limit states design concept. This challenge also includes the establishment of the numerical modelling of the prestressed concrete sleepers using the dynamic finite element model updating calibrated against the modal parameters obtained in Chapter 3, the static test results to appear in Chapter 5, and the impact responses to appear in Chapter 6 onwards.

## CHAPTER 5

### INVESTIGATIONS ON STATIC ULTIMATE LOAD-CARRYING CAPACITY OF PRESTRESSED CONCRETE SLEEPERS

Railway sleepers are the key components of railway infrastructure, being used to distribute axle loads to ground. Knowledge of failure mechanisms of concrete sleepers is required for their design criteria and for better insight into the development of the limit states design concept. This chapter focuses on the determination of maximum positive and negative bending moments of concrete sleepers. The sectional analyses have been conducted, which are in good agreement with the experimental results. It should be noted that the design moments obtained from the manufacturers are lower than the calculated decompression moments, implying that the sleepers are designed to meet the fatigue load criteria. Cracking in concrete sleepers is usually detected at rail seats and mid span regions because of large bending stresses resulted from wheel/rail interactions. Therefore, in this chapter the ultimate load-carrying capacity of sleepers at these sections is investigated. It is noticed that although the fracture toughness is high, the ductility of sleepers is relatively low.

#### 5.1 OVERVIEW

Concrete sleepers have a major role in distributing axle loads to formation. The axle loads could be considered static or quasi-static when the speeds of trains are quite moderate (Gustavson, 2000). However, in general, the axle loading tends to physically behave like the dynamic impact pulses due to the continual moving ride over track irregularities and faster speeds. These dynamic effects would then deteriorate the mechanical properties of the track components and undermine the load-carrying capacity of the concrete sleepers (Kaewunruen and Remennikov, 2005a; 2005b). Although concrete sleepers are affected by the dynamic loading, the practical design standards still relies on the sectional analysis and static behaviour of the sleepers. There have been a number of publications addressing the dynamic wheel load factors, in order to perform the design calculations for concrete sleepers using quasi-static analysis and

procedure (Murray and Cai, 1998; Remennikov, 2004). In addition, theoretical concepts of strength, ductility, stability, fracture mechanics, and so on, mostly refer to the static behaviour.

In Australia, Standards Australia (2003) revised the conventional design of railway prestressed concrete sleepers and fastening assemblies. Also, the maximum design flexural moments in sleepers can be statically calculated from the pressure distribution in Figure 5.1. It is found that the maximum positive moment occurs at the rail seat, whilst the maximum negative moment remains at the middle of sleepers. The maximum positive design bending moment at railseat ( $M_{R+}$ ) for standard and broad gauge sleeper ( $g > 1.5$  m) can be read

$$M_{R+} = R(L-g)/8 \quad (5.1)$$

for narrow gauge sleeper, the formula becomes

$$M_{R+} = R(L-g)/6.4 \quad (5.2)$$

In contrast, the maximum negative design bending moment at mid span ( $M_C$ ) for concrete sleepers with track gauge of 1.6m or greater is

$$M_C = 0.5 [Rg - Wg(L-g) - W(2g-L)^2/8] \quad (5.3)$$

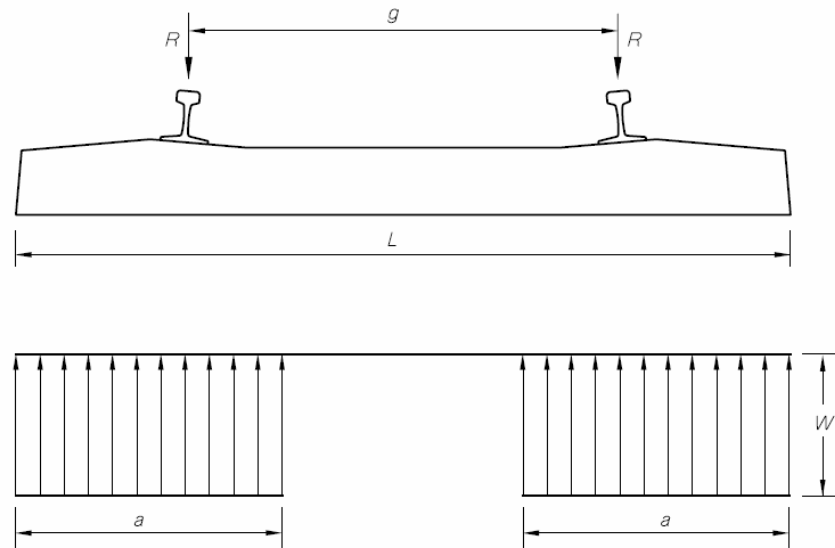
where

$$W = 4R/(3L-2g) \quad (5.4)$$

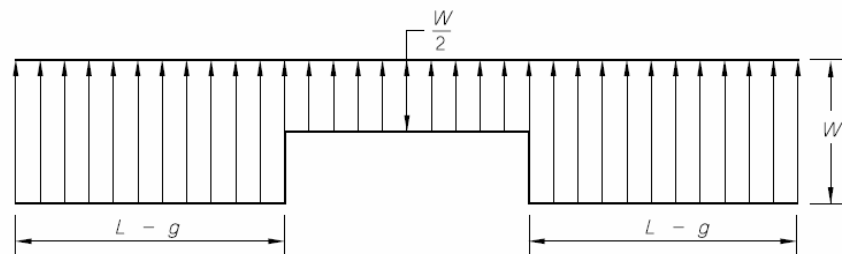
The design formula for sleepers with track gauge of 1435 mm read

$$M_C = R [2g - L]/4 \quad (5.5)$$

If the track gauge is less than 1435mm, the purchaser shall specify the negative design bending moment. However, for sleepers with track gauge of 1067 mm, it should not less than 14 kNm. Concept of permissible stresses has been governed in the 2003 release. The Standard also gives consideration that need not to check sleeper section for stresses other than flexural stresses, e.g. shear, if the design is complied with all clauses in the Standard. It is noteworthy that for prestressed concrete sleepers, the influence of the dead load can be ignored and the design load can be expressed by the wheel load alone (Wakui and Okuda, 1999).



a) Pressure distribution for maximum positive rail seat and centre moments.



b) Pressure distribution for maximum negative centre moments  
for track gauge of 1600 mm and greater.

**Figure 5.1** Pressure distribution (AS1085.14, 2003)

In this chapter, the results of static testing of prestressed concrete sleepers are presented. The load-carrying capacities of railway concrete sleepers at railseat and at the centre of sleepers are highlighted. At the centre section, the negative bending moment was applied through the four-point-load bending test. The similar setup was also adopted in positive bending moment test program at railseat section. The testing programs were

designed in accordance with AS1085.14-2003 Prestressed concrete sleepers and AS1085.19-2001 Resilient fastening assemblies (Standards Australia, 2001; 2003). It should be noted that AUSTRAK broad gauge sleeper was employed in both negative and positive bending moment tests. All tests were performed using full-scale sleepers without cutting, scaling, dividing, nor adjusting the sleepers. The detailed experimental program will be presented in the next section. Failure mechanisms, crack propagation, and post-failure behaviour of concrete sleepers will be discussed.

The concrete sleepers in this study are designed with Pandrol eClip system using rail pads. Based on the available data (E-mail from Steve Douglas, 2005), the design moments of prestressed concrete sleepers are as follows.

#### **AUSTRAK:**

##### **Broad gauge sleeper**

Rail Seat Section	+ 23.4 kNm
	- 15.7 kNm
Middle Section	+ 9.4 kNm
	- 17.9 kNm

##### **Narrow gauge sleeper**

Rail Seat Section	+ 25.0 kNm
	- 18.0 kNm
Middle Section	+ 19.0 kNm
	- 18.0 kNm.

The experiments are aimed at underpinning the data from the sectional analyses (by manual calculation and by a computer package, Response-2000) as well as understanding the static ultimate behaviours of the railway prestressed concrete sleepers. It is believed that the prestressed concrete sleepers were cast under high quality control, which results in the consistent properties of the sleepers at each casting batch. Two patterns of load-carrying capacity are of structural-design interest and will be evaluated. The first one is the maximum negative moment of sleeper, which corresponds with the middle section. The later one is the maximum positive moment of sleeper, especially at rail seat. The test setups were carried out complying with

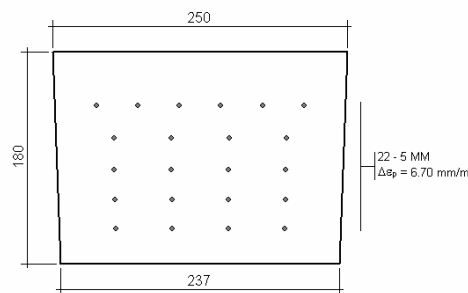


Australian Standards: AS1085.14-2003 Prestressed concrete sleepers and AS1085.19-2001 Resilient fastening assemblies (Standards Australia, 2001; 2003). AS1085.14-2003 indicates the boundary conditions, location of supports, and characteristics of loading. The strain measurements on top and bottom fibres at the surface of concrete sleepers were performed according to AS1085.14-2003 requirements.

## 5.2 NEGATIVE MOMENT TEST AT MID-SPAN

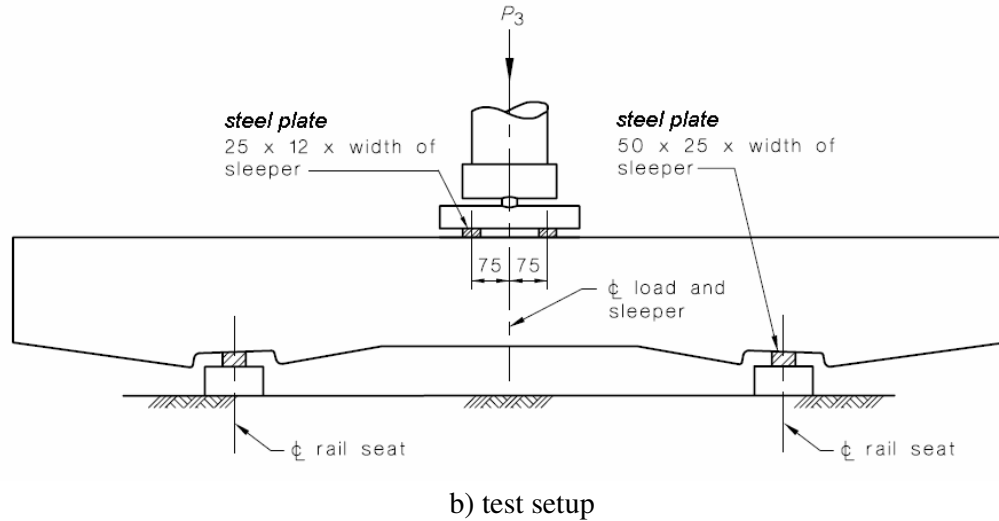
The schematic diagram for the experimental setup of the centre negative moment test is shown in Figures 5.2(a) and 5.2(b). The strain gauges were installed 10 mm from the top and bottom surfaces at the centre of sleeper. Linear variable displacement transformer (LVDT) was used to measure deflection at the load point. The rotations at supports that represent the gauge rotations were measured using inclinometers. The test program was carried out using displacement control with loading rate of approximately 10 kN/min, as prescribed by AS1085.14. The equipment used in these tests includes:

- LVDT at middle span,
- Inclinometers at rail seat supports,
- Strain gages and wires at top and bottom fibres,
- Load cell,
- Loading frame,
- DataLogger, and
- Electronic load control.



a) up-side-down cross section at mid span

**Figure 5.2** Centre-negative moment test (AS1085.15-2003, L1)



**Figure 5.2** Centre-negative moment test (AS1085.15-2003, L1)

Figures 5.3 and 5.4 show the experimental setup and instrumentation for the negative moment test at the middle section. The maximum experimental load was 133 kN, which is equivalent to the mid-span bending moment of about 45 kNm. It was found that the hand calculations showed very good agreement with the experimental results. The ultimate load from the hand calculations (general prestressed concrete theory) is 132 kN (or bending moment of 44.8 kNm), whereas the ultimate resistance of 139 kN (or bending moment of 47 kNm) was predicted by Response-2000 (Bentz, 2000).



**Figure 5.3** Experimental setup for centre-negative moment test



a) LDVT



b) Inclinometer

**Figure 5.4** Instrument in the test

### 5.2.1 Load-deflection relationship

The load-deflection relation is presented in Figure 5.5. The moment-deflection curve is shown in Figure 5.6. The crack initiation load was detected visually during each test as well as determined by the use of the load-deflection relation. Crack initiation was defined as the intersection between the load-deflection relations in stages I and II as shown in Figure 5.7. This simplified definition was employed to obtain a consistent method for the crack initiation load determination (Gustavson, 2000). This method provides a slightly higher cracking load than that from the first deviation point from the linear elastic part of load-deflection relationship. Comparisons of measured and visualized crack initiation loads showed very good agreement. The visually determined crack initiation load was about 79 kN while the measured one was about 75 kN.

### 5.2.2 Energy absorption characteristics

Energy absorption characteristics reflect how much the structure can dissipate the work done by external forces. The energy absorption capacity can be computed from the area of the load-deflection curve. This energy absorption has led to the prediction of forces and distances that could significantly affect the structure. In this study, the energy

absorption capacity was calculated using a direct integration method; Newmark's Beta (0.5) or the so-called trapezoidal rule. The energy absorption capacity of the AUSTRAK concrete sleeper from the centre negative moment test is shown in Figure 5.8. This picture indicates the amount of inelastic deformation absorbed by the sleeper at different deformation levels.

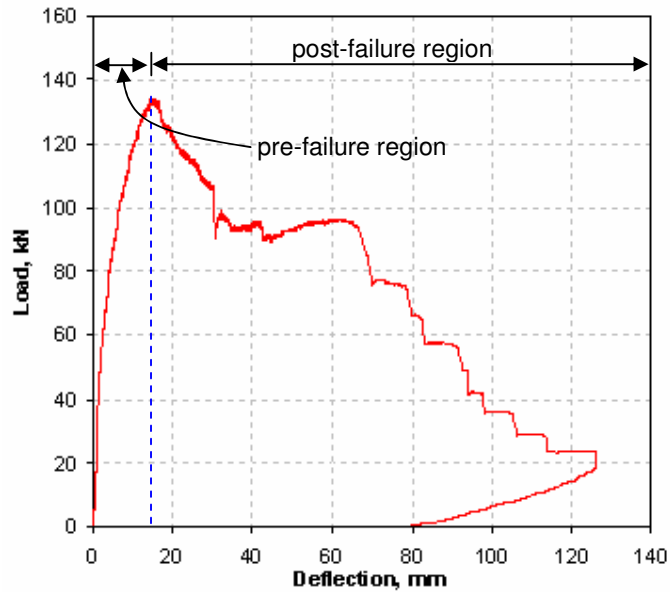


Figure 5.5 Load-deflection curve of centre negative moment test

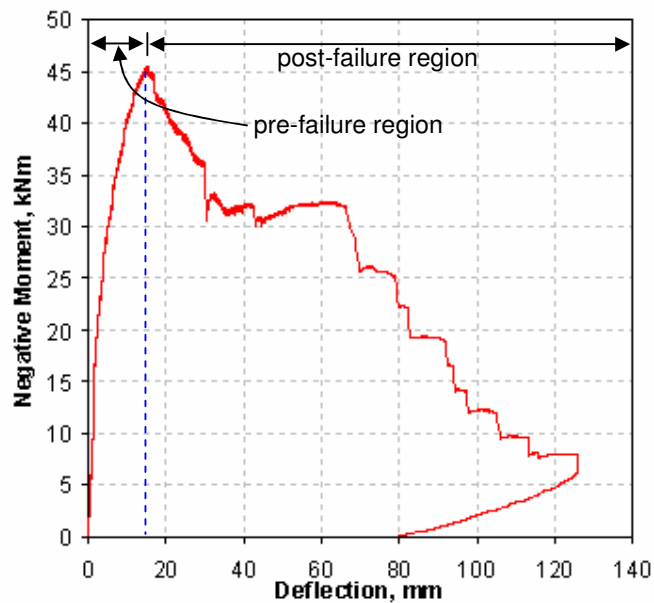
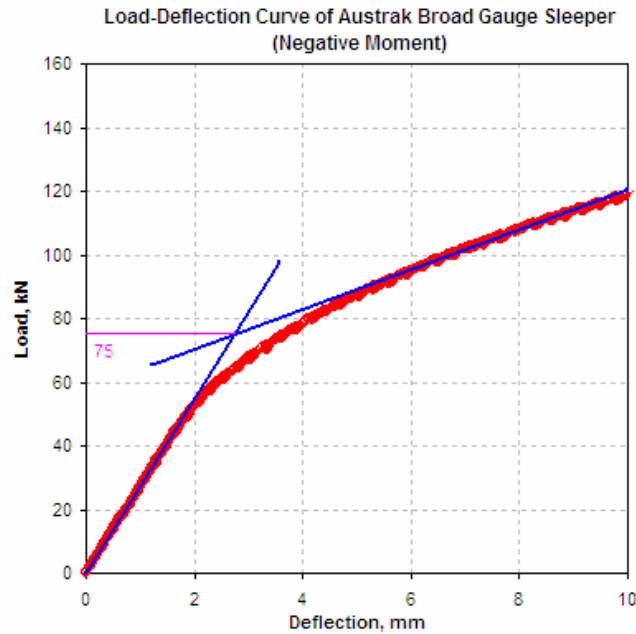
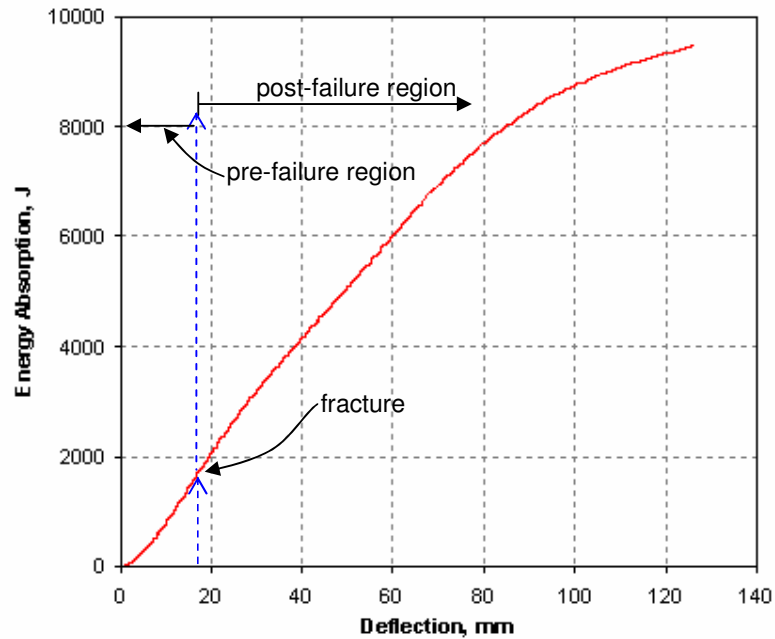


Figure 5.6 Moment-deflection curve of centre negative moment test



**Figure 5.7** Measured cracking load of centre negative moment test



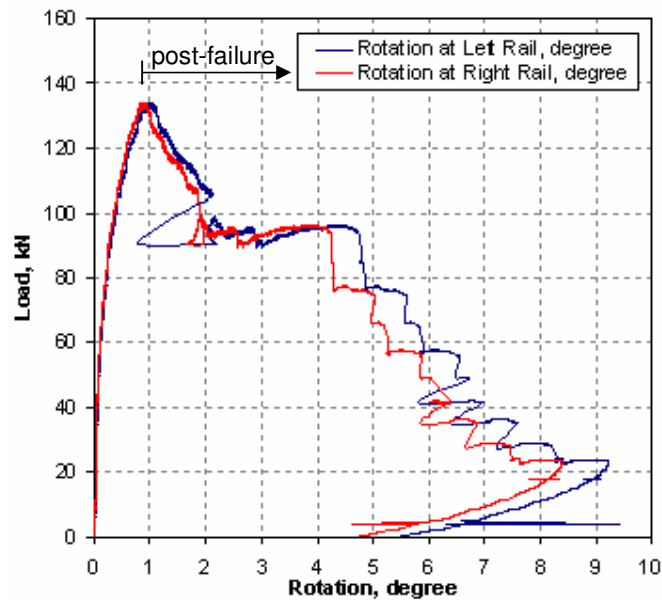
**Figure 5.8** Energy absorption characteristic due to centre negative moment test

The bending failure of the test concrete sleeper occurs at the first peak in the load-deflection curve, as can be seen in Figure 5.5. At the first peak, the concrete at the top fibre of rail seat start to crush while major bending cracks arise from the bottom fibre. The sudden failure could be noticed right after the load approaches the peak capacity. The remaining uncracked portion of concrete and the yielding wires could still sustain

the applied load until the first wire snaps. The failure mechanism will be described in details in later section. Figure 5.8 shows that maximum energy absorbed by the sleeper prior to the brittle failure is about 1,800 J. In contrast, only 100 J of energy can generate cracking in mid-span section of the tested concrete sleeper. It should be noted that the total energy absorbed after the fracture was mostly due to the high strength prestressing wires.

### 5.2.3 Rotational capacity

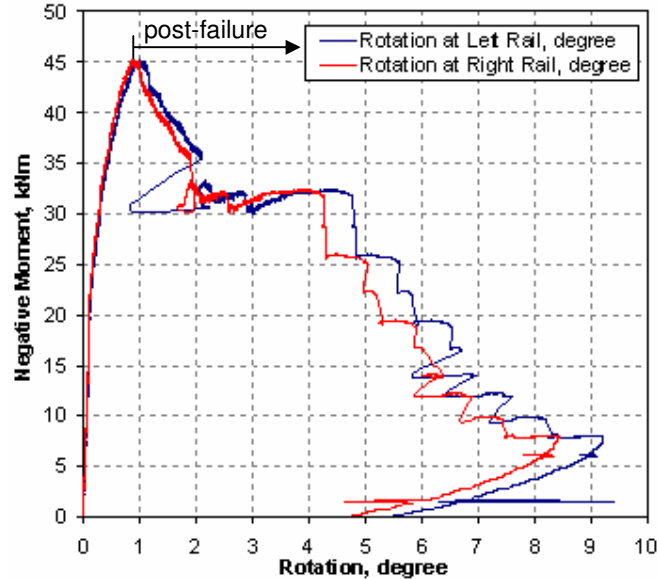
Excessive rotation of rails can cause derailment of rolling stocks. To determine these rotations, the inclinometers were mounted at both supported ends as shown in Figure 5.4(b). The rotational capacity under applied load and moment is presented in Figures 5.9 and 5.10, respectively. It was found that the left and right hand side rotations were identical before the sleeper fails. The maximum angle of rotation at failure was about 1 degree at which the maximum static load carrying capacity of the mid-span cross section was reached.



**Figure 5.9** Load-rotation relation from centre negative moment test

The angle of rotation that is associated with the first cracking of the mid-span cross section for the test specimen is about 0.2 degree. It should be noted that the angle of

rotation at first cracks of concrete sleepers implies the allowable angle of rotation designed in accordance with AS1085.14 (2003).



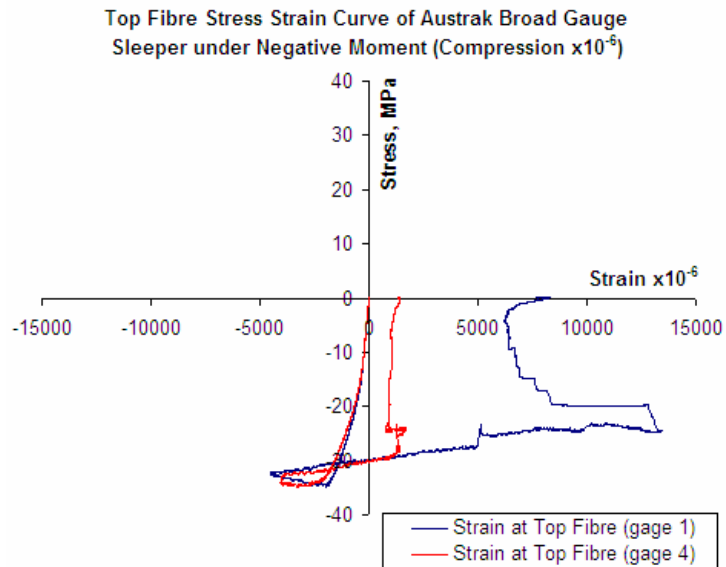
**Figure 5.10** Moment-rotation relation from centre negative moment test

#### 5.2.4 Stress-strain curves

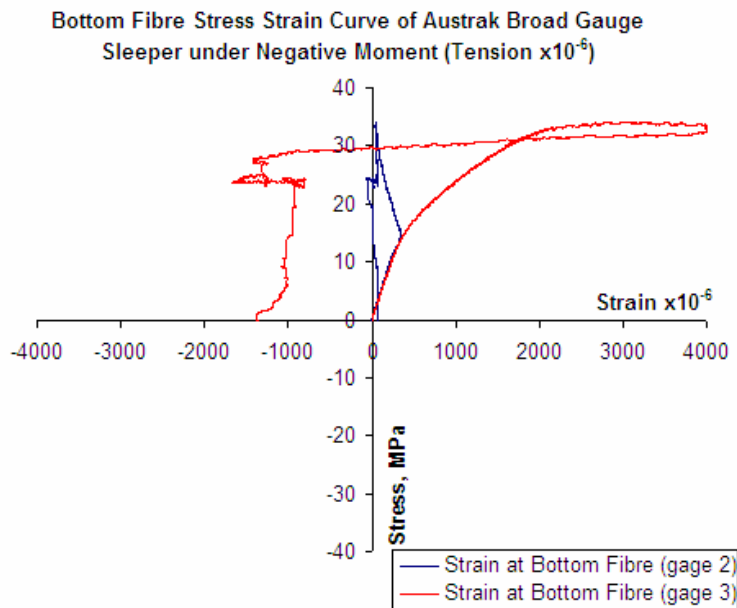
Four strain gages were installed to determine the strain behaviour at the top and bottom fibres. The stress strain curves for compressive and tensile strains at top and bottom fibres, respectively, are displayed in Figures 5.11 and 5.12. The corresponding stresses due to the applied bending moment can be calculated using the bending stress function ( $My/I$ ) that is based on the neutral axis of the gross section. From the experiments, it is clear that the crushing and spalling of concrete occurred within the top-fibre compressive zone of the sleepers under the applied load.

It was found that the ultimate compressive strain of concrete was about 0.004 before the brittle failure. As the high-strength concrete was usually used in the manufacture of concrete sleepers, the compressive strain of 0.004 is relatively high compared with the ultimate strain of normal strength concrete (20 to 40 MPa), which is around 0.003 (Rangan, et al., 1998). The strain records then changed the sign as the concrete bursts in tension.

The ultimate tensile strain of the concrete before cracking was found at about 0.0004, which is about 10 percent of the ultimate compressive strain. It was found that, once the strain of concrete exceeded the tensile strain, the concrete started cracking. Then, the strains changed the sign due to the shrinkage of concrete after cracking in tension.



**Figure 5.11** Compressive stress-strain curve of centre negative moment test



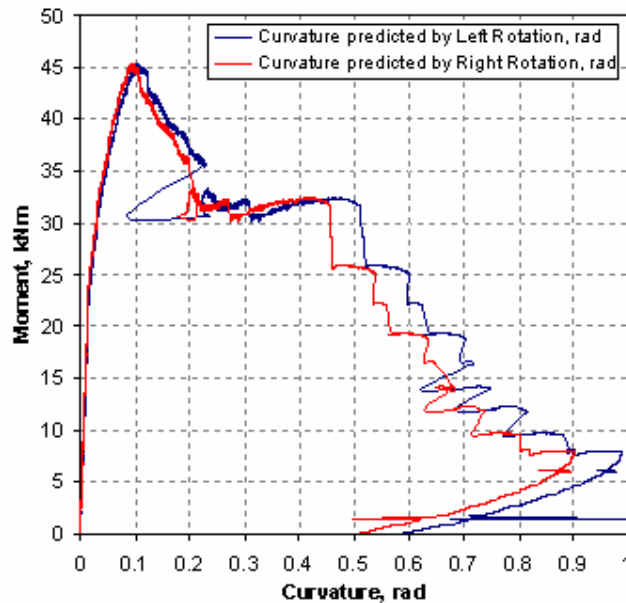
**Figure 5.12** Tensile stress-strain curve of centre negative moment test



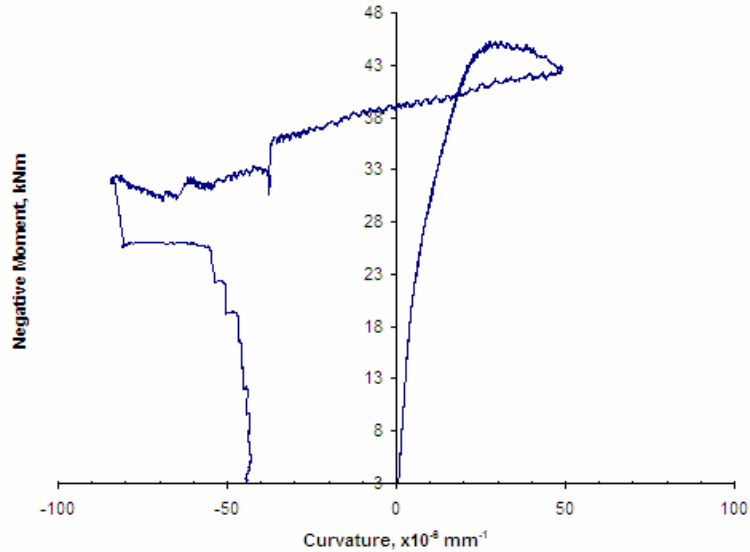
### 5.2.5 Mode of failure

Visible vertical crack due to the pure bending at the mid span initially appeared at 79 kN load. The concrete sleeper failed in flexure at the ultimate load of 133.3 kN, which results in 16 mm deflection at middle span and about 1 degree rotations at both ends. At this ultimate state, the sleeper absorbed energy of about 1,500 J. The detailed failure mechanisms pre- and post-failure will be discussed later in Section 5.2.6.

Moment-curvature relationship of a concrete sleeper can be found from the end rotations through the structural theory (Rangan, et al., 1998). Figure 5.13 illustrates the moment-curvature relationship based on the rotation measurements. By contrast, the moment-curvature relationship can also be computed from linear strain diagram (between gage distance of 170 mm) as shown in Figure 5.14. It should be noted that these relations were on linear deformation basis. However, those results were in quite good agreement during pre-failure loading range.



**Figure 5.13** Moment-curvature relation of negative middle section – End rotations



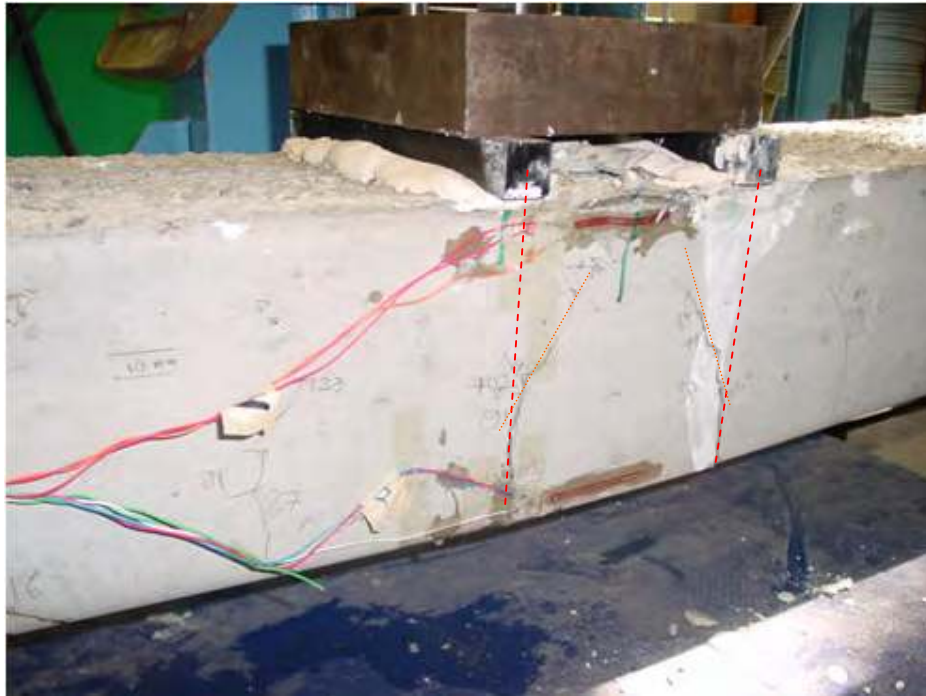
**Figure 5.14** Moment-curvature relation of negative middle section – Strain diagram

### 5.2.6 Post-failure mechanisms and crack propagation

Knowledge of failure mechanisms enhances the design procedures of engineering structures. Both pre-and post-failure characteristics are of critical concern for design engineers who need to incorporate these characteristics during design process. In particular, post-failure behaviour of prestressed concrete sleepers has not been thoroughly studied so far. Thereby, this investigation focuses on response of concrete sleepers from elastic stage to first and to complete collapse. This study will provide new information on the ductility of concrete sleepers and their post-failure behaviour.

The first crack during the test was a flexure crack appearing in the line of loading, see Figure 5.15. As the load was increased, the flexure-shear cracks formed at each side after the bending cracks stopped at a distance of about one third of the sleeper depth. All cracks were initiated at the base of the sleeper and propagated towards the compressive zone beneath the applied load. When the load reached the maximum, the concrete crushed and spalled as seen in Figure 5.16. At this stage, the applied load decreased while the deformation continued from that about 16 mm. The prestressing wire seemed to govern the sleeper strength and slightly yield. Combined flexure and shear failure seems to be suitable to explain the crack behaviour. The behaviours of the sleeper after failure could be explained based on its load-deflection curve. At certain deflections, the prestressing wires started to damage one by one, resulting in a sudden significant vertical drop of load in load-deflection curve, approximately 10 kN per wire damage.

The wire damage started from the lowest layer of such prestressing wires as can be seen from Figure 5.17.



**Figure 5.15** Initial flexure cracks at middle span of AUS-BG Sleeper



**Figure 5.16** Failure of middle span of AUS-BG Sleeper

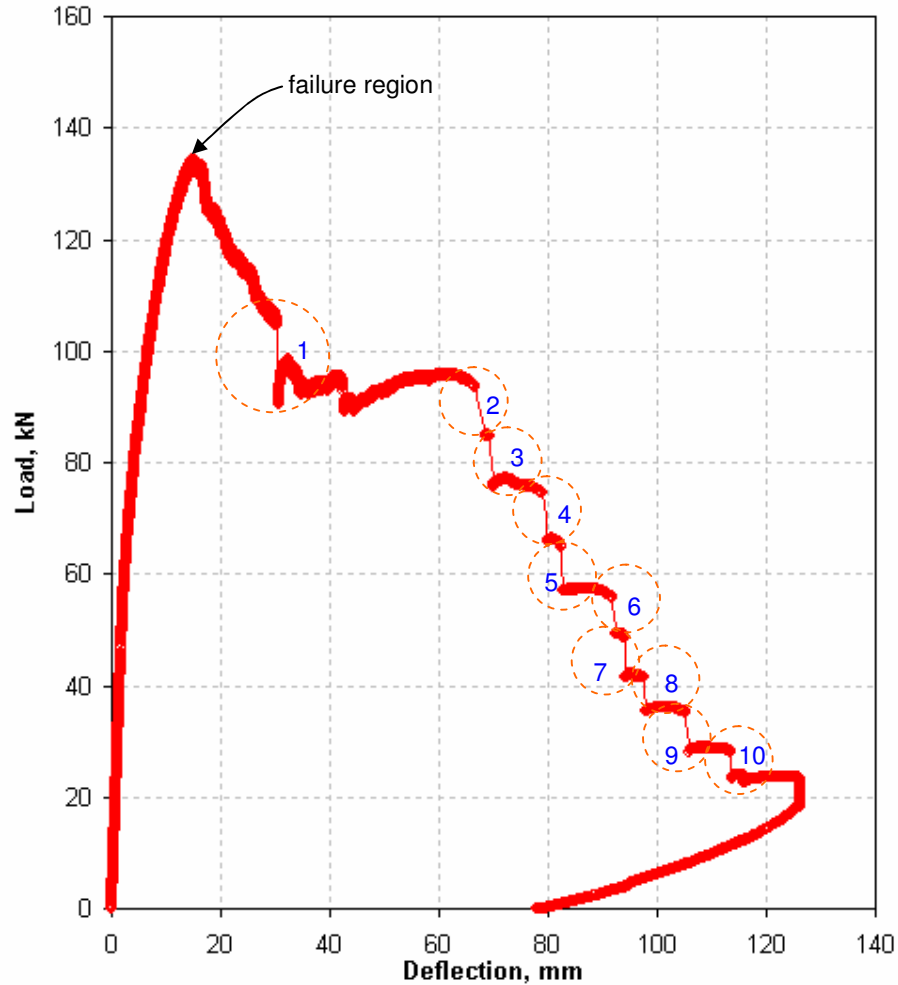


**Figure 5.17** Damage of the lowest-layer prestressing wires of AUS-BG Sleeper

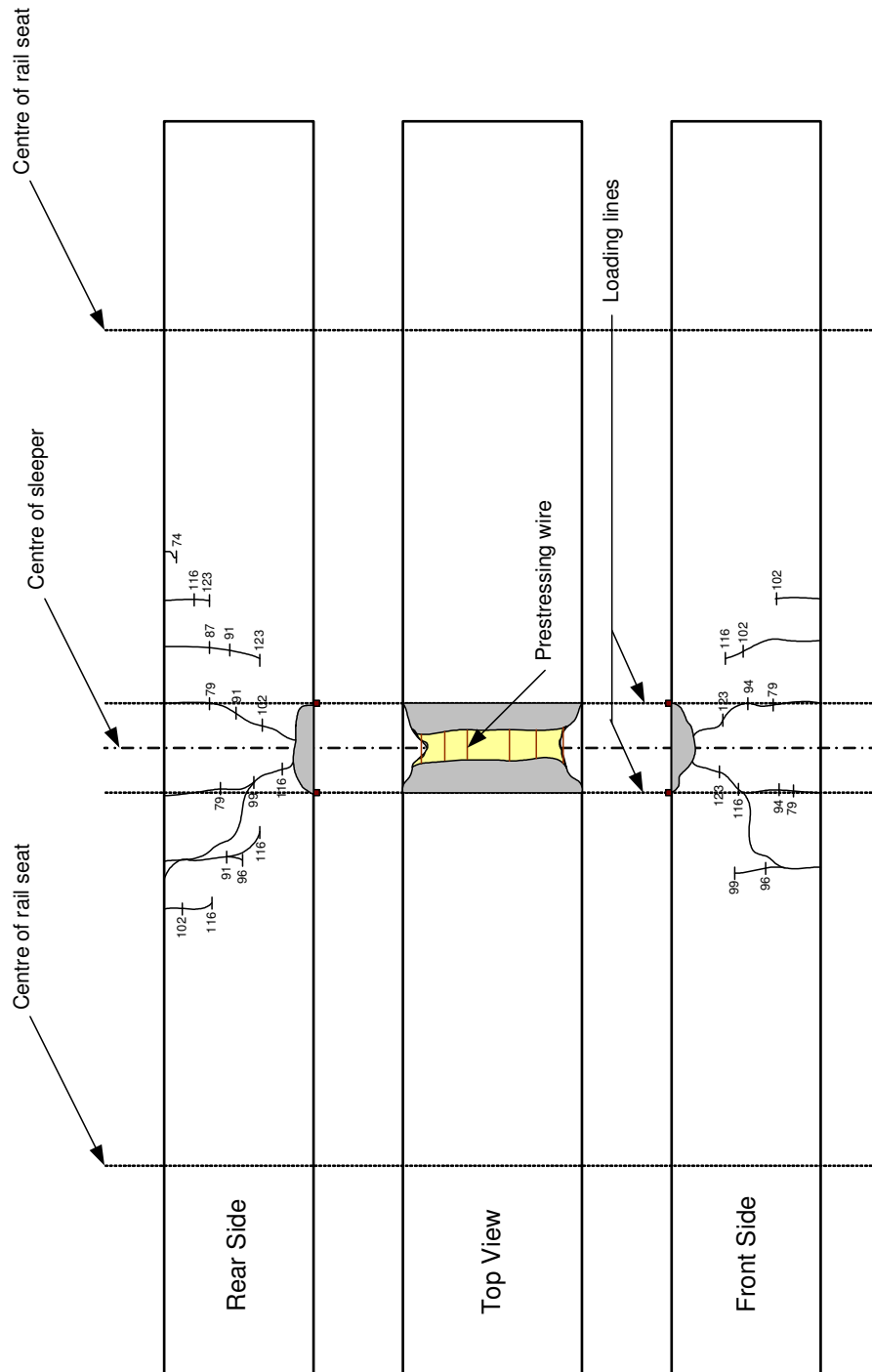
Recalling the load-deflection curve of this test in Figure 5.18, each dash circle in the curve indicates the damage of each wire starting from the lowest layer of prestressing. Each sudden drop releases the breaking noise and loses the carrying load about 10 kN. Definitely, ten wires were damaged and about 100 kN load-carrying capacity was disappeared. It also showed that the concrete sleeper tended to have very small ductility. At the failure region, it was found that the yielding deformation was almost negligible. On the other hand, the failure tended to be sudden and brittle. The flexural ductility index of the tested concrete sleeper was about 1.

The crack propagation during the test is outlined in Figure 5.19. Both sides of sleeper have similar crack behaviour. At top surface subjecting to applied load, the influence zone of crushing covers all area between loading lines. The area between the loading lines was under the high compression and tends to have the local stress concentration due to the short bending span on the superficial concrete surface. Overall, the sleeper mid-span cross-section performed well under the bending moment. Cracks propagated mostly due to the bending effect. The stress-strain curves showed that at failure the fracture of concrete forms at the top fibre as the ultimate compressive strain of concrete

was reached, and the shear diagonal cracks incurred to connect between the concrete crushing and the significantly opened bending cracks. Also, the prestressing wires tended to yield and the tendon strains reached the rupture failure strength. As a result, there were significant drops of the load carrying capacity as the wires start to snap one by one.



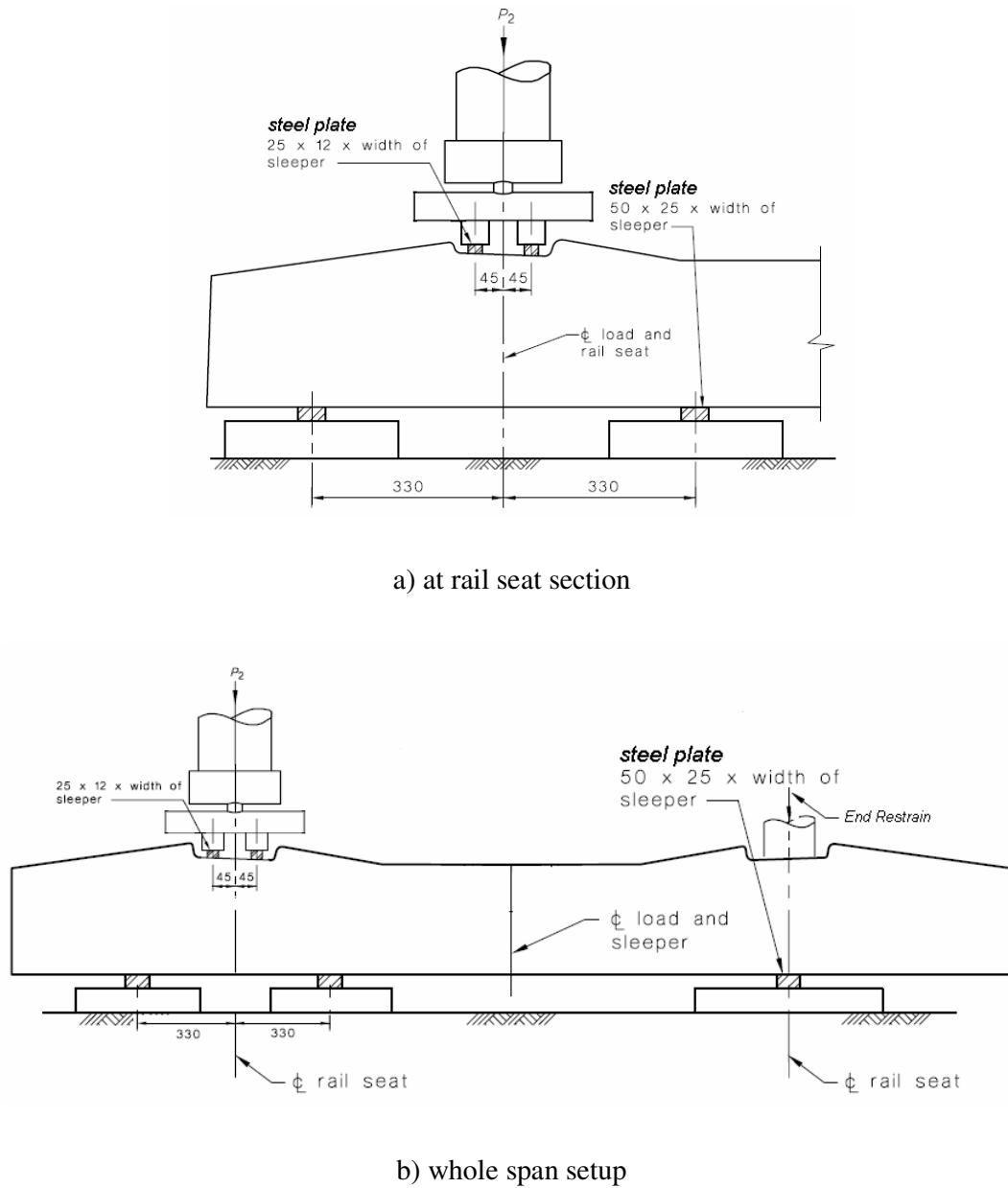
**Figure 5.18** Load-deflection analysis of AUS-BG Sleeper



**Figure 5.19** Crack pattern of AUS-BG Sleeper

### 5.3 POSITIVE MOMENT TEST AT RAILSEAT

The schematic diagram for the experimental setup of rail-seat positive moment test is shown in Figure 5.20. The test setup is similar to previous test. However, the location of measurements was changed to the centre line of rail seat instead. In this test, the inclinometer was also used and another rail seat was preloaded and clamped.



**Figure 5.20** Rail Seat-positive moment test (AS1085.15-2003, P2)

The test was carried out at the same loading rate (about 10 kN/min). The equipment required in these tests included:

- LVDT for sleeper deflections at loading line,
- Strain gages and wires installed at loading line and at middle span for obtaining both top- and bottom-fibre strains,
- Load cell,
- Laser deformation measurement of loading steel column,
- Inclinometers at supports,
- DataLogger, and
- Electronic load control.

Figure 5.21 shows the real setup and instrument for the maximum positive moment test at rail seat section. Vertical seat was used to keep the loading path in vertical plane. The maximum experimental load was found to be 585 kN, which is equivalent to bending moment of about 63 kNm. Shear strength deficiency governed the observed failure mode. It was found that the predicted ultimate load from Response-2000 (Bentz, 2000) was 539 kN (or bending moment of 58 kNm).

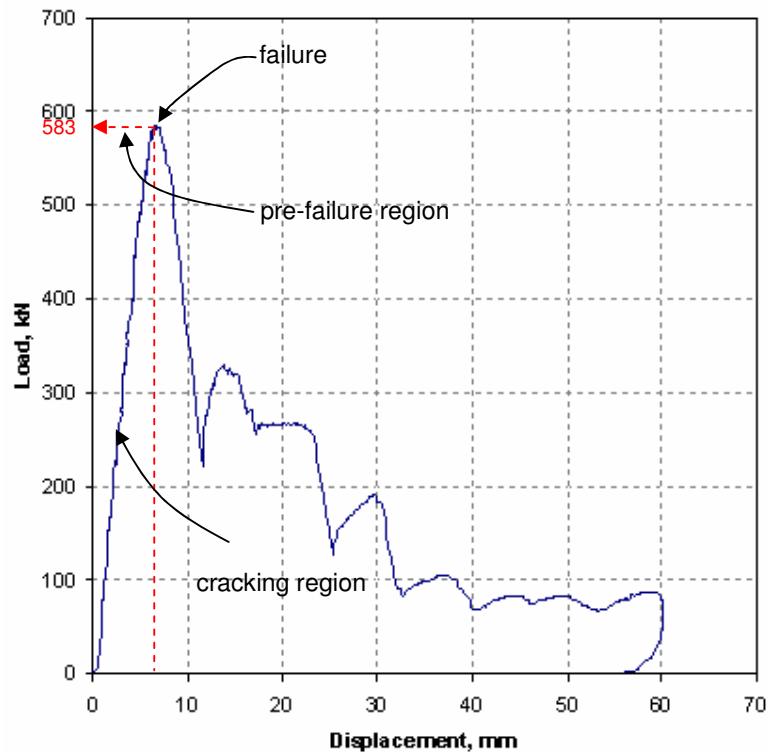


**Figure 5.21** Experimental setup for rail seat- positive moment test



### 5.3.1 Load-deflection relationship

The load-deflection relation for the railseat cross-section of the tested concrete sleeper is presented in Figure 5.22, whereas the moment-deflection curve can be seen in Figure 5.23. The crack initiation load was detected visually during each test as well as determined by the use of the load-deflection relation. Crack initiation was defined as the intersection between the load-deflection relations of the average data in stages I and II as shown in Figure 5.24. Comparisons of measured and visualized crack initiation loads showed quite good agreement. The crack initiation load determined by visual observation was about 240 kN, while the measured one was about 235 kN.



**Figure 5.22** Load-deflection curve of rail seat positive moment test

At the very beginning stage when the load was applied at railseat, the vertical displacement of the railseat was linearly proportional to the applied load and bending moment up until the tensile strains at the bottom fibre almost reach the ultimate tensile strength. Once the strain reached the tensile strength, the concrete started cracking and the nonlinear relation between load and deflection appeared. When the top-fibre strain of concrete approached the ultimate compressive strength, the fracture of concrete occurred as will be discussed in Section 5.3.5.

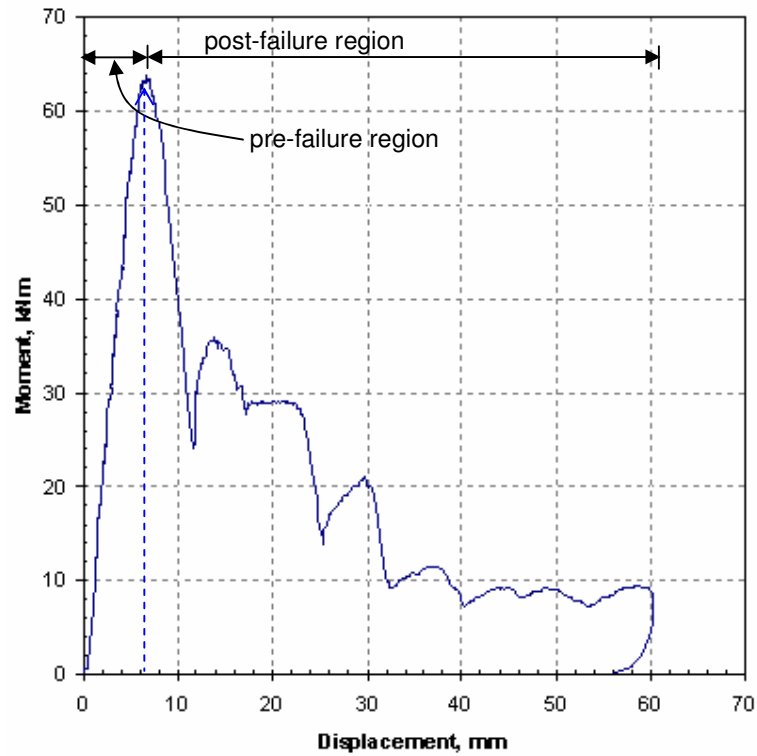


Figure 5.23 Moment-deflection curve of rail seat positive moment test

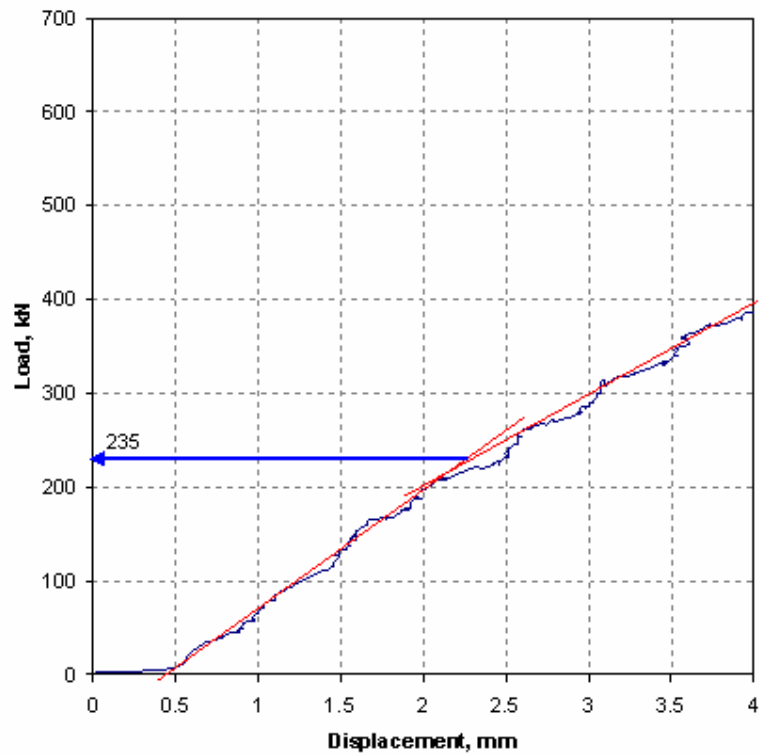
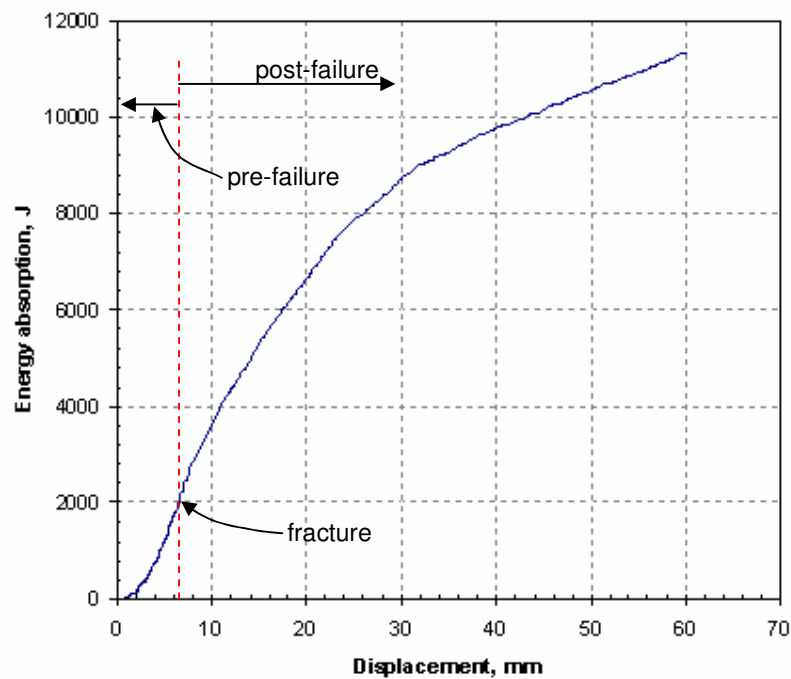


Figure 5.24 Measured cracking load of rail seat positive moment test

### 5.3.2 Energy absorption characteristics

As aforementioned, the energy absorption capacity reflects how much the structure can dissipate the work done by external forces. The energy absorption characteristics determined from the rail seat positive moment test are shown found in Figure 5.25. It should be noted that the failure is indicated when the major fracture of concrete occurs at the top fibre of railseat. At fracture, energy given to deform sleeper railseat vertically to about 6.5 mm was about 2,000 J, which is slightly higher than that of mid-span cross-section. On the other hand, an amount of 250 J of energy is required to cause cracking in the railseat of the tested concrete sleeper.

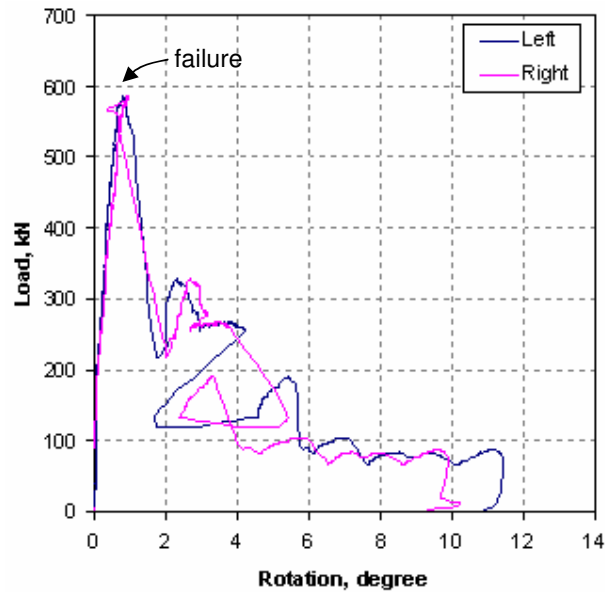


**Figure 5.25** Energy absorption characteristic due to rail seat positive moment test

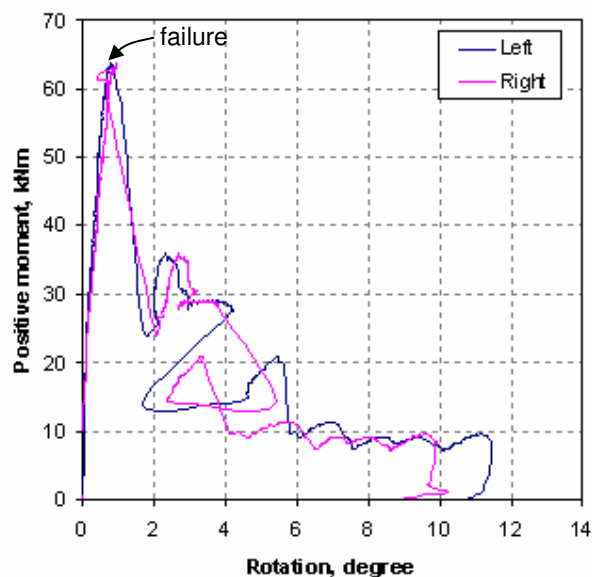
### 5.3.3 Rotational capacity

In this railseat test, the inclinometers were mounted coincident with both supports. Although the rotations at these setup supports play an insignificant role on the rail gauge, they provide important information in relation to the curvature at the inflection point between positive bending moment at railseat and negative bending moment at mid span. The rotational capacity under applied load and moment is presented in Figures 5.26 and 5.27, respectively. It is found that the left and right hand side rotations were

fairly similar before the sleeper fails. The angle of rotation that is associated with the fracture of railseat section is about 0.8 degree. The allowable angle of rotation that causes cracking at the railseat is found to be about 0.1 degree. It should be noted that the rotations of angle, which cause cracking and failure at rail seat of the tested concrete sleeper, are less than those at mid-span of the tested concrete sleeper. This is because the shear span ratio of the railseat test setup is much less than that of the mid-span test setup.



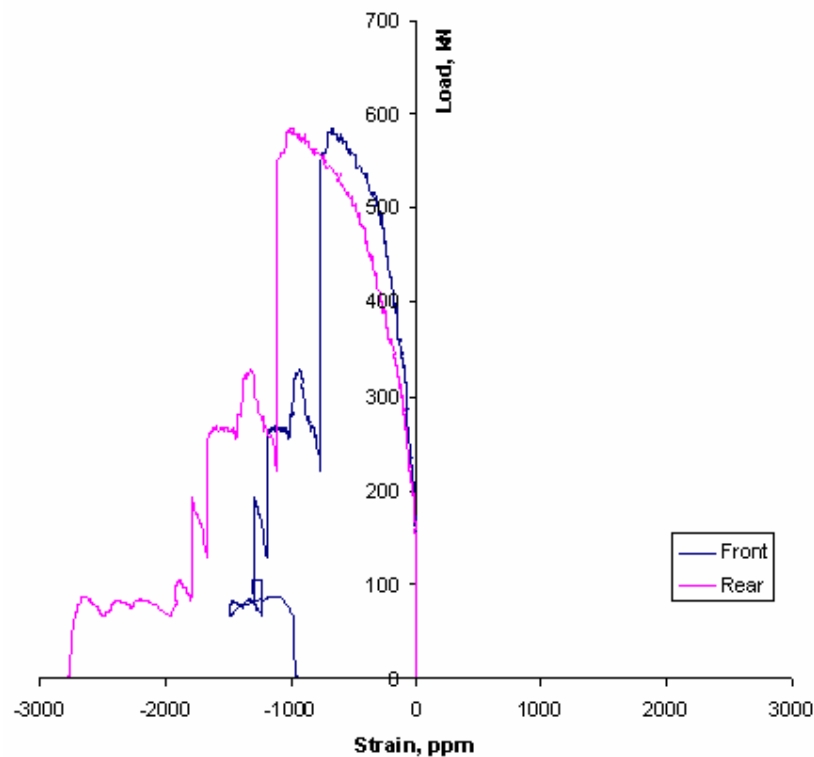
**Figure 5.26** Load-rotation relation from centre negative moment test



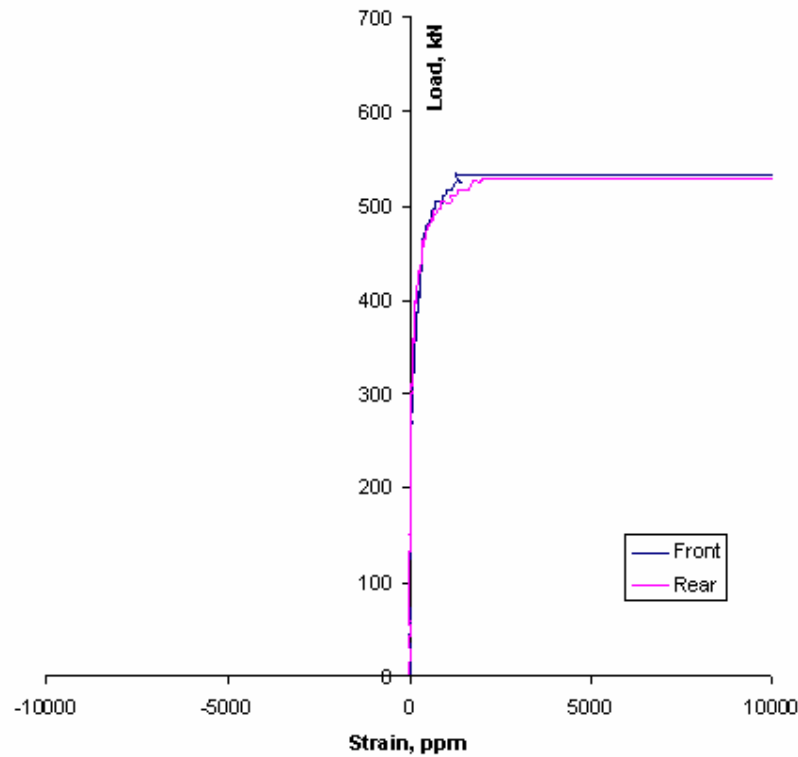
**Figure 5.27** Moment-rotation relation from centre negative moment test

### 5.3.4 Load-strain curves

Six strain gages were installed to determine the strain behaviour at the top and bottom fibres of both rail seat and middle sections. The load-strain curves for compressive and tensile strains at top and bottom fibres of rail seat section are displayed in Figures 5.28 and 5.29. From the experiments, it was found that the crushing and spalling of concrete did not occur at the top-fibre compressive zone of sleepers when the sleeper failed. It was found that the maximum compressive strain at top fibre of railseat was 0.0012. The load-strain curves showed that the ultimate strains were not reached, which implies that the failure mode was not due to purely flexure. It was also found that the maximum tensile strain of concrete at bottom fibre was about 0.001 at which the ultimate tensile strain of concrete was reached and the cracking occurred.



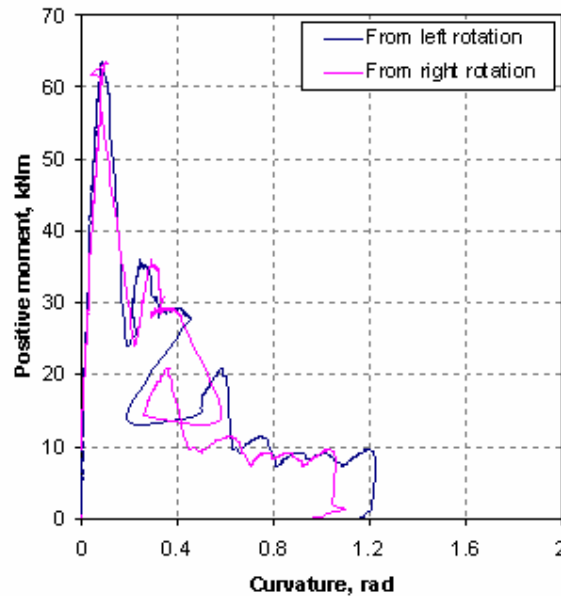
**Figure 5.28** Compressive stress-strain curve of railseat positive moment test



**Figure 5.29** Tensile stress-strain curve of railseat positive moment test

### 5.3.5 Mode of failure

Interestingly, visible vertical cracks due to pure bending initially occurred at surfaces of the sleeper's rail seat about 240 kN load. However, the concrete sleeper failed due to deficient shear strength at the ultimate load of 583 kN, which allows nearly 7 mm deflection at rail seat centre. At this ultimate state, the sleeper absorbed energy of about 2,000 J. Some diagonal shear cracks initiated at 525 kN load and dominated until the sleeper failed. It can be seen that the failure mode is of shear-bending damage. The detailed post-failure mechanisms will be discussed in Section 5.3.6. Moment-curvature of concrete sleeper at rail seat section can be approximated from the end rotations as shown in Figure 5.30. The moment curvature relations were promising during the pre-failure stage.

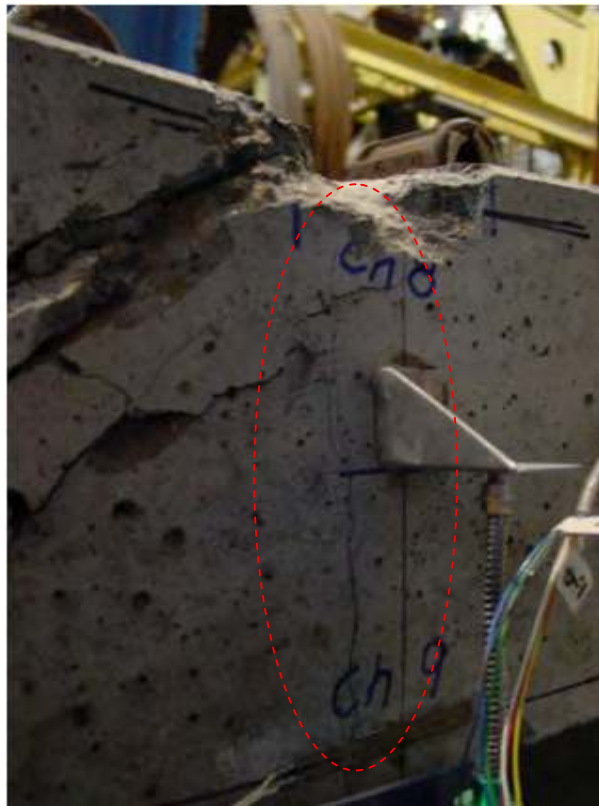


**Figure 5.30** Moment-curvature relation of positive rail seat section – End rotations

### 5.3.6 Post-failure mechanisms and crack propagation

In this later test, the first crack during the test was a flexural crack appearing close to the centre between loading lines, see Figure 5.31. However, as the load was increased, the flexure cracks formed further slightly. The cracks were initiated at the base of the sleeper and propagated towards the compressive zone beneath the applied load. The sleeper did not show any visible shear cracks prior to the imminent load of 580 kN. When the load reached the maximum at 580 kN, the sleeper seemed to have a sudden brittle failure from shear diagonal crush and spalling of concrete along the diagonal crack without any appreciable deflection warning as seen in Figure 5.32. The ultimate vertical displacement of sleeper at rail seat is nearly 7 mm. At ultimate failure, the prestressing wires were observed and found little yielding of few wires but no damage of any wires, see Figure 5.33. Shear-bending failure is considered suitable for this test behaviour of the positive rail seat moment test. The major shear diagonal failure occurs in the external span, which coincides with the maximum shear force. After the sleeper was damaged, the loading has been applied further to evaluate the residual strength and post-failure behaviours. The concrete crush was removed as shown in Figure 5.34. It was noticed that the wires got damage one by one, until the sleeper collapsed and become unstable. Referring to the load-deflection curve (see Figure 5.35), linear

proportion between load and deflection was found at the very beginning. At failure, the large shear diagonal cracks incurred resulting in the sudden drop of load carrying capacity. After the concrete showed the brittle failure mode, the sleeper gained a bit more strength from the wires and aggregate friction. When the tensile stress of wires exceeded the rupture strength, the wires snapped individually. The crack propagation was plotted all sides (front, rear, and top view) of surface in Figure 5.36. It was found that a first set of bending cracks started at the beginning by degrees, but the remarkable diagonal cracks rapidly formed when the shear stress governed. The small longitudinal cracks along the top fibre of concrete could also be observed in the top view.



**Figure 5.31** Flexure cracks at rail seat





**Figure 5.32** Crush and spalling along diagonal crack at rail seat



**Figure 5.33** Prestressing wire inspection at rail seat

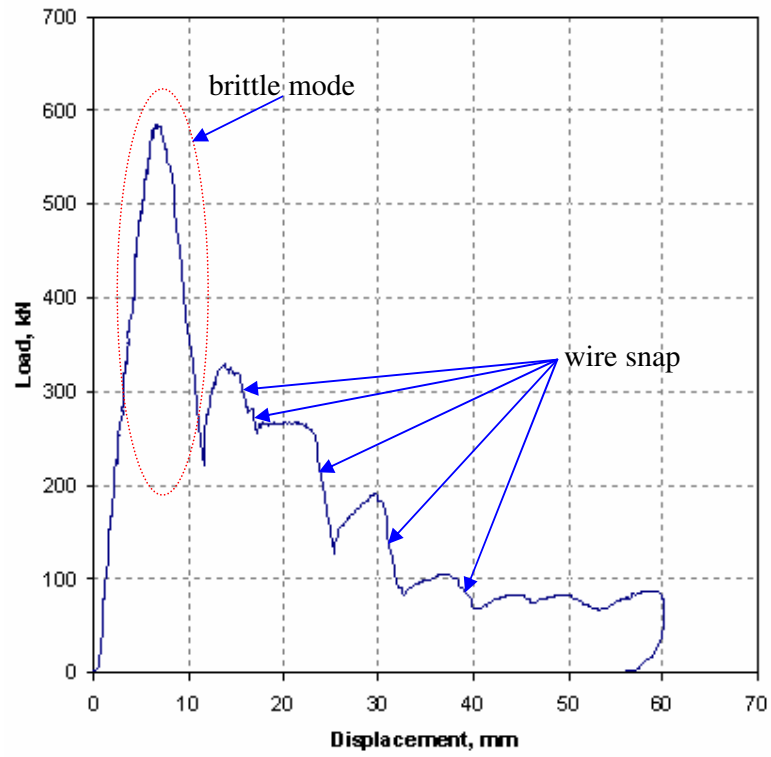


a) at applied-load rail seat



b) at another restrained rail seat (no crack found)

**Figure 5.34** Remaining concrete core at rail seat



**Figure 5.35** Load-deflection curve of rail seat positive moment test

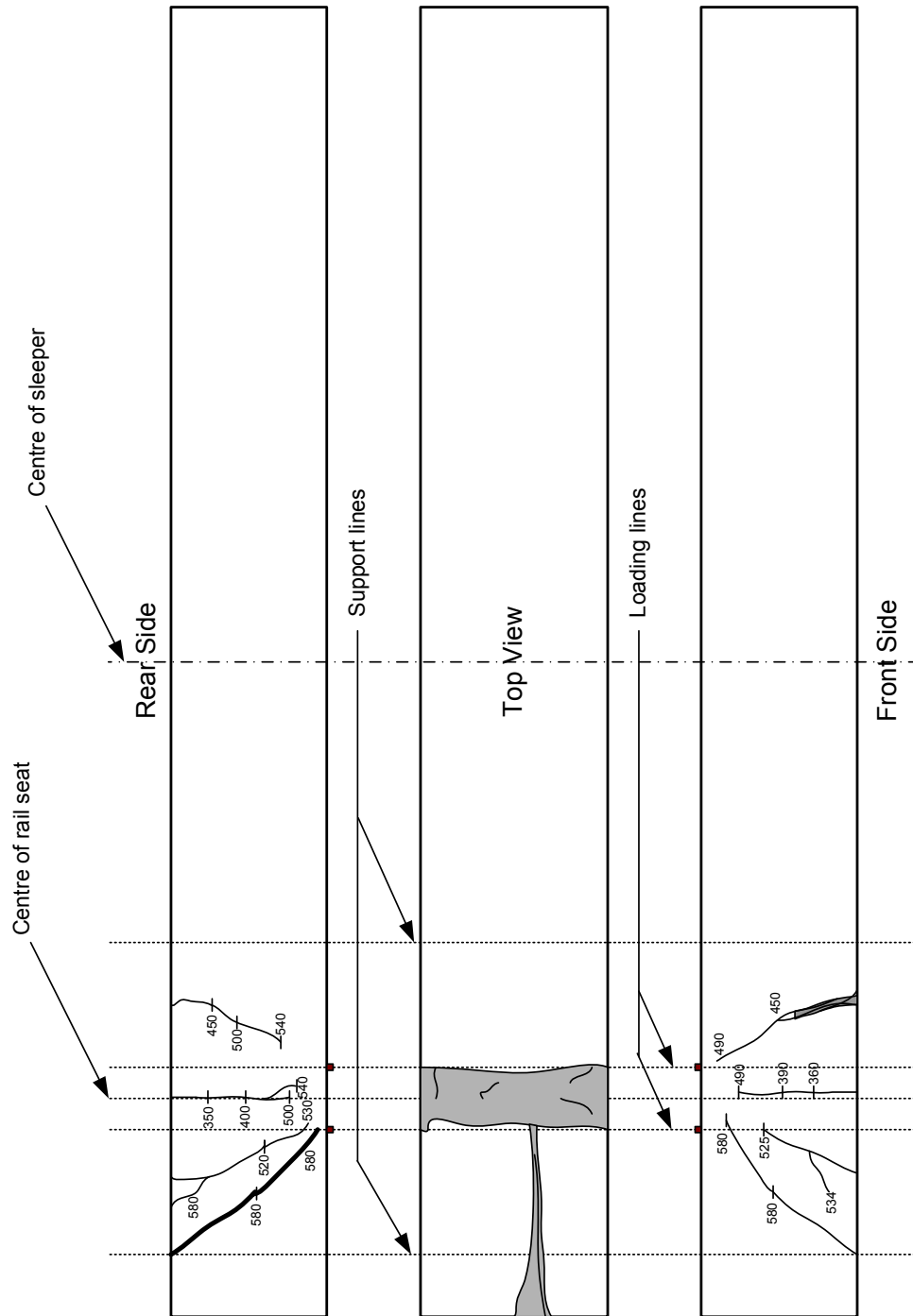


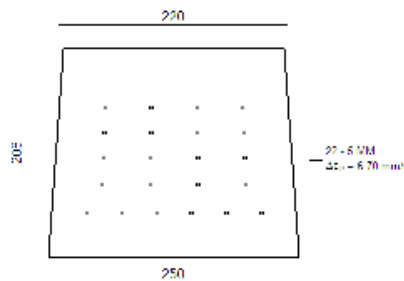
Figure 5.36 Crack pattern at railseat.

## 5.4 SECTIONAL ANALYSIS

Design and analysis of prestressed and reinforced concrete elements subject to bending require an understanding of their sectional capacity. The sectional capacity takes the stress and strain relationships under flexural moment into account. This study makes use of a computer program for sectional analysis, Response-2000, which is based on the modified compression field theory (Bentz, 2000).

### 5.4.1 Railseat section

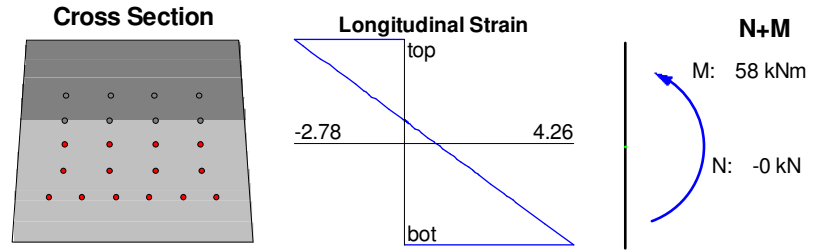
The rail seat section is presented in Figure 5.37. The cylinder compressive strength of concrete at release is 30 MPa and at 28 days is 55 MPa. The nominal prestress force per sleeper is 550 kN, or 25 kN for each wire.



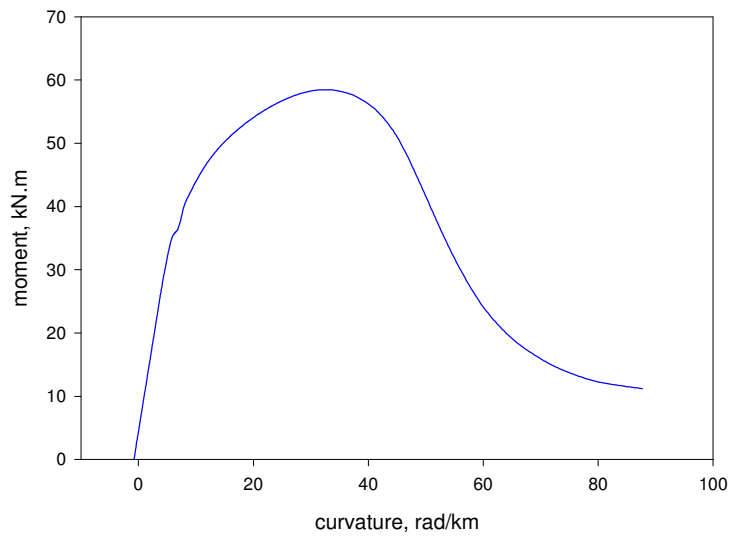
**Figure 5.37** Rail seat section of AUS-BG Sleeper

#### *a) Positive Moment Capacity*

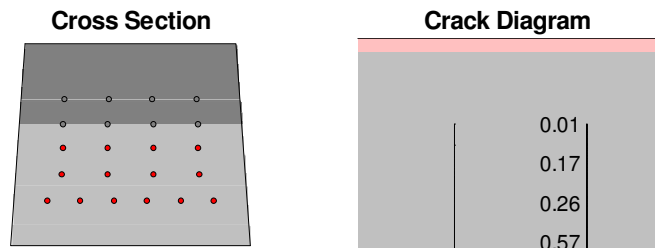
Sectional analysis of AUS-BG Sleeper for ultimate positive moment of rail seat section is shown in Figure 5.38. Figure 5.39 displays the moment curvature relationship and Figure 5.40 presents the crack width of the sleeper at ultimate load. It is found that the ultimate moment is 58 kNm, while the decompression moment is about 24.5 kNm.



**Figure 5.38** Ultimate positive behaviour of AUS-BG Sleeper at rail seat



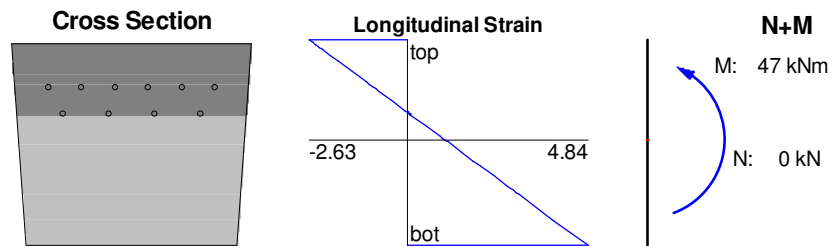
**Figure 5.39** Positive moment-curvature of rail seat section of AUS-BG Sleeper



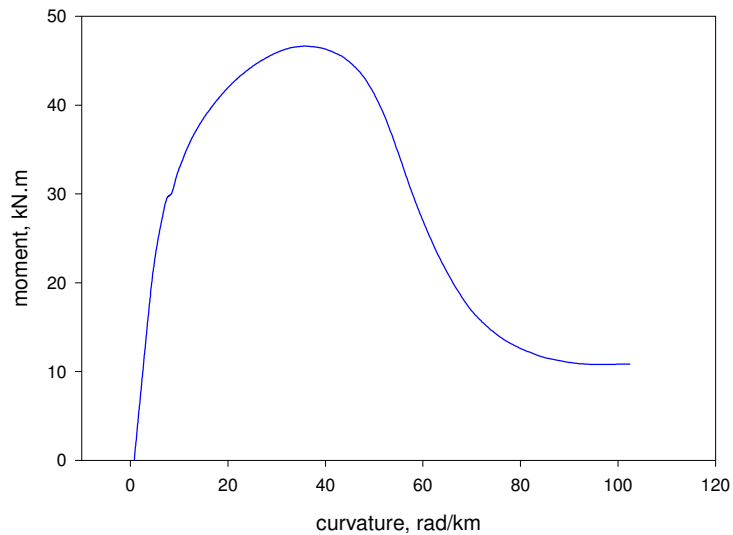
**Figure 5.40** Crack width of AUS-BG Sleeper at ultimate, positive rail seat moment

### b) Negative Moment Capacity

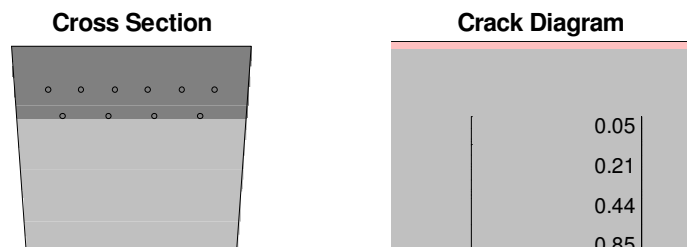
Analogously, sectional analysis of AUS-BG Sleeper for ultimate negative moment of rail seat section is shown in Figure 5.41. Figure 5.42 displays the moment curvature relationship and Figure 5.43 presents the crack width of the sleeper at ultimate load. It is found that the ultimate negative moment is 47 kNm, while the decompression moment is about 15.5 kNm.



**Figure 5.41** Ultimate negative behaviour of AUS-BG Sleeper at rail seat



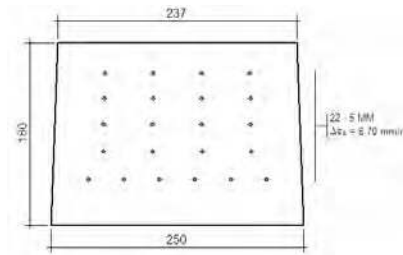
**Figure 5.42** Negative moment-curvature of rail seat section of AUS-BG Sleeper



**Figure 5.43** Crack width of AUS-BG Sleeper at ultimate, negative rail seat moment.

### 5.4.2 Mid-span section

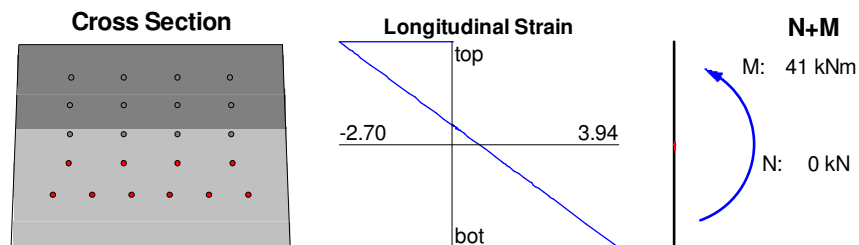
The middle section is displayed in Figure 5.44. The cylinder compressive strength of concrete at release is 30 MPa and at 28 days is 55 MPa. The nominal prestress force per sleeper is 550 kN, or 25 kN for each wire.



**Figure 5.44** Middle section of AUSTRAK broad gauge Sleeper

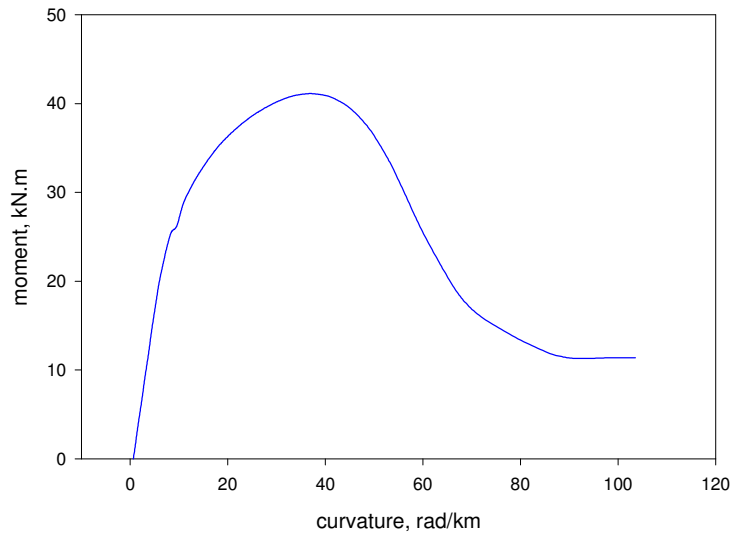
#### a) Positive Moment Capacity

Sectional analysis of AUS-BG Sleeper for ultimate positive moment of middle section is shown in Figure 5.45. Figure 5.46 displays the moment curvature relationship and Figure 5.47 presents the crack width of the sleeper at ultimate load. It is found that the ultimate moment is 41 kNm, while the decompression moment is about 15 kNm.

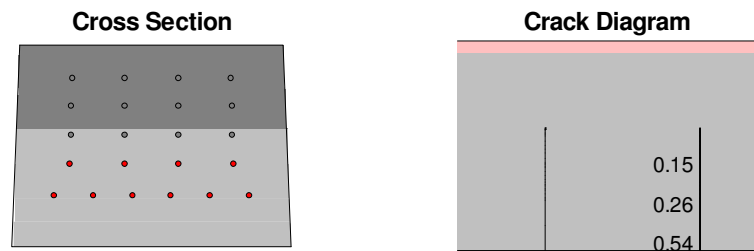


**Figure 5.45** Ultimate positive behaviour of AUS-BG Sleeper at centre





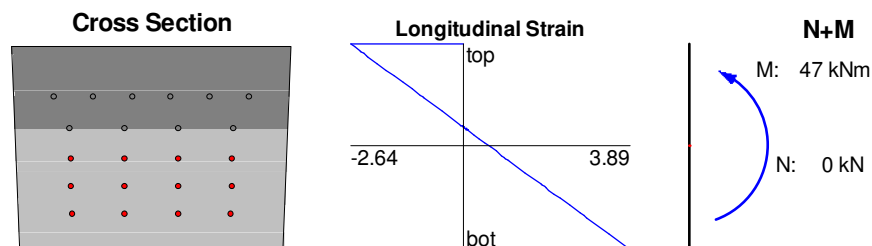
**Figure 5.46** Positive moment-curvature of middle section of AUS-BG Sleeper



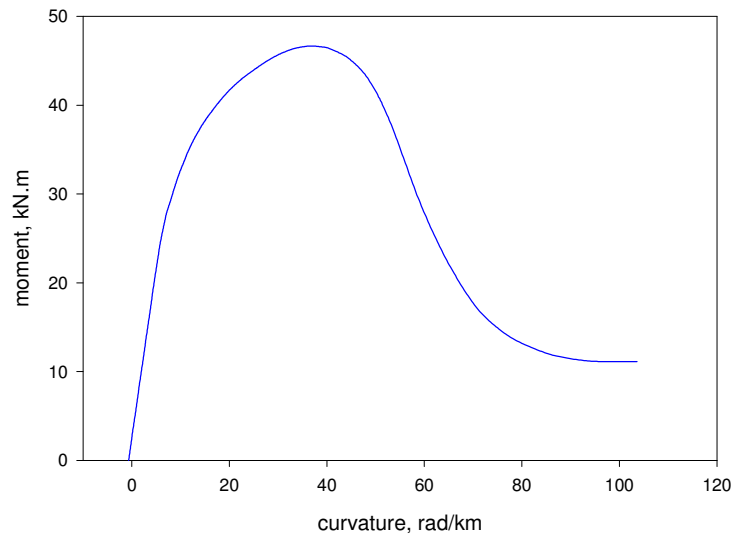
**Figure 5.47** Crack width of AUS-BG Sleeper at ultimate, positive centre moment

*b) Negative Moment Capacity*

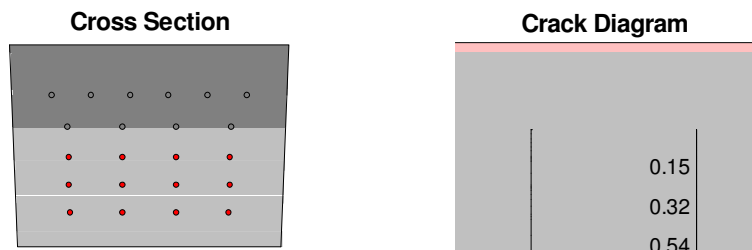
Analogously, sectional analysis of AUS-BG Sleeper for ultimate negative moment of middle section is shown in Figure 5.48. Figure 5.49 displays the moment curvature relationship and Figure 5.50 presents the crack width of the sleeper at ultimate load. It is found that the ultimate negative moment is 47 kNm, while the decompression moment is about 19 kNm.



**Figure 5.48** Ultimate negative behaviour of AUS-BG Sleeper at centre



**Figure 5.49** Negative moment-curvature of middle section of AUS-BG Sleeper



**Figure 5.50** Crack width of AUS-BG Sleeper at ultimate, negative centre moment.

## 5.5 SUMMARY

Railway sleeper is a fundamental part of railway infrastructure, in order to distribute axle loads to ground. Static behaviours of concrete sleepers are the first step to get better insight into the limit states concept of design. In this chapter, the technical procedures and testing methods for determining static performance of the prestressed concrete sleepers have also been presented. The emphases are placed on determination of maximum positive and negative bending moments of the concrete sleepers. Applying load at rail seat is the way to carry out the maximum positive moment, whilst the ultimate negative flexural moment can be found by means of pushing the sleeper at middle span in opposite direction.

According to the experiments, the failure modes, maximum loads, visualized and measured cracking loads of each section of concrete sleeper tested have been summarized in Table 5.1.

**Table 5.1** Test results of concrete sleepers

Type/Section	Experimental results			
	Visualized cracking load, kN	Measured cracking load, kN	Maximum load, kN	Failure Mode
<b>AUSTRAK Broad Gauge Sleeper</b>				
Middle	79	75	133.3	Flexure
Rail Seat	240	235	583	Shear-flexure

The sectional analyses have been conducted using Response-2000 based on modified compression field theory. The theoretical results of all sections of prestressed concrete sleepers have been achieved. The results are in very good agreement with the hand calculation based on general prestressed concrete theory. The decompression moments are almost identical while the ultimate moments of Response-2000 are up to 10% higher than those from hand calculation. Interestingly, the design moments obtained from designers are slightly lower than calculated decompression moments, implying that the current sleepers under designed conditions behave within the elastic compressive range. According to the sectional analyses, the moment capacity of each section has been tabulated in Table 5.2. The factor of about 2.5 times decompression moment seems to attain the ultimate moment.

**Table 5.2** Prediction of static performance of concrete sleepers

Type/Section	Decompression moment, kNm		Ultimate moment, kNm	
	Positive	Negative	Positive	Negative
<b>AUSTRAK Broad Gauge Sleeper</b>				
Rail Seat	+24.5	-15.5	+58	-47
Middle	+15	-19	+41	-47

It should be noted that the prestressed concrete sleeper is designed capable of resisting the fatigue loading of more than  $10^6$  cycles (Warner et al., 1998) since the decompression moments are larger than the design moments ( $M_{design} < M_{decom}$ ), hence always keeping the whole sleeper section in elastic compressive zone during normal smooth traffics.

The comparison between the prediction from sectional analyses and the experimental results from static tests can be summarized in Table 5.3.

**Table 5.3** Experimental results of static performance of concrete sleepers

Type/Section	Cracking moment, kNm		Ultimate moment, kNm	
	Experiment	Prediction	Experiment	Prediction
Rail Seat	+25	+27	+63	+58
Middle	-24	-22	-45	-47

The experimental results from static tests give very good correlation with the sectional analysis data. Cracking moments from experimental curves are quite close to those from measured cracking ones, computed from the intersection of two initial slopes of a load-deflection curve. Flexural failure seems to govern the negative bending behaviour of the sleepers. Nevertheless, the shear diagonal failure tends to suddenly happen to the rail seat section under positive moment. Ductility of sleepers can be considered fairly low.

## CHAPTER 6

### IMPACT TESTING OF PRESTRESSED CONCRETE SLEEPERS

On railway track structures, dynamic impact loads with very high magnitude but short duration are often caused by wheel or rail abnormalities such as flat wheels, dipped rails, etc. The possibility of the large impact loading to cause an extreme failure to an in-situ concrete sleeper could be very low about once or twice in the design life cycle. However, until now, the behaviour of the in-situ prestressed concrete sleepers under the severe impact loading has not been well comprehended. A high-capacity drop-weight impact testing machine was thus constructed at the University of Wollongong, in order to evaluate impulsive resistance of prestressed concrete sleepers under impact loads. This chapter describes the details of the high-capacity impact testing machine, as well as the instrumentation, flexural toughness, and energy absorption mechanisms for railway prestressed concrete sleepers. The impact tests were carried out using the prestressed concrete sleepers manufactured in Australia. A track test bed was simulated in laboratory and calibrated against the frequency response functions obtained from the experimental modal analysis. Simulation of impact loads, similar to the wheel impact loads, in the laboratory conditions is also discussed.

#### 6.1 OVERVIEW

It is believed, based on the industry experience, that prestressed concrete sleepers have reserves of strength that are untapped. It is thus important to ascertain the spectrum and amplitudes of forces applied to the railway track, to understand more clearly the manner in which track components respond to those forces, and to clarify the processes whereby concrete sleepers in particular carry those actions. In addition, cracks in concrete sleepers have been visually observed by many railway organizations, including the field trials. As noted in a review report (Murray and Cai, 1998), the principal cause of cracking is the infrequent but high-magnitude wheel loads produced by a small percentage of “bad” wheels or railhead surface defects. Those loads are of short duration but of very high magnitude. As an example, the typical loading duration

produced by the wheel flats could vary between 1 and 10 msec, while the force magnitude could reach up to 600 kN per rail seat. Existing design philosophy for prestressed concrete sleepers is based on the allowable stress principle taking into account only the quasi-static wheel loads, which results in overly conservative design for concrete sleepers (Remennikov and Kaewunruen, 2007). Limit states design concept, which considers the probabilistic dynamic loading condition, is a more logical entity for development of the new design approach for prestressed concrete sleepers. Current knowledge is insufficient so as to constitute the new limit states design concept. The research tasks are required to perform fundamental studies of the loading conditions, the static behaviour, the dynamic response, and the impact resistance of the prestressed concrete sleepers (Remennikov and Kaewunruen, 2007). A major research effort at the University of Wollongong is to evaluate the ultimate capacities of concrete sleepers under static and impact loads.

The emphasis of this chapter is placed on the experimental verification of the ultimate impact resistance and failure modes of railway prestressed concrete sleepers. The prestressed concrete sleepers used were designed in accordance with Australian Standard: AS1085.14 (Standards Australia, 2003). The support condition provided by the track was simulated using multiple layers of resilient material and validated against the in-field and laboratory vibration measurements.

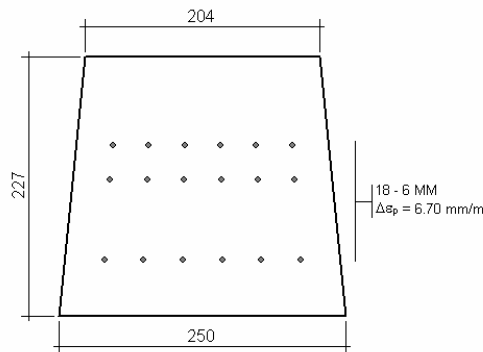
## **6.2 TEST SPECIMENS**

The prestressed concrete sleepers were supplied by an Australian manufacturer, under a collaborative research project of the Australian Cooperative Research Centre for Railway Engineering and Technologies (Rail CRC). The typical prestressed concrete sleepers, which are often used in broad gauge tracks, were selected for these tests. The dimensions and shape of the prestressed concrete sleeper are shown in Table 6.1. High strength concrete material was used to cast the prestressed concrete sleepers, with the characteristic compressive strength at 28 days of 55 MPa, and the prestressing steel wires were made from high strength steel with the rupture strength of 1860 MPa. The cored samples, drilled from the sleepers, were taken to confirm the material properties of the tested concrete sleepers, in accordance to the Australian Standard AS1012.14 (Standards Australia, 1991). The average compressive strength of concrete at the test

age of about two years was 80 MPa. It is believed that the high strength steel prestressing wires are of high quality and the strength will not change during time in service. Cross section of the prestressed concrete sleepers at railseat can be seen in Figure 6.1.

**Table 6.1.** Dimensions and masses of the test sleepers (Austrak Broad Gauge Sleeper)

Mass (kg)	Gauge length (m)	Total length (m)	At railseat (m)		At centre (m)	
			width	depth	width	depth
299.5	1.60	2.85	0.22	0.21	0.22	0.18



**Figure 6.1** Cross sectional area of the test specimens

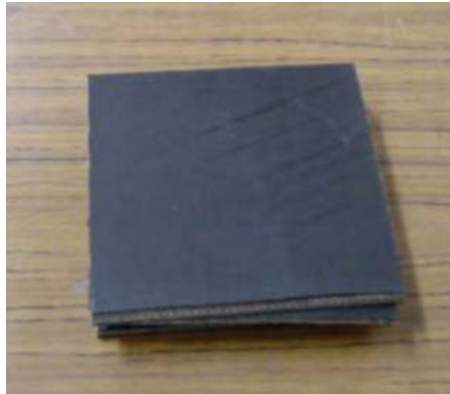
### 6.3 SUPPORT CONDITIONS

In real track, a sleeper is supported by a layer of loose, coarse, granular materials with high internal friction, so-called 'ballast'. It is often a mix of crushed stone, gravel, and crushed gravel through a specific particle size distribution. Using a typical ballast bed leads to difficulties in controlling the boundary conditions in either the experiments or the numerical simulations. To equally distribute supporting pressures underneath the sleepers' soffit, to retain strength after multiple high-velocity impact blows, and to re-arrange the test setup, an alternative approach that uses polymeric materials (or '*rubber mat*') to replace the real ballast has been adopted for a specific use in Australian Standard, AS1085.19J (Standards Australia, 2001).

### 6.3.1 Alternative support

Railway ballast plays a vital role in ballasted railway tracks as it provides the support to the railway superstructure and redistributes train/track loads from railway sleepers to the track subgrade. The ballast is made of loose, coarse, granular materials with high internal friction. It is often a mix of crushed stone, gravel, and crushed gravel through a specific particle size distribution. Studies of impact responses of railway track components have been extensively carried out both computationally and experimentally at the University of Wollongong, Australia. Computer modeling of track assembly has been developed for use in the validations of predicted responses of such track components, in particular the railway sleepers. An appropriate way to make possible the verifications between those results is to devise laboratory setups, which are identical to the models. Using a characteristic ballast bed leads to difficulties in controlling the boundary conditions in either the experiments or the numerical simulations, to equally distribute supporting pressures underneath the sleepers' soffit, to retain strength after multiple high-velocity impact blows, and to re-arrange the test setup. An alternative method referred to as '*alternative support procedure*' using polymeric materials (hereafter called '*rubber mat*') to replace the real ballast has been adopted for a specific use in Australian Standard, AS1085.19J (2001). It states that when the support is subjected to an increase in static load from 50 kN to 60 kN at a railseat, it shall allow a vertical displacement between 0.1 mm and 0.5 mm (inclusive). Experimental modal testing technique was chosen for the simulation of the optimum parameters of the alternative supporting structure for concrete sleepers. Modal testing gives the modal data in terms of natural frequencies, damping constants, and corresponding mode shapes of a system. These data are extracted from frequency response functions (FRFs) obtained from instrumented impact hammer tests and can be used for the formulation of a dynamic model of the railway track system.

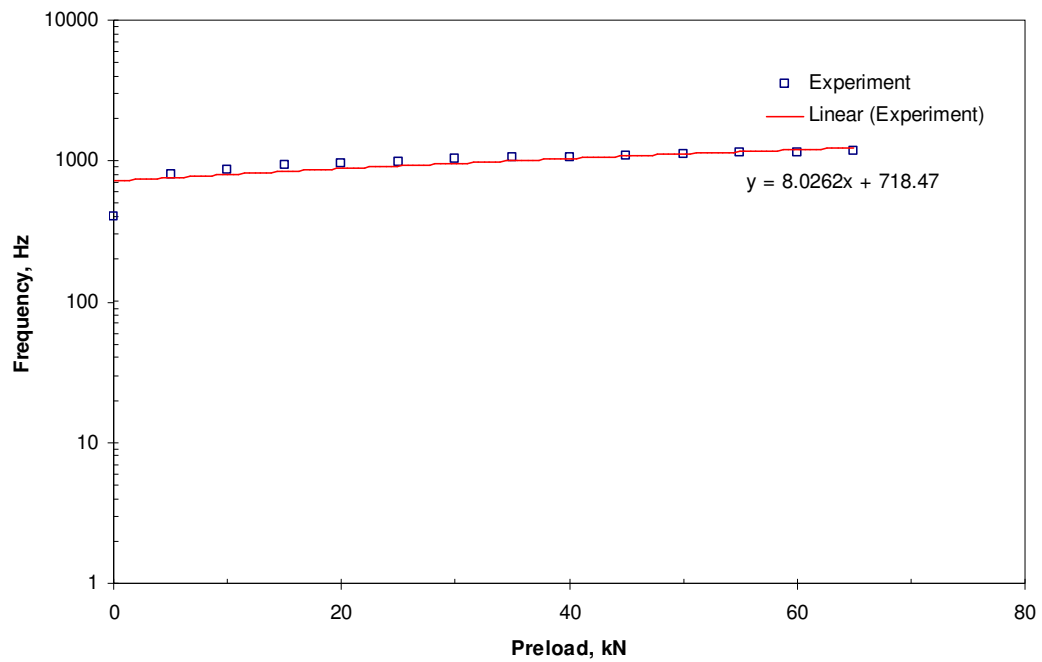




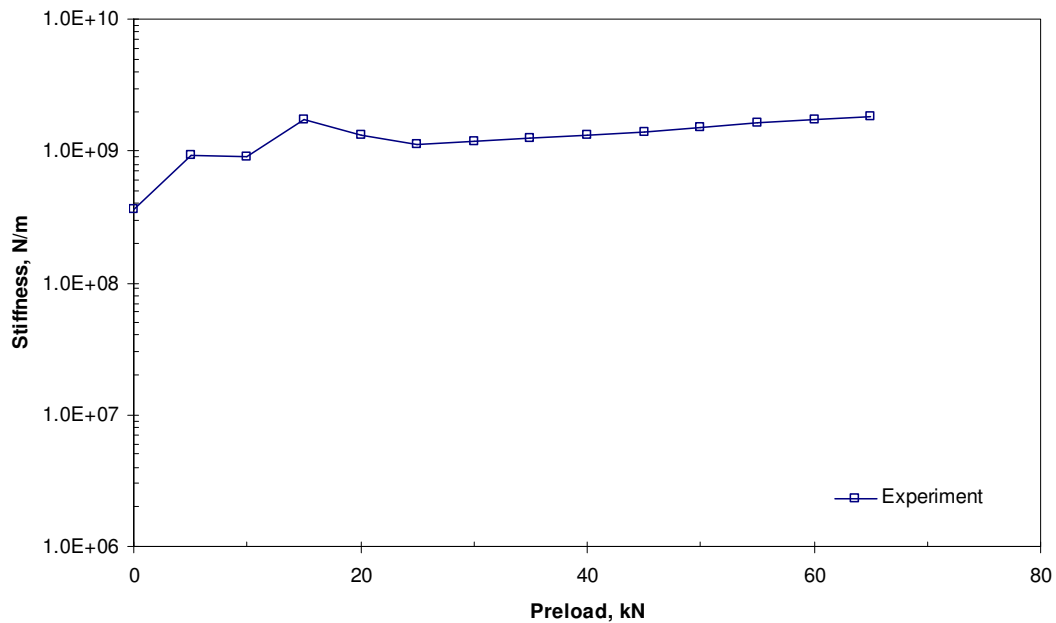
**Figure 6.2** Conveying belt used in mining processes

### 6.3.2 Test sample

A variety of rubber materials were selected and tested. The preliminary tests involved load-deflection analysis to meet the Australian Standard (AS1085.19J-2001). A universal testing machine instron was used to apply compression uniformly over the area of the rubber pieces (150x150 mm), and to develop the load-deflection curves. Several types of rubber materials were evaluated for their properties but only the conveying belt provided satisfactory results. It was found that the conveying belts used in the mining industry (see Figure 6.2) provide very good resistance to static loading. Under static preloads, the conveying belt performs very well in terms of dynamic properties. Modal testing was performed and the modal data was extracted using an optimisation algorithm. The experimental procedures and analytical formulations can be found in Chapter 3. Figure 6.3 shows the dynamic properties of a single-layer conveying belt: a) natural frequency; b) dynamic stiffness; and c) damping factor. The modal data reflect the consistently high stiffness of the material under preloads. Based on the current data obtained from available types of rubber materials, the conveying belt was selected for the use as an alternative support (so-called ‘rubber mat’). Subsequently, in order to simulate variable support conditions for concrete sleepers, the best mix of varying the number of layers of the conveying belts was the main challenge in this investigation.

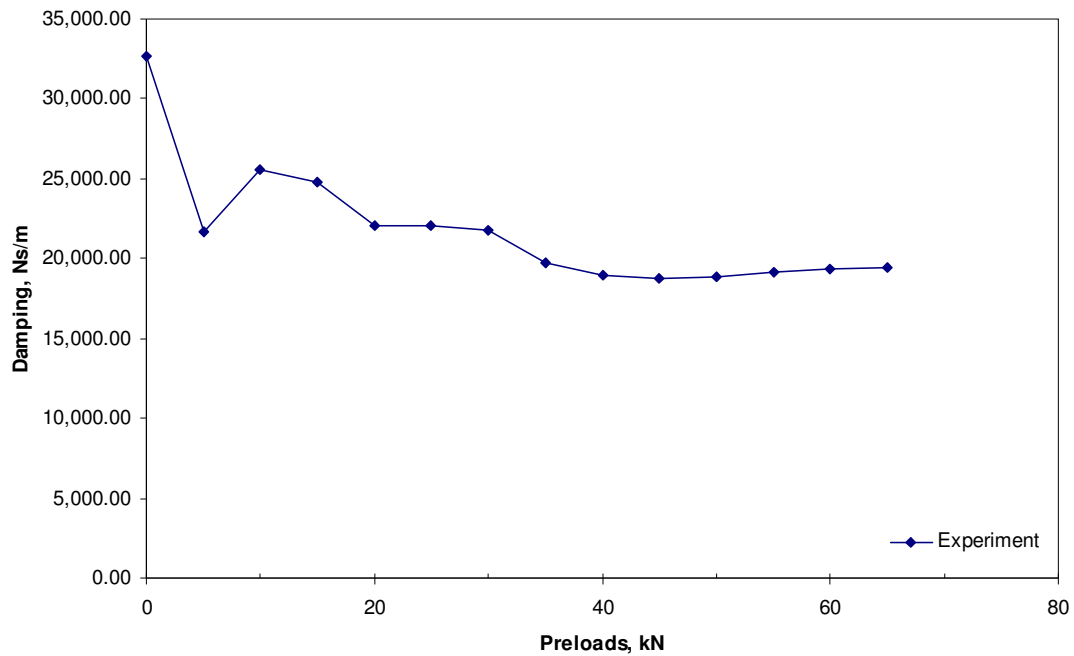


a) natural frequency vs. preload



b) dynamic stiffness vs. preload

**Figure 6.3** Dynamic properties of a single-layer conveying belt: a) natural frequency; b) dynamic stiffness; and c) damping factor



c) damping factor vs. preload

**Figure 6.3** Dynamic properties of a single-layer conveying belt: a) natural frequency; b) dynamic stiffness; and c) damping factor

### 6.3.3 Load-displacement analysis

The rubber mat was arranged for the proper size close to the area of the railseat (150x150 mm). The universal testing machine was used to apply compression to rubber specimens with varying numbers of layers of the rubber mat, from one to six layers. Since the stiffness of a single layer of the conveying belt is very high as described in Figure 6.3(b), the series arrangement of rubber mats lowers the flexibility of the whole

system like a series of springs ( $\frac{1}{k_{total}} = \frac{1}{k_1} + \frac{1}{k_2} + \dots$ ), where  $k_{total}$  is the stiffness of

combined system,  $k_i$  is the stiffness of the  $i^{\text{th}}$  layer. Figure 6.4 depicts the load-deflection test setups for a) two layers and b) six layers of rubber mat. The load deflection curves are presented in Figure 6.5. It is found that six layers of the rubber mat fit the strength requirement of the alternative support prescribed in the Australian Standard (2003). The inclusive vertical displacement under a load increment between 50 kN and 60 kN is 0.15 mm. The energy absorption and dissipation capacities of the different mixes of the

rubber mat are tabulated in Table 6.2. It is found that six layers of the rubber mat provide the largest energy dissipation or about 15 times that of a single layer. The six-layer mix was also found to be more suitable for the impact test setup at the University of Wollongong. From these test data, it was determined that 6 layers of the rubber mat make it possible to replicate the ballast as an alternative support for experimentation purposes.

**Table 6.2.** Energy absorption and dissipation capacities of rubber mat

Number of Layers	Energy Absorption	Energy Dissipation
	kN-mm	kN-mm
1	8.10	1.04
2	15.2	5.92
3	20.5	7.90
4	27.3	11.3
5	33.2	13.6
6	39.8	15.7

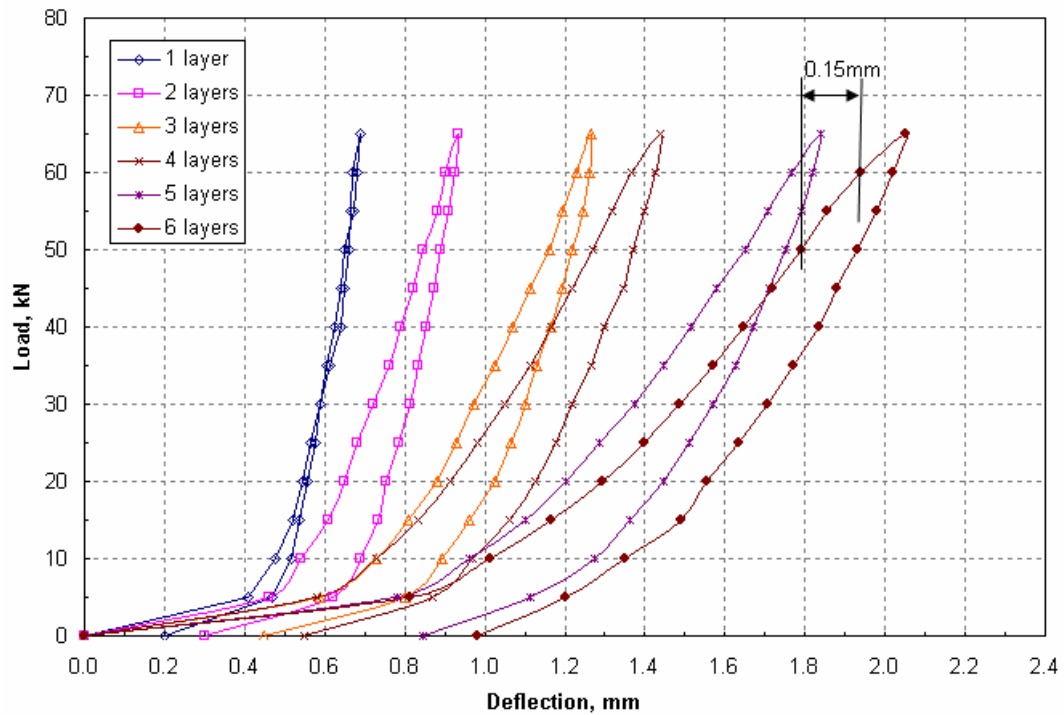


a) two layers



b) six layers of the rubber mat

**Figure 6.4** Load-deflection test setups



**Figure 6.5** Load-deflection curves of rubber mat

### 6.3.4 2DOF modal analysis

An efficient way to evaluate and monitor the track stiffness was developed and widely accepted, based on the method of 2DOF assembly. In this methodology, the rail and sleeper were considered as rigid masses with the ballast and rail pad as the spring-dashpot elements. Application of this theory was also adopted for railway ballast replication. An assembly of rail, rail pad, and sleeper block with known properties, as well as a predetermined ballast bed was built up for previous studies. Figure 6.6a) shows the assembly for 2DOF tests, Figure 6.6b) shows the rubber mat (six layers), and Figure 6.6c) shows the ballast bed test box. The experimental demonstrations have been presented in this chapter for four cases: 1) when the assembly is laid on a single layer of rubber mat; 2) when the assembly is on three layers; 3) when the assembly is on six layers (best mix); and 4) when the assembly is on the ballast bed.



a) assembly for 2DOF tests

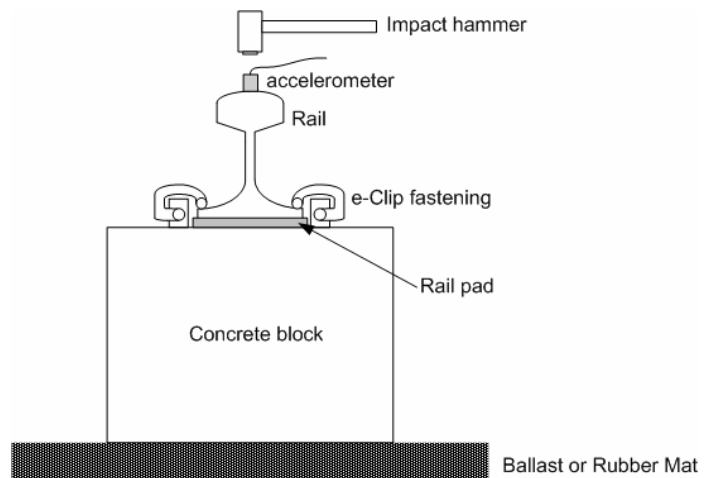


b) rubber mat



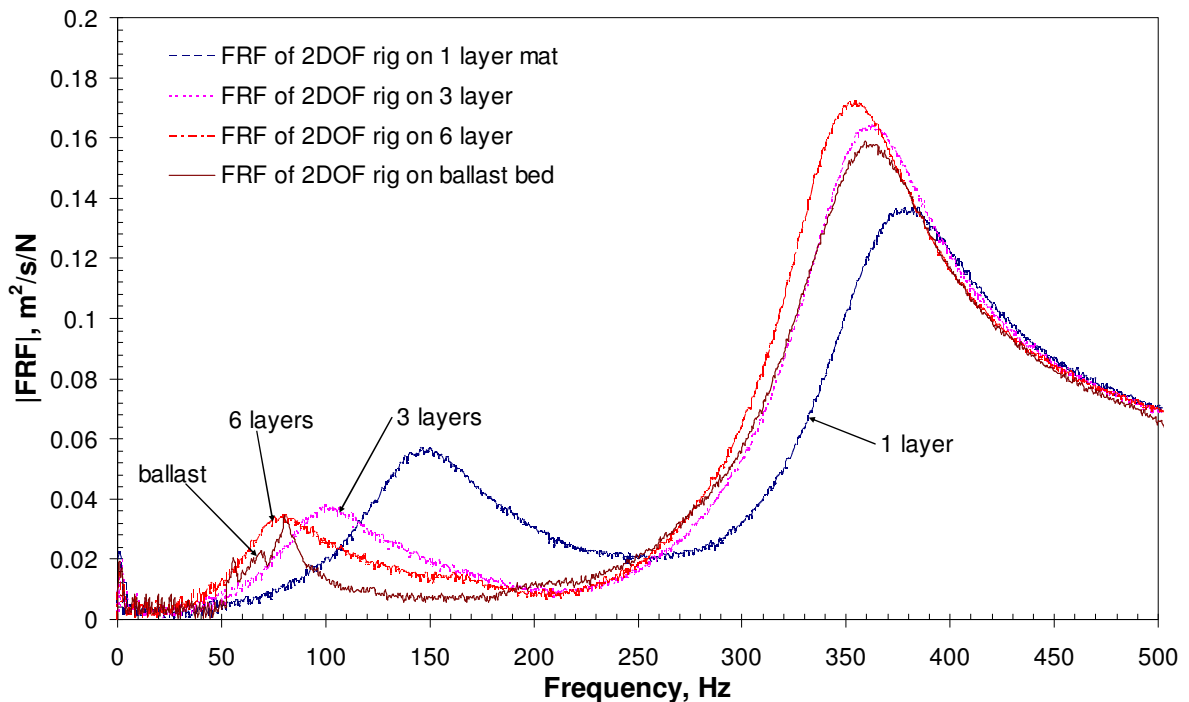
c) ballast bed test box

**Figure 6.6** Experimental rigs



**Figure 6.7** Schematic test setup for 2DOF modal testing

To measure the vibration response of the track assembly, an accelerometer was attached to the top surface of the railhead, as illustrated in Figure 6.7. The railhead was impacted vertically with an instrumented hammer and the measurements were taken within a frequency range of 0–800 Hz. The FRF was then measured by the Bruel&Kjaer PULSE modal testing system, which was connected to a computer. Measurement records also extended to the impact forcing function and the coherence function. It is known that the FRFs describe the modal parameters of the vibrating rail system. Figure 6.8 presents the FRFs of those experimental demonstrations. It is noticed from the magnitudes and resonance frequencies that FRFs in the cases of 3 and 6 layers lie fairly close to the FRF in the case of the ballast bed in both resonance bands.



**Figure 6.8** Frequency response functions of 2DOF test rig under different conditions

The extraction of these dynamic properties was achieved using a curve-fitting approach as described in Chapter 3. In this approach, the FRF of the model was tuned to be as close as possible to the recorded FRF in both frequency bands around the resonant frequencies. Curve-fitting routines can be found in many general mathematical computer packages (e.g. MATLAB, Mathematica, Maple), or using specialized curve-fitting computer codes (e.g. DataFit). Based on the Fast Fourier Transform (FFT)

method, Table 6.3 gives the modal data extracted from the FRFs shown in Figure 6.8 wherein the correlation indices found are less than a 1% error. From Table 6.3, one can notice that only the stiffness and damping values of the 6-layer rubber mat match reasonably the response of the ballast bed. It can also be seen that there is a highly nonlinear relationship between the number of layers of the rubber mat and their dynamic stiffness, whereas only a little effect on damping factors can be noticed.

**Table 6.3.** Modal data of rubber mat using 2DOF test assembly

Number of Layers	Stiffness (kN/mm)	Damping (Ns/mm)
1	97.1	23.1
3	33.9	21.3
6	17.5	16.6
ballast bed	10.0	25.8

### 6.3.5 MDOF modal analysis

The track test bed was constructed earlier as shown in Figure 6.6(c) in order to investigate the full-scale dynamic sleeper/ballast interaction. To assess the precision and effectiveness of the rubber mat in full scale, confirmation of the MDOF modal results should be investigated. In this study, the test specimen was an Australian-manufactured prestressed concrete sleeper, as given in Table 6.1. The dimensions of the test sleeper are tabulated in Table 6.1. The experimental setups are presented in Figure 6.9: (a) on the ballast bed and (b) on the 6-layer rubber mat. The excitation points were located on the top surface of the sleeper at every 150 mm along the perimeter. It was found that the number of these positions is sufficient to represent the vibration modes of interest and the best position for mounting the accelerometer is at the end of the sleeper.





a) on ballast bed

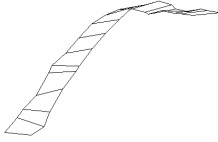
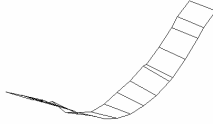
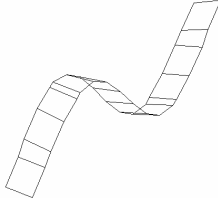
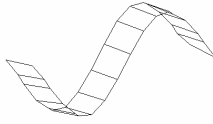
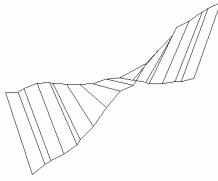
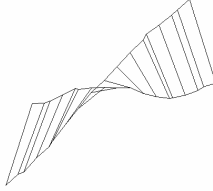
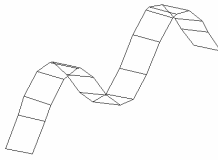
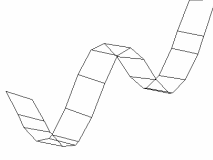
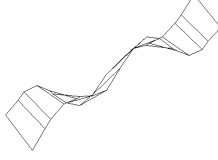
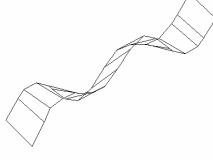
b) on 6-layer rubber mat

**Figure 6.9** Experimental setups for a) on ballast bed and b) on 6-layer rubber mat

In this study, an accelerometer had a fixed position whilst an instrumented impact hammer was roved along the excitation points. The instruments used in this study were a PCB accelerometer, the PCB impact hammer, and the Bruel&Kjaer PULSE vibration analyser. Using the hammer to excite vibrations in the sleeper over the frequency range 0 to 1600 Hz, the 10-time average vibration responses represented by the FRFs were obtained using the PULSE system. Then, processing the recorded FRFs by the STAR Modal Analysis Package gave the natural frequencies and modal damping constants of the sleeper. The first processing procedure in STAR is the geometric definition where the sleeper was modeled using wire meshes through the plane coordinates. The FRFs obtained were computed for the set of frequency spectra. The vibration peaks in the spectra were identified. Damped natural frequencies, dashpot values, and graphical corresponding mode shapes were calculated from the peaks based on peak picking and polynomial fitting analyses.

The results of the vibration tests are depicted in Table 6.4. In this table, the first five modes of vibration are presented. It can be seen clearly that the first five resonance frequencies, corresponding mode shapes, and damping coefficients are mutually consistent in both ballast and rubber mat conditions. For all conditions, the lowest frequency corresponded to the fundamental bending mode, the second frequency to the second bending mode, the third frequency to the lowest torsional mode, the fourth frequency to the third bending mode, and the fifth frequency to the second torsional mode. Of all five modes, the most significant change in natural frequencies between the ballast and rubber mat conditions was the first bending mode. The maximum discrepancy between resonant frequencies of ballast and rubber mat conditions is 15%, while the damping factor difference is about two times. It should be noted that the important frequencies of sleepers are associated with the second and third modes of flexural vibration. Under dynamic conditions, the railway sleepers tend to crack at those two resonances. Apparently, the consistencies of those resonant frequencies and damping constants between ballast and rubber mat conditions can be concluded from the MDOF modal testing.

**Table 6.4** Comparison of modal parameters of test sleeper with different support conditions

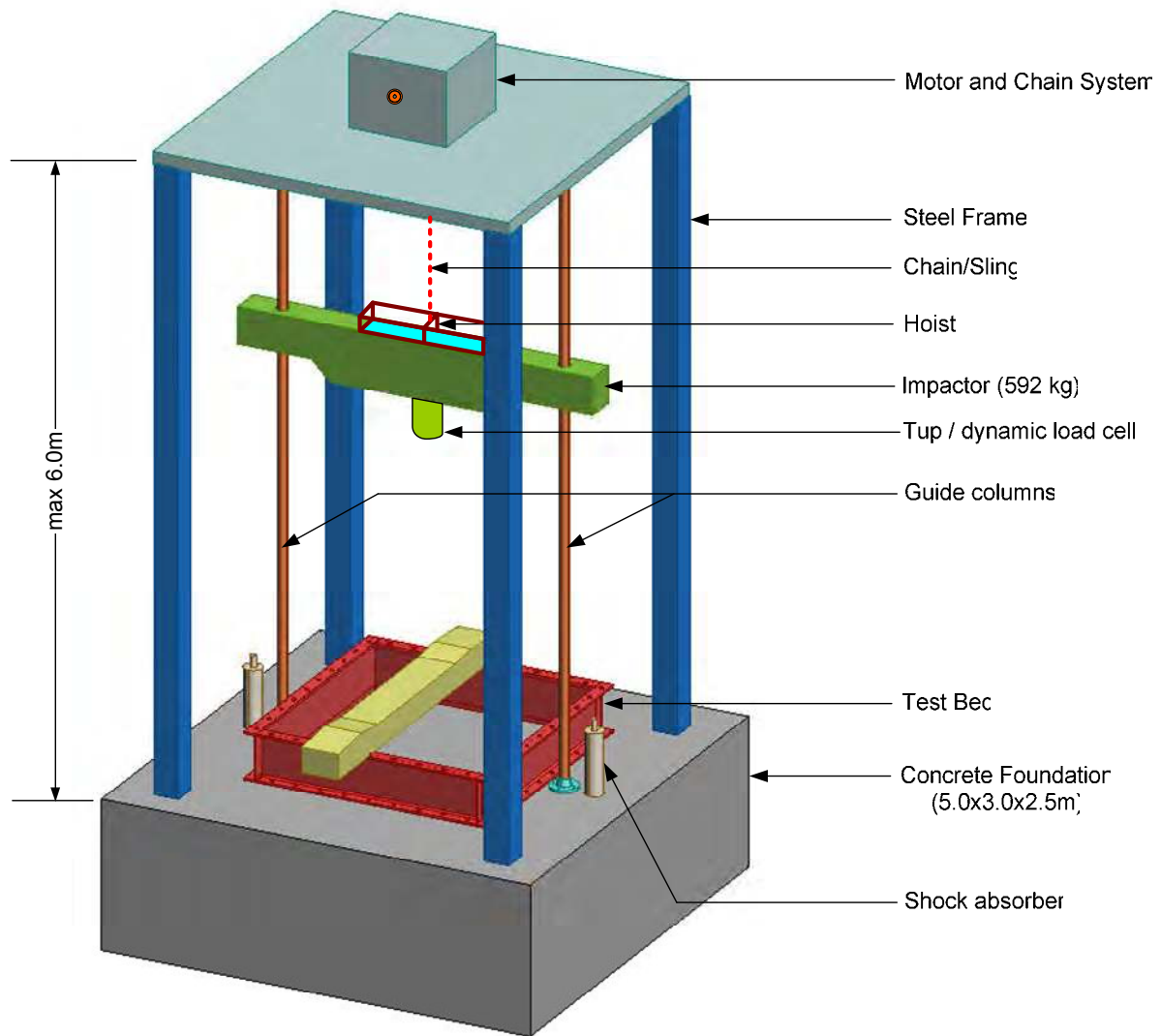
Mode	Ballast Condition		Rubber Mat Condition	
	Frequency (Hz)	Damping (%)	Frequency (Hz)	Damping (%)
1	 150.21 (1 <sup>st</sup> bending)	5.16	 177.88 (1 <sup>st</sup> bending)	12.68
2	 334.13 (2 <sup>nd</sup> bending)	5.05	 333.35 (2 <sup>nd</sup> bending)	3.04
3	 449.05 (1 <sup>st</sup> twisting)	8.05	 460.06 (1 <sup>st</sup> twisting)	4.00
4	 617.98 (3 <sup>rd</sup> bending)	3.20	 616.73 (3 <sup>rd</sup> bending)	1.85
5	 963.88 (2 <sup>nd</sup> twisting)	1.77	 959.29 (2 <sup>nd</sup> twisting)	1.08

## 6.4 IMPACT TESTING FACILITY

In this study, the drop height and drop mass were selected to simulate a typical impact load due to a wheel flat of 20-25 mm, which could generate an impact of over 600 kN. The weight of the projectile was set as 5.81 kN (592 kg), and therefore, the drop height becomes the only variable. The experimental setup thus required for specific energy absorption capacity for particular sleeper, in order to back calculating for the optimum drop height. The drop height was adjusted from a series of pre-test experiments to cause complete collapse under one blow. To eliminate surrounding noise and ground motion, the concrete sleepers were set up and placed on a strong isolated floor in the laboratory. The strong isolated floor is made of reinforced concrete using high strength concrete. The large concrete mass is of 5 x 3 x 2.5 m over a compacted sand bed and surrounded by 50 mm-thick shock absorber material. Figure 6.10 shows the construction of the strong isolated floor. The annex of steel rods each with a threaded hole was installed to provide the screw support for any universal setup in the future. For instance, at a railseat was installed the impact plate to transfer the load to the specimens and the rail was mounted to the strong floor using the thread bars at the other railseat. The roller was attached to the steel drop mass through runners guiding the descent of the drop weight hammer. This type of guiding arrangement provides very low friction during a free fall. The hammer was hoisted mechanically to the required drop height (ultimate resistance of the sleeper) and released by an electronic quick release system. The impact test rig is capable of fitting the test specimen and its fixture with a working area of 1800 x 5000 mm.



**Figure 6.10** Steel frame for the strong floor



**Figure 6.11** Schematic layout of the drop-weight impact test rig

#### 6.4.1 High-capacity drop-weight impact testing machine

The schematic of the impact testing machine is illustrated in Figure 6.11. The core of the test rig is the free-fall hammer that can be dropped from a maximum height of 6 m, or equivalent to the drop velocity up to 10 m/s. The impact load was monitored and recorded by the dynamic load cell connected to the computer. Efficiency of drop weight hammer has been obtained through the calibration tests done using high speed camera, which will be described later. It is found that due to friction of guiding runner the hammer's experimental velocity reduces to 98% of theoretical velocity ( $V_t$ ). To achieve

the prescribed impact velocity, the required drop height is adjusted by the coefficient  $(\frac{1}{0.98^2}) = 0.96$ . Based on the energy conservation theory, the relationship between the drop height ( $h$ ) and the drop velocity ( $V$ ) reads

$$0.98V = \sqrt{2gh} \quad (6.1)$$

$g$  is the gravitational acceleration ( $= 9.81 \text{ m/s}^2$ ). A series of impact tests on concrete sleepers were conducted using the same test setup as described above. A special attention was paid to the different drop heights on the prestressed concrete sleepers to achieve the different damage severity levels. The variable applied loading and strain rate can also be obtained. This experimental test rig can be used to investigate the failure and energy absorption mechanisms, impact load history (from the dynamic load cell), accelerations, and crack propagation of any engineering structure.

#### 6.4.2 Calibration of impactor using a high-speed camera

Table 6.4 presents the efficiency of the impact test rig evaluated using the high speed camera. The theoretical free falling velocity is computed from the conservation of energy. The measured free falling velocity is calculated from the moving time frames corresponding with movement of the object. The identical marks on the impactor and a reference column were calibrated to be 100 mm long. The moving time frames were captured as the mark on the impactor moves fully pass by the other mark on the reference column. Three drop tests were done at each drop height and the average drop velocity can be obtained. Tendency of the efficiency, which is gently decreased as the drop height increases, can be found. Averagely at all drop heights, the loss of the drop velocity is about only 2 percent.

**Table 6.4** Efficiency of high capacity impact testing machine

Drop height (m)	Measured free falling velocity (m/s)	Theoretical free falling velocity (m/s)	Efficiency (%)
1	4.33	4.43	97.76
2	6.12	6.26	97.70
5	9.65	9.90	97.43
average			97.62

## 6.5 TEST INSTRUMENTATION

### 6.5.1 Measurement devices

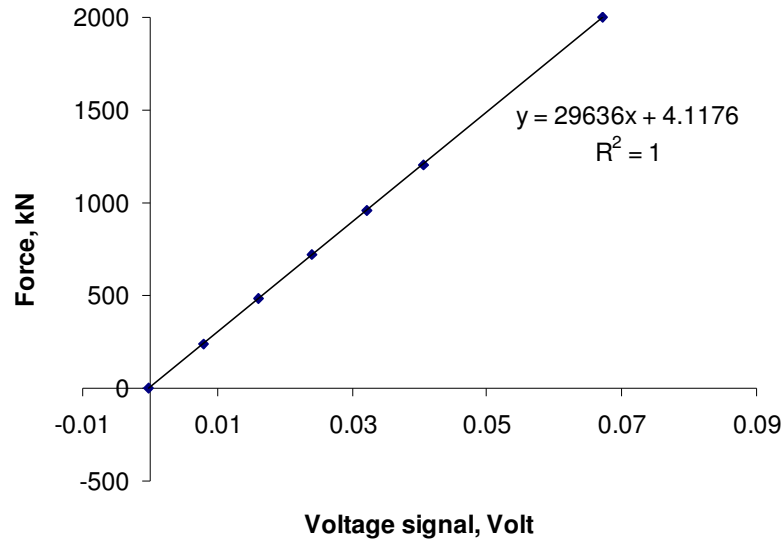
At each drop height, the measurements in an impact testing include the impact load history, the accelerations, the crack width, and the damage severity. The device for measuring the impact load history is the dynamic load cell. The accelerations were captured by using the accelerometers, and the crack width was obtained by using the magnifier glass telescope. The strain measurements were done by using the foiled strain gauges.

a) The dynamic load cell (Type Interface Model 1200)

The impact load history is the contact force between the impactor and the test specimen as the drop-weight hammer strikes the rail. It is measured by the dynamic load cell as shown in Figure 6.12. The specification of the dynamic load cell can be found in the interface website (<http://www.interfaceforce.com>). The calibration curve (as shown in Figure 6.13) was developed by using the universal testing machine in the highbay laboratory at the University of Wollongong. The maximum capacity of the dynamic load cell is as much as 1200 kN.



**Figure 6.12** 1200 kN standard high capacity load cell (<http://www.interfaceforce.com>)



**Figure 6.13** Calibration curve for the 1200 kN standard high capacity load cell



**Figure 6.14** 3200B Dytran Accelerometer (<http://www.dytran.com>)

b) The accelerometers

The piezoelectric accelerometers used in the experiments are Dytran Series 3200B quartz shock accelerometers, which are designed to measure the mechanical shock events with the amplitude of up to 10,000g (where g is the Earth's gravitational acceleration or about  $9.81 \text{ m/s}^2$ ). This series of accelerometers are the low impedance voltage mode (LIMV) instrumentation of which the output signals are in unit of mV/g. Their mounted resonant frequency is 133 kHz and the bias voltage is 8.3 VDC. Figure 6.14 shows the typical perspective of the 3200B accelerometer used. The inner body is electrically isolated from the mounting surface so as to eliminate the ground loop noise interfering with the measurements. The calibration for the accelerometers was obtained



by the manufacturer (Dytran, 2007). Table 6.5 shows the common specification of 3200B Dytran accelerometer. In this investigation, the accelerometers were installed at three positions: at railseat, at mid span, and at the end of sleeper.

**Table 6.5** Common specification of 3200B Dytran accelerometer

Specification	Value	Unit
Discharge time constant, NOM	1.0	sec
Low frequency -3db point, NOM	0.16	Hz
Low frequency -5db point, NOM	0.50	Hz
Transverse sensitivity, Max	3.0	%
Output impedance, NOM	100	Ohms
Output voltage bias, NOM	+11	VDC
Supply current range	2 to 20	mA
Compliance (supple) voltage range	+18 to +30	VDC
Operating temperature range	-60 to +250	Degree Fahrenheit
Size (Hex x Height)	3/8 x 0.64	Inches
Weight	6	Grams
Connector, top mounted	10-32	Micro-coaxial
Material, housing/connector	17-4 PH	Stainless steel
Mounting provision, 3200B/3200BT/3200BM	1/4-28/10- 32/M6 x 1.0	Integral Stud
Environmental seal	Epoxy	
Isolation, case to mounting surface	10	megOhms

c) The magnifier glass telescope

To measure an interfacial crack width, the magnifier glass telescope was employed. With a resolution of 0.1 mm, the telescope can read up to 5 mm of the crack width. The telescope focus is adjustable as to zoom in or out the concrete surface.

d) The foiled strain gauges

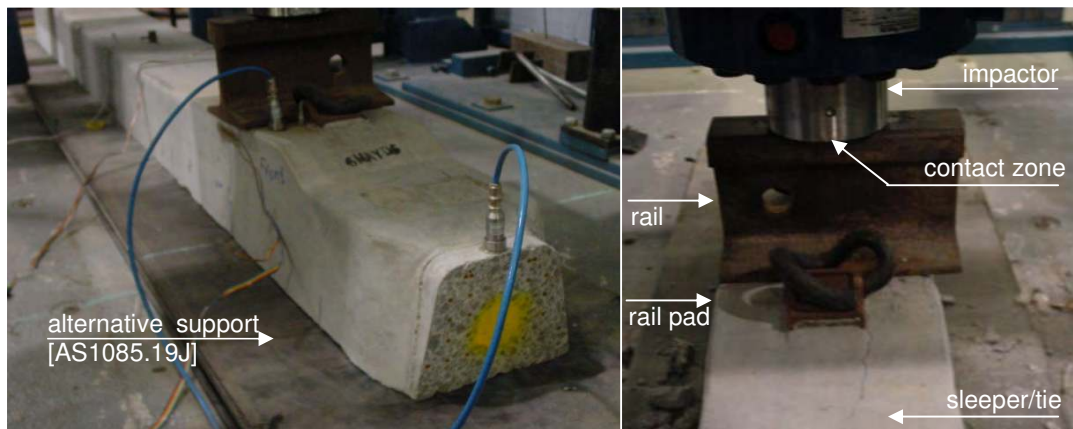
The foiled strain gauges used are the OCP series of BCM Sensor Technologies. The gauge resistance is  $120.0 \pm 0.1$  with the gauge factor of  $2.11 \pm 1.10$ . The 40 mm length of the gauge is chosen to be suitable for concrete material (porous media). The Davidson EA10 adhesive material was used in order to glue the strain gauges to the clean concrete surface. Strain measurements were focused on the top and the bottom fibres at railseat and at mid span so as to back calculate the curvature of the concrete sleeper and the resultant bending moment under impact loading.

### 6.4.2 Data acquisition system

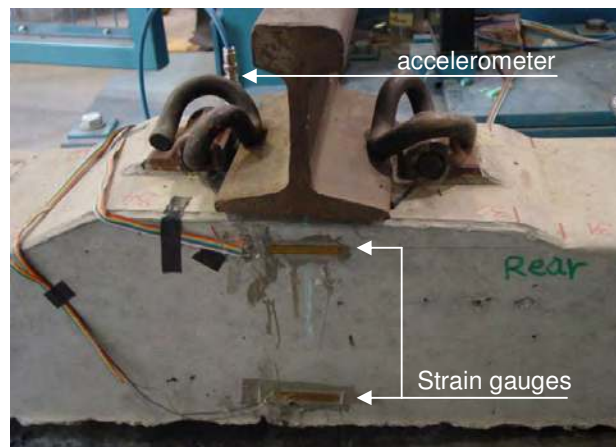
The built-in chassis with coupled SCXI and SCI channels from National Instruments were used to acquire the experimental signals from the 24-channel strain gauge unit, the 4-channel digital voltage platform, and the 8-channel acceleration box (see Figure 6.15). The data acquisition system was triggered by the impact loading signal from the freely drop-weight hammer itself during a test. Subsequently, the impact load history, the accelerations, and the strain signals can be captured. Ten-kHz low-pass filtering and the frequency ban filtering between 45 and 55 Hz were utilised. It should be noted that the instrumental chassis allow a maximum of 10-Volt signal entering to the system. Signal conditioning units were then used to decrease the high voltage signals where appropriate. LabView8 was programmed to obtain, process, analyse, and record the experimental data to a computer. Signals in voltage (e.g. impact load history and acceleration) were converted to the particular units (e.g. kN or g's) by using the calibration curves and sensitivity values of the particular device as described above. Spectral analysis feature in LabView8 can facilitate the test data in time domain transformed into frequency domain if preferred. Also, the recording mode can be selected for a specific point number or a continuous mode. Figure 6.16 shows the experimental setup for an impact test.



**Figure 6.15** National Instrument DAQ



a) in-situ condition setup



b) instrumentation

**Figure 6.16** A setup of the in-situ prestressed concrete sleeper

## 6.6 IMPACT ANALYSIS

### 6.6.1 Effect of inertia load

It should be noted that in these experiments the impact load is recorded from the tup or the dynamic load cell attached to the impactor. In addition, it is well-known that the inertia forces play a major role on the actual bending load applied to the test specimens. Therefore, the true bending load  $P_b(t)$  is the difference between the recorded impact load history  $P_i(t)$  and the generalized inertia load  $P_i(t)$ , as follows (Banthia et al, 1989).

$$P_b(t) = P_f(t) - P_i(t) \quad (6.2)$$

For any particular setup, the inertia load  $P_i(t)$  can be computed from the virtual work expression as follows.

$$P_i(t)\delta u_0 = \int m \cdot a(t)\delta u(x)dx \quad (6.3)$$

where  $a(t)$  is the acceleration along the sleeper in  $x$  direction,  $\delta u_0$  is a given virtual displacement,  $\delta u(x)$  is the generalised virtual displacement, and  $m$  is the mass per unit length of the test specimen (Banthia et al, 1989).

### 6.6.2 Energy of the impactor

Kinetic energy of the impactor during the strike on a specimen can be evaluated based on the acceleration of the drop-weight hammer,  $a_h(t)$ . The energy spent by the drop-weight hammer ( $E_h$ ) is given by (Bhattacharya et al, 2006)

$$E_h = \int M \cdot a_h(t)du \quad (6.4)$$

where  $u_t$  is the displacement at time  $t$ .

On the other hand, the potential energy ( $E_p$ ) of the drop-weight hammer at a certain height, which would be the same amount of the kinetic energy in Equation (6.4), can be read as

$$E_p = Mgh \quad (6.5)$$

where  $M$  is the drop mass (592 kg);  $g$  is 9.81 m/s<sup>2</sup>; and  $h$  is the drop height.

### 6.6.3 Energy loss in the impactor

According to Wang (1996), the energy loss in impactor ( $\Delta E$ ) due to frictions in contact zones can be calculated from the integration of impact force signal as follows.

$$\Delta E = \frac{1}{2} M \left( \left[ \frac{1}{M} \int P_f(t)dt - 0.98\sqrt{2gh} \right]^2 - 2gh(0.98)^2 \right) \quad (6.6)$$

The factor 0.98 is the efficiency of the test rig.  $M$  is the drop mass (592 kg);  $P_i(t)$  is the impulse load history;  $g$  is  $9.81 \text{ m/s}^2$ ; and  $h$  is the drop height.

#### 6.6.4 Energy absorbed by a test specimen

Virtual work done by an external force  $\delta W$  (impact load  $P$  in this case) can be written in a virtual work form as follows.

$$\delta W = P \delta u_o \quad (6.7)$$

where  $\delta u_o$  is the virtual displacement at the load point.

Based on Birch et al. (1988), the actual energy absorbed by the sleepers ( $E_A$ ) can be approximated from the multiplication between the mean plastic impact load and the displacement integrated from the acceleration responses, as follows.

$$E_A = P_{mp} u_o(t) \quad (6.8)$$

$$\text{and, } u_o(t) = \int_0^t \int_0^t \ddot{u}_o(t) dt dt \quad (6.9)$$

where  $P_{mp}$  is the mean plastic impact force (recorded from dynamic load cell). It can be obtained from the average between the maximum impact force and the summit of the elastic loading portion of impact load history. In addition,  $\ddot{u}_o(t)$  is the acceleration at the load point of time  $t$ , and  $u_o$  is a displacement at the load point of time  $t$ .

### 6.7 SIMULATION OF IMPACT LOADS

The nature of loading conditions on railway tracks is mostly of regular loading patterns due to passage of wheels of rolling stock, as described in details in Chapter 4. Dynamic forces on a railway track caused by abnormal impacts due to wheel flats, rail dips, etc. are usually highly impulsive with short durations and high frequency contents. There have been a number of investigations on the wheel/rail impacts due to wheel and rail imperfections and track abnormalities. However, the effect of railway track

environments including ballast and rail pads has yet been addressed. Intensive studies on the impact resistance of railway concrete sleepers have been conducted at the University of Wollongong, Australia. In order to understand more clearly the manner in which track components respond to those forces, and to clarify the processes whereby concrete sleepers in particular carry those actions, it is vital to ascertain the spectrum and amplitudes of forces applied to tracks. In addition, artificial impacts replicating the generic actual wheel/rail interaction must be identified, prior to investigating the shock responses of the railway concrete sleepers.

This section presents the experimental studies into the effects on dynamic loading conditions of track environments including the ballast support condition and rail pads. An assembled in-situ concrete sleeper has been constructed and subjected to artificial shock loading using a large capacity drop-weight hammer. The attempts to simulate the repeated impacts due to general wheel flats or engine burns are demonstrated so as to investigate of probabilistic impact failure of the concrete sleepers. The shock loadings under various track environments have been quantitatively monitored and recorded by National Instrument multi-channel PXI-SCXI using LabView8. These impacts could eventually lead to cracking and failure of the sleepers, and hence are important in the context of developing the new reliability-based design approach for the railway prestressed concrete sleepers.

In this investigation, the new high capacity impact machine, as depicted in Figure 6.15, has been developed to evaluate the possibility to simulate the shock loading conditions. The prestressed concrete sleepers were supplied by an Australian manufacturer, under a collaborative research project of the Australian Cooperative Research Centre for Railway Engineering and Technologies (Rail CRC). The sleepers are arranged under the actual in-situ condition, using the alternative method, in accordance with AS1085.19 (Standards Australia, 2003). To produce different shock quantity, the drop height and the softening media (to reduce contact stress) are the experimental parameters to be varied.



a) Wide perspective

**Figure 6.17** High-capacity drop-weight impact machine at the University of Wollongong



b) Close-up impactor

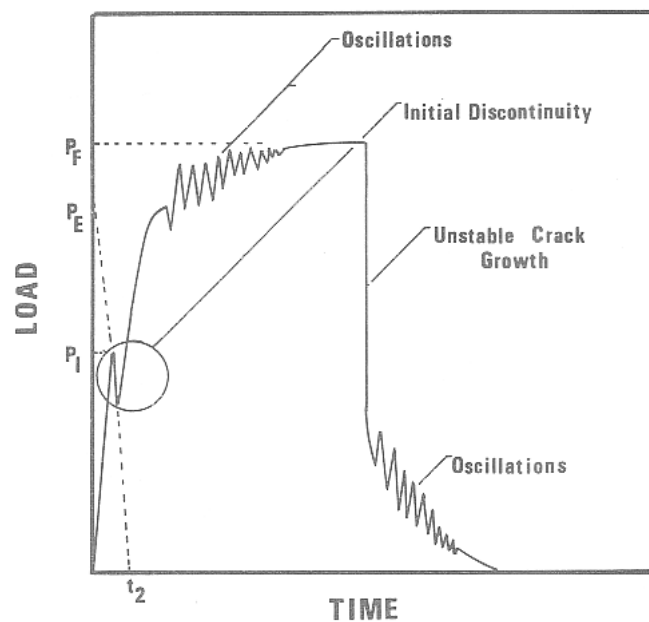
**Figure 6.17** High-capacity drop-weight impact machine at the University of Wollongong

### 6.7.1 Drop impact tests

Artificial impacts simulating actual probabilistic loads can be rendered using a free falling mass. This drop-weight technique is one such feasible option as it can be conveniently facilitated and is the economical option. Therefore, the high-capacity drop-weight impact testing machine, which is currently the largest in Australia, has been developed as depicted in Figure 6.17 (a). To eliminate surrounding noise and ground motion, the concrete sleepers were set up and placed on a strong isolated floor in the laboratory. The thick rubber mat was used to replicate the ballast support. It was found that the test setup represents the concrete sleepers in general soft track systems (Esveld, 2001; and Standards Australia 2003). To apply impact loads, the drop hammer (see Figure 6.17(b)) used has the weight of 5.81 kN. At the railseat was installed the rail with fastening system to transfer the load to the specimens. The roller was attached to the steel drop mass through runners guiding the descent of the drop weight hammer. The hammer was hoisted mechanically to the required drop heights and released by an



electronic quick release system. The core of the test rig is the free-fall hammer that can be dropped from a maximum height of 6 m, or equivalent to the maximum drop velocity of 10 m/s. The impact load was monitored and recorded by the dynamic load cell connected to the computer. Table 6.6 shows the experimental programs to investigate the effects on the impact load characteristics of drop height, track environment, and contact stress. The drop heights were varied between 0.1 m and 0.8 m. The rail pad used in the test setup is the HDPE type. Two different support conditions represent the real 'hard' and 'soft' tracks in practice. It is important to note that the effect of inertia forces plays a vital role on the impact loading history (Saxton, et al., 1974). The schematic of load-time history for a tough material is presented in Figure 6.18.



**Figure 6.18** Schematic impact load history for a tough material (Saxton, et al., 1974); time  $t_2$  results from a linear extrapolation.

**Table 6.6** Experimental programs for impact load duplication

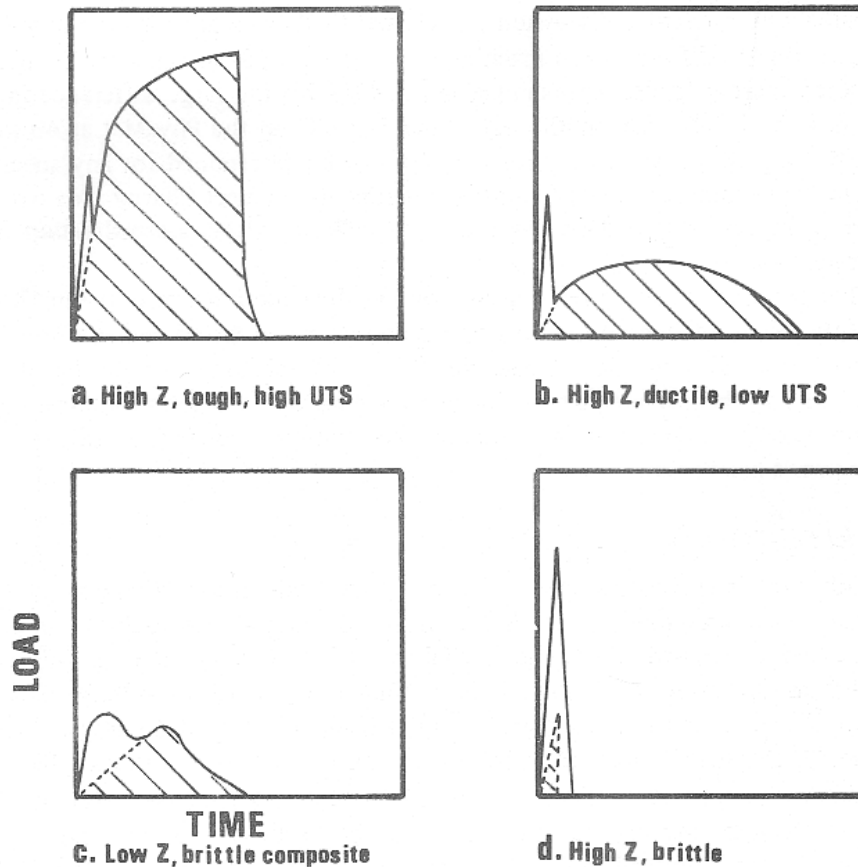
No	Drop height (m)	Use of rail pad [Y: yes; N: no]	Support condition	Use of softening media
1	0.2, 0.4, 0.6, 0.8	Y	Soft	direct contact 1mm neoprene 2mm neoprene 3mm neoprene
2/3	0.2, 0.4	Y/N	Soft	direct contact 1mm neoprene 2mm neoprene 3mm neoprene
4/5	0.2, 0.4	Y/N	Hard	direct contact 1mm neoprene 2mm neoprene 3mm neoprene

In general, the impact load history as shown in Figure 6.18 is the superposition between the inertial force and the bending resistance action during the impulsive event (Wang, 1996). The inertial force is the rapid, short peak of impact due to the striking drop mass on the contact zone. The inertial force increases and then decreases quickly as the velocity of the test specimen increases. The oscillations at the beginning of the impact load history also caused by the elastic strain energy in the impactor (tup), resulting in the impact stress wave. Saxton, et al. (1974) identified the typical load history and the true mechanical load (bending resistance load) as illustrated in Figure 6.19. In the interpretation,  $Z$  is the mechanical or acoustical impedance of the test specimen, which reads (Wang, 1996)

$$Z = c\rho = \sqrt{\frac{E}{\rho}} \cdot \rho = \sqrt{E\rho} \quad (6.10)$$

where  $c$  is the speed of elastic wave propagation (dilation sound speed),  $\rho$  is the density and  $E$  is the elastic modulus of the test specimen. From Figure 6.19, the contribution of the inertia force represents the first sharp peak of the impact load history, while the cross-hatched area is the true mechanical resistance response of the test specimen, which is the actual bending load. It should be noted that the reinforced or prestressed concrete structures are considered as reasonably ductile (Wang, 1996). They have a medium ductility and medium impedance when compared with ductile steel and brittle composite materials. Most likely, the impact load history of the prestressed concrete sleepers should lie in the case (a), (b), or (c), depending on the experimental setup. The

peak bending load can thus be evaluated from the second peak or the third peak (Server, 1978) in the plot of impact load history obtained from the dynamic load cell.

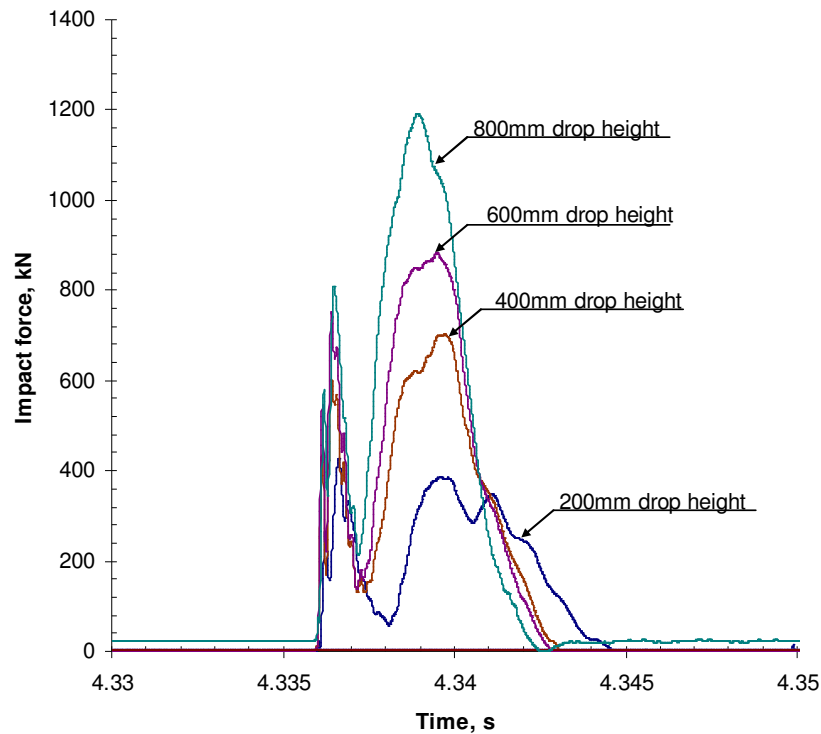


**Figure 6.19** Schematic impact load histories for general materials (Saxton, et al., 1974)

### 6.7.2 Impact loads

In the first case, the full installation of in-situ sleeper has been carried out to replicate the real condition on the track. From Chapter 3, the dynamic stiffness of the new HDPE pad (High density polyethylene 7.5 mm thick) is about 1,200 MN/m. The conveyor belt in mining industry is found suitable for use as the alternative support. The impact forces measured from the dynamic load cell from direct contact between rail and impactor are presented in Figure 6.20. Very small bending crack was firstly detected at the drop height of 600 mm but the small shear cracks were also found after few blows at the drop height of 800 mm. However, no major failure can be observed. From the test undertaken it is evident that the sleeper exhibits a significant amount of reserved

strength. Figure 6.20 shows that the higher drop heights provide the larger magnitude of impact loading, but slightly reduce the shock duration. The magnitude of the shock loading associated with the flexure of the sleeper varies from 380 to 1,150 kN while the duration remains in a small range between 4 and 6 ms. It should be noted that the first peaks are related to the contact stresses at the contact zone between the impactor and the railhead. The actual flexural responses of the sleeper are most likely due to the second peaks. The first peak can be filtered by using the low-frequency-pass feature in LabView, so that only the impact load history with associated bending frequency would be recorded.



**Figure 6.20** Impact forces at different drop heights

Tables 6.7-6.10 present the impact load characteristics under various conditions. It is found that the impact force magnitude increases up to 20 to 25 % when using the rail pad in the soft track, while it ascends as much as 45 to 50 % in the hard track. On the other hand, the duration gently reduces either when the support condition is stiffer or when the rail pad is very stiff (or when no use of rail pad). It appears when considering the similar experimental setups that the shock quantities (including magnitude and

duration) tend to be more susceptible to the rail pad effect in the hard track than those in the soft track. The support condition seems to dominate the impact responses as well as the corresponding behaviour of the concrete sleepers. Remarkably, the rail pad plays a role on the man-made shock loading quantities, as it tends to attenuate the impact stresses (reducing the magnitude of force) and filter the impulse frequencies (extending the time duration of impact). This is because the in-situ sleepers on the soft track possess the global track modulus less than the hard track. Also, it is well known that the contact force quantity largely depends on the contact stiffness (Cai, 1992). The magnitude of impacts was found to increase as the contact stiffness, whilst the pulse duration is inversely proportional to the contact stiffness. Then, it is clearly found that the rail pad provides the resilient support as a spring to the rail (Cai, 1992), thus weakening the contact stiffness.

**Table 6.7** Impact load characteristics in the soft track with rail pad

Softening media	Drop height			
	0.2m.		0.4m	
	Impact characteristics		Impact characteristics	
	Magnitude, kN	Duration, ms	Magnitude, kN	Duration, ms
Direct contact	426	7	700	7
1mm Neoprene	362	9	611	8
3mm Neoprene	327	9	466	9
5mm Neoprene	300	11	419	10

**Table 6.8** Impact load characteristics in the soft track without rail pad

Softening media	Drop height			
	0.2m.		0.4m	
	Impact characteristics		Impact characteristics	
	Magnitude, kN	Duration, ms	Magnitude, kN	Duration, ms
Direct contact	564	6.5	904	5
1mm Neoprene	322	2	858	5.5
3mm Neoprene	436	8	530	8
5mm Neoprene	359	9	493	8.5

**Table 6.9** Impact load characteristics in the hard track with rail pad

Softening media	Drop height			
	0.2m.		0.4m	
	Impact characteristics		Impact characteristics	
	Magnitude, kN	Duration, ms	Magnitude, kN	Duration, ms
Direct contact	441	8	761	6.5
1mm Neoprene	429	8.5	622	8
3mm Neoprene	386	9	563	8.5
5mm Neoprene	313	11	365	10

**Table 6.10** Impact load characteristics in the hard track without rail pad

Softening media	Drop height			
	0.2m.		0.4m	
	Impact characteristics		Impact characteristics	
	Magnitude, kN	Duration, ms	Magnitude, kN	Duration, ms
Direct contact	675	5.5	1036	4
1mm Neoprene	503	6.5	905	5.5
3mm Neoprene	485	8	800	7
5mm Neoprene	400	9	475	9

The influence on artificial shock quantities of the softening media to reduce the contact stress between the impactor and the railhead is established from the above experiments. Regardless of the effects of the use of rail pad or the support conditions, the softening media significantly affects the shock loading quantities. It is discovered that the thicker the softening media, the lesser the impact magnitude but the larger the pulse duration. The effect of the softening media is constantly similar (about 25-30 % decrease) at all conditions, whether in the soft or the hard track, or whether with or without the use of rail pad. Based on this study, the impact loads can be simulated from the combined use of drop height and softening media.

## 6.8 SUMMARY

This chapter presents the use of a high-capacity impact testing machine developed at the University of Wollongong, in order to investigate the impact behaviour of an in-situ

railway prestressed concrete sleeper. The instrumentation was described in details so as to achieve the adequate experimental results. The fracture energy and energy losses under dynamic conditions of the in-situ prestressed concrete sleepers as a performance indicator of damage for the selected limit states, were qualitatively demonstrated.

The traditional method for railway ballast replication (for use as an alternative support) requires small parts of the material for testing and therefore the difficulties and inconvenience may appear. In this chapter, experimental techniques and applications of experimental modal analysis for railway ballast replication have been established. This study was initially developed for use in impact testing of railway track components at the University of Wollongong, Australia. The additional objective of this study is to develop the experimental techniques to evaluate the modal data and imitate the dynamic signatures of alternative supporting materials, aimed at their uses in experimentations. This chapter also presents the experimental results of both 2DOF and MDOF modal tests. The laboratory demonstrations have proved the effectiveness, efficiency, and precision of the replication techniques by using dynamic signatures (FRFs) and modal parameters such as the natural frequency, the damping coefficient, and the corresponding mode shape, by means of the instrumented hammer impact technique.

From Chapter 4, it is well known that the wheel or rail abnormalities were found to cause the large impact load during the dynamic interaction between the wheel and rail. The impact load characteristics are typically of high magnitude but short duration. In general, the force magnitude varies between 300 and 400 kN, with the pulse duration from 1 to 10 ms. This magnitude of impact corresponds roughly the fifty-year return period, which is about only once in the design life span of concrete sleepers. The research conducted at the University of Wollongong, Australia, aims to understand more clearly the manner in which track components respond to those forces, and to clarify the processes whereby the concrete sleepers in particular carry those actions. It is therefore very important to ascertain the statistics related to the spectrum and amplitudes of forces applied to tracks, as well as to develop a methodology to replicate the impacts.

## CHAPTER 7

### PROGRESSIVE IMPACT RESPONSES OF PRESTRESSED CONCRETE SLEEPERS

In general, railway tracks suffer with the extreme loading conditions, which are attributable to the train operations with either wheel or rail abnormalities such as flat wheels, dipped rails, etc. These loads are of very high magnitude but short duration, as well as they are of low-possibility occurrence during the design life of the prestressed concrete sleepers. In spite of the most common use of the prestressed concrete sleepers in railway tracks, their impact responses and behaviours are not deeply appreciated nor taken into the design consideration. The experimental investigations presented in this Chapter were aimed at understanding the progressive dynamic behaviours of prestressed concrete sleepers in railway track structures under incremental impact loading, in order to form the state of the art of limit states design concept for prestressed concrete sleepers. Series of repeated impact tests for the in-situ prestressed concrete sleepers were carried out, ranging from a low drop height to the ultimate drop height where the ultimate failure occurred. The cumulative impact damage and crack propagation are highlighted in this Chapter. The effects of track environment including soft and hard tracks together with the relationship between the resultant bending moment of prestressed concrete sleepers and the applied impact force as a design guideline were also presented.

#### 7.1 OVERVIEW

All static, quasi-static, and impact loads are very important in design and analysis of railway track and its components. Generally, dynamic shock loading corresponds to the frequency range from 0 to 2,000 Hz due to modern track vehicles. The shape of impact loading varies depending on various possible sources of such loading, e.g. wheel flats, out-of-round wheels, wheel corrugation, short and long wavelength rail corrugation, dipped welds and joints, pitting, and shelling. Wheel/rail irregularities induce high dynamic impact forces along the rails that may greatly exceed the static wheel load. In

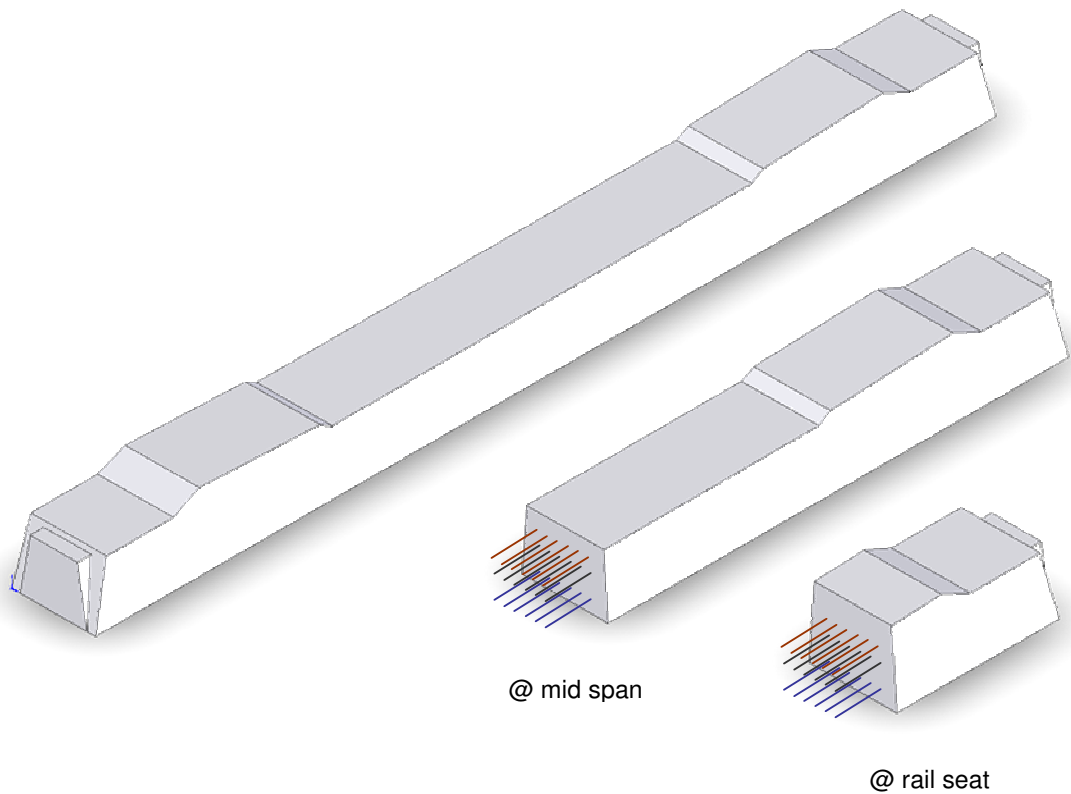


all cases, the impact forces are significantly dependent on the train speed. These impulses would occur repetitively during the roll. Loss of contact between wheel/rail, so-called “wheel fly”, will occur if the irregularity is large enough, or the speed is fast enough. However, the impact force could be simplified as a shock pulse acting after the static wheel load is removed. The typical magnitude of impact loads from the reviewed cases (Remennikov and Kaewunruen, 2007a) varies roughly between 200 kN and up to 750 kN, depending on the causes and the traveling speed of train. The durations of such loads are quite similar, varying between 1 and 10 msec. However, the representative values of the first peak ( $P_1$ ) of the forces caused by dipped joints should be about 400 kN magnitude with 1 to 5 msec time duration. For the second peak ( $P_2$ ), the average values are about 80 kN magnitude and 5 to 12 msec time duration. Therefore, it should be taken into account that the typical duration of impact wheel forces varies widely between 1 and 12 msec (Wakui and Okuda, 1999; Esveld, 2001; Remennikov and Kaewunruen, 2007a).

In practice, cracks in the concrete sleepers have been visually observed by many railway organizations. As noted in a review report by Murray and Cai (1998), the principal cause of cracking is the infrequent but high-magnitude wheel loads produced by a small percentage of “bad” wheels or railhead surface defects. Those forces are the impact loading condition as described above. However, most of the cracks found were not critical nor significant that would lead to the failure of a prestressed concrete sleeper or a railway track as a whole. Leong (2007) performed the probabilistic load analyses of railway tracks in Queensland, Australia. Two railway networks for the heavy haul lines transporting coals were equipped with a number of sensors and impact load detectors. The prediction formulae for the impact loads in relation to the return period (inversely proportionate to the possibility of occurrence) have been established in his investigations. It is found that the impact load of about 400-600 kN is associated with around fifty years of return period, or on the other hand, the possibility of occurrence is approximately 1 to 2 percent. Nonetheless, the recorded data shows that the larger impact force can also be achieved, which might be ascribed to the dipped joint in rail connection.

This chapter examines the progressive dynamic behaviour of railway prestressed concrete sleepers subjected to impact loading. The prestressed concrete sleepers were

designed complied with Australian Standard: AS1085.14 (2003). The test specimens were kindly supplied by an Australian manufacturer, AUSTRAK. Figure 7.1 shows the general sample cross-sections of a prestressed concrete sleeper. Drop-weight impact hammer was used to apply multiple impacts directly to the railseat at certain drop heights on the basis of the test arrangement. The impact pulses were recorded using the high capacity load cell connected to the National Instrument data acquisition system. The dynamic measurements also include fibre dynamic strains and accelerations. The use of softening media placed on top to railhead as to reduce the contact stress was adopted. Neoprene rubber was used varying thicknesses: 1.5 mm, 3 mm, and 5.5 mm. Then, the simplified relationships between railseat bending moment and impact force can be obtained. Impact damage and crack propagation at each drop test was recorded.



**Figure 7.1** General profile and cross-sections of prestressed concrete sleepers

## 7.2 EXPERIMENTAL PROGRAM

The details of test specimens have been given in Chapter 6. The cross section of the prestressed concrete sleepers at railseat can also be seen in Figure 6.1. The alternative support condition is adopted for use in this study.

Table 7.1 shows a series of test program with the particular emphasis on the different target levels of impact force acting on the prestressed concrete sleepers. The series of impact test program were conducted using the same test setup as described above. The special attention was paid to the different drop heights on the prestressed concrete sleepers to achieve the target conditions, including the crack propagations and the crack widths. This study experimentally investigates the influence of ballast supports on the accumulative failure and load-carrying mechanisms, impact load history (from the dynamic load cell), accelerations, and crack propagation. Two different support conditions, including ‘soft track’ and ‘hard track’, have been calibrated against the vibration modal parameters of ballast support in actual tracks (Kaewunruen and Remennikov, 2007c). The soft track can be considered as thin ballast bed (about 100-150 mm in depth), while the hard track represents the thick layer of the ballast bed (more than 250 mm in depth). The experimental setups for support conditions were in accordance with AS1085.19 (2001), as illustrated in Figure 6.14 of Chapter 6. This setup was verified to be sufficient for the investigations of prestressed concrete sleepers’ behaviour at railseat (Wakui and Okuda, 1999). The method of superposition can also be utilized to understand the behaviour of the prestressed concrete sleepers at mid span. As a result, many railway companies have simplified by using simply a half sleeper for their tests.

**Table 7.1.** Summary of experimental programs.

Support condition	Drop Height Used (m)	Softening media (between impactor and rail)
Soft track	0.1-1.4 (every 0.1 m)	1.) 5.5 mm neoprene
		2.) 3.0 mm neoprene
		3.) 1.5 mm neoprene
		4.) without any
Hard track	0.1-1.0 (every 0.1 m)	1.) 5.5 mm neoprene
		2.) 3.0 mm neoprene
		3.) 1.5 mm neoprene
		4.) without any

## 7.3 RELATION BETWEEN IMPACT FORCE AND DYNAMIC MOMENT

### 7.3.1 D-TRACK for dynamic analysis of railway tracks

Cai (1992) developed a finite element model aimed at establishing a comprehensive theoretical model of rail tracks, in order to evaluate the dynamic behaviours of railway track and wheel/rail interaction. This model is known as Dynamic Analysis of Rail Track Structures (so-called D-TRACK). The two-dimensional finite element model consists of three subsystems: a rolling stock vehicle, wheel/rail contact interface, and track structure. The vehicle is modeled by a single double-axle bogie with four DoFs. Although the bogie side frame and rotatory inertia are considered, only transversely symmetric vibration (only two wheels of unsprung masses and a side frame on one rail) can be represented. However, Cai and Raymond (1992; 1994) found that the vehicle components would not contribute significantly to high frequency wheel/rail contact forces. The wheel/rail contact interface is modeled using the Hertzian contact theory. By employing the 4th order Runge-Kutta method, the iterative computation of wheel/rail contact forces is undertaken in the time domain.

The track structure is combined with steel rails, which are discretely supported by flexible sleepers. It was found that the Timoshenko beam theory is the most suitable for simulating both the rails and sleepers (Cai, 1992; Grassie, 2005; and Kaewunruen and Remennikov, 2006). D-Track allows the varied data inputs for the sleeper cross-section and ballast properties along the sleeper length. Connection between rails and sleepers is modeled through linear spring-dashpot elements representing the rail pad stiffness and the damping coefficient. The track bed (comprising of ballast, subballast and subgrade) is modeled as a continuous array of linear spring-dashpot elements. The estimate of the track modulus can be used to validate the effect of ballast and subgrade layering (Cai et al., 1994).

Steffens (2004) investigated the potential of D-Track for further development under the research umbrella of RailCRC and found that D-Track is capable of performing four types of analysis of the railway track system:

- Free vibration characteristics of track i.e. natural frequency and mode shapes of individual track components and the entire track as an integral structure;

- Dynamic responses of track in the frequency domain i.e. frequency response characteristics of the entire track, and of the rail and the sleeper as integral components of the track;
- Dynamic responses of track under a stationary impact load i.e. rail-sleeper displacement, acceleration, shear stresses, rail seat forces and ballast pressures at any wayside location along the track; and also rail and sleeper deflection and stress wave shapes across the track;

Dynamic responses of track and wheelset to moving wheel-rail interaction for the input of excitation sources from any out-of-round wheel/rail abnormalities. The predicted dynamic responses include the onboard and wayside reactions.

### 7.3.2 Benchmarking

D-Track model has been updated and further developed under the commercial linkage with the original developer (Steffens, 2005). To verify the analytical results, the benchmarking programs were conducted. The first benchmarking was done by Steffens (2005) and the second benchmarking was finalized by Leong (2007).

- **Benchmark I**

Steffens and Murray (2005) conducted a benchmarking test to investigate the dynamic response of tracks. The simulations were based on a standard gauge passenger vehicle traveling at the constant speeds at 100 and 160 km/hr, and with a variety of wheel/rail contact defects. Table 7.2 shows the list of participants in Benchmark I. It was found that the computer models in the benchmarking exercises have widely different theoretical background. Table 7.5 gives the list of benchmarking scenarios for simulations. Two types of track structures were considered and about three different wheel/rail contact conditions were evaluated (Steffens, 2005).

Benchmark I provided the common ground solutions. It was found that the D-TRACK model has shown a reasonable agreement to other models under most circumstances. The sleeper model of D-TRACK was found to be more suitable and more realistic for the track structures than the other models. The general agreement of D-TRACK with the TRACK and DIFF results for the sleepers indicates strong confidence and reliability (Steffens and Murray, 2005). It was also recommended that a second benchmark compare analytical results to real on-track data.

**Table 7.2.** Benchmark participants

Computer Model	Exercise	Research and Development Institutions
DARTS	Benchmark II	Delft University of Technology, the Netherlands
DTRACK	Benchmark I & II	DynTrack Systems, USA and Rail Innovation Australia Pty
DIFF	Benchmark I & II	CHARMEC, Sweden
NUCARS <sup>TM</sup>	Benchmark I & II	Transportation Technology Center, Inc. USA
SUBTTI	Benchmark I & II	Technical University of Berlin, Germany
TRACK	Benchmark I	Stuart Grassie Engineering Solutions, UK
VICT	Benchmark I	Southwest Jiaotong University, China
VIA	Benchmark II	University of Valencia, Spain

**Table 7.3.** Benchmark I scenarios (Steffens, 2005)

No.	Vehicle Type	Train Speed (km/hr)	Ballast Track Structures	Wheel/rail Contact Condition
I-1	Passenger	160	Concrete sleepers	No irregularity
I-2	Passenger	160	Concrete sleepers	Worn wheel flat
I-3	Passenger	160	Concrete sleepers	Dipped rail joint/weld
I-4	Passenger	100	Timber sleepers	No irregularity
I-5	Passenger	100	Timber sleepers	Worn wheel flat
I-6	Passenger	100	Timber sleepers	Dipped rail joint/weld

- **Benchmark II**

Updated version of D-TRACK was succeeded by Leong (2007). The modifications and upgrades of D-TRACK include the use of very high stiffness values of rail pads, the output layout, the additional part of wheel/rail contact conditions, the calculation of the sleeper centre bending moments, and the material database upgrades. Leong et al. (2007) performed a second benchmarking test that adopted the new version

of D-TRACK, in order to compare the analytical results against other computer models' results and the field data obtained in Melbourne site, Australia.

Table 7.4 shows eight scenarios for the second benchmarking exercise. Benchmark II showed that the D-Track results are quite accurate with the field data and other track models' analytical results. Table 7.5 summarizes the correlation between the computer models and the field data (Leong, 2007). Based on the second benchmarking exercise, D-Track is found to be a suitable package for dynamic analysis of railway track structure.

**Table 7.4.** Benchmark II scenarios (Leong, 2007)

No.	Wagon Type	Train Speed (km/hr)	Gross Vehicle Mass (kg)	Rail Profile
II-1	RQTY Container	101.7	52,000	Geelong
II-2	RQTY Container	110.8	78,000	Melbourne
II-3	RKWF Structural	75.0	28,000	Geelong
II-4	RKWF Structural	83.1	100,000	Melbourne
II-5	RQTY Container	101.7	52,000	Geelong
II-6	RQTY Container	110.8	78,000	Melbourne
II-7	RKWF Structural	75.0	28,000	Geelong
II-8	RKWF Structural	83.1	100,000	Melbourne

**Table 7.5.** Correlation between computer packages' analytical results and field data (Leong, 2007)

Correlation	DARTS	DIFF	D-TRACK	NUCARS	SUBTTI	VIA	Field Data
DARTS	☺	☑	☑	☒	☒	☑	☑
DIFF	☑	☺	☑	☒	☒	☑	☑
D-TRACK	☑	☑	☺	☑	☒	☑	☑
NUCARS	☒	☒	☑	☺	☑	☒	☒
SUBTTI	☒	☒	☒	☑	☺	☒	☒
VIA	☑	☑	☑	☒	☒	☺	☑

### 7.3.3 Case studies: computer simulations

Thirty-six case scenarios, given in Table 7.6, were compiled using DTRACK (Murray and Leong, 2006). The analytical studies were initially carried out in order to benchmark the analytical results and in order to evaluate the wheel/rail impact forces. The case studies include the various data inputs as to represent the different functions, and the variety of material properties and support conditions of railway tracks. The analytical results have been investigated to obtain the relationships between impact loads transferring onto a railseat and the resultant bending moment at the railseat (Kaewunruen and Remennikov, 2007d). Figure 7.2 shows the analytical relationship between impact load and railseat bending moment. The analytical results yield the scattered data of different track properties and operational functions as shown in Figure 7.2. It is found that the heavy and light tracks possess different relationships between the railseat moment and impact force. The function between railseat moment ( $M^*$ ) and impact force ( $I$ ) for the light track is about  $M^* = 0.03I$  while  $M^* = 0.06I$  can be used for heavy tracks. These analytical solutions provide the general approximation for uses in track designs as the correlation errors are less than 15%. For structural design purpose, the analytically-based moment envelope to be used as a guess design guideline for prestressed concrete sleepers read

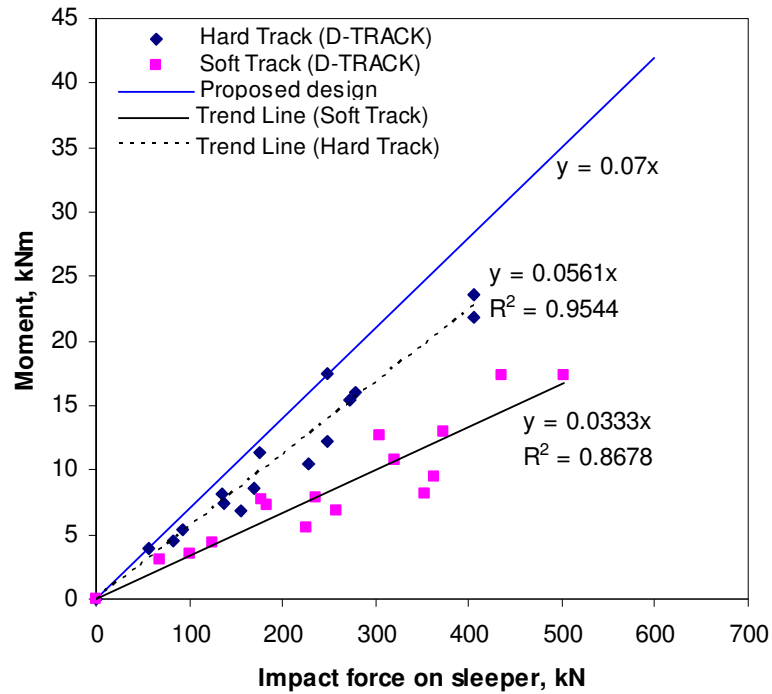


$$M^* = 0.07I \quad (2)$$

where  $M^*$  is the resultant bending moment at railseat and  $I$  is the impact force transferring onto the railseat.

**Table 7.6.** D-TRACK simulation scenarios (Murray and Leong, 2006)

No.	Wagon Type	Train Speed (km/hr)	Wheel flat sizes (mm)	Track Type
D-1	90 tonne coal wagon	80	25	Narrow gauge, 60 kg/m rail, heavy duty sleepers, 250 mm thick ballast
			50	
			75	
D-2	55 tonne freight car	80	25	Narrow gauge, 60 kg/m rail, heavy sleepers, 250 mm thick ballast
		100	50	
			75	
D-3	30 tonne passenger carriage	80	25	Narrow gauge, 60 kg/m rail, heavy duty sleepers, 250 mm thick ballast
		120	50	
		160	75	
D-4	55 tonne freight car	80	25	Narrow gauge, 50 kg/m rail, low profile sleepers, 150 mm thick ballast
		100	50	
			75	
D-5	30 tonne passenger carriage	80	25	Narrow gauge, 50 kg/m rail, low profile sleepers, 150 mm thick ballast
		120	50	
		160	75	
D-6	90 tonne coal wagon	80	25	Standard gauge, 60 kg/m rail, heavy duty sleepers, 250 mm thick ballast
			50	
			75	



**Figure 7.2.** Analytical relation between bending moment and impact force at a railseat.

#### 7.3.4 Case studies: experiments

To evaluate the relationship between railseat bending moment and the associated impact force, the drop heights were kept at low levels that would not create major cracks in the concrete. The drop heights were increased step by step until all strain gauges were broken due to the large dynamic tension at bottom fibre and compression at top fibre. Impact forces measured from the dynamic load cell (tup load) are presented in Figure 7.3. (Remennikov and Kaewunruen, 2007b). Examples of acceleration responses are illustrated in Figure 7.4. The dynamic strains at top and bottom fibres were captured using the dynamic strain gauges, as shown in Figure 7.5. The curvature at the railseat can be computed based on the assumption that strain plane is linear and remains plane after the deformation. The moment-curvature relationship for uncracked up till cracked sections is then employed for obtaining the resultant bending moment at the railseat of railway prestressed concrete sleeper (Kaewunruen and Remennikov, 2007d). The impact tests were identical for both support conditions: light and heavy tracks.

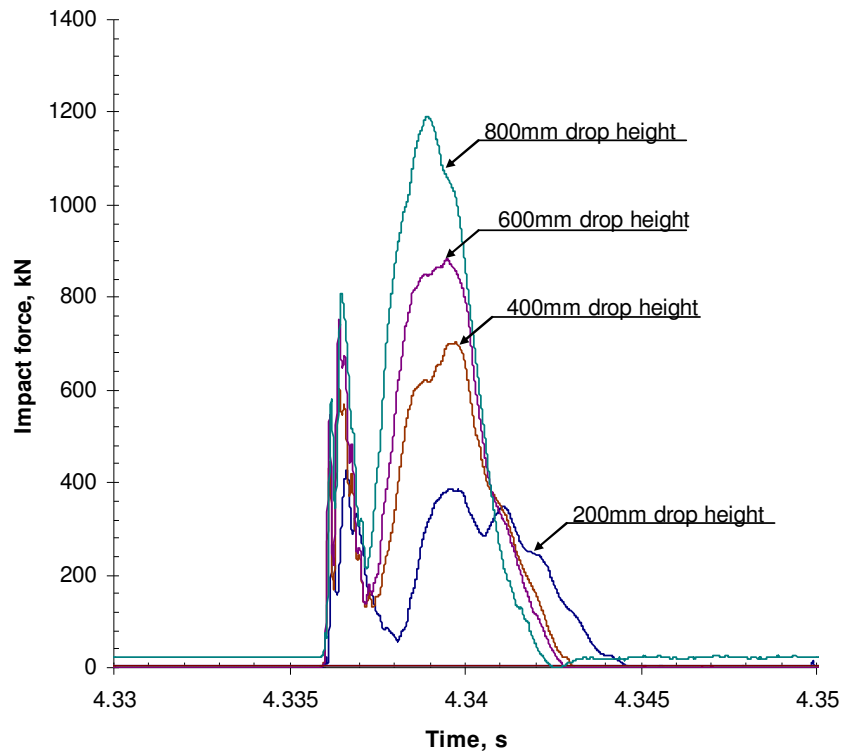
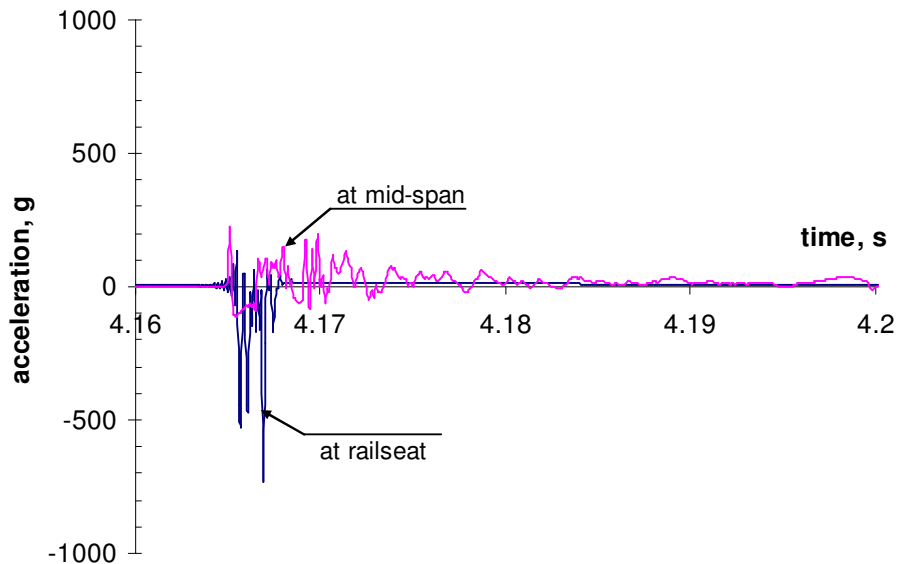
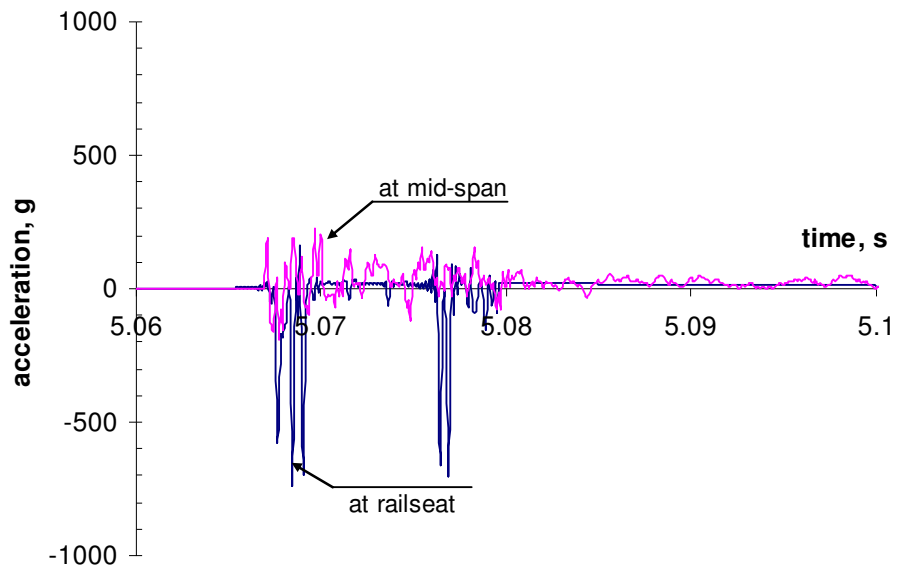


Figure 7.3. Example of typical impact forces from the impact testing.

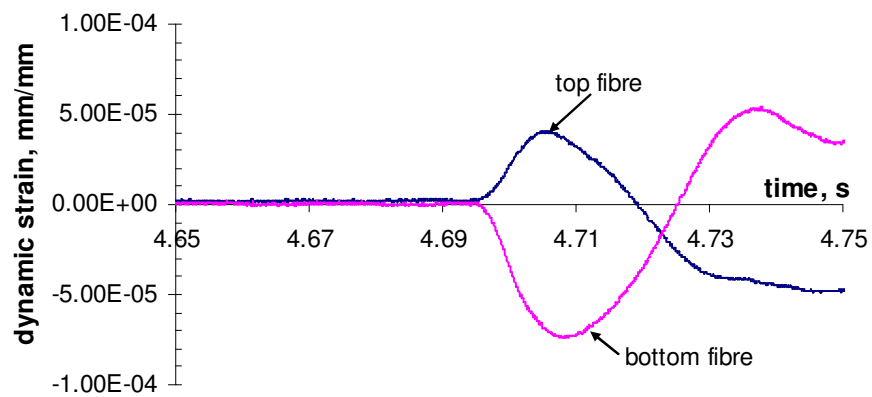


a) soft track environment

Figure 7.4. Accelerations due to 200 mm drop height

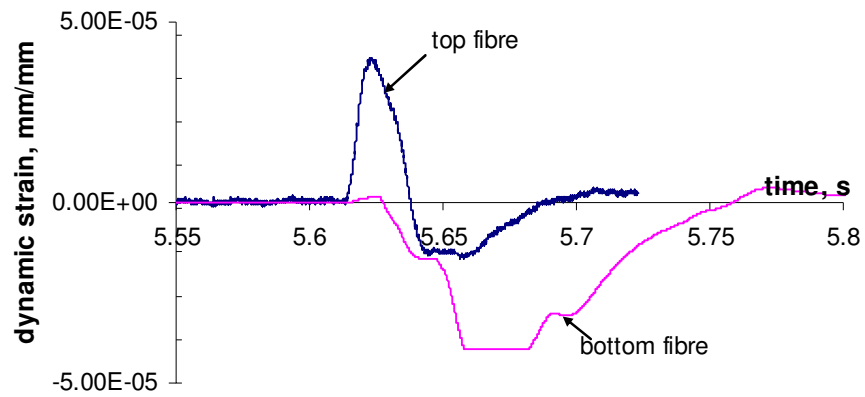


b) hard track environment

**Figure 7.4.** Accelerations due to 200 mm drop height

a) soft track environment

**Figure 7.5.** Dynamic strain at sleeper railseat due to 200 mm drop-weight impact



b) hard track environment

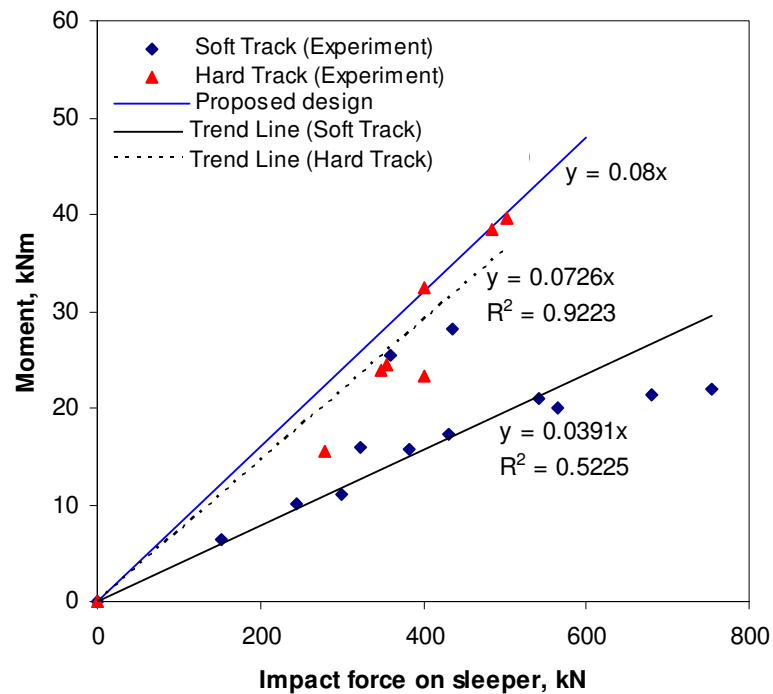
**Figure 7.5.** Dynamic strain at sleeper railseat due to 200 mm drop-weight impact**Figure 7.6.** Experimental relation between bending moment and impact force at a railseat.

Figure 7.6 depicts the experimental relationships between the railseat bending moment and impact force acting directly on the railseat. Comparing Figure 7.6 with Figure 7.2, the experimental results show that the test setup well simulates the actual light and heavy tracks. However, it was found that the experimental results were slightly dispersed. The relationship between the artificial impacts and railseat moment for soft track is about  $M^* = 0.04I$  and for hard track is approximately  $M^* = 0.07I$  with the correlation index of about 52 and 92 percent, respectively. The experimentally-based moment envelope for a guess design guideline for prestressed concrete sleepers read

$$M^* = 0.08I \quad (7.1)$$

Although the best way to determine the bending moment along the railway sleepers is to employ the advanced dynamic analysis of railway tracks (i.e. D-TRACK), a design guideline presented would allow convenience and would be preferable in railway practice as the analytical and experimental results in this study confirm and provide the faster and adequate means to predict the bending moment on the sleepers from the anticipated wheel/rail interaction. It should be noted that the impact force on sleeper railseat is roughly about 70 percent of the wheel/rail interaction force (Murray and Cai, 1998).

## 7.4 IMPACT PERFORMANCE

### 7.4.1 Crack propagations

Based on the statistical data of the frequency of occurrence of impact loads and their magnitudes, the impact tests on prestressed concrete sleepers were designed to simulate wheel/rail interface forces by varying the height of drop and the contact stiffness to achieve the required magnitudes and durations of the load pulses (Remennikov et al., 2007). Also, an impact load can be back-calculated for the equivalent return period. The crack initiation was detected visually during the test as well as the impact load was determined by the National Instrument's device. Table 7.7 presents the first crack identification and associated return periods of loading. It is found that the initial cracks could occur in the hard track more rapid than in the soft track. On the other hand, the possibility of occurrence of the impact load causing the first crack in the soft track is

much lower than that in the hard track. It is also found that the first dynamic cracks in the prestressed concrete sleepers either in the soft or the hard tracks are always due to excessive flexures.

**Table 7.7.** Impact crack identification of railway prestressed concrete sleepers

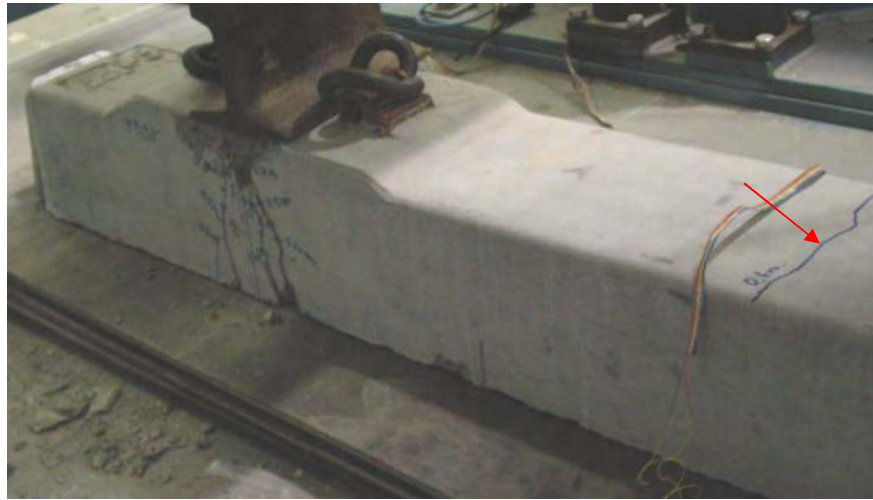
Support condition	Drop height (m)	Impact force (kN)	Return period of loading*	Crack type
Soft track	0.2	560	50 years	bending
Hard track	0.1	400	9 months	bending

\*based on a field data from a site in Central Queensland (Leong, 2007).

Figure 7.7 depicts the progressive impact behaviour of prestressed concrete sleeper in the soft track environment. Very small flexural cracks were initially detected starting from a drop height of 200 mm. Small shear cracks were also found after several impacts from a drop height of 500 mm. However, no major failure was observed in these single impact load experiments. The prestressed concrete sleepers were also subjected to gradually increasing impact loads until failure of the sleepers occurred. The crack widths at each stage were measured using the magnified telescope. For impact loads between 150 and 600 kN (see Figure 7.7a), the crack widths were about 0.01 to 0.02 mm. The crack widths increased from 0.02 to 0.08 mm when subjected to impact loads with magnitudes between 700 to 1,000 kN (see Figure 7.7b). At this stage, spalling of the concrete at the top of railseat section could be detected. When the impact forces were increased up to 1,500 kN, the crack widths also increased up to 0.5 mm (see Figure 7.7c). The top surface crack at mid-span could also be noticed as illustrated in Figure 7.7d. However, it was found that the severity of the top surface crack is relatively low as the crack width is about 0.02 mm.



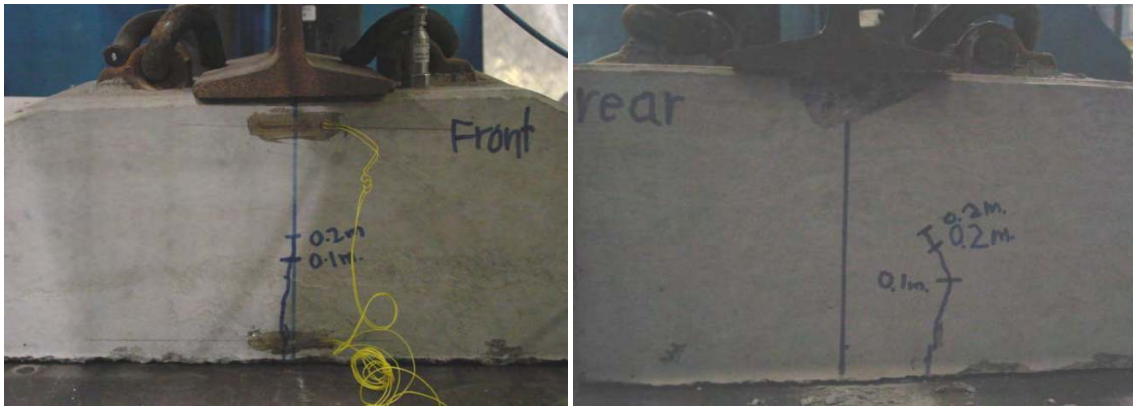




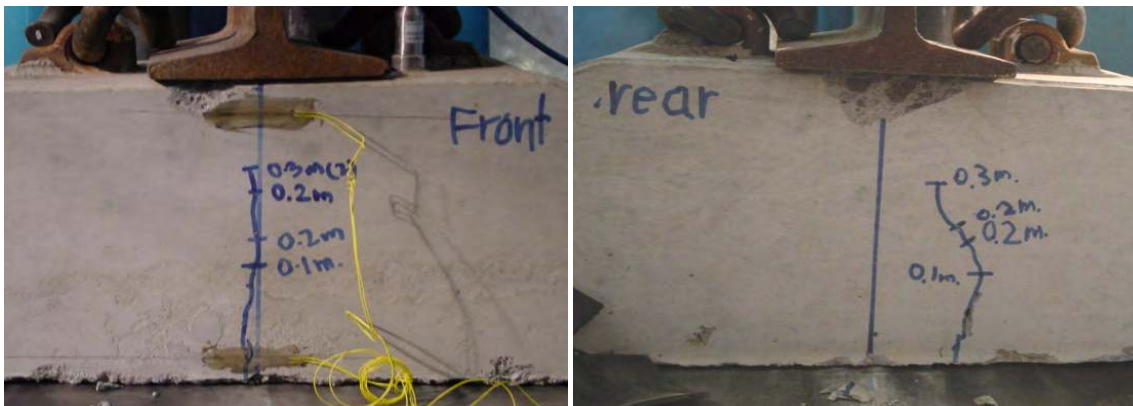
d) crack on top surface

**Figure 7.7.** Progressive impact response of a railway sleeper in soft track environment

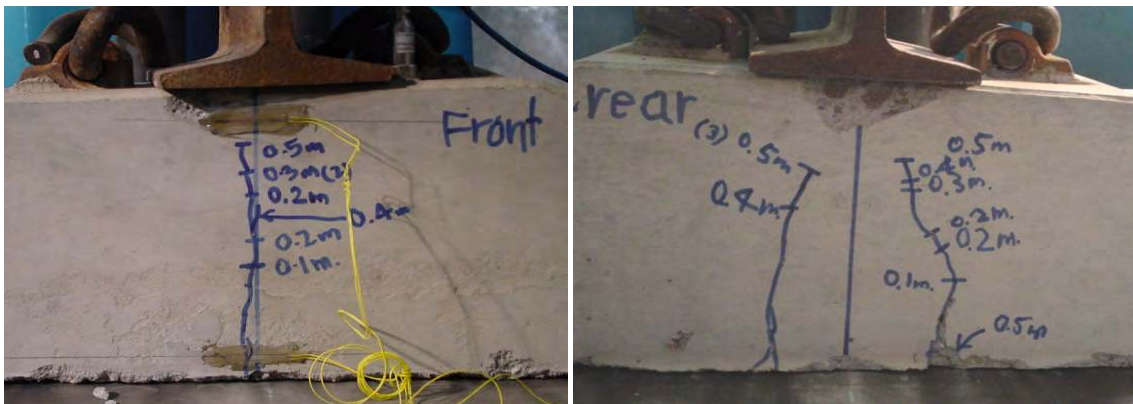
Figure 7.8 depicts the progressive impact behaviour of prestressed concrete sleeper in the hard track environment. The small flexural cracks were initially observed starting from a drop height of 100 mm. Small diagonal cracks were also found after several impacts from a drop height of about 500 to 600 mm. Neither could major bending or shear failure be noticed in the initial series of the impact load tests. As a result, gentle increments of impact load were applied to the prestressed concrete sleepers until major damage of the sleepers occurred. Using the magnified telescope, the crack widths at each stage were measured. For impact loads less than 500 kN (see Figure 7.8a), the crack widths were about 0.01 to 0.02 mm. The crack widths increased from 0.02 to 0.12 mm when subjected to impact loads with magnitudes between 500 to 850 kN (see Figure 7.8b). At this stage, small spalling of the concrete at the top of railseat section could be detected. When the impact forces were increased up to 1,200 kN, the crack widths also increased up to 0.3 mm (see Figure 7.8c). Spalling of the concrete was significantly enlarged when the impact forces were recorded at between 1,200 kN and 1,800 kN, as depicted in Figure 7.8d. Apart from vertical cracks, a few of longitudinal cracks across the prestressed concrete sleeper could also be detected as shown in Figure 7.8e. Although there were more cracks occurring in the hard track environment, the size of crack widths is comparatively small, ranging from 0.01-0.02 mm.



a) impact forces less than 500 kN



b) impact forces between 500 and 850 kN



c) impact forces between 850 and 1,200 kN

**Figure 7.8.** Progressive impact response of a railway sleeper in hard track environment



d) impact forces between 1,200 and 1,800 kN



e) cracks on top surface

**Figure 7.8.** Progressive impact response of a railway sleeper in hard track environment

#### 7.4.2 Progressive failure

Table 7.8 summarizes the progressive impact failure conditions. It is found that under the accumulative damage the hard track seems to occur at very large impact load. This could be explained on the basis of Hertzian contact theory (Cai and Raymond, 1994;

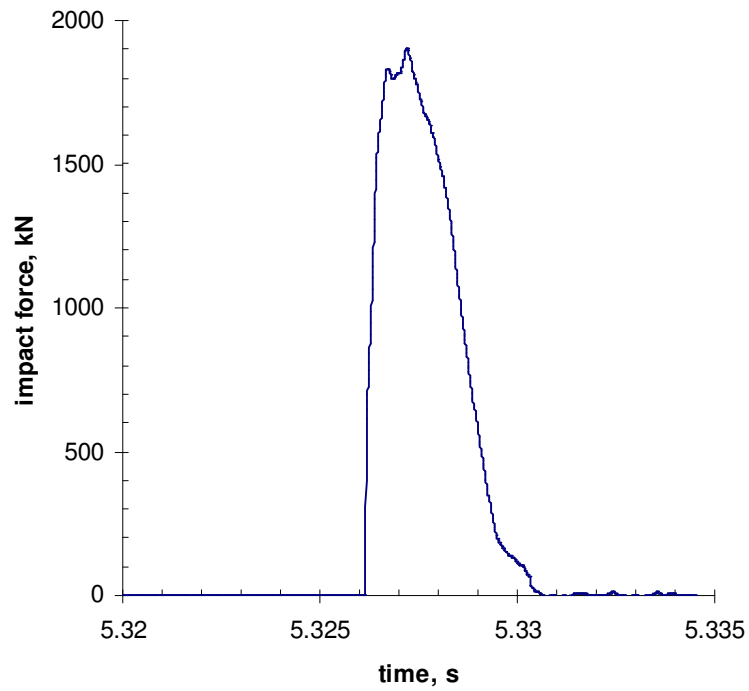
Barke and Chiu, 2005) as the high wheel/rail contact stiffness would give the large contact force. It should be noted that the wheel/rail contact stiffness were exponentially dependent to both the support stiffness and the drop height. Consequently, due to the high drop height and very stiff support, the impact force on the prestressed concrete sleeper is significantly ascended. At the same time, the high loading rate would result in high strain rate and would complement the strength of concrete material and prestressing wires (Gustavson, 2002; Delhomme, et al., 2005; Kaewunruen and Remennikov, 2007e). Overall, it was found that the ultimate impact force of the identical prestressed concrete sleeper in the soft track environment would be slightly higher than that in the hard track environment.

**Table 7.8.** Accumulative impact damage of railway prestressed concrete sleepers

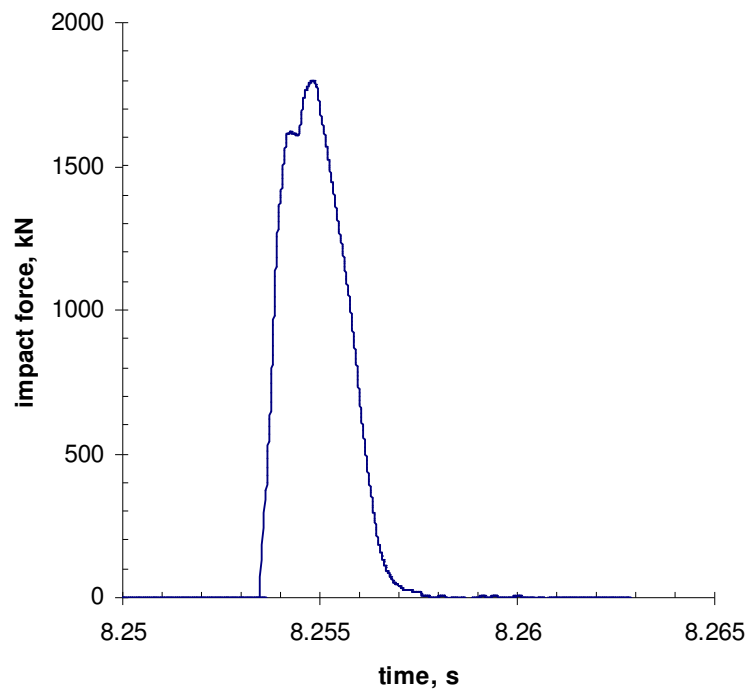
Support condition	Drop height (m)	Impact force (kN)	Return period of loading*	Failure mode
Soft track	1.4	1,910	over several million years	Disintegrated
Hard track	1.0	1,780		Disintegrated

\*based on a field data from a site in Central Queensland (Leong, 2007).

The ultimate impact forces failing the prestressed concrete sleeper were recorded and are presented in Figure 7.9. Figure 7.10 illustrates the impact failure of the sleepers in the soft track environment. The ultimate impact load carrying capacity was reached at about 1,910 kN, when the sleeper railseat section has disintegrated. The failure mode was associated with both flexural and longitudinal splitting actions. The splitting fractures were aligned along the prestressing tendons as illustrated in Figure 7.10b. It was found that these splitting fractures were occurred due to the lack of bonding along the prestressing tendons when the impact stress waves move along the composite section of concrete and tendons whereas the mechanical properties are much different. Based on the probabilistic analysis of dynamic loading, the magnitude of the ultimate impact load that caused failure of the prestressed concrete sleeper would be equivalent to that with a return period of several million years.



a) soft track environment



b) hard track environment

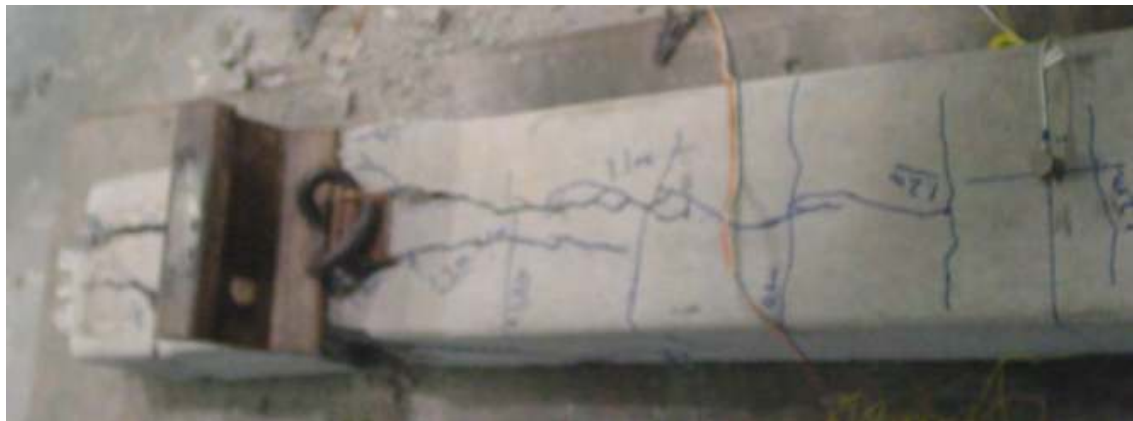
**Figure 7.9.** Ultimate impact forces failing railway concrete sleepers (after the low-frequency-pass filtering)



a) interfacial damage

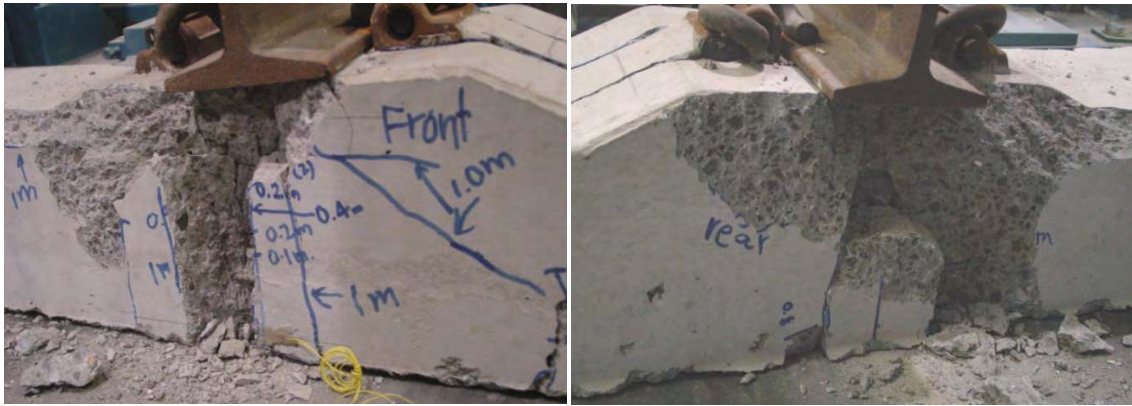


b) disintegration



c) top surface cracks

**Figure 7.10.** Impact failure at 1,910 kN of a railway sleeper in soft track environment



a) interfacial damage



b) disintegration and top surface cracks

**Figure 7.11.** Impact failure at 1,780 kN of a railway sleeper in hard track environment

Figure 7.11 shows the impact failure of the sleepers in the hard track environment. The ultimate impact load capacity was detected at about 1,780 kN, when the sleeper railseat section has been dismantled. Similarly, the failure mode was combined with both flexural and longitudinal splitting actions. The splitting fractures were aligned along the prestressing tendons in the identical analogy to the prestressed concrete sleeper in the soft track environment. On the statistical basis of dynamic loading, the size of the ultimate impact load failing of the prestressed concrete sleeper would be equivalent to that with a return period of several million years. From Figures 7.10 and 7.11, it is

noticeable that the progressive impact failure is rather localized at railseat, although some minor cracks could be visually inspected on top surface of the prestressed concrete sleepers in either the soft track or the hard track environments.

## 7.5 IMPACT DAMAGE CLASSIFICATION

An indicator to estimate the life expectancy of structures subjected to repeated loading is the cumulative damage. The damage accumulation mechanism can be evaluated from the critical crack length in relation to the depth of structural member (Fryba, 1996). The assessment method has been successfully developed for the fatigue life assessment of railway bridges. However, the fatigue damage theory is based on the fatigue stress and not suitable for railway concrete sleepers subjected to periodic impacts. As a result, the impact damage accumulation characteristics of the concrete sleepers are developed as a guide tool for the residual life prediction of the concrete sleepers. The hypotheses of the damage accumulation and fracture mechanics are adopted for this study (Fryba, 1996).

The relationships between the damage index and the cumulative load impulse are shown in Figure 7.12. The damage index  $D$  is the ratio between the maximum bending crack length  $c_{max}$  and the total depth of the sleeper  $d$  or  $D = c_{max}/d$ . This ratio provides a means for damage quantification and classification for the prestressed concrete sleepers subjected to impact loading. The load impulse  $I$  is the area under the impact load history diagram, which can be simulated as a half sinusoidal function. The cumulative load impulse is the summation of impulses at each stage during the experiments. In addition, if  $W$  represents the net impact energy absorbed at failure, then

$$\frac{w_1}{W} + \frac{w_2}{W} + \frac{w_3}{W} + \dots + \frac{w_n}{W} = 1 \quad (7.2)$$

where  $w_i$  is the impact energy input of the 1<sup>st</sup> load impulse and  $w_n$  is the impact energy input of the  $n^{\text{th}}$  load impulse. The cumulative impulse ratio  $I_R$  can be formulated using the theory of linear cumulative damage (Milton, 1945), where it is assumed that

$\frac{w_1}{W} = \frac{I_1}{I_f}$ . The relation between  $I_I$  and  $I_f$ , which are the impulse due to the 1<sup>st</sup> load

impulse and the total load impulse to failure, respectively, read

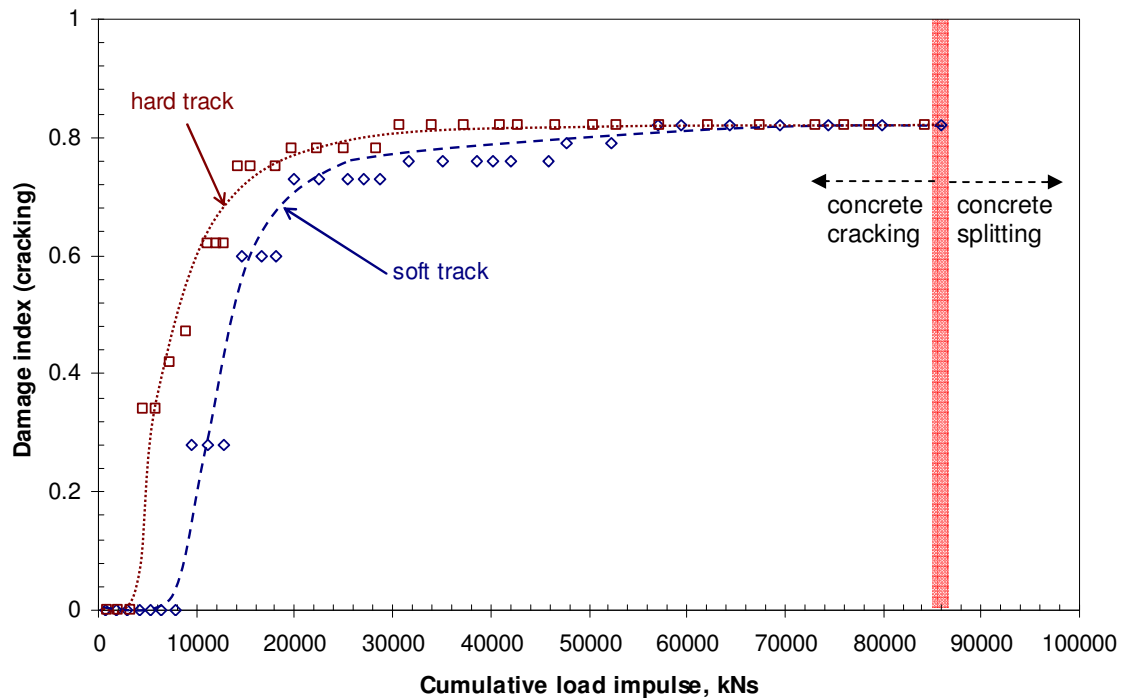


$$\frac{I_1}{I_f} + \frac{I_2}{I_f} + \frac{I_3}{I_f} + \dots + \frac{I_n}{I_f} = 1 \quad (7.3)$$

then, the cumulative impulse ratio  $I_R$  can be written as follows:

$$I_R = \sum_i \frac{I_i}{I_f} \quad (7.4)$$

where  $i$  is the number of impact loads which impart the impulse level greater than the cracking impact load threshold as tabulated in Table 7.7.

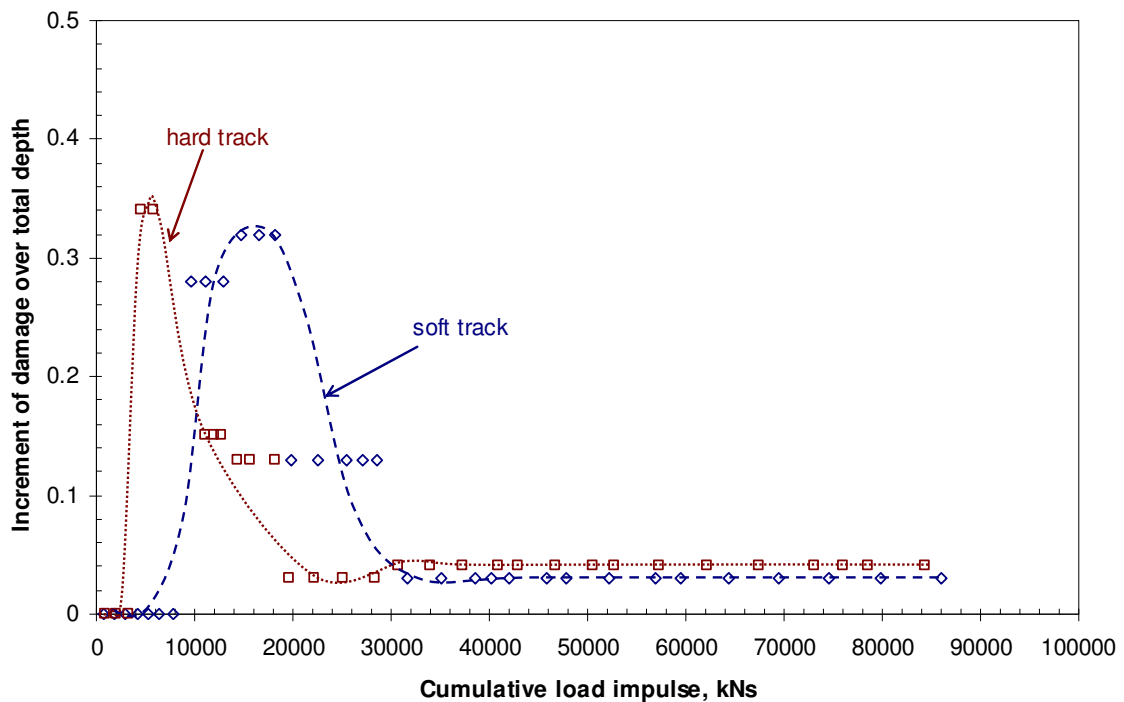


**Figure 7.12.** Cracking damage index of railway concrete sleepers in different track environments

It is found that the concrete sleepers in the hard tracks tend to fail under lower cumulative load impulse compared with those in the soft track environments. The slopes of the curve imply the damage rate of the concrete sleepers. It was found that cracking rate of concrete sleepers in the hard tracks is faster than those in the soft tracks. Surprisingly, the ultimate crack lengths of the concrete sleepers in hard and soft tracks were found very close or about 85 percent of sleeper depth at rail seat. Figure 7.12 also points out that if the cumulative load impulse reaches the ultimate load impulse to failure, the mode of failure will change from concrete cracking to concrete splitting as described above. Based on this concept, the residual life prediction of the concrete

sleepers can be carried out with the use of impact load data and their probability of occurrence obtained from a force detection system located in the particular railway tracks.

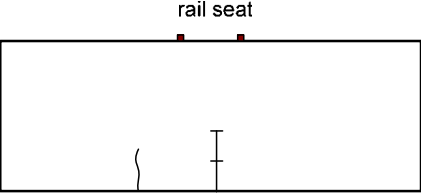
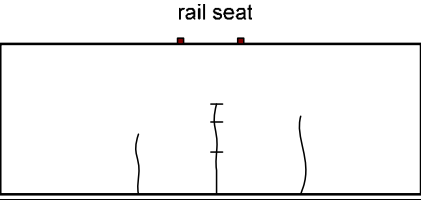
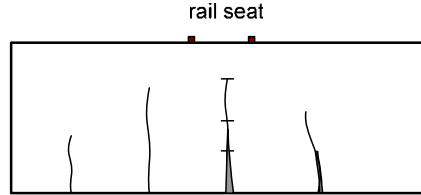
Figure 7.13 shows the crack increments due to the cumulative impulse before the concrete sleepers disintegrated. The crack increments were measured from the difference between the total crack length and the initial crack length. It is found that majority of cracks in hard track condition progressively occurred due to the small impact loads but only small and uniform increments propagated further. In contrast, the distribution of crack damage is wider for the concrete sleepers in soft track environment, and the uniform crack propagation can be noticed under severe impact loading conditions.



**Figure 7.13.** Incremental damage of railway concrete sleepers in different track environments

Based on the progressive impact tests of the concrete sleepers, damage classification of concrete sleepers under loading conditions can be presented in Table 7.9. The damage classification refers to the assessment of concrete sleepers in track systems, and is associated with cumulative impulse ratio  $I_R$  and damage index  $D$ , based on cumulative crack length in the concept of fracture mechanics (Fryba, 1996).

**Table 7.9** Damage classification of prestressed concrete sleepers

Damage Level	Description	Damage index, $D$	Cumulative impulse ratio, $I_R$
1. Light damage (reusable)	<p>Few small cracks incur in the concrete sleeper. The cracks grow quickly but significant crack widths can not be observed. The maximum crack length measured from soffit is not significant and do not affect the resistance of the sleeper.</p> 	0-0.50	0-0.20
2. Medium damage (reusable in light tracks)	<p>Cracks incur in the concrete sleeper. The cracks grow consistently and the crack widths can be observed of about 1 to 2 mm. The maximum crack length measured from soffit is remarkable but tends not to weaken the capacity of the sleeper.</p> 	0.50-0.75	0.20-0.65
3. Severe damage (non-reusable)	<p>Major cracks can be detected in the concrete sleeper. Although the cracks grow consistently, the crack widths are significant. The concrete spalling and dust can be noticed. The crack length measured from soffit grows largely and tends to significantly weaken the capacity of sleeper.</p> 	0.75-1.0	0.65-1.0

## 7.6 SUMMARY

Impact loading conditions on railway tracks are often caused by wheel or rail abnormalities such as flat wheels, dipped rails, etc. The cracks in railway concrete sleepers have been often observed due to the impact load, even though the possibility of occurrence for this large magnitude load is very low and it could be once or twice in their design life span of fifty to a thousand years. Current design method for prestressed concrete sleepers does not consider the ultimate behaviour under such impact loads. The widespread notion about the reserved strength of a concrete sleeper has raised the concern to develop its new ultimate limit states design concept. As a result, a high-capacity drop weight impact testing machine was constructed at the University of Wollongong, in order to evaluate the ultimate capacity of prestressed concrete sleepers under impact loads. The emphasis of this chapter is placed on the experimental investigations as to evaluate progressive impact behaviour, failure modes, and crack propagation of railway prestressed concrete sleepers under extreme impact loading.

This study includes the analytical and experimental investigations of the relationship between railseat bending moment and the impact force of prestressed concrete sleepers under impact loading, as a design guideline for track design engineers. The relationships between wheel/rail interface impact force and flexural moment acting at railseat of railway concrete sleepers are investigated experimentally and numerically. It is found that each particular track exhibit distinctive relationship and the best way to determine the bending moment along the railway sleepers is to employ the advanced dynamic analysis of railway tracks. However, in railway practice, the analytical and experimental results in this study confirm and provide the faster and adequate means to predict the bending moment on the sleepers from the anticipated wheel/rail interaction. The empirical moment envelope can be re-written as  $M^*=0.08I$ . This equation is found to be conservative for use in the dynamic design for prestressed concrete sleepers.

Based on the dynamic crack propagations, it is found that the initial cracks could occur in the hard track more rapid than in the soft track. On the other hand, the possibility of occurrence of the impact load causing the first crack in the soft track is much lower than that in the hard track. The first cracks due to impacts in the prestressed concrete sleepers

either in the soft or the hard tracks are always due to flexures. The impact failure modes at both support conditions were associated with both flexural and longitudinal splitting actions. The splitting fractures were aligned along the prestressing tendons. Due to the lack of concrete and tendon bonding, the impact stress waves travelling along the composite section become the key indicator for the combined failure mode. The probabilistic analysis of dynamic loading showed that the magnitude of the ultimate impact load causing the failure of the prestressed concrete sleeper would be equivalent to that with a return period of several million years. This implies the over-conservative design of the current Australian Standard for prestressed concrete sleepers.

By using the concept of damage accumulation, the relationships between cumulative damage of concrete sleepers and given impulse enable the predictions of residual life of the concrete sleepers under severe impact loads. It is noticed that the hard track condition rapidly exacerbates cracking in the concrete sleepers. The crack increment distribution of the hard track concrete sleepers was found in a relatively narrow range of impulse compared with the soft track concrete sleeper. However, uniform and small progress of cracks can be detected under more severe impact loading conditions. Based on the progressive impact testing, the damage classification of prestressed concrete sleepers has been proposed.

Next chapter presents investigations that include the repeated impact responses and the residual fracture toughness of prestressed concrete sleepers since these will lead to the better understanding of the limit states condition of prestressed concrete sleepers.

## CHAPTER 8

### REPEATED IMPACT BEHAVIOUR AND RESIDUAL CAPACITY OF PRESTRESSED CONCRETE SLEEPERS

So far, it is well known that the concrete sleepers in any track system are affected mostly by the dynamic impact loads. The severity level of impact damage depends largely on the magnitude of impact forces as well as the in-service experience of the concrete sleepers. The magnitudes of impact forces have been categorised by the building code of Australia (BCA), on the considerations of the importance of design structures and the possibility of load occurrence. The possibility of occurrence infers the repetition of the design load acting on the structures in a number of years. Understanding into the behaviour and the residual capacity of concrete sleepers under the repeated impact loads will allow track engineers to carry out the performance-based design for concrete sleepers. Nonetheless, the impact behaviours of concrete sleepers under repeated impact loads have not been investigated. This Chapter thus identifies the responses of prestressed concrete sleepers in railway track structures under both single and repeated impact loads associated with the design probability of occurrence (and return period). The fifty time repetition of loading implicates the possibility to upgrade the use of the concrete sleeper subject to the tested loads as a year return period. The residual capacities of the damaged prestressed concrete sleepers become a highlight of this study. The results exhibit the reserved strength of the prestressed concrete sleepers, which is untapped and long believed of its existence. The effects of track environment including soft and hard tracks are also demonstrated in this Chapter.

#### 8.1 OVERVIEW

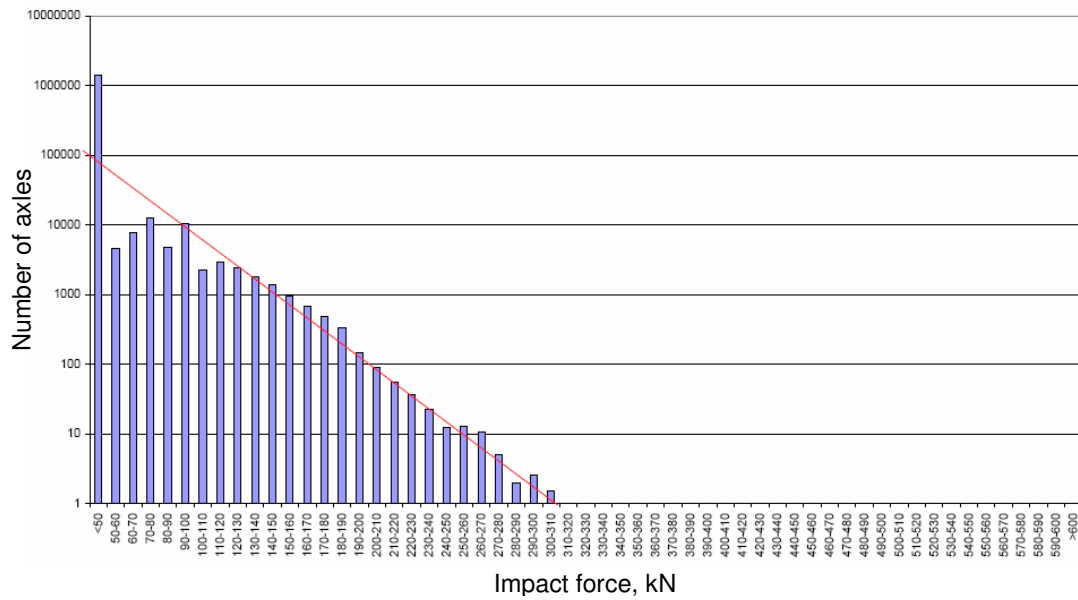
A recent study showed that there is a potential possibility for railway sleepers subject to severe impact loads (Leong, 2007). In general, the dynamic load characteristics considered in design and analysis include the magnitudes of impact loading and the variety of pulse durations. The loading and strain rate effects tend to complement the strength of materials whilst the high loading magnitude devastates the structural

members. In structural design and analysis, the public safety must not be compromised so the design loads must be appropriate and associated with the long return periods which would optimally provide the low probability of occurrence on structures during their design life. For further explanation, a design load that is associated with 50 year return period has the likelihood of occurrence that the design load might happen only once in 50 years regardless of the structural life span.

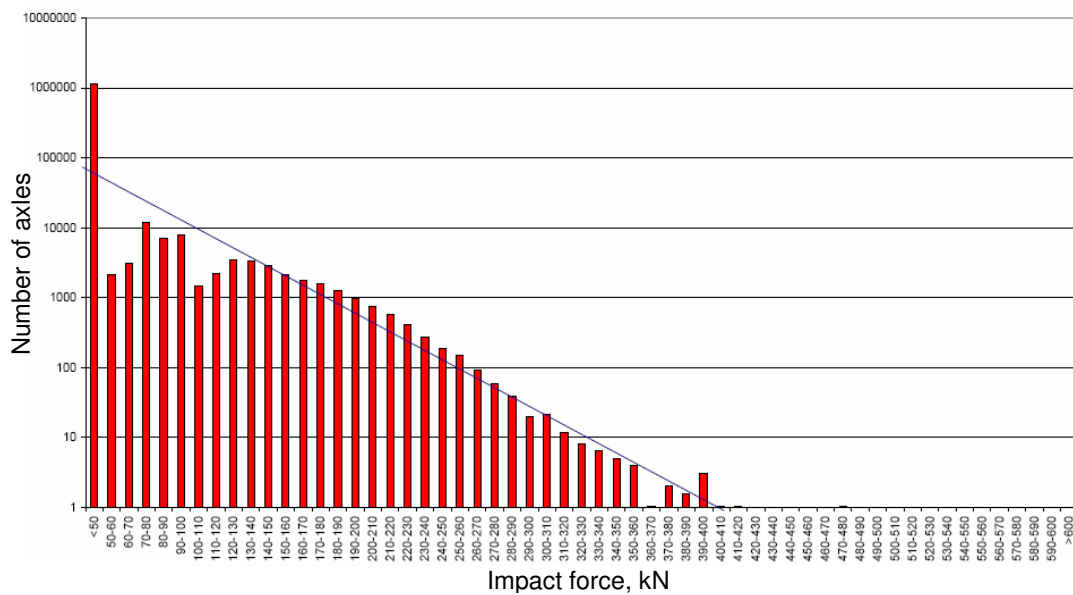
Wheel load is an important factor in design and analysis of railway track and its components. The design load ( $F^*$ ) for the limit states design concept takes into account both the static ( $F_s$ ) and dynamic ( $F_i$ ) wheel loads. There are three main steps in designing the concrete sleepers. First, the design actions or loads are to be determined based on the importance level of the track ( $F^* = 1.2 F_s + 1.5 F_i$ ). Then, the design moment can be achieved by converting the design load to sleeper moment using advanced railtrack dynamic analysis or the design formulation as described in Chapter 7. Last, the strength and serviceability of the prestressed concrete sleepers can be optimized in accordance with AS3600 Concrete structures (Standards Australia, 2001). The proposed limit states design methodology and procedure can be found in details in Chapter 10.

The building code of Australia (BCA) in conjunction with Standards Australia indicates the importance levels of structures for determining the probabilistic wheel loads for track design at ultimate limit states, upon the consequences of failure of the structures. As the design criteria for railway sleepers (with 50 to 100 years design life), loading with 100 years return period should be considered for the Category 1 tracks (infrequent traffic, interstates); 500 years return period for Category 2 tracks (regular, freight); and 2,000 years return period for Category 3 tracks (inner city suburban, heavy haul). For design and analysis of prestressed concrete sleepers, certain design loads associated with probabilistic return periods (related to the importance level of the structure) must be considered. The dynamic responses of prestressed concrete sleepers in railway track structures under repeated impact loads associated with the design probability of occurrence (and return period) have not yet been adequately addressed, although they are the key indicator for determining the reserved strength mechanism and performance-based optimisation (Murray and Cai, 1998).

Leong (2007) showed the statistical data of wheel loading obtained from railway networks in Queensland, Australia. Using probabilistic analysis, the possibility of occurrence related to the magnitude of impact loading on railway sleepers can be predicted. Figure 8.1 shows a statistical data of actual loading obtained from a railway network in North Queensland (Martin and Leong, 2006).



a) at Braeside



b) at Raglan

**Figure 8.1** A typical statistical data of loading on tracks (Leong, 2007)



From Figure 8.1, the relationships between the impact forces  $I$  and the return periods  $R$  can be written as follows:

$$\text{For Braeside, } \frac{1}{R} = 10^{-0.0191I+5.92} \quad (8.1)$$

$$\text{For Raglan, } \frac{1}{R} = 10^{-0.010I+4.1} \quad (8.2)$$

These formulae can be used to determine the impact force factor, which is based on the return periods and consequences of changing operations, such as speeds or wheel/rail defects (Leong, 2007), as will be described in Chapter 10.

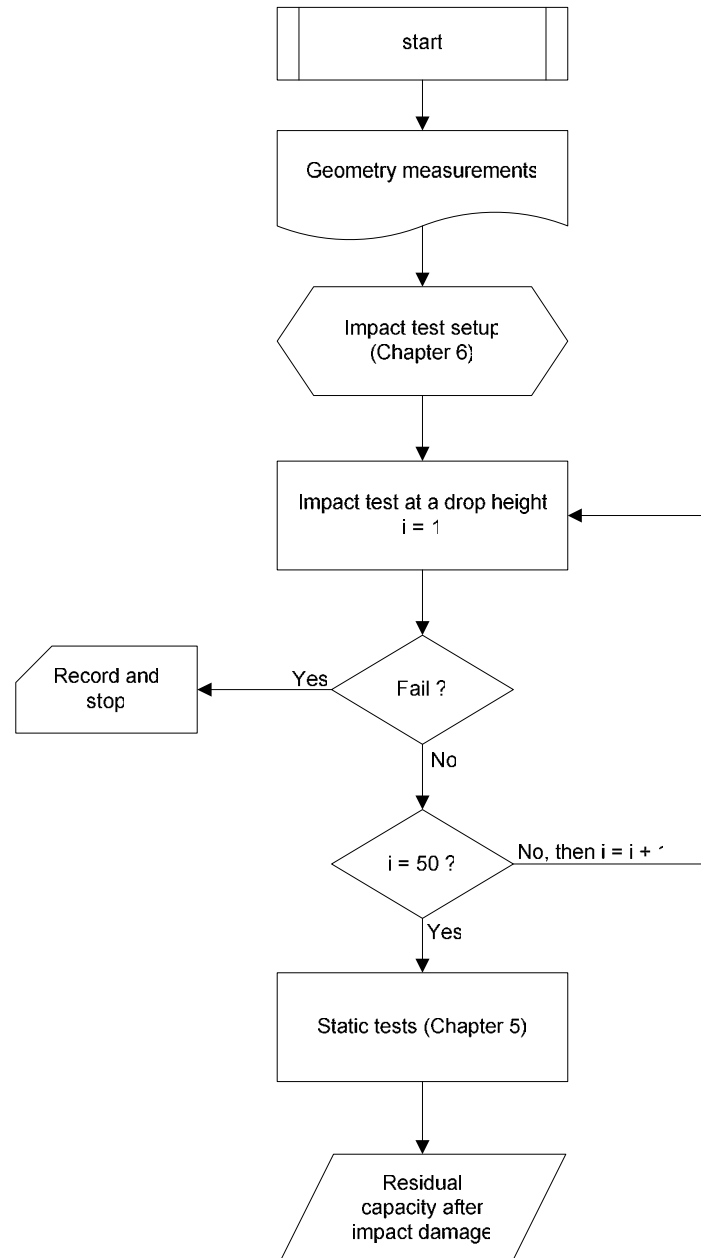
This chapter investigates the repeated impact responses and behaviour of railway prestressed concrete sleepers subjected to a variety of repeated impact loads. The prestressed concrete sleepers used were designed to comply with Australian Standard: AS1085.14 (2003). The test specimens were supplied by an Australian manufacturer, AUSTRAK. Drop-weight impact hammer was used to apply multiple impacts directly to the railseat at identical drop heights in order to repeat the pulse characteristics at each return period. The impact pulses were captured using the high capacity load cell connected to the National Instrument data acquisition system. The dynamic measurements also include dynamic strains and accelerations. The softening media placed on top of the railhead to reduce the contact stress was used. Neoprene rubber pads with thickness of 1.5 mm were used to control the duration of load pulses. Impact damage and crack propagation at each drop test were recorded. After each repeated impact test, the static test (as described in Chapter 5) was carried out to identify the residual capacity of a damaged prestressed concrete sleeper. The results show that a concrete sleeper damaged by an impact load could possess significant reserve capacity sufficient for resisting the axle load of about 1.05 to 1.10 times of the design axle loads. Also demonstrated are the effects of track environment including soft and hard tracks on the repeated impact behaviour and residual capacity of the prestressed concrete sleepers.

## 8.2 EXPERIMENTAL PROGRAM

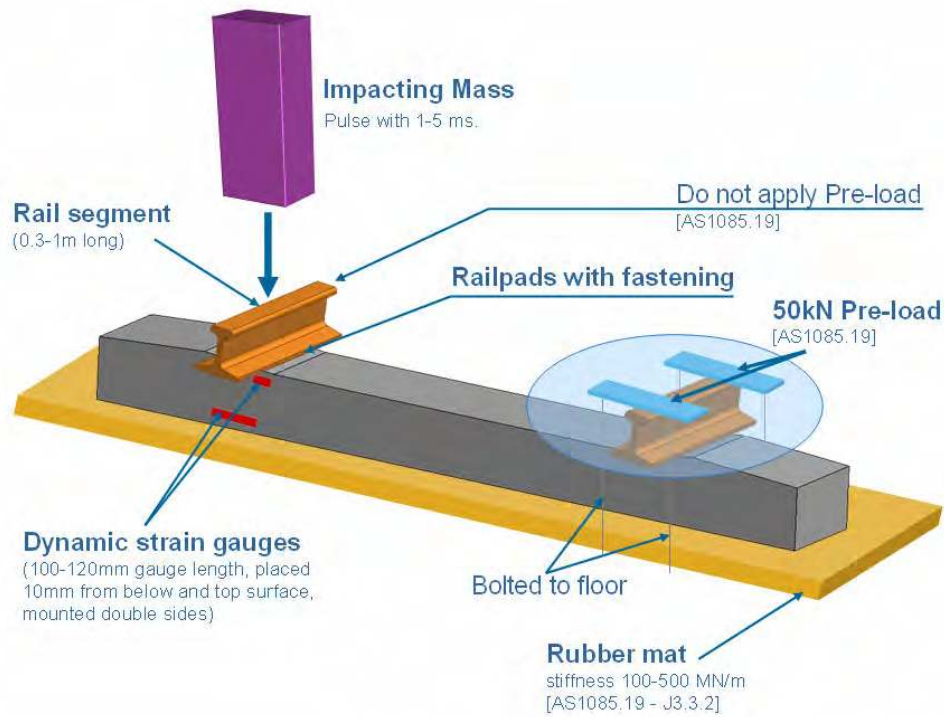
The details of the test specimens have been given in Chapter 6. The cross section of the prestressed concrete sleepers at railseat can also be seen in Figure 6.2. The alternative support condition for sleepers is adopted for the use in this study. The test setups for impact tests were described previously in Chapter 6, while the details of static test setups were earlier demonstrated in Chapter 5. In this study, the prestressed concrete sleepers are subjected to certain identical impact magnitudes. There are two phases of the experiments. The first phase is to evaluate the behaviours under 50 identically repeated impacts. The rationale for the 50 identical drop tests was that the sleepers are generally designed for 50 years and the potential of the concrete sleepers subject to increased wheel loads (associated with annual return period) was sought. The later phase is to identify the once-off impact behaviours (single drop) of the sleepers under the same sets of pulse magnitudes. Those impact tests have the same set of the impact force magnitudes, including 500 kN (associated with 50 years return period), 740 kN (associated with 2,000 years return period), and 810 kN (associated with 10,000 years return period). These probabilities were obtained from the field data (Leong, 2007)

Figure 8.2 presents the schematic flowchart of the investigations of concrete sleepers under impact and static loadings to evaluate the responses to repeated impacts and the consequent fracture toughness of the prestressed concrete sleepers. Table 8.1 shows a series of test program with the particular emphasis on the different target levels of impact force acting on the prestressed concrete sleepers. The series of impact test program were conducted using the same test setup as described in Chapter 6. Figure 8.3 presents the schematic setup of the prestressed concrete sleepers under impact testing. The special attention was paid to the identical drop height on the prestressed concrete sleepers to achieve the structural conditions under 50 repeated impact loads. In addition to the impact, acceleration, and dynamic strain signals, the data measurements include the crack propagations and the crack widths at each drop test. This chapter experimentally investigates the influence of ballast supports on the residual load-carrying capacity, repeated impact responses, and dynamic crack propagation. For comparison with those results in Chapter 7, two support conditions termed ‘soft track’ and ‘hard track’ were calibrated against the vibration modal parameters of the ballast support in actual tracks (Kaewunruen and Remennikov, 2007c). As aforementioned, the

soft track can be considered as thin ballast bed (about 100-150 mm in depth), while the hard track represents the thick layer of the ballast bed (more than 250 mm in depth). The experimental setups for support conditions were in accordance with AS1085.19 (2001), as illustrated in Figure 6.14 of Chapter 6 and Figure 8.3. The tests followed the schematic flowchart in Figure 8.2 but the magnitudes of impacts varied as follows: 500 kN, 740 kN, and 810 kN, as tabulated in Table 8.1.



**Figure 8.2** Flow chart of the repeated impact and residual capacity toughness tests



**Figure 8.3** Schematic experimental setup for impact testing

**Table 8.1.** Summary of impact and static testing programs

Support condition	Impact force (kN)	Related return period (years)	Number of blows	Subjecting static test
Soft track	500	50	1	✓
			50	✓
	740	2000	1	✓
			50	✓
	810	10,000	1	✓
50	✓			
1,500	millions	1	✓	
Hard track	500	50	1	✓
			50	✓
	740	2000	1	✓
			50	✓
	810	10,000	1	✓
50	✓			
1,500	millions	1	✓	

### 8.3 CRACK PROPAGATION UNDER SINGLE IMPACT CONDITIONS

Cracks in the prestressed concrete sleepers were visually observed after each drop test. This type of crack is referred to as the residual crack as the cracks were closed in the unloaded conditions. Measurements of crack widths and lengths were carried out after each impact using the magnifying glass telescope. The length of the residual cracks is the main indicator for the durability and serviceability of the prestressed concrete sleeper in practice (Wang, 1996). It should also be noted that the lengths of the residual crack and the maximum opened crack due to dynamic impact are fairly close.

#### 8.3.1 Cracks of prestressed concrete sleeper in soft track condition

##### 8.3.1.1 Single impact load of 500 kN

The first cracks that formed in the sleeper under the impact load of 500 kN were 'hair line' flexural cracks at the bottom fibre of loaded railseat. It is important to note that there is no crack occurred at the other railseat. Figure 8.4 shows the crack pattern of the prestressed concrete sleeper under the single impact of 500 kN. It is found that there is no major crack occurred. The average crack length measured from both front and rear faces is about 97.5 mm, while the crack width is around 0.01-0.02 mm. Clearly, under the 50 year-return-period loading, the sleeper seemed to possess a large amount of reserved strength.



a) front face

b) rear face

**Figure 8.4** Cracks in a sleeper in soft track after a single impact of 500 kN

### 8.3.1.2 Single impact load of 740 kN

The first cracks that formed in the sleeper under the impact load of 740 kN were also flexural cracks arising from the bottom fibre of loaded railseat, whilst no crack can be observed at the other end. Figure 8.5 shows the crack pattern of the prestressed concrete sleeper under the single impact of 740 kN. It is found that the lengths of cracks are quite significant, which are more than half of the sleeper's cross section. The average crack length measured from both front and rear faces is about 137.5 mm, while the residual crack width is around 0.01-0.03 mm.



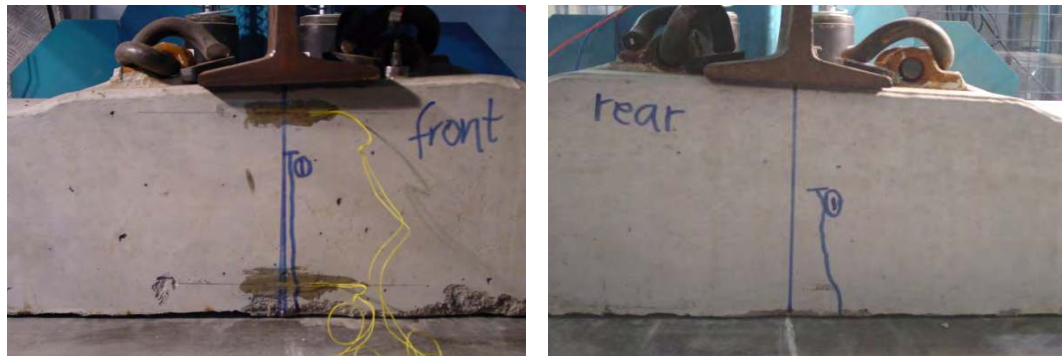
a) front face

b) rear face

**Figure 8.5** Cracks in a sleeper in soft track after a single impact of 740 kN

### 8.3.1.3 Single impact load of 810 kN

The first cracks in the sleeper under the impact load of 810 kN were flexural cracks arising from the bottom fibre of loaded railseat, whilst there is no crack noticeable at the other railseat. Figure 8.6 shows the crack pattern of the prestressed concrete sleeper under the single impact of 810 kN. It is found that the lengths of cracks are considerable, which are a bit less than those under 740 kN. The average crack length measured from both front and rear faces is about 125.5 mm, while the residual crack width is around 0.02-0.03 mm.



a) front face

b) rear face

**Figure 8.6** Cracks in a sleeper in soft track after a single impact of 810 kN

#### 8.3.1.4 Single impact load of 1,500 kN

The first set of cracks in the sleeper under the impact load of 1,500 kN were a combination of flexural cracks arising from the bottom fibre and spalling of concrete in the top fibre (under compression) of loaded railseat. On the other hand, there is no crack observable at the other railseat or at the mid span. Figure 8.8 shows the crack pattern of the prestressed concrete sleeper under the single impact of 1,500 kN. It is found that the lengths of cracks are substantial, as three cracks can be clearly noticed. The longest (centre) crack length measured from both front and rear faces is about 160.5 mm, while the residual crack widths are varied from 0.02 mm to 0.08 mm.



a) front face

b) rear face

**Figure 8.8** Cracks in a sleeper in soft track after a single impact of 1,500 kN

### 8.3.2 Cracks of prestressed concrete sleeper in hard track condition

#### 8.3.2.1 Single impact load of 500 kN

The first cracks that formed in the sleeper under the impact load of 500 kN were tiny flexural cracks at the bottom fibre of loaded railseat. It is noted that there is no crack occurred at both the other railseat and the mid span. Figure 8.9 shows the crack pattern of the prestressed concrete sleeper under the single impact of 500 kN. The cracks occurred are rather insignificant. The average crack length measured from both front and rear faces is about 112.5 mm, while the crack width is around 0.01-0.02 mm. Clearly, under the 50 year-return-period loading, the sleeper in the hard track condition also tends to own a large amount of untapped strength.



a) front face

b) rear face

**Figure 8.9** Cracks in a sleeper in hard track after a single impact of 500 kN

#### 8.3.2.2 Single impact load of 740 kN

The first cracks that formed in the sleeper under the impact load of 740 kN were small flexural cracks at the bottom fibre of loaded railseat. It is noted that there is no crack occurred at both the other railseat and the mid span. Figure 8.10 shows the crack pattern of the prestressed concrete sleeper under the single impact of 740 kN. The cracks occurred are rather insignificant. The average crack length measured from both front and rear faces is about 141.5 mm, while the crack width is around 0.01-0.03 mm.





**Figure 8.10** Cracks in a sleeper in hard track after a single impact of 740 kN

### 8.3.2.3 Single impact load of 810 kN

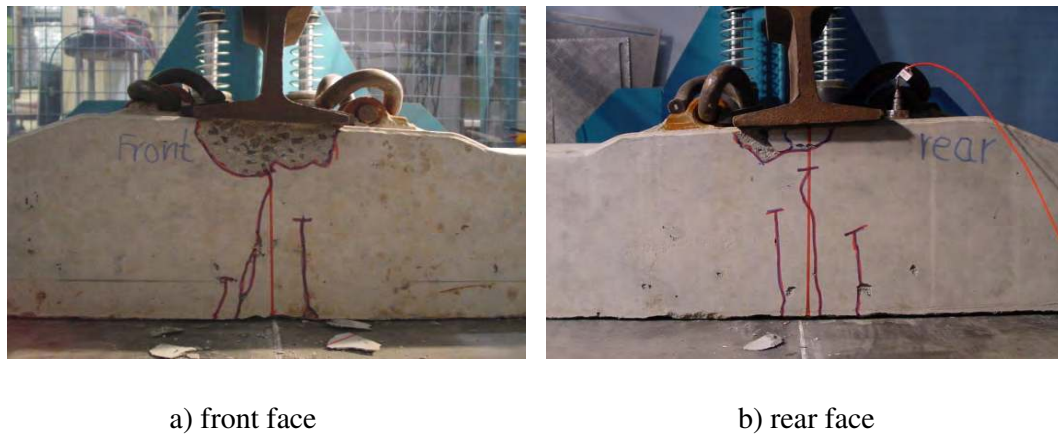
The first cracks in the sleeper under the impact load of 810 kN were flexural cracks arising from the bottom fibre of loaded railseat, whilst there is no crack noticeable at the other railseat. Figure 8.11 shows the crack pattern of the prestressed concrete sleeper under the single impact of 810 kN. It is found that the lengths of cracks are a bit lesser than those under 740 kN. However, there is a spalling of concrete in top fibre (under compression) of the sleeper. The average crack length measured from both front and rear faces is about 133.5 mm, while the residual crack width is around 0.03-0.04 mm.



**Figure 8.11** Cracks in a sleeper in hard track after a single impact of 810 kN

### 8.3.2.4 Single impact load of 1,500 kN

The first set of cracks in the sleeper under the impact load of 1,500 kN were a combination of flexural cracks arising from the bottom fibre and spalling of concrete in the top fibre (under compression) of loaded railseat. On the other hand, there is no crack observable at the other railseat or at the mid span. Figure 8.12 shows the crack pattern of the prestressed concrete sleeper under the single impact of 1,500 kN. It is found that the lengths of cracks are substantial, as three cracks can be visibly noticed. The longest (centre) crack length measured from both front and rear faces is about 168.5 mm, while the residual crack widths are varied from 0.04 mm to 0.08 mm.



**Figure 8.12** Cracks in a sleeper in hard track after a single impact of 1,500 kN

### 8.3.3 Crack propagations under single impact loading

Figure 8.13 shows the relation between the impact loads and the crack length propagation of the prestressed concrete sleeper under the impact testing conditions. It is found that the average discrepancy in the crack length between the soft and hard tracks is about 7 percent. As concurrently found in Chapter 7, it is clear that the dynamic crack propagation of the prestressed concrete sleeper in hard track environment is higher than that in soft track environment.

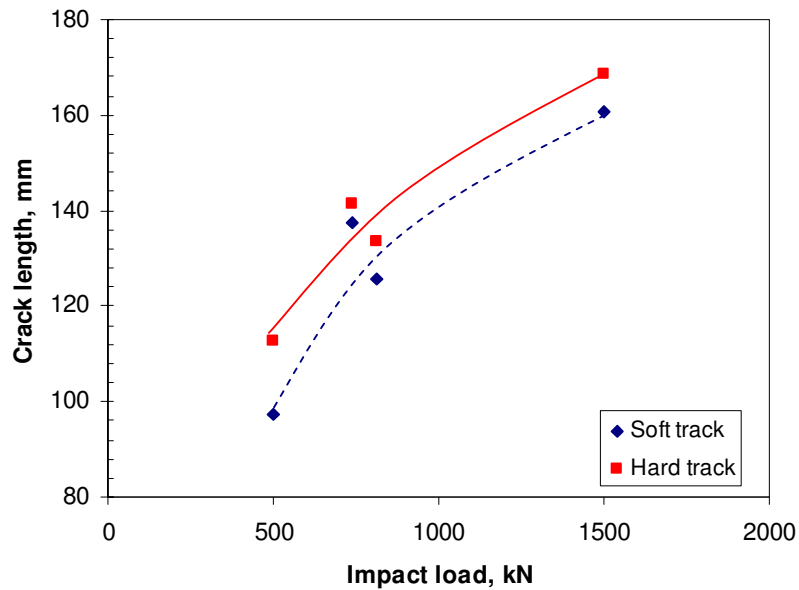


Figure 8.13 Crack propagations in the sleepers under single impact loads

## 8.4 CRACK PROPAGATION UNDER REPEATED IMPACT CONDITIONS

### 8.4.1 Cracks of prestressed concrete sleeper in soft track condition

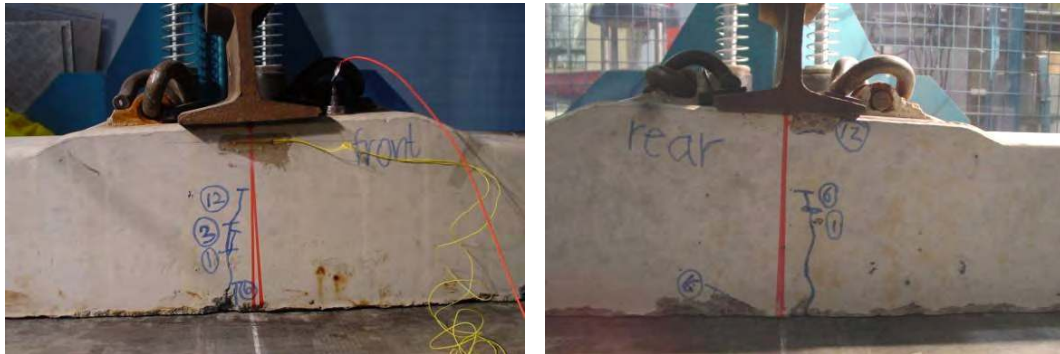
#### 8.4.1.1 Repeated impact loads of 500 kN

The first cracks that formed in the sleeper under the repeated impact load of 500 kN were ‘hair line’ flexural cracks at the bottom fibre of loaded railseat. It should be noted that there is no crack in the other railseat of sleeper. After 50 identical impact drop tests, there is no significant crack in the sleeper as demonstrated in Figure 8.14. It is however found that few small cracks occurred after the 16<sup>th</sup> blow at mid span as shown in Figure 8.15. Clearly, the sleeper seemed to have a large portion of reserved strength.

#### 8.4.1.2 Repeated impact loads of 740 kN

The first cracks that formed in the sleeper under the repeated impact load of 740 kN were small flexural cracks at the bottom fibre of loaded railseat. After 50 identical impact drop tests, there is no significant crack in the sleeper as demonstrated in Figure 8.16. However, it is observable that there are few cracks at the mid span of the

prestressed concrete sleeper, as illustrated in Figure 8.17. Overall, the sleeper tends to be able to resist larger load, or has a large portion of reserved strength.



a) front face

b) rear face

**Figure 8.14** Cracks in a sleeper in soft track after 50 repeated impact of 500 kN



**Figure 8.15** Cracks in a sleeper mid-span in soft track after 50 drops of 500 kN



**Figure 8.16** Cracks in a sleeper in soft track after 50 repeated impact of 740 kN

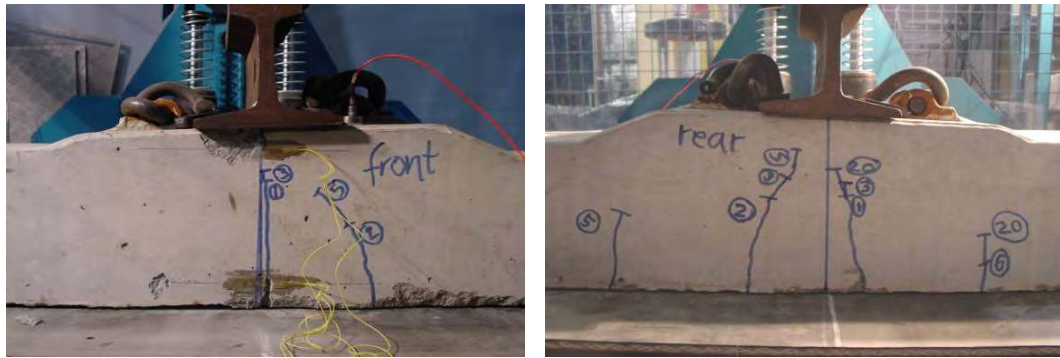


**Figure 8.17** Cracks in a sleeper mid-span in soft track after 50 drops of 740 kN

#### 8.4.1.3 Repeated impact loads of 810 kN

The first set of cracks that formed in the sleeper under the repeated impact load of 810 kN were fairly small flexural cracks at the bottom fibre of loaded railseat. After 50

identical impact drop tests, there is no major crack in the sleeper as demonstrated in Figure 8.18. However, it is observable that there are few cracks at the mid span and the spalling of concrete at the top fibre of railseat of the prestressed concrete sleeper, as illustrated in Figures 8.18 and 8.19. Overall, the sleeper tends to be able to resist larger load, or has a large amount of reserved strength.



a) front face

b) rear face

**Figure 8.18** Cracks in a sleeper in soft track after 50 repeated impact of 810 kN



**Figure 8.19** Cracks in a sleeper mid-span in soft track after 50 drops of 810 kN

## 8.4.2 Cracks of prestressed concrete sleeper in hard track condition

### 8.4.2.1 Repeated impact loads of 500 kN

The first cracks that formed in the sleeper under the repeated impact load of 500 kN were small flexural cracks at the bottom fibre of loaded railseat. It should be noted that there is no crack in the other railseat of sleeper. After 50 identical impact drop tests, there is no significant crack in the sleeper as demonstrated in Figure 8.20. It is found that few small cracks occurred after 50 blows at mid span as shown in Figure 8.21. Clearly, the sleeper seemed to have a large portion of reserved strength.



a) front face

b) rear face

**Figure 8.20** Cracks in a sleeper in hard track after 50 repeated impact of 500 kN

### 8.4.2.2 Repeated impact loads of 740 kN

The first cracks that formed in the sleeper under the repeated impact load of 740 kN were small flexural cracks at the bottom fibre of loaded railseat. It should be noted that there is no crack in the other railseat of sleeper. After 50 identical impact drop tests, there is no significant crack in the sleeper as demonstrated in Figure 8.22. Several of small cracks can be found after 50 blows at mid span as shown in Figure 8.23. It exhibits that the sleeper has a large potential of reserved strength.



**Figure 8.21** Cracks in a sleeper mid-span in hard track after 50 drops of 500 kN



a) front face

b) rear face

**Figure 8.22** Cracks in a sleeper in hard track after 50 repeated impact of 740 kN





**Figure 8.23** Cracks in a sleeper mid-span in hard track after 50 drops of 740 kN



a) front face

b) rear face

**Figure 8.24** Cracks in a sleeper in hard track after 50 repeated impact of 810 kN

#### 8.4.2.3 Repeated impact loads of 810 kN

The first set of cracks that formed in the sleeper under the repeated impact load of 810 kN were few small flexural cracks at the bottom fibre of loaded railseat. However, it should be noted that there is no crack in the other railseat of sleeper. After 50 identical impact drop tests, there is no significant crack in the sleeper as shown in Figure 8.24.

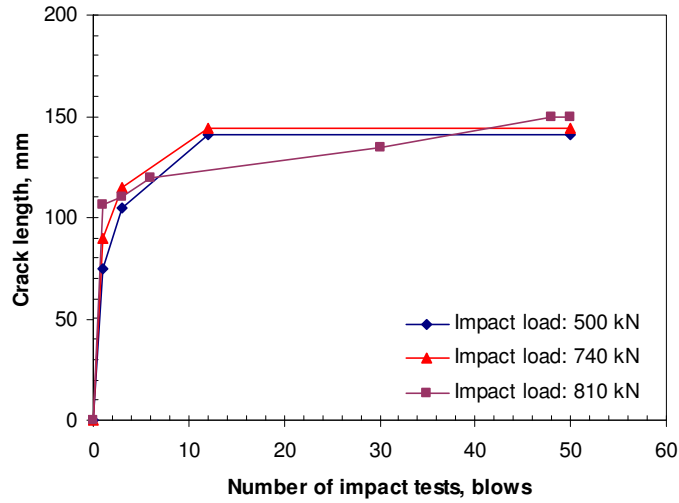
Few of small cracks can be found at mid span of the prestressed concrete sleeper after 50 blows as shown in Figure 8.25. It implies that the sleeper has a large amount of strength that is untapped.



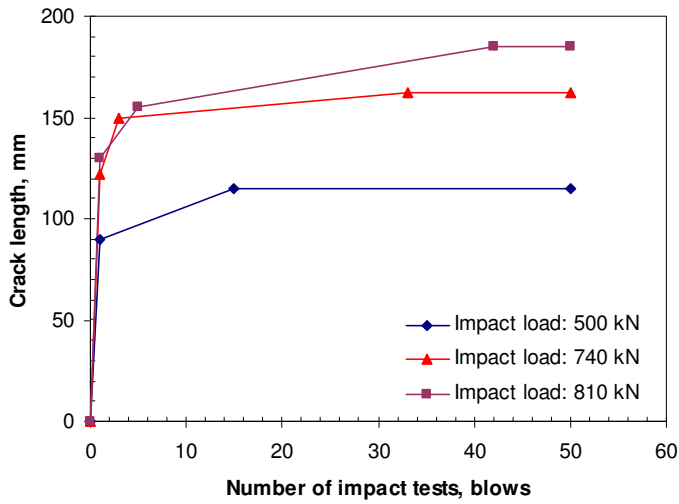
**Figure 8.25** Cracks in a sleeper mid-span in hard track after 50 drops of 810 kN

### 8.4.3 Crack propagations under multiple impact loading

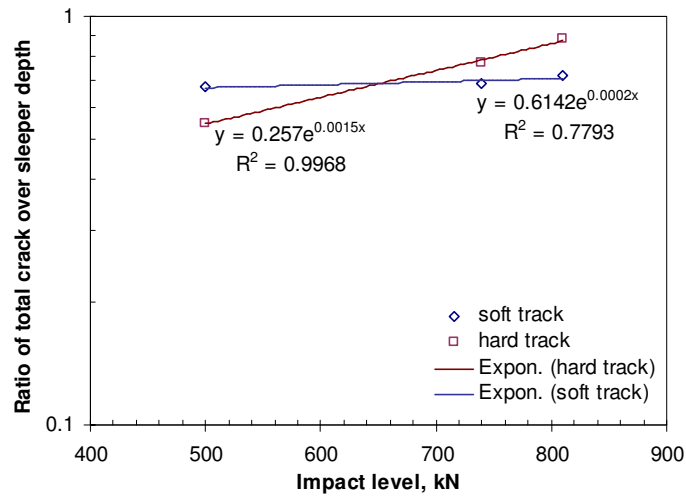
Figure 8.26 show the relations between the number of impact blows and the crack length propagation of the prestressed concrete sleeper under soft and hard track environments. It is found that the average discrepancy in the crack length between the soft and hard tracks is about 5.5 percent. As earlier discovered, it is apparent that, in general, the dynamic crack propagation of the prestressed concrete sleeper in hard track environment is higher than that in soft track environment. Figure 8.26(c) shows that the semi-logarithm relationship between normalised crack length and the impact load levels. The linear trends of the relationships can be observed.



a) soft-track sleepers under multiple impact loads



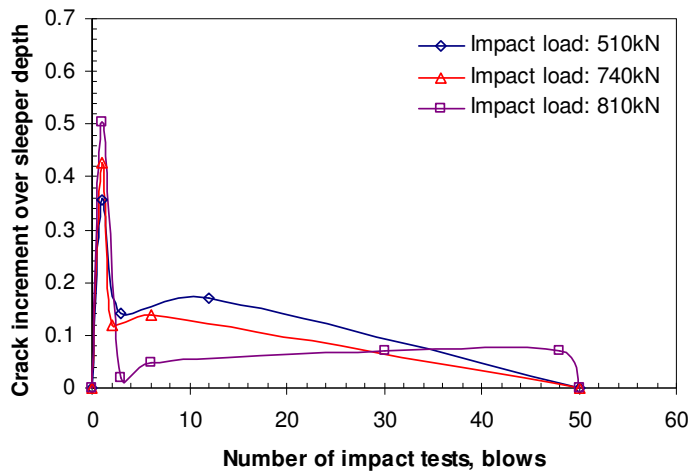
b) hard-track sleepers under multiple impact loads



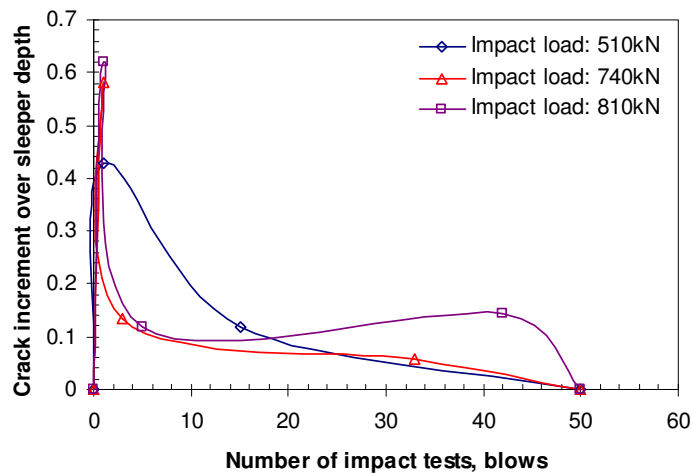
c) total crack lengths at different impact load levels

Figure 8.26 Crack propagations in concrete sleepers under multiple impact loads

Figure 8.27 show the distributions of percent crack increments of the prestressed concrete sleeper under soft and hard track environments against the number of impact blows. The results of crack propagations in both soft- and hard-track sleepers show that the low level of impact load tends to spread the crack propagation in a wider range compared with those subject to the higher levels of impact loading. It was also found that once the crack reached the critical lengths, which are about 80 percent of total sleeper depth (at rail seat), the crack did not further develop or only infinitesimal crack length could be caused by more blows of impacts.



a) soft-track sleeper



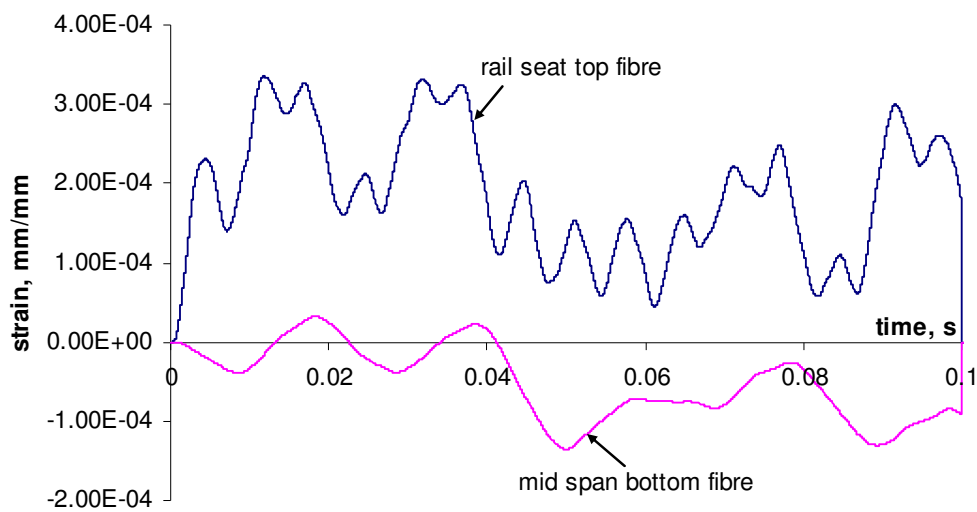
b) hard-track sleeper

**Figure 8.27** Crack distributions in the concrete sleepers under multiple impact loads

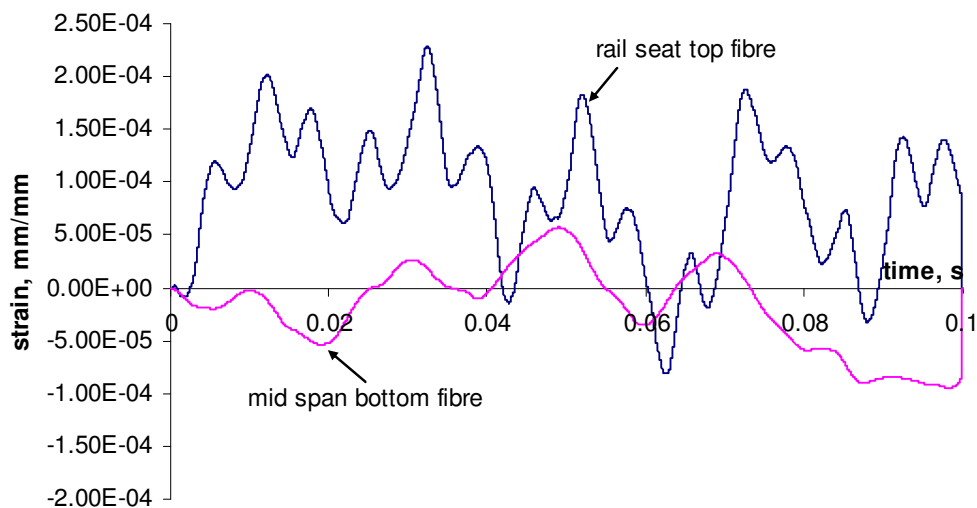
## 8.5 SINGLE IMPACT RESPONSES

### 8.5.1 Dynamic strains

The dynamic strains can be captured using the strain gauges at the top and bottom fibres of the prestressed concrete sleepers. At each drop, the dynamic strains were captured and converted to the associated dynamic moment. Figure 8.28 shows the example to the dynamic strains due to the impact load of 500 kN.



a) soft track environment



b) hard track environment

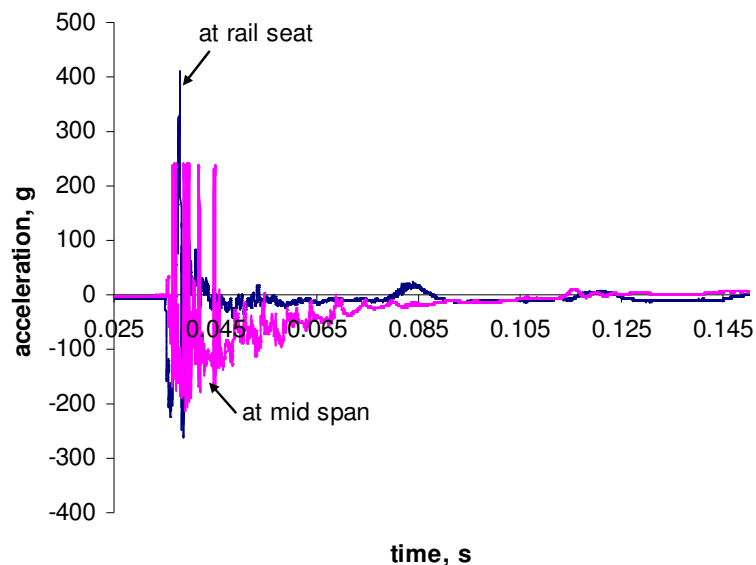
**Figure 8.28** Strains due to the impact load of 500 kN

It is found that, at either the railseat top fibre or the mid span bottom fibre due to 500 kN impact, the dynamic strains shift in a wider range for the prestressed concrete sleeper in hard track environment. The strains in hard-track sleepers move in both positive and negative ranges of bending moments. The dynamic strains due to other impacts also present similar phenomena.

### 8.5.2 Accelerations

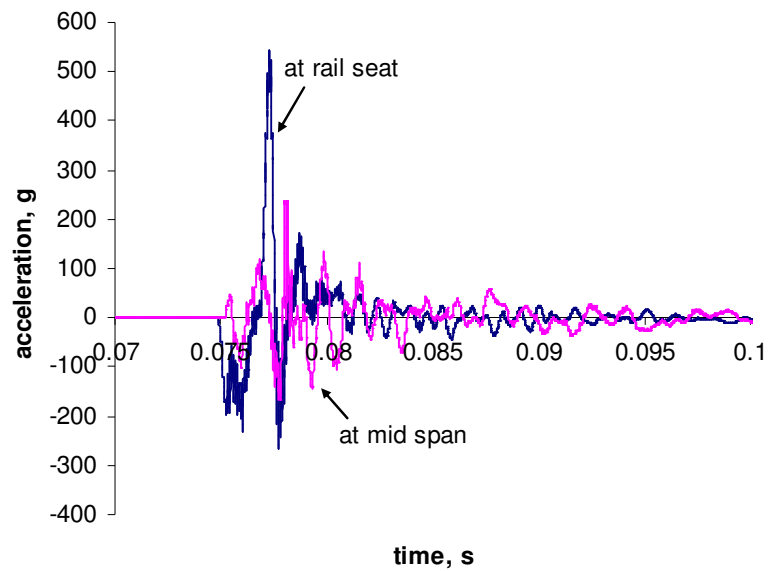
The acceleration responses were obtained by mounting the accelerometers at the railseat, at the loaded end, and at the mid-span of the prestressed concrete sleepers. At each drop, the accelerations were recorded as to compare with the numerical study in the future. Figure 8.29 shows the example to the acceleration responses due to the impact load of 500 kN.

It is found that the track environment plays a role in the acceleration responses at both railseat and at mid span of the prestressed concrete sleepers. The maximum amplitudes of the accelerations of the sleeper in soft track condition are about +400g at railseat and about +230g at mid span, while those of the sleeper in hard track condition are +600g and +255g at railseat and at mid span, respectively. In addition, the acceleration responses due to other impact magnitudes show the similar trend.



a) soft track environment

**Figure 8.29** Acceleration responses due to the impact load of 500 kN



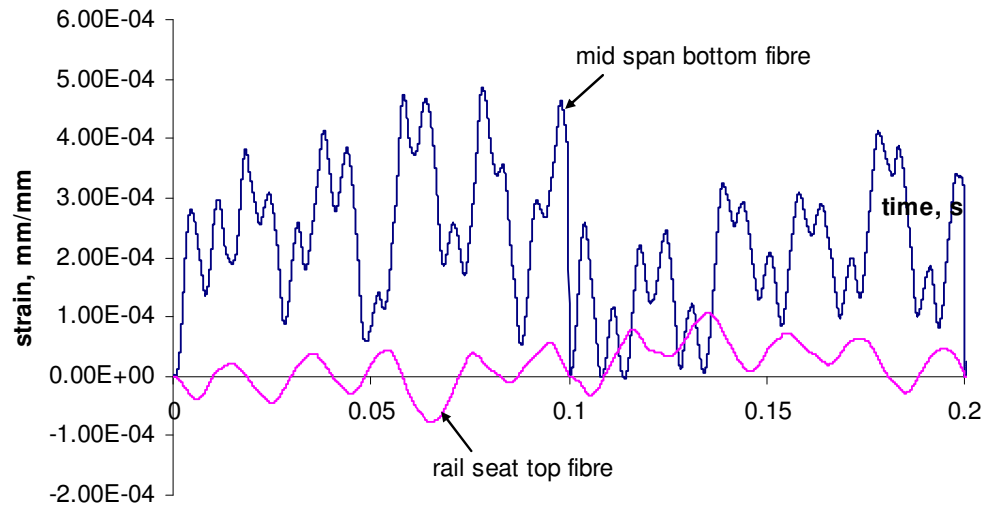
b) hard track environment

**Figure 8.29** Acceleration responses due to the impact load of 500 kN

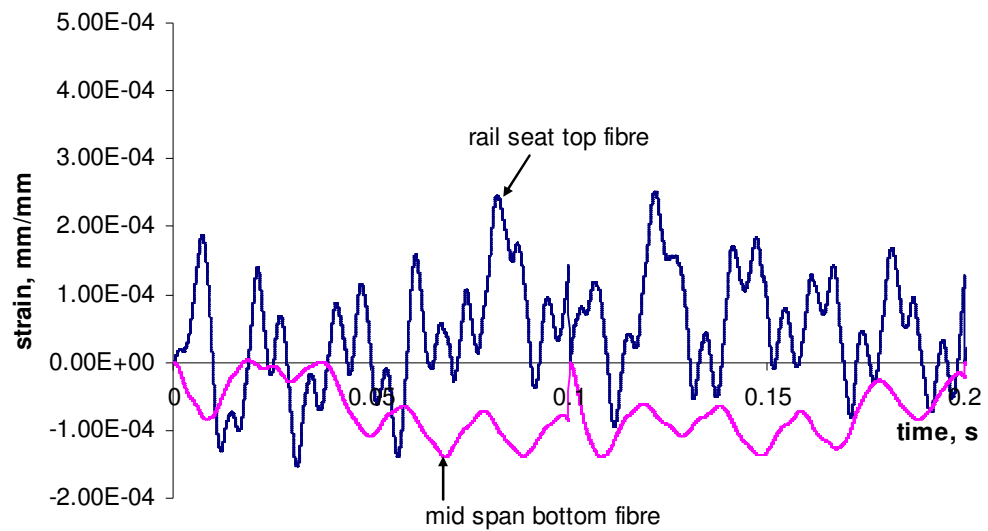
## 8.6 REPEATED IMPACT RESPONSES

### 8.6.1 Dynamic strains

The dynamic strains along both top and bottom fibres of the prestressed concrete sleepers change at each time. In these experimental investigations, the strain gauges were calibrated each test to record the offset dynamic strain signals. Figure 8.30 presents the dynamic strain signals at after 10 drop impact tests. It is found that the dynamic strains after 10 drop impact tests are slightly lower than those at the first drop test, as shown in Figure 8.29. Figures 8.31 and 8.32 show the dynamic strains after 20 and 50 drop impact tests, respectively. The similar trend also occurs at the higher impact loads. Overall, the figures exhibit that the sleepers subjected to multiple drop impacts tend to have more cracks and those cracks are opened. The cracks become larger and wider, which result in the lower range of the dynamic strains at both railseat and mid-span.



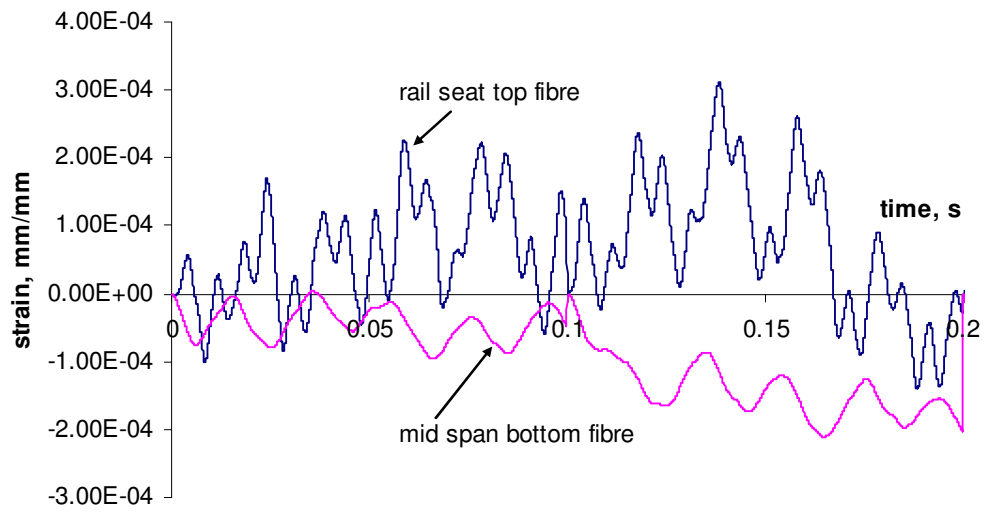
a) soft track environment



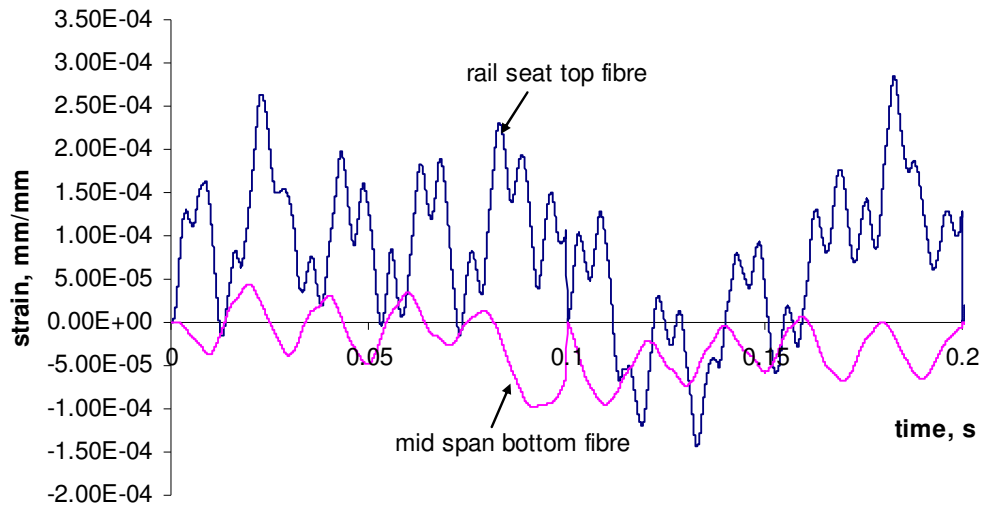
b) hard track environment

**Figure 8.30** Dynamic strains after 10 drop tests of impact load of 500 kN



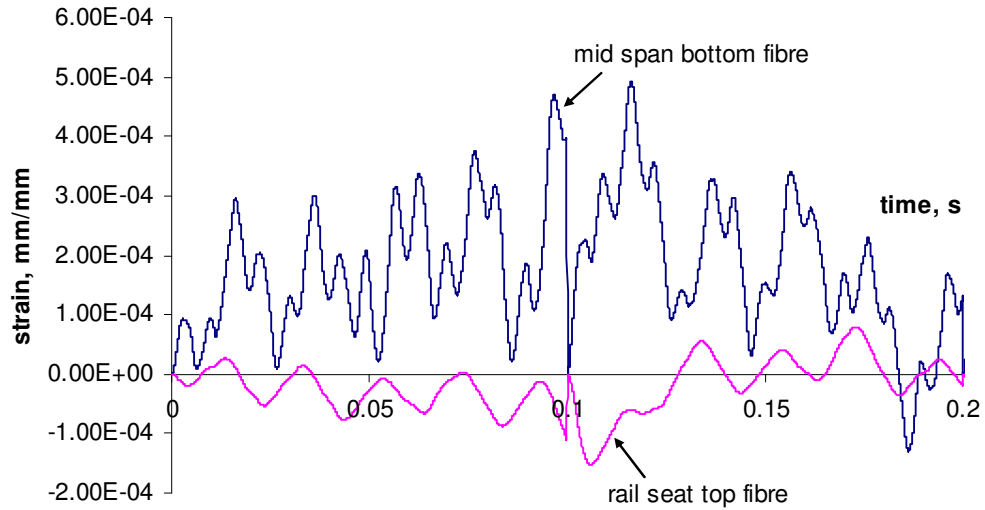


a) soft track environment

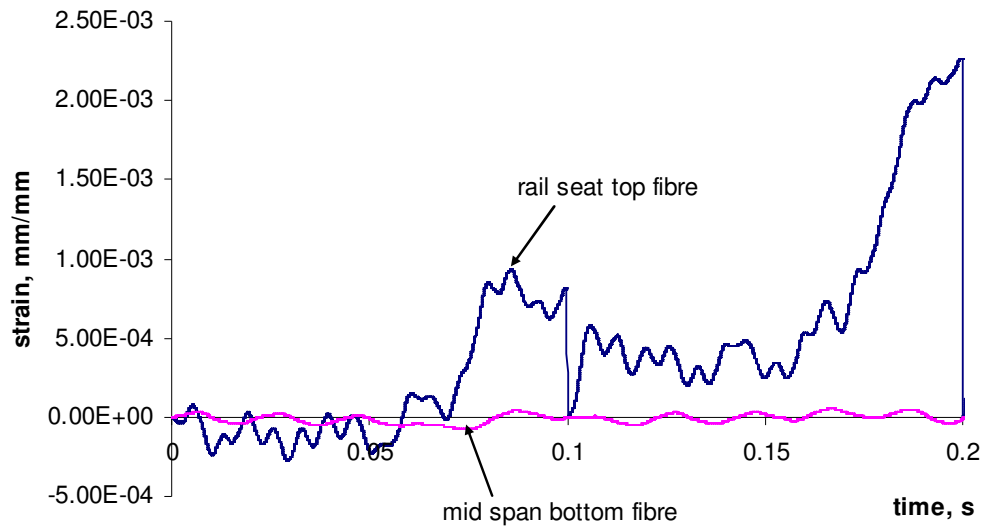


b) hard track environment

**Figure 8.31** Dynamic strains after 20 drop tests of impact load of 500 kN



a) soft track environment

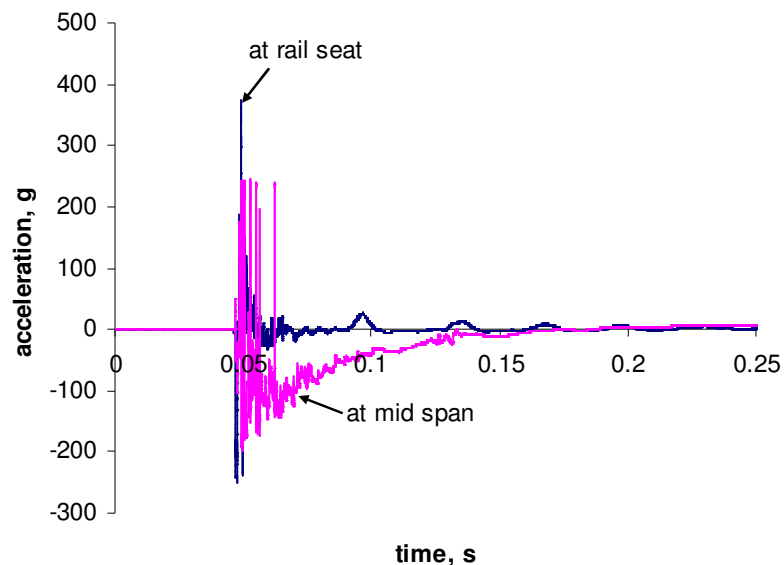


b) hard track environment

**Figure 8.32** Dynamic strains after 50 drop tests of impact load of 500 kN

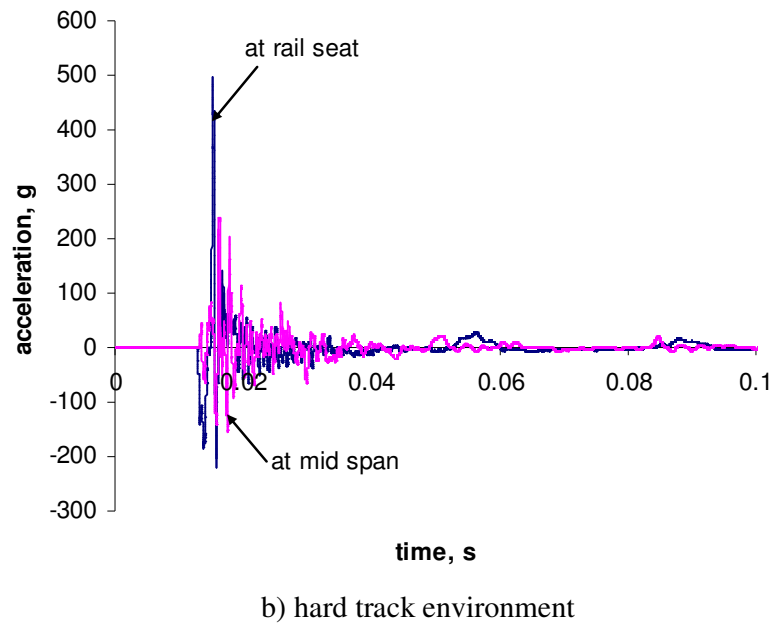
### 8.6.2 Accelerations

In these experimental investigations, the accelerations were recorded using high-amplitude accelerometers. The accelerations at the loaded railseat and at mid span of the prestressed concrete sleepers were obtained at each drop test. Figure 8.33 presents the acceleration responses after 10 drop impact tests. It is found that the magnitudes of the acceleration responses after 10 drop impact tests are slightly lower than those at the first drop test, as shown in Figure 8.29. Figures 8.34 and 8.35 illustrate the acceleration responses after 20 and 50 drop impact tests, respectively. It should be noted that the similar trend also occurs for the sleepers under the higher impact loads, so that those plots are excluded in this chapter. Overall, it exhibits that the sleepers subjected to multiple drop impacts tend to provide lesser dynamic stiffness due to larger cracks. This leads to the slightly larger range of the acceleration responses at both railseat and mid-span of the prestressed concrete sleepers. However, when considering the overall acceleration responses after 50 impact drops, the effect of cracks in the sleepers is not significant.

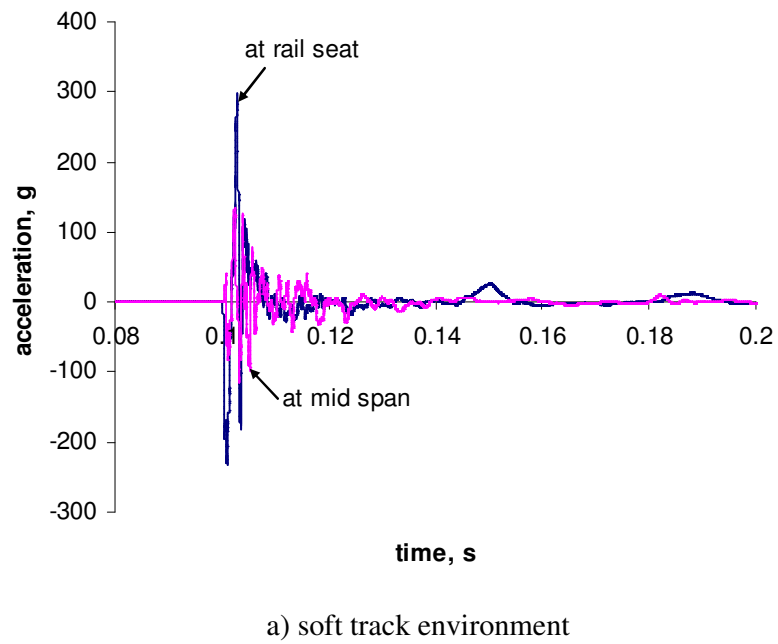


a) soft track environment

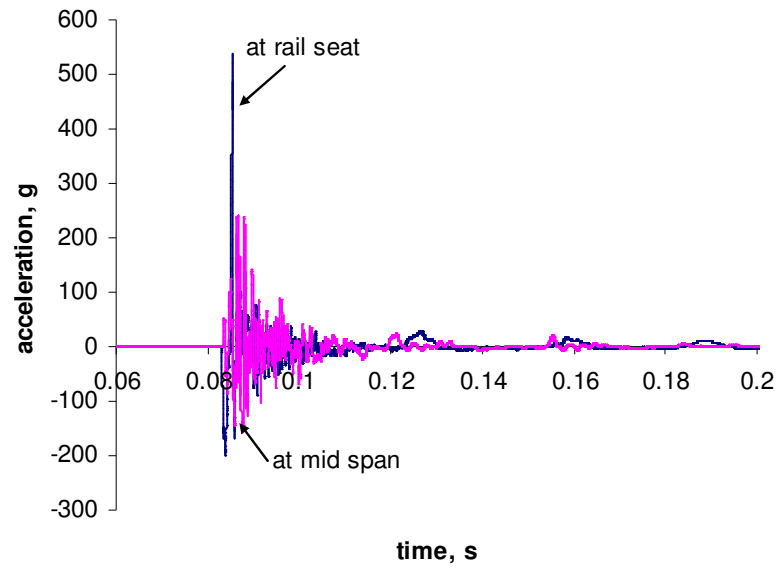
**Figure 8.33** Accelerations after 10 drop tests of impact load of 500 kN



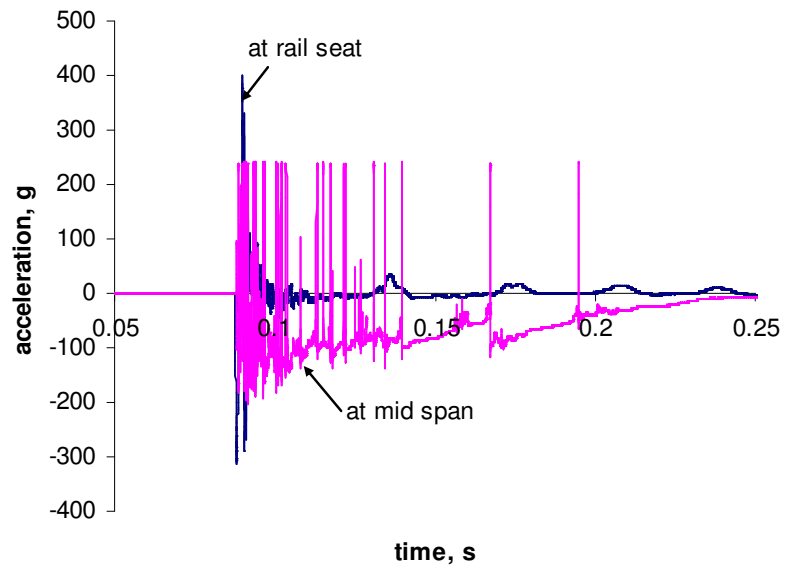
**Figure 8.33** Accelerations after 10 drop tests of impact load of 500 kN



**Figure 8.34** Accelerations after 20 drop tests of impact load of 500 kN

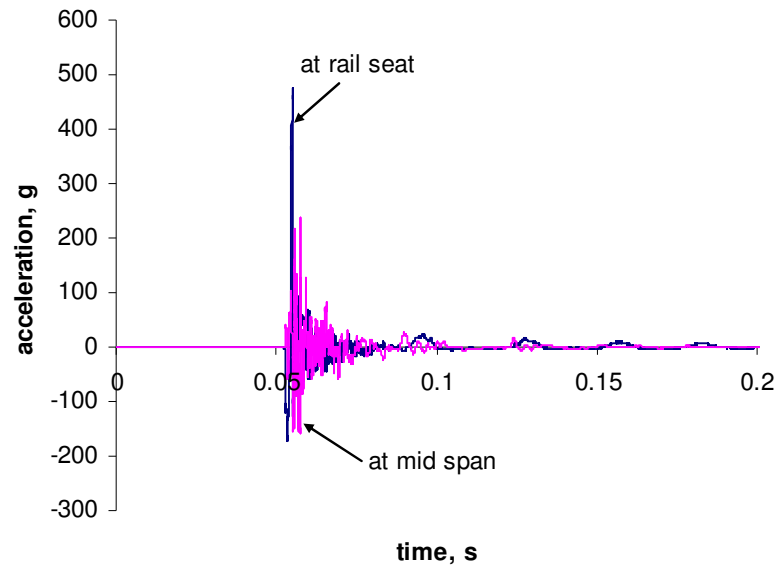


b) hard track environment

**Figure 8.34** Accelerations after 20 drop tests of impact load of 500 kN

a) soft track environment

**Figure 8.35** Accelerations after 50 drop tests of impact load of 500 kN



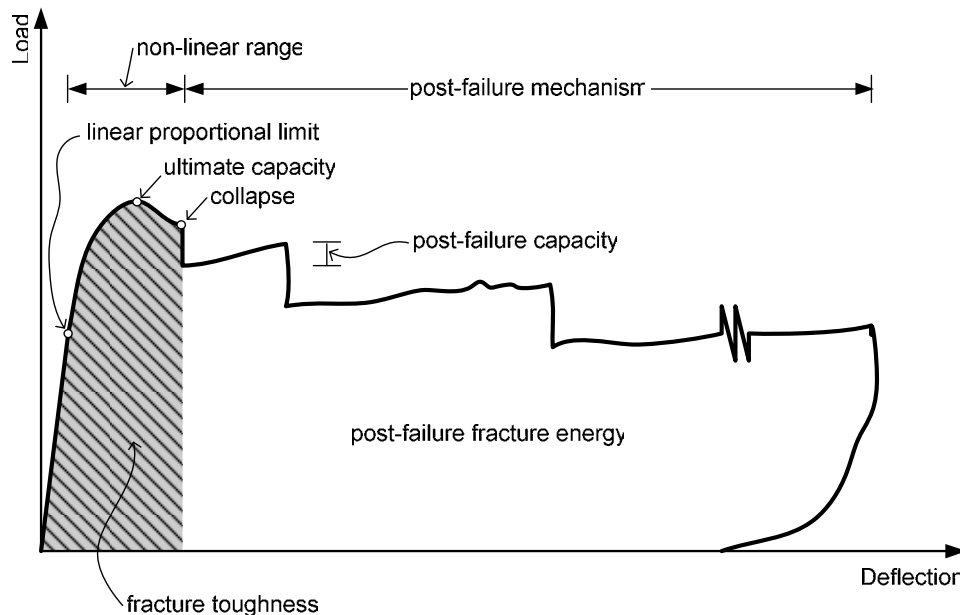
b) hard track environment

**Figure 8.35** Accelerations after 50 drop tests of impact load of 500 kN

## 8.7 RESIDUAL CAPACITY

After completing 50 drop tests, it is clear that the sleepers have a great potential that they could withstand further loading. As a result, the damaged sleepers are subjected to the static testing as described in Chapter 5, as to evaluate the residual load carrying capacity and the residual fracture toughness of the prestressed concrete sleepers. Through the static tests, the residual load carrying capacity is plotted against the railseat deflection. The fracture toughness can subsequently be identified by the integration (area under the curve) of the load-deflection relationship. There are two sets of the damaged sleepers, including those under single impacts and those under repeated impacts. The single impact tests relate to the pulse magnitudes of 500 kN, 740 kN, 810 kN, and 1,500 kN, while the repeated impact tests are associated with the pulse magnitudes of 500 kN, 740 kN, and 810 kN. The effect of the support conditions (soft and hard tracks) on the residual capacity is to be discussed. The comparison between residual capacities of those cases is the highlight in this section.

In general, the full load deflection curve can be found in Figure 8.36. The first stage of the curve is the elastic stage when the materials behave linearly in elastic range. Then, the nonlinear behaviour takes place when the principal stress reaches the proportional yield stress and the materials make use of the nonlinear portion of the strength. Until the structural member reaches the ultimate capacity or stability failure, the nonlinear portion dominates. At the ultimate point, the load deflection curve drops at certain extent due to the yielding of high strength strands and spalling of concrete. The strength beyond this ultimate capacity, if the member is further loaded, is referred to as the residual fracture toughness in the post failure mechanism. The post failure mechanism can be clearly seen in Figure 8.36 as well. It exhibits that the strands still provide the strength hardening effects to the residual load carrying capacity and the energy absorption mechanism until they reach the rupture capacity. The hardening effect is significant when more tendons remain and the effect decreases as the remaining number of tendons diminishes.



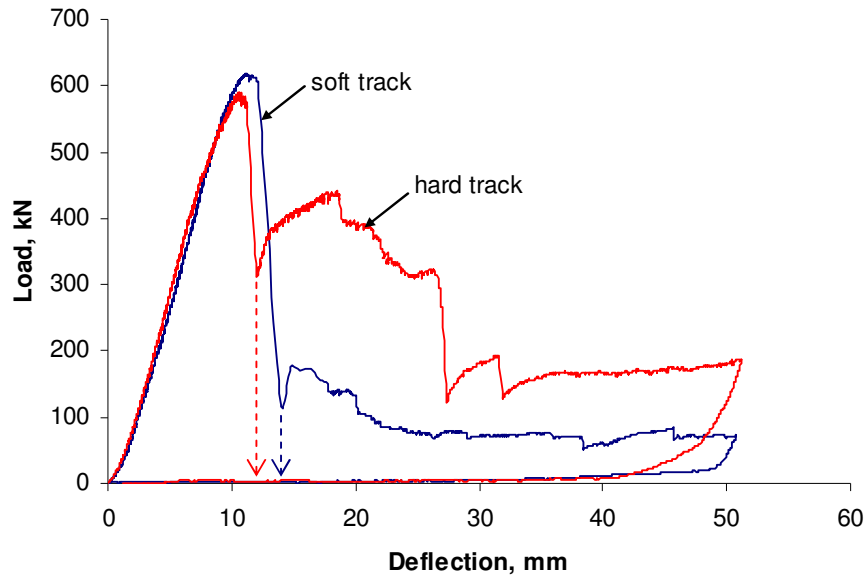
**Figure 8.36** Schematic full load-deflection curve of structural member

## 8.7.1 Residual capacity of prestressed concrete sleeper under single impacts

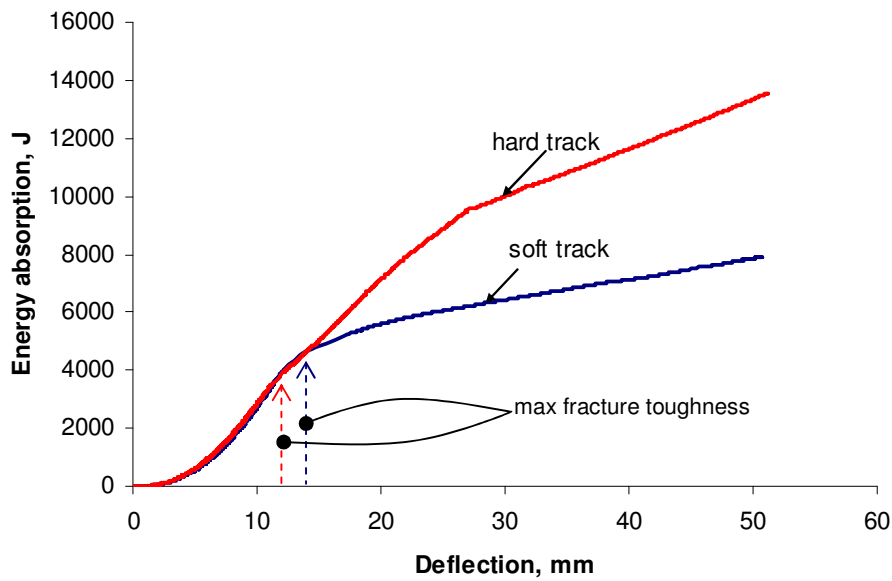
### 8.7.1.1 After subjecting the impact load of 500 kN

Figures 8.37 and 8.38 show the residual load-deflection curve and the energy absorption mechanism of the prestressed concrete sleeper after subjecting to the single

impact load of 500 kN, respectively. It clearly shows from the residual load-deflection curve that the sleeper can still provide a large deflection before collapsing at ultimate failure point. The failure load of the hard-track sleeper is slightly lesser than the soft-track one. However, the residual fracture toughness energy of the hard-track sleeper seems significantly higher.

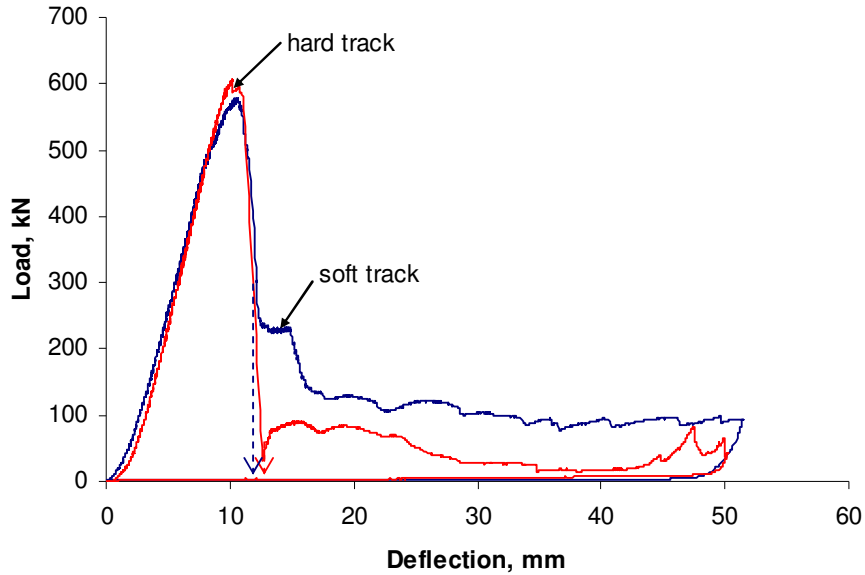


**Figure 8.37** Residual load-deflection relation for sleepers subjected to a 500 kN impact

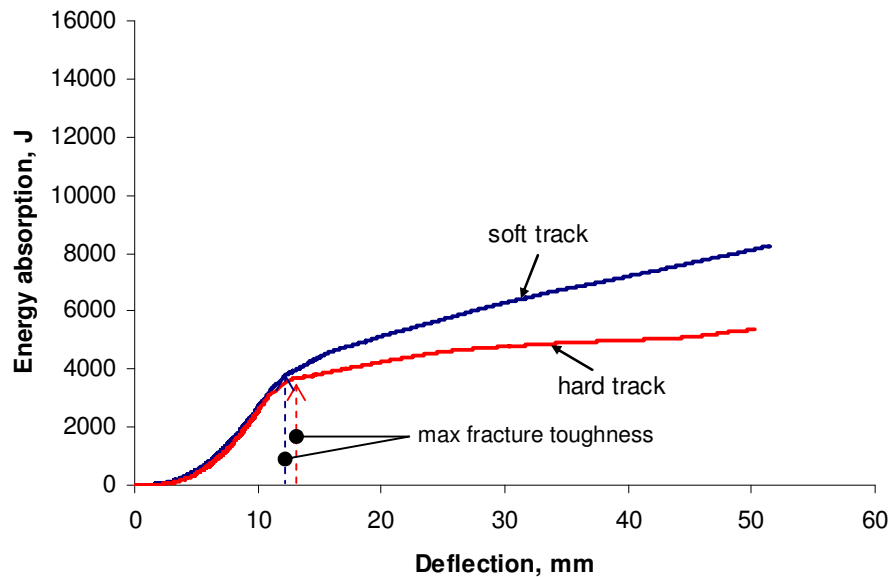


**Figure 8.38** Residual energy absorption for sleepers subjected to a 500 kN impact





**Figure 8.39** Residual load-deflection relation for sleepers subjected to a 740 kN impact

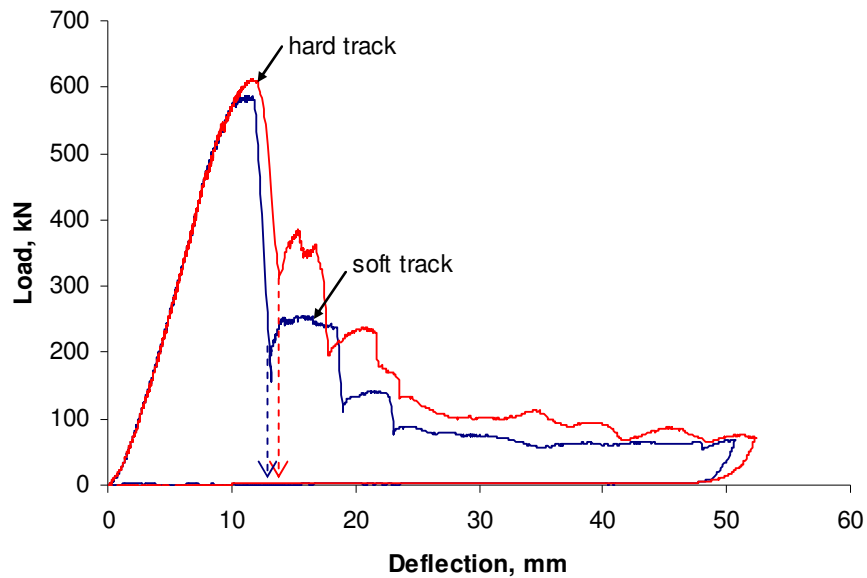


**Figure 8.40** Residual energy absorption for sleepers subjected to a 740 kN impact

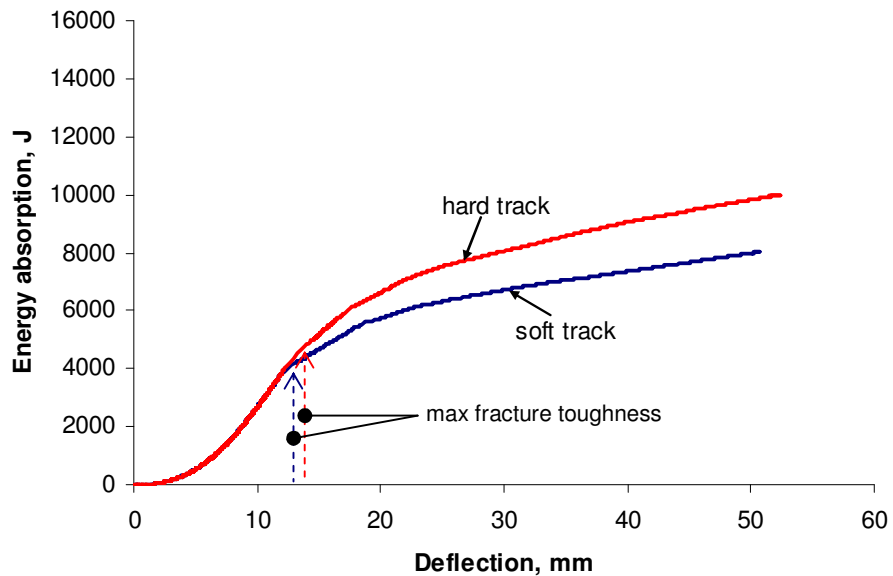
### 8.7.1.2 After subjecting the impact load of 740 kN

Figures 8.39 and 8.40 show the residual load-deflection curve and the energy absorption mechanism of the prestressed concrete sleeper after subjecting to the single impact load of 740 kN, respectively. It clearly shows from the residual load-deflection curve that the sleeper can still provide a large deflection before collapsing at ultimate

failure point. Although the failure load of the hard-track sleeper is similar to the soft-track one, the residual fracture toughness energy of the hard-track sleeper seems significantly lesser. This is because the sleeper carried more internal damage in terms of local bonding and internal cracks.



**Figure 8.41** Residual load-deflection relation for sleepers subjected to a 810 kN impact



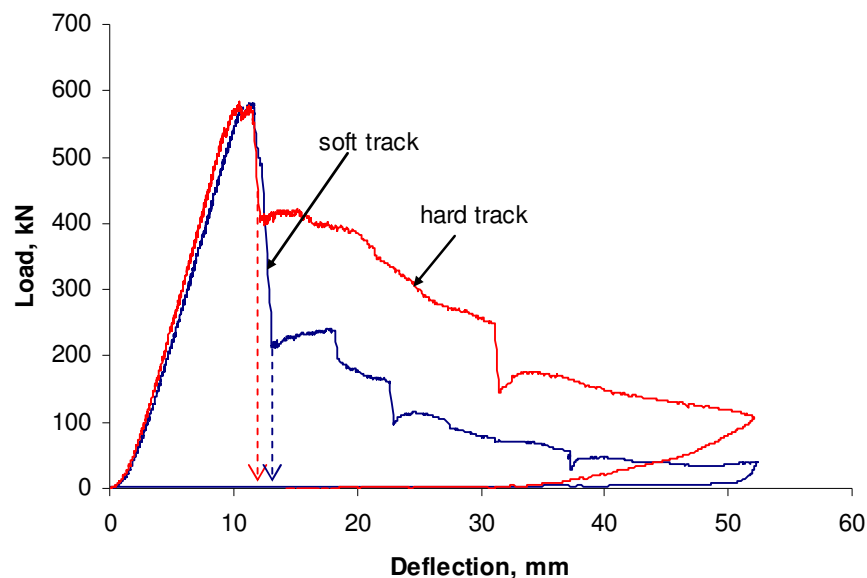
**Figure 8.42** Residual energy absorption for sleepers subjected to a 810 kN impact

### 8.7.1.3 After subjecting the impact load of 810 kN

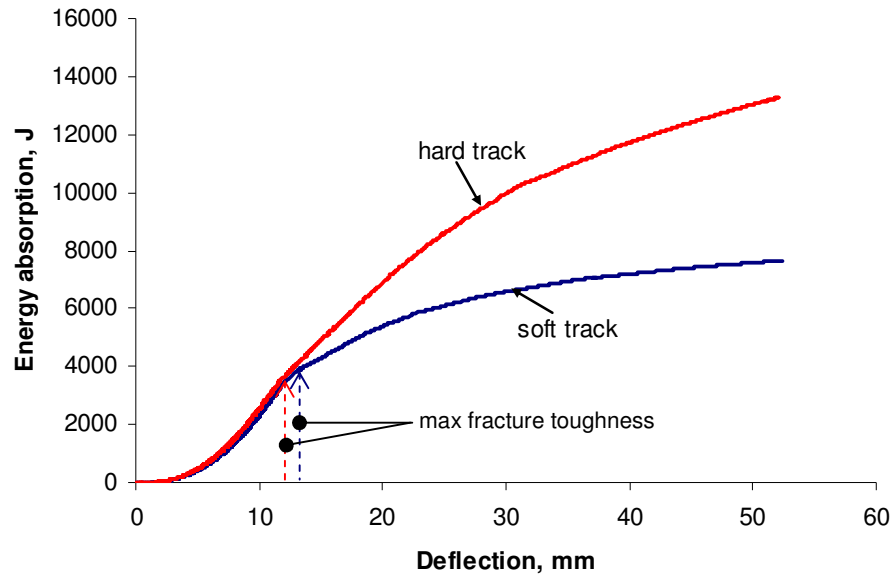
Figures 8.41 and 8.42 show the residual load-deflection curve and the energy absorption mechanism of the prestressed concrete sleeper after subjecting to the single impact load of 810 kN, respectively. It shows that at a high impact load the sleeper in either soft or hard track can still provide a large deflection before collapsing at ultimate failure point. However, the effect of the track conditions seems not significant as the failure loads as well as the residual fracture toughness energy are fairly similar. It should be noted that at higher impact loading there are more cracks occurred in the hard-track sleeper. These cracks allow the sleepers to behave and fail in a ductile mode. On the other hand, the sleeper with few hair cracks (in soft track) tends to fail in a shear brittle mode and consequently provides poor residual fracture toughness energy.

### 8.7.1.4 After subjecting the impact load of 1,500 kN

Figures 8.43 and 8.44 show the residual load-deflection curve and the energy absorption mechanism of the prestressed concrete sleeper after subjecting to the single impact load of 1,500 kN, respectively. It shows that at a high impact load the sleeper in either soft or hard track can still provide a large deflection before collapsing at ultimate failure point. However, the effect of the track conditions seems insignificant to the failure loads but cracks play a dominant role in the residual fracture toughness energy.



**Figure 8.43** Residual load-deflection relation for sleepers subjected to a 1,500 kN impact



**Figure 8.44** Residual energy absorption for sleepers subjected to a 1,500 kN impact

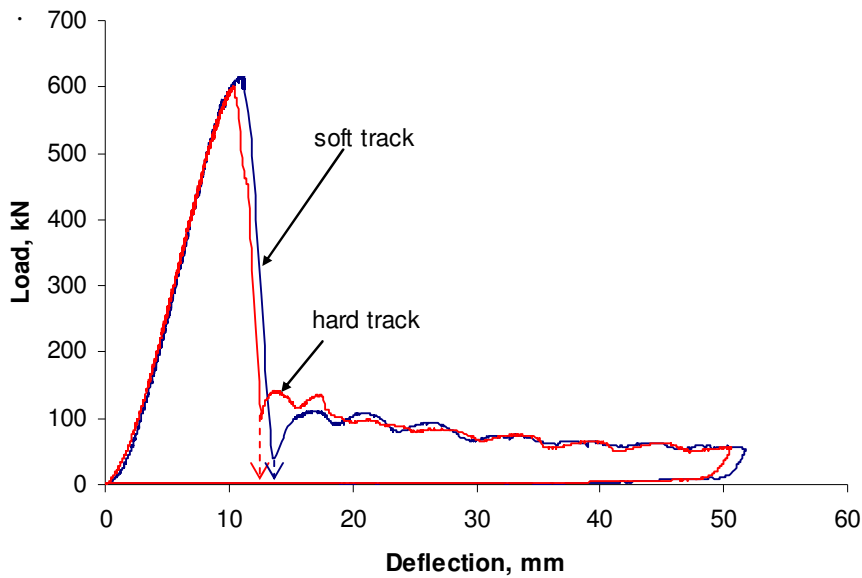
Overall, the impact magnitude tends to have little influence on the prestressed concrete sleepers in soft track environment. In contrast, the sleepers in hard track environment are sensible to the impact magnitudes and are likely to absorb more fracture toughness energy when the dynamic bending moment is larger and more major cracks occur. However, at the ultimate failure, it seems that there is no remarkably influential factor, which considerably degrades the sleepers under these single impact events.

## 8.7.2 Residual capacity of prestressed concrete sleeper under repeated impacts

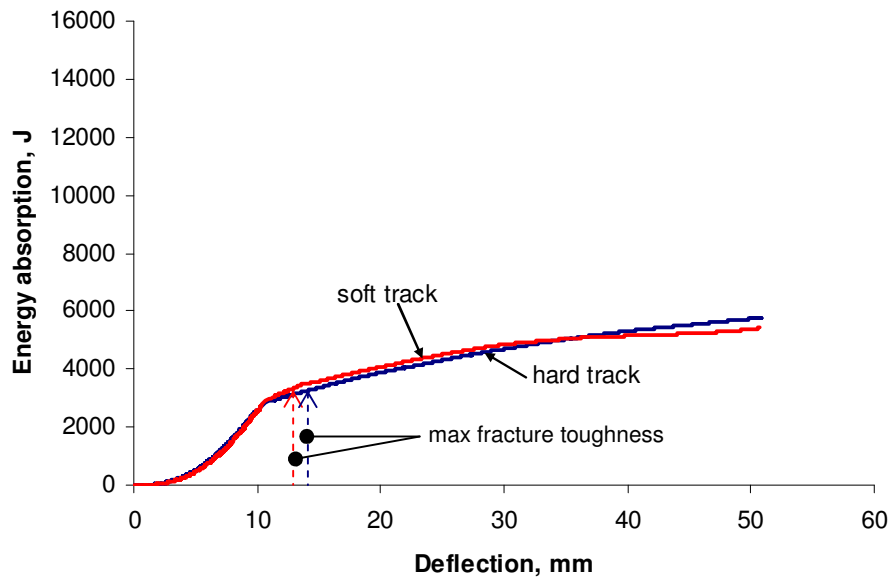
### 8.7.2.1 After subjecting the impact load of 500 kN

Figures 8.45 and 8.46 show the residual load-deflection curve and the energy absorption mechanism of the prestressed concrete sleeper after subjecting to 50 repeated impact loads of 500 kN, respectively. It clearly shows from the residual load-deflection curve that the sleepers can still provide a large deflection before collapsing at ultimate failure point but they have poor performance in the post failure behaviours. The effect of the soft and hard track environments seems insignificant to the residual fracture toughness energies. This is because the repeated impacts substantially degrade the

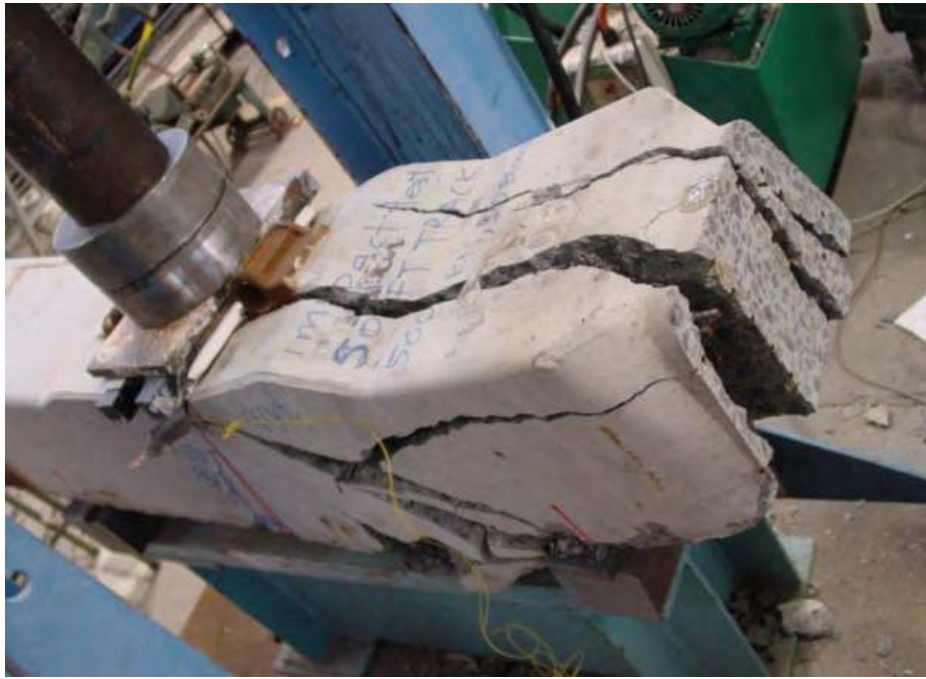
bonding between the concrete and the prestressing steels. As a result, the weak surface can be located along the tendon alignments. The failure mode of the prestressed concrete sleepers becomes the splitting mode along the tendon alignments, as shown in Figure 8.47. Once the sleeper loses its bonding strength between the tendons and concrete, the residual fracture energy mechanism is remarkably poor.



**Figure 8.45** Residual load-deflection relation for sleepers subjected to 50 repeated impact loads of 500 kN impact



**Figure 8.46** Residual energy absorption for sleepers subjected to 50 repeated impact loads of 500 kN impact



a) soft track environment

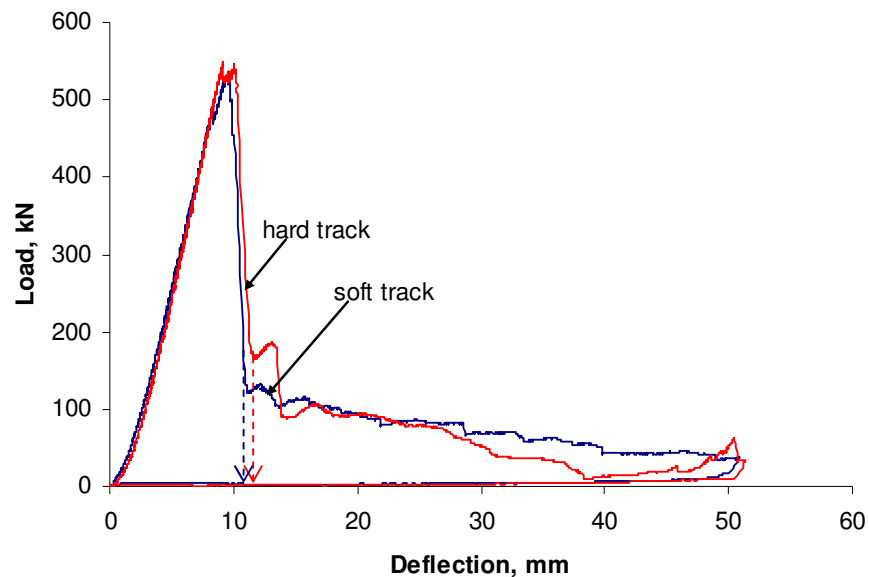


b) hard track environment

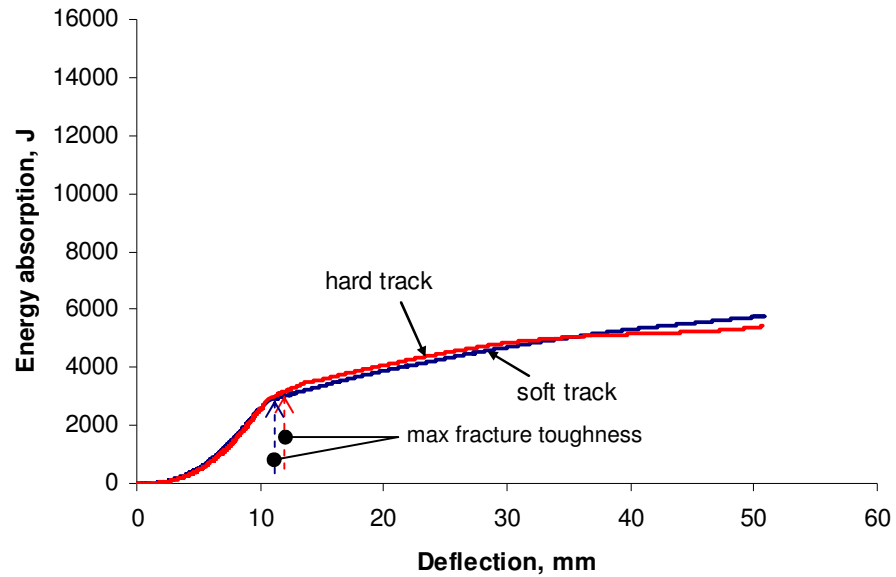
**Figure 8.47** Residual static failure mode of the sleepers subjected to 50 repeated impact loads of 500 kN impact

### 8.7.2.2 After subjecting the impact load of 740 kN

Figures 8.48 and 8.49 show the residual load-deflection curve and the energy absorption mechanism of the prestressed concrete sleeper after subjecting to 50 repeated impact loads of 740 kN, respectively. The residual load-deflection curves exhibit that the sleepers can still provide a reasonable deflection before reaching at ultimate failure point. However, they show poor performance for the post failure energy absorption mechanism. The effect of the soft and hard track environments tends to be insignificant for the residual fracture toughness energy. The fact is that the repeated impacts substantially degrade the bonding between the concrete and the prestressing steels. As a result, the weak surfaces occur along the tendon alignments. The failure mode of the prestressed concrete sleepers becomes the splitting mode along the tendon alignments, as shown in Figure 8.50. Once the sleeper losses its bonding strength between the tendons and concrete, the residual fracture energy mechanism is remarkably poor.



**Figure 8.48** Residual load-deflection relation for sleepers subjected to 50 repeated impact loads of 740 kN impact



**Figure 8.49** Residual energy absorption for sleepers subjected to 50 repeated impact loads of 740 kN impact



a) soft track environment

**Figure 8.50** Residual static failure mode of the sleepers subjected to 50 repeated impact loads of 740 kN impact



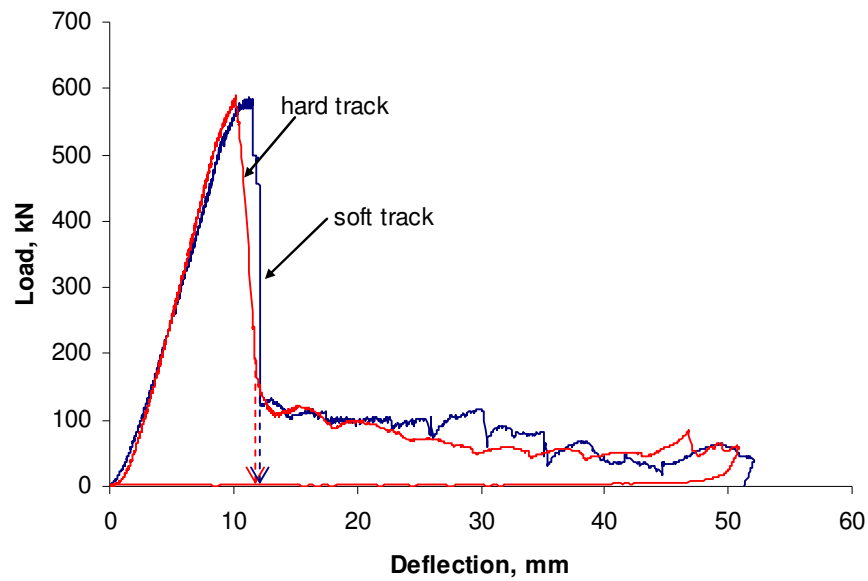


b) hard track environment

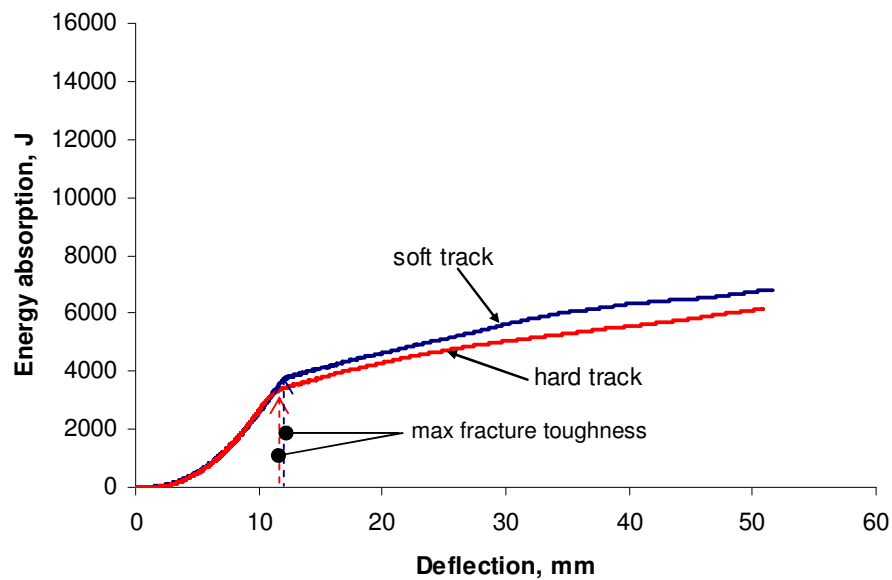
**Figure 8.50** Residual static failure mode of the sleepers subjected to 50 repeated impact loads of 740 kN impact

### 8.7.2.3 After subjecting the impact load of 810 kN

Figures 8.51 and 8.52 show the residual load-deflection curve and the energy absorption mechanism of the prestressed concrete sleeper after subjecting to 50 repeated impact loads of 810 kN, respectively. The residual load-deflection curves exhibit that the sleepers can still provide a fair deflection before failing at ultimate capacity. The effect of the soft and hard track environments is insignificant for the residual fracture toughness energy. The post failure energy absorption mechanisms of the sleepers indicate that the repeated impacts considerably degrade the bonding between the concrete and the prestressing steels. As a result, the weak surfaces occur along the tendon alignments. The failure mode of the prestressed concrete sleepers becomes the splitting mode along the tendon alignments, as shown in Figure 8.53. Once the sleeper loses its bonding strength between the tendons and concrete, the residual fracture energy mechanism is poor as dependent on the amount of lost bonding surface.



**Figure 8.51** Residual load-deflection relation for sleepers subjected to 50 repeated impact loads of 810 kN impact



**Figure 8.52** Residual energy absorption for sleepers subjected to 50 repeated impact loads of 810 kN impact



a) soft track environment



b) hard track environment

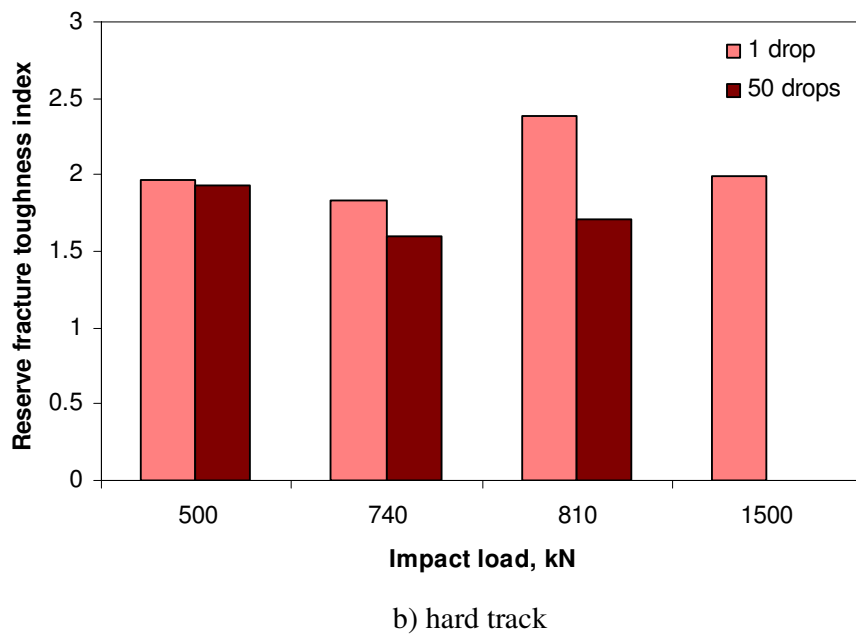
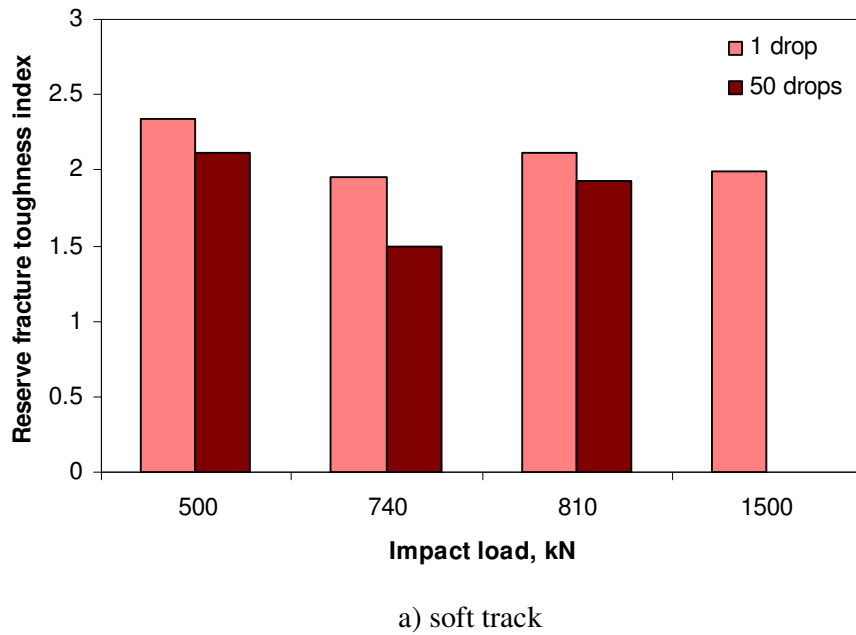
**Figure 8.53** Residual static failure mode of the sleepers subjected to 50 repeated impact loads of 810 kN impact

Overall, under repeated impact loading, the sleepers are considered as having a large amount of reserved strength that is untapped. Through, the static testing, the load deflection relationships as well as energy absorption mechanisms can be identified. The results exhibit that the sleepers under the certain impacts can withstand the ultimate failure load comfortably, regardless of different support conditions. The failure modes of the prestressed concrete sleepers damaged from repeated impacts are rather the splitting mode along the deteriorated tendon alignments. Consequently, the residual fracture toughness energy of the prestressed concrete sleepers is fairly poor.

### **8.7.3 Reserve strength of prestressed concrete sleepers**

The residual energy absorption mechanisms imply the reserve strengths of the prestressed concrete sleepers. Figure 8.54 shows the reserve fracture toughness indices of the concrete sleepers under different conditions. The reserve fracture toughness index here is the ratio between fracture toughness of dynamically damaged concrete sleeper and that of the undamaged, uncracked concrete sleeper (obtained from Chapter 5).

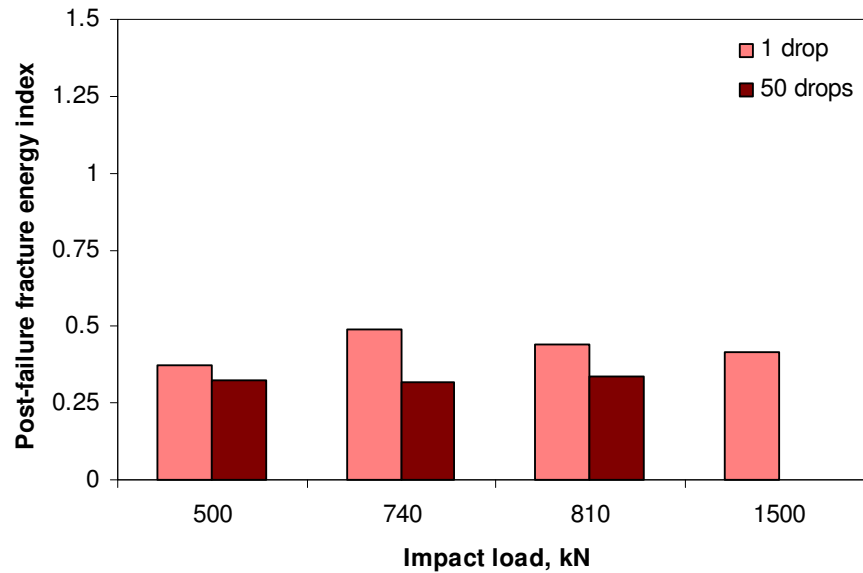
It is found that in general the concrete sleepers potentially have the large amounts of reserve fracture toughness. Overall, the reserve fracture toughness indices are more than 1.5. This is because the fractures and cracks in concrete sleepers, caused by the impact loads, attenuate the stress concentration around the tensile region of the concrete sleepers. As the tensile regions play a vital role on fracture formation and failure mode, those cracks allow more flexibility and unleash the flexural toughness of the concrete sleepers. The test results show that the reserve fracture toughness indices are averagely 2.10 and 1.85 for the soft-track sleepers under 1 and 50 impact drops, respectively. Also, they are about 2.04 and 1.75 for the hard-track sleepers under 1 and 50 impact drops. The mean differences between the in-service experiences (1 and 50 impact drops) were found to be 14 and 17 percent for soft- and hard-track sleepers. The more experienced concrete sleepers tend to provide lesser reserve fracture toughness because the repetitive impact stress wave deteriorates the bonding along the prestressing wires, especially in the hard track environment where the support condition imparts significant flexural moments. As a result, the splitting failure mode would occur in a faster manner relative to those sleepers with lesser in-service experiences.



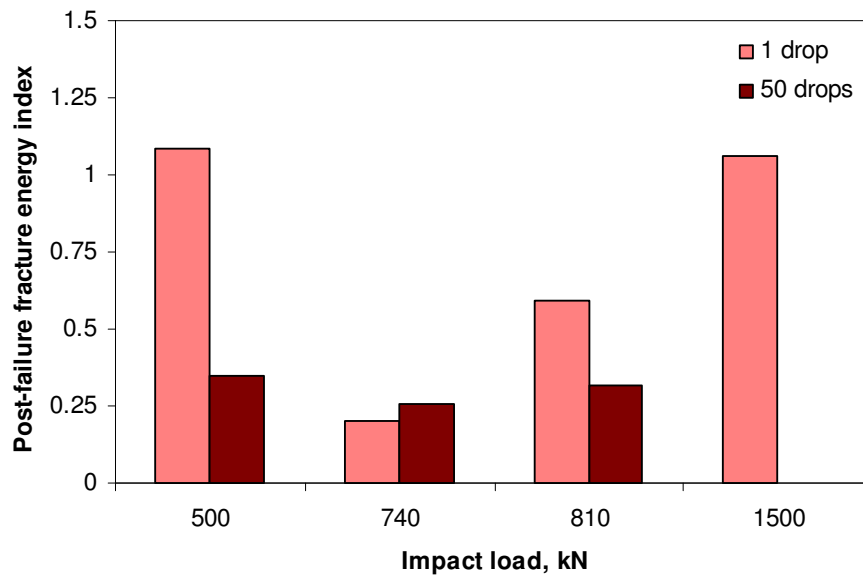
**Figure 8.54** Reserve fracture toughness of the concrete sleepers

The post-failure fracture energy is the energy absorbed by a concrete sleeper after the failure was identified up until the sleeper is completely devastated or the load-carrying capacity become very low and negligible. Figure 8.55 shows the post-failure fracture energy indices of the concrete sleepers. The post-failure fracture energy index represents the ratio between the post-failure fracture energy of damaged concrete

sleeper and that of undamaged concrete sleeper obtained earlier in Chapter 5. In general, the post-failure fracture energy of the damaged concrete sleepers is most likely to be lower than that of the undamaged sleeper. The average post-failure fracture energy indices of the soft-track sleepers under an impact drop and under 50 impact drops are about 0.42 and 0.32, respectively. Those of the hard-track sleepers are 0.73 and 0.30, respectively.



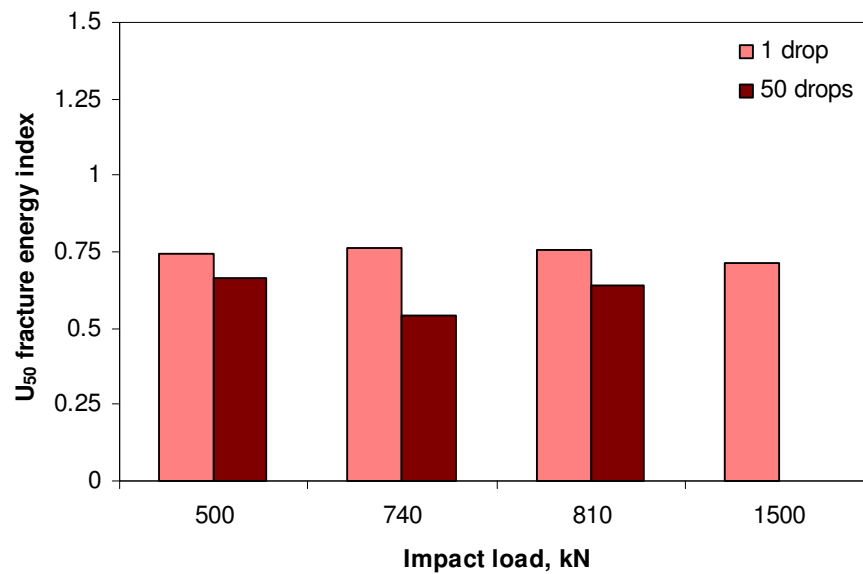
a) soft track



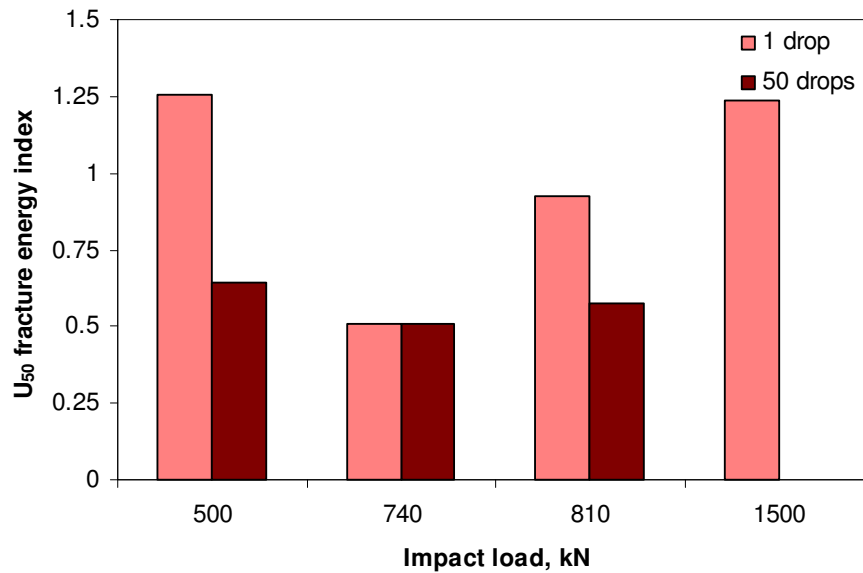
b) hard track

**Figure 8.55** Post-failure fracture energy of the concrete sleepers

The overall post-failure fracture energy absorptions are relatively low because the internal concrete cracking and prestressing wire debonding were developed during impact repetitions. As a result, less energy would be demanded for forming internal cracks and stretching the steel reinforcement.



a) soft track



b) hard track

**Figure 8.56** Post-failure fracture energy of the concrete sleepers

Figure 8.56 illustrates the total fracture energy absorbed by the concrete sleepers to vertically deform about 50 mm, so-called  $U_{50}$ . The total fracture energy is the summation of the reserve fracture toughness and the post-failure fracture energy. The actions and causes are resulted from the combination of cracks in concrete and deterioration of bonds between the wires and concrete as described above. The  $U_{50}$  fracture energy index is computed from the ratio between the total fracture energy of damaged sleeper and that of undamaged sleeper.

Interestingly, it is found that the damaged sleepers tend to possess the lower total fracture energy absorptions than the new sleeper. The average  $U_{50}$  fracture energy indices are about 0.74 and 0.61 for the soft-track sleepers under a single and 50 impact drops, respectively. They are also found to be around 0.98 and 0.57 for the hard-track sleepers under a single and 50 impact drops, respectively. From the experimental results, it is clear that the sleepers with more impact loaded experience would have less residual total fracture energy absorption.

The residual energy absorption mechanisms show that the indicator to predict the residual capacity and reserve strength includes the concrete cracking severity and the debonding level of the prestressing wires in the concrete sleepers due to the severe impact loads. Although there were cracks in concrete sleepers, the remaining prestressing force has kept the cross-section close after impact loading and the sleeper could provide further load resistance with increased flexibility. The residual failure consequences of the damaged concrete sleeper are found to be fairly different to the failure mode of the new concrete sleeper. However, it is noteworthy that only the fracture toughness portion in the total energy absorption region is useful for railway track design purpose. The post-failure mechanism provides the insight into the residual behaviour and the prospective strategy for mitigation of the concrete sleepers under severe impact loading conditions.

## 8.8 SUMMARY

The imperfections on either wheel or rail provide a potential for railway sleepers to subject to large extent of impact loading with the various pulse magnitudes and



durations. For analysis and design taking into account the extreme action, the behaviour and capacity of the prestressed concrete sleepers are required. In general, those impact loads are of very high magnitude and they are of low-possibility occurrence during the design life of the prestressed concrete sleepers. For example, a 50 year-return-period load has the likelihood of occurrence that the extreme load might happen only once in 50 years regardless of the structural life span. The building code of Australia (BCA) in conjunction with Standards Australia indicates the importance levels of structures for determining the probabilistic loads for track design at ultimate limit states, upon the consequences of failure of the structures. In a design consideration (50 to 100 years design life), it is important to note that the loading with 100 years return period should be considered for the Category 1 tracks (less importance); 500 years return period for Category 2 tracks (medium importance); and 2,000 years return period for Category 3 tracks (very high importance).

This chapter thus identifies the dynamic behaviours and responses of prestressed concrete sleepers in railway track systems under either single or repeated impact loads associated with the design probability of occurrence (and return period). The residual capacities of the damaged prestressed concrete sleepers due to those impact actions are discussed in this chapter. The residual capacity implies the reserved strength of the prestressed concrete sleepers, which is untapped and believed of its existence by railway industry. Effects of track environment including soft and hard tracks on the probabilistic impact responses and residual capacity of the prestressed concrete sleepers are also presented in this chapter. The test specimens were the prestressed concrete sleepers designed complied with Australian Standard: AS1085.14 (2003). They were kindly supplied by an Australian manufacturer, AUSTRAK. Drop-weight impact hammer was used to apply multiple impacts directly to the railseat at identical drop heights as to repeat the pulse characteristics at each return period. Measurements include the dynamic impact load history, dynamic strains, and acceleration responses. In these investigations, to reduce the contact stress between railhead and impactor, neoprene rubber with the thicknesses of 1.5 mm was used as the softening media placed on top to railhead. After each repeated impact test, the static test (as described in Chapter 5) are carried out as to identify the residual capacity of the damaged prestressed concrete sleepers.

Based on the dynamic crack propagations, it is found that the initial cracks could occur in the hard track more rapid than in the soft track. The first cracks due to impacts in the prestressed concrete sleepers either in the soft or the hard tracks are always due to flexures. The testing results reveal that the larger impact, the larger and wider are the cracks. Under a single impact load testing, it is found that the track environments (soft and hard tracks) play a sensible role on the crack propagation of the prestressed concrete sleepers. The hard track support tends to provide faster and longer cracks in the sleepers than the soft support does. The average increment in the crack length between the hard and soft track supports is approximately 7 percent. Under repeated impact loading conditions, few more bending cracks at bottom fibre of the prestressed concrete sleepers exist after each impact. The residual cracks are relatively small but the spalling of concrete in compression zone becomes larger when subjected to more and higher impact drops. It is found that the difference in the crack length between the soft and hard tracks is averagely 5.5 percent. The dynamic crack propagation of the prestressed concrete sleeper in hard track environment grows faster and higher than that in soft track environment. After either single or 50 impact drop tests, the damage in the sleepers is not significant. As a result, the damaged sleepers were later determined for the residual capacity under static testing.

It should be noted that the hard track environments allows the sleepers to reasonably vibrate, resulting in the small dynamic negative strains in positive zone. The opened cracks in the sleepers are also the cause that the dynamic strains at both railseat and mid-span fluctuate in a low range, since the concrete is no longer homogenous. It shows that the sleepers subjected to multiple drop impacts tend to provide lesser dynamic stiffness due to larger cracks, leading to the slightly larger range of the acceleration responses at both railseat and mid-span of the prestressed concrete sleepers. However, it is clear that hair cracks have insignificant influence on the vibrations or acceleration responses of the prestressed sleepers. Interestingly, this finding is concurrent with previous research at Chalmers University of Technology in Sweden (Gustavson, 2002).

As aforementioned that the sleepers were subjected to static testing, it is found that the failure modes of the sleepers under repeated impact loading are associated with both flexural and longitudinal splitting actions. The splitting fractures were aligned along the

prestressing tendons, as previously found in the progressive impact failure (Chapter 7). Due to the repetition of compression and tension in the bonding between concrete and tendon, the tendon surface alignments are weakened from the repeated impact tests. Consequently, the residual fracture toughness energy after the ultimate static failure of prestressed concrete sleepers remains minimal, regardless of the track support conditions. On the other hand, under a single impact event, the impact magnitude tends to have little influence on the residual fracture toughness of prestressed concrete sleepers in soft track environment, whilst the sleepers in hard track environment are sensible to the impact magnitudes and are likely to absorb more fracture toughness energy when the dynamic bending moment is larger and more major cracks occur. However, to consider only the energy absorption at the ultimate failure, it seems that there is no remarkably influential factor, which considerably degrades the sleepers under these single impact events.

The reserve strength capacity of the concrete sleepers can be extracted from the fracture toughness portion in the residual energy absorption diagrams. The experimental results clearly exhibit that overall the damaged concrete sleepers tend to possess large amounts of reserve strength, which is about 50 percent of the fracture toughness of the new concrete sleeper. Reserve strength would depend on the prestressing steel and concrete interaction under remaining prestressing force at the cross-section and the increased flexibility due to concrete cracks formed by the impact loads.

## CHAPTER 9

### NUMERICAL ANALYSES OF PRESTRESSED CONCRETE SLEEPERS

This chapter deals with the numerical investigations of the static and impact behaviours of railway prestressed concrete sleepers under static and dynamic loads. A three-dimensional nonlinear finite element model of a prestressed concrete sleeper was developed using the general purpose finite element package, ANSYS10. The model was initially validated against static test results. Using SOLID65 solid element, the compressive crushing of concrete is facilitated using plasticity algorithm while the concrete cracking in tension zone is accommodated by the nonlinear material model. Since the cross section of concrete sleeper is fully pre-stressed, the smeared crack analogy is impracticable. Discrete reinforcement modelling with truss elements, LINK8, is then more suitable to utilize. The pre-tensioning was modelled using an initial strain in the tendon elements. Perfect bonding between concrete and pre-stressing wires was assumed. Comparison with experimental static load-deflection response is presented for a prestressed concrete sleeper. Through the linkage between ANSYS and LS-Dyna, the finite element model was subsequently extended to account for the ballast support and in-situ conditions for use in the impact analysis. The calibration of the extended model was successfully achieved by using vibration data. Drop-weight impact tests were carried out in the identical setup for verifications of the impact model. Validations were conducted where possible. Convergence of both analytical and experimental results shows very good agreements between drop impact experiments and numerical simulations.

#### 9.1 OVERVIEW

Concrete structural components require the understanding into the responses of those components to a variety of loadings. There are a number of methods for modelling the concrete structures through both analytical and numerical approaches. Finite element analysis (FEA) is a numerical technique widely applied to the concrete structures based on the use of the nonlinear behaviour of materials. FEA provides a tool that can

simulate and predict the responses of reinforced and prestressed concrete members. A number of commercial FEA codes are available to the researchers, along with the advanced modules for complex analyses. The use of FEA has increased because of progressing knowledge and capability of computer package and hardware. Any attempts for engineering analyses can be done conveniently and fast using such versatile FEA packages. These result in the modernization of structural modelling by new-generation practical engineers, in order to verify their structural designs. Nonlinear material models have been integrated in many of general purpose finite element codes, i.e. ABAQUS, ANSYS, STRAND7, or MSC.NASTRAN. Those nonlinear models play a vital role in nonlinear response analyses since each material component tends to possess the complicated stress-strain behaviours. Among those packages, ANSYS (2006) provide a three-dimensional element (Solid65) with the nonlinear model of brittle materials similar to the concrete materials. The element features in a smeared crack analogy for cracking in tension zones and a plasticity algorithm to take into account the concrete crushing in compression zones. It is an eight noded solid isoparametric element with the integration points for the cracking and crushing checks. The linear elastic behaviour governs the analyses until exceeding either the specified tensile or compressive strengths. Once the principal stresses at the integration points reach the tensile and compressive strength, the cracking or crushing of concrete elements can be formed. Then, the cracked or crushed regions will form in perpendicular with the locally redistributed residue stresses to the direction of principal stress. These require the nonlinear iterative solver with high performance computer (Barbosa and Ribeiro, 1998; Fanning, 2001; Padmarajaiah and Ramaswamy, 2001).

Railway sleeper is an important component of track structure. It mainly helps distribute loads from the rail foot to underlying ballast bed. It has been found that most of loading on tracks are dynamic loads that have effects on the deterioration of the railway tracks' components and undermine the load resistant performance of the railway concrete sleepers (Gustavson, 2000; Kaewunruen and Remennikov, 2005a). Understanding into relationships between static and dynamic responses is mandatory. There have been few studies related to modelling of prestressed concrete sleepers. Most of them predicted the static sagging behaviour of the concrete sleepers (Gustavson, 2002). Prediction of the rotational and translational behaviour under normal track loading, which creates the hogging moment, has rarely been found in literature. The objective of this study was to

develop a numerical model where nonlinear material properties of concrete sleepers can be included in the detailed analyses for static and dynamic investigations in the future. Due to its availability to industry, a commercial FEA package is preferable in order to use the model in general design practice. A three-dimensional nonlinear finite element model of a railway prestressed concrete sleeper was developed by a general purpose finite element analysis package, ANSYS10. Concrete section was modelled using SOLID65 solid element where the compressive crushing of concrete is facilitated using plasticity algorithm and the concrete cracking in tension zone is accommodated by the nonlinear material model.

In normal practice, the railway concrete sleeper is designed to resist prestressing force fully throughout the whole cross section. This makes the smeared crack analogy unsuitable for the replacement of prestressing tendons in the fully prestressed concrete sleeper. The use of a truss element, LINK8, for discrete reinforcement modeling, is then more practicable. An initial strain real-constant feature in ANSYS appropriately substituted the pre-tensioning forces in the tendon elements. However, it was assumed that perfect bonding between concrete and pre-stressing wires occurs during loading exposure. The static full-scale experiment was conducted to validate this FE model (see Chapter 5). The experimental details were based on the associated Australian Standards. Comparison with experimental load-deflection response and rotational capacity are presented for a specific type of prestressed concrete sleepers. Also, since free-falling drop tests require significant amount of resources and are time consuming, a convenient means to attain the understanding into the impact behaviours is to use the numerical impact simulations. Finite element analysis (FEA) provides a tool that can simulate and predict the responses of reinforced and prestressed concrete members. This results in the modernization of structural engineers, in order to either verify their '*structural designs*' or trial the '*virtual experiments*'. The calibrated finite element model was extended to include ballast support and in situ conditions. The extended model has been linked to LS-Dyna (Livermore Software Technology Corporation, 1998) for impact analysis and validated against the drop impact tests. The emphasis of this chapter is placed on the numerical verifications and applications of the static and impact load responses of the railway prestressed concrete sleeper. The prestressed concrete sleepers used for modelling were designed in accordance with Australian Standard: AS1085.14 (Standards Australia, 2003). The support condition provided by the track was simulated

using multiple layers of resilient material and validated against the in-field and laboratory vibration measurements.

## 9.2 MATERIAL MODEL

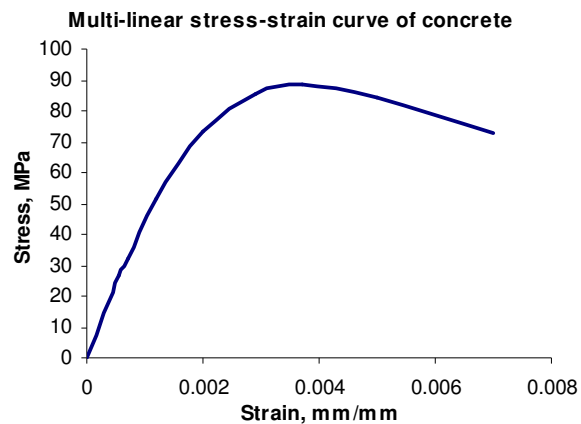
In the static analysis, ANSYS10 is employed for the nonlinear model of prestressed concrete sleeper. Concrete part was modeled using a three-dimensional solid element, SOLID65, which has the material model to predict the failure of brittle elements. SOLID65 is defined with eight nodes – each with three degrees of freedom: translations in nodal x, y, and z directions. This element is capable of cracking in tension and crushing in compression. Plastic deformation and creep can also be captured. The cracking is determined by the criterion of maximum tensile stress, called ‘*tension cutoff*’. Concrete crushes when the compressive principal stress (von Mises stress) on the failure surface surpasses the *Willam-Warnke* failure criterion dependent on five material parameters (Willam and Warnke, 1974). To simulate the behaviour of prestressing wires, a truss element, LINK8, were used to withstand the initial strain attributed to prestressing forces, by assuming perfect bond between these elements and concrete. LINK8 requires users to input ‘real constants’ to define reinforcement geometry, material behaviour, and prestressing strain. Note that this truss element cannot resist neither bending moments nor shear forces.

Nonlinear elastic behaviour of concrete can alternatively be defined by the multi-linear stress-strain relationships. The modulus of elasticity of concrete ( $E_c$ ) can be found based on AS3600 (2001) as given by  $E_c = 5050\sqrt{f'_c}$  and the tensile strength of concrete at 28 days ( $f'_{ct}$ ) is  $0.4\sqrt{f'_c}$ , with the value of  $f'_c$  equal to 88.5 MPa (based on tests of the cored samples) and Poisson’s ratio was assumed to be 0.3. The multi-linear isotropic stress-strain curve for the concrete can be computed by (MacGregor, 1992):

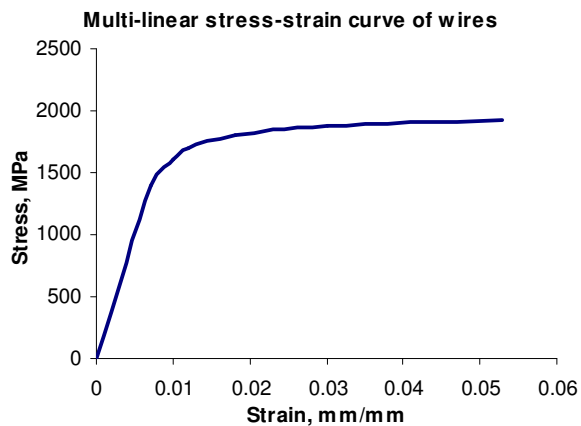
$$f = \frac{E_c \varepsilon}{1 + \left(\frac{\varepsilon}{\varepsilon_0}\right)^2}, \quad \varepsilon_0 = \frac{2f'_c}{E_c}, \quad \text{and} \quad E_c = \frac{f}{\varepsilon} \quad (9.1a, b, c)$$

In Equation (9.1), note that  $f$  is stress at any strain ( $\varepsilon$ ) and  $\varepsilon_0$  is the strain at the ultimate compressive strength at 28 days,  $f'_c$ .

For prestressing wires, the bi-linear elasto-plastic material models can be used as well as the multi-linear isotropic model from the manufacturer's data. The 0.2% proof stress is 1,700 MPa and the ultimate stress is 1,930 MPa. The modulus of elasticity of prestressing wire is 190,000 MPa. Figure 9.1 shows the schematic material models for static analysis. Table 9.1 tabulates the summary of material models used in finite element analysis. Four cases of material models have been investigated in this study.



a) concrete



b) prestressing steel

**Figure 9.1** Material models for static analysis



Load-deflection behaviour of concrete structures typically includes three stages. Stage I shows the linear behaviour of uncracked elastic section. Stage II allows initiation of concrete cracking and Stage III relies relatively on the yielding of steel reinforcements and the crushing of concrete. This results in the nonlinear response analysis of concrete structures. In nonlinear iterative algorithms, ANSYS10 utilizes Newton-Raphson method for the incremental load analysis.

**Table 9.1** Material models used in finite element analyses.

Model	Concrete Model		Prestressing Wire Model	
	Tension	Compression	Distribution	Material Properties
MAT1	Linear Elastic	Linear Elastic	Discrete	Linear Elastic
MAT2	Linear Elastic	Multi-linear Isotropic	Discrete	Linear Elastic
MAT3	Linear Elastic	Multi-linear Isotropic	Discrete	Multi-linear Isotropic
MAT4	Cracking	Multi-linear + Crushing	Discrete	Multi-linear Isotropic

For impact simulations, the FE model was extended to include rails, rail pads, ballast bed, and falling mass. The extended finite element model was calibrated using vibration data (see Chapter 3). The updated finite element model was then transferred to LS-Dyna explicit dynamic analysis program (Livermore Software Technology Corporation, 1998). The simulation results were achieved by assigning the initial velocity to the drop mass to generate an impact event, similarly to the actual drop tests.

In the impact model, the impactor is modelled using rigid solid elements with the density of  $7850 \text{ kg/m}^3$ . The weight of the projectile was set as 5.81 kN (592 kg). The elastic modulus of the steel (205 GPa) is adopted for the impactor. For the rail pads, the linearly elastic solid elements were used with the elastic modulus of 200 MPa. The ballast support is also modelled with the solid elements using the linearly elastic moduli ranging from 200 MPa to 1,000 MPa for the sensitivity analysis. The interface between the concrete sleeper and the ballast was simulated using contact surfaces.

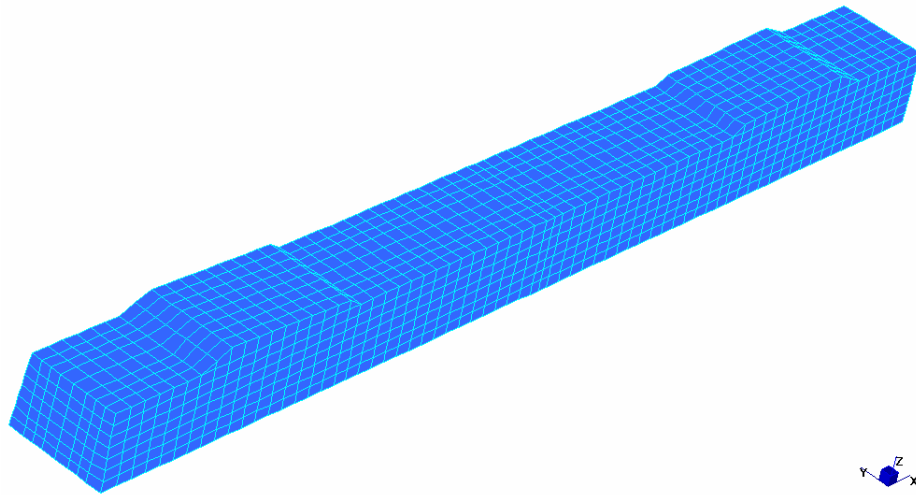
### 9.3 FINITE ELEMENT MODELLING

The finite element modelling is divided into two parts for static and impact analysis. The main aim is to achieve the numerical simulations that could predict the static responses as well as the impact loads and behaviours under the dynamic conditions. To maintain the acceptable functionality and viability of industry, the commercial finite element packages (ANSYS and LS-DYNA) are employed in the three-dimensional modelling in this numerical study. It is important to note that the numerical results can also be attained precisely using the two dimensional finite element models, of which the data are available elsewhere (Kaewunruen and Remennikov, 2006; 2007).

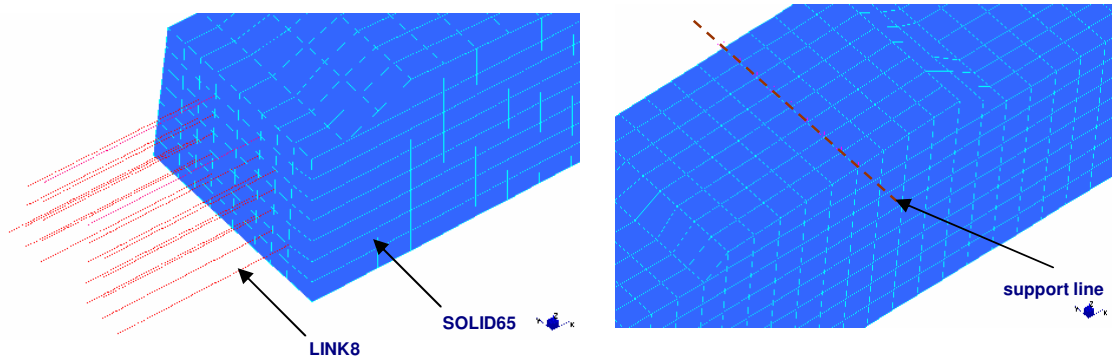
#### 9.3.1 Static modeling

The three-dimensional model of railway prestressed concrete sleeper has been developed in ANSYS10 as illustrated in Figure 9.2a. Dedicated solid bricks (SOLID65) represent the concrete and the embedded three-dimensional spar elements (LINK8) are used as the prestressing wires, as shown in Figure 9.2b. The pre-tensioning was modeled using an initial strain in the tendons corresponding to prestressing forces in the preliminary load stage. The nonlinear material models were specified in the '*material properties*' feature, while the initial strain and prestressing wire diameters could be defined in '*real constants*'. Figure 9.2c shows the boundary conditions imposed along the related nodes. The model would be loaded to failure in a manner consistent with the experimental data.

A technique used for load-deflection analysis involves with the use of applied displacements to facilitate the smooth convergence of loading, in accordance with the experimental programs. Then, the maximum displacement at mid span can be calculated. There were three steps towards final solutions. First, no load was applied since the initial strain was defined. The time at the end of the prestrain load step is 1. Second, the self-weight was added in a load step. The uniformly distributed loading is done by applying gravitational acceleration of  $9.81 \text{ m/s}^2$  in the negative global z direction. The typical mass density of concrete ( $2,400 \text{ kg/m}^3$ ) was entered in as a function of the gravitational acceleration (density/g). The last step was to define the load step until failure of the prestressed concrete sleeper, with consistency to the testing data.



a) Three-dimensional full-scale model



b) Connectivity between solid and bar elements

c) Boundary conditions

**Figure 9.2.** Finite element mesh of railway prestressed concrete sleeper

### 9.3.2 Impact modelling

For the static analysis, a three-dimensional model of a typical railway prestressed concrete sleeper was developed initially in ANSYS (1998) as illustrated in Figure 9.2. The dedicated solid bricks represent the concrete and the embedded three-dimensional spar elements are used as the prestressing wires. The pre-tensioning was modelled using an initial strain in the tendons corresponding to the prestressing forces at final stage (sustained prestressing force after all losses). In this study to determine the impact

analysis in LS-Dyna, the concrete part of the sleeper was modelled using a three-dimensional solid element, which has the material model to predict the failure of brittle materials (MAT72R2). However, the tendons are modelled using truss elements, which cannot resist neither bending moments nor shear forces. Non-linear elastic behaviour of concrete can alternatively be defined by the multi-linear stress-strain relationships. The static modulus of elasticity of concrete ( $E_c$ ) can be found based on AS3600 (2001) using the compressive strength of 80 MPa. For impact simulations, the FE model was extended to integrate rails, rail pads, ballast bed, and falling mass, as illustrated in Figure 9.3. The extended finite element model was calibrated using vibration data (from Chapter 3). The updated finite element model was then converted to LS-Dyna format (Livermore Software Technology Corporation, 1998). To simulate the nature of the free uplift behaviours between sleeper and ballast, between sleeper and rail pads, between rail pads and rails, and between the railhead and impactor, contact surfaces have been treated to those contact interaction areas. The impact simulations were achieved by assigning the initial velocities to the drop mass to generate an impact event, similarly to the actual drop tests in laboratory.

The multi-linear isotropic dynamic stress-strain curve for the concrete and prestressing wires can be calculated based on the consideration of the effect of strain rate. Based on the assumption of perfect bond between prestressing wires and concrete, the dynamic material properties of concrete and prestressing wires can be determined as follows (Wakui and Okuda, 1999).

*Concrete:*

$$\sigma = f'_{c,dyn} \left[ 2 \frac{\epsilon}{\epsilon_{c0,dyn}} - \left( \frac{\epsilon}{\epsilon_{c0,dyn}} \right)^2 \right] \quad (9.2)$$

$$\frac{f'_{c,dyn}}{f'_{c,st}} = 1.49 + 0.268 \log_{10} \dot{\epsilon} + 0.035 [\log_{10} \dot{\epsilon}]^2 \quad (9.3)$$

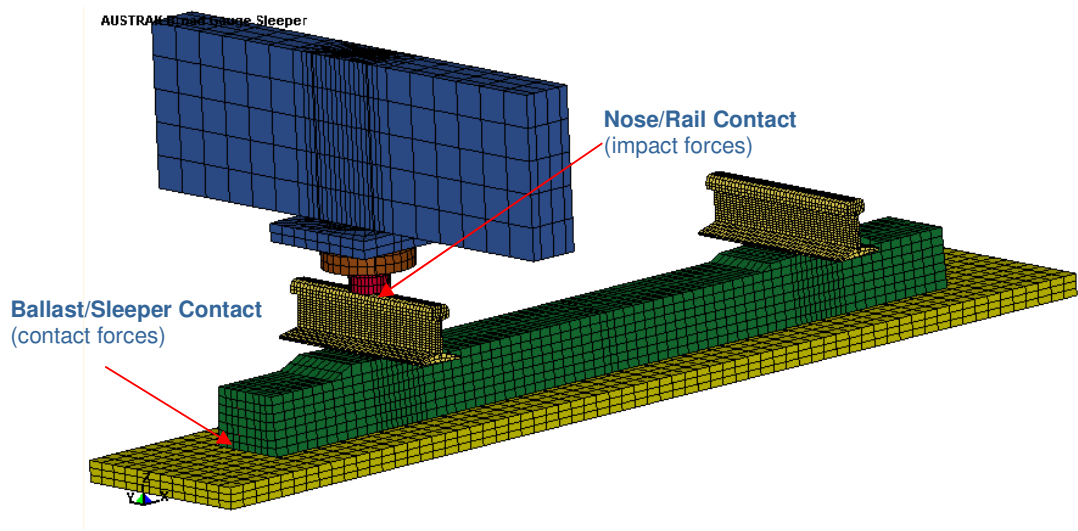
$$\frac{\epsilon_{c0,dyn}}{\epsilon_{c0,st}} = 1.24 + 0.053 \log_{10} \dot{\epsilon} \quad (9.4)$$

where  $\sigma$  is the dynamic stress,  $f_{c,dyn}$  is the dynamic compressive strength,  $f_{c,st}$  is the static compressive strength of concrete,  $\varepsilon$  is the dynamic strain,  $\varepsilon_{c0,st}$  is the static ultimate strain, and  $\dot{\varepsilon}$  is the strain rate in concrete fibre.

*Prestressing wires:*

$$\frac{f_{y,dyn}}{f_{y,st}} = 10^{0.38 \log_{10} \dot{\varepsilon}^{-0.258}} + 0.993 \quad (9.5)$$

where  $f_{y,dyn}$  is the dynamic upper yield point stress,  $f_{y,st}$  is the static upper yield point stress of prestressing wires (about 0.84 times proof stress), and  $\dot{\varepsilon}$  is the strain rate in tendon.

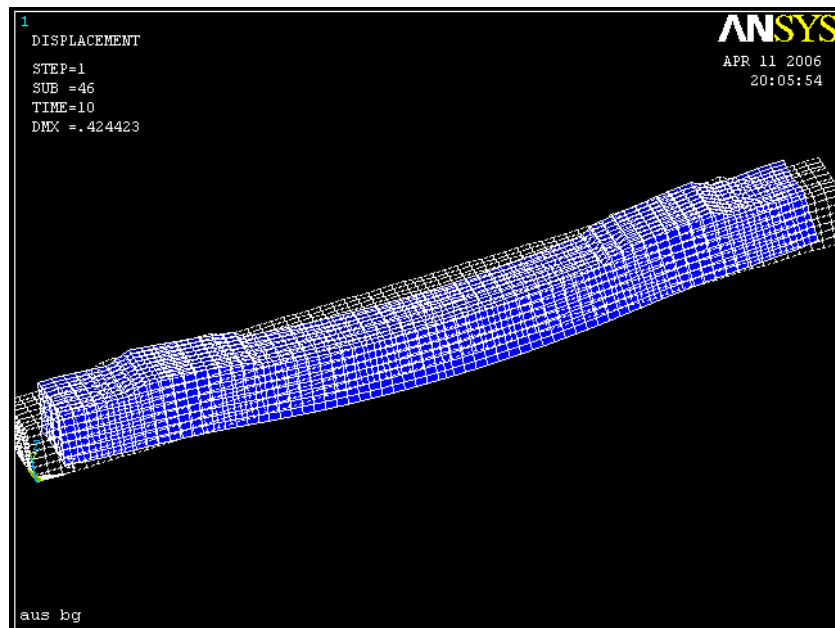


**Figure 9.3** Impact model of a prestressed concrete sleeper

In the impact test setup, the alternative support was adopted by using layers of conveying belts. For the numerical impact analyses, the support condition was modelled using elastic brick elements. The contact surfaces were treated at the top layer of support elements to the concrete sleeper. The engineering properties were obtained earlier from Chapter 6. Variation of the support properties is an important parameter for the numerical analysis.

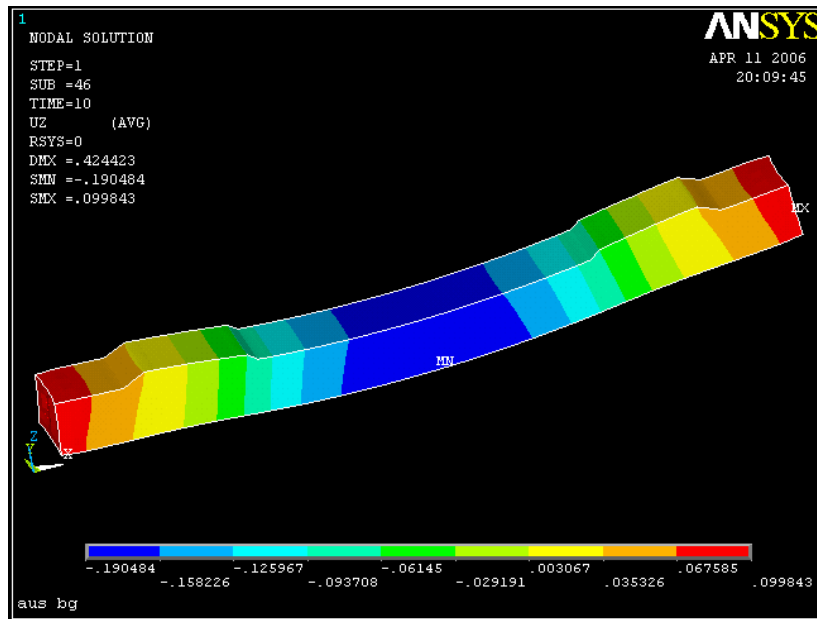
## 9.4 NONLINEAR STATIC ANALYSIS

The deformation and stress diagrams of the concrete sleeper due to only prestressing force (Stage I) are illustrated in Figure 9.4. Both top and bottom fibre stresses are identical to those calculated manually (Warner, et al., 1998). The results from various material models are similar since only the initial linear parts of elasticity were employed in this early stage. The effect of the self-weight in Stage 2 is quite small when added up to the displacements due to the pre-tension. The comparison of experimental load-deflection responses is plotted with the finite element results in Figure 9.5.

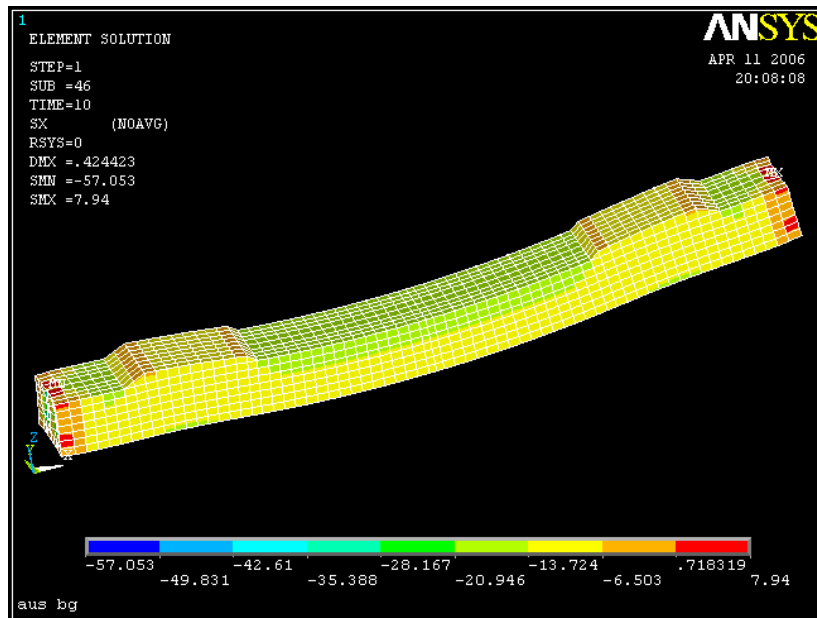


a) wire frame of the pre-camber shape

**Figure 9.4** Pre-camber, displacement, and fibre stress diagrams due to pre-tensioned strain.

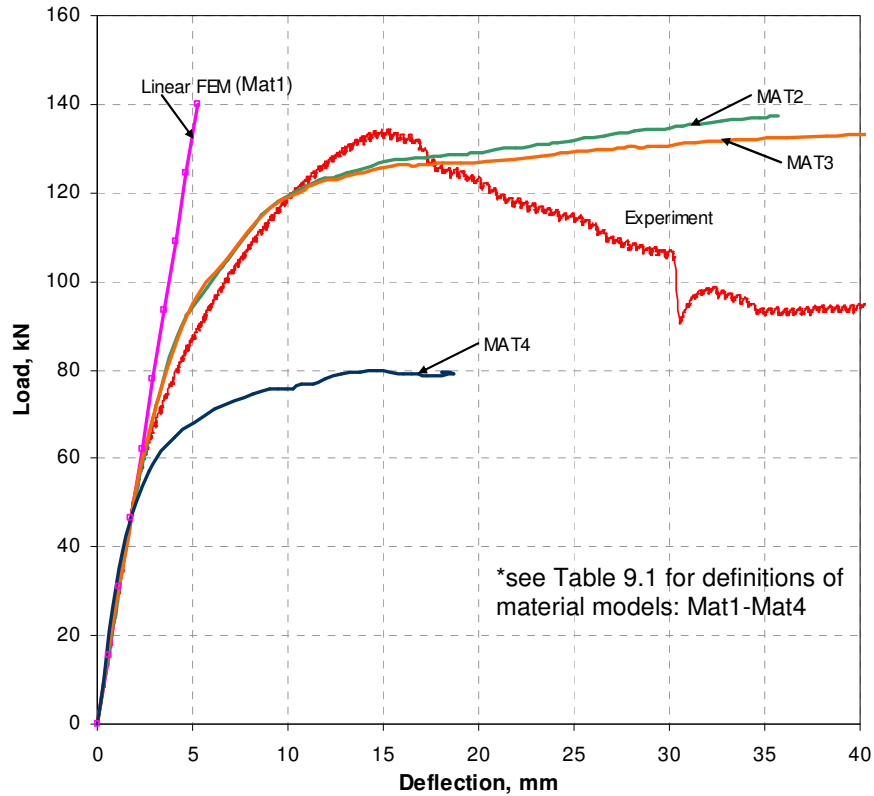


b) displacement contour



c) total fibre stress

**Figure 9.4** Pre-camber, displacement, and fibre stress diagrams due to pre-tensioned strain.



**Figure 9.5** Load-deflection responses

From Figure 9.5, it is found that MAT1 model can predict the linear range (from 0 to 65 kN of loading) of static behaviour of the concrete sleeper. The nonlinear material models, MAT2 and MAT3, give similar results in the same loading range. However, it can be found in the nonlinear range that MAT2 model seems to well represent the experimental load-deflection curve, while MAT3 model yields slightly smaller than MAT2 model when subjected to larger displacements (after 10-15 mm). To obtain the deflection of 15 mm, the static loads of about 126 and 125 kN are needed in MAT2 and MAT3 models, which are, respectively, at 4.5% and 5.3% differences from the experimental results. When using both cracking and crushing model into MAT4, it is noticed that the analytical results are far from the experimental ones because of the low tensile strength of concrete used. This causes the load-deflection response much lower than others. The discrepancy of the numerical and experimental results in the deflection range greater than 20 mm is due to the inadequacy of material model to capture the brittle failure of concrete and simulate the bonding and damage of prestressing wires. At this condition, the test results show that the concrete suddenly crushed and brittle failure



occurred with the damage of prestressing wires. Concurrently, the numerical analysis diverted and terminated.

From this numerical study, the experimental and numerical results were in good agreement. The finite element model is consequently found sufficient for further impact simulation. By extending the model, the material models and functionality of elements remain and make it more convenient for railway industry.

## **9.5 PREDICTION OF IMPACT LOADS AND RESPONSES**

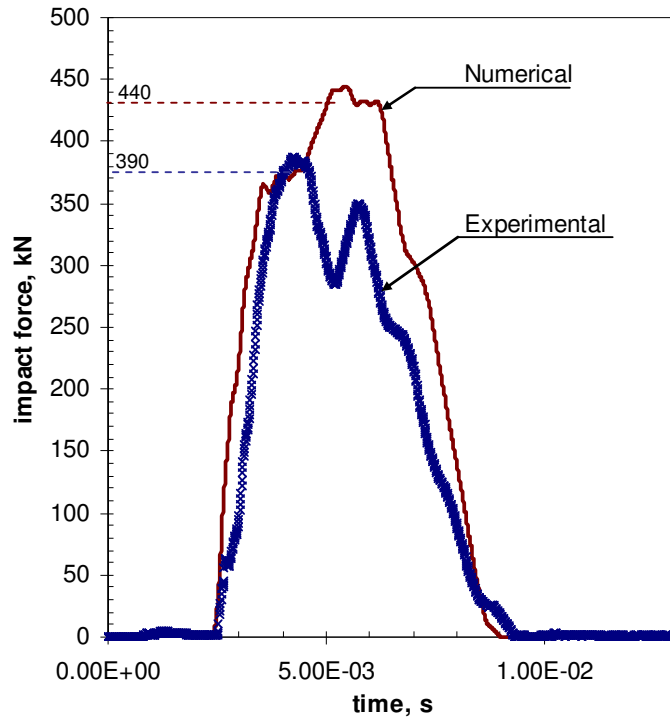
### **9.5.1 Model verification**

The prestressed concrete sleepers used in this study were supplied by an Australian manufacturer. Experimental setup and impact tests were arranged in accordance with the Australian Standards (2001). The accelerometers were used to measure the dynamic responses at mid-span and railseat, as presented in Chapters 7 and 8. The contact force between the impactor and the steel rail was recorded using the dynamic load cell connected to the data acquisition system. For the verification purpose, the drop height used in the impact tests was 0.1m since there was the measurement limitation for the accelerometers employed. The in-situ conditions of railway concrete sleeper were replicated, as can be seen in Chapter 6. Comparison between numerical and experimental results can be seen in Figure 9.6. It is found that the finite element model is sufficient for predicting impact responses of the prestressed concrete sleepers. The trends of peak acceleration responses are quite close to each other, although there is certain phase difference.

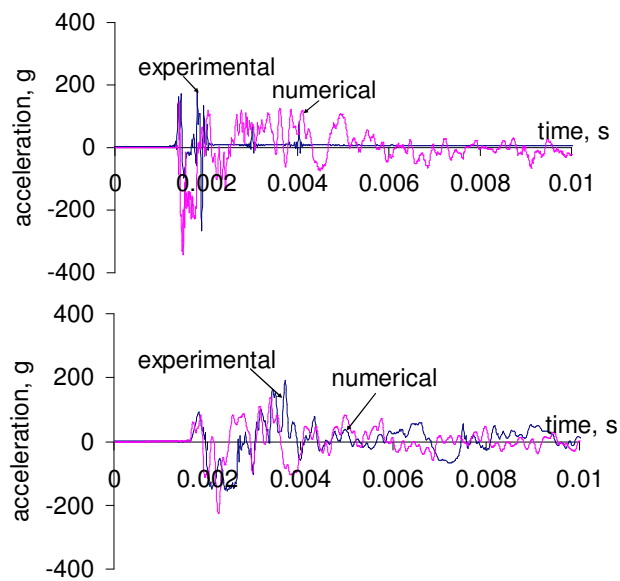
### **9.5.2 Impact simulations**

In general, the main track components that require maintenance or renewal apart from the sleeper itself include the ballast bed and rail pads. The ballast bed requires re-packing and tamping every six months or so depending on the characteristics of gravels used at particular locations. It degrades through the breakage of gravel, resulting in the large settlement of railway tracks. Rail pads deteriorate through the age of use. The wearing process can be incurred due to the impact loads or asymmetrical burden on the

pads. Once the rail pad deteriorates, its properties also change. Based on this understanding, the parametric studies have been conducted and discussed in this section.



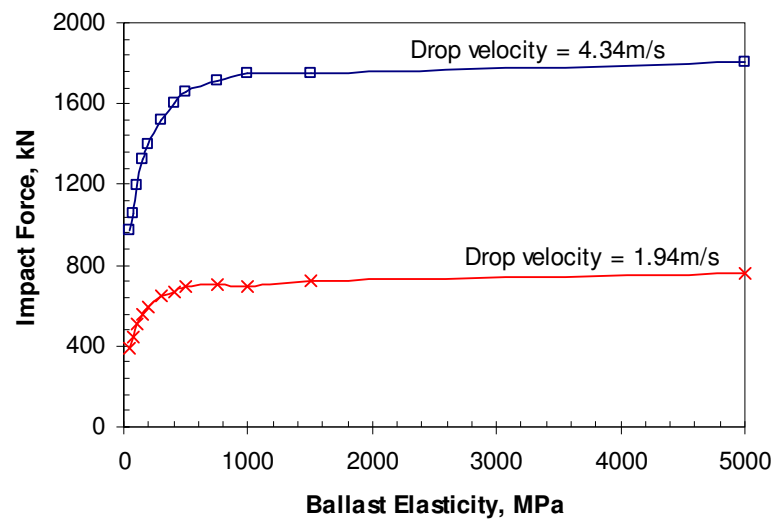
a) contact shock load



b) acceleration at railseat (top); at mid-span (bottom)

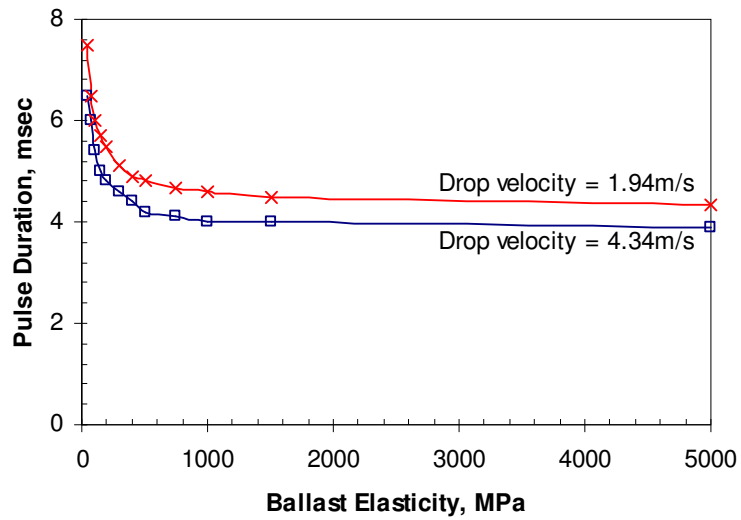
**Figure 9.6** Comparison of numerical and experimental results (0.1 m drop)

In the impact analysis, the drop velocity is also varied to evaluate the effect of drop heights on the impact force occurring on railway track structures. On the other hand, this analysis provides the insight into the effect of railway track environments on the contact impact forces due to the identical causes and the responses of concrete sleepers to such loading. For example, a wheel, with 10mm wheel flat on a specific vehicle and running at 80 km/hr, generates different contact impact forces on tracks with different environments. However, this study focuses only on ballast and rail pad parameters as they play key role on the interface impact force characteristics and there responses of prestressed concrete sleepers.

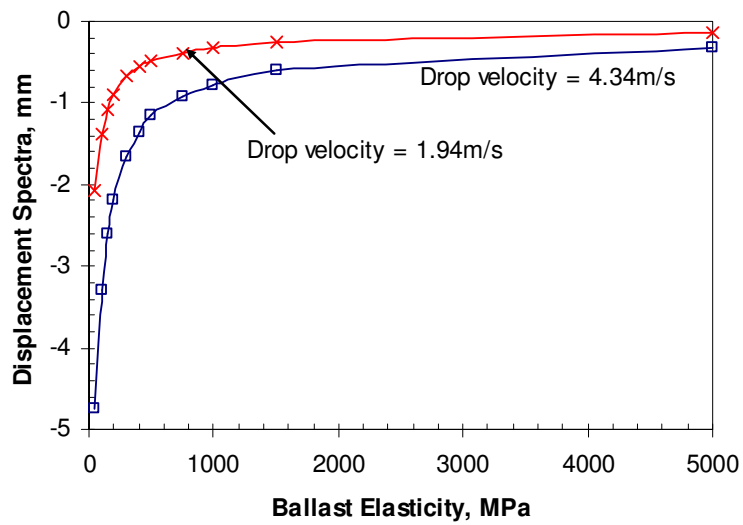


a) impact load

**Figure 9.7** Influence of ballast elasticity on contact impact forces and dynamic responses

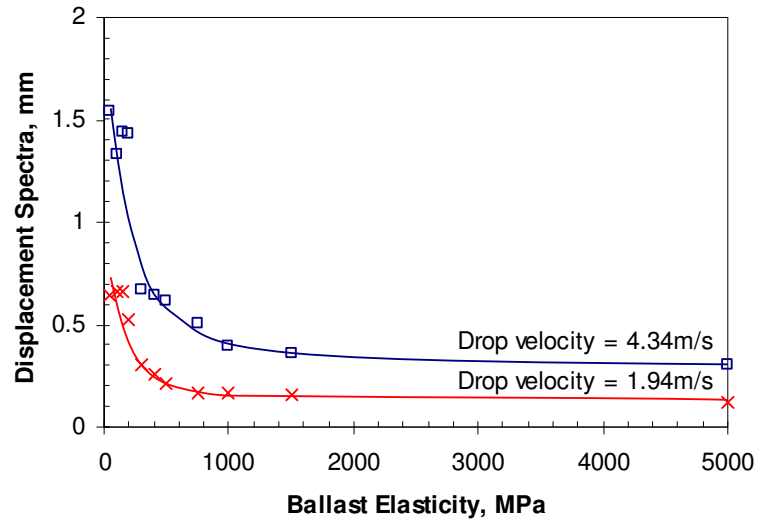


b) impact force duration

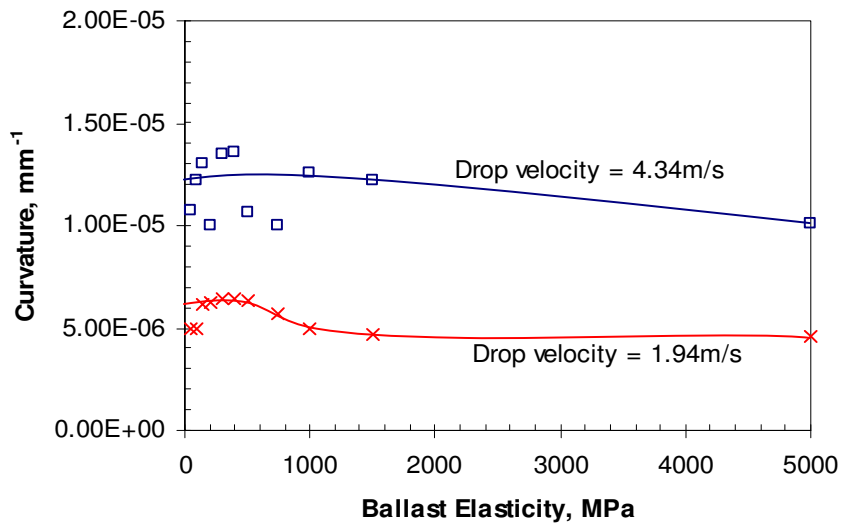


c) displacements at loaded railseat

**Figure 9.7** Influence of ballast elasticity on contact impact forces and dynamic responses



d) displacements at loaded railseat



e) bending curvature at railseat

**Figure 9.7** Influence of ballast elasticity on contact impact forces and dynamic responses

a) Effect of ballast bed

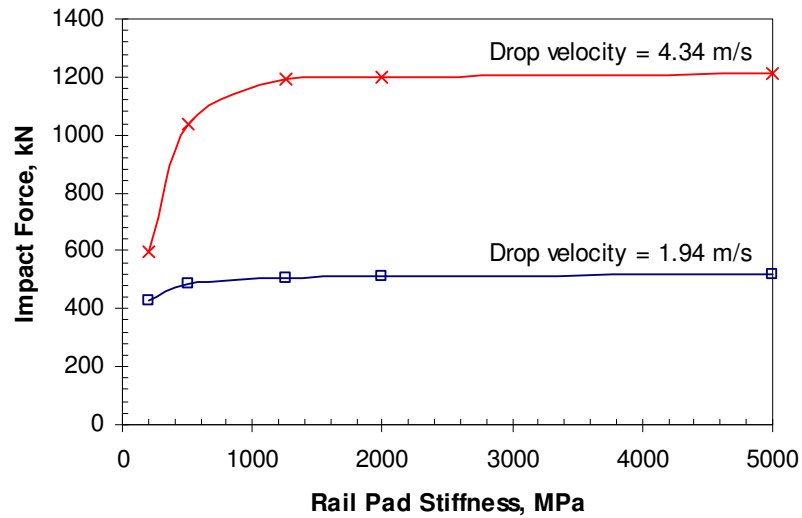
The influence of the ballast strength on the contact impact forces and dynamic responses of prestressed concrete sleepers is presented in Figure 9.7. Clearly, the ballast stiffness in the low range between 50 MPa and 1500 MPa plays substantial role in both

the impact force magnitude (Figure 7a) and the corresponding pulse duration (Figure 7b). The contact forces increase dramatically during that low range whilst the effect of ballast elasticity becomes insignificant when the stiffness is large. Analogously, the impact duration, which will affect the resonance responses of railway sleepers, decrease greatly in the low range of ballast stiffness, and vice versa. These behaviours can be detected for either very low velocity impacts at 1.94 m/s (equivalent to the drop height of 0.2 m in the test rig) or even at 4.34 m/s (equivalent to the drop height of 1 m in the test rig). It can be observed that the impact force magnitude varies from 390 kN to 670 kN and from 970 kN to 1,800 kN, while the duration changes from 7.5 msec to 4.3 msec and from 6.5 msec to 4.0 msec, for drop velocities of 1.94 m/s and 4.34 m/s, respectively. The displacement spectra (the maximum dynamic displacement responses) are plotted against the ballast strength in Figures 9.7c (at railseat) and 9.7d (at mid-span). However, it is discovered from Figure 9.7e that the ballast stiffness has little effect on the impact responses in terms of bending curvatures of the railway concrete sleeper.

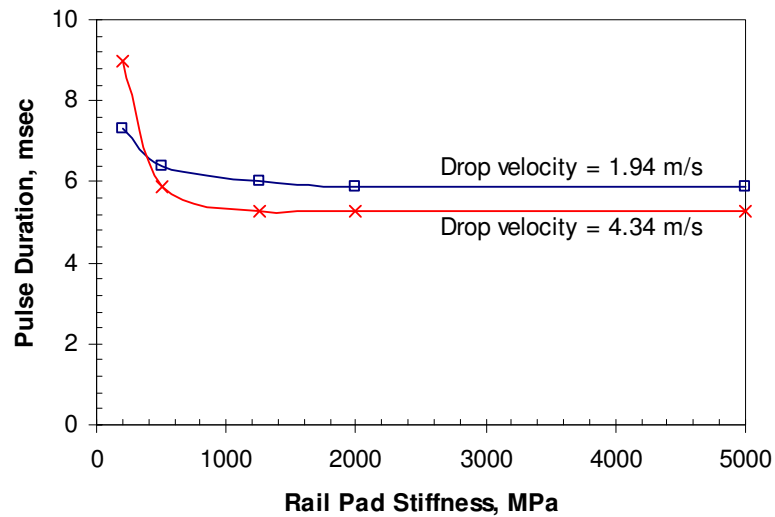
#### b) Effect of rail pads

Figures 9.8a and 9.8b depict the influence of the rail pad stiffness on the contact impact force magnitude and duration, while Figures 9.8c and 9.8d show the effect on the displacement response spectra at railseat and mid-span of the sleeper, respectively. At the stiffness range between 200 MPa and about 750 MPa, the substantial changes of impact force characteristics (both magnitude and duration) can be observed. However, the greater rail pad parameters are unlikely to affect the impact force magnitude and duration. The impact force magnitude varies from 400 kN to 500 kN and 600 kN to 1,200 kN, while the associated duration diminishes from 7.5 msec to 6.0 msec and from 9.0 msec to 5.3 msec, for the drop velocities of 1.94 m/s and 4.34 m/s, respectively. Alternatively, the rail pads tend to reduce the impact force from the rail foot as shown in Figure 9.9a and help attenuate the flexural responses in the prestressed concrete sleeper as presented in terms of curvature changes in Figure 9.9b. The impact reduction is calculated from the difference between the contact impact force at rail interface and the load burden that is distributed to rail seat of the sleeper. In contrast, the impact attenuation is considered from the effect of rail pad stiffness on the changes of sleeper curvature. From Figure 9.9a, it is apparently found that the softer the rail pad, the larger

the force reduction. In addition, the soft rail pad considerable attenuate the impact forces, resulting small flexures.

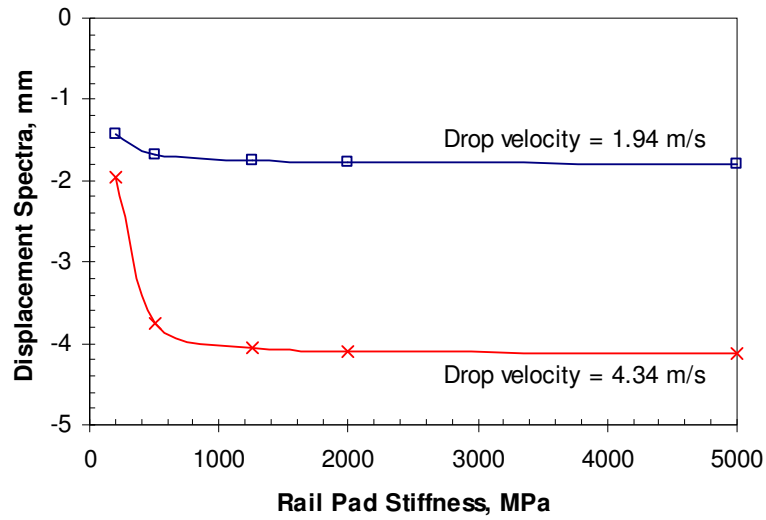


a) impact force magnitude

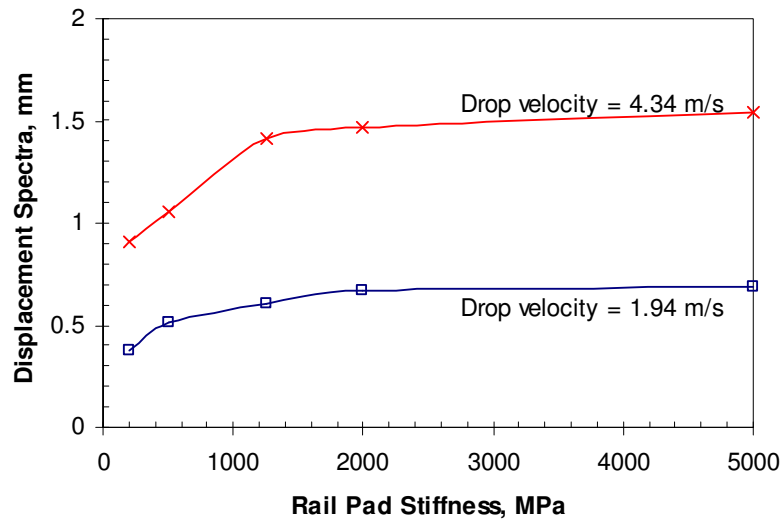


b) impact force duration

**Figure 9.8** Influence of rail pad stiffness on contact impact forces and dynamic responses



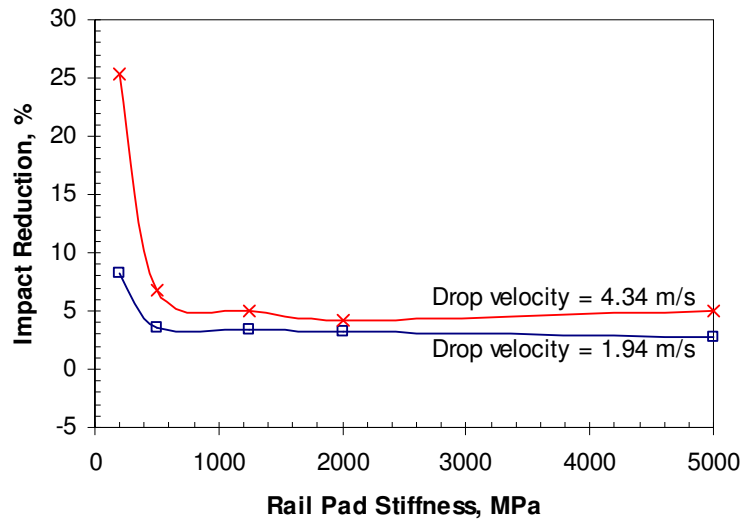
c) displacement responses at railseat



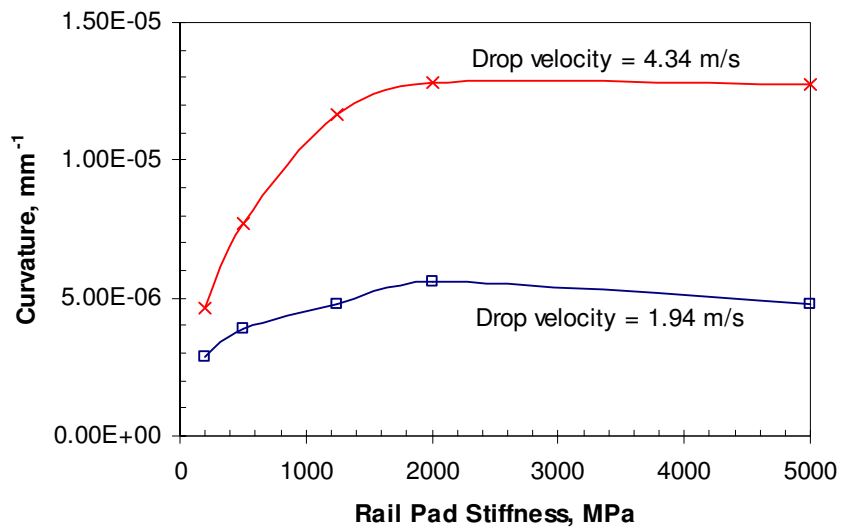
d) displacement responses at mid-span

**Figure 9.8** Influence of rail pad stiffness on contact impact forces and dynamic responses





a) impact force reduction



b) bending curvature

**Figure 9.9** Influence of rail pad stiffness on impact responses of the prestressed concrete sleeper

## 9.6 SUMMARY

This chapter presents the results of finite element analyses to investigate the static and impact behaviour of prestressed concrete sleeper. Commercial finite element packages, ANSYS10 and LS-Dyna, were employed in static and impact studies, respectively. Initially, the finite element model of a prestressed concrete sleeper was developed. The concrete elements and steel prestressing wires were modeled using SOLID65 and LINK8 elements, respectively. The prestressing was applied using an initial strain to LINK8 elements in the discrete manner. Applied displacement method was used in the static analyses due to the fast and smooth convergence of numerical iterations. The hogging moment test of railway concrete sleeper was carried out, to evaluate its performance under such loading. It was found that only known compressive strength of concrete, measured from exacted cores, and existing formulas are sufficient to model the prestressed concrete sleeper. Apparently, the nonlinear material models can well capture the nonlinear static behaviours of concrete sleeper. The results also show that the tensile strength based on  $0.4\sqrt{f'_c}$  is unsuitable for the high strength concrete. The finite element model was then extended using finite element model updating technique. Linkage between ANSYS and LS-Dyna helps develop the numerical impact modelling. Drop impact tests were carried out to validate the numerical shock simulations. It is found that the extended model can be used to predict impact responses of prestressed concrete sleepers.

The low-velocity impact analysis has been carried out in this chapter. Initially, the three-dimensional finite element model was developed for static analysis. It has then been appended the track components to ensure the in-situ conditions found in actual tracks. A commercial finite element package, LS-Dyna, has been employed for impact analysis and validation against the drop impact tests. The emphasis of this study is placed on the elastic responses whereas the drop heights are limited to impart the low-velocity shocks. The further study on nonlinear behaviours will be presented in the future. This chapter firstly point out the influences of track components, particularly the ballast support and rail pads, on the elastic impact behaviour of the railway prestressed concrete sleepers.

Clearly, the ballast bed has strong influence over the contact impact force characteristics including magnitude and duration, particularly in the stiffness range lower than 1,500 MPa. On the other hand, the high stiffness of ballast insignificantly affects those characteristics. This finding confirms the preliminary results done earlier that the effect of high ballast stiffness is insignificant (Wakui and Okuda, 1999). It is also found that the ballast bed has slight effect on the impact responses of prestressed concrete sleepers. As a result, it is reasonably adequate to use the elastic brick element for modelling the ballast bed in the dynamic simulations. In addition, the rail pads tend to play vital role on both the contact impact force characteristics and the responses of prestressed concrete sleepers. The softer rail pads are likely to have more substantial influences on the impact reduction and impact attenuation.

## CHAPTER 10

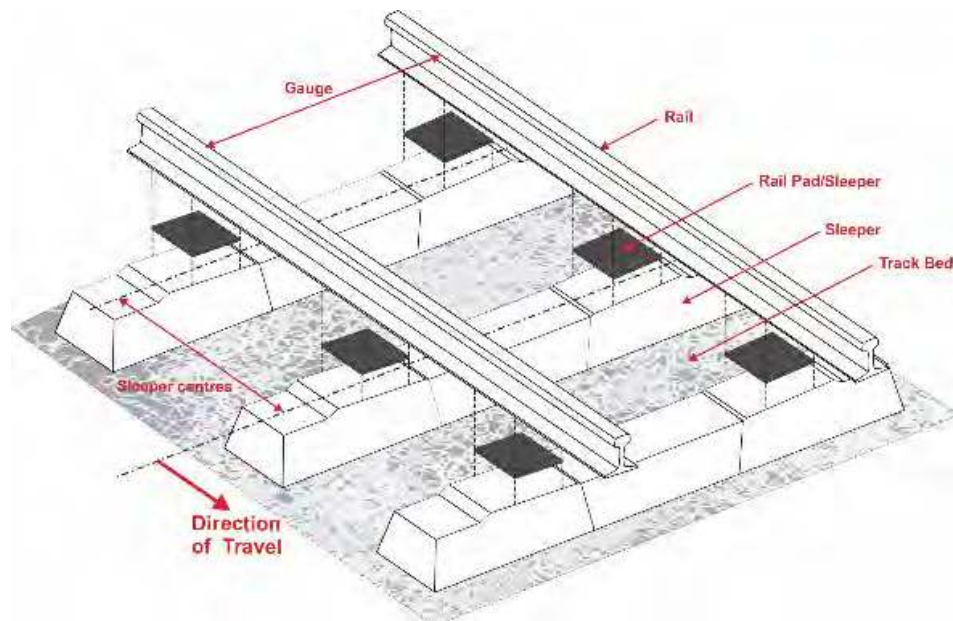
### DEVELOPMENT OF LIMIT STATES DESIGN CONCEPT FOR PRESTRESSED CONCRETE SLEEPERS

Premature cracking of prestressed concrete sleepers has been found in railway tracks. The major cause of cracking is the infrequent but high-magnitude wheel loads produced by a small percentage of “bad” wheels or rail head surface defects which are crudely accounted for in AS 1085.14 by a single load factor. The current design philosophy, outlined in AS 1085.14, is based on assessment of permissible stresses resulting from quasi-static wheel loads and essentially the static response of concrete sleepers. In order to shift the conventional methodology to a more rational design method that involves more realistic dynamic response of concrete sleepers and performance-based design methodology, a significant research effort within the framework of the CRC for Railway Engineering and Technologies is currently underway to perform comprehensive studies of the loading conditions, the dynamic response, and the dynamic resistance of prestressed concrete sleepers.

The collaborative research between the University of Wollongong (UoW) and Queensland University of Technology (QUT) has addressed such important issues as the spectrum and amplitudes of dynamic forces applied to the railway track, evaluation of the reserve capacity of typical prestressed concrete sleepers designed to the current code AS 1085.14, and the development of a new limit states design concept. This chapter presents the results of the extensive investigations at UoW and some related research at QUT aimed at predicting wheel impact loads at different return periods (based on the field data from impact detectors) together with an experimental investigation of the ultimate impact resistance of prestressed concrete sleepers required by a limit states design approach. The chapter also describes the reliability concepts and rationales associated with the development of limit states format codes and the issues pertaining to conversion of AS 1085.14 to a limit states design format.

## 10.1 OVERVIEW

Railway is the world's safest transportation system for either passengers or merchandise across distant areas. Track structures guide and facilitate the safe, cost-effective, and smooth ride of trains. Figure 10.1 recalls the main components constituting typical ballasted railway track (Steffens, 2005). Its components can be subdivided into the two main groups: superstructure and substructure. The most obvious components of the track such as the rails, rail pads, concrete sleepers, and fastening systems form a group that is referred to as the superstructure. The substructure is associated with a geotechnical system consisting of ballast, sub-ballast and subgrade (formation) (Esveld, 2001). Both superstructure and substructure are mutually vital in ensuring the safety and comfort of passengers and a satisfactory quality of ride for passenger and freight trains. Note that in Australia, UK, and Europe, the common term for the structural element that distributes axle loads from rails to the substructure is 'railway sleeper', while 'railroad tie' is the usual term used in the US and Canada. This chapter will adopt the former term hereafter.



**Figure 10.1** Typical ballasted railway tracks from D-Track (Steffens, 2005)

The main functions of sleepers are to: (1) transfer and distribute loads from the rail foot to underlying ballast bed; (2) hold the rails at the proper gauge through the rail fastening system; (3) maintain rail inclination; and (4) restrain longitudinal, lateral and vertical movements of the rails (Esveld, 2001). Typical load conditions on railway track structures have been presented previously in Chapter 4 while common design procedures for Australian railway tracks in AS1085.14 (Standards Australia, 2003). The permissible stress design approach makes use of an empirical function taking into account the static wheel load ( $P_0$ ) with a dynamic impact factor ( $\phi$ ) to account for dynamic vehicle/track interactions:

$$P_D = \phi P_0 \quad (10.1)$$

where  $P_D$  is the design wheel load,  $P_0$  is the quasi-static wheel load, and  $\phi$  is the dynamic impact factor ( $>1.0$ ).

Significant research attention has been devoted to the forces arising from vertical interaction of train and track as these forces are the main cause of railway track problems when trains are operated at high speed and with heavy axle loads. It has been found that wheel/rail interactions induce much higher-frequency and much higher-magnitude forces than simple quasi-static loads. These forces are referred to as '*dynamic wheel/rail*' or '*impact*' forces. The summary of typical impact loadings due to train and track vertical interaction has been presented in Chapter 4 with particular reference to the shape, magnitude and duration of impact loads found in railway track structures.

Current Australian and international design standards for prestressed concrete (PC) sleepers are based on the permissible stress concept where various limiting values or reduction factors are applied to material strengths and load effects (Standards Australia, 2003; Kaewunruen and Remennikov, 2007). Empirical data collected by railway organisations suggests that railway tracks, especially railway PC sleepers, might have untapped strength that could bring potential economic advantage to track owners. The permissible stress design approach does not consider the ultimate strength of materials, probabilities of actual loads, risks associated with failure, and other factors which could lead to overdesigning the PC sleepers. A research programme to investigate the actual load carrying capacity of PC sleepers was initiated as a collaborative project between

UoW, QUT and the industry partners (QR, RailCorp, Austrak, Rocla) within the framework of the Australian Cooperative Research Centre for Railway Engineering and Technologies (Rail-CRC). The main objective was the conversion of the existing Australian design code for PC sleepers into limit states design format, in order to account for the statistical nature, probability and risk of failure.

Murray and Leong (2005; 2006) proposed a limit states design concept and load factors for a revamped standard AS1085.14. The expressions for predicting the impact loads at different return periods (based on field data from impact detectors at two sites) were proposed. It was suggested that a simple pseudo-static (using factored load) approach can be used in the design procedures of PC sleepers under routine traffic. For concrete sleepers under non-routine traffic, a dynamic analysis was suggested as part of a design process. The research team of the Rail-CRC Project has undertaken statistical, probabilistic and experimental studies to investigate the ultimate resistance of the PC sleepers in a manner required by a limit states design approach (Leong, 2007; Kaewunruen and Remennikov, 2005a; 2005b).

In addition to experimental investigations in this project, conversion of the existing design standard into new limit states design format required a comparative examination of the safety margin and probability of failure of PC sleepers designed in accordance with both permissible stress and limit states provisions. It is well known that the performance of structural systems depends on the weakest element with lowest reliability, as show in Chapter 4. To achieve uniform performance and reliability in structural designs for different design principles, the reliability-based approach is the most suitable, in order to either maintain consistent levels of desirable structural reliabilities or overcome the differences of such reliabilities (Kaewunruen and Remennikov, 2006d). From a review of the literature, very few studies were found devoted to the development of the limit states design method for PC sleepers. A preliminary reliability assessment exercise for PC sleepers has been discussed in the later section.

This chapter proposes the use of reliability-based approach in the conversion of the existing design code for PC sleepers to limit states design format. Experimental results complementing the reliability concepts for the impulsive response and ultimate resistance of PC sleepers are also presented in this Chapter. An example of the

reliability assessment of an Australian-manufactured PC sleeper is presented to evaluate the influence of dynamic load amplification on the target reliability indices and probabilities of failure.

## 10.2 CURRENT DESIGN STANDARD AS1085.14-2003

Australian Standard AS1085.14-2003 (2003) prescribes a design methodology for PC sleepers. The *life cycle* of the sleepers based on this standard is 50 years. The design process relies on the permissible or allowable stress of materials. A load factor is used to increase the static axle load to incorporate dynamic effects. The design load is termed '*combined quasi-static and dynamic load*' which has a specified lower limit of 2.5 times static wheel load. Load distribution to a single sleeper, rail seat load, and moments at rail seat and centre can be obtained using tables provided in AS1085.14. It should be noted that the ballast pressure underneath sleepers is not permitted to exceed 750 kPa for high-quality ballast as described by AS2758.7 (1996).

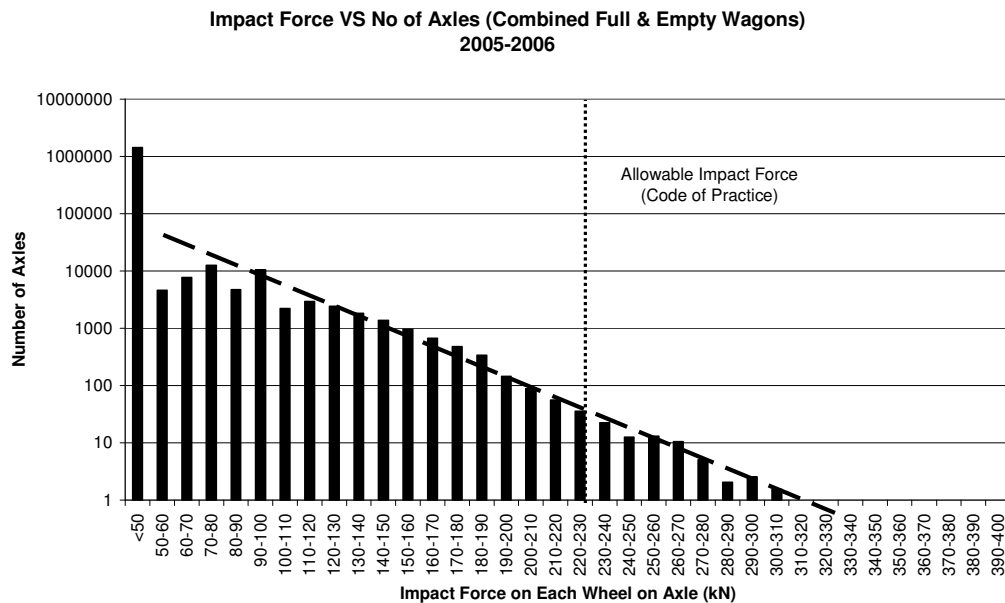
Factors to be used for strength reduction of concrete and steel tendons at transfer and after losses can be found in the standard, ranging between 40% to 60% reduction. However, the minimum pre-camber compressive stress at any cross-section through the rail seat area is set at 1 MPa after all losses (loaded only from prestress). It should be noted that 25% loss of prestress is to be assumed for preliminary design or when there is no test data. A lower level of 22% loss has been generally found in final design of certain types of sleepers (see details in AS1085.14 Appendix E, 2003). The standard testing procedures in AS1085.14 (2003) have been recommended for strength evaluation of PC sleepers.

Past practice has indicated that utilisation of this standard is adequate for flexural strength design. AS1085.14 states that if the design complies with AS1085.14, there is no need for consideration to checking stresses other than flexural stresses, because the permissible stress design concept limits the strengths of materials to relatively low values compared to their true capacity. Under the design loads, the material is kept in the elastic zone so there is no permanent set. In particular, sleepers that comply with AS1085.14 have all cross sections of the sleepers fully in compression, under either pre-camber or design service loads. This approach ensures that an *infinite* fatigue life is



obtained and *no* cracking occurs. Sleepers designed in this way therefore have a significant reserve of strength within their 50 year life cycle under normal service loads.

In reality, impact forces due to wheel/rail interactions may subject the sleepers to dynamic loads that are much larger than the code-specified design forces. Large dynamic impact forces may initiate cracking in the concrete sleepers; indeed, testing at UoW has shown shear failure can also occur at or near the flexural limit. However, concrete sleeper flexural failures have rarely been observed in railway tracks, showing the conservative nature of the existing design process. To develop an ultimate limit states design approach, a study of the response of concrete sleepers to high-magnitude short-duration loading is required. The earlier proposal of allowing cracks in sleepers (by Wakui and Okuda, 1999) could also be considered in a limit states design approach.



**Figure 10.2** Frequency of occurrence of impact forces, derived from (Leong, 2007)

### 10.3 STATISTICS OF DYNAMIC LOAD ON TRACKS

The Defined Interstate Network Code of Practice in Volume 5, Part 2 - Section 8, 2002 (Australasian Railway Association, 2002) prescribes a maximum allowed impact force of 230 kN to be applied to the rail head by passing train wheels. That impact may come about from a variety of effects, including flats worn on the wheel tread, out-of-round wheels, and defects in the wheel tread or in the rail head. Leong (2007) showed that the

largest impact forces are most likely from wheel flats; because such flats strike the rail head every revolution of the wheel, severe flats have the potential to cause damage to track over many kilometres.

Despite the Code of Practice requirement, there is little published data able to be found showing the actual range and peak values of impact for normal operation of trains, and certainly none were found for the defined interstate network. The value of 230 kN is therefore a desired upper limit rather than a measure of real maximum forces encountered on track.

A comprehensive investigation of actual impact forces was undertaken by Leong (2007) as part of the Rail CRC project at QUT. Over a 12 month period he gathered data from two Teknis Wheel Condition Monitoring stations located on different heavy haul mineral lines. The forces from a total of nearly 6 million passing wheels were measured, primarily from unit trains with 26 to 28 tonne axle loads, in both the full and empty states.

An analysis of Leong's data from one of those sites is shown as a histogram Figure 10.2. The vertical axis shows the number of axles on a log scale, while on the horizontal axis is the measured impact force from the Teknis station. Note that the impact force in Figure 10.2 is the dynamic increment above the static force exerted by the mass of the wagon on a wheel. Over 96% of the wheels created impact forces less than 50 kN. The bulk of the graph in Figure 10.2 therefore, is comprised of only the remaining 4% of wheels. However, that small percentage still comprised over 100,000 wheels throughout the year of the study, and they caused impact forces as high as 310 kN. The sloping dashed line in the graph represents a line of best fit to the data for these 100,000 wheel forces.

The vertical dotted line in Figure 10.2 represents the Code of Practice maximum impact force of 230 kN – even though the heavy haul lines from which the data came are not part of the defined interstate network, it's clear that in normal operation very large impact forces can occur which greatly exceed the Code of Practice specification (Australasian Railway Association, 2002).

The distribution of high impact wheel forces in the histogram columns of Figure 10.2 lies along the sloping, dashed straight line, which means the distribution would appear

as a logarithmic curve on a graph with a linear scale on the vertical axis. Now, the vertical axis in Figure 10.2 is the number of impacting wheels per year, so if the rate of occurrence of such impacts over the year of the study is representative of impacts over a longer period, then extrapolation of that sloping dashed line will provide the frequency of occurrence of impact forces greater than 310 kN.

On that basis, one could predict that an impact force of 380 kN would occur at the rate of 0.1 axles per year, or once in every 10 years; an impact of 450 kN would occur on average once in every 100 years. This process naturally leads on to the concept of a return period for impact force, which Murray and Leong (2006) developed to produce equation (2).

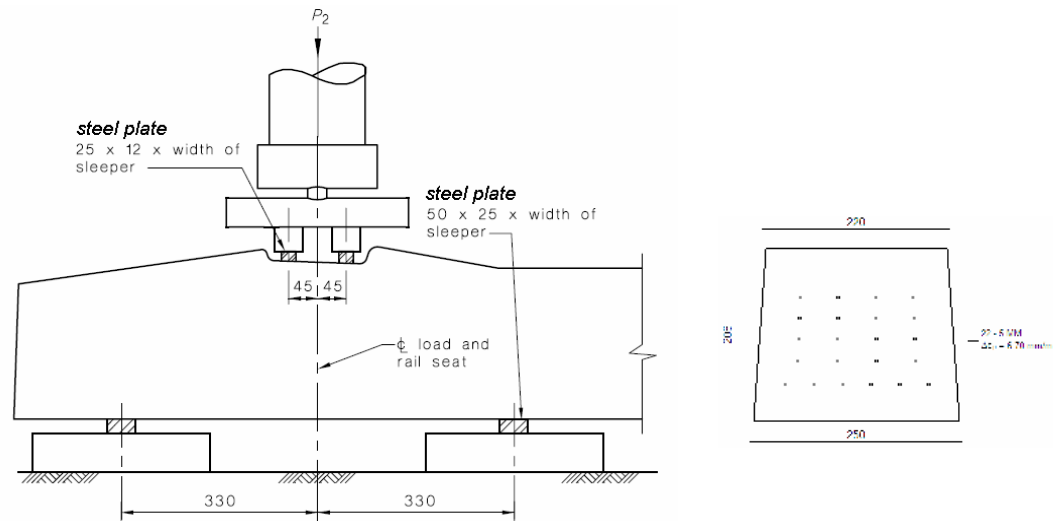
$$\text{Impact Force (kN)} = 53(5.8 + \log R) \quad (10.2)$$

where R is the return period in years of a given level of impact. It should be emphasised that this impact force is that which is applied by a wheel to the rail head. To determine the impact force applied to components further down the track structure, such as the sleeper or ballast, appropriate measures should be applied which allow for force sharing amongst support elements and allow for the not insignificant dynamic behaviour of the track. Equation (10.2) is used later in this chapter to help assess the probability of failure of concrete sleepers in the heavy haul lines which were monitored as part of this study.

#### **10.4 CAPACITY OF PRESTRESSED CONCRETE SLEEPERS**

The experimental programme to investigate the performance of PC sleepers under impulsive loads has been undertaken at UoW. The prestressed concrete sleepers were supplied by Australian manufacturers Rocla and Austrak, as part of the collaborative research project supported by the Australian Cooperative Research Centre for Railway Engineering and Technologies (Rail CRC). The sleepers were broad gauge with the gauge length of 1.60 m commonly used in heavy haul coal lines. For better understanding into the capacity of prestressed concrete sleepers, this section repeatedly and briefly makes use of some previous results. More details in-depth on the behaviours of sleepers can be found in Chapters 5-9.

A series of static tests on the concrete sleepers was performed in accordance with the Australian Standards (2001, 2003). A positive four-point bending moment test was conducted based on the assumption that the sleepers would behave similar to those in-situ (Standards Australia, 2003). It should be noted that the initial strain of prestressing wires is about 6.70 mm/m, and each prestressing wire has a specified minimum proof stress of 1860 MPa. The average compressive strength of cored concrete was 88 MPa. This value was corrected according to AS1012.14 (1991). The details of static responses, rotational capacity, post-failure mechanisms, and residual load-carrying capacity of the prestressed concrete sleepers under static loading can be found in Chapter 5. Figure 10.3 reminds the setup for static testing. A load cell was used to measure the applied load, while an LDVT was mounted at the mid-span to obtain the corresponding deflections. Strain gauges were affixed to the top and bottom surfaces of the test sleeper and on both sides. The transducers were connected to a computer for recording experimental data. The applied loading rate was 0.5 mm per minute.

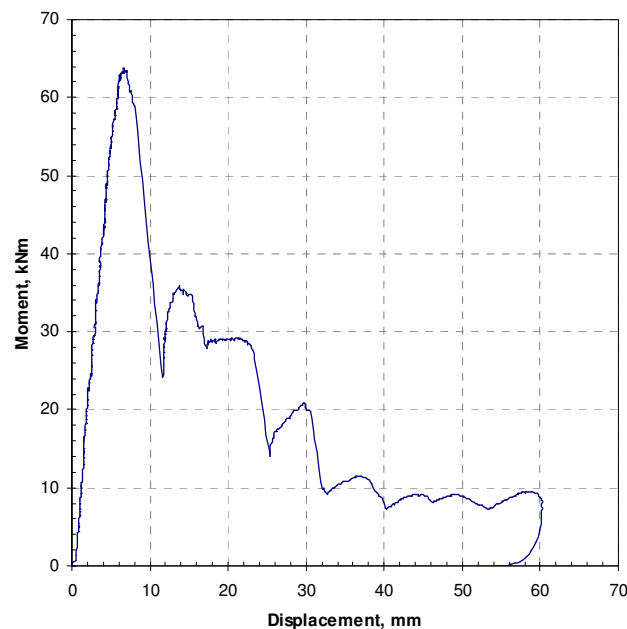


**Figure 10.3** Static test setup

A new high-capacity drop-weight impact testing machine has recently been developed at the University of Wollongong, as depicted in Chapter 6. To eliminate surrounding noise and ground vibration, the concrete sleepers were placed on a strong shock-isolated concrete floor in the laboratory. Thick rubber mats were used to replicate the ballast support. It was found that the test setup could accurately represent the support conditions for concrete sleepers found in typical track systems (see Chapter 6). To apply

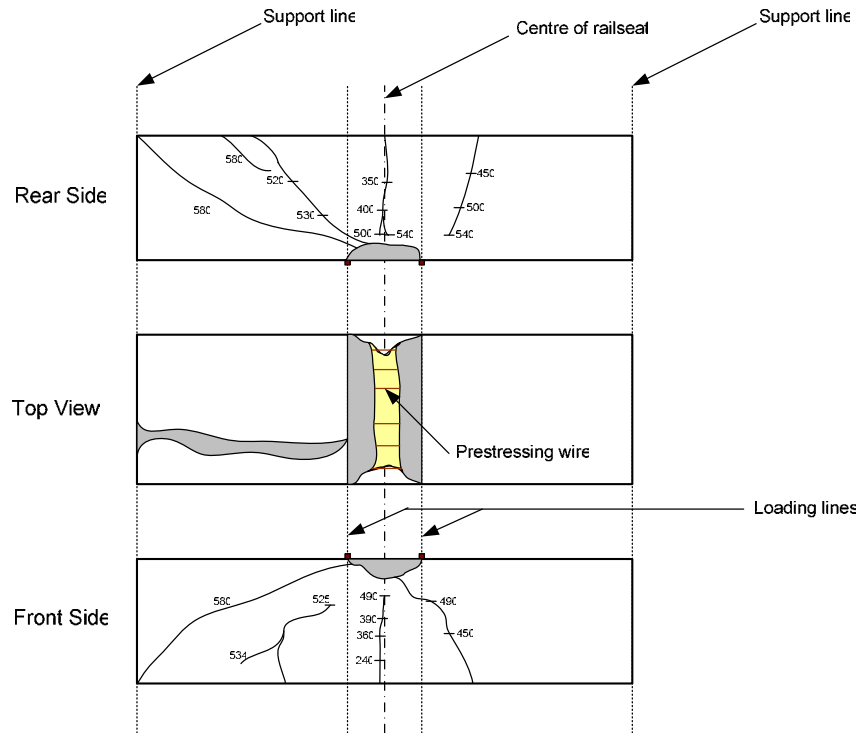
impact loads, a drop hammer with a falling mass of 591 kg was used. The rail, with its fastening system for transferring the load to the specimens, was installed at the railseat. The drop-hammer was hoisted mechanically to the required height and released. Impact load was recorded by the dynamic load cell.

The reliability of the drop hammer machine had been evaluated earlier through calibration tests using a high speed camera. It was found that the hammer's experimental velocity was about 98% of the theoretical velocity. Experimental setup and impact tests were arranged in accordance with the Australian Standards. The in-situ conditions of railway concrete sleepers were replicated. A separate study was performed in order to simulate the impact loads recorded in tracks by means of the drop hammer machine and numerical impact simulations. A typical dynamic moment-deflection relationship at the railseat for PC sleepers is presented in Figure 10.4. The crack initiation load was detected visually during each test as well as determined by the use of the load-deflection relationships.



**Figure 10.4** A static moment-displacement relationship (at railseat)

Figure 10.5 illustrates the crack propagation in a PC sleeper under static monotonically increasing loading. The initial cracking moment was about 26 kNm. The maximum static load capacity was found to be about 583 kN, which is equivalent to bending moment at railseat of about 64 kNm.



**Figure 10.5** Crack propagation of PC sleeper under static loading (at railseat)

Based on the statistical data of the frequency of occurrence of impact loads and their magnitudes (see Section 3), the impact tests on PC sleepers were designed to simulate wheel/rail interface forces by varying the height of drop and the contact stiffness to achieve the required magnitudes and durations of the load pulses. Typical impact force-time histories can be measured by the dynamic load cell. Very small flexural cracks were initially detected starting from a drop height of 600 mm. Small shear cracks were also found after several impacts from a drop height of 800 mm. However, no major failure was observed in these single impact load experiments (see Chapter 8).

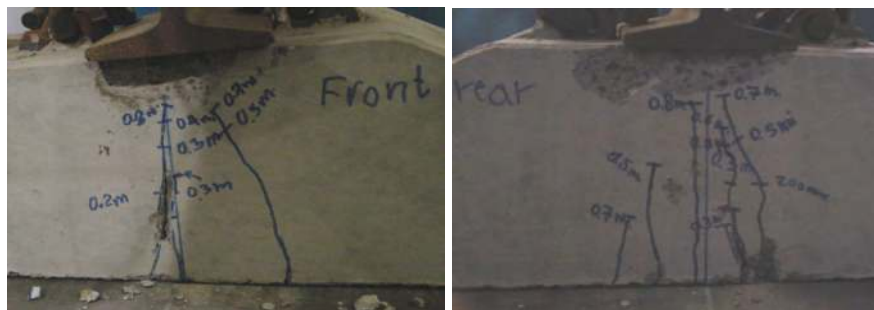
The PC sleepers were also subjected to gradually increasing impact loads until failure of the sleepers. Figure 10.6 depicts the progressive impact behaviour of a PC sleeper in the soft track environment. The crack widths at each stage were measured using the magnified telescope. For impact loads between 150 and 600 kN (see Figure 10.6a), the crack widths were about 0.01 to 0.02 mm. The crack widths increased from 0.02 to 0.08 mm when subjected to impact loads with magnitudes between 700 to 1,000 kN (see Figure 10.6b).



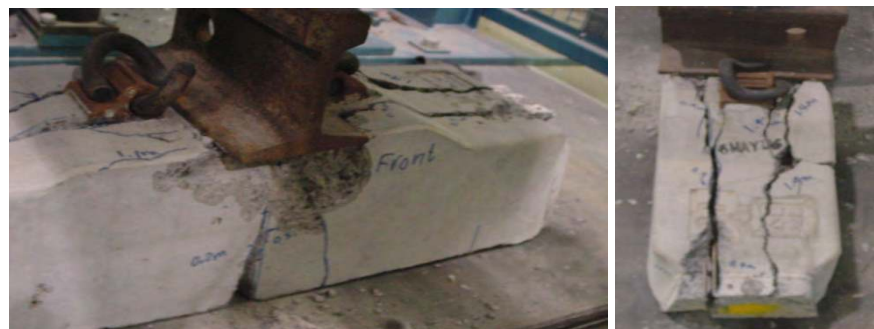
a) impact forces between 150 and 600 kN



b) impact forces between 700 and 1,000 kN



c) impact forces between 1,000 and 1,500 kN



d) impact failure at 1,600 kN

**Figure 10.6** Progressive impact response of a PC sleeper in soft track environment  
(see more details in Chapter 7)

At this stage, spalling of the concrete at the top of railseat section could be detected. When the impact forces were increased up to 1,500 kN, the crack widths also increased up to 0.5 mm (see Figure 10.6c). The ultimate impact load carrying capacity was reached at about 1,600 kN, when the sleeper railseat section has disintegrated. The failure mode was associated with both flexural and longitudinal splitting actions. The splitting fractures were aligned along the prestressing tendons as illustrated in Figure 10.6d.

Based on the probabilistic analysis of dynamic loading, the magnitude of the ultimate impact load that caused failure of the PC sleeper would be equivalent to that with a return period of several million years.

## 10.5 RELIABILITY CONCEPT

The errors and uncertainties involved in the estimation of the loads on and the behaviour of a structure may be allowed for in strength design by using load factors to increase the nominal loads and using capacity factors to decrease the structural strength. The purpose of using any factors is to ensure that the probability of failure under the most adverse conditions of structural overload remains very small, which may be implicit or explicit in the rules written in a code. In earlier structural design codes that employed the traditional *working stress design* e.g. AS 1250-1981 Steel Structures (Standards Australia, 1981), and in the current AS1085.14 sleeper code, safe design was achieved by using *factors of safety* to reduce the failure stress to permissible working stress values, but ultimately the purpose was to limit the likelihood of failure.

The specified maximum allowed stresses in AS1085.14 are expressions of ultimate strengths of isolated members divided by the factors of safety SF. Thus

$$\text{Working stress} \leq \text{Permissible stress} \approx \text{Ultimate stress} / \text{SF} \quad (10.3)$$

All structural design codes except AS1085.14 have been converted to a limit state design approach. Limit state deems that the strength of a structure is satisfactory if its calculated *nominal capacity (resistance)*, reduced by an appropriate capacity factor  $\phi$ , exceeds the sum of the nominal load effects multiplied by various load factors  $\gamma$ , so that



$$\Sigma (\gamma \times (\text{Nominal load effects})) \leq \phi \times \text{Nominal capacity} \quad (10.4)$$

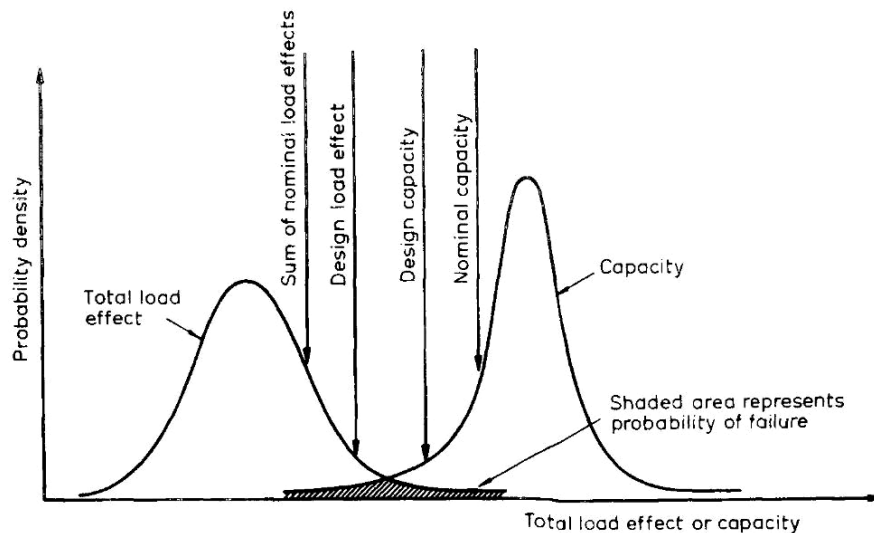
or

$$\text{Design load effect} \leq \text{Design capacity} \quad (10.5)$$

where the nominal load effects are the appropriate bending moments, axial forces or shear forces, determined from the nominal applied loads by an appropriate method of structural analysis (static or dynamic).

Although the limit states are described in deterministic form, the load and capacity factors involved are usually derived from *probabilistic models* based on statistical distributions of the loads and the capacities as illustrated in. Figure 10.7. The probability of failure  $p_F$  is indicated by the region for which the load distribution exceeds that for the structural capacity.

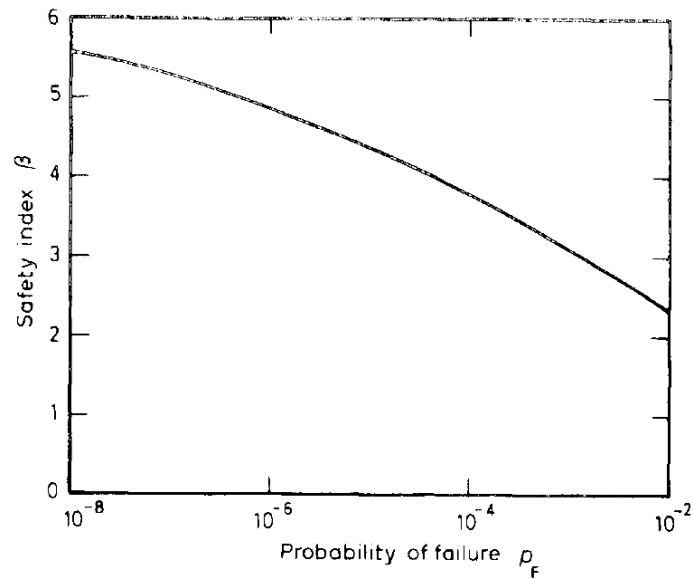
In limit state codes, the probability of failure  $p_F$  is usually related to a parameter  $\beta$ , called the *safety index* or *reliability index*, by the transformation in Equation (10.6) (Standards Australia, 2005).



**Figure 10.7** Probabilistic density functions for reliability (Standards Australia, 1981)

$$\Phi(-\beta) = p_F \quad (10.6)$$

where the function  $\Phi$  is the cumulative frequency distribution function. The relationship between  $\beta$  and  $p_F$  shown in Figure 10.8 indicates that an increase of 0.5 in  $\beta$  implies a decrease in the probability of failure by approximately one order of magnitude.



**Figure 10.8** Relationship between safety index and probability of failure (Standards Australia, 2005)

## 10.6 CONVERSION OF AS1085.14

In the conversion of the existing design code AS1085.14 to a new limit states format, the concept of a safety index may be used to ensure that the use of the new code will lead to a satisfactory level of structural reliability. This could be done by first selecting typical prestressed concrete sleepers that had been designed according to the current working stress code. The safety indices of these sleepers would then be computed using idealised but realistic statistical models of their loads and structural capacities. These computed safety indices would be used to select target values for the limit state formulation. The load and capacity factors for the limit state design method would be varied until the target safety indices are met with reasonable precision. This procedure is called the *code calibration procedure*.

As an example, the calibration procedure and the safety indices  $\beta$  for ultimate limit state

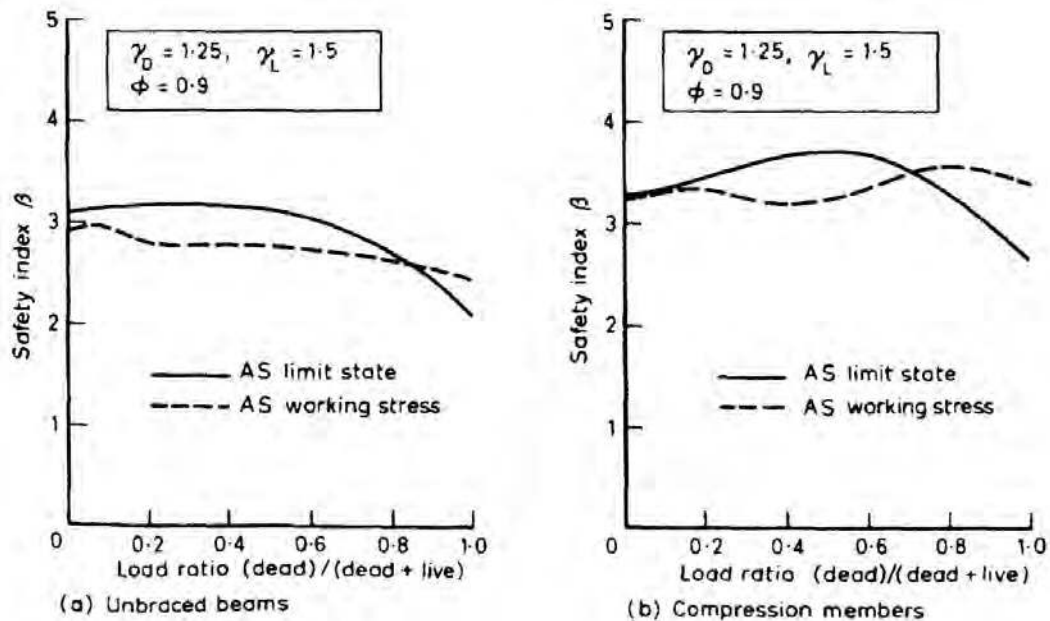
designs according to the Australian limit state code AS 4100 Steel Structures (Standards Australia, 1981b) are compared in Figure 10.9 with those of the previous working stress code AS 1250-1981 for steel beams and columns (Standards Australia, 1981a). These comparisons show that the limit state formulations with a dead load factor of 1.25, live load factor of 1.5 and a capacity reduction factor of 0.9 offer designs with a reasonably consistent safety index in the range of 3.0 to 3.5 compared to the working stress designs of steel beams and columns.

An essential feature of the new limit states design format is that design criteria will be related to specified limit states, and particularly to ultimate limit states such as structural collapse. Another feature of the new format is that the *design values* of resistance  $R^*$ , loads  $Q^*$  and load effects  $S^*$  (such as for example the bending moment at a rail-seat cross-section) are specified in terms of their *characteristic values*  $R_k$ ,  $Q_k$  and  $S_k$  and associated design coefficients  $\phi$ ,  $\gamma_Q$  and  $\gamma_S$  as follows:

$$R^* = \phi R_k \quad (10.7)$$

$$Q^* = \gamma_Q Q_k \quad (10.8)$$

$$S^* = \gamma_S S_k \quad (10.9)$$



**Figure 10.9** Safety indices for steel beams and columns (Standards Australia, 1981)

Typically, extreme values such as 5 and 95 percentile values (of distributions similar to Figures 10.7 and 10.8) are chosen for characteristic values in specifying design values for checks concerned with ultimate limit states, while average values are typically used in checks concerned with serviceability limit states.

In the process of converting AS1085.14 to a new limit states format, it is proposed that the opportunity is taken to examine the structural reliability of both the existing and proposed concrete sleeper codes to endeavour to obtain some specified consistency in structural reliability in the formulation of the new design code, as demonstrated in the following paragraphs.

The statistical characteristics of resistance and loads may be stated in terms of *random variables* that will be denoted by  $X_1, X_2, \dots, X_N$ . For the simplified case where the parameters considered do not vary with time, the probability of failure is defined as

$$p_F = \text{Probability} \{g(X_1, X_2, \dots, X_N) < 0\} \quad (10.10)$$

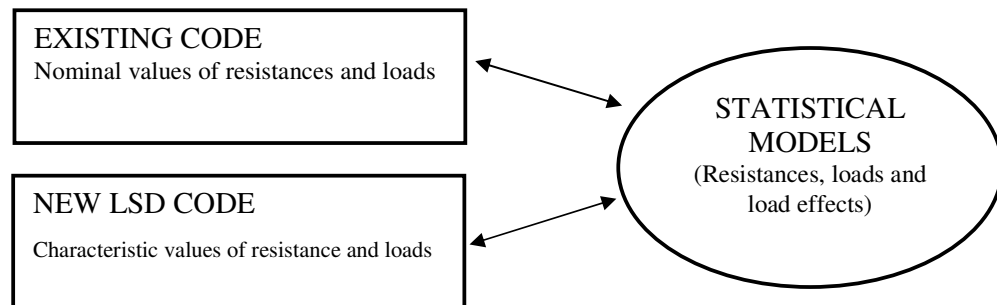
where  $g(X_1, X_2, \dots, X_N)$  may be a general function of the random variables  $X_1, X_2, \dots, X_N$  that represents the limit states equations for a selected structural member. If the statistical values of the random variables are known, Equation (10.5) may be solved for the probability of failure using the methods of structural reliability analysis. From the relationship between  $\beta$  and  $p_F$  given in Figure 10.8, the safety index could be determined.

It should be noted that Equation (10.6) and Figure 10.8 lead to numbers for the safety index that are convenient for evaluations of comparative safety of various designs of prestressed concrete sleepers.

Conceptually, the conversion of the existing design code to a new code written in limit states format should be undertaken through a calibration procedure which could comprise the following steps:

1. Derive statistical models of structural resistances (concrete, prestressing steel) and loads (e.g. impact loads at wheel/rail interface) and load effects (e.g. bending moments at rail seat cross-section).
2. Using these models, safety indices could be evaluated for existing designs of concrete sleepers according to the current code AS1085.14.
3. Using the values of safety indices obtained in Step 2, values of target safety indices could be chosen for a new limit states design code.
4. The load and resistance factors of the proposed new code could be selected so that, the associated safety indices are close to the chosen target values.

The essential information required for the calibration procedure that should be generated by the research teams at QUT and UoW is illustrated schematically below.



## 10.7 LIMIT STATE DESIGN OF PRESTRESSED CONCRETE SLEEPERS

According to Leong (2007), Australian railway organisations would condemn a sleeper when its ability to hold top of line or gauge is lost. These two failure conditions can be reached by the following actions:

- abrasion at the bottom of the sleeper causing loss of top;
- abrasion at the rail seat causing a loss of top;
- severe cracks at the rail seat causing the ‘anchor’ of the fastening system to move and spread the gauge;
- severe cracks at the midspan of the sleeper causing the sleeper to ‘flex’ and spread the gauge;

- severe degradation of the concrete sleeper due to alkali aggregate reaction or some similar degradation of the concrete material.

Since abrasion and alkali aggregate reaction are not structural actions causing failure conditions, only severe cracking leading to sleeper's inability to hold top of line and gauge will be considered as the failure conditions defining a limit state related to the operations of a railway system.

A challenge in the development of a limit states design concept for prestressed concrete sleepers is the acceptance levels of the structural performances under design load conditions. Infinite fatigue life of sleepers *cannot* be retained after allowing cracks under impact loads. Degree of reliability is also an important factor that needs to be taken into account. The Australian Standard AS 5104-2005 (Standards Australia, 2005) prescribes the general principles for reliability for structures, and indicates that limit states can be divided into the following two categories:

1. ultimate limit states, which correspond to the maximum load-carrying capacity or, in some cases, to the maximum applicable strain or deformation;
2. serviceability limit state, which concerns the normal use.

Leong (2007), and Murray and Leong (2006a; 2006b) noted that for railway concrete sleepers the limit state categories could be different from the traditional structural approach and should take into consideration the track's ability to continue operating in an event of exceedance of a limit state. Therefore, the following three limiting conditions (Leong, 2007) have been proposed that would be relevant to the design of railway concrete sleeper:

#### *Ultimate Limit State*

A single once-off event such as a severe wheel flat that generates an impulsive load capable of failing a single concrete sleeper. Failure under such a severe event would fit within failure definitions causing severe cracking at the rail seat or at the midspan.

#### *Damageability (or Fatigue) Limit State*

A time-dependent limit state where a single concrete sleeper accumulates damage progressively over a period of years to a point where it is considered to have reached

failure. Such failure could come about from excessive accumulated abrasion or from cracking having grown progressively more severe under repeated loading impact forces over its lifetime.

### *Serviceability Limit State*

This limit state defines a condition where sleeper failure is beginning to impose some restrictions on the operational capacity of the track. The failure of a single sleeper is rarely if ever a cause of a speed restriction or a line closure. However, when there is failure of a cluster of sleepers, an operational restriction is usually applied until the problem is rectified.

For the purpose of this discussion chapter, only the ultimate limit state for a single concrete sleeper is considered in the development of the reliability-based design procedure for concrete sleepers. An experimental programme will be developed to characterise the uncertainties of the calculation models for the resistances of concrete sleepers in the ultimate limit state.

If the ultimate limit state for a concrete sleeper is associated with the flexural failure, equation (10.6) could be defined as

$$M^* \leq \phi M_u \quad (10.11)$$

where the ultimate moment capacity,  $M_u$  is determined from AS 3600 code (2001), and  $M^*$  is the design bending moment due to the design static wheel load combined with the design impact wheel load caused by wheel or rail irregularities (e.g. wheel flats). In the reliability analysis format, equation (10.8) can be represented by the following limit state function

$$g_{\text{ult}}(\mathbf{X}) = \Theta_R M_u - \Theta_S \times \text{Applied moment} \quad (10.12)$$

where  $M_u$  is the random variable that could be expressed as a function of the basic random variables describing the ultimate resistance of the selected cross section; the sleeper *Applied moment* is the random variable due to the design wheel impact load and described by a probability curve of flexural moments in sleeper;  $\Theta_R$  and  $\Theta_S$  are the model uncertainty coefficients.

As described in section 3 earlier, Murray and Leong (2006a; 2006b) proposed a method by which the ultimate limit state wheel/rail impact design forces may be calculated based on data drawn from a QR WILD impact detector on a heavy haul coal line. But the problem with converting the design wheel/rail force to the design sleeper moment is still open for discussion.

Murray and Leong (2006a; 2006b) emphasised the need for computer dynamic track analysis using such package as DTRACK to compute the design sleeper moment. While in principle this approach could be viable, it could lead to a complication with formulating statistical ultimate limit state models of concrete sleepers for their reliability assessment and for the model calibration in the conversion process to a new limit states design code format. Equation (10.12) will become

$$g_{\text{ult}}(\mathbf{X}) = \Theta_R M_u - \Theta_S \times M^* \quad (10.13)$$

(applied moment,  $M^*$  is to be determined from computer analysis - DTRACK) where the design sleeper moment does not have an analytical representation and equation (10.11) cannot be solved to find the safety indices  $\beta$ . Therefore, it is very important to carry out an experimental investigation of the relationship between impact wheel load and the resulting bending moments with a view to establishing a simplified analytical expression that could be incorporated in the limit state functions like equation (10.11) for conducting the reliability assessment studies on prestressed concrete sleepers.

The impact tests to establish the relationship between the impact load and the railseat bending moment have been carried out using a new drop hammer machine at UoW as illustrated in Chapters 6-7. In the impact tests, the fall height of an anvil was increased step-by-step up to the maximum height from which the resulting bending moments would not exceed the cracking moment capacity. The duration of impact loads was kept almost constant at about 4-5 msec regardless of the fall height (by varying the softening media placed between the impactor and the railhead). To provide support in interpreting the data from the tests, finite-element modelling of sleepers subjected to impact loads and DTRACK simulations were also used. The findings from these studies showed that the results of UoW experiments were very close to those obtained from DTRACK (see Chapter 7).



Wheel load is the main factor in design and analysis of railway track and its components. The proposed methodology for the calculation of the design wheel load and the design approach of the limit states concept for strength and serviceability are in concurrence with the current design standards: AS1170-2002 Loading on structures; and AS3600-2001 Concrete structures (the new amendment to appear in early 2008). There are three main steps in designing the concrete sleepers on the basis of the new limit states design concept: first, the determination of design loads ( $F^*$ ); second, the analysis of design moment or actions ( $M^* = 0.8F^*$  or D-TRACK); and third, the structural design and optimisation of concrete sleepers ( $M^* \leq \phi M_u$ , AS3600).

The design wheel load ( $F^*$ ) for the limit states design concept takes into account both the static ( $F_s$ ) and dynamic ( $F_i$ ) wheel loads (Leong, 2007), as presented follows. It should be noted that the factors 1.2 and 1.5 are derived from the statistical data and probability analysis of loading actions in general. It is not the permission to overload any type of structures.

$$F^* = 1.2 k_{tf} F_s + 1.5 F_i \quad (10.14)$$

$$F_i = k_r k_t k_{vf} P_{axle} \quad (10.15)$$

where

$F^*$  = ultimate limit state wheel/rail design force applied to rail head, kN

$F_i$  = design wheel/rail impact force, kN

$F_s$  = design static wheel load, kN

$k_t$  = factor allowing for type of track (track importance factor)  
see Table 10.1

$k_{tf}$  = factor allowing for quality of maintenance on rail track  
see Table 10.2

$k_r$  = factor associated with the basic return period of loading,  $R_b$   
(impact load factor)

$k_{vf}$  = factor allowing for quality of maintenance on vehicle wheels  
see Table 10.3

$P_{axle}$  = nominal axle load in tonnes

$R_b$  = basic return period of load occurrence in years  
see Table 10.1

It should be noted that the impact load factor  $k_r$ , which is the factor associated with the basic return period of loading ( $R_b$ ), can be obtained from the statistical data of loading. Leong (2007) carried out the probabilistic analysis of the impact loads (excluding static axle force) detected by WILD impact detector. Based on the statistical traffic data (Murray and Leong, 2006) as presented in Chapter 8, the impact load factor  $k_r$  can be written as follows:

$$k_r = 11.6 + 2 \log_{10} \left[ \frac{1}{5} \frac{R_b V_t}{P_{axle}} \right] \quad (10.16)$$

where  $V_t$  is the estimated traffic volume in MGT per annum.

**Table 10.1** Track importance categories and related factors (Leong, 2007)

<b>Track Importance Category</b>	<b>Line Characteristics</b>	<b>Track Importance factor (<math>k_t</math>)</b>	<b>Basic Return Period of Loading (<math>R_b</math>)</b>
Category I	Sleepers in low to medium trafficked lines for which delays to services caused by speed restrictions or by track possession for maintenance are not usually of serious consequence.	1.0	100
Category II	Sleepers in railway lines in which safety is an important design consideration and which carry mixed traffic producing a significant income to business; such as lines between major city centres carrying medium speed passenger and freight trains.	1.1	500
Category III	Sleepers in railway lines that are critically important in terms of safety, revenue or business reputation, such as high speed inter-city passenger lines, suburban passenger lines, or important heavy haul mineral lines.	1.2	2,000

**Table 10.2** Track maintenance factor,  $k_{tf}$  (Leong, 2007)

<b>Track Maintenance Group</b>	<b>Track Maintenance Characteristics</b>	<b>Track Maintenance factor (<math>k_{tf}</math>)</b>
Group I	A very high standard of track maintenance in general, which only few dipped welds or rail head out-of-round defects can be detected.	1.0
Group II	This group includes railway lines which are ground regularly but a certain frequency of occurrence of squats, shells, and the like are tolerated. Likewise the dipped welds are not uncommon but perhaps are limited to 0.3mm dip or peak.	1.2
Group III	This group includes railway lines with irregular grinding, and/or in which dipped welds are common and are often larger than 0.3mm dip or peak.	> 1.2

**Table 10.3** Wheel maintenance factor,  $k_{vf}$  (Leong, 2007)

<b>Wheel Maintenance Group</b>	<b>Wheel Maintenance Characteristics</b>	<b>Wheel Maintenance factor (<math>k_{vf}</math>)</b>
Group I	A very high standard of wheel maintenance in which wheel tread defects are detected and removed quickly. The maximum wheel tread defects tend to be small.	1.0
Group II	This group includes railway lines on which the vehicles usually run has an impact detector and the data is fed to the operator to assist in identification and rectification of wheel defects. The wheel maintenance standard in this group is not the highest standard achievable in vehicle maintenance. The early detection of wheel defects reduces the risks of further damage to the railway track.	1.2
Group III	This group includes situations where vehicles are subjected only to visual inspection and detection by drivers.	> 1.2

## 10.8 RELIABILITY ANALYSIS OF PRESTRESSED CONCRETE SLEEPERS

The case study on the reliability analysis has been conducted to achieve a preliminary target value. The 2700 mm long Australian-manufactured broad gauge sleeper was originally designed for both metropolitan and country tracks with the following parameters:

Track gauge	1600 mm
Rail size	53/60 kg
Maximum axle load	25 tonne
Maximum train speed	115 kph
Sleeper spacing	685 mm
Design rail seat load	187 kN

This sleeper was designed according to AS 1085.14 (Standards Australia, 2003) to satisfy permissible stresses at transfer and at service. The sleeper design will be assessed using the reliability-based approach to calculate the safety index  $\beta$ . The limit state function  $g(\mathbf{X})$  (see equation (10.3)) with respect to permissible stress criteria can be formulated as follows:

$$g(\mathbf{X}) = \text{permissible stress} - \text{fibre stress} \quad (10.17)$$

The rail seat section is designed such that the extreme top and bottom fibres satisfy stress constraints as prescribed by AS 1085.14:

*Concrete:*

At transfer:  $f'_{cp} = 30$  MPa;  $f_{ci} = 0.5 f'_{cp} = 15$  MPa;  $f_{ti} = 0.25 \sqrt{f'_{cp}} = 1.37$  MPa

At final:  $f'_c = 55$  MPa;  $f_c = 0.45 f'_c = 24.8$  MPa;  $f_t = 0.4 \sqrt{f'_c} = 2.97$  MPa

*Prestressing steel:*

At transfer:  $f_p = 1700$  MPa;  $f_{pe@t} = 0.7 f_p = 1190$  MPa

At final:  $f_p = 1700$  MPa;  $f_{pe@f} = 0.8 f_p = 1360$  MPa

In general, the stresses at the top and bottom fibres ( $\sigma_t$  and  $\sigma_b$ , respectively) are

$$\sigma_t = -\frac{P}{A_g} \pm \frac{P \cdot e \cdot y_t}{I_g} \mp \frac{M \cdot y_t}{I_g} \quad (10.18)$$

$$\sigma_b = -\frac{P}{A_g} \mp \frac{P \cdot e \cdot y_b}{I_g} \mp \frac{M \cdot y_b}{I_g} \quad (10.19)$$

where  $P$  is the prestressing force,  $e$  is the effective eccentricity,  $M$  is the bending moment at the rail seat,  $A_g$  is the gross sectional area,  $I_g$  is the gross moment of inertia of the cross section,  $y_t$  is the distance between top fibre and neutral axis of the cross section, and  $y_b$  is the distance between bottom fibre and neutral axis of the cross section.

The current design procedure based on the QR PSC Design spreadsheet provides the designed railseat section as shown in Figure 10.3 with fibre stresses at each stage. The design data is adopted from QR drawings. The sleeper is designed for the axle load of 25 tons, sleeper spacing of 685 mm, and the dynamic amplification factor ( $j$ ) of 2.5. The length of sleeper  $L$  is 2.695 m and the centre-centre gauge  $g$  is 1.680 m.

The railseat load,  $R$  can be read:  $R = j \cdot Q (DF)/100$  where  $j$  is the design load factor (2.5),  $Q$  is static wheel load (125 kN), and  $DF$  is the axle load distribution factor (55% for 600mm spacing). For standard and broad gauge sleepers, at railseat, the positive moment  $M_R^+ = R(L-g)/8$  while the negative moment  $M_R^- = \max\{0.67 M_R^+, 14\text{MPa}\}$ . The wheel load is 125 kN and the designed railseat load is equal to 172 kN. Table 10.4 presents the sectional stresses of the Austrak broad gauge sleeper at the final stage. It should be noted that the stresses  $\sigma_t$  and  $\sigma_b$  are calculated using equations (10.18) and (10.19).

**Table 10.4** Design results for the selected PC sleeper

Moment	Value of Moment, kNm	Location	Total Stress, MPa	Allowable Stress, MPa	Check
MR+	21.8	Top fibre	19.61	24.75	OK
		Bottom fibre	-1.71	-2.97	OK
MR-	14.6	Top fibre	-2.09	-2.97	OK
		Bottom fibre	18.97	24.75	OK

Limit state functions for bending strength can be defined as

$$\text{At the top fibre:} \quad g_t(X) = \alpha_1 \bar{\sigma}_t - \alpha_2 \sigma_t$$

$$\text{At the bottom fibre:} \quad g_b(X) = \alpha_1 \bar{\sigma}_b - \alpha_2 \sigma_b$$

where  $\bar{\sigma}_t$  and  $\bar{\sigma}_b$  are the permissible stresses at the top and bottom fibres, respectively, at any stage (transfer/initial and final stages -  $f_{ci}$ ,  $f_{ti}$ ,  $f_c$ ,  $f_t$ ,  $f_{pe@t}$ , and  $f_{pe@f}$ ), and  $\alpha_1$  and  $\alpha_2$  are the model variation coefficients with respect to the resistance and the action, respectively.

The definition of limit state functions involves the use of appropriate strength models. These models should be realistic rather than code-based conservative approximations.

In particular, the limit functions for  $M_R^+$  of railseat section at final stage are:

$$g_t(X) = \Theta_R(0.85f'_c) - \Theta_S \left[ \frac{0.76P}{A_g} - \frac{0.76P \cdot e \cdot y_t}{I_g} + \frac{R(L-g)}{8} \cdot \frac{y_t}{I_g} \right] \quad (10.20)$$

$$g_b(X) = \Theta_R(0.6\sqrt{f'_c}) - \Theta_S \left[ \frac{0.76P}{A_g} - \frac{0.76P \cdot e \cdot y_b}{I_g} - \frac{R(L-g)}{8} \cdot \frac{y_b}{I_g} \right] \quad (10.21)$$

In equations (10.20) and (10.21), the flexural compressive strength of concrete  $R_c = 0.85f'_c$  and the characteristic flexural tensile strength  $R_t = 0.6\sqrt{f'_c}$  (AS3600-2100) are used as the permissible stresses to more realistically represent the strength models. Note that 0.76 is coefficient that accounts for the prestressing losses (24%).

In addition, based on the permissible stresses prescribed in AS1805.14, the limit functions for  $M_R^-$  of railseat section at final stage are:

$$g_t(X) = \Theta_R(0.4\sqrt{f'_c}) - \Theta_S \left[ -\frac{0.76P}{A_g} + \frac{0.76P \cdot e \cdot y_t}{I_g} + \max \left\{ \frac{0.67R(L-g)}{8}, 14 \right\} \cdot \frac{y_t}{I_g} \right] \quad \dots(10.22)$$

$$g_b(X) = \Theta_R(0.45f'_c) - \Theta_S \left[ \frac{0.76P}{A_g} + \frac{0.76P \cdot e \cdot y_b}{I_g} + \max \left\{ \frac{0.67R(L-g)}{8}, 14 \right\} \cdot \frac{y_b}{I_g} \right] \quad \dots(10.23)$$

Note that coefficient 0.67 is used to calculate the negative railseat moment and the constant term '14' is the minimum railseat negative bending moment in kNm.

**Table 10.5** Statistical model of the selected PC sleeper.

Basic variables	Symbol	Distribution type	Units	Mean value	Standard deviation	Coefficient of variation
<u>Loads</u>						
Static wheel load	$Q_{st}$	Log-normal	kN	125	31.25	0.25
Dynamic load factor	$j$	Log-normal		2.5	0.625	0.25
Axle load distribution factor	$DF$	Constant		0.55		
<u>Resistances</u>						
Permissible tension at transfer ( $f_{cp} = 30$ MPa)	$f_{ti}$	Normal	MPa	1.37	0.2466	0.18
Permissible compression at transfer ( $f_{cp} = 30$ MPa)	$f_{ci}$	Normal	MPa	15.0	2.25	0.15
Permissible tension at service ( $f_c = 55$ MPa)	$f_t$	Normal	MPa	2.97	0.5346	0.18
Permissible compression at service ( $f_c = 55$ MPa)	$f_c$	Normal	MPa	24.8	3.72	0.15
Concrete compressive strength	$f'_c$	Normal	MPa	66.0	9.9	0.15
Prestressing steel yield stress	$f_p$	Normal	MPa	1768	44.2	0.025
Area of prestressing steel	$A_{ps}$	Normal	m <sup>2</sup>	432	5.4	0.0125
Prestressing nominal force	$P$	Normal	kN	550.0	33	0.06
<u>Sleeper dimensions</u>						
Length	$L$	Constant	m	2.7		
Depth (rail seat)	$h$	Constant	m	0.208		
<u>Track parameters</u>						
Track gauge	$g$	Constant	m	1.6		
Sleeper spacing	$S$	Constant	m	0.685		
Track stiffness	$k_T$	Constant	MN/m <sup>2</sup>	100		
Railpad stiffness	$k_p$	Constant	MN/m <sup>2</sup>	400		
<u>Model uncertainties</u>						
Uncertainty of resistance	$\Theta_R$	Normal		0.99		0.06
Uncertainty of load effect	$\Theta_S$	Normal		1.0		0.2

\*Distribution patterns and coefficients of variation adopted from Al-Harthy (1992)

The rail seat section is shown in Figure 10.3. The basic random variables in this study are the permissible stresses at transfer and at final stages, the permissible prestressing

force at transfer and at final stages, compressive and tensile strength of concrete, allowable tensile stress of prestressing wires, sleeper dimensions (sectional area, width, length, & depth), effective eccentricity ( $e$ ), area of prestressing wires, and model coefficients. The statistical properties of the basic random variables used in the reliability analysis of selected PC sleeper are given in Table 10.5.

The reliability index  $\beta$  can be obtained by using the stress limit functions:

$\beta_{ti}$  = reliability index with respect to top fibre stress at initial stage;

$\beta_{bi}$  = reliability index with respect to bottom fibre stress at initial stage;

$\beta_{tf}$  = reliability index with respect to top fibre stress at final stage;

$\beta_{bf}$  = reliability index with respect to bottom fibre stress at final stage;

$\beta_{wi}$  = reliability index with respect to wire stress at initial stage;

$\beta_{wf}$  = reliability index with respect to wire stress at final stage; and

$\beta_{cf}$  = reliability index with respect to cross-sectional stress at final stage.

where  $\beta = \min \{ \beta_{ti}, \beta_{bi}, \beta_{tf}, \beta_{bf}, \beta_{wi}, \beta_{wf}, \beta_{cf} \}$

In this example, only  $\beta_{tf}$  and  $\beta_{bf}$  will be determined. Five random variables include  $P$ ,  $f'_c$ ,  $Q$ ,  $\Theta_R$ , and  $\Theta_S$ . Other parameters are treated as being deterministic in the reliability analyses.

---

*Limit State Function:  $g(X) = R - S$*

---

Taking into account that the total design load acting on a sleeper includes both static and dynamic components,  $Q = Q_{st} + Q_{dyn} = Q_{st}(1 + Q_{dyn}/Q_{st})$ , the limit functions could be arranged such that the dynamic amplification factor  $Q_{dyn}/Q_{st}$  becomes the chief independent parameters with respect to which the reliability indices will be calculated.

Therefore, the limit functions for  $M_R^+$  of railseat section at final stage are:

$$g_t(X) = \Theta_R(0.85f'_c) - \Theta_S \left[ \frac{P}{57671} - \frac{0.76P}{200363} + \frac{0.55 \times Q_{st}(1 + Q_{dyn}/Q_{st}) \times (2695 - 1680)}{8 \times 1657000} \right] \quad \dots(10.21)$$



$$g_b(X) = \Theta_R(0.6\sqrt{f'_c}) - \Theta_S \left[ \frac{P}{57671} + \frac{0.76P}{209069} - \frac{0.55 \times Q_{st}(1 + Q_{dyn}/Q_{st}) \times (2695 - 1680)}{8 \times 1729000} \right] \quad \dots(10.22)$$

Also, the limit functions for  $M_R^-$  of railseat section at final stage are:

$$g_t(X) = \Theta_R(0.6\sqrt{f'_c}) - \Theta_S \left[ \frac{P}{57671} - \frac{0.76P}{200363} - \frac{0.67 \times 0.55 \times Q_{st}(1 + Q_{dyn}/Q_{st}) \times (2695 - 1680)}{8 \times 1657000} \right] \quad \dots(10.23)$$

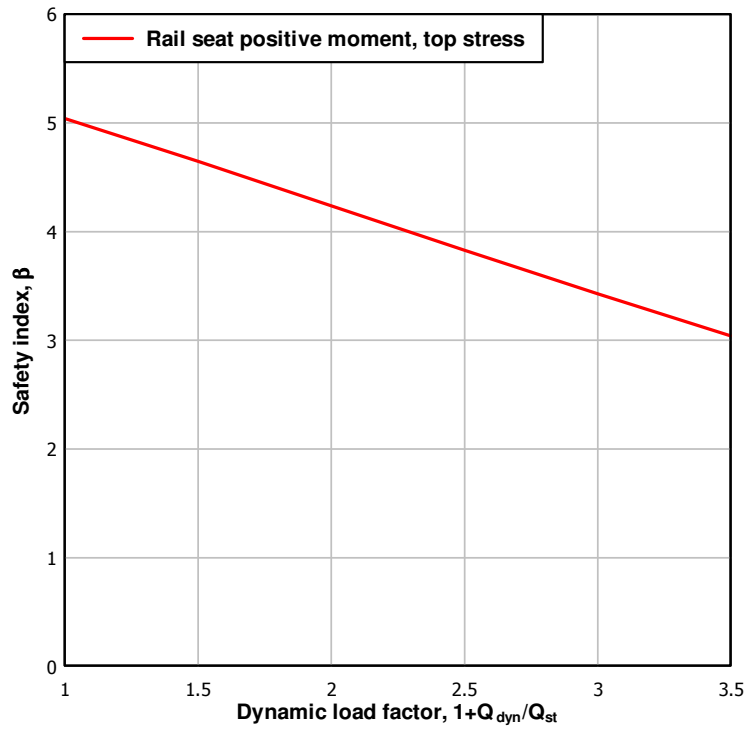
$$g_b(X) = \Theta_R(0.85f'_c) - \Theta_S \left[ \frac{P}{57671} + \frac{0.76P}{209069} + \frac{0.67 \times 0.55 \times Q_{st}(1 + Q_{dyn}/Q_{st}) \times (2695 - 1680)}{8 \times 1729000} \right] \quad \dots(10.24)$$

Using the structural reliability analysis program COMREL (RCP GmbH, 2004), the reliability indices can be calculated as provided in Table 10.6. The effect of the variation of the dynamic load factor on the reliability indices can be seen in Figures 10.10 and 10.11. It should be noted that the reliability indices can also be used as the design parameter in some cases (Kumaran et al., 2003).

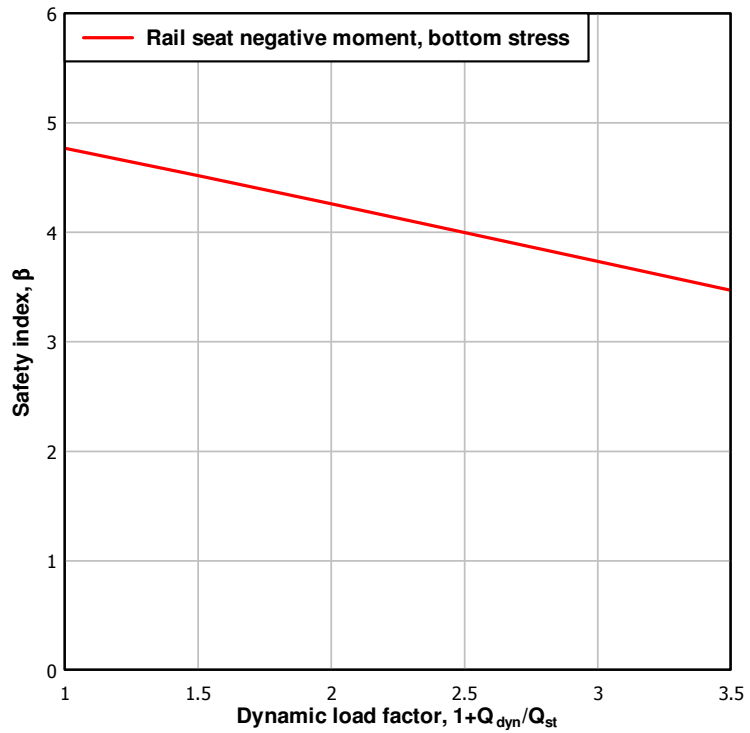
**Table 10.6** Reliability indices of railseat section of Austrak broad gauge sleepers

Moment	Reliability Index	FORM <sup>a</sup>	Probability of failure, $p_F$
$M_R^+$	$\beta_{tf}$ (top fibre stress at final stage)	3.829	6.43E-5
	$\beta_{bf}$ (bottom fibre stress at final stage)	1.872	3.06E-2
$M_R^-$	$\beta_{tf}$ (top fibre stress at final stage)	2.692	3.55E-3
	$\beta_{bf}$ (bottom fibre stress at final stage)	3.998	3.19E-5

<sup>a</sup>first-order reliability method



**Figure 10.10** Safety indices (rail seat positive moment)



**Figure 10.11** Safety indices (rail seat negative moment)

## 10.9 ECONOMIC ASPECTS OF THE NEW DESIGN APPROACH

Limit states design concept has proven to be more logical entity for a new design approach associated with the actual behaviours of concrete sleepers under the impact loading condition. The new design concept will bring out the ultimate capacity of concrete sleeper for exploitation. The experimental results indicated the reserve strength in which the new design approach can save the construction material usage and reduce the individual cost of a sleeper. Alternatively, possible options are to enable the passage of heavier trains on existing concrete sleepers through increased axle loads.

Based on a specific case study by Murray and Leong (2006), it was found that the impact load per railseat at the 2,000 year return period was about 740 kN. From experiments in Chapter 7, the sleeper can withstand the ultimate impact loads of at least 1,800 kN in total ( $F^*$ ). The experimental results in Chapter 8 show that the fracture toughness of the sleeper damaged by a single impact of 740 kN is relatively no less than that of the undamaged sleeper. If the sleeper would thus be redesigned for the increased axle load of 30 tonnes, the new limit states design concept gives an estimate  $F^* = 1.2 \times 1 \times 150$  (static) + 540 (dynamic) = 722 kN (Murray and Leong, 2006; Leong, 2007). Compared with the data obtained from the manufacturer (as shown in Chapter 5), the wheel load can be increased (from 25 tonnes to 30 tonnes) of about 16 percent.

Leong (2007) identified the effect of train speeds on the impact loads on tracks. It was found that at the train speed of 120 km/h, the impact force associated with 2,000 year return period would be 850 kN (at Braeside). The total design force based on the new design concept would be about 1,000 kN. A test result in Chapter 8 shows that the sleepers under 1,500 kN impact loading either in soft- or in hard track environment were still in good condition with sufficient residual energy absorption capacity. Accordingly, in addition to increasing wheel load, the speed of trains can also be increased. However, before doing so, the track engineers must consider the safety in terms of other aspects, e.g. curved track, vibrations, and so on.

Using current design standard AS1085.14-2003, the cross section of the tested sleeper is designed for axle load of about 23 tonnes. However, it is found that the ultimate moment capacity is about 64 kNm or  $\phi M_u = 0.8(64) = 51$  kNm. Using Equation (7.1)  $M^* = 0.08F^*$ , an approximation of  $F^* = 640$  kN can be found. Using the previous

results in the case studies (Murray and Leong, 2007), the design wheel load of 640 kN was found equivalent to the axle load of about 27 tonnes. Based on the data from industry partners, this has proven that the new limit states design concept will save the cost of new sleepers about 15 percent of an individual cost.

The benefits would also have a potentially large flow-on effect. Cheaper but more reliable tracks mean added passenger comfort and security, less materials wastage, and reductions in insurance fees for merchandise. This all could add up to social, environmental, and financial gains.

### **10.10 SUMMARY**

The current design of railway prestressed concrete sleepers, stated in AS 1085.14, is based on the permissible stress concept. The design process is based on the quasi-static wheel loads and the static response of concrete sleepers. To shift to a more rational design method involves significant research effort within the framework of the CRC for Railway Engineering and Technologies.

The collaborative research between the University of Wollongong (UoW) and Queensland University of Technology (QUT) has involved all important facets such as the spectrum and amplitudes of dynamic forces applied to the railway track, evaluation of the reserve capacity of typical prestressed concrete sleepers designed to the current code AS 1085.14, and the development of a new limit states design concept. This chapter presents the background information and some research outcomes of the Rail-CRC research project aimed at developing the new limit states design concept for prestressed concrete sleepers.

The chapter also describes the reliability concepts and rationales associated with the development of limit states format codes and the issues pertaining to conversion of AS 1085.14 to a limit states design format. The use of a reliability-based approach in the conversion of the existing code to the new limit states format has also been demonstrated. The target reliability indices  $\beta$  to be used for the code calibration can be obtained from the reliability analysis of existing design procedures and the newly proposed method to design the prestressed concrete sleepers. An example of the reliability analysis of the Austrak broad gauge sleeper is also discussed.

## CHAPTER 11

### CONCLUSIONS AND RECOMMENDATIONS

The initial aim of this research project was to experimentally and numerically evaluate the impact responses of the prestressed concrete sleepers in track systems. The comprehensive review has however highlighted the extremely limited research work previously done in this field and associated area. In order to achieve this target goal, a lot of research was carried out in collaboration with a team from the University of Wollongong (UoW) and Queensland University of Technology (QUT). While QUT had previously addressed important issues such as the spectrum and amplitudes of dynamic forces applied to a railway track, UoW performed the evaluations of the reserve capacity of typical prestressed concrete sleepers designed to the current AS1085.14 code, and the development of a new limit states design concept.

This research effort within the framework of the CRC for Railway Engineering and Technologies (RailCRC) involved comprehensive studies of the loading conditions, dynamic response, and resistance of prestressed concrete sleepers. The ultimate goal of the collaborative project was to shift the conventional methodology to a more rational design method that involves a more realistic dynamic response from concrete sleepers and performance-based design methodology. This is because the current design philosophy, as outlined in AS 1085.14, is based on the assessment of permissible stresses resulting from quasi-static wheel loads and essentially the static response of concrete sleepers, making it unduly conservative and very costly for the railway construction.

This thesis mainly presents the results of the extensive investigations at UoW. Experimental and numerical investigations for the static, dynamic, and impact resistance of prestressed concrete sleepers were discussed. It also proposed the reliability-based concepts and rationales associated with the development of limit states format codes for the conversion of AS 1085.14 to a limit states design format.

## 11.1 CONCLUSIONS

This thesis has presented the static, dynamic, and impact behaviour of prestressed concrete sleepers under various conditions. There are two main parts which compliment the aim of this study, including a determination of the dynamic properties of railway track components, and the experimental and numerical investigations for the behaviour and capacity of the prestressed concrete sleepers under static, dynamic, and impact loads.

### 11.1.1 Determining the dynamic properties of railway track's components

Rail tracks are a fundamental part of railway infrastructure. Its components can be classified into two main categories: superstructure and substructure. The most observable parts of the track such as the rails, rail pads, concrete sleepers, and fastening systems are referred to as superstructure while the substructure is associated with a geotechnical system consisting of ballast, sub-ballast, and subgrade. In this study the dynamic testing of railway track and its components, particularly concrete sleepers and rail pads can lead to the dynamic model updating for numerical analysis and an alternative experimental setup. The results can be used as a benchmark for health monitoring of a railway track and its components.

Most of data available for the dynamic modelling of track components are based on an experimental modal testing technique, although there exists an extremely limited extent of available data for various conditions for the track components. To our knowledge, very few investigations have been conducted to study the dynamic interaction between the ballast and the railway track or its components such as sleepers, adjacent sleepers, and global systems connected by the rail track. In addition, although the field tests seem to be realistic, the experiments may lead to unreliable results because of many unpredictable factors in the rail track, for instance, the nonlinearities in the track that are attributed to voided sleepers, rail impurities, track corrugations, and worn pads. This thesis has presented new results of the dynamic properties of the railway track and its components, in particular for rail pads and concrete sleepers.

**a) Rail Pads**

An alternative, innovative rail pad tester was devised based on the SDOF vibration response measurement for determining the dynamic properties of rail pads subjected to large preloads. This approach enables testing of new types of rail pads as well as identifying the influences of incremental preloading on their dynamic characteristics. It was discovered that the preloads could significantly affect the natural frequencies and the corresponding dynamic properties of the studded rubber pads and that their damping mechanism is much more susceptible to preloads than the HDPE pads.

The dynamic properties of structural/mechanical components can be used for a number of applications to railway track dynamics such as analysis, modelling, and for monitoring the structural degradation rate. The applications of the test rig and experimental modal testing to determine and monitor the rate of structural degradation of rail bearing pads were also presented. Based on a linear regression of the results, it could be approximated that the per-MGT rate of rail pad degradation in terms of dynamic stiffness is about 2.18 MN/m and the rate for the damping is approximately 19.63 Ns/m. It should be noted that this is a 5.5 mm thick, high-density polyethylene (HDPE) pad. This information is imperative to track maintenance and renewal divisions in order to make decision and optimise track uses.

**b) Prestressed Concrete Sleepers**

The vibration characteristics and dynamic interaction of concrete sleepers and ballast support system are very important for developing a realistic dynamic model of railway track capable of predicting its dynamic responses. The results of the experimental modal analysis for prestressed concrete sleepers under different boundary conditions were presented. The dynamic effects of sleeper/ballast interaction of four types of prestressed concrete sleepers manufactured in Australia were evaluated using an impact hammer excitation technique over the frequency range of interest: from 0 to 1600 Hz. It was found that the resonant frequencies and damping ratios associated with the lower mode of vibration of prestressed concrete sleepers were considerably affected by the support boundary conditions. However, the influence of the ballast condition was reduced in the higher frequency range. The dominant effect of the in-situ support was placed on the modal damping in the ballast-sleeper interaction. In addition, the mode

shapes, which can indicate the deteriorated state of concrete sleepers, were affected by the ballast condition. In summary, the in-situ boundary condition had a remarkable influence on the natural frequency, modal damping, and vibration mode shape of prestressed concrete sleepers, especially in the low frequency range. It is recommended that the determined parameters of concrete sleepers be used in modelling of railways tracks where the effect of the boundary condition and dynamic sleeper/ballast interaction will be taken into account.

### **c) In situ Railway Track**

The free vibration behaviour of global railway tracks were investigated experimentally and computationally using an in-situ ballasted track simulated in the laboratory at University of Wollongong. Using the modal testing technique, the experimental modal results can be obtained. For the sake of better understanding into dynamic track behaviours, two and three dimensional finite element (FE) models of the global track were developed using a FE package, STRAND7. Numerical solutions based on the natural frequency analysis were validated against experimental results of the natural frequencies and corresponding mode shapes of railway track. Symmetrical and asymmetrical modes of vibration were discovered which shows that wheel loading frequencies might deteriorate the support and components of railway tracks. The results showed that the dynamic mode shapes of railway track in good condition are rather symmetrical. The first bending modes of concrete sleepers can damage the ballast and accelerate cracking in rail track sleepers at mid span. The second and the third bending modes tend to accelerate cracks in sleepers at rail seats.

### **d) Field Trials**

Accelerating the degradation of railway tracks creates many problems for railway track engineers. The in-field dynamic testing in combination with track modelling is thus an efficient strategy for identifying the current condition of railway track structure and its components.

In the field investigations described previously, experimental modal testing was carried out and the modal results were obtained from the field measurements and used to assess the current state of the railway track. For practical purposes, this thesis integrates field measurements, experimental modal analysis, and finite element



modelling to evaluate the dynamic parameters of in-situ railway track components. Based on the discrete support model, a railway track can be simplified as a two-degree-of-freedom (2DOF) dynamic system. An analytical formulation of the 2DOF model was developed in order to extract the modal properties of track components from the field dynamic testing results obtained using an instrumented hammer impact technique. A railway track site in Central Queensland managed by Queensland Rail (QR) was selected for the field tests. Six sleeper-fastening-rail assemblies were randomly selected for dynamic testing. The frequency response functions (FRFs) were recorded by using Bruel & Kjaer PULSE vibration analyser in a frequency domain between 0 and 1600 Hz, although in practice only 0 to 600 Hz was sufficient for the optimisations. The results showed that the correlation of the curve fitting seems to be very good in both methods: FFT and MS. However, FFT tends to fit the experimental data better. The dynamic properties at the track site with good conditions are consistent because the stiffness of pad and ballast lies in the narrow ranges of 800-1500 MN/m for rail pads and 150-470 MN/m for ballast. Nonetheless, damping for rail pads varied from 1 to 58 kNs/m and from 140 to 270 kNs/m for ballast.

The advantages of this approach are the non-destructive testing technique and criteria used to evaluate the integrity of the track structure. They could be used by the railway industry to evaluate the current state and monitor of the structural health of railway tracks. Three samples including major defects found in general track problems, e.g. loosening e-Clip and cracked sleeper, were clearly illustrated. The modal result of a full-scale concrete sleeper was discovered and it highlighted the dynamic influences over the cracks of concrete sleepers. These results can supply a track maintenance engineer with important information on the current state of the railway track and also as a benchmark for health monitoring. In addition, the experimentally determined resonance frequencies and the dynamic properties of the track components can provide an important input into the dynamic analysis of railway track package for determining the maximum speed and axle load for future upgrades or functional changes.

### **11.1.2 Capacity of prestressed concrete sleepers**

The typical dynamic impact loading imparted by wheel/rail interaction and wheel/rail/track irregularities were rigorously reviewed. This comprehensive overview

started with the general static and dynamic forces on railway track structures but its primary emphasis was placed on the typical impact loadings, which are attributed to certain sources, such as rail corrugation, wheel flats and shells, worn wheels and rail profiles, bad welds or joints, switches, and track imperfections. Typical shapes of the dynamic, impact axle force waves in time history domain generally found on railway track structures were reviewed.

All static, quasi-static, and impact loads are very important in design and analysis of railway track and its components. Generally, dynamic/impact loading is associated with frequencies ranging from 0 to 2000 Hz due to modern track vehicles. The shape of impact loading varies depending on various possible sources of such loading, e.g. wheel flats, out-of-round wheels, wheel corrugation, short and long wavelength rail corrugation, dipped welds and joints, pitting, and shelling. Wheel/rail irregularities induce high dynamic impact forces along the rails that may greatly exceed the static wheel load. In each instance, the impact forces are significantly dependent on the train speed. These impulses would occur repetitively during the roll. Loss of contact between the wheel and the rail, so-called “wheel fly”, will occur if the irregularity is large enough, or the speed is fast enough. Nevertheless, the impact force could be simplified as a shock pulse acting after the static wheel load is removed.

In summary, the typical magnitude of impact loads from the above cases varies roughly between 100 kN and up to 750 kN, depending on the causes and the traveling speed of the train. The durations of such loads are quite similar, varying between 1 and 10 msec. However, the representative values of the first peak ( $P_1$ ) of the forces caused by dipped joints should be about 400 kN magnitude with 1 to 5 msec time duration. For the second peak ( $P_2$ ), the average values are about 80 kN magnitude and 5 to 12 msec time duration. Therefore, it should be taken into account that the typical duration of impact wheel forces varies widely between 1 and 12 msec.

On the basis of this review, there is high potential that the wheel defects would damage the whole tracks so the impact load due to a wheel flat was considered in this study. There was also the need to develop the experiment programs to achieve the impact resistance behaviours of prestressed concrete sleepers. The first step of the experimental study was to simulate the impact pulses of interest and then apply those impact forces onto the setup in-situ railway prestressed concrete sleepers. Subsequently, the numerical

modelling is an effective and significant option because the repetitive experimental investigations in this regard would be time and resources consuming, and costly. It provided the virtual tests to develop the broader and deeper perspectives than those of the limited experiments. Currently, there is no analytical or numerical model for predicting the dynamic responses of prestressed concrete sleepers to impact loading. This study would thus provide the profound insight into the impact behaviours of railway concrete sleepers under various conditions.

As aforementioned, cracking in prestressed concrete sleepers has been investigated by many railway organisations. The principal cause of cracking is the infrequent but high-magnitude wheel loads produced by a small percentage of “bad” wheels or rail head surface defects which are crudely accounted for in AS 1085.14 by a single load factor. The current design philosophy, outlined in AS 1085.14, is based on an assessment of permissible stresses resulting from quasi-static wheel loads and essentially the static response of concrete sleepers. To shift the conventional methodology to a more rational design method that involves more realistic dynamic response of concrete sleepers and performance-based design methodology, a significant research effort within the framework of the CRC for Railway Engineering and Technologies is imperative to perform comprehensive studies of the loading conditions, the dynamic response, and the dynamic resistance of the prestressed concrete sleepers. Collaborative research between the University of Wollongong (UoW) and Queensland University of Technology (QUT) has addressed important issues such as the spectrum and amplitudes of dynamic forces applied to a railway track, evaluation of the reserve capacity of typical prestressed concrete sleepers designed to the current code AS 1085.14, and the development of a new limit states design concept.

In order to devise a new limit states design concept, research effort at the University of Wollongong is committed to performing comprehensive studies of loading conditions, static behaviour, dynamic response, impact resistance of the prestressed concrete sleepers, and the ultimate capacity of concrete sleepers under both static and impact loads. This challenge also includes the establishment of the numerical modelling of the prestressed concrete sleepers using the dynamic finite element model updating calibrated against the modal parameters obtained in Chapter 3, the static test results to appear in Chapter 5, and the impact responses and residual capacity described in Chapters 7 and 8.

### a) Static capacity

Railway sleepers are an important part of railway infrastructure that distribute axle loads to ground. Investigating the static behaviour of concrete sleepers is the first step to gaining a better insight into the limit states concept of design. The emphases in this evaluation are placed on the determination of maximum positive and negative bending moments of the concrete sleepers at railseat and mid-span, respectively. Applying a load at the rail seat is the way to carry out the maximum positive moment, whilst the ultimate negative flexural moment can be found by means of pushing the sleeper at the middle span in opposite direction.

From the experiments, the failure modes, maximum loads, visualised and measured cracking loads of each section of concrete sleeper tested under static load can be found, as illustrated in Table 5.1. It is found that the failure mode of the sleeper under hogging moment at mid span tends to be flexural failure, whilst the failure mode under sagging moment at railseat seems to be combined shear-flexural failure. In addition, the prediction of the sectional capacity can be carried out using Response-2000 based on modified compression field theory. The theoretical results of all sections of prestressed concrete sleepers are in very good agreement with the experimental results and the manual calculation based on general prestressed concrete theory. The decompression moments are almost the same while the ultimate moments of Response-2000 are up to 10% higher than those from experimental results. Cracking moments from experimental curves are quite close to those from measured cracking ones, computed from the intersection of two initial slopes of a load-deflection curve. Flexural failure seems to govern the negative bending behaviour of the sleepers. Nevertheless, the shear diagonal failure tends to suddenly happen to the rail seat section under a positive moment. The ductility of sleepers can be considered as fairly low. Interestingly, the design moments obtained from designers are slightly lower than calculated decompression moments, which imply that the current sleepers under designed conditions behave within the elastic compressive range. It should be noted that a prestressed concrete sleeper is designed capable of resisting a fatigue loading of more than  $10^6$  cycles (Warner et al., 1998) because the decompression moments are larger than the design moments ( $M_{\text{design}} < M_{\text{decom}}$ ), and hence always keeping the whole sleeper section constantly in the elastic compressive zone during normal smooth traffics.

### **b) Impact testing**

A high-capacity impact testing machine was developed at the University of Wollongong to investigate the impact behaviour of an in-situ railway prestressed concrete sleeper. The traditional method for simulating railway ballast (for use as an alternative support) in laboratory requires small parts of the potential material to be tested, which is difficult and inconvenient. In this thesis, experimental techniques and applications of experimental modal analysis for railway ballast replication were established. This study was initially developed for use in impact testing of railway track components at the University of Wollongong. The additional objective of this study is to develop experimental techniques to evaluate the modal data and imitate the dynamic signatures of alternative supporting materials, aimed at their uses in experimentations. Laboratory demonstrations have proven the effectiveness, efficiency, and precision of replication techniques by using dynamic signatures (FRFs) and modal parameters such as natural frequency, damping coefficient, and corresponding mode shape, by means of the instrumented hammer impact technique.

It is well known that wheel or rail abnormalities were found to cause large impact loads during their dynamic interaction between the wheel and rail. The impact load characteristics are typically of high magnitude but short duration. In general, the force magnitude varies between 300 and 400 kN and the pulse duration from 1 to 10 ms. This magnitude of impact corresponds roughly with the fifty-year return period, which is only about once in the design life span of concrete sleepers. This thesis therefore ascertained the statistics related to the spectrum and amplitude of forces applied to tracks, as well as developed a methodology to replicate the impacts.

The effects on the dynamic loading conditions of the track environment including the condition of ballast support and rail pads were evaluated. The techniques of free falling mass and alleviating contact stress were demonstrated through the extensive experimental programs. With particular reference to the track environment, the rail pad plays a more significant role on the quantity of artificial shock than the support conditions. Using rail pad clearly demonstrates the preclusion of excessive dynamic stress from the rails to the railway sleepers. However, the support condition is most likely to be involved with the global track modulus and the sleeper's inertia, which is directly proportional to the impulse magnitude and vice versa. In spite of the sound

effects of the track environment, the softening media dominantly diminish the contact stress and shock loading magnitude but enlarge the impact duration. This intensive experience will lead to an estimation of the combined use of drop height and softening media, in order to simulate the impact forces in the laboratory from the actual ones on the tracks.

### **c) Progressive impact responses of prestressed concrete sleepers**

Also presented were the analytical and experimental investigations of the relationship between the railseat bending moment and the impact force of prestressed concrete sleepers under impact loading, as a design guideline for track design engineers. Every track exhibits a distinctive relationship and the best way to determine the bending moment along the railway sleepers is to employ the advanced dynamic analysis of railway tracks. In railway practice, the analytical and experimental results in this firmed study confirm and provide a faster and adequate means for predicting the bending moment on the sleepers from the anticipated wheel/rail interaction. The empirical moment envelope can be used as  $M^*=0.08I$ . This equation is found to be conservative for uses in the dynamic design for prestressed concrete sleepers at the ultimate limit states.

Based on dynamic crack propagations, it is found that the initial cracks could occur more rapidly in the hard track rather than in the soft track. On the other hand, the possibility of occurrence of the impact load causing the first crack in the soft track is much lower than that in the hard track. The first cracks due to impacts in the prestressed concrete sleepers in either the soft or the hard tracks are always due to flexures. The impact failure modes in both support conditions were associated with both flexural and longitudinal splitting actions. Splitting fractures were aligned along the prestressing tendons. Due to the lack of concrete and tendon bonding, the impact stress waves travelling along the composite section become the key indicator for a combined failure mode. The probabilistic analysis of dynamic loading showed that the magnitude of the ultimate impact load causing failure of the prestressed concrete sleeper would be equivalent to that with a return period of several million years. This implies that the current Australian Standard for prestressed concrete sleepers is overly conservative.

#### **d) Repeated impact behaviour and residual capacity of prestressed concrete sleeper**

The imperfections on either wheel or rail provide a potential for railway sleepers to be subjected to heavy impact loads with various pulse magnitudes and durations. The statistical data of loading on track can provide the equivalent return period for the particular magnitude of impact loading. The building code of Australia (BCA) in conjunction with Standards Australia indicates the importance levels for determining the probabilistic loads for track design at ultimate limit states of structures, upon the consequences of failure of the structures. In a design consideration (50 to 100 years design life), it is important to note that a loading with 100 years return period should be considered for Category 1 tracks (less importance); 500 years return for Category 2 tracks (medium importance); and 2,000 years return for Category 3 tracks (very high importance). In this study, the dynamic behaviour and response of prestressed concrete sleepers in railway track systems under either single or repeated impact loads were considered associated with the design probability of occurrence or the equivalent return period. The residual capacity of the damaged prestressed concrete sleepers due to those impact actions was described. The residual capacity implies the reserved strength of the prestressed concrete sleepers, which is untapped and is believed of its existence by railway industry for decades.

Based on dynamic crack propagations, the initial cracks could occur more rapidly in the hard track than in the soft track. The first cracks due to impacts in the prestressed concrete sleepers in either the soft or the hard tracks are always due to flexures. The testing results exhibit that the greater impact, the longer and wider cracks. Under the single impact load testing scheme, the track environments (soft and hard tracks) play a sensible role in propagating the cracks in the prestressed concrete sleepers. The hard track support tends to provide faster and longer cracks in the sleepers than the soft support does. The average increment in the crack length between the hard and soft track supports is approximately 7 percent. Under repeated impact loading conditions, there were more bending cracks in bottom fibres of the prestressed concrete sleepers existed after each impact. These residual cracks are relatively small but concrete spalling in compression zone becomes larger when subjected to more and higher impact drops. The difference in the crack length between the soft and hard tracks is averagely 5.5 percent. Dynamic crack propagation of the prestressed concrete sleepers in a hard track

environment grows faster and higher than that in a soft track environment. After either one or 50 impact drop tests, the damages in the sleepers are not significant. As a result, the damaged sleepers were later determined for the residual capacity under static testing.

It should be noted that a hard track environment allows the sleepers to vibrate enough to cause small dynamic negative strains in the positive zone. Opened cracks in the sleepers are also the cause that the dynamic strains at both railseat and mid-span fluctuate in a low range, since the concrete is no longer homogenous. This shows that the sleepers subjected to multiple impact drops tend to provide lesser dynamic stiffness due to larger cracks, leading to a slightly larger range of the acceleration responses at both railseat and mid-span of the prestressed concrete sleepers. However, it is clear that hairline cracks do not significantly affect the vibrations or acceleration responses of the prestressed sleepers. Interestingly, this finding is concurrent with previous research by other researchers.

As aforementioned, the damaged sleepers were again subjected to static testing where the failure modes of the sleepers under repeated impact loading were associated with both flexural and longitudinal splitting actions. These splitting fractures were aligned parallel to the prestressing tendons, as previously found in the progressive impact failure. Due to the repetition of compression and tension in the bond between concrete and tendon, the tendon surface alignments were weakened from the repeated impact tests. Consequently, the residual fracture toughness after the ultimate static failure of prestressed concrete sleepers remains minimal, regardless of the conditions of track support. On the other hand, the impact magnitude after a single impact event tends to have little influence on the residual energy toughness of prestressed concrete sleepers in a soft track environment, whilst the sleepers in a hard track environment are sensible to the impact magnitudes and are likely to absorb more fracture toughness when the dynamic bending moment is larger and more major cracks occur. However, only to consider the energy absorption at the ultimate failure, it seems that there is no remarkably influential factor, which considerably degrades the sleepers under these single impact events.



### e) Numerical analysis of prestressed concrete sleepers

The numerical results using finite element analyses to investigate the static and impact behaviour of prestressed concrete sleepers were presented. Commercial finite element packages, ANSYS10 and LS-Dyna, were employed in static and impact studies respectively to extend their use in other related industrial projects. The applied displacement method was used in the static analyses because of its fast and smooth convergence of numerical iterations. The model was calibrated by the hogging moment test of railway concrete sleeper. It was found that only the known compressive strength of concrete, measured from exacted cores, and existing formulas are sufficient to model the prestressed concrete sleeper. Apparently, the nonlinear material models can well capture the nonlinear static behaviour of concrete sleeper. The results also showed that the tensile strength based on  $0.4\sqrt{f'_c}$  is unsuitable for high strength concrete, whilst twice of the standard tensile strength provided better solutions. The finite element model was then extended using finite element model updating technique. Linkage between ANSYS and LS-Dyna helps develop numerical impact modelling. Drop impact tests were carried out to validate the numerical shock simulations. It was found that the extended model can be used to predict the impact responses of prestressed concrete sleepers.

For impact analysis, the three dimensional finite element model, which was developed for static analysis, has been appended other track components, including rail pads, rails, and ballast support. The low-velocity impact analysis was carried out after the model verification. The emphasis of this study was placed on the elastic responses whereas the drop heights are limited to impart the low-velocity shocks. This study pointed out the influences of track components, particularly the ballast support and rail pads, on the impact behaviour of the railway prestressed concrete sleepers.

Clearly, the ballast bed has strong influence over the contact impact force characteristics including magnitude and duration, particularly in a stiffness range lower than 1,500 MPa. On the other hand, very high stiffness of ballast insignificantly affects those characteristics. This finding confirmed the some results done by other researchers that the effect of high ballast stiffness is insignificant. It was also found that the ballast bed has slight effect on the impact responses of prestressed concrete sleepers. In addition, the rail pads tend to play vital role on both contact impact force characteristics

and responses of prestressed concrete sleepers. The softer rail pads are likely to have substantial influences on the dynamic force reduction and impact attenuation.

#### **f) Development of limit states design concept for prestressed concrete sleepers**

The current design of railway prestressed concrete sleepers, as stated in AS 1085.14, is based on the permissible stress concept. Their design process is based on quasi-static wheel loads and static response of concrete sleepers. To shift to a more rational design method involves a significant research effort within the framework of the CRC for Railway Engineering and Technologies. The collaborative research between the University of Wollongong (UoW) and Queensland University of Technology (QUT) has involved all the important facets such as the spectrum and amplitudes of dynamic forces applied to the railway track, evaluation of the reserve capacity of typical prestressed concrete sleepers designed to the current code AS 1085.14, and the development of a new limit states design concept.

The reliability concept is suitable for use as the calibration methodology for the limit states format codes and issues pertaining to conversion of AS 1085.14 to a limit states design format. The use of a reliability-based approach in the conversion of the existing code to the new limit states format was demonstrated. The target reliability indices  $\beta$  to be used for the code calibration can be obtained from the reliability analysis of existing design procedures as a case study and the newly proposed method for designing prestressed concrete sleepers in Chapter 10.

### **11.2 RECOMMENDATIONS FOR FUTURE RESEARCH**

Although a number of comprehensive investigations were presented, a future challenge for research and development of railway products and construction is still remained. The key areas that are currently insufficient are pointed out in two different aspects: first, the dynamic properties of railway track's components and their uses; and second, the behaviour and capacity of prestressed concrete sleepers

### **11.2.1 Dynamic properties of railway track's components**

More comprehensive results of condition assessments of railway tracks are limited as a field test is very expensive. Future field tests would provide a better insight in terms of track degradation and the effect of train operations on the structural track conditions, which would result in the optimum renewal and maintenance of track components. Due to the limitations of the worn pads, the degradation rates can be statistically improved when more worn rail pads are obtained from the industry partners. The optimum renewal period will be a new challenge for future studies.

Small cracks in concrete sleepers have an insignificant influence on the track response and its impact behaviour. The limit states design proposes to allow small crack to develop. Future investigation would therefore focus on the new technology, which non-destructively monitors the major cracks in sleepers using the vibration signal or the ultrasonic/radar echo. This non-destructive testing system can be integrated into the existing or new track systems to form a 'smart track', which would provide the decision support system to the track managers in order to optimise the track maintenance and schedule the effective logistics of train operations.

The numerical model can also be used in the applications of damage detection in railtrack systems and the track components using the in-depth understanding of dynamical sensitivity and stochastic analysis. The advanced prediction and neural networks model for structural condition identification, damage detection, and health monitoring of railway tracks and their components are the technological frontier of research into computer aided engineering. A statistical study of the strength of track components and materials is the cutting edge for the reliability analysis of the components, which would lead to the life cycle analysis and risk-based design of railway track system. Understanding the dynamic behaviour of the track components would allow for future train/track design upgrade, the development of train speed, and contingency planning.

### **11.2.2 Capacity of prestressed concrete sleepers**

The limitation of only testing in a laboratory environment prevails in this study. Sensing technology, including an optical fibre sensor, is the new area of measuring and

monitoring the condition of railway track and its' components. It can be an integral part of the instrumented railway sleepers, which can be used as in research and development, as well as sensing to evaluate the in-field behaviour of the sleepers and investigate the dynamic loading statistical data on the railway network. The dynamic loading condition will help the track designers satisfy the cost-effective design, while maintain the ample public safety. It should be noted that the cost-effective design will reduce the material wastage, including concrete and steel. The minimal use of concrete will directly minimise the carbon emission to atmosphere, which is a main cause of global warming. Also, the in-field capacity can be implicated from the data obtained from the sensors. Wireless sensing technology for measuring and monitoring of cracks in concrete sleepers would be the new area of sleeper research. The sleeper may include nanotubes, which are able to detect cracks or internal defects via measurable resistance signals and can '*wirelessly*' transfer the signal to the maintenance train.

The effect of rail pads has not been properly evaluated in the current research. The different uses of various rail pads could also largely attenuate the impact forces on the rail heads, giving less dynamic load on the sleepers and formation. The use of different rail pads to evaluate the impact behaviour and capacity of the prestressed concrete sleepers should be considered in the future. Due to the limitations of type and number of sleepers used in the tests, the reliability assessment can still be improved. Future research should consider the experimental investigations of new other types of sleepers, including different topology, shapes, strength of concrete and steels, types and sizes of prestressing tendons, and other added materials (i.e. steel fibre, GFRP), and stirrups to improve the capacity and ductility of the concrete sleepers. New carbon-free materials as a replacement of concrete and novel cementitious chemistry for reducing the causes of green house effect and climate change are currently the hot research topics for environmental-friendly sleepers. Unfortunately, the preload control at the railseat during the impact tests is not in the scope of this study. More tests on varied preload conditions could be done in the future.

This study assumed that the high strain rate effect complimented the strength of the sleepers at their ultimate states, so the effect of the strain rate was not thoroughly been evaluated. There are a number of key factors that can be investigated including the variation of impact magnitudes and pulse durations, the random stiffness of ballast support, and more repetitions of multiple impacts. The serviceability of concrete

sleepers including the cracks, deflection, rail gauge rotation, impact fatigue strength, as well as dynamic creep and shrinkage can be the interesting research topics.

In the experiments on impact, only a single end is subjected to an impact load. This is because it was assumed that the possibility of a dual impact on both wheels is relatively low. However, dual impact loading at both railseats can be investigated in the future. The current numerical study does not consider the statistical data of track components. The future research may involve the probabilistic and stochastic finite element modelling of the concrete sleepers in track system. It would lead to the performance-based and reliability-based design optimizations of the concrete sleepers, which is a very interesting research area.

## REFERENCES

### R1. References from literature survey

- Abbate, S. (1998), *Impact on Composite Structures*, Cambridge University Press, USA.
- ACI Committee 544 (1990), Measurement of properties of fibre reinforced concrete, *ACI Manual of Concrete Practice Part 5*, 544, 2R-6.
- Adachi, T., Tanaka, T., Sastranegara, A., Yamaji, A., Kim, S-K., and Yang, I-Y., (2004). Effect of transverse impact on buckling behavior of a column under static axial compressive force. *International Journal of Impact Engineering*, **30**: 465-475.
- Andersson, C. and Dahlberg, T. (1999) Load impacts at railway turnout crossing. *Vehicle System Dynamics*; **33**(Supplement): 131-142
- Andersson M, Murray M, Ferreira L, Lake N. (2004) Collection and use of railway track performance and maintenance data. In: *Proceedings of CORE 2004 – Conference on Railway Engineering*, Darwin, Australia.
- Ahlbeck, D.R. and Hadden, J.A. (1985) Measurement and prediction of impact loads from worn railroad wheel and rail surface profiles. *ASME Journal of Engineering for Industry*; **107**: 197-205
- Ahlbeck, D.R., Tuten, J.M., Hadden, J.A., and Harrison, H.D. (1986), Development of safety criteria for evaluating tie track in the Northeast Corridor, 1, Battelle's Columbus Laboratories, *Report No.DOT/FRA/ORD-86/08.1*, June.
- Al-Harthy, AS. (1992) *Reliability analysis and reliability-based design of prestressed concrete structures*, PhD Thesis, Department of Civil Engineering, University of Colorado at Boulder, USA.
- Allemang, R. (1993), Modal Analysis – Where do we go from here?, *International Journal of Analytical and Experimental Modal Analysis*, 8(2) April, 79-91.
- Allemang, R. and Brown, D. (1986), Multiple – Input experimental modal analysis – A survey, *International Journal of Modal Analysis*, January, 37-43.
- Alias, J. (1986) Characteristics of wave formation in rails. *Rail International*; **17**(11): 17-23
- Ando, T., Kishi, N., Mikami, H., and Matsuoka, K.G. (2000), Weight falling impact tests on shear-failure type RC beams without stirrups, *Proceedings of Structures under Shock and Impact IV*, Cambridge, England, July, 351-360.

- Ando, T., Kishi, N., Mikami, H., Sato, M., and Matsuoka, K.G. (1999), Experimental study on impact resistance of bending failure type of RC beams, *Proceedings of the 7th EASEC*, Kochi, Japan, August, 27-29, 1075-1080.
- ANSYS, 10. (2006) *ANSYS v.10 Documentation Manual*.
- Barbosa, A.F., Ribeiro, G.O., (1998) Analysis of reinforced concrete structures using ANSYS nonlinear concrete model In: Idelsohn, S., Onate, E., and Dvorkin, E. (Eds.), *Computational Mechanics: New trends and applications*, pp. 1-7.
- Barke DW. and Chiu WK., (2005) A review of the effects of out-of-round wheels on track and vehicle components. *Proc Instn Mech Engrs Part F.*, 219, 151-175.
- Bhattacharya S., Krishnamurthy K.C., Rajendran R., Prem sai R., and Basu S. (2006) Impact studies on structural components using a free-flight drop tower. *Experimental Techniques*, 18: 52-58.
- Bentz, E.C. (2000), Reinforced concrete sectional analysis using the modified compression theory, *Ph.D. Thesis*, Department of Civil Engineering, University of Toronto, Canada.
- Birch R.S., Jones N., and Jouri W.S., (1988) Performance assessment of an impact test rig, *Proceedings of the Institution of Mechanical Engineers, Part C.*, **202**(4): 275-285.
- Bona, M.E. (2004) The effect of straightening and grinding of welds on track roughness, *Master of Engineering Research Thesis*, Queensland University of Technology, Australia.
- Banthia, N.P., Mindess, S., and Bentur, A., (1987). Impact behaviour of concrete beams. *Materials and Structures*, **20**: 293-302.
- Banthia, N., Mindess, S., and Bentur, A. (1989), Impact testing of concrete using drop-weight impact machine, *Experimental Mechanics*, 29(1), 63-69.
- Brown, D. (1982), Keynote Speech Modal Analysis – Past, Present and Future, *Proceedings of the 1<sup>st</sup> International Modal Conference*, Union College, New York.
- Cai, Z. (1992), Modelling of rail track dynamics and wheel/rail interaction, *Ph.D. Thesis*, Department of Civil Engineering, Queen's University, Ontario, Canada.
- Cai, Z. and Raymond, G.P. (1992). Theoretical model for dynamic wheel/rail and track interaction, *Proceedings of Institution of Engineers Australia's National Conference*, p. 127-131.

- Cai, Z. and Raymond, G.P. (1994). Modelling the dynamic response of railway track to wheel/rail impact loading, *International Journal of Communication Systems*, 2(1), 95-112.
- Cai, Z. and Raymond, G. P. (1994), Use of a generalized beam/spring element to analyze natural vibration of rail track and its application, *International Journal of Mechanical Sciences*, 36, 863-876.
- Cai, Z., Raymond, G. P., and Bathurst, R. J., (1994). Natural vibration analysis of rail track as a system of elastically coupled beam structures on Winkler foundation, *Computers & Structures*, 53(6), 1427-1436.
- Carrascal, IA., Casado, JA., Polanco, JA., Gutierrez-Solana, F. (2007) Dynamic behavior of railway fastening setting pads. *Engineering Failure Analysis* 14(2): 364-373.
- Colla, C., Krause, M., Maierhofer, CH., Höhberger, H. -J., and Sommer, H. (2002), Combination of NDT techniques for site investigation of non-ballasted railway tracks, *NDT & E International*, 35(2), 95-105.
- Clark RA., Dean, PA., Elkins JA., & Newton, SG. (1982). An investigation into the dynamic effects of railway vehicles running on corrugated rails, *Journal of Mechanical Engineering Science*; 24(2): 65-76.
- Clark R. (2004) Rail flaw detection: overview and needs for future developments. *NDT&E International*, 37(2): 111-118.
- Dahlberg T, Nielsen J (1991, April) Dynamic Behaviour of Free-Free and In-situ Concrete Railway Sleepers. *Proceedings of International Symposium on Precast Concrete Railway Sleepers*, Madrid, Spain.
- Dahlberg, T. (2003) Railway track dynamics – a survey. *Technical Report*. Department of Solid Mechanics/IKP, Linköping University, Sweden.
- DataFit, (2005). *User's Manual*, Oakdale Engineering, Oakdale, PA, USA.
- Dean, F.E., Harrison, H.D., Prause, R.H., and Tuten, J.M. (1983), Investigation of the effects of tie stiffness on the impact loading of concrete ties in the Northeast Corridor, Battelle's Columbus Laboratories, *Report No. DOT/FRA/ORD-83/05*, April.
- Delhomme, F., Mommessin. M., Mougin, J.P., and Perrotin, P., (2005). Behavior of a structurally dissipating rock-shed: experimental analysis and study of punching effects, *International Journal of Solids and Structures*, 42(14), 4204-4219.



- De Man, A.P. (1996). Determination of dynamic track properties by means of excitation hammer testing, *Railway Engineering International 1996 Edition*, (4), 8-9.
- De Man, A.P. (2002). DYNATRACK: A survey of dynamic railway track properties and their quality, *Ph.D. Thesis*, Faculty of Civil Engineering, Delft University of Technology, The Netherlands.
- De Man, A.P. and Esveld, C. (2000). Recording, estimating, and managing the dynamic behavior of railway structures, *Proceedings of Symposium Leuven*. The Netherlands.
- Douglass, S. (2005) *Personal contact via E-mail*, Australia.
- Dukkipati, R.V. and Dong, R. (1999) Impact loads due to wheel flats and shells. *Vehicle System Dynamics*; **31**: 1-22.
- Dytran Instruments Inc. *Model series 3200B calibration and operation manual for the University of Wollongong*, CA, USA, 2007.
- Ewins, D.J. (1995). *Modal Testing: Theory and Practice*, Research Studies Press, Taunton.
- Esveld, C., Van't Zand, J., Scheepmaker, P.N., and Suiker, A.S.J. (1996). Dynamic behavior of railway track, *Railway Engineering International 1996 Edition*, 2, 17-20.
- Esveld, C. (1997). Track structures in an urban environment., *Proceedings of Symposium K.U. Leuven*, The Netherlands. 1-21.
- Esveld, C., Kok, A.W.M, and De Man, A. (1998). Integrated numerical and experimental research of railway track structures, *Proceedings of the 4<sup>th</sup> International Workshop on Design Theories and their Verification of Concrete slabs for Pavements and Railroads*, Portugal.
- Esveld, C. (2001) *Modern Railway Track*, MRT Press. The Netherlands.
- Fahey, S. O'F. and Pratt, J. (1998). Frequency domain modal estimation techniques, *Experimental Techniques*, Sep/Oct, 22(5), 33-37.
- Fanning, P., (2001) Nonlinear models of reinforced and post-tensioned concrete beams, *Electronic Journal of Structural Engineering*, vol. 2, pp. 111-119, [Available Online: <http://www.ejse.org>]
- Fenander, A. (1997). Frequency dependent stiffness and damping of railpads, *Proceedings of Institute of Mechanical Engineering Part F*, 211, 51-62.
- Fenander, A. (1998). A fractional derivative railpad model included in a railway track model, *Journal of Sound and Vibration*, 212(5), 889-903.

- Fermer, M. & Nielsen, JCO. (1994) Wheel/rail contact forces for flexible versus solid wheels due to tread irregularities. *Vehicle System Dynamics*; **23**: 142-157.
- FIP Commission on Prefabrication. (1987). *Concrete Railway Sleepers – FIP State of Art Report*, Thomas Telford Ltd., London, UK.
- Ford, R. (1988a) Modal analysis of a concrete railway sleeper, *Research Note AVG/RN881122-1*, School of Mechanical and Industrial Engineering, University of New South Wales, Australia.
- Ford, R. (1988b) Vibration responses of systems comprising a concrete sleeper, rail section, and various types of rail pads, *Research Note AVG/RN881122-2*, School of Mechanical and Industrial Engineering, University of New South Wales, Australia.
- Fryba, L. (1996) *Dynamics of railway bridges*, Thomas Telford, Czech Republic.
- Gopalaratnam, V.S., Shah, S.P., and John, R. (1984), A modified instrumented Charpy test for cement-based composites, *Experimental Mechanics*, 24(2), 102-111.
- Grassie, S.L., Gregory, R.W., Harriswon, D., and Johnson, K.L. (1982) The dynamic response of railway track to high frequency vertical excitation, *Proceedings of the Institution of Mechanical Engineers, Part C, Journal of Mechanical Engineering Science*; **24**(2): 77-90.
- Grassie, S.L. and Cox, S.J. (1984). The dynamic response of railway track with flexible sleepers to high frequency vertical excitation, *Proceedings of Institute of Mechanical Engineering Part D*, 24, 77-90.
- Grassie, S.L. (1987). Measurement and attenuation of load in concrete sleepers, *Proceedings of Conference on Railway Engineering*, Perth, September 14-16, 125-130.
- Grassie, S.L. (1989a). Resilient rail pads: Their dynamic behavior in the laboratory and on track, *Proceedings of Institute of Mechanical Engineering Part F*, 203, 25-32.
- Grassie, S.L. (1989b). Behavior in track of concrete sleepers with resilient rail pads, *Proceedings of Institute of Mechanical Engineering Part F*, 203, 97-101.
- Grassie, S.L. and Kalousek, J. (1994) Rail corrugation: characteristics, causes and treatments, *Proceedings of the Institution of Mechanical Engineers, Part F, Journal of Rail and Rapid Transit*; **207**(F1): 57-68.
- Grassie, S.L. (1996) Models of railway track and train-track interaction at high frequencies: Results of benchmark test, *Vehicle System Dynamics*; **25**(Supplement): 243-262.

- Gustavson, R. (2000), Static and dynamic finite element analyses of concrete sleepers, *Licentiate of Engineering Thesis*, Department of Structural Engineering, Chalmers University of Technology, Sweden.
- Gustavson, R., (2002). Structural behaviour of concrete railway sleepers. *PhD Thesis*, Department of Structural Engineering, Chalmers University of Technology, Sweden.
- G+D Computing (2002) *Using STRAND7 Introduction to the Strand7 finite element analysis system*, G+D Computing Pty Ltd.
- G+D Computing (2005) *STRAND7 Theoretical Manual*, G+D Computing Pty Ltd.
- Hay, W.M. (1982) *Railroad Engineering*, 2<sup>nd</sup> edition, John Wiley & Sons, Inc.
- He, H. and Fu, Z. (2001), *Modal Analysis*, Butterworth – Heinemann Publishers, Great Britain.
- Hetenyi, K. (1976). *Beams on Elastic Foundation: Theory with applications in the fields of civil and mechanical engineering*, University of Michigan Press.
- Hillmasen, S. and Smith, R.A. (2005) Discussion: Benefits of lower-mass trains for high speed rail operations. *Transport, Proceedings of the Institution of Civil Engineers*; **158**: 179-182.
- Hughes, B.P. and Al-Dafiry, H., (1995). Impact energy absorption at contact zone and supports of reinforced plain and fibrous concrete beams. *Construction and Building Materials*, **9**: 239-244.
- Igwemezie, J.O. and Mirza, M.S. (1989) Impact load distribution in concrete bridge ties, *Journal of Structural Engineering*, ASCE, 115, 527-542.
- Igwemezie, J.O., Kenedy, S.L., and Cai, Z. (1992) Calibration of railway track for dynamic loads, *Report No.91-7*, Canadian Institute of Guided Ground Transport, Queen's University, Ontario, Canada
- Indraratna, B. and Salim, W. (2005) *Mechanics of Ballasted Rail Tracks A Geotechnical Perspective*. Taylor & Francis, London.
- Iyengar, K.T.S.R. and Ramu, S.A. (1979) *Design Tables for Beams on Elastic Foundations and Related Structural Problems*, Applied Science Publishers Ltd.
- Jeffs, T. and Tew, G.P. (1991) *A Review of Track Design Procedures. Vol. 2 Sleepers and Ballast*. Railways of Australia.
- Johansson, A. and Nielsen, JCO. (2003) Out-of-round railway wheels-wheel-rail contact forces and track response derived from field tests and numerical simulations.

- Proceedings of the Institution of Mechanical Engineers Part F: Rail and Rapid Transit*; **217**(2): 135-145
- Kishi, N., Nakano, O., Matsuoka, K.G., and Ando T. (2001a), Experimental study on ultimate strength of flexural-failure-type RC beams under impact loading, *Transactions, SMiRT 16*, Washington DC, 2001.8, #1525, 1-7.
- Kishi, N., Ikeda, K., Mikami, H., and Yamaguchi, E. (2001b), Dynamic behavior of RC beams under steel weight impact loading - effects of nose-shape of steel weight, *Proceedings of 3rd CONSEC*, Vancouver, Canada, 660-667.
- Kishi, N., Mikami, H., Matsuoka, K.G., and Ando T. (2002a), Impact behavior of shear-failure-type RC beams without shear rebar, *International Journal of Impact Engineering*, (27), 955-968.
- Kishi, N., Mikami, H., and Ando, T., (2002b). Impact-resistant behaviour of shear-failure-type RC beams under falling-weight impact loading. In: *Proceedings of the 7<sup>th</sup> International Conference on Structures under Shock and Impact*, p. 499-508.
- Knothe, K. and Grassie, S.L. (1993). Modelling of railway track and vehicle/track interaction at high frequencies, *Vehicle System Dynamics*, 22(3-4), 209-262.
- Knothe, K., Yu, M. and Ilias, H. (2003). Measurement and Modelling of Resilient Rubber Rail-Pads. In: K. Popp und W. Schiehlen (Ed.), *System Dynamics and Long-term Behaviour of Railway Vehicles, Track and Subgrade*, Springer Verlag, Berlin Heidelberg, Germany, pp. 265-274.
- Kumaran, G., Menon, D., and Nair, K.K. (2002) Evaluation of dynamic load on railtrack sleepers based on vehicle-track modelling and analysis. *International Journal of Structural Stability and Dynamics*; **2**(3): 355-374.
- Kumaran, G., Menon, D., and Nair, K.K. (2003) Dynamic studies of railtrack sleepers in a track structure system. *Journal of Sound and Vibration*, 268, 485-501.
- Kumaran, G., Menon, D., and Nair, K.K. (2003) Reliability analysis and design of PSC railtrak sleepers. *Proceedings of Conference on Applications of Statistics and Probability in Civil Engineering*, Rotterdam, pp.1667-1673.
- Lee, ML., Chiu, WK., and Koss, LL. (2005) A numerical study into the reconstruction of impact forces on railway track-like structures. *Structural Health Monitoring*; **4**(1): 19-45.
- Leong, J., (2007). Development of a limit state design methodology for railway track. *Master of Engineering Thesis*, Queensland University of Technology, QLD, Australia.

- Leong, J., Steffens, D., and Murray, M.H., (2007). Examination of railway track dynamic models. *Proceedings of International Heavy Haul Conference*, June 11-13, Kiruna, Sweden.
- Liang, B. and Zhu D., (2001). Dynamic analysis of the vehicle-subgrade model of a vertical coupled system, *Journal of Sound and Vibration*, (245), 79-92.
- Lilja, J. (2006) Preliminaries for probabilistic railway sleeper design, *Licentiate of Engineering Thesis*, Department of Applied Mechanics, Chalmers University of Technology, Sweden.
- Livermore Software Technology Corporation, (1998) *LS-DYNA theoretical manual*. Livermore Software Technology Corporation, May.
- Lundqvist A. & Dahlberg, T. (2005) Load impact on railway track due to unsupported sleepers. *Proceedings of the Institution of Mechanical Engineers Part F: Rail and Rapid Transit*; **219**: 67-77.
- MacGregor, J.G., (1992) *Reinforced Concrete Mechanics and Design*, Prentice-Hall, Inc., Englewood Cliffs, New Jersey, USA.
- Maes, J., Sol, H., Guillaume, P. (2006) Measurements of dynamic railpad properties. *Journal of Sound and Vibration* 293(3-5): 557-565.
- Melchers, R.E. (1987) *Structural Reliability: Analysis and Prediction*, Ellis Horwood, Chichester, England.
- Milton, A. (1945) Cumulative damage in fatigue. *ASME Journal of Applied Mechanics* 12(1), 159-164.
- Mindess, S., Yan, C., and Venuti, W.J. (1991a), Impact and fatigue of prestressed concrete railroad sleepers, *Proceedings of the Fatigue and Fracture in Steel and Concrete Structures*, Madras, India, 537-547.
- Mindess, S., Yan, C., and Venuti, W.J. (1991b), Impact resistance of fibre reinforced prestressed concrete railroad sleepers, *Proceedings of ACI International Conference on Evaluation and Rehabilitation of Concrete Structures and Innovations in Design*, Hong Kong, 1, 183-199.
- Mindess, S., Yan, C., and Venuti, W.J. (1992), Impact resistance of prestressed concrete railroad sleepers, *Proceedings of International Symposium on Precast Concrete Railway Sleepers*, Madrid, Spain, 487-504.
- Mitchell, L. (1986), Signal processing and the Fast Fourier Transform (FFT) Analyser: A survey, *International Journal of Modal Analysis*, January, 24-36.

- Murray, M. and Cai, Z. (1998) Prestressed concrete sleepers – literature review, *ARA Project Report Ref: 15250*, Australasian Railway Association, Inc., December.
- Murray, M. and Leong, J. (2005) *Discussion paper: Limit states design of concrete sleepers – Stage I*, CRC for Railway Engineering and Technologies, Australia.
- Murray, M.H. and Leong, J., (2006a; 2006b). Limit states design of railway sleepers. *RailCRC Research Discussion Paper: Stage I and II*, CRC for Railway Engineering and Technologies, Australia.
- Narayanan RM, Jakub JW, Li D, Elias SEG. (2004) Railroad track modulus estimation using ground penetrating radar measurements. *NDT&E International*, 37(2): 141-151.
- Newton, SG. and Clark, RA. (1979) An investigation into the dynamic effects on the track of wheel flats on railway vehicles. *Journal of Mechanical Engineering Science*; **21**(4): 287-297.
- Nielsen, JCO. and Igeland, A. (1995) Vertical dynamic interaction between train and track – influence of wheel and track imperfections, *Journal of Sound and Vibration*; **187**(5): 825-839.
- Nielsen, JCO and Johansson, A. (2000) Out-of-round railway wheels – a literature survey. *Proceedings of the Institution of Mechanical Engineers, Part F, Journal of Rail and Rapid Transit*; **214**(F2): 79-91.
- Nielsen, JCO., Oscarsson, J. (2004) Simulation of dynamic train-track interaction with state-dependent track properties. *Journal of Sound and Vibration* 275: 515-532.
- Oscarsson, J. (2002) Dynamic train-track interaction: Variability attributable to scatter in the track properties. *Vehicle System Dynamics* 37(1): 59-79.
- Plenge, M. and Lammering, R. (2003). The dynamics of railway track and subgrade with respect to deteriorated sleeper support. In: K. Popp und W. Schiehlen (Ed.), *System Dynamics and Long-term Behaviour of Railway Vehicles, Track and Subgrade*, Springer Verlag, Berlin Heidelberg, Germany, pp. 295-314.
- Rail Safety and Standards Board. (1993) Permissible Track Forces for Railway Vehicles, London, *Group Standard GM/TT0088*, Issue 1, Revision A, [Online <http://www.rgsonline.co.uk>]
- Rail Safety and Standards Board. (1995) Commentary on Permissible Track Forces for Railway Vehicles, London, *Technical Commentary GM/RC2513*, Issue 1, [Online <http://www.rgsonline.co.uk>]
- RCP GmbH, (2004) *COMREL User Manual – Demo Version*, Germany.

- Remennikov, A.M. (2003) A Review of Methods for Predicting Bomb Blast Effects on Buildings, *Journal of Battlefield Technology*, 6(3) 5-10.
- Rochard, B.P. and Schmid, F. (2004) Benefits of lower-mass trains for high speed rail operations. *Transport, Proceedings of the Institution of Civil Engineers*; **157**: 51-64.
- Sadeghi, J. (1997), Investigation of characteristics and modeling of railway track system, *PhD Thesis*, School of Civil, Mining, and Environmental Engineering, the University of Wollongong, Australia.
- Sato, Y., Odaka, T., and Takai, H. (1988) Theoretical analyses on vibration of ballasted track. *Quarterly Reports of Japan Railway Technical Research Institute*; 29(1): 30-32.
- Saxton, H.J., Ireland, D.R., and Server, W.L., (1974) Analysis and control of inertial effects during instrumented impact testing, *Instrumented Impact Testing, ASTM STP563*, American Society for Testing and Materials, 50-73.
- Selig, E.T. and Waters, J.M. (1994). *Track geotechnology and substructure management*, 1<sup>st</sup> Ed., Technology Development and Application Committee, on behalf of the Railways of Australia.
- Sjoberg, M. (2002). On dynamic properties of rubber isolators, *Ph.D. Thesis*, Department of Vehicle Engineering, Kungl Tekniska Hogskolan Royal Institute of Technology, Stockholm, Sweden.
- Smutny, J. (2004). Measurement and analysis of dynamic and acoustic parameters of rail fastening, *NDT&E International*, 37, 119-129.
- Standards Australia. (1981) *AS 1250-1981 Allowable stress design for steel beams and columns*, Standards Australia.
- Standards Australia. (1991) *AS1012.14-1991 Method of testing concrete – Method for securing and testing cores from hardened concrete for compressive strength*, Standards Australia.
- Standards Australia. (1998) *AS 4100-1998 Design of steel structures*, Standards Australia.
- Standards Australia, (2001). *AS3600-2001 Design of Concrete Structures*, Standards Australia.
- Standards Australia, (2001). *AS1085.19-2001 Railway track material - Part 19: Resilient fastening assemblies*, Standards Australia.

- Standards Australia, (2003). *AS1085.14-2003 Railway track material - Part 14: Prestressed concrete sleepers*, Standards Australia
- Standards Australia, (2005). *AS 5104-2005 Reliability-based design of structures*, Standards Australia.
- Steffens, D.M. (2005). Identification and development of a model of railway track dynamic behavior, *M.Eng. Thesis*, School of Civil Engineering, Queensland University of Technology, QLD. Australia.
- Steffens, D. and Murray, M.H., (2005). Establishing meaningful results from models of railway track dynamic behaviour, *Proceedings of International Heavy Haul Conference*, June 14-16, Rio De Janeiro, Brazil.
- Stewart, M.G. and Attart, M.M. (1998) Structural reliability and model errors for high strength concrete column design, *Research Report No.159.01.1998*, University of Newcastle, Australia.
- Sukontasukkul, P. and Mindess, S., (2003). The shear fracture of concrete under impact loading using end confined beams. *Materials and Structures*, **36**: 372-378.
- Sukontasukkul, P., Mindess, S., and Banthia, N.P., (2004). Effect of loading rate on damage of concrete. *Cement and Concrete Research*, **34**: 2127-2134.
- Thompson, D.J., van Vliet, W.J., and Verheij, J.W. (1998). Developments of the indirect method for measuring the high frequency dynamic stiffness of resilient elements, *Journal of Sound and Vibration*, 213(1), 169-188.
- Timoshenko S. (1926) Method of analysis of statistical and dynamical stresses in rail. In: *Proceedings of Second Int. Congress for Applied Mechanics*, Zurich, 407-418.
- Van't, Z. (1993). Assessment of dynamic characteristics of rail pads, *Railway Engineering International 1994 Edition*, 23(4), 15-17.
- Vincent, G. (2001). Modal analysis and numerical modeling of a concrete railway sleepers, *M.Eng. Thesis*, Department of Structural Engineering, Chalmers University of Technology, Göteborg, Sweden. 128 pp.
- Verheij, J.W. (1982). Multi-path sound transfer from resiliently mounted shipboard machinery, *Ph.D. Thesis*, TNO Institute of Applied Physics, Delft University of Technology, the Netherlands.
- Wakui, H. and Okuda, H. (1999). A study on limit-state design method for prestressed concrete sleepers. *Concrete Library of Japan Society of Civil Engineers*; 33(1): 1-25.



- Wang, N. (1996). Resistance of Concrete Railroad Ties to Impact Loading, *Ph.D. Thesis*, Department of Civil Engineering, University of British Columbia, Canada.
- Warner, R.F., Rangan, B.V., Hall, A.S., and Faulkes, K.A., (1998), *Concrete Structures*, Addison Wesley Longman, Melbourne, Australia.
- Weaver, W.Jr., Timoshenko, S.P., and Young D.H. (1990). *Vibration Problems in Engineering*, 4<sup>th</sup> ed., John Wiley & Sons.
- Willam, K.J. and Warnke, E.P., (1974) Constitutive model for triaxial behaviour of concrete, Seminar on Concrete Structures Subjected to Triaxial Stresses, *Proceedings of International Association of Bridge and Structural Engineering Conference*, Bergamo, Italy.
- Wu, T.X. and Thompson, D.J. (1999), The effects of local preload on the foundation stiffness and vertical vibration of railway track, *Journal of Sound and Vibration*, 219(5), 881-904.
- Wu, T.X., & Thompson, D.J. (2004) The effects of track nonlinearity on wheel/rail impact. *Proceedings of the Institution of Mechanical Engineers Part F: Rail and Rapid Transit*; 218(1): 1-15.
- Ye, X., Wang, N., and Mindess, S., (1994). Effect of loading rate and support conditions on the mode of failure of prestressed concrete railroad ties subjected to impact loading, *Cement & Concrete Research*, 24(7): 1386-1298
- Zaveri, K. (1985). Modal Analysis of Large Structures – Multiple Exciter Systems, Naerum Offset, Denmark.
- Zhai, W. and Cai, Z. (1997) Dynamic interaction between a lumped mass vehicle and a discretely supported continuous rail track. *Computers and Structures*; 63(5): 987-997.

---

**R2. References from the author's publications*****Book Chapters (Refereed)***

- Kaewunruen, S. and Remennikov, A.M., 2008, "Trends in vibration-based structural health monitoring of railway sleepers." Chapter In *Mechanical Vibration: Measurement, Effect, and Control*, Nova Science Publishers, USA.
- Kaewunruen, S. and Remennikov, A.M., 2008, "Application of vibration measurements and finite element model updating for structural health monitoring of ballasted railtrack sleepers with voids and pockets." Chapter In *Mechanical Vibration: Measurement, Effect, and Control*, Nova Science Publishers, USA.
- Kaewunruen, S. and Remennikov, A.M., 2008, "Dynamic properties of railway track and its components: A state-of-the-art review." Chapter In *Acoustic Properties of Solids*, Nova Science Publishers, USA. in press.
- Kaewunruen, S. and Remennikov, A.M., 2008, "Dynamic properties of railway track and its components: Recent finding and future research directions." Chapter In *Acoustic Properties of Solids*, Nova Science Publishers, USA. in press.
- Remennikov, A.M. and Kaewunruen, S., 2009, "Reliability based design of railway prestressed concrete sleepers." Chapter In *Reliability Engineering Advances*, Nova Science Publishers, USA. (accepted).

***Peer-reviewed Journals***

- Kaewunruen, S. and Remennikov, A.M., 2008, Dynamic effect of vibration signatures of cracks in railway prestressed concrete sleepers. *Advanced Materials Research*, 41-42: 233-239, (republished from SIF2008 Proceedings).
- Kaewunruen, S. and Remennikov, A.M., 2008, Probabilistic impact fractures of railway prestressed concrete sleepers. *Advanced Materials Research*, 41-42: 259-264, (republished from SIF2008 Proceedings).
- Kaewunruen, S. and Remennikov, A.M., 2008, Nonlinear transient analysis of railway concrete sleepers in track systems. *International Journal of Structural Stability and Dynamics*, in press.
- Kaewunruen, S. and Remennikov, A.M., 2007, Effect of a large wheel impact burden on flexural response and failure of railway concrete sleepers in track systems. *Engineering Failure Analysis*, in press.

- Kaewunruen, S. and Remennikov, A.M., 2007, Impact capacity of railway prestressed concrete sleepers. *Materials and Structures*, (tentatively accepted).
- Remennikov, A.M. and Kaewunruen, S., 2007, A review on loading conditions for railway track structures due to train and track vertical interaction. *Structural Control and Health Monitoring*, in press.
- Kaewunruen, S. and Remennikov, A.M., 2007, Experimental determination of the effect of wet/dry ballast on dynamic sleeper/ballast interaction. *ASTM J of Testing and Evaluation*, in press.
- Kaewunruen, S. and Remennikov, A.M., 2007, On free vibrations of voided concrete sleepers in railway track system. *Proceedings of IMechE Part F Journal of Rail and Rapid Transit*, 221(4): 495-508.
- Kaewunruen, S. and Remennikov, A.M., 2007, An alternative rail pad tester for measuring dynamic properties of rail pads under large preloads. *Experimental Mechanics*, in press.
- Kaewunruen, S. and Remennikov, A.M., 2007, Experimental simulation of railway ballast using resilient materials and its validation by modal testing. *Experimental Techniques*, in press.
- Kaewunruen, S. and Remennikov, A.M., 2007, Field trials for dynamic characteristics of railway track and its components using impact excitation technique. *NDT&E International*, 40(7), 510-519.
- Kaewunruen, S. and Remennikov, A.M., 2007, Effect of improper ballast tamping/packing on dynamic behaviors of on-track railway concrete sleeper. *International Journal of Structural Stability and Dynamics*, 7(1), 167-177.
- Kaewunruen, S. and Remennikov, A.M., 2007, Experimental and numerical studies of railway prestressed concrete sleepers under static and impact loads. *Civil Computing: Special Issue on Computer Application in Civil Engineering*, AIT-ACECOMS, August, 25-28 (invited).
- Kaewunruen, S. and Remennikov, A.M., 2006, Sensitivity analysis of free vibration characteristics of an in-situ railway concrete sleeper to variations of rail pad parameters. *Journal of Sound and Vibration*, 298(1-2), 453-461.
- Remennikov, A. and Kaewunruen, S., 2006, Experimental investigation on dynamic railway sleeper/ballast interaction. *Experimental Mechanics*, 46(1), 57-66.

- Kaewunruen, S. and Remennikov, A.M., 2006, Non-destructive testing (NDT): A tool for dynamic health monitoring of railway track structures. *Materials Australia*, 39(6), 14-16 (invited).
- Remennikov, A. and Kaewunruen, S., 2005, Determination of dynamic properties of rail pads using instrumented hammer impact technique. *Acoustics Australia*, 33(2), 63-67.

### ***Peer-reviewed Conferences***

- Kaewunruen, S. and Remennikov, A.M., 2008, Dynamic effect of vibration signatures of cracks in railway prestressed concrete sleepers. *International Conference on Structural Integrity and Failure - SIF2008*, July 9 - 11, Perth, Australia, [CD Rom].
- Kaewunruen, S. and Remennikov, A.M., 2008, Probabilistic impact fractures of railway prestressed concrete sleepers. *International Conference on Structural Integrity and Failure - SIF2008*, July 9 - 11, Perth, Australia, [CD Rom].
- Kaewunruen, S. and Remennikov, A.M., 2008, An experimental evaluation of the attenuation effect of rail pad on flexural behaviour of railway concrete sleeper under severe impact loads. *Australasian Structural Engineering Conference - ASEC2008*, June 26 - 27, Melbourne, Australia, [CD Rom].
- Kaewunruen, S. and Remennikov, A.M., 2008, Reliability assessment of railway prestressed concrete sleepers. *Australasian Structural Engineering Conference - ASEC2008*, June 26 - 27, Melbourne, Australia, [CD Rom].
- Remennikov, A.M., Murray, M.H., and Kaewunruen, S., 2007, Conversion of AS1085.14 for railway prestressed concrete sleeper to limit states design format. *AusRAIL Plus 2007*, Dec 2-6, Sydney, Australia, [CD Rom].
- Kaewunruen, S. and Remennikov, A.M., 2007, Low-velocity impact analysis of prestressed concrete sleepers. *Concrete Institute of Australia's 23rd Biennial Conference 07*, October 18-20, Adelaide, Australia, 659-668.
- Remennikov, A.M. and Kaewunruen, S., 2007, Resistance of railway concrete sleepers to impact loading. *7th International Conference on Shock and Impact Loads on Structures*, Oct 17-19, Beijing, China, 489-496.
- Remennikov, A.M. and Kaewunruen, S., 2007, Experimental determination of energy absorption capacity for railway prestressed concrete sleepers under impact loading. *International Conference on Structural Engineering and Construction - ISEC2007*, Sep 26-28, Melbourne, Australia, 381-386.

- Remennikov, A.M. and Kaewunruen, S., 2007, Simulating shock loads in railway track environments: experimental studies. *14th International Congress on Sound and Vibration*, July 9-12, Cairns, Australia, [CD Rom].
- Kaewunruen, S. and Remennikov, A.M., 2007, Response and prediction of dynamic characteristics of worn rail pads under static preloads. *14th International Congress on Sound and Vibration*, July 9-12, Cairns, Australia, [CD Rom].
- Kaewunruen, S. and Remennikov, A.M., 2007, Relationship between wheel/rail interface impact and railseat flexural moment of railway prestressed concrete sleeper. *Society of Experimental Mechanics (SEM) Annual Conference and Exhibition 2007*, June 3- 6, Springfield, Massachusetts, USA, [CD Rom].
- Kaewunruen, S. and Remennikov, A.M., 2007, Influence of voids and pockets on the vibration characteristics of prestressed concrete sleepers. *Society of Experimental Mechanics (SEM) Annual Conference and Exhibition 2007*, June 3- 6, Springfield, Massachusetts, USA, [CD Rom].
- Kaewunruen, S. and Remennikov, A.M., 2007, Investigations on static and dynamic performance of railway prestressed concrete sleepers. *Society of Experimental Mechanics (SEM) Annual Conference and Exhibition 2007*, June 3- 6, Springfield, Massachusetts, USA, [CD Rom].
- Remennikov, A.M. and Kaewunruen, S., 2006, Impact resistance of reinforced concrete columns: experimental studies and design considerations. *19th Australasian Conference on the Mechanics of Structures and Materials*, Nov 29 - Dec 1, Christchurch, New Zealand, 817-824.
- Kaewunruen, S. and Remennikov, A.M., 2006, Laboratory measurements of dynamic properties of rail pads under incremental preload. *19th Australasian Conference on the Mechanics of Structures and Materials*, Nov 29 - Dec 1, Christchurch, New Zealand, 319-324.
- Kaewunruen, S. and Remennikov, A.M., 2006, Non-destructive evaluation for dynamic integrity of railway track structure. *International Conference on Structural Integrity and Failure - SIF2006*, Sep 27 - 29, Sydney, Australia, 294-299.
- Kaewunruen, S. and Remennikov, A.M., 2006, Post-failure mechanism and residual load-carrying capacity of railway prestressed concrete sleeper under hogging moment. *International Conference on Structural Integrity and Failure - SIF2006*, Sep 27 - 29, Sydney, Australia, 331-336.

- Kaewunruen, S. and Remennikov, A.M., 2006, Nonlinear finite element modelling of railway prestressed concrete sleeper. *10th East Asia-Pacific Conference on Structural Engineering and Construction*, Aug 3 - 5, Bangkok, Thailand, Vol. 4, 323-328.
- Kaewunruen, S. and Remennikov, A.M., 2006, Rotational capacity of railway prestressed concrete sleeper under static hogging moment. *10th East Asia-Pacific Conference on Structural Engineering and Construction*, Aug 3 - 5, Bangkok, Thailand, Vol. 5, 399-404.
- Remennikov, A.M., Kaewunruen, S., and Ikaunieks, K., 2006, Deterioration of dynamic rail pad characteristics. *Conference of Railway Engineering 2006*, Apr 30 - May 3, Melbourne, Australia, 173-179.
- Kaewunruen, S. and Remennikov, A.M., 2005, Integrated field measurements and track simulations for condition assessment of railway tracks. *the 1st International Conference on Structural Condition Assessment, Monitoring, and Improvement*, Dec 12-14, Perth, Australia, 391-398.
- Kaewunruen, S. and Remennikov, A.M., 2005, Monitoring structural degradation of rail bearing pads in laboratory using impact excitation technique. *the 1st International Conference on Structural Condition Assessment, Monitoring, and Improvement*, Dec 12-14, Perth, Australia, 399-405.
- Remennikov, A.M. and Kaewunruen, S., 2005, Investigation of vibration characteristics of prestressed concrete sleepers in free-free and in-situ conditions. *Australian Structural Engineering Conference 2005*, Sep 11-14, Newcastle, Australia [CD Rom].
- Kaewunruen, S. and Remennikov, A.M., 2005, Applications of experimental modal testing for estimating dynamic properties of structural components. *Australian Structural Engineering Conference 2005*, Sep 11-14, Newcastle, Australia [CD Rom].
- Under review***
- Kaewunruen, S. and Remennikov, A.M., 2008, "Impact responses of railway prestressed concrete sleepers under repeated severe impact loads." *IES Journal Part A: Civil and Structural Engineering*, (submitted).

- Kaewunruen, S. and Remennikov, A.M., 2008, "Crack propagations of prestressed concrete sleepers in railway track systems subjected to once-off and repeated severe impact loads." *ASCE Journal of Structural Engineering*, (submitted).
- Kaewunruen, S. and Remennikov, A.M., 2008, "Residual energy toughness of prestressed concrete sleepers in railway track structures subjected to repeated probabilistic impact loads." *International Journal of Impact Engineering*, (submitted).
- Kaewunruen, S. and Remennikov, A.M., 2007, "Progressive impact behaviours of prestressed concrete sleepers in railway track environments." *Engineering Structures*, (submitted).
- Kaewunruen, S. and Remennikov, A.M., 2007, "Dynamic flexural influence on railway concrete sleepers in track systems of a wheel impact." *Engineering Failure Analysis*, (submitted).
- Kaewunruen, S. and Remennikov, A.M., 2007, "Influence of ballast conditions on flexural responses of railway concrete sleepers in track systems." *Concrete In Australia, Journal of Concrete Institute of Australia*, (submitted).
- Kaewunruen, S. and Remennikov, A.M., 2007, "Transient load effects on flexural responses of railway concrete sleepers in track systems." *Computers and Concrete*, (submitted).
- Kaewunruen, S. and Remennikov, A.M., 2007, "Impact testing of in-situ railway prestressed concrete sleepers." *Procs of ICE - Structures and Buildings, Special issue 2008 on Impact Engineering* (submitted).
- Kaewunruen, S. and Remennikov, A., 2008, "Relation between impact energy and fracture toughness of prestressed concrete sleepers." *2008 Permanent Way Institute Convention, Oct 27 - 29, Sydney, Australia*, (submitted).
- Kaewunruen, S. and Remennikov, A., 2008, "Probabilistic impact assessment of railway prestressed concrete sleepers." *2008 Permanent Way Institute Convention, Oct 27 - 29, Sydney, Australia*, (submitted).
- Kaewunruen, S. and Remennikov, A., 2008, "Vibrations of statically preloaded railway sleepers." *11th East Asia-Pacific Conference on Structural Engineering and Construction, Nov 19 - 21, Taipei, Taiwan* (submitted).
- Kaewunruen, S. and Remennikov, A., 2008, "Effects of holes and web openings on sectional capacities of prestressed concrete sleepers." *11th East Asia-Pacific*

Conference on Structural Engineering and Construction, Nov 19 - 21, Taipei, Taiwan (submitted).

Kaewunruen, S. and Remennikov, A., 2008, "State-dependent properties of rail pads." *20th Australasian Conference on the Mechanics of Structures and Materials*, Dec 19 - 21, Toowoomba, Queensland, Australia (submitted).

Remennikov, A.M., Murray, M.H., and Kaewunruen, S., 2008, "Dynamic design guidelines for railway prestressed concrete sleepers." *20th Australasian Conference on the Mechanics of Structures and Materials*, Dec 19 - 21, Toowoomba, Queensland, Australia (submitted).

#### ***Technical Reports:***

Kaewunruen, S., and Remennikov, A. 2006, Use of reliability-based approach for conversion of AS1085.14 to limit states design of railway prestressed concrete sleepers, *Research Discussion Paper*, CRC Railway Engineering and Technology, Australia, November, 21p.

Kaewunruen, S., and Remennikov, A. 2005, Static behaviors and testing of railway prestressed concrete sleepers, *Research Report*, CRC Railway Engineering and Technology, Australia, December, 61p.

Kaewunruen, S., and Remennikov, A. 2005, Typical dynamic, impact loading on railway tracks, *Research Report*, CRC Railway Engineering and Technology, Australia, September, 21p.

Kaewunruen, S., and Remennikov, A. 2005, In-field dynamic testing and measurements of railway tracks in Central Queensland, *Research Report*, CRC Railway Engineering and Technology, Australia, April, 26p.

Kaewunruen, S., and Remennikov, A. 2004, A state-of-the-art review report on vibration testing of ballasted track components, *July-Dec Research Report*, CRC Railway Engineering and Technology, Australia, December, 20p.

#### ***Public Presentations***

Kaewunruen, S. and Remennikov, A., 2008, Limit states design concept for railway concrete sleeper. *Concrete Institute of Australia Technical Seminar*, June, Brisbane, Australia.



- Kaewunruen, S. and Remennikov, A., 2007, Impact studies towards the development of a new design concept for railway concrete sleeper. *HDR Student Conference 2007*, Sep 26, Wollongong, Australia.
- Remennikov, A. and Kaewunruen, S., 2006, Dynamic analysis of railway tracks with particular reference to concrete sleepers. *Rail CRC Showcase & Review 2006*, Feb 15-16, Sydney, Australia.
- Kaewunruen, S. and Remennikov, A., 2005, Determining dynamic properties of structural/mechanical elements based on single- and 2-DOF idealisations. *CME Seminar Series 2005*, Nov 2, Wollongong, Australia.
- Kaewunruen, S. and Remennikov, A., 2005, Railway track dynamics - Innovating theory into practice. *HDR Student Conference 2005*, Sep 29, Wollongong, Australia.
- Kaewunruen, S. and Remennikov, A., 2005, Field investigation for structural health assessment of railway tracks. *Rail CRC Student Workshop 2005*, June 22-24, Brisbane, Australia.
- Remennikov, A. and Kaewunruen S., 2004, Experimental and numerical investigation of dynamic properties of railway track components. *Rail-CRC Theme 2 Workshop: Innovative/Automated Track Maintenance & Upgrading Technologies*, August 27, Stampford Airport Hotel, Sydney, Australia.

### **Media Releases**

- 1.) Students' Newsletter, Engineers Australia (February, 2008)
- 2.) University media: <http://media.uow.edu.au/news/2007/0706a/index.html>
- 3.) Mercury Newspaper (09/07/2007)
- 4.) Rhizome Magazine (2007) Issue 2, p21
- 5.) Rail Express (2006)
- 6.) Rail CRC Newsletter (2005)

# APPENDIX

---



### Safe Work Procedure

<b>Process/Equipment:</b> High capacity impact testing machine	<b>Location:</b> Highbay Laboratory (4G28)	
<b>Procedure Developed by:</b> Sakdirat Kaewunruen	<b>Approved by:</b> A/Prof M. Hadi	<b>Date:</b> 12/03/2007

**Referenced UOW Guidelines, legislation, codes of practice, Australian Standards etc:** All users must be trained prior to use the apparatus including a competency test to ensure that the user can use the apparatus safely.

**Personal Protective Equipment Required** (Check the box for required PPE):

															
<input checked="" type="checkbox"/>	<input type="checkbox"/>	<input type="checkbox"/>	<input type="checkbox"/>	<input type="checkbox"/>	<input checked="" type="checkbox"/>	<input type="checkbox"/>	<input type="checkbox"/>	<input checked="" type="checkbox"/>	<input type="checkbox"/>	<input type="checkbox"/>	<input checked="" type="checkbox"/>	<input type="checkbox"/>	<input type="checkbox"/>	<input type="checkbox"/>	<input type="checkbox"/>

<b>Activity</b> <i>(Steps in the process/task)</i>	<b>Hazards Identified</b> <i>(What could cause an injury)</i>	<b>Risk Score</b> <i>(How harmful is it)</i>	<b>Controls</b> <i>(What can be done to minimise the risk of injury)</i>
Ensure the work area is safe.	-Tools, oil left on floor -Incorrectly kept heavy parts and electric cables	M	-Ensure Tidy/clean work area -Make sure all parts are securely positioned, and watch for electric cables
Inspection of pressure lines, cable, and control panel	- Damage or leak in pressure lines - Damage or defect of sling - Malfunction of control panel	H	-Check the pressure lines for leak and damage -Check often the integrity of sling and clamp -Check the electronic control panel and winch battery
Preparation of test	-Handling of access to impact machine -Assembling the specimens	H	-Lift the drop mass to the safe position -Use the control panel to open all gates -Use crane for the assembly -Wear safety shoes and gloves -Have an appropriate training to operate the machine
Pre testing	-Operation of the impact machine	H	-Make sure the test area is clear before operating the machine -No one is allowed to access the test area once the machine is already operated or the falling mass is lifted from ground. -Wear glasses to avoid possible eye contact with the flying objects -Use earplug all the time of operation and testing

<b>Process/Equipment:</b> High capacity impact testing machine		<b>Location:</b> Highbay Laboratory (4G28)	
<b>Procedure Developed by:</b> Sakdirat Kaewunruen		<b>Approved by:</b> A/Prof M. Hadi	<b>Date:</b> 12/03/2007
Testing (falling impact)	-Application of impact force	H	-Ensure the test area is clear and all gates are closed before dropping the mass -Wear protective stuffs all the time -Be aware of flying objects
End of test	-Access to the machine -Removal of specimen -Dismantling the arrangement	H	-Use the control panel to operate the machine -Before open any gate using the control panel, ensure that the drop mass is locked at the safe position. -Use appropriate tools for dismantling the arrangement -Use crane to move the damaged specimens
Finishing	-Leaving the crane in an improper way -Incorrectly kept tools and parts -Spilled oil/water on the floor -power and electric cables -Left door opened	M	-Lower crane jib and keep in a safe place -Keep tools and parts in a safe and secure position -Clean the apparatus and work area -Ensure electric cables are properly placed, and power is off. -All gates must be closed after finishing.